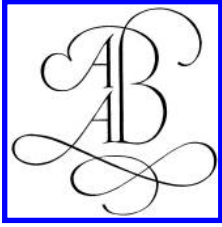


TUNNELLING. A DECADE OF PROGRESS

GeoDelft 1995–2005



BALKEMA – Proceedings and Monographs
in Engineering, Water and Earth Sciences

Tunnelling. A Decade of Progress

GeoDelft 1995–2005

Editors

A. Bezuijen
GeoDelft, The Netherlands

H. van Lottum
GeoDelft, The Netherlands



LONDON/LEIDEN/NEW YORK/PHILADELPHIA/SINGAPORE

Copyright © 2006 Taylor & Francis Group plc, London, UK

All rights reserved.

Except for

A. Bezuijen, A.M. Talmon, F.J. Kaalberg, & R. Plugge, 'Field measurements of grout pressures during tunnelling of the Sophia Rail Tunnel' is reprinted from: *Soils & Foundations* 44(1), pp. 39–48. © 2004 Japanese Geotechnical Society. Used with permission.

A. Bezuijen & A.M. Talmon, 'Grout pressures around a tunnelling, influence of grout consolidation and loading on lining' is reprinted from: *Tunnelling and Underground Space Technology* 19 (4-5), Underground space for sustainable urban development. Proceedings of the 30th ITA-AITES World Tunnel Congress, pp. 443–444. © 2004 Elsevier. Used with permission.

T. Hashimoto, J. Brinkman, T. Konda, Y. Kano, & A. Feddema, 'Simultaneous backfill grouting, pressure development in construction phase and in the long-term' is reprinted from: *Tunnelling and Underground Space Technology* 19 (4-5), Underground space for sustainable urban development. Proceedings of the 30th ITA-AITES World Tunnel Congress, p. 447. © 2004 Elsevier. Used with permission.

A. Bezuijen & A.M. Talmon, 'Grout the foundation of a bored tunnel' is reprinted from: Proceedings BGA International Conference on Foundations, Dundee, September 2003, pp. 129–138. © 2003 London, Telford. Used with permission.

A.M. Talmon & A. Bezuijen, 'Muck discharge by the screw conveyor of an EBP tunnel boring machine' is reprinted from: *Geotechnical Aspects of Underground Construction in Soft Ground*, Proceedings of the 3rd International Symposium, Toulouse, France 23–25 October 2002, pp. 173–178. © 2002 Specificque. Used with permission.

A. Bezuijen, 'The influence of soil permeability on the properties of a foam mixture in a TBM' is reprinted from: *Geotechnical Aspects of Underground Construction in Soft Ground*, Proceedings of the 3rd International Symposium, Toulouse, France 23–25 October 2002, pp. 221–226. © 2002 Specificque. Used with permission.

R.H.B. Rijkers, B.R. Hemmen, N.M. Naaktgeboren & H. Weigl, 'In-situ frost heave loads in artificially frozen ground for tunnelling' is reprinted from: *Geotechnical Aspects of Underground Construction in Soft Ground*, Proceedings of the 3rd International Symposium, Toulouse, France 23–25 October 2002, pp. 379–386. © 2002 Specificque. Used with permission

F.B.J. Barends, 'Unseen Features Jeopardise Underground Construction' is reprinted from: Proceedings of 25 Years Jubilee Symposium of Engineering Geology in the Netherlands, Delft, The Netherlands, 10 December 1998, pp. 19–30. © 1998 Ingeokring. Used with permission.

H.J.A.M. Hergarden, J.W. Plekkenpol & J.S. van der Schrier, 'Shield tunnelling in saturated sand, face support pressure and soil deformation' is reprinted from: *Tunnelling* 97. Proceedings of the 8th International Symposium, pp. 91–102. © 1997 Institute of Mining and Metallurgy. Used with permission.

P. van den Berg, J.S. van der Schrier & H.J.A.M. Hergarden, 'Constructing underground: Influencing geotechnical equilibrium' is reprinted from: *ICUSESS 92*. Proceedings of the 5th International Conference in Underground Space and Earth Sheltered Structures, pp. 760–770. © 1992 Delft University Press. Used with permission.

No part of this publication or the information contained herein may be reproduced, stored in a retrieval system, or transmitted in any form or by any means, electronic, mechanical, by photocopying, recording or otherwise, without written prior permission from the publisher.

Although all care is taken to ensure the integrity and quality of this publication and the information herein, no responsibility is assumed by the publishers nor the author for any damage to property or persons as a result of operation or use of this publication and/or the information contained herein.

Published by: Taylor & Francis/Balkema
P.O. Box 447, 2300 AK Leiden, The Netherlands
e-mail: Pub.NL@tandf.co.uk
www.balkema.nl, www.tandf.co.uk, www.crcpress.com

ISBN 0 415 39133 4

Printed in Great-Britain

Table of Contents

Preface	IX
Introduction	XI
<i>Part 1: Field Measurements</i>	
<i>Introduction to Field Measurements</i>	
Monitoring soft soil tunnelling in the Netherlands: an inventory of design aspects <i>P. van den Berg, K.J. Bakker & J. Rots</i>	5
Ground deformations due to the boring of the Second Heineoord Tunnel <i>E.P. van Jaarsveld, J.W. Plekkenpol & C.A. Messemaeckers van de Graaf</i>	11
ETAC two-component grout field test at Botlek rail tunnel <i>A. Feddema, M. Möller, W.H. van der Zon & T. Hashimoto</i>	19
Pore pressures in front of tunnel, measurements, calculations and consequences for stability of tunnel face <i>A. Bezuijen, J.P. Pruiksma & H.H. van Meerten</i>	27
The influence of soil permeability on the properties of a foam mixture in a TBM <i>A. Bezuijen</i>	35
Pressure gradients and muck properties at the face of an EPB <i>A. Bezuijen, J.F.W. Joustra, A.M. Talmon & B. Grote</i>	43
In-situ frost heave loads in artificially frozen ground for tunnelling <i>R.H.B. Rijkers, B. Hemmen, N.M. Naaktgeboren & H. Weigl</i>	51
Monitoring and modelling during tunnel construction <i>A. Bezuijen & A.M. Talmon</i>	61
<i>Part 2: Grout Behaviour</i>	
<i>Introduction to Grout Behaviour</i>	
Modelling the grouting process around a tunnel lining in a geotechnical centrifuge <i>H.E. Brassinga & A. Bezuijen</i>	71
Grout pressures around a tunnel lining <i>A.M. Talmon, L. Aanen, A. Bezuijen & W.H. van der Zon</i>	77
Field measurements of grout pressures during tunnelling of the Sophia Rail Tunnel <i>A. Bezuijen, A.M. Talmon, F.J. Kaalberg & R. Plugge</i>	83
Grout the foundation of a bored tunnel <i>A. Bezuijen & A.M. Talmon</i>	95
Simultaneous backfill grouting, pressure development in construction phase and in the long-term <i>T. Hashimoto, T. Konda, J. Brinkman, A. Feddema & Y. Kano</i>	101

Grout pressures around a tunnel lining, influence of grout consolidation and loading on lining <i>A. Bezuijen & A.M. Talmon</i>	109
Laboratory testing of grout properties and their influence on backfill grouting <i>A. Bezuijen, W.H. van der Zon & A.M. Talmon</i>	115
 <i>Part 3: Model Testing</i>	
<i>Introduction to Model Testing</i>	
The influence of a bored tunnel on pile foundations <i>A. Bezuijen & J.S. van der Schrier</i>	127
Shield tunnelling in saturated sand – face support pressure and soil deformations <i>J.W. Plekkenpol, J.S. van der Schrier & H.J.A.M. Hergarden</i>	133
Blow-out pressures measured in a centrifuge model and in the field <i>A. Bezuijen & H.E. Brassinga</i>	143
The stability of a tunnel face in soft clay <i>A. Bezuijen & A. van Seters</i>	149
Simulation of the EPB-shield TBM in model tests with foam as additive <i>A. Bezuijen & P.E.L. Schaminée</i>	157
Muck discharge by the screw conveyor of an EPB Tunnel Boring Machine <i>A.M. Talmon & A. Bezuijen</i>	165
Geotechnical centrifuge tests to verify the long-term behaviour of a bored tunnel <i>H.M.A. Pachen, H.E. Brassinga & A. Bezuijen</i>	171
 <i>Part 4: Numerical Analysis</i>	
<i>Introduction to Numerical Analysis</i>	
Constructing underground: influencing geotechnical equilibrium <i>P. van den Berg, J.S. van der Schrier & H.J.A.M. Hergarden</i>	181
Stress distribution due to tunnel excavation <i>A.J. Grashuis & J.A.M. Teunissen</i>	189
Soil loads acting on shield tunnels: comparison between bedded beam model and finite element calculations <i>J.T. van der Poel, H.J.A.M. Hergarden & H.R.E. Dekker</i>	195
3D analysis of soft soil tunnelling <i>S.J.M. van Eekelen, P. van den Berg, K.J. Bakker & F. Jonker</i>	203
Three dimensional numerical simulation of tunnelling <i>J.A.M. Teunissen, J. Brinkman & P.S. Jovanovic</i>	211
Simplified three-dimensional numerical modelling of shield tunnel advancement <i>A.R. Koelewijn & A. Verruijt</i>	217
 <i>Part 5: Miscellaneous</i>	
<i>Introduction to Miscellaneous</i>	
Souterrain The Hague: clogging of groundwater wells above a gel layer during construction of an underground tram station <i>H.J. Luger, E.E. van der Hoek & A.F. van Tol</i>	227

Souterrain The Hague: imperfections in jet-grout layers <i>A.F. van Tol & J.B. Sellmeijer</i>	235
Souterrain The Hague: scouring in case of sand boils through a jet-grout layer <i>D.R. Mastbergen, W.G.M. van Kesteren & A.F. van Tol</i>	241
The use of the underground space in deltaic areas <i>F.B.J. Barends & W.L. Leendertse</i>	247
Unseen features jeopardise underground construction <i>F.B.J. Barends</i>	263
Managing soil deformations due to tunnelling in the Netherlands <i>J. Brinkman</i>	273
Influence of pore pressure at tunnel face <i>A. Bezuijen</i>	277

Contribution by year

1992

- Constructing underground: influencing geotechnical equilibrium 181
P. van den Berg, J.S. van der Schrier & H.J.A.M Hergarden

1994

- The influence of a bored tunnel on pile foundations 127
A. Bezuijen & J.S. van der Schrier
- The use of the underground space in deltaic areas 247
FB.J. Barends & WL. Leendertse

1995

- Stress distribution due to tunnel excavation 189
A.J. Grashuis & J.A.M. Teunissen

1996

- Soil loads acting on shield tunnels: comparison between bedded beam model and finite element calculations 195
J.T. van der Poel, H.J.A.M. Hergarden & H.R.E. Dekker

1997

- Monitoring soft soil tunnelling in the Netherlands: an inventory of design aspects 5
P. van den Berg, K.J. Bakker & J. Rots
- Shield tunnelling in saturated sand – face support pressure and soil deformations 133
J.W. Plekkenpol, J.S. van der Schrier & H.J.A.M. Hergarden
- 3D analysis of soft soil tunnelling 203
S.J.M. van Eekelen, P. van den Berg, K.J. Bakker & F. Jonker

1998

- Unseen features jeopardise underground construction 263
FB.J. Barends

1999

- Ground deformations due to the boring of the Second Heinenoord Tunnel 11
E.P. van Jaarsveld, J.W. Plekkenpol & C.A. Messemaeckers van de Graaf

2001

- ETAC two-component grout field test at Botlek rail tunnel 19
A. Feddema, M. Möller, W.H. van der Zon & T. Hashimoto
- Pore pressures in front of tunnel, measurements, calculations and consequences for stability of tunnel face 27
A. Bezuijen, J.P. Pruiksma & H.H. van Meerten
- Modelling the grouting process around a tunnel lining in a geotechnical centrifuge 71
H.E. Brassinga & A. Bezuijen

Grout pressures around a tunnel lining <i>A.M. Talmon, L. Aanen, A. Bezuijen & W.H. van der Zon</i>	77
Blow-out pressures measured in a centrifuge model and in the field <i>A. Bezuijen & H.E. Brassinga</i>	143
Simulation of the EPB-shield TBM in model tests with foam as additive <i>A. Bezuijen & P.E.L. Schaminée</i>	157
Three dimensional numerical simulation of tunnelling <i>J.A.M. Teunissen, J. Brinkman & P.S. Jovanovic</i>	211
Simplified three-dimensional numerical modelling of shield tunnel advancement <i>A.R. Koelewijn & A. Verruijt</i>	217
 <i>2002</i>	
The influence of soil permeability on the properties of a foam mixture in a TBM <i>A. Bezuijen</i>	35
In-situ frost heave loads in artificially frozen ground for tunnelling <i>R.H.B. Rijkers, B. Hemmen, N.M. Naaktgeboren & H. Weigl</i>	51
The stability of a tunnel face in soft clay <i>A. Bezuijen & A. van Seters</i>	149
Muck discharge by the screw conveyor of an EPB Tunnel Boring Machine <i>A.M. Talmon & A. Bezuijen</i>	165
Managing soil deformations due to tunnelling in the Netherlands <i>J. Brinkman</i>	273
 <i>2003</i>	
Grout the foundation of a bored tunnel <i>A. Bezuijen & A.M. Talmon</i>	95
Souterrain The Hague: clogging of groundwater wells above a gel layer during construction of an underground tram station <i>H.J. Luger, E.E. van der Hoek & A.F. van Tol</i>	227
Souterrain The Hague: imperfections in jet-grout layers <i>A.F. van Tol & J.B. Sellmeijer</i>	235
Souterrain The Hague: scouring in case of sand boils through a jet-grout layer <i>D.R. Mastbergen, W.G.M. van Kesteren & A.F. van Tol</i>	241
 <i>2004</i>	
Field measurements of grout pressures during tunnelling of the Sophia Rail Tunnel <i>A. Bezuijen, A.M. Talmon, F.J. Kaalberg & R. Plugge</i>	83
Simultaneous backfill grouting, pressure development in construction phase and in the long-term <i>T. Hashimoto, T. Konda, J. Brinkman, A. Feddema & Y. Kano</i>	101
Grout pressures around a tunnel lining, influence of grout consolidation and loading on lining <i>A. Bezuijen & A.M. Talmon</i>	109
Influence of pore pressure at tunnel face <i>A. Bezuijen</i>	277

2005

Pressure gradients and muck properties at the face of an EPB <i>A. Bezuijen, J.F.W. Joustra, A.M. Talmon & B. Grote</i>	43
Monitoring and modelling during tunnel construction <i>A. Bezuijen & A.M. Talmon</i>	61
Laboratory testing of grout properties and their influence on backfill grouting <i>A. Bezuijen, W.H. van der Zon & A.M. Talmon</i>	115
Geotechnical centrifuge tests to verify the long-term behaviour of a bored tunnel <i>H.M.A. Pachen, H.E. Brassinga & A. Bezuijen</i>	171

Preface

Delta areas all over the world are attractive places to live and work. They have tremendous economic potential; but living there also means to live in the permanent threat of flooding and subsidence of the soft soil. Civil and hydraulic engineering are key factors in managing these challenges and providing sustainable solutions. Apart from the constant threat of water on the one hand and the soft soil on the other, the Netherlands face an additional problem as well. The claims on the available space in the Netherlands are becoming bigger and bigger. A solution to cope with this problem has been found in a totally new dimension: the underground. However, building underground in the soft soils of the Dutch delta is not without risks when the available knowledge and experience is limited. The last decade a lot of research has been carried out in the Netherlands related to underground construction in soft soil. This book presents a collection of papers related to this field.

Tunnels in Holland had been traditionally constructed by dredging a trench and sink down caissons in the trench. The impact on above ground activities is temporarily but large, and tunnel boring would be a viable alternative. However, the soft soil has long been an impassable obstacle, and only in 1999 the first large diameter bored tunnel in the Netherlands, the Second Heinenoord tunnel, was completed. From the beginning on it was decided that this tunnel should be a study object as well and this approach has been the beginning of a successful knowledge development strategy. During the construction an extensive monitoring program was performed. Unexpected effects occurred: the settlement trough was narrower than predicted and the soil and pore water stress distribution were quite different from what was expected based on the experience from tunnels outside the Netherlands.

From this first experience it became clear that knowledge development was heavily needed. GeoDelft (within the context of the Delft Cluster consortium, an open network of knowledge institutes in and near Delft, founded in 1999) decided to focus on the fundamental long term aspects. Herein they could easily hook on to the running programme of COB, the Netherlands Centre for Underground Construction that was directed primarily on applied research to acquire practical knowledge. The COB-programme was therefore a very relevant source of research questions, and the COB-approach of developing knowledge in one tunnel project and applying it in the next was thought to be fruitful. The different parts of the Delft Cluster programme have therefore been coupled directly to COB within the framework of 'Joint Practical Research of Bored Tunnels' (GPB). In addition GeoDelft developed a fruitful cooperation with a Japanese partner, the Geo Research Institute in Osaka.

Coupling of GeoDelft – Delft Cluster research to practical projects guaranteed the availability of field laboratories. In that way it became possible to perform extensive measurements, but also to do experiments and to apply and validate the acquired knowledge and models. A clear example is the optimization of the grouting process throughout a number of tunnel projects. In the Second Heinenoord tunnel it appeared that the subsidence of the surface area was quite sensitive to the amount and pressure of grout injected in the tail void of the TBM, and this generated a string of research projects in numerical and physical modelling and field verification. During the construction of the Botlek Rail Tunnel GeoDelft and WL|Delft Hydraulics performed tests with a two component grout, and in the Sophia Rail Tunnel an extensive measurement and evaluation programme has been completed. By the knowledge developed in those cases, the grouting process can now be predicted accurately, so that the tunnel which will shortly be bored in the subsoil deep under the pile foundations of old Amsterdam can be looked forward with confidence.

A second example of a field laboratory in the framework of the GPB consortium was the Westerschelde tunnel. The construction of this 6.6 kilometre long tunnel under the Westerschelde waterway experienced rather extreme conditions as the deepest point lies at 60 metres below sea level. A number of transverse links, each with a length of 12 meters, had to be constructed between the two bored tunnels by way of emergency exits. Their construction was done using soil freezing. It was the first time that this technology was used in the Netherlands on that scale in such an extreme condition. Delft Cluster partners GeoDelft and TNO cooperated in the research how and how much the frozen environment would deform the transverse tubes. The results from this project will also benefit to other Dutch tunnel and other underground construction projects.

Not only the effects on the surroundings, but also the structure of the concrete tunnel itself is subject of the Delft Cluster research. In the Heinenoord case it already appeared that in the soft Dutch soil the behaviour of the stiff structure is fundamentally different from what the existing models predicted. Although the models suggested

that the construction phase is not indicative for the design conditions of the tunnel segments, it appeared to be of paramount importance. The stamps with which the TBM is pushed forward find their reaction forces in the already placed tunnel segments. Possible damage mechanisms to the segments were investigated in a full scale test set-up at the Technical University of Delft. In the Botlek tunnel an extensive set of measurements has been performed. The results of these tests have led to an optimized form of the segments and to modifications in the joints, notches and reinforcement of the segments.

These examples show the power of combination the knowledge of the soil, of soil/construction interaction and of construction material properties. The last decade important steps have been made in order to be able to construct bored tunnels in the very soft soil conditions in the densely populated Western part of the Netherlands. Underground construction in a controlled way is an enormous challenge, especially the coming years, when a number of tunnels will be constructed underneath the old city centres of Amsterdam, Rotterdam and The Hague. The set of papers presented in this volume gives an overview of the research work carried out the last decade by GeoDelft and their partners, especially within the Delft Cluster network and the COB consortium.

Peter van den Berg,
Director Research GeoDelft.

Introduction

Shield tunnelling was introduced in the Netherlands only recently. The first large shield tunnel was the Second Heinenoord tunnel. The Tunnel Boring Machine (TBM) for this project started in March 1997, preliminary works in 1995. Within a decade, 6 bored tunnels were realized. Some of them were challenging projects pushing the limits of tunnelling technology. The list of tunnels includes the by then largest diameter shield tunnel, the tube with the fastest drilling velocity, a tunnel up to 60 m below the sea water level and an EPB tunnel bored in sand with a high water pressure.

Field measurements, model and laboratory testing were performed for each tunnel to increase understanding in the mechanisms involved when in boring a tunnel in soft soil with a high water table. GeoDelft was always involved in the geotechnical aspects of this research. The contribution of GeoDelft was not limited to the 'traditional' geotechnical fields: face stability and settlement trough, but there were also contributions to the field of bore technology and freezing. Results of this research have been published in articles and conference proceedings.

Aim of this book is to present an overview of the contribution of GeoDelft to this research. Existing articles and papers are the core of this book. The contents of these has not been changed, only the layout has been harmonized for this book and some pictures that were not available in sufficient quality have been changed or have been removed (pictures were removed only when not essential for the text). The first contributions have been written in 1992, when the idea came up that shield tunnelling in the Netherlands is a realistic possibility, the last contributions are from 2005.

In this way the book not only presents pure technical contents, but it also presents how the ideas evolve on what research is relevant to improve the knowledge on tunnelling. The oldest publications concentrate on what will be the advantages of tunnelling, Mid-nineties the face stability and the stability of surrounding pile foundations became an issue. Physical and numerical models were made to investigate face stability and stability of pile foundations. From the results obtained in the first tunnelling projects it became clear that tail void grouting is a critical process to minimize surface and subsurface settlement. Grout flow properties were investigated in a Delft Cluster project and in field measurements at the Sophia Rail tunnel.

The most recent publications in this book show the influence of the grouting process on the force distribution on the lining and the influence on the grout pressure distribution. The Botlek tunnel was made using an EBP (Earth Pressure Balance) shield. This triggered some EPB-shield related research on face stability and, properties and the influence of ground water flow on foam stability.

It was tempting to present the articles in chronological order to show the development in the research. Looking to the individual papers however, it appears that the historical development is less strait forward than the more general picture sketched above. Some papers deal with older subjects but were published later, to contribute to a certain conference. It is therefore decided to present the papers by subject. 4 chapters present 4 focus points in the research on tunnelling performed by GeoDelft. These focus points are:

- Field measurements
- Grout behaviour.
- Model testing
- Numerical analysis.

The last chapter presents some papers, which do not fit directly within one of these focus points. Each chapter has a short introduction before the contributions of that chapter.

Introduction to Field Measurements

This chapter comprises some results that were obtained from field measurements. Field data were obtained from the Second Heinenoord Tunnel, the Botlek Rail Tunnel and Sophia Rail tunnel.

Papers dealing with the first two tunnels focus on the tunnel face (pore pressures, pressure distribution), for the last tunnel it is focused on the grout pressures. Field measurements of the first blow out of a tunnel face in The Netherlands, which occurred during drilling of the Second Heinenoord Tunnel, are also presented in this book, not in this chapter however. In a paper from 2001 the measured pressures at the blow out are compared with the pressures of blow out experiments in a centrifuge and therefore this paper is collected in the chapter over model tests.

The content of the first paper in this section was made before measurements on the Second Heinenoord Tunnel started. It therefore presents what should be measured and not what is measured. The next paper presents some measurements results and shows a comparison of the measured ground deformations with a Finite Element Model. It shows that the measured grout pressures deviate considerably from the assumed pressures, or as it was stated in the conclusions of the paper: "Above mentioned phenomena desire a more accurate model of the back fill grouting procedure". This was one of the reasons to start a research programme on grout behaviour, which is dealt with in the next chapter.

The third paper presents the results of measurements performed at the Botlek Rail Tunnel. A two component grout that was used for the Second tube was tested and the results were analyzed and compared with the results of measurements on 'traditional' grout that was used for the first tube of the same tunnel.

The paper "Pore pressures in front of tunnel, measurements, calculations and consequences for stability of tunnel face" presents one of the main findings from the measurements at the Second Heinenoordtunnel": the excess pore water pressures that exist in the soil in front of the TBM. This excess pore water pressure can have consequences for the stability of the tunnel face as is elucidated in the paper by using analytical and numerical methods. A prediction was made what will be the consequences for Green Heart Tunnel (that was in the design phase during the writing of the paper)

when the TBM reaches a polder. It became clear that there was a risk for a blow out. The recommendations based on these calculations were taken over by the contractor and owner of the Green Heart Tunnel, resulting in extra precautions (Aime et al., 2004).

The interaction between a sandy soil and foam, as present at the face of an EPB shield was studied in the fourth paper using the measurements performed during drilling of the Botlek Rail Tunnel. It was shown that excess pore pressures as measured in front of a slurry shield can also be present in front of an EPB shield, depending on the permeability of the subsoil. The permeability of the subsoil also influences the foam properties. In case of permeable subsoil it is possible for the foam to expel the pore water in front to the tunnel face. This will lead to 'dry foam'. In case of less a permeable saturated soil the pore water will remain in the muck leading to 'wet foam' with different qualities.

The next paper in this section deals with the pressure distribution at the tunnel face and the pressure drop in the screw conveyer of the EPB shield that was used for the Botlek Rail Tunnel. It is shown that the pressure distribution at the tunnel face is not only governed by the density of the muck, but the yield stress of the slurry also plays a role as well as grain stresses that can occur in the muck. It is further shown that the pressure distribution in the screw conveyer can be influenced by arching that can occur in front of the entrance of the screw conveyer.

Artificial Freezing is an important technique quite often used to make cross passages between two tunnels. The fore last paper in this chapter presents measurements on frost heave and frost related stresses that were measured during construction of the cross passages of the Western Scheldt Tunnel. Frost heave pressures appear to be influenced by the measurement direction with respect to the freezing tubes and the permeability of the soil that was frozen.

The last paper in this chapter showed how a combination of field and laboratory measurements can be used successfully to increase the knowledge on tunnelling. It presents some measurements that are, according to the authors of the paper, examples how progress was made using a combination of measurements and calculation methods.

Monitoring soft soil tunnelling in the Netherlands: an inventory of design aspects

Recherches aux tunnels en sol tendre aux Pays-Bas: Un inventaire des aspect de construction

Klaas Jan Bakker

Centre for Underground Construction CUR/COB/Delft University of Technology, The Netherlands

Peter van den Berg

Delft Geotechnics, The Netherlands

Jan Rots

TNO Delft, The Netherlands

ABSTRACT: In the Netherlands the monitoring of two tunnel boring projects is scheduled. In order to derive a meaningful scheme of instrumentation and measurements, an inventory was made of particular problems related to boring in soft soil has been made. First a description of the geological situation in the Netherlands is given. Secondly the Dutch approach to monitoring is explained. And finally an overview of the typical problems relating to tunnel boring in soft soil (based on the Dutch situation) is produced.

RESUME: Aux Pays-Bas on a décidé d' exécuter deux projets pour la construction des tunnels avec la methode de percer. Pour obtenir un dessin efficace d'instruments et mesurages, un inventaire des problèmes de percer en fond doux a fait. Aussi une description de la situation geologique aux Pays-Bas a exhibé. Pour finir, une tour d'horizon des problems de percer en fond doux (pour la situation aux Pays-Bas) a donné.

1 INTRODUCTION

In 1993 the Dutch minister of Transport and Public Works decided for having two 'pilot' projects with bored tunnelling. For the first time in the Netherlands, tunnels with larger diameter would be build using a boring technique, instead of immersed tunnelling. Though smaller diameter tunnels of up to approximately 3 m diameter had be realised with boring techniques, up to now boring larger diameters tunnels was looked upon as unfavourable with respect to costs and risks. Designers related these risks especially to the soft soil conditions, in the upper zone of the dutch soil.

However, the increasing demand on available space and the increasing public consensus that avoiding hinder during construction and operation has a value too and has to be considered in the weighing of design alternatives, leads to the demand for underground alternatives and building techniques; including bored tunnels.

For that it was decided to have pilot projects. With the aim of gaining experience and to develop

knowledge. The pilot projects will be accompanied by research, involving the prediction, monitoring and evaluation of actual tunnel behaviour. To set-up the predictions and monitoring scheme, an inventory was made of the typical problems to be expected while boring in the Dutch soft soil.

The pilot projects chosen are:

- 1) *The Second Heinenoord tunnel* for road transport
- 2) *The Botlek Spoortunnel* for rail transport

Both tunnels are passing the "Oude Maas" river and located just south of the city of Rotterdam. The second Heinenoord tunnel will have a two tube tunnel with an outer diameter of 8.3 meter, and will be constructed using a slurry-shield (TBM). The lining thickness will be 0.35 meter reinforced concrete segmented rings. The total length of the tunnel will be approximately 900 m. The Botlek Railway tunnel will be a two tube tunnel too, depending on the choice single or double stack transit, the outer diameter will be 8.35 m or 9.5 m. The lining thickness might be 0.4 m or 0.5 m respectively. The total length for the bored tunnel will be approx. 1800 m.

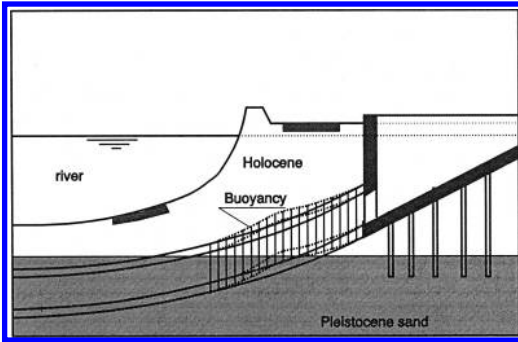


Figure 1. Beam Action of a tunnel in non homogeneous soil.

2 MONITORING PROJECTS

The execution of the 2^e Heineoord tunnel; the boring will start in January 1997, whereas the Botlek railway tunnel will start approximately a year after, in spring 1998. The monitoring of the projects is commissioned to the CUR/COB (Dutch Centre for Underground Construction) committee K100. The preparation of the monitoring, especially for the part that is focussed on the 2^e Heineoord tunnel was initiated late 1993. And started with an inventory. The global plan for the monitoring was formulated simultaneously. The leading thesis for the definition of monitoring project was; 'Measuring is knowing' and secondary to that; 'A predicted measurement has added value'. Therefore, a preliminary phase for the monitoring project is making predictions.

Among other models, K100 has chosen to make predictions with Continuum models such as with Finite Elements. This reflects the view that on the longer term there is more benefit; more added value, related to using 'integral models'. Models which are not limited to an aspect of a design, but where it is possible to analyse several aspects based on one model, one topology of the construction. Continuum models such as 2D and 3D Finite Element models fit in with this perspective.

This reflects the Dutch philosophy for structural design, especially for constructions which go beyond our experience. That is to analyse the 'new' structure rigorously with 'models', both empirical, analytical, physical and numerical. This in contradistinction with the 'observational method of design' such as often used in the United Kingdom or Japan.

3 GEOLOGY OF THE NETHERLANDS

Both tunnels are located in the western part of the country in an area in which the soft to very soft layers (undrained shear strength less than 40 kPa and

sometimes even less than 10 kPa) have a thickness of about 15 to 20 meter. Due to sea attacks, braiding rivers and tidal effects, the subdivision of these upper layers strongly differs at a short distance. In contrast to many projects in other countries, in the Netherlands it is almost impossible to plan a tunnel in, predominantly, one homogeneous layer. In many cases the tunnel boring machine has to excavate many different materials (peat, soft clay, sand and gravel) during the same track.

The top-section of the stratigraphy of the western part of the Netherlands consists of peat and soft to very soft clay (formed during the holocene period) laying on top of a thick layer of sand, coarse sand and gravel (formed during the pleistocene period). In this part of the country, the groundwater level is almost at the soil surface. The pleistocene sand layers were formed during the glacial periods. During these periods the water level of the North Sea was relatively low and during inter-glacial periods the sea level was relatively high. During times of high sea level, the west coast was below sea level and marine clays were deposited, but, generally speaking, sedimentation related to (braided) river systems dominated. Coarse sands and gravels were deposited during glacial periods and windblown sands during inter-glacial periods.

At the beginning of the holocene period, the last sea level rise started and tidal zones reached the south west of the Netherlands again. Peat formation started nearby in the floodplains. These peat layers were sometimes overlain by marine clay and were sometimes eroded by the sea. About 5000 years ago a coastal barrier system was developing: dune forming started. In the areas behind the coastal barrier, out of reach of the aggressive sea, thick peat layers were formed. Locally, these layers were eroded by the sea again and were (partly) replaced by marine clay sediments.

4 INVENTORY OF PROJECT ISSUE'S

According to Peck (1969), the main problems relating to bored tunnelling are;

- **keeping a stable boring front**
- **limiting the impact on the surrounding soil and foundations and**
- **keeping the tunnel safe and operational during use**

Typical aspects which might lead to problems in relation to boring in the Dutch situation might be;

- the geology; very soft soil on top of pleistocene sand
- piled foundations in the Dutch city's,
- groundwater level almost at the soil surface

In order to draw up the inventory of all the aspects on which monitoring of the 'pilot' projects would have to be focused, first a partial inventory was made on

the following aspect fields (for which research and development proposals had been made):

- Risk assessment and safety
- Exploration and monitoring of the subsoil
- Boring and tunnel technology
- Design models for deformation and dynamics
- Integral maintenance and Management
- Environmental aspects

Monitoring was part of all these proposals. The task of committee K100 was to extract a coherent combination of instrumentation and experiments, which would serve the demand of all the aspect fields. Part of this task included was ordering the priority of all the proposals to optimize the profit of the monitoring scheme, and to fit this in on the budget. The result of this is an integrated 'bundle' of research which is under execution as one project.

5 TYPICAL DUTCH PROBLEMS WITH RESPECT TO BORED TUNNELLING

5.1 Feasibility of boring

The feasibility of boring is among other authors described by Peck (1969).

Aspects relating to this feasibility are:

- 1) Front stability
- 2) Excavation efficiency with respect to the soil encountered
- 3) Maintenance and unexpected wear of cutter bits
- 4) Unexpected objects

Front stability; For a slurry shield, such as is foreseen for the 2^e Heineoord tunnel, the working pressure for the slurry support is on the underside bounded by 'active' failure of the soil; if the support pressure is too low to maintain equilibrium in the soil mass. Whereas it is bounded at the upper side by a passive failure of the soil; if the support pressure is too high, a blow out or uncontrolled loss of support fluid might appear.

In Fig. 2 it is illustrated how the boundaries for the support pressure P_a are affected by the strength of the soil. In the figure it is indicated how the boundaries for the support pressure will be affected if the soil gets weaker; narrowing the bandwidth which is available for the support pressure.

In Fig. 3 it is indicated what it means if the uncertainty with respect to the upper and lower bound is taken into account, sketching the probability density of instability. For soft soils; weak soils, a problem might be encountered if the safe range between lower and upper limit leaves a too small range for operating the working pressure of the face support.

A complicating factor might arise if the vertical soil stresses are partially determined by water loading

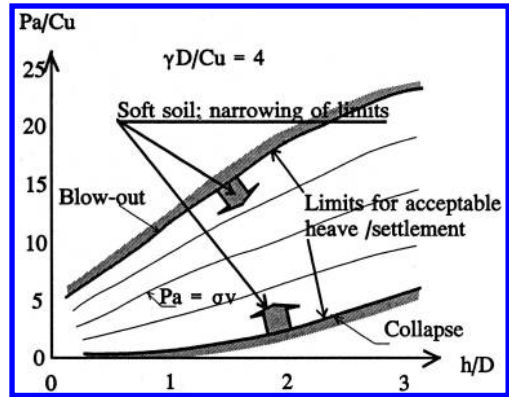


Figure 2. Face support pressure required for stability acc. to Mair (1987).

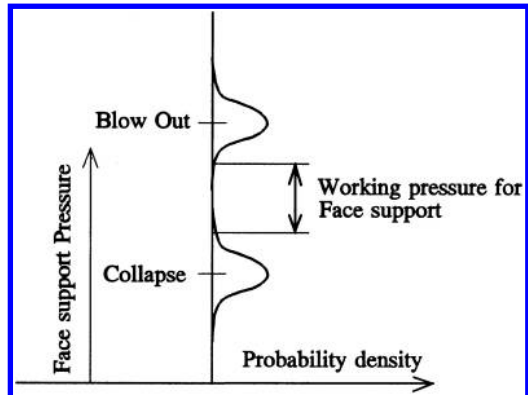


Figure 3. Stability range for face support pressure.

under the influence of tidal movements. The machine driver might have to compensate his slurry support pressure as a function of the tidal movements.

Maintenance and wear of cutter bits; is most likely not too much affected by soft soil. Too 'sticky' behaviour of clay might give more problems.

Excavation efficiency; if there is a large diversity in soil layers; e.g. in the upper holocene layers, the excavation efficiency might be influenced. It will be difficult then, to optimize the type of TBM on a single type of soil. During a tunnel drive of only hundreds of meters, several types of soil might and will be encountered, often only in thin layers. The boring front might not be homogenous; and may exist of very diverse materials, with very diverse permeabilities. This coupled with the probability of water bearing layers, might give problems with respect to local instabilities. For situations with a large fluctuation in soil layers it will be advised to reduce the speed of excavation in order to secure that the 'cake' formation on the front is not too much influenced by a too high speed.

Unexpected objects; In the Netherlands subsoil fossil wood might be encountered. During exploration for the sand closures during the Delta project, where large amounts of sand were needed, special interest was given to this aspect. Seismological surveys in the Eastern Scheldt estuary indicated the existence of fossil wood in the subsoil. In practice no practical problems were encountered. The encountering of tree trunks however cannot be excluded.

In the northern parts of the Netherlands, in the zone that was covered with ice in the last glacial period, boulders were carried by the Ice from the Scandinavian zone's to the Netherlands. The megalithic chambered tombs which can be found in the province 'Drente' are artifacts of that. Boulders might be encountered North of the line 'Haarlem Nijmegen in the Netherlands, and on the 'Utrecht chain off Hills'.

5.2 Buoyancy

As the weight of the tunnel lining and installation is less than the soil (including the groundwater) that is removed, the structure is not in vertical equilibrium. In order to gain equilibrium an initial upward movement will develop, initiating a stress redistribution above, and a stress relieve under the tunnel until equilibrium is reached. The effects of this aspect are related to the beam action of a tunnel, see Fig 2. and section 5.3.1 of this paper.

5.3 Soil-Stiffness

5.3.1 Soil-Stiffness effects on the beam action

As the stiffness of the soil might have a variation along the length of the tunnel, as is illustrated in figure 1, equilibrium might not only be derived from the equilibrium of the successive rings but also because the tunnel tube acts as a 'beam on elastic foundation' This effect is related with the parameter $\frac{\pi}{\lambda}$ (Hetényi 1946), according to:

$$\pi/\lambda = \pi \sqrt[4]{\frac{4E_b I_b}{K}} \quad (1)$$

which might be interpreted as a measure of the length scale on which a disturbance might spread. where:

E_b = the Young's modulus for the material of the 'tube'

I_b = Moment of Inertia for bending of the tube

K = subgrade reaction modulus for the soil

The Moment of Inertia for a thin lined tube is approximated by:

$$I_{buis} \approx \frac{\pi}{8} dD^3 \quad (2)$$

where:

D = Diameter of the tube

d = thickness of the lining

Taking into account that a continuous bedding is assumed both under and on top of the tunnel, the subgrade reaction for the tube is approximated as:

$$K \approx 2Dk_g \quad (3)$$

where for the subgrade reaction modulus for the soil;

$$k_g \approx \frac{E_g}{2D} \quad (4)$$

is assumed, with:

E_s = Young's modulus for the soil.

If one takes into account that:

$$\frac{E_b}{E_g} \approx 1000 \text{ à } 10000 \quad (5)$$

although reducing this ratio by factor 2 for the fact that semi 'elastic' material (Kaubit) is used in the joint between rings to avoid stress concentrations. The lining thickness is approximated as:

$$d \approx \frac{D}{20} \quad (6)$$

combination of all this yields:

$$\frac{\pi}{\lambda} \approx \pi \sqrt[4]{\frac{4}{20} * 0.5 * (1 \text{ à } 10 * 10^3) \frac{\pi}{8} D^4} \approx (7.9 \text{ à } 14D) \quad (7)$$

Which means that for the staged construction of a tunnel tube, and for situation where there is a distinct difference in subgrade reaction modulus, one has to take into account that for a length of approximately 8 to 14 times the diameter of the tube, reckoned from the point of 'disturbance' there is a diminishing effect on bending moments and shearing forces in the tube.

The lower the stiffness of the soil, and/or the higher the stiffness of the tube (larger diameter), the more the assumption that every ring in the tube is in distinct equilibrium with the supporting soil, had to be doubted.

More generally; a low stiffness of the soil brings larger deformation corrections to derive equilibrium from soil reactions.

5.3.2 Soil stiffness effects on bending moments in the lining

For the stress distribution in the tunnel rings, the model developed by Duddeck (1980) and later on evaluated on with respect to the influence of the stiffness of the

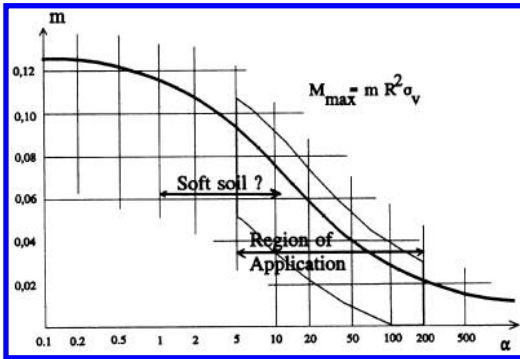


Figure 4. Maximum bending moments in the lining as a function of the stiffness ratio α , acc to Duddeck (1985).

bedding can be used to illustrate the influence of soft soil. The model itself can be regarded as a Winkler type with a curved beam on continuous elastic bedding. In the limiting case this model describes the results for a ring with static loading instead of a spring reaction. Which means that for the bending moments in a tunnel lining, the effect of the relative stiffness can be ‘visualized’ as a reduction factor on the Rigid solution, as a function of the elasticity parameter;

$$\alpha = \frac{E_g R^3}{E_b J_d} = \frac{E_g D^3}{8 E_b J_d} \quad (8)$$

The rigid solution, for a deep tunnel with tangential interaction, which is taken here for reasons of illustration, can be described by:

$$M_{\max} \approx \frac{\sigma_v - \sigma_h}{16} D^2 \quad (9)$$

Where

σ_v = vertical soil stress
 σ_h = horizontal soil stress

For $\sigma_h = K_0 \sigma_v$ and $m = \frac{(1-K_0)}{4}$ this can be read as $M_{\max} = m \sigma_v R^2$ such as indicated in Figure 4. The Figure is drawn for $K_0 = 0.5$.

Duddeck (1985), indicated a region of application between $5 < \alpha < 200$ which would give a reduction of bending moment with respect to the ‘rigid’ situation (no stress redistribution) with a percentage of 20 to 80%.

If we evaluate this for the Dutch soft soil situation, considering that the segmental bending stiffness for a unit with is $I_d = \frac{1}{12} d^3$; and if we assume again that $d = \frac{D}{20}$; evaluating a range for $\frac{E_b}{E_g} \approx 1 \cdot 10^3$. Then, for the soft soil conditions, this leads to;

$$\alpha \approx \frac{12 \cdot 10^3 E_g}{E_b} = \frac{12 \cdot 10^3}{(1 \cdot 10000)} \approx (1 \cdot 12) \quad (10)$$



Figure 5. Deformation of a segmental lining.

Which means that for soft soil conditions we are only nearly within the region of application such as indicated by Duddeck, and now the expected reduction is much less; only 10 to 30%.

5.3.3 Axial equilibrium

At the stage of entering the receiving shaft, the axial stresses at the front, will diminish, and so the axial stresses in the tube. These axial stresses in the tube contribute to the shear force capacity of the tube, and so a procedure has to be developed to secure the shear capacity between the rings at all stages of construction.

5.4 Segmental lining

The effect of soil-structure interaction, and the effect of the stiffness ratio between soil and structure are discussed above in section 5.3 Not discussed yet is that the lining is composed of segments. Segmental tunnel linings can be viewed upon as an assembly of ‘blocks’, connected by joints. Basically, the situation is similar to other stacked structures like masonry, brickwork and precast concrete assemblies. The behaviour of these structures can be assessed using block mechanics. In particular, a nonlinear finite element strategy whereby the segments are modelled by continuum elements and the joints by interface elements might be attractive. The nonlinear behaviour will be mainly concentrated in the relatively weak and flexible joints while the relatively strong concrete segments can be modelled as linear elastic. With this approach the total strength, stiffness/flexibility of the assembly can be predicted.

In Figure 5, an illustrative result is given of one of the predictions which was made to prepare the ‘Instrumented rings’. One of the results of these predictions was the observation that not only the monitoring of stresses within the elements, but also the differential displacements between elements has to be measured. Special instrumentation for that is scheduled.

Finally; the analysis of segmental behaviour is important, especially in the case of soft soil, as the lining build from loose elements with prestresses in fact inherently represents an *unstable* structure, so that large joint openings and segment movements might occur if the proper attention is not paid to this issue.

5.5 Influence of tunnelling on pile foundations

In the western part of the Netherlands, most buildings are founded on piles. The reason for that is discussed in section 3 of this paper. The length of the piles is 15 to 20 meter or even more. The tunnel boring process will take place at or around the same depth.

Normally, during tunnelling a larger volume of soil is removed than the volume of the tunnel itself. Using the present techniques, in many cases this volume loss may be around 1% of the tunnel volume. This volume loss influences the state of stress in the surrounding soil. This may lead to additional settlement of the piles and a reduction of the bearing capacity of the foundation.

The interaction between loaded foundation piles and a tunnel under construction is a complicated mechanical problem. The problem is typically 3-dimensional and the stress distribution in the soil around a driven pile is still a point of discussion. Although at the moment software and hardware is available, suitable for modelling this problem in a 3-dimensional finite element model, the results need validation either by full scale or by model tests in the centrifuge.

Recently, the problem was modelled Delft Geotechnics, centrifuge, (Bezuijen and van der Schrier, 1994). The tunnelling process was simulated by a model tunnel: a cylinder with a diameter which can be varied in a controlled way. Six piles at different distances from the tunnel, loaded to 75% of the ultimate bearing capacity, have been used to investigate the pile-tunnel-interaction. During the test, in which the diameter of the tunnel was reduced, the settlement of the piles was monitored. Three different tests were performed: one preliminary test with limited instrumentation for a tunnel in homogeneous, saturated sand and two subsequent tests with a layered soil model analogous to the typical Dutch conditions, i.e. a (holocene) clay layer on top of a (pleistocene) sand layer.

Based on the test results it was concluded that additional pile settlement due to tunnelling can be quite significant, if the volume loss is about 1% or more and the distance between the pile and the tunnel is about or less than one tunnel diameter. More settlement was measured during the test in which the tunnel was located for a substantial part in the foundation (sand) layer. Extrapolation of the test results indicate that, if the tunnel is not located in the foundation layer,

but in the overlaying clay layer, the influence of the tunnelling process is less significant: larger volume losses or shorter distances between tunnel and pile seem to be acceptable than.

During construction of the 2nd Heineoord Tunnel full scale tests will be carried out using concrete and wooden piles. In the old cities in the western part of the country many buildings are founded on wooden piles. The results of this full scale test will be compared to the results of 3-dimensional finite element predictions and the results of the centrifuge tests.

6 CONCLUDING REMARKS

- In order to control the deformation behaviour of a segmental lining it is recommended to pay attention to the beam action of a tunnel.
- Special attention should be given to the stability of segments in the lining, as the empirical analysis with Winkler theory, in combination to the view that a segmental lining with ‘joints’ will loose stability if the subgrade reaction modulus of the soil is too small.
- The interaction between tunnelling and pile-foundations needs further research.

The coöperation of Mr. W.L. Leendentse, program-director of the ‘Centre for Underground Construction’ in Gouda, is gratefully acknowledged.

REFERENCES

- Bezuijen, A. and van der Schrier, J.S. (1994) The influence of a bored tunnel on pile foundations. Proc. Conf. Centrifuge 94 (Lee and Tan, eds.). Balkema, Rotterdam, pp. 681–686
- Duddeck, H. Empfehlungen zur Berechnung van Tunneln im Lockergestein Die Bautechnik 10/1980
- Duddeck, H. (1984) Analysis of Linings for Shielddriven Tunnels, Proc. Int symp. on tunnelling in soft and water-bearing ground, Lyon 27–29 nov 1984, Balkema Rotterdam
- Hetényi, M. (1946) Beams on Elastic Foundation The University of Michigan Press
- Mair, R.J. (1987) Tunnel face support pressure, soft Clay, Proc. 8th Asian regional conference on SMFE. 2, 290 JSSMFE, Tokyo
- Peck, R.B. (1969) Deep excavations and Tunnelling in soft Ground. 7th ICSMFE Mexico

Ground deformations due to the boring of the Second Heineoord Tunnel

Déformations au sol causées par le forage du second tunnel de Heineoord

E.P. van Jaarsveld

Delft Geotechnics, Delft, The Netherlands

J.W. Plekkenpol

Centre of Underground Space Technology (d.b. Public Works Rotterdam), Gouda, The Netherlands

C.A. Messemaeckers van de Graaf

Centre of Underground Space Technology (d.b. Holland Railconsult BV), Gouda, The Netherlands

ABSTRACT: During the construction of the bored 'Second Heineoordtunnel', an extensive research programme was carried out. This paper presents the ground deformations, measured at the Northern monitoring area. The 950 m long tunnel comprises two tubes, each with an outer diameter D of 8.3 m. The measured ground deformation varies between 7 and 37 mm. It appears that there is an almost linear relation between the ground settlement and the volume of injected grout. From the measured vertical and horizontal ground deformations it is concluded that the model, used for the predictions, overestimates the width of the settlement trough and gives incorrect values of the soil deformations and soil stresses around the lining. A grouting pressure model has been developed which results in a better analysis of the ground deformations next to the tunnel lining and a better prediction of the settlement trough.

RÉSUMÉ: Lors de la construction du second tunnel de Heineoord déjà foré, un programme de recherche étendu a été effectué. Le présent article présente les déformations au sol mesurées à la zone de surveillance nordique. Le tunnel de 950 m de long comporte 2 tunnels de diamètre extérieur 8,3 m. Les mesures de déformations varient entre 7 et 37 mm. Les résultats de l'étude montrent une relation quasi linéaire entre le tassement du sol et le coulis injecté par volume. Les déformations mesurées poussent à la conclusion que le modèle de prédiction utilisé surévalue la largeur de tassement de la cuvette et produit un calcul incorrect des déformations du sol et des tensions du sol autour de la doublure du tunnel. Un nouveau modèle décrivant les pressions de colmatage du coulis a été développé. Il effectue une meilleure analyse des déformations au sol au voisinage de la doublure du tunnel et améliore le calcul du tassement de la cuvette.

Keywords: Tunnelling, Ground deformations, FEM models

1 INTRODUCTION

A few kilometres south of the city of Rotterdam, the 'Second Heineoordtunnel' has been bored in the period between 1996 and 1998. In order to obtain experience with shield tunnelling in Dutch soft soil conditions, the project was designated as a pilot project. Therefore, an extensive research programme was carried out during construction. This paper describes a part of the results of the geotechnical research programme. Other research topics were the behaviour of the lining and the tunnel boring machine. The total

research programme was commissioned by the Centre of Underground Construction (COB).

The tunnel crosses the river 'Oude Maas' and was bored using a pressurised slurry shield. The 950 m long tunnel comprises two tubes, each with an outer diameter D of 8.3 m. The cover varies between 0.8 times the diameter near the entry and exit point and approximately 1 times the diameter below the deepest point of the river. A longitudinal profile of the tunnel is given in [Figure 1](#). For the research programme, two monitoring areas have been prepared. One on the northern bank of the river and one on the southern

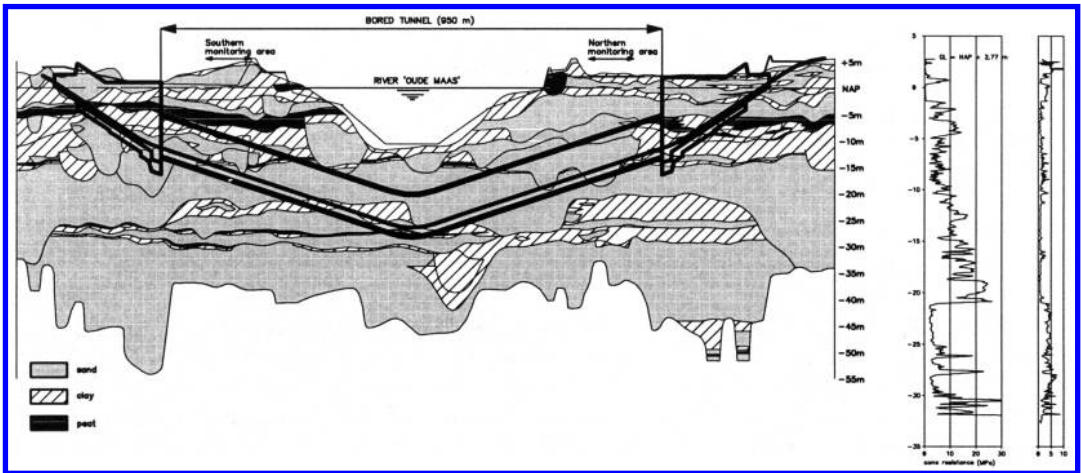


Figure 1. Longitudinal profile and typical CPT result at northern monitoring area.

bank. This paper describes the results of the research programme performed at the northern bank only. Presented displacements are displacements caused during each passage of the TBM. A few days before passing of the TBM, all displacements were reset to zero.

2 SOIL CONDITIONS

The geotechnical profile of Figure 1 was established from 82 Cone Penetration Tests and 15 boreholes. Because of the presence of old river beds and gullies, large variations in soil conditions occur. At the monitoring areas on the river banks, the ground level is NAP +2 m to NAP +3 m (Dutch reference level). In general the Holocene layer extends to a depth of NAP -15 m and consists of peat, clay and loose to medium dense sand layers. Beneath this Holocene layer 8 m dense to very dense sand occurs, followed by a 2 m thick stiff silty clay layer. Beneath this clay layer, mainly dense sand was encountered. At the northern monitoring area, the Holocene layer however mainly consists of sand. A typical CPT result at the northern monitoring area is shown in Figure 1.

The river is connected to the North Sea. The water level in the river and the ground water table at the river banks are influenced by tidal action. At the northern monitoring area, the average ground water table is 3 m below ground level.

3 INSTRUMENTATION

For monitoring of the soil deformations and stress variations, two monitoring areas were set up. The northern monitoring area is $75 \times 50 \text{ m}^2$. In this area the average

cover of the tunnel is 15 m. An overview of the installed instrumentation is given in Figure 2:

- A. 53 settlement markers installed in 4 rows: 2 rows in the tube axes and 2 rows perpendicular the tube axes
- B. 4 inclinometers: 2 above the tube axes, 2 next to the tubes to a depth of NAP -24 m
- C. 6 extensometers: 2 above the tube axes, 4 next to the tubes to a depth of NAP -18.5 m
- D. 3 piezometers within the driving range of the tubes for measuring water pressure in front of the TBM. During the passage of the TBM, the piezometers were destroyed
- E. 4 earth pressure cells installed at a distance of 2 m and 4 m from the first tube. Each pressure cell measured the water pressure and the soil pressure in 3 orthogonal directions
- F. 1 open standpipe
- G. 1 reference point

4 PREDICTIONS

Before construction, soil deformations and stress variations were predicted using several calculation methods. Green field settlements were calculated using analytical and empirical formulas, such as Sagaseta and Peck. Two and three dimensional FEM calculations were used to predict horizontal and vertical soil deformations and stress variations.

All predictions were based on an area of the settlement trough of 1% of the tube area. In the FEM analyses, the tail effect was modelled by applying a contraction of the borehole. This method results in soil displacements towards the tube. The results will be discussed in the following chapter.

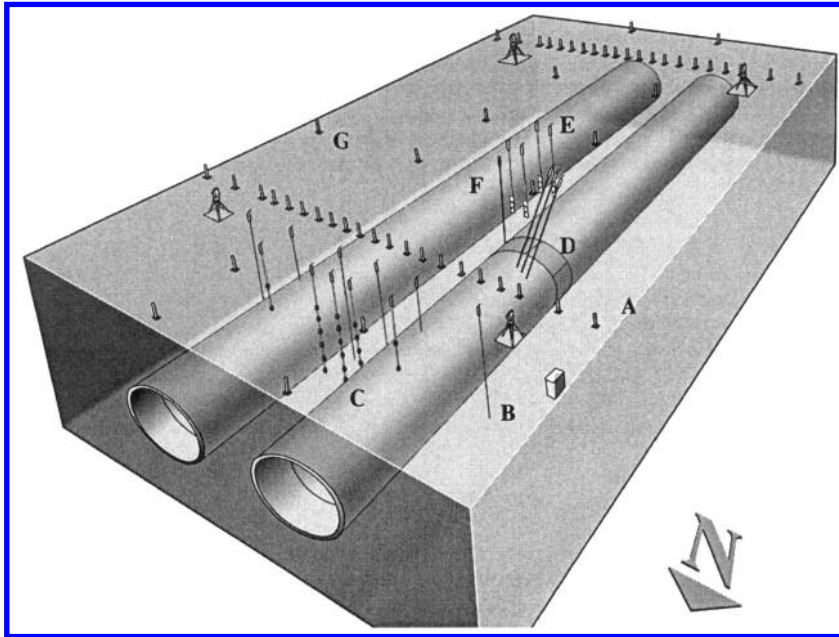


Figure 2. Overview of northern monitoring area.

5 RESULTS

The measured green field settlements above the tube axes are presented in Figure 3. Up to a distance of approx. 5 to 10 m ahead of the TBM, almost no settlements occur. While the TBM passes, the settlements rapidly increase. At a distance of 20 to 30 m behind the face, the settlements remain constant, which indicate that time dependent settlements are small. After the first passage, the maximum settlement at 32 m (4D) behind the face varies between 22 and 37 mm. After the second passage of the TBM, the maximum settlement varies between 7 and 17 mm.

The relatively small settlements at the front of the TBM indicate that soil displacements due to front effects remain small. Apparently, settlements that occur above the face are caused by (spreading) soil deformations due to overcutting and tail effects. The variation of the measured maximum settlement is mainly determined by a variation in the volume of injected grout. In Figure 4 the maximum settlements are given against the volume of injected grout. From this Figure it appears that there is a linear relation between the volume of injected grout and the maximum settlement.

The predicted vertical ground deformations at 4D behind the face are shown in Figure 5. The displacements were calculated by applying a uniform contraction of the bore hole in a FEM analysis. During the calculations, an area of the settlement trough of

1% was assumed. The predicted maximum settlement at ground level is 18 mm.

The vertical ground deformations, measured by the extensometers at 4D behind the face, are also presented in figure 5. After the first passage, the maximum settlement at ground level is 26 mm. The area of the settlement trough at ground level is 0.76% of the cross section of area of the tube. With depth, the area of the settlement trough increases from 0.84% at NAP -3.5 m to 0.85% at NAP -6.5 m. The measured settlement above the tube axis appears to be larger than predicted, whereas the width of the trough appears to be smaller than predicted.

In Figure 5, also the vertical ground deformations measured above the second tube are given. Compared to the settlements above the first tube, the settlements above the second tube remain small. This is mainly caused by a larger volume of injected grout during the second passage of the TBM. The maximum settlement at ground level is 8 mm. The area of the settlement trough at ground level is 0.23%. With depth, the area of the settlement trough slightly increases from 0.23% at NAP -3.5 m to 0.24% at NAP -6.5 m.

The horizontal displacements perpendicular to the tube axis and at 4D behind the face are given in Figure 5b. By contracting the bore hole, an almost constant horizontal displacement of 7 mm has been calculated at 2 m next to the tube.

Next to the first tube only a small displacement of 3 mm towards the tube was measured. Up to ground

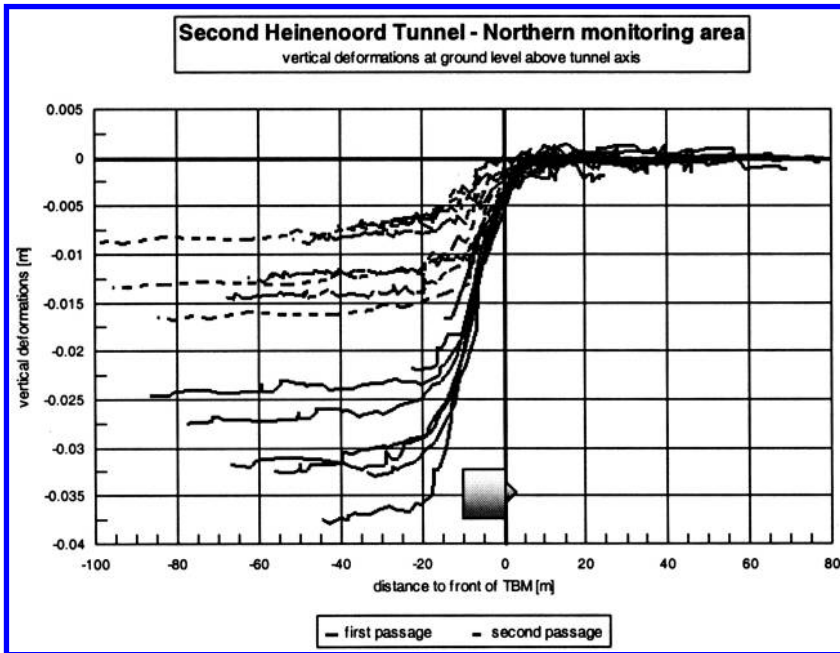


Figure 3. Greenfield settlements above tube axes.

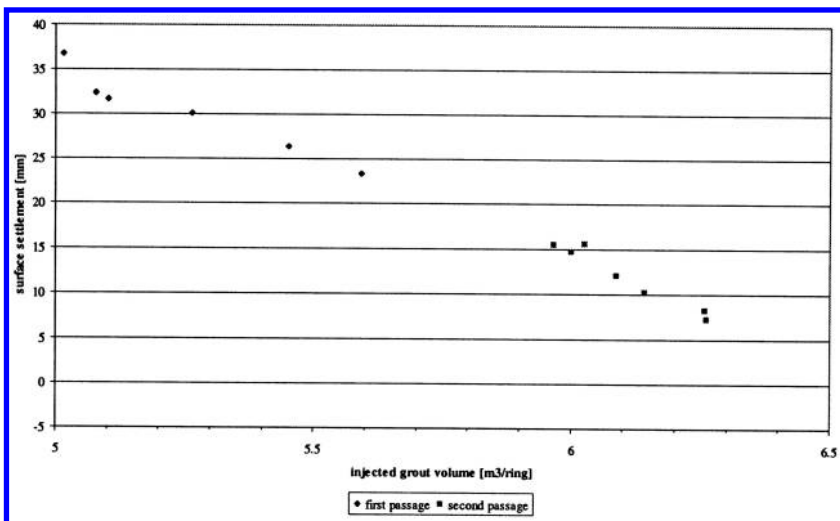


Figure 4. Relation between maximum settlement and volume injected grout.

level the horizontal displacements increase to 10 mm. Next to the second tube small displacements in the direction away from the tube are measured. The maximum displacement at the side of the tube axis is 2 mm.

It appears that, using a contraction model, the width of the settlement trough and the horizontal displacements are overestimated. The contraction model will

predict a stress release above and at the side of the tube, which will result in ground displacement towards the tube and a wide settlement trough. From the measured displacements it appears that the displacements perpendicular to the tubes vary. The ground displacement and therefore the stress release above the tube axis are larger than the displacement next to the tube axis.

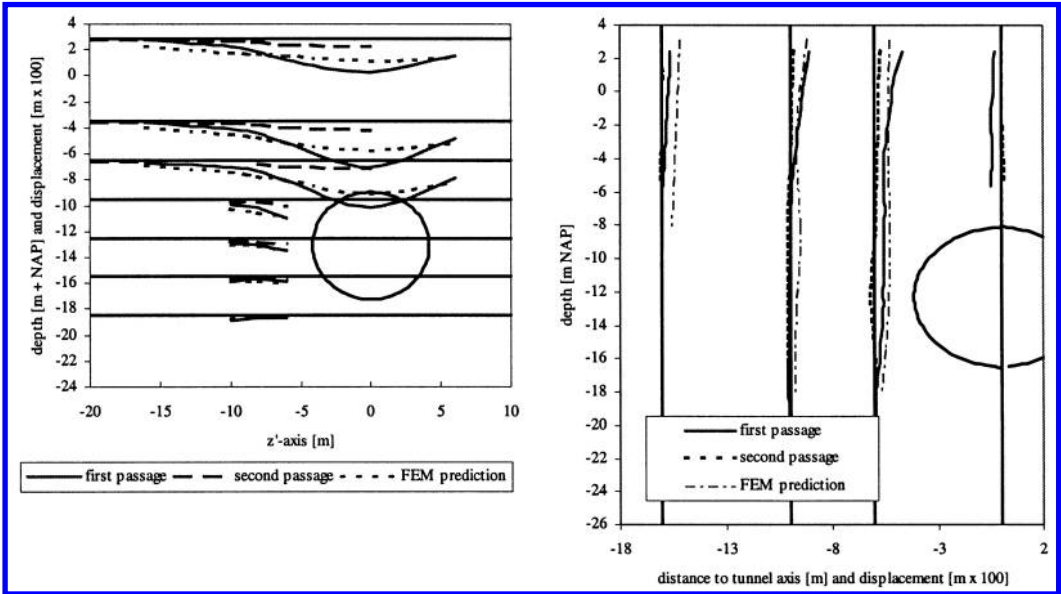


Figure 5. Vertical (a) and horizontal (b) ground deformations at 32 m behind the face.

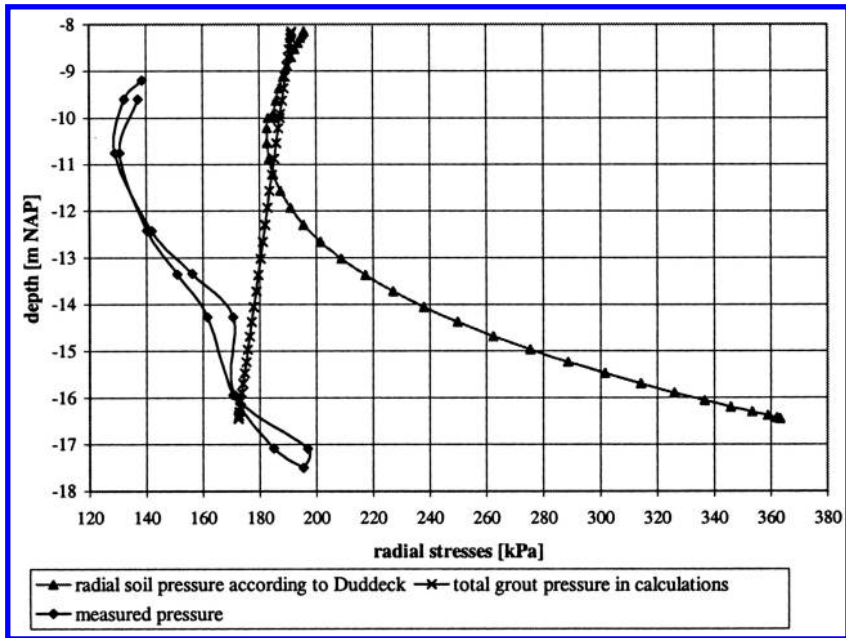


Figure 6. Pressure distribution around the lining at the first tube.

At the second tube, even a displacement away from the tube is measured, which will result in a stress increase. The pressure cells installed next to the tube also measured this stress increase.

6 GROUTING PRESSURE MODEL

The predictions were performed using a contraction model. This model will result in an incorrect

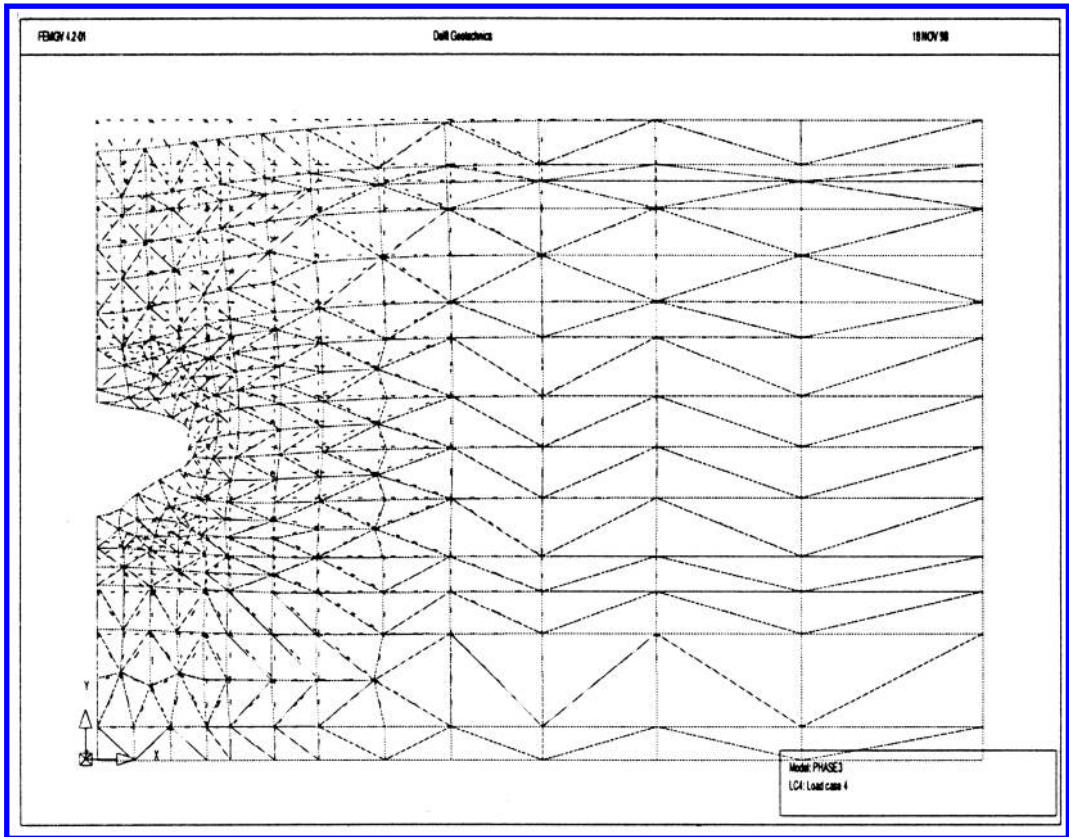


Figure 7. Deformed mesh using grouting pressure model.

deformation of the borehole and an overestimation of the width of the settlement trough. To come to a more realistic model of the boring process, a more accurate modelling of the grouting process is desired. To fill the tail void, grout is injected under high pressure. The pressurised grout will support the tunnel lining and the surrounding soil layers and prevents excessive soil deformations. The pressure distribution within the injected grout depends on the injection pressure, the material properties of the grout, the number of injection points, location of the injection points and the dimension of the tail void.

A grouting pressure model has been developed, in which the pressure distribution within the tail void can be applied, whereafter the deformations that occur can be calculated. This model has been used for back analyses of the measured displacements. From stress measurements on the lining and back analyses of the measured displacement it appears that, compared to the initial K_0 -stresses, a rather uniform pressure distribution will be created around the lining due to the grouting pressure. In Figure 6 the initial K_0 -pressures, the measured pressures and the calculated pressures

for the first tube are presented. The calculated pressures were determined by back analysing the measured ground deformations.

In Figure 7 the deformed element model is given. From this figure it appears that a non-uniform deformation of the bore hole occurs due to the application of the pressures, presented in Figure 6. The applied grouting pressure will not only result in a better calculation of the soil deformations around the bore hole, but will also result in an accurate analysis of the ground settlement.

7 CONCLUSIONS

At the Northern monitoring area the final settlements varied from 7 to 37 mm. It appeared that, using a slurry shield machine, the settlements due to front effects remain small. The settlements are mainly caused by tail effects. Because the subsoil mainly consists of sand, the time-dependent settlements are negligible. The settlement trough appears to be smaller than predicted. The ground displacements and therefore the

incremental stresses perpendicular to the tubes vary strongly. The ground displacement and therefore the stress release above tube axis are larger than the displacement next to the tube axis. At the second tube, even a displacement away from the tube is measured, which will result in a stress increase.

Above mentioned phenomena desire a more accurate model of the back fill grouting procedure. This model will provide better values of the ground deformations adjacent to the tunnel lining and a better prediction of the settlement trough.

ETAC two-component grout field test at Botlek rail tunnel

A. Feddema

GeoDelft, Delft, The Netherlands

M. Möller

Studiedienst BTC, The Netherlands

W.H. van der Zon

GeoDelft, Delft, The Netherlands

T. Hashimoto

Geo Research Institute, Osaka, Japan

ABSTRACT: This paper describes the experiences and test results of a field test during the construction of the Botlek rail tunnel (port of Rotterdam), where the Japanese 2-component grout, ETAC, has been used. In this test the assumed advantages of the ETAC product compared to more traditional grouts have been examined. A difference is made between a grout (the ETAC material) and a mortar (the traditional materials).

1 GENERAL INTRODUCTION

The existing Botlek bridge over the Oude Maas river is a bottleneck for freight transport along the Port Railway of Rotterdam. The bridge is often raised to allow ships to pass and does not have sufficient capacity for a second track. In order to remove this bottleneck, the two track Botlek rail tunnel is being constructed. The tunnel is part of the BetuweRoute project. Its total drilled length is 1,850 metres. The tunnel exist of 2 tubes with an internal diameter of 8.65 m laying at a distance of one times the diameter from each other. The project is carried out by the BoorTunnelCombinatie Botlek using an Earth Pressure Balance shield (EPB) type of tunnel boring machine (TBM). The construction period is 1998 until 2001. The project has been commissioned by Railinfrabeheer of Dutch Rail (NS RIB).

The area where the tunnels are constructed has the largest pipe and cable density in Europe. This is the backbone of the Port of Rotterdam. Numerous of these pipes and cables are crossing over the tunnel. Among these are pipes for various chemicals. The pipes are concentrated in so-called "pipe streets". Damage to these pipes could have catastrophic economical and environmental consequences.

2 INTRODUCTION ETAC TWO-COMPONENT GROUT

For over twenty years a two-component grout has been used by the Japanese for the filling of tail voids in shield tunnelling. The tail voids are caused by the fact that the outer diameter of a TBM is larger than the outer diameter of the tunnel lining. It is necessary to fill these tail voids, because not filling them may result in the collapse of the surrounding soils. This will lead to excessive settlements of the soil, causing damage to the surroundings.

The ETAC grout injection test was carried out by three parties. The composition of the project team, supporting these tests consisted of members of all three parties involved; Nederlandse Bouwstoffen Combinatie (NBC), BTC Studiedienst Boren and Combinatie (NBC), BTC Studiedienst Boren and GeoDelft (GD). Furthermore the project was supported by the producer of the ETAC material, the TAC Corporation, and by the Geo Research Institute of Osaka. Both from Japan.

3 PROJECT OBJECTIVES

The project objectives were to conduct a test in which the expected advantages of ETAC could be proven and

to gain experience in working with the ETAC material. The expected advantages of ETAC compared to conventional grouts and mortars are:

1. *More efficient tunnel boring process*

In this part of the evaluation the realisation of the test is presented in respect to:

- The mechanics (components of the ETAC production plant and the lay-out of the site).
- The methods (process handling, process parameters, material consumption and material specifications).
- The quality (analysis of time related to progress and stagnations).

2. *Faster and better support of the tunnel lining*

Here the relation between the ETAC process parameters and the acting forces in the TBM is studied. A relation between the ETAC and TBM process parameters on one side and the occurrence of ring damages was also studied.

3. *Reduced influences to the surroundings*

The evaluation of this part of the study was divided into:

- The acting forces in the tail voids. An analysis of the injection and tail void pressures was made for the ETAC grout as well as the standard mortar. Here the relations amongst the mutual process parameters were studied.
- The influences of the grouting process on the surroundings.

4 LOCATION, METHODS AND DATA

4.1 *Description of the test areas*

The location of the test site was divided into four separate test areas (see table 1). Along the drilled part of the tunnel a total of six monitoring locations are arranged. Monitoring location 2 is used to perform the ETAC test; monitoring location 3 is used as reference location for the BTC-Botlek mortar.

Both monitoring locations are equipped with settlement plates, extensometers, inclinometers and monitoring rings. The monitoring rings consist of pre-installed pressure cells in the lining segments and are used to measure grout and soil pressures on the outside of the tunnel lining.

4.2 *Steering principals injection process*

Injection of the tail voids has a direct influence on the settlement behaviour of the surface and the quality of the tunnelling process. The tail void injection serves as a backfill and a foundation for the individual tunnel segments. The injection pressure must be sufficient

Table 1. Test areas.

Test area	Monitoring situation	Injection process	Injection pressure
1	location 2	ETAC grout	high
2	location 2	ETAC grout	low
3	location 2	ETAC grout	optimal
4	location 3	BTC-Botlek mortar	standard

to fill these tail voids completely. However the maximum allowed pressure should not be exceeded and may also not lead to leakage of the tail seals of the TBM. Therefore the applied injection pressures and injection volumes must be maintained and controlled during the injection process.

The controlling of the ETAC grouting system is based upon controlling the injection pressure and injected volume of the two-components of the ETAC grout. The injected volume depends upon the pressure development during boring.

During the injection process of the BTC-Botlek mortar the control parameter is the injected volume of the mortar. Here a maximum pressure is maintained that should not be exceeded.

The amount of mortar, that should be injected, depends on the contour cut of the excavation wheel and the outside diameter of the tunnelling.

5 TUNNEL BORING PROCESS

5.1 *Injection methods*

Injection method BTC-Botlek mortar

Here the tail void will be filled with mortar through six injection openings (lisenes) in the mantle of the shield of the TBM. Each lisene consists of two pipes, where the second pipe is used as a spare (see figure 1).

Injection method ETAC two-component grout

Here the lisenes were not used, because the lisenes are not suitable to keep the two components apart from each other before they enter the tail void. Because the ETAC was used as a test the TBM was not modified. Therefore the ETAC grout was injected directly into the tail void during the test through special made pre-installed openings in the tunnel lining. The ETAC grout was injected through two injection openings located at the top section of the tunnelling, as shown in figure 1.

5.2 *Quality*

5.2.1 *Time analysis of the tunnel boring process*

During the construction of a shield tunnel the time necessary to build the tunnel can be divided in operational time and non-operational time of the TBM.

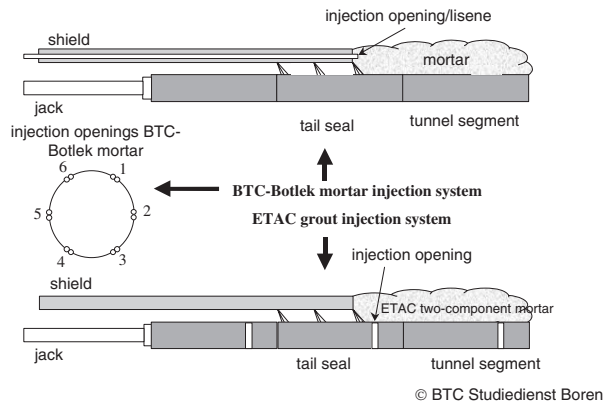


Figure 1. Injection methods (BTC-Botlek mortar and ETAC).

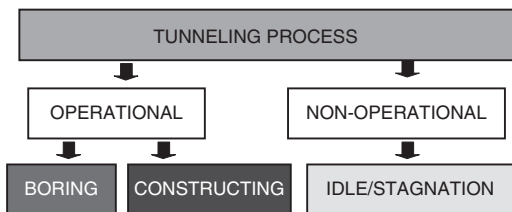


Figure 2. Construction "cycle".

The actual boring and construction of a tunnel ring is the operational time. These two matters are the basic parameters of the construction cycle. When this construction cycle is disturbed in such a way that there is stagnation in the process we speak of non-operational time. The non-operational time is also a part of the realisation time of the tunnel.

5.2.2 Performance indicators

Lessons learned from an earlier time analysis performed by the BTC Studiedienst Boren during the "Second Heineoord tunnel" project, showed that the performances of the different tunnel boring processes are hard to define. Therefore the BTC Studiedienst Boren has defined performance indicators, with which the tunnel boring process could be reviewed unambiguously:

- **Effectiveness (indicator: availability of systems)**
The effectiveness of the tunnel boring process is distinguished by the ratio of the operational time and the total realisation time.
- **Efficiency (indicator: efficiency of actions)**
The efficiency of the tunnel boring process is defined as the realised production per unit of operational time. Thus the non operational time will not be taken in consideration.

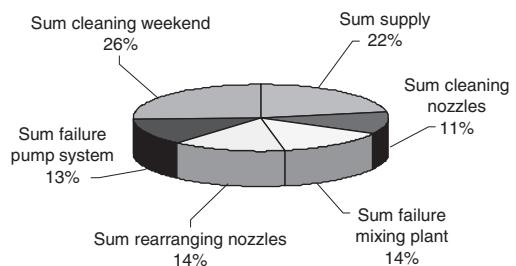


Figure 3. Distribution of idle time of ETAC-system.

5.2.3 Time analysis ETAC

The average boring cycle time of the ETAC test areas was 66 minutes. The average ring building time was 67 minutes. Due to non operational time of the ETAC plant, the tunnel boring process has been interrupted for a total of 648 minutes. The total idle time of the system was 4341 minutes. The average cycle time was 236 minutes per ring. From this time analysis it is concluded that 26% of the idle time in the ETAC system was caused by cleaning and preparations activities on behalf of weekend leaves.

5.2.4 Time analysis BTC-Botlek mortar

During boring with BTC-Botlek mortar the average boring time was 70 minutes. Construction of the rings took an average time of 61 minutes. Idle time of the tunnel boring process in this test area was 3807 minutes, of which 987 minutes was caused by the mortar system.

More than half of the idle time was caused by the cleaning of the fixed mortarcontainer on the TBM. Time was also consumed by cleaning and preparation time on behalf of the weekend leaves. These two phenomena are inherent to this type of mortar system.

There was also time lost due transport of the mortar. This idle time was caused by:

- The fact that preparation of the mixture in the mortar installation started too late.
- Stagnation of the transport of the mortar through the tunnel.
- The pumping of the mortar from the mortar carriage into the fixed mortar container.

5.2.5 Analysis of performance indicators

The quality assurance of the tunnel boring process is valued by means of performance indicators. There are two of these indicators: the **effectiveness** and the **efficiency**.

- **Effectiveness (indicator: availability of systems)**

ETAC test areas

The effectiveness during injection with ETAC grout was 56% according to the time analysis described above. Thus, the tunnel boring process was interrupted during 44% of the total process due to stagnations.

BTC-Botlek test area

The effectiveness of this test area was 59%. So the tunnel boring process was for 41% of the process time interrupted due to stagnations.

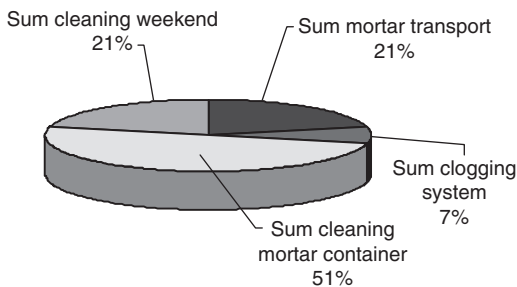


Figure 4. Distribution of idle time of the BTC-Botlek mortar system.

- **Efficiency (indicator: suitability of actions)**

ETAC test areas

The efficiency of the tunnel boring process with the ETAC grout was 0.45 according to the time analysis. This corresponds with a non disturbed construction cycle of 2 hours and 13 minutes.

BTC-Botlek test area

The efficiency of the tunnel boring process with the BTC-Botlek mortar was 0.46 according to the time analysis. This corresponds with a non disturbed construction cycle of 2 hours and 10 minutes.

5.2.6 Performance forecast

The production and/or progress of the tunnel boring process can be forecasted with the determined performance.

From table 2 one can conclude that the tunnel boring process was more successful with the BTC-Botlek mortar than with the grout. However, the idle time caused by problems in the mortar system itself was not accounted for in the analysis mentioned below.

The idle time caused by this factor is 15% with ETAC grout and 26% with BTC-Botlek mortar. The part of the idle time caused by problems in the BTC mortar system was significantly higher than in the ETAC grout system. This is remarkable because the TBM itself is completely set for the BTC-Botlek mortar. From this the conclusion can be drawn that a tunnel boring process with use of the ETAC grout is less vulnerable to interruptions in the system and therefore a higher production could be made.

6 INTERACTION WITH THE TUNNELLING

A conclusion, concerning the interaction of the fillings of the tail voids and the tunnelling has been drawn by judging the appeared damages (damages to the tunnel segments) of the tunnelling.

6.1 Observed damages at the ETAC test areas

There were 192 damages observed in the ETAC test areas, given an average of 4.6 occurred damages per

Table 2. Progress forecast tunnel boring process.

	Tunnel boring process with ETAC grout	Tunnel boring process with BTC-Botlek mortar
Available time daily shift	24 hours	24 hours
Effectiveness	56%	59%
Operational time	13 hours 26 minutes	14 hours 9 minutes
Non operational time	10 hours 34 minutes	9 hours 51 minutes
Efficiency	0.45 ring per hour	0.46 ring per hour
Daily production	6.0 rings	6.5 rings

ring. It seems that there is a relation between the injection pressure, the injected volume and the amount of occurred damages when using the ETAC grout. The test area that has been injected with the highest injection pressure, had the least damages. More damages were observed in the test area where the ETAC grout was injected through only one injection nozzle instead of the common two injection nozzles. This was due to a technical problem with the injection system caused by a human error.

6.2 Observed damages at the BTC-Botlek mortar test area

At 122 rings damages have been observed in this test area, meaning an average of 2.9 damages per ring. No relations could be found between the injection pressure and injection volume on one hand and the observed ring damages on the other hand. Or: no interaction between the BTC-Botlek mortar and the tunnelling was observed.

7 SURFACE DEFORMATIONS

7.1 Surface deformations monitoring location 2 – ETAC test areas

The vertical surface deformations that occurred in monitoring location 2 along the tunnel axis are shown in figure 5.

From figure 5 two groups of surface deformation lines can be recognised. The group with the lowest deformations are situated at test area no. 1 (where the highest injection pressures were applied), with the exception of one settlement plate. The level of deformations in this test area range between 11 and 15 mm. The difference of the results in this test area probably lies in the vertical deformations that occur in front of the TBM. A rising of the surface of approximately 4 mm at a distance of 0 meters from the front of the TBM was observed, whereas settlement plate 179 does

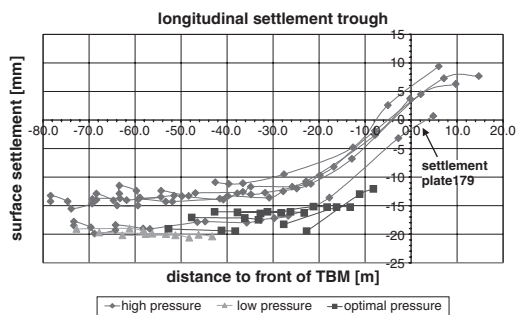


Figure 5. Surface settlement versus distance to front of TBM with ETAC.

not have this heaving of the surface in front of the TBM. When the final settlement for settlement plate 179 is corrected for this difference of 6 mm the final surface settlement at this location fits with the readings of the other settlement plates in test area no. 1 (19 mm).

In the test areas no. 2 and 3 (respectively low and optimal injection pressures) there were no measurements available before the passage of the front of the TBM. Therefore it was not possible to make a proper analysis of the total settlements.

The total surface settlements at the ETAC test area range between 11 and 21 mm.

7.2 Surface deformations monitoring location 3 – BTC Botlek mortar reference area

The surface deformations that occurred at monitoring location 3 are shown in figure 6. This figure shows that there was a surface settlement of 5 to 8 mm before the passing of the front of the TBM. It also shows that there is no difference in slope of the settlement curves. The maximal final settlements range between 25 mm and 37 mm.

7.3 Inclinerometers

The maximal horizontal deformations (obtained by measurements with inclinometers) at monitoring location no. 2 and 3, are shown in figure 7. The results of the horizontal deformations that occurred at monitoring location no. 2 are 50 times enlarged, whereas the horizontal deformations at monitoring location no. 3 are enlarged by a factor of 100.

The maximal horizontal displacement next to the tunnel in monitoring location no. 2 is 10 mm, whereas the maximum horizontal deformation in monitoring location no. 3 is 45 mm. Figure 7 shows, that the soil at monitoring location no. 2 moves towards the tunnel above the tunnel and from the tunnel below the tunnel. The soil at monitoring location no. 3 moves throughout the depth in the direction of the tunnel.

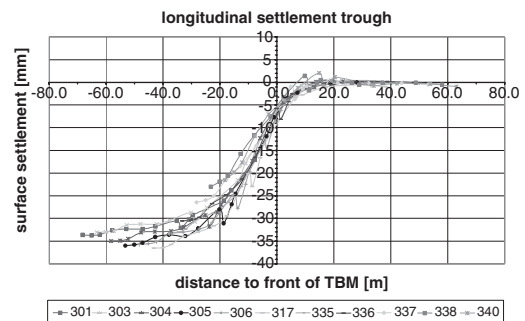


Figure 6. Surface settlement versus distance to front of TBM with BTC-Botlek mortar.

7.4 Analysis

Both the horizontal and the vertical deformations of the soil are significantly less in the test areas injected with ETAC, compared to the deformations measured in the test area injected with the BTC-Botlek mortar. It can be stated that this could be caused by the different behaviour of the ETAC material. The ETAC

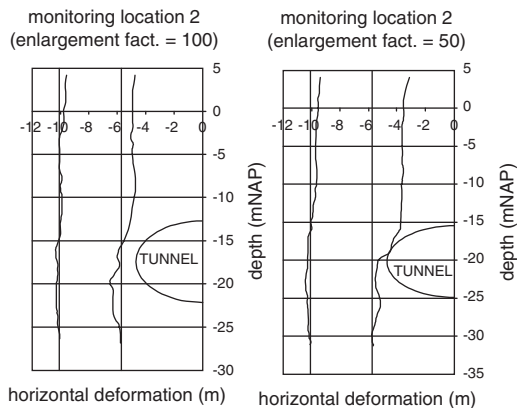


Figure 7. Maximum horizontal deformations.

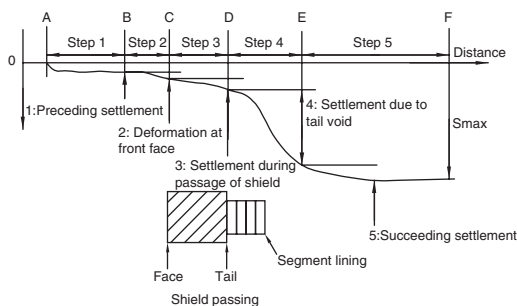


Figure 8. Phases of surface deformations during the tunnel boring process [1].

grout forms a plastic, clay-like gel within 15 seconds after injection. Successively, the ETAC will harden, and reaches a strength of 250 kPa after only 1 hour. This means that the grout is no longer liable to distortion.

A comparison is made between the test results of the ETAC field-test and results at other shield tunnels obtained from international literature and the Second Heineoord tunnel project the first shield tunnel in The Netherlands. The surface deformations are divided into five phases (see figure 8). It should be noted that this kind of division does not take the influence of 3D-effects on these phases into account.

The differences of the relative parts of the deformations, in percentages of the final deformation, are shown in table 3. Here phase 1 and 2 as well as phase 4 and 5 are presented as one, in order to make a comparison with other projects possible.

Table 3 shows that there is hardly any difference between the test results of monitoring location 2 and 3 (the ETAC test areas and the BTC-Botlek mortar test area). The results also match quite well with the results obtained from the literature for non-cohesive soils (sandy soils).

However, there is a difference between the ETAC test areas (monitoring location no. 2) and the BTC-Botlek mortar reference area (monitoring location no. 3), when the absolute figures are compared to each other. The results of this analysis are presented in table 4. It is not useful to compare the results from

Table 4. Absolute influences of the different phases of the tunnel boring process to the surface deformations for ETAC field test.

	Part of total surface deformation [mm]		
	Monitoring location 2	Monitoring location 3	Factor location 3/ location 2
Phase 1/2	4	7	1.75
Phase 3	7	11	1.57
Phase 4/5	10	15	1.50
Total	21	33	1.57

Table 3. Relative influences of different phases of the tunnel boring process to the surface deformations.

source	soil type/project	Part of total surface deformation [%]		
		Phase 1/2	Phase 3	Phase 4/5
Literature [2]	Non cohesive	20	37	43
	Cohesive	10	16	72
Heineoord [2]	North I	15	45	40
	North II	15	45	40
	South II	10	25	65
ETAC field-test	Monitoring location 1	21.4	34.7	44
	Monitoring location 2	21.1	34.7	44.2

the Second Heinenoord tunnel project with the ETAC field-test, as the soil at both locations differs too much.

The average vertical surface deformations at monitoring location no. 2 (ETAC) are a factor 1.5 to 1.75 lower than at monitoring location no. 3 (BTC-Botlek mortar). This may be caused by the 3D-effects. A larger loss in the tail voids (phase 4 and 5) automatically results in a larger deformation over the shield (phase 3).

8 CONCLUSIONS

8.1 *Efficiency tunnel boring process*

The tail void injection system using the ETAC grout is a new development, it is still in its “infancy”. The normal tail void injection system with conventional mortar however is a fully optimised process, due to the fact that the constructors have more experience in using this system. It is therefore difficult to make a comparison between the two systems. By means of the set performance indicators it can be concluded that the tunnel boring process in the test area where the regular BTC-Botlek mortar was used, is more efficient than at the test areas where the ETAC grout was used.

However, the idle time due to problems in the mortar system were significant higher in the test area where the BTC-Botlek mortar was used. This is remarkable considering the fact that the TBM is set to the use of this mortar. It can be concluded that a tunnel boring process using ETAC grout is less vulnerable to disturbances, so a higher production rate can be accomplished when using the ETAC grout system. This was the main reason why BTC-Botlek decided to use ETAC for the construction of the second tube of the Botlek rail tunnel. Therefore the TBM was modified by constructing special injection tubes for ETAC that could be inserted inside the existing injection openings in the shield of the TBM. Also the ETAC injection control system was integrated in the TBM control system.

8.2 *Interaction tunnelling*

It seems that there is a relation between the injection pressure and the number of damages to the tunnelling where ETAC grout was used. More damages occurred in the test area where only one injection opening was

used. Fewer damages occurred in the test area where high injection pressures were applied.

Comparing both injection techniques, it can be concluded that there were fewer damages in the test area where the BTC-Botlek mortar was used.

It should be noticed that there are other factors than the injection technique and the injection method used that affect the interaction between the tunnelling and the filling of the tail voids. It was observed that the friction of the shield increased in the test areas where the ETAC grout was used. It was not clear whether this was caused by the interaction of the ETAC grout or a change in geology.

During the construction of the second tube the number of damages was much less than during the ETAC test.

8.3 *Surface deformations*

Both the absolute horizontal and vertical deformations in the soil were significant lower where the ETAC grout was used. It can be stated the different behaviour of the ETAC material is responsible for this phenomenon. The ETAC grout forms a plastic, clay-like, gel within 15 seconds after injection. Successively, the ETAC will harden, and reaches a strength of 250 kPa after only 1 hour. This means that the grout is no longer liable to distortion.

There were no differences observed in the **relative distribution** of the vertical surface deformations over the 5 different boring phases between the ETAC grout and the BTC-Botlek mortar. The observed values match the values found in the literature for non-cohesive (sandy) soils. However the **absolute** deformations are a factor 1.5 lower in the areas where ETAC grout was used.

During the construction of the second tube the surface settlements ranged between 10 and 20 mm at the monitoring areas used for the field test.

REFERENCES

- Feddema A., Möller M., Zon van der W., August 2000, Praktijkproef ETAC groutinjectie BTC-Botlek, report CO-384800/68 GeoDelft, BTC Studiedienst, NBC
- Litjens, P.P.T., Eerste orde evaluatie K100, Beschouwing boor-/volumeverlies en deformaties (analytisch), deel II, K100-W-105-A, september 1999, CUR/COB

Pore pressures in front of tunnel, measurements, calculations and consequences for stability of tunnel face

Adam Bezuijen, Jitse P. Puijsma & Hans H. van Meerten
Delft Geotechnics, The Netherlands

ABSTRACT: As a part of a measurement campaign the pore pressures were measured in front of a tunnel during drilling with a slurry shield in sand. It was found that during drilling the pore pressure in front of the tunnel up to a distance of 2 tot 3 times the tunnel diameter is higher than the hydrostatic pressure. This is caused because drilling prevents plastering of the bentonite at the tunnel face. Calculations show that this excess pore pressure increases the minimum pressure necessary for stability of the tunnel face and has also consequences for the maximum allowable pressure at the tunnel face. The paper describes the measurements, what mechanism prevents the plastering in front of the tunnel during drilling, speed of plastering by the bentonite slurry during stand still and consequences for stability of the drilling process

1 INTRODUCTION

A measurement and monitoring programme has been performed during the drilling of the 2nd Heinenoord-tunnel (Bakker et al. 1999). The aim of this programme was to investigate the relevant mechanism during drilling for the soft soil conditions that are present in most of The Netherlands.

This paper deals with only one aspect of these measurements, the excess pore pressures that were measured in front of the tunnel face during drilling. It will show the origin of these excess pore pressures and the consequences for the stability of the tunnel face during drilling. The minimum and maximum allowable pressures to achieve a stable tunnel face are studied. For the minimum allowable pressure usually calculation methods as suggested by Anagnostou & Kovári (1994) or Jancsecz & Steiner (1994) are used. Consequences for these calculation methods will be discussed. An example is presented for the maximum allowable pressure. There are indications that consequences of excess pore pressures on the maximum allowable pressure are also present in other situations (Bezuijen & Brassinga 2001).

2 MEASUREMENTS

Pore pressure gauges (PPTs) were mounted in the tunnel track as a part of the measurement campaign. The total instrumentation, measuring deformations and pressures, in one of the measurement fields is shown in

Figure 1. The PPTs in the tunnel track were in use until destruction by the TBM. Results will be discussed for a PPT located in sand. Excess pore pressures were measured in front of the TBM during drilling. However, the pore pressure decreased until hydrostatic pressure when the drilling stopped. The result of one of the gauges is shown in Figure 2.

When the TBM reaches the PPTs, the passing of the cutters on the TBM can be seen in the measured pore

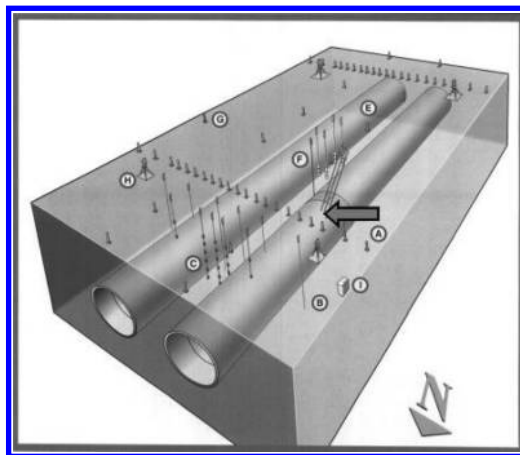


Figure 1. Artist impression measurement field. The arrow indicates the pore pressure gauges in front of the TBM. Results of the gauge in the middle are used this paper. (Bakker et al. 1999).

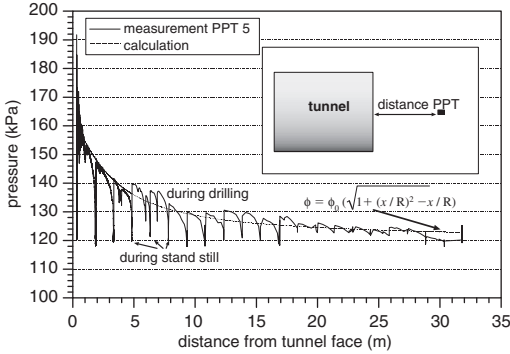


Figure 2. Measured excess pore pressure in front of a slurry shield and approximation.

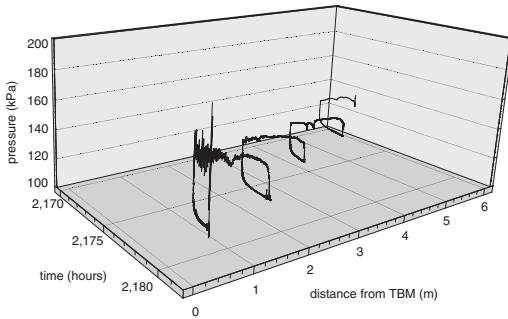


Figure 3. 3D presentation of the measured excess pore pressure in front of a slurry shield.

pressures as variations in the pressure. The pressure decrease during a stand still can be seen in the 3-D plot, Figure 3, where the pressure is presented as a function of both the distance from the tunnel and the time. From this plot it is clear that when there is no progress in the drilling (the distance remains constant) the pressure decreases. The pressure starts to increase when drilling started on the distance between the gauge and the tunnel decreases.

The measurements show that there is a plastering of the tunnel face by bentonite when drilling stops, but that there is no plastering during drilling. The reason for that will be explained in the next section.

3 PRESSURE CALCULATIONS

If there is no plastering of the tunnel face at all, it is possible to calculate the excess pore pressure by means of groundwater flow computations. The actual 3D boundary value problem reduces to a rather simple problem

if we calculate the pressure in front of the tunnel at the tunnel axis, assuming a constant excess pore pressure over the tunnel face, a homogeneous soil and no influence of the surface. For such a situation the solution of the piezometric head at the tunnel axis leads to:

$$\phi = \phi_0(\sqrt{1 + (x/R)^2} - x/R) \quad (1)$$

Where ϕ is the excess piezometric head above the hydrostatic level at a distance x from the tunnel face. ϕ_0 the excess piezometric head at the tunnel face and R the radius of the tunnel. This solution is plotted with the measurements in Figure 2 and showed good agreement.

With this solution it is also possible to understand why the bentonite at the tunnel face cannot provide plastering during drilling. The hydraulic gradient in front of the tunnel can be calculated by taking the derivative of Equation (1). At the tunnel face ($x=0$) this leads to the equation:

$$i = \phi_0 / R \quad (2)$$

with i the hydraulic gradient. The pore water velocity (v_p) in front of the tunnel can be written as:

$$v_p = \frac{ki}{n} \quad (3)$$

where k is the permeability of the sand and n the porosity. When a tunnel with a diameter of 10 m (5 m radius) is drilled in sand with a permeability of 10^{-4} m/s and a porosity of 40% (average values for this tunnel), the velocity of the pore water will be $2.5 \cdot 10^{-4}$ m/s. Bentonite cannot penetrate faster than the velocity of the pore water. If the drilling advances with 1 mm/s, this means that the drilling goes faster than the bentonite penetrates. Bentonite will penetrate, but every time a cutter of the rotor passes, it will take away all bentonite and there is no possibility to form a filter cake.

This means that the excess pore pressure measured is not caused because the bentonite does not plaster well enough. It is caused because drilling goes faster than bentonite penetration into the sand for this tunnel.

4 PLASTERING

When drilling stops, a filter cake will build up due to the mud spurt and consolidation of the bentonite slurry (Bezuijen 1997). Using the results of experiments (Huisman 1998) and the permeability of the soil, it is possible to derive the course of the pressure in the soil just in front of both the tunnel face and the slurry

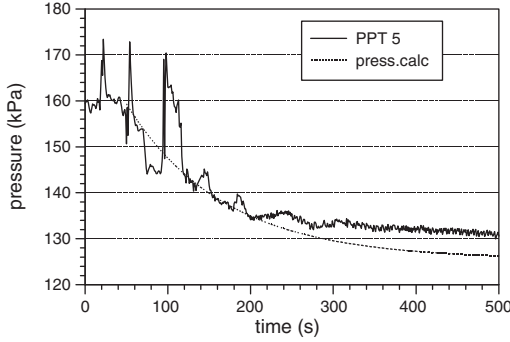


Figure 4. Measured and calculated pressure in the soil in front of a tunnel face during a stop in the drilling when a filter cake is built.

cake when drilling stops. At the axis close to the tunnel face there will be 1-dimensional flow. In that situation the pressure, written as a piezometric head, in front of the tunnel due to the mud spurt (the most important mechanism) can be written as:

$$\phi_{ms} = \frac{x\psi + nk_{ws}\phi_0 + k_s(\phi_0 - \Gamma x)}{x\psi + nk_{ws} + k_s} \quad (4)$$

where ϕ_{ms} is the piezometric head in the soil in front of the tunnel face, ϕ_0 is the piezometric head at the tunnel face, x the distance the bentonite has penetrated into the soil, n the porosity, k_{ws} the permeability of the consolidated slurry, k_s the permeability of the soil for slurry, Γ the ratio between applied piezometric head and final penetration of the bentonite slurry as measured in a plastering test, in which bentonite penetrates into a sand sample using a predefined pressure difference (Huisman 1998). ψ is the 1-dimensional flow resistance in the soil in front of the tunnel without bentonite (caused by groundwater flow only) and is defined as:

$$q = \psi(\phi_{ms} - \phi_\infty) \quad (5)$$

with q the specific discharge and ϕ_∞ the piezometric head at a large distance from the tunnel ($=0$ when the other values are presented as excess values). Since the thickness of the bentonite layer that penetrate into the soil during the mud spurt is very small compared to the dimensions of the tunnel, this layer can be neglected to determine ψ . Using Equation (2) and Darcy's law $q = k \cdot i$ it is found:

$$\psi = k / R \quad (6)$$

x in Equation (4) varies with time and is determined by the amount of slurry that has flown into the soil and can be solved using the equation:

$$\frac{dx}{dt} = \frac{q}{n} = k_s \left(\frac{\phi_0 - \phi_{ms}}{x} - \Gamma \right) \quad (7)$$

To check the validity of these equations the results of PPT 5 measurements were used during the last drilling stop before the gauge was destroyed by the TBM. The result is shown in Figure 4 together with the result of a calculation using the measured Γ (133) and $\phi_0 - \phi_\infty = 3.5$ m, $n = 0.4$, $\psi = 2.5 \cdot 10^{-5}$ 1/s, $k_s = 5 \cdot 10^{-5}$ m/s and $k_{ws} = 2.5 \cdot 10^{-8}$ m/s. The result showed reasonable agreement apart from pressure peaks that are present in the measured signal, probably because the rotor is still turning.

Analysing laboratory results Huisman (1998) found that better agreement between measurements and calculations could be obtained if also the blocking of the pores by bentonite particles is taken into account by an empirical blocking factor. These field data do not clearly prove the need for such a factor.

5 CONSEQUENCES FOR STABILITY

Calculation methods for the stability of the tunnel face normally do not take into account the influence of excess pore pressure on the stability. It is generally assumed that the pressure at the tunnel face is directly applied to the grains, which means that implicitly a perfect plastering is assumed. Using the wedge shape failure mechanism as suggested by Horn (1961), Anagnostou & Kovári (1994) and Jancsecz & Steiner (1994), the influence of the excess pore water can be explained, see Figure 5. The figure shows a 3 dimensional plot of the failure surface and two 2 dimensional cross-sections. In the left 2 dimensional cross-section the situation as assumed in the various calculation methods is presented, the cross-section at the right presents the situation with excess pore pressures in the sand. Stability is obtained because the tunnel face pressure supports the triangle column ABCDEF.

It is clear that this support is less effective in the situation with excess pore pressure. As indicated in the figure, the net force to support the triangle is less. On the other hand, the excess pore pressure will also create a vertical gradient over the block CDEFGHIJ resulting in a reduction of the force from this block on the triangle.

To investigate the influence of the excess pore pressure on the stability, the analytical calculation methods as described by Anagnostou & Kovári (1994) and Jancsecz & Steiner (1994) has been adapted by Broere (2000) and as described in CUR/COB (2000).

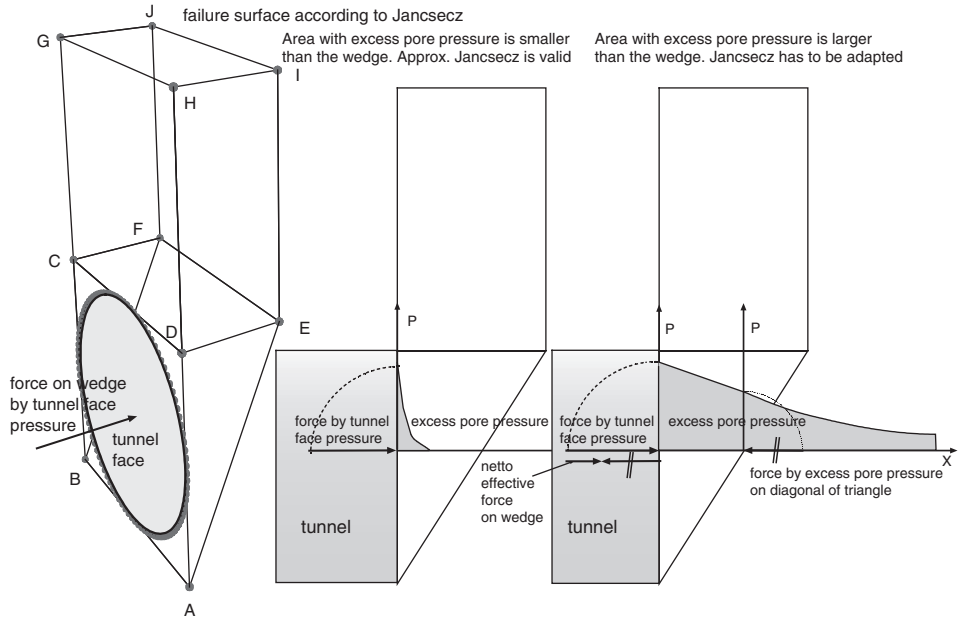


Figure 5. Sketch, influence of pore pressure on stability tunnel face. What is mentioned about the approach of Jancsecz is also valid for the other “wedge shaped solutions” mentioned in the text.

Both models showed comparable results, a significant increase in the minimum allowable tunnel face pressure to achieve a stable front.

These models are analytical models and therefore it was necessary to simplify the problem to come to a solution. To check these solutions it was decided to run some calculations with the numerical model that will be described in the next section.

6 NUMERICAL ANALYSIS

6.1 Element mesh

To determine the influence of excess pore pressures on the stability of the tunnel face, a flow-stress analysis was performed with the finite element program DIANA. In this analysis, a potential flow problem is solved and the resulting pressures are transferred to the stress (deformation) analysis. To simplify the problem, a homogeneous subsurface was assumed with a concrete tunnel. A 3D model was made with 3440 20-node elements and a total of 16159 nodes, see Figure 6.

The modelled tunnel has a length of 45 m, an inside diameter of 10 m and a wall thickness of 0.5 m. The top of the tunnel lies 15 m below the surface. The total length of the model is 90 m. In the stress analysis, the tunnel wall is modelled linear elastically and the soil with a Mohr-Coulomb model. The soil is assumed to be fully saturated sand, so the water level is at the surface.

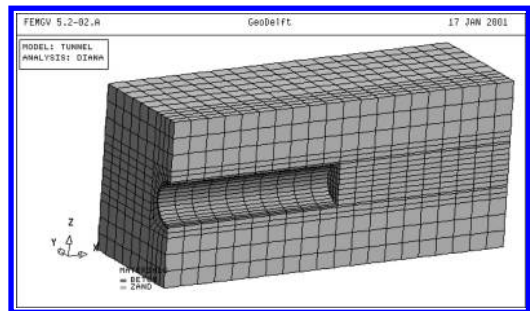


Figure 6. Element mesh used in the numerical calculations.

The calculation was made using effective stresses, so the weight of the water is subtracted from the total weight of the soil. The following parameters were used for the sand: Young’s modulus 48.7 Mpa, poisson ratio 0.3, ρ_{wet} 2000 kg/m³, cohesion 1 kPa, friction angle 32.5° and angle of dilation 2.5°.

6.2 Potential flow simulation

The bentonite slurry at the tunnel face has a slightly higher density than water. In the flow calculations this small difference is neglected, expressing the flow problem in excess pressures, the tunnel face pressure was assumed to be constant. The calculation was made

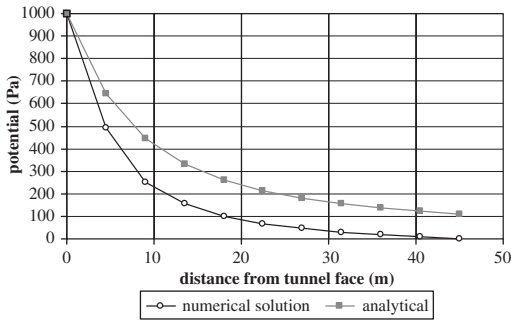


Figure 7. Calculated excess pressure in front of the tunnel (numerical calculation and approximation, Equation (1)).

for 1kPa pressure on the tunnel face. At all other boundaries, the pressures are set zero except for the symmetry plane and tunnel wall which are taken as impermeable. The soil has a permeability of 10^{-4} m/s. However, the potential flow is expressed in excess pore pressures and therefore this value has to be divided by the specific weight of water resulting in a permeability of 10^{-8} m²/sPa. This value was used in the calculations. The numerical solution of the potential flow problem in line with the tunnel axis and starting at the bore face is presented in Figure 7 together with the result of Equation 1.

6.3 Tunnel face stability calculations

The pressure field resulting from the potential flow simulation is applied as a load in the deformation analysis to determine stability of the tunnel face. There are three load cases: weight, tunnel face pressure and excess pore pressures resulting from the flow calculation. The flow calculation is a linear one, which means that if a pressure of 2 kPa instead of 1kPa was applied on the tunnel face, the solution is the same, except that all pressures are twice as large.

This idea can be used in the stability calculation. In the beginning a certain pressure is applied on the tunnel face. Then, the excess pore pressures are multiplied with a factor to input the correct pressures. During the stability calculation, the pressure at the tunnel face is lowered and the excess pore pressure loads are lowered correspondingly until the tunnel face collapses.

In reality, if the bentonite slurry builds a filter cake at the bore face, this will make the face less permeable. This aspect is difficult to model with elements, but can be modelled in a different way. When a thin filter cake is present, the pressure gradient is large in this cake, causing a pressure drop over a relatively small distance. Then if a pressure of 1 kPa is applied on the tunnel face, the pressure just after the filter

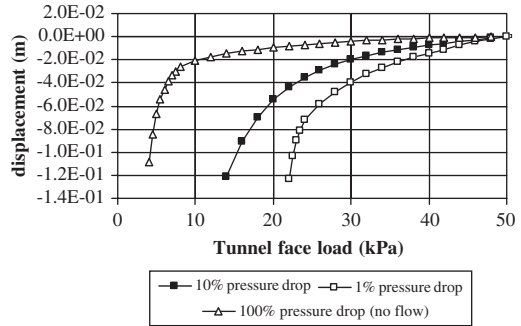


Figure 8. Horizontal displacement of the tunnel face as a function of the applied pressure and the percentage of pressure drop that occurs at the tunnel face.

Table 1. Results numerical calculations.

Pressure drop over cake (%)	Pressure (kPa)
1	24.5
10	18.0
100 (no flow)	5.0

cake is lower. To describe this, we introduced a factor $(1 - \alpha)$ with which the excess pore pressures are multiplied. If $\alpha = 0$ then there is no filter cake or pressure drop, so the excess pore pressure is the same as the applied pressure. If $\alpha = 1$, the filter cake is fully impermeable and all excess pore pressures are zero, so in this case a standard stability calculation is modelled with only weight and tunnel face pressure. We have calculated three cases with 1%, 10% and 100% pressure drop over the filter cake giving $\alpha = 0.01$, $\alpha = 0.1$ and $\alpha = 1$ respectively. As calculation results, the horizontal displacements of the bore face centre are shown as a function of the applied pressure, see Figure 8.

From the figure it can be seen that the tunnel face collapses at higher tunnel face pressures (is less stable) for the case with the lowest pressure drop over the filter cake, which has the highest excess pore pressures in the sand. Collapse in a numerical model happens when the stiffness matrix becomes singular and no equilibrium can be obtained, depending on the element type this can be different from collapse in reality, therefore a collapse criterion was obtained from model tests. In centrifuge tests the bore face collapsed at a deformation of 0.7% of the tunnel diameter. In this case this means 7 cm. The pressures for this stability criterion presented in Table 1, which shows that stability is better for lower excess pore pressures.

The trend found in the numerical calculations confirmed the results found in the analytical models. However, the minimum allowable pressures, as found

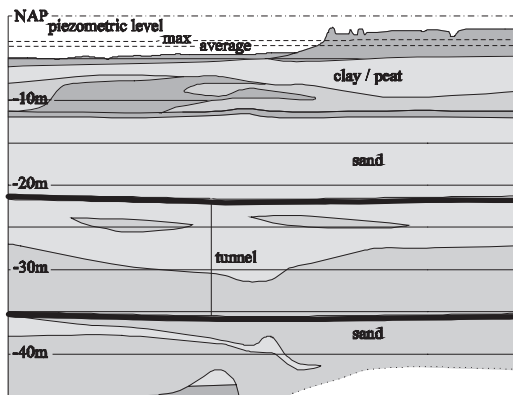


Figure 9. Geotechnical profile tunnel in polder.

with this numerical method are lower than according to calculation methods as described by Broere (2000) and in CUR/COB (200).

7 CONSEQUENCES FOR MAX. PRESSURE

The section above has dealt with the consequences for the face stability at minimum pressure. However, depending on the situation it is possible that the excess pore pressure influence the maximum allowable drilling pressure. An example of such a situation is discussed below.

In view of the excess pore pressures measured at the 2nd Heinenoord tunnel it was decided to determine the possible risks of these excess pore pressures for another Dutch tunnelling project. The hypothesis that there might be a large risk involved arises from the geohydrological conditions in this polder area of Holland: relatively high piezometric levels compared to a low surface level. Calculations were made to check this in the design phase for a large tunnel project (14.9 m diameter) crossing a deep polder (Surface level = SL - 5 m; groundwater head average = SL - 3.5 m, maximum = SL - 3 m). The depth of the tunnel is shown in Figure 9. In the normal situation the weight of the (semi)confining top soil layer, consisting of only 7 m of peat and soft clay, just equals the upward forces from the groundwater underneath. A surplus of water pressure can disturb this vulnerable equilibrium state (bursting of the top layer).

The minimum slurry pressures, which are needed for a stable tunnel face during drilling were for this situation calculated using the analytical model of Broere (2000). As minimum excess pore pressure in front of the cake a value of 28.3 kPa was determined (2.83 m surplus water head).

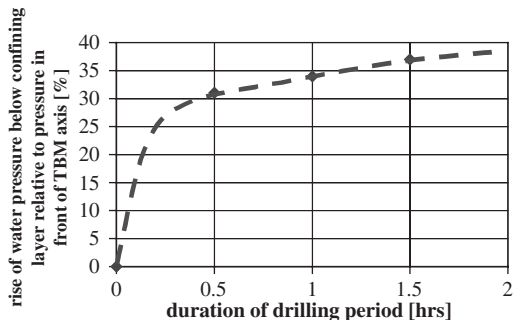


Figure 10. Calculated pressure build up when drilling starts.

The slurry pressure can only be transmitted to the groundwater in the period that the slurry cake is cut from the soil face by the rotating cutting wheel of the TBM. As argued before, there will be no cake formation during drilling and drilling of one ring takes between 0.5 and 1.5 hours. However, the water pressure will not adopt directly to the slurry pressure during drilling due to the time dependent damping effect in the groundwater aquifer caused by the elastic storage capacity. The groundwater effects just below the (semi)confining top were calculated with the finite difference groundwater program MODFLOW. The 10*5 km² axial symmetrical model was multilayered (13 anisotropic model layers for the aquifer) and the input was: flow resistance top aquifer $c = 10000$ days, total transmissivity aquifer $kD = 1600$ m²/day, storage capacity $S = 1.10^{-3}$ [-], anisotropy factor $kh/kv = 3$.

The calculated surplus water pressure depended on the duration of the drilling period as shown in Figure 10. The calculated extra water head below the confining layer is 1.05 m. The calculation results led to the conclusion that the stated hypothesis concerning bursting risk is true. Measures to overcome problems, e.g. by monitoring and adaptation of the drilling procedure or even hydrological solutions must be considered in this situation.

8 CONCLUSIONS

It is shown that the measured excess pore water pressures in front of the tunnel face are mainly caused by the groundwater flow conditions and hardly by the slurry properties. During stand still plastering occurs. The formulation for this plastering, presented in this paper, presents reasonable results, but needs the input of plastering experiments. The excess pore pressures during drilling have consequences for as well the minimum and maximum pressures that can be allowed at the tunnel face.

ACKNOWLEDGMENT

HSL-Noord, COB, Delft Cluster.

REFERENCES

- Anagnostou G. & Kovári K. 1994. The face stability of Slurry-shield-driven Tunnels. *Tunnelling and Underground Space Technology*, Vol 9. No.2. pp 165–174.
- Bakker K.J., Boer F. de, & Kuiper J.C. Extensive independent research programs on 2nd Heinoord tunnel and Botlek Rail tunnel. *Proc. XII ECSMGE, Amsterdam*, 1999.
- Bezuijen A. 1997. Plastering and mud spurt during drilling (in Dutch). BTL-report 27.
- Bezuijen A. & Brassinga H.E. 2001. Blow-out pressures measured in a centrifuge model and in the field *Proc. Int. Symp. on Modern Tunneling Science and Techn. Kyoto*.
- Broere W. & Tol A.F. van, 2000. Influence of infiltration and Groundwater flow on Tunnel stability. *Proc. Int. Conf. on geotechnical aspects of underground construction in soft grounds*, eds. Kusakabe O. Fujita K and Niyazaki Y.
- CUR/COB 2000, Directive for the design of drilled tunnels for roads and tunnels. *Final report commission L500* (in Dutch).
- Horn N. 1961. Horizontal Erddruck auf senkrechte Abschlussflächen von Tunnelröhren. *Landeskonferenz der Ungarischen Tiefbauindustrie*. pp. 7–16.
- Jancsecz S. & Steiner W. 1994. Face support for a large Mix-shield in heterogeneous ground conditions, *Tunneling '94*, 531–550.
- Huisman M. 1998. Static plastering, Theory and experiments, *BTL-report 34, WL / Delft Hydraulics J1384* (in Dutch).

The influence of soil permeability on the properties of a foam mixture in a TBM

A. Bezuijen

GeoDelft, Delft, The Netherlands

ABSTRACT: The penetration velocity of foam into the soil at the front face of an EPB TBM is investigated. It is shown that groundwater flow determines this penetration velocity in saturated conditions and soil permeabilities of around 10^{-4} m/s or less. An approximate method to calculate the excess pore pressure and hydraulic gradient in the soil in front of the tunnel is presented. The results of this method are compared with field measurements. It appears that the difference between a slurry shield and an EPB shield is only small. It is further shown that the groundwater flow can also have a dominating influence on the moisture content in the muck. This can mean that only a limited reduction of permeability in the mixing chamber is possible. Furthermore the calculations show that in some cases only a limited pressure drop will be present over the front face, which has consequences for the way the stability of the front face is calculated.

1 INTRODUCTION

Foam is often used in an EPB (Earth Pressure Balanced) TBM (Tunnel Boring Machine) to improve soil conditions for boring of a tunnel, especially in granular material. The foam increases the porosity between the grains, reduces the permeability and increases compressibility. The amount of foam to be added is based on experience or trial and error when no experience is available. The mixture can be 'too wet' or 'too dry' in the eyes of the experts.

Field measurements (Joustra, 2002) and model experiments (Bezuijen 2000) have shown that 'too wet' or 'too dry' in a saturated sand does not only depend on the foam properties, the foam injection ratio (FIR) and foam expansion ratio (FER), but also depends on the interaction between foam and groundwater. In permeable sand the excess pressure in the foam with respect to the pore water will cause a groundwater flow from the tunnel face. As a result the foam will replace the pore water and the mixture in the mixing chamber will be relatively dry. In less permeable conditions the foam will not be able to replace the pore water and the mixture will be wet and much less foam will be needed to increase the porosity of the sand compared to permeable conditions.

The paper deals with the interaction between foam, grains and groundwater in granular material. Some functions of the foam when drilling granular material will be dealt with briefly. The paper concentrates on the interaction with ground water flow. The flow

equation is derived for a simplified situation. This equation is used to estimate the flow velocity in front of the tunnel face and the penetration of foam in the soil. Consequences are discussed.

2 THEORY

2.1 *Functions of foam*

The main functions of foam were already mentioned in the introduction:

- Increasing the porosity between the grains. Measurements showed that the porosity is increased to values higher than the maximum porosity (Joustra, 2002). This leads to negligible grain stresses between the grains and reduces the torque necessary to turn around the rotor through the sand-water-foam mixture.
- Reduction of the permeability. A large permeability can lead to a water flow in the soil-water-foam mixture resulting in differences in porosity over the mixing chamber with the possibility of liquefaction.
- Increasing of the compressibility. During boring with a TBM the front face pressure has to be more or less constant, to avoid instability in the soil. This is controlled by controlling the soil removal through the screw conveyer in a EPB shield. A compressible mixture in the mixing chamber will allow for difference in soil removal without large fluctuations in the pressure.

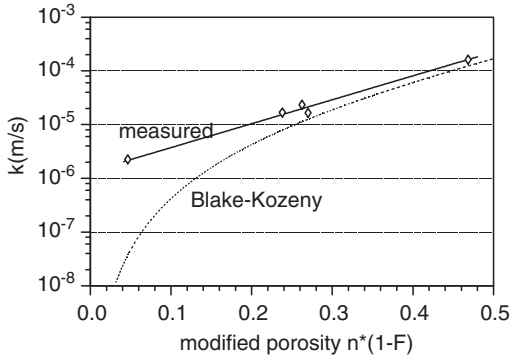


Figure 1. Permeabilities measured in a foam mixture compared with the Blake-Kozeny equation assuming that the foam only reduces the porosity. Figure modified from Kleinjan & Hannink (1999). F is the volume of air.

A consequence of the first function is that the excess pressure in the mixing chamber is a pore pressure. This will cause a groundwater flow from the tunnel face into the soil. The permeability of the mixture and or the flow properties of the subsoil determine the amount of water that flows into the tunnel face.

2.2 Groundwater flow

Permeability of the mixture

Only the air content determines the relative permeability of the mixture, compared to the permeability of the same mixture but without air. The properties of the foam have no influence and therefore theory for unsaturated flow can be used (Zhou & Rossen, 1995). However, for relatively high water contents in medium coarse sand an even simpler approach is possible. Experiments showed (Kleinjan & Hannink, 1997) that for relatively high water contents the permeability of a sand-water-foam mixture can be estimated assuming that the foam leads to bubbles with diameters of the same order as the mean diameter of the sand. Measurements were fitted with the Blake-Kozeny equation:

$$k = \frac{\rho g D_p^2}{150 \mu} \frac{n^3}{(1-n)^2} \quad (1)$$

Where k is the permeability, ρ the density of the water, g the acceleration of gravity, μ the dynamic viscosity, D_p the mean grain size (approx. D_{15}) and n the porosity.

Figure 1 shows that there is reasonable agreement between the measurements and the calculated values of the permeability for 'porosities' higher than 0.24. Porosities is between quotes because to perform the calculation it is assumed that foam is stable between

Table 1. Calculated permeabilities of a foam mixture where the porosity of the sand is increased from 0.4 to 0.55 by drilling and foam injection using foam with a FER of 10.

Perc. replacement (-)	Modified porosity (-)	Permeability	
		Fitted (m/s)	Theory (m/s)
0	0.3	2.9×10^{-5}	1.7×10^{-5}
10	0.27	2.1×10^{-5}	1.1×10^{-5}
20	0.24	1.6×10^{-5}	7.2×10^{-6}
50	0.15	6.2×10^{-6}	1.4×10^{-6}
90	0.03	1.8×10^{-6}	8.6×10^{-9}

the grains and that the porosity is not the usual porosity of the grains only but the porosity of the sand-foam mixture (thus the foam decreases the porosity of that mixture). Agreement is less at low porosities, because such low porosities can only be reached which a lot of foam. The foam bubbles will deviate from the sphere and Equation (1) is not valid for such low porosities. Results as presented in Figure 1 can be used to calculate the amount of replacement of the pore water by the foam necessary to have a real reduction of the permeability at the front face. A reasonable porosity increase of the sand grains themselves during drilling is from 0.4 to 0.55. This increase will lead to a decrease of the modified porosity (of grains and bubbles). The amount of this decrease depends on the amount of pore water that is replaced by the foam. The values found, using the volume balance, are shown in Table 1.

The results show that according to the measurements the sand water foam mixture will always have a certain permeability. A significant reduction of the permeability is only possible when a significant part of the pore water is replaced by foam.

Flow in front of the tunnel

The groundwater flow in front of a TBM will be determined by the soil layering, the depth of the tunnel and the properties of the mixture in the mixing chamber. For a particular situation this 3-dimensional flow problem can be solved in detail only numerically. To get an idea about the flow properties some approximations were used. A tunnel is located in a homogeneous granular soil deep below the soil surface. The flow from the mixing chamber into the soil is evenly distributed over the front face. Furthermore quasi-static conditions are assumed.

With these assumptions the flow problem can be schemed as shown in Figure 2.

Starting point of the calculation is the increase in piezometric head caused by a point source on the surface of a half space. A half space because only the flow in the soil in front of the tunnel face is taken into account.

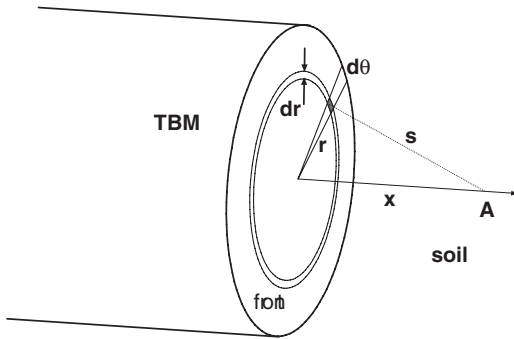


Figure 2. Sketch of tunnel face for flow computation.

The distribution of the piezometric head for such a situation can be written as:

$$\phi = \frac{Q}{2\pi ks} \quad (2)$$

With, ϕ the increase in piezometric head, Q the discharge of the point source, k the permeability of soil in the half space and s the distance between the point source and the point where the piezometric head is measured. For an uniformly distributed load as at the tunnel face the increase in piezometric head for one small area as indicated in Figure 2 can be written as:

$$d\phi = \frac{q r dr d\theta}{2\pi ks} \quad (3)$$

with q the specific discharge. For a point A in front of the tunnel on the axis of the tunnel, all points on the circle indicated in Figure 2, will have the same contribution to the piezometric head.

Integration over the circumference of the circle leads to:

$$d\phi = \frac{q r dr}{ks} \quad (4)$$

Integration over all circles from $r=0$ to $r=R$ and using: $s = \sqrt{x^2 + r^2}$ leads to:

$$\phi = \frac{q}{k} (\sqrt{x^2 + R^2} - x) \quad (5)$$

If the discharge is not known, but the piezometric head is known at the surface of the half space where the tunnel is located, the tunnel face, the equation can be written as:

$$\phi = \phi_0 (\sqrt{1 + (x/R)^2} - x/R) \quad (6)$$

With ϕ_0 the piezometric head in the sand just in front of the tunnel face.

In this situation the piezometric head in the soil in front of the tunnel is only a function of the distance from the tunnel and the piezometric head just in front of the tunnel face, but does not depend on the permeability of the soil.

Rewriting Equation (5) to Equation (6) can be done because it was assumed beforehand that there was a uniform flow at the tunnel face. This assumption is not true in case of a constant piezometric head, but is used here as an approximation. Numerical calculations and measurements for a slurry shield have shown that it is a reasonable approximation (Bezuijen et al, 2001). Using numerical calculations It was shown that the approximation is reasonable for the piezometric head along the tunnel axis for C/D values of 1 or larger, where C is the cover of the tunnel and D the diameter.

The amount of penetration of the foam or slurry in front of the tunnel depends on the flow velocity at the tunnel face. Foam can only penetrate when the pore water is removed. The gradient in the pore water can be calculated from Equation (6). Differentiation results in the gradient at the tunnel face for a given excess pore pressure. At the tunnel face ($x=0$) this leads to the equation:

$$i = \phi_0 / R \quad (7)$$

with i the hydraulic gradient. The pore water velocity (v_p) in front of the tunnel can be written as:

$$v_p = \frac{ki}{n} = \frac{k\phi_0}{nR} \quad (8)$$

where k is the permeability of the sand and n the porosity.

This last equation also gives the velocity, which with foam can penetrate in front of the tunnel during drilling. If this velocity is larger than the drilling velocity, all pore water will be replaced by foam and the muck will be relatively dry. However, if this velocity is smaller than the drilling velocity there will always remain pore water in the soil that is excavated from the tunnel face and the foam will be relatively wet. Another consequence is that less foam is necessary, because some of the pore water is not replaced by foam.

Another way to describe the flow in front of a tunnel face was presented by Hoefsloot (2001) and Broere (2001). They used equations for unsteady flow in a semi-confined aquifer to calculate the pore pressure distribution. This is not followed here because not all soil layer distributions can be schemed to a semi-confined aquifer and the difference between both methods is limited close to the tunnel face, which is the situation most of interest for this paper. It is assumed here that it is more important to incorporate the 3-dimensional flow than the non-stationary flow,

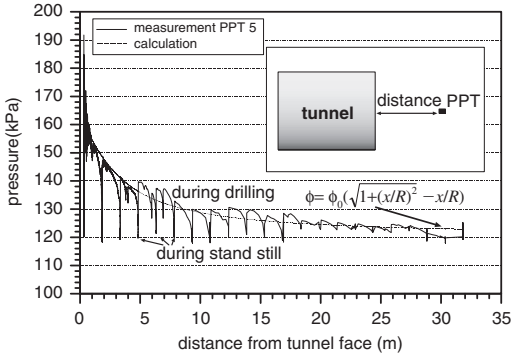


Figure 3. Measured excess pore pressure in front of a slurry shield and approximation (2nd Heinenoord Tunnel).

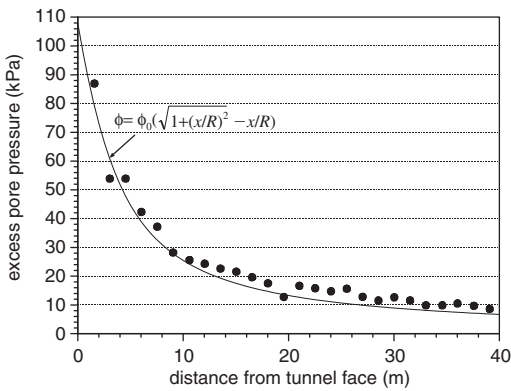


Figure 4. Measured excess pore pressure in front of an EPB shield (●) and approximation (Botlek Rail Tunnel, MQ 1 South). Relatively impermeable subsoil (measurement data from Hoefsloot, 2001).

although this assumption has to be proved by further measurements. However, it should be taken into account that the gradient can be less than calculated here in case a tunnel is located in a thin semi-confined aquifer with a long leakage length.

3 MEASUREMENTS

Although only an approximation, the formula derived in this paper fitted quite well with measurements performed in front of a TBM at the 2nd Heinenoord Tunnel, see Figure 3, where a slurry shield was used. It also fitted well with one of measurement locations during drilling of the Botlek Rail Tunnel where an EPB shield was used, see Figure 4. At another location on the Botlek Rail Tunnel track, the calculated pressures further from the front face were too low, Figure 5. Here a semi-confined aquifer was present with a

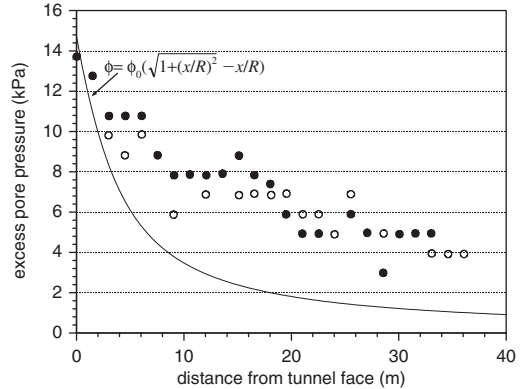


Figure 5. Measured excess pore pressure in front of an EPB shield (● pore pressure gauge 1, ○ pore pressure gauge 2) and approximation (Botlek Rail Tunnel, MQ4 South). Relatively permeable subsoil (measurement data from Hoefsloot, 2001).

leakage length, estimated by Hoefsloot (2001), of 707 m and this influences the results.

Only point measurements of maximum excess pore pressure are presented for the Botlek Rail tunnel because the measured excess pore water pressure has to be corrected for the tide.

The figures for the Botlek used the data as presented by Hoefsloot (2001). It should be noted that the excess pressures are rather low in Figure 5. It is also possible that a small error in the determination of the tidal pressures causes the deviation.

4 CONSEQUENCES

4.1 Wet and dry foam

Starting with the pressure in the mixing chamber there can be a pressure drop at the tunnel face due to cake forming when a slurry shield is used or by penetration of foam in case of a EPB shield. Bezuijen (2001) elaborates the penetration of bentonite in case of a slurry shield. Here it is concentrated on a EPB shield. The maximum gradient in the soil in front of the tunnel face occurs when ϕ_0 is equal to the average pressure in the mixing chamber. For such a situation the pore water velocity is given with Equation (8) with ϕ_0 equal to the pressure in the working chamber. This equation predicts at what velocity the pore water is expelled, but it also presents the velocity that the foam can penetrate into the soil in front of the tunnel face. If the drilling velocity is higher than the penetration velocity of the foam, then pore water will partly remain in the excavated soil. If the drilling velocity is lower, then the foam will replace the pore water, or the foam is stopped by the granular material causing a pressure drop over the tunnel face.

One of the functions of foam is to increase the porosity between the grains, which enables the grains to move with respect to each other. Due to the possibility to expel pore water the increase of porosity is not only determined by the FIR (Foam Injection Ratio, defined as the volume of foam divided by the in situ volume of foam on which that foam volume is injected). It also depends on the drilling speed, the radius of the tunnel, the permeability of the soil and the excess pressure in the mixing chamber. Using the definitions for the porosity and the FIR and equation (3) and assuming homogeneous conditions, thus no segregation of the soil-water-foam mixture, it can be derived:

$$n_m = \frac{n - \frac{k\phi_0}{Rv_d} + FIR}{1 - \frac{k\phi_0}{Rv_d} + FIR} \quad (9)$$

Where n_m is the porosity of the grains in the mixing chamber and n the in situ porosity in the soil. In the derivation it is assumed that $n - k\phi_0/(Rv_d) > 0$.

It is clear that for a constant ϕ_0 and FIR n_m can change as drilling velocity or permeability of the soil change. To keep the porosity constant it is necessary to increase the FIR when the drilling speed is decreased or a sand layer with a higher permeability is encountered.

Pore water that is not replaced by foam during the drilling will remain in the mixture and will result in a 'wetter' foam in the muck than originally injected. The amount of water in the foam is defined with the FER (Foam Expansion Ratio, defined as the total foam volume divided by the water volume in the foam). Again using Equation (8) and the definitions of the FER, the porosity and the FIR it is possible to calculate the FER in a muck (FER_s , with 'foam water' and the remaining pore water):

$$FER_s = \frac{FER}{1 + \frac{FER}{FIR} \left(n - \frac{k\phi_0}{Rv_b} \right)} \quad (10)$$

Where the FER is the Foam Expansion Ratio of the injected foam.

In the case of a low permeability soil and a relatively high FER of the original foam it is possible that the resulting FER_s is completely independent for the original FER. For $k\phi_0/(nRv_b) \ll 1$ and $n \cdot FER/FIR \gg 1$ the equation reduces to:

$$FER_s = \frac{FIR}{n} \quad (11)$$

For this situation 'drier foam' will not help if the resulting muck looks 'too wet'. It is only possible to

increase the FIR (but this will also increase the porosity in the muck and reduce the friction in the screw conveyer) or to reduce drilling speed to replace more pore water in front of the tunnel face. As mentioned in Section 2.2 such 'wet' muck will also have a relatively large permeability and therefore it can be unstable.

4.2 Pressure drop at the tunnel face

The name of the drilling method (earth pressure balance shield) suggests that the shield controls the earth pressure. This earth pressure is not a very well defined term in soil mechanics. Soil mechanics defines total stresses, pore water pressures and effective stresses. Earth pressures most likely corresponds with the total stresses. However, as was mentioned before, using foam will result in a porosity in the mixing chamber that is higher than the maximum porosity and thus the effective stress in the mixing chamber will be zero. This means that a change in pressure in the mixing chamber will be a change of pore pressure. During the drilling through fine sand at the measurement location MQ 1, of which Figure 4 shows results, the pore pressure present in the mixing chamber is equal to the pore pressure in the soil just in front of the tunnel. For that situation the stability of the tunnel face is not determined by controlling the total pressure but by controlling only the pore pressure in the soil. In such a situation the stability of the front face with respect to the minimum allowable pressure has to be calculated taking into account the influence of the excess pore pressure and using methods as described by Broere (2001) and Bezuijen et al (2001). The situation is very much comparable to a slurry shield. With respect to the stability of the soil at the tunnel face there is no difference. As mentioned in Bezuijen et al (2001) during drilling with a slurry shield in fine sand, it was also found that there was hardly a pressure drop over the front face of the tunnel during drilling and that plastering only occurred during stand still.

In the coarse sand that was encountered in measurement location MQ 4 an excess pore pressure in the mixing chamber of approx. 60 kPa was applied (Joustra, 2002). It appears from Figure 5 that in this case only 1.5 m water corresponding with an excess pore water pressure of approximately 15 kPa was found in the soil in front of the tunnel, which means that in this case there is a considerable pressure drop at the tunnel face.

The reason for the difference in behaviour for these 2 locations is the difference in permeability and due to that the difference in penetration velocity of the foam, see Table 2.

In MQ 1 the groundwater flow limited the penetration of the foam into the soil. In MQ 4 this is much less the case.

Maidl (1995) and Quebaud et al (1998) have reported experiments where foam penetrated into sand

Table 2. Parameters for the 2 measurement locations.

Parameter	MQ 1	MQ 4
Permeability (m/s)	5.8×10^{-6}	3.0×10^{-4}
Porosity soil (-)	0.4	0.38
Excess pressure front (kPa)	180	60
v_p , Equation (8) (m/s)	3.3×10^{-5}	9.9×10^{-4}
Drilling velocity (m/s)	7.5×10^{-4}	6.6×10^{-4}
Perc. penetration in front (%)	4.4	100

using a high pressure gradient over the foam and sand. In these experiments the foam penetrated fast for 30 to 60 mm (depending on the type of sand), but the penetration slowed down afterwards. This means that some penetration in the sand is necessary before a pressure drop can be maintained over the foam. Due to the limited penetration such a pressure drop was not possible at location MQ 1. In MQ 4 the penetration velocity of the foam was just a bit higher than the drilling velocity and therefore it was possible to maintain a pressure drop over the front face.

5 MUCK SAMPLES

An additional way to validate the theory developed would be to extract muck samples from the mixing chamber in a tunnel project. This was done for the Botlek Rail tunnel. Results were summarised by Joustra (2002) and Rodenhuis (2002). However, it appeared from their results that reality is more complex than theory. In a real tunnelling situation the drilling speed is not constant, the excess pressure varies, the FIR varies, the mixture is not homogeneous over the mixing chamber and sometimes air escaped during tunnelling. Therefore it is not possible to make a general comparison between measurements and calculations. No samples were taken for MQ1. Samples taken for MQ4 (10 samples for 2 tubes) showed an average density of 1600 kg/m^3 , larger than would be expected if all pore water was expelled by the foam (1410 kg/m^3 for foam with an expansion ratio of 10). However, Joustra (2002) also showed that the mixing chamber was not filled homogeneously. From pressure measurements in the mixing chamber it is reasonable to assume that air was concentrated in the top of that chamber. Since this air has to come from the mixture the density of the samples taken at the height of the axis of the TBM will have a higher density. It was reported that at another location a sample taken at the axis of the TBM contained only air.

These results showed that a homogeneously filled mixing chamber is not always a present during drilling. Further research would be necessary to determine for what conditions a homogeneous muck could be expected.

6 CONCLUSIONS

The research presented here led to the following conclusions:

1. Excess pore pressures, as measured in front of an EPB shield tunnel, can be described in the same way as for a slurry shield.
2. The penetration of foam into the soil in front of the TBM is, in case of soils with a low permeability, determined by the groundwater flow and not by the properties of the foam.
3. Due to the limited penetration of the foam in soils with a low permeability, there will be hardly a pressure drop at the tunnel face and the pressure in the working chamber will result in a comparable pore pressure in the soil just in front of the tunnel. Due to this the effective stress just in front of the tunnel will be small in such cases. This should be taken into account in calculations for the stability of the front face.
4. In case of a limited penetration of foam the possibilities to influence the properties of the mixture, as the permeability, are restricted. The water content of the mixture is to a large extent determined by the pore water present in the sample and much less by the foam properties.

ACKNOWLEDGEMENTS

The author would like to acknowledge BTL (Research foundation: Horizontal Drilling & Tunnelling.) and COB (Centre for Underground Construction) for their permission to publish the results. The commission F310 is acknowledged for analysing the data that came from the TBM of the Botlek Rail Tunnel and were essential for this research and for stimulating discussion during the meetings, Arno Talmon for co-operation and useful comments on the manuscript.

REFERENCES

- Bezuijen A. 2000. Model experiments using foam, simulating the drilling with an EPB shield, *GeoDelft report CO-51010*.
- Bezuijen A., Pruiksma J.P., Meerten H.H. van 2001. Pore pressures in front of tunnel, measurements, calculations and consequences for stability of tunnel face. *Proc. Int. Symp. on Modern Tunneling Science and Techn. Kyoto*.
- Broere W. 2001. Tunnel Face Stability & New CPT Applications. Ph.D. Thesis, *Delft University of Technology, Delft University Press, 2001*.
- Hoefsloot F.J.M. 2001. Waterspanningen voor het boorfront: een eenvoudig geohydrologisch model. *Geotechniek oktober. pp. 26-33*.

- Joustra J.W.F. 2002. Aanvullende data-analyse praktijkonderzoek Botlek-spoortunnel-het EPB process. *Delft University of Technology, Report 2001.BT.5566*.
- Kleinjan J.A., Hannink G. 1997. EPB-schild, Zand-waterschuimmengsels, schuim, grondbrij, *BTL-report 57*.
- Maidl U. 1995. Einsatz von Schaum für Erddruckshilde – Theoretische Grundlagen de Verfahrenstechnik- *Bauingenieur 70 487–495 Springer-Verlag*.
- Quebaud S., Sibai M., Henry J.-P. 1998. Use of chemical foam for improvements in drilling by earth-pressure balanced shields in granular soils. *Tunnelling and Underground Space Technology, Vol. 13, No. 2, pp. 173–180*.
- Rodenhuis S. 2002. Evaluatiefase A Noordelijke buis MQ 2, 4 en 5, Vergelijk tussen Noord- en Zuidbuis. *COB report F300-W-018-04*.
- Zhou Z.H., Rossen W.R. 1995. Applying fractional flow theory to foam processes at the ‘limiting capillary pressure’ *SPE Adv. Technol. 3, 154*.

Pressure gradients and muck properties at the face of an EPB

A. Bezuijen

GeoDelft, Delft, The Netherlands

A.M. Talmon

WL | Delft Hydraulics, Delft, The Netherlands

J.F.W. Joustra

Tunnel Engineering Consultants (TEC)/Witteveen + Bos

B. Grote

T & E Consult

ABSTRACT: Measurements are presented that were performed in the pressure chamber and screw conveyor of an EPB TBM. The TBM operated in saturated sand with a high water table. Foam was applied for soil conditioning. Different from a slurry shield there was no direct relation between vertical the pressure gradient and the density of the muck in the pressure chamber. The pressure measurements differ considerably for different rings. The density and saturation of the mixture was measured by taking samples from the pressure chamber during excavation. Densities found indicate a porosity just higher than the maximum porosity of the sand. A pressure drop of approximately 1 bar was found when the muck passes from the pressure chamber to the screw conveyor. Explanations are presented in the paper.

1 INTRODUCTION

The Botlek Rail Tunnel was the second bored tunnel in The Netherlands and the first one that was completed using an EPB shield. A considerable part of the tunnel was bored through Pleistocene sand under a high water table, see Figure 1. The water table was up to 23 m above the tunnel axis. Foam was used to stabilize the tunnel face.

The support pressure acting at the tunnel face can be seen as a combination of an absolute pressure and the vertical pressure gradient. In an EPB shield, the average pressure is controlled by the screw conveyor and valves; the vertical pressure gradient is determined by a combination of the excavation process and material properties and cannot be controlled. Yet this gradient

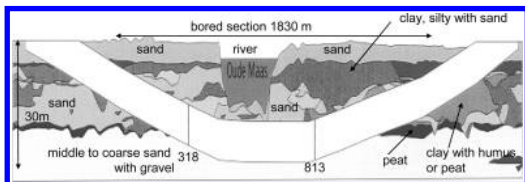


Figure 1. Geotechnical profile. The numbers indicate the approximate positions of evaluated rings, see further text.

is of importance because it determines the pressure at the crown of the tunnel for a given pressure at the axis. The pressure gradient at the tunnel face of a slurry shield is determined by density of the slurry at the tunnel face. For an EPB-shield there appear to be more mechanisms determining the gradient.

The paper deals with the pressure gradients measured, the densities and saturation of the mixture samples taken, the pressure drop in the muck at the transition between pressure chamber and the screw conveyor and presents possible explanations.

2 MEASUREMENTS

2.1 Density measurements

A sampling device was developed in order to determine the exact composition of the muck inside the excavation chamber. This device simply consisted of a piece of pipe with some valves directly attached to the pressure bulkhead. By carefully opening the valves, some muck was allowed to flow out from the pressured excavation chamber through the sampling device. By subsequently closing the valves an exactly known volume of muck was extracted, which would be analysed

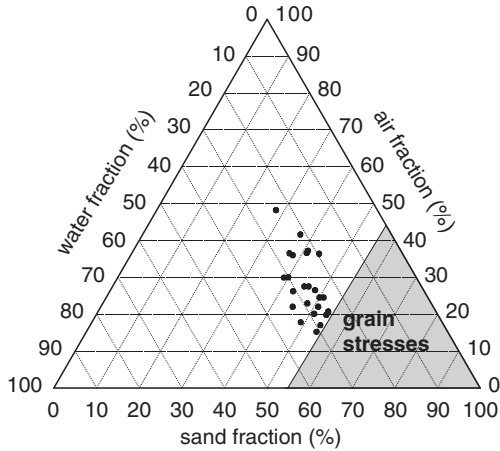


Figure 2. Measured sand, water and air fractions by sampling through the pressure bulkhead.

in a laboratory. In this way, the porosity and water content of the mixture could be determined and could be converted to the relative volumes of the different phases of the muck (solid, liquid and gas) as shown in Figure 2.

A total of more than 20 samples of muck have been extracted from the centre of the excavation chamber at 6 different locations along the tunnel alignment. Although muck with a relatively high consistency proved problematic to collect because of its inability to flow easily, samples taken in a short time span were very comparable.

The results show that all samples have a sand fraction that is lower than the minimum fraction to develop grain stresses in the sand. For some samples however, the density is close to the density where grain stresses can be expected.

2.2 Pressure measurements

2.2.1 Instrumentation in pressure chamber

The total pressure was measured at the bulkhead at 9 locations and the pore water pressure at 3, see Figure 3. The pore pressure gauges could be cleaned by a small water jet to avoid blocking of the filter. The status of the boring process was monitored as well as the amount of injected foam.

2.2.2 Pressures and vertical gradients

Pressures were measured during excavation of the Botlek Rail Tunnel at various locations at the pressure bulkhead; see for an example Figure 4. The average vertical pressure gradients determined from these pressures are shown in the upper plot of Figure 4. (All figures with measurements present the ring number in the caption that was drilled during the measurement.

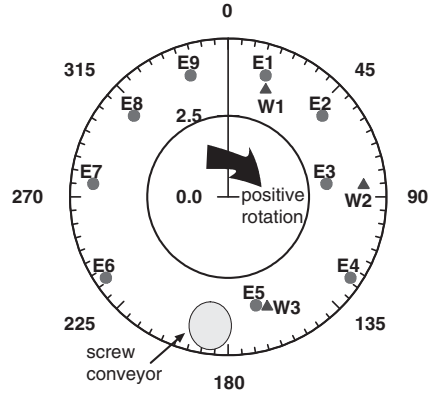


Figure 3. Position of instruments in the TBM looking from the tunnel to the TBM and definition of rotation.

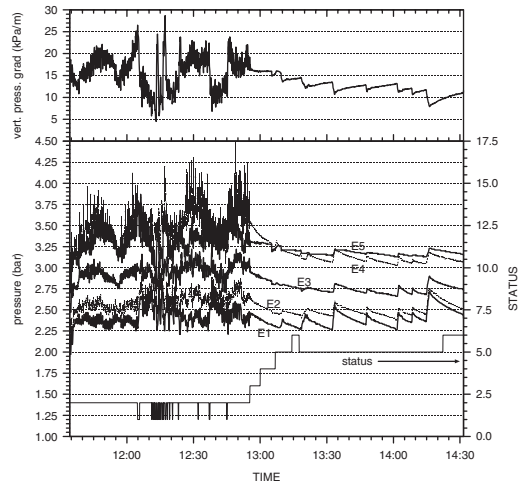


Figure 4. Ring 318 N. Pressures measured at the bulkhead, status of the TBM and the gradient determined from the pressures. Only a part of the pressure readings is shown, but all readings (E1 – E9) are used to calculate the gradient.

S is the south tunnel, N the north, location of the rings is shown in Figure 1). It shows that the gradient can be high during excavation but decreases when excavation stops (shown with the status, 2 means excavation, all other values mean stand still, see Table 1). The values measured for the vertical gradient can be put in perspective realizing that the gradient of the total vertical pressure in the not yet excavated soil is approximately 20 kPa/m, the density of the foam-water-soil mixture is approximately 13 kPa/m and the pore pressure has a gradient of 10 kPa/m. The measurements show that the measured gradients can be higher than 20 kPa/m,

Table 1. Meaning of the status bit (Figure 4, lower part).

Status	Meaning
1	Temporary stop during excavation
2	Excavation
3	End of excavation phase
4	Start of ring building phase
5	Actual ring erection
6	Pause after ring erection

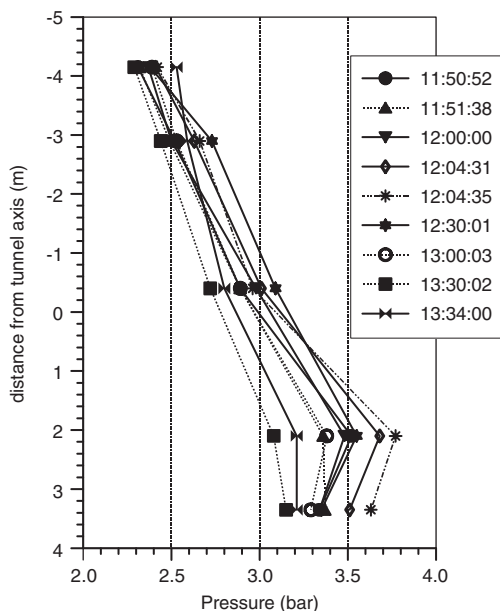


Figure 5. Ring 318 N. Pressure distributions along the gauges E1 until E5 for various times. Up to 12:30:01 the TBM is drilling, later times represent pressures during ring building.

but also lower than 10 kPa/m. The vertical pressure gradient decreases during ring building. The vertical pressure gradient determines, together with the average pressure, how well the TBM can counterbalance the in-situ soil stress, which is of importance to limit soil deformations.

Another way to present the pressure measurements for the same ring is shown in Figure 5. It shows the pressures from gauges E1 until E5 for different time steps. It can be seen that there is a more or less linear pressure increase with depth apart from the lowest measurement position (E5) with various gradients. The pressure decreases at the position of E5, because this gauge is close to the screw conveyor, where the mixture is removed from the pressure chamber.

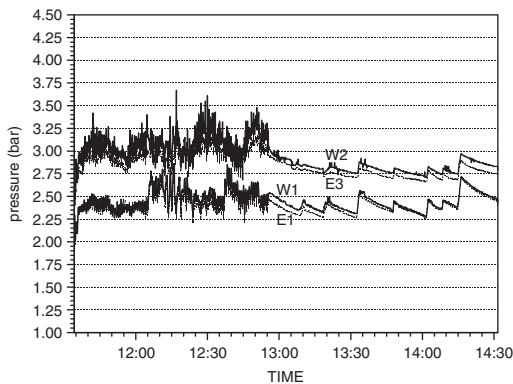


Figure 6. Ring 318 N. Total pressures and pore pressures compared.

2.2.3 Effective stress

Pore pressure gauges were installed near some total pressure gauges, see Figure 3, to determine the effective stress in the soil water foam mixture. Results of both total pressure gauges and pore pressure gauges are shown in Figure 6. It is clear that both pressures are comparable, which means that the effective stress in the mixture is negligible. W3 did not function and therefore could not be compared with E5.

Figure 6 shows the pressures measured for only one ring. The conclusion that there is hardly any effective stress in the mixture is a more general one for this boring (Joustra, 2002). Although there are some indications, that there is an effective stress near transducers E4 and E6 during the excavation of some rings, for example the large pressure variations measured during excavation between 12:00 and 13:00 (Figure 4) (see also Bezuijen et al. 2005). The conclusion that there is hardly any effective stress is also confirmed by the density measurements performed. It was found that in most cases the porosity of the samples was above the maximum porosity (see Section 2.1). A porosity lower than the maximum porosity is necessary to have a grain skeleton and effective stresses.

2.2.4 Pressures near the screw conveyor

The muck was removed from the pressure chamber by a screw conveyor. The screw conveyor was 15 m long from the entrance to the valve controlled outlet and made an angle of 23 degrees with the horizontal. The pressures were measured at 3 locations in the conveyor. Positions of the pressure gauges in the screw conveyor together with the vertical position of the pressure gauges in the bulkhead are shown in Figure 7. Results of measurements are shown in Figure 8 and Figure 9. The TBM excavates at the left side of these plots, where the pressures are fluctuating and there is no excavation at the right side

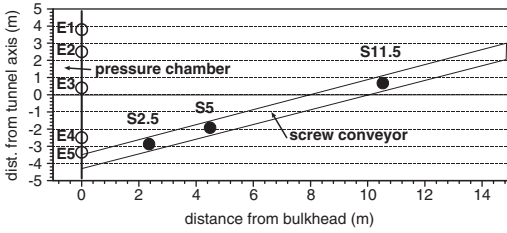


Figure 7. Position of pressure gauges on bulkhead and in the screw conveyor.

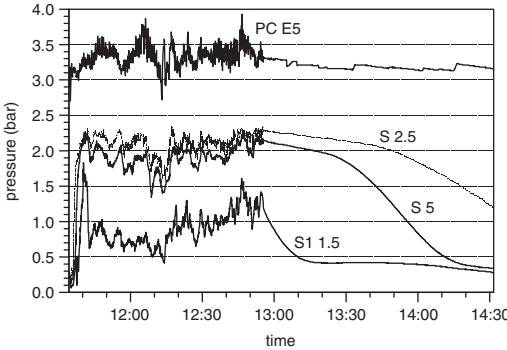


Figure 8. Ring 318 N, pressures in the pressure chamber (PC) screw conveyor (S).

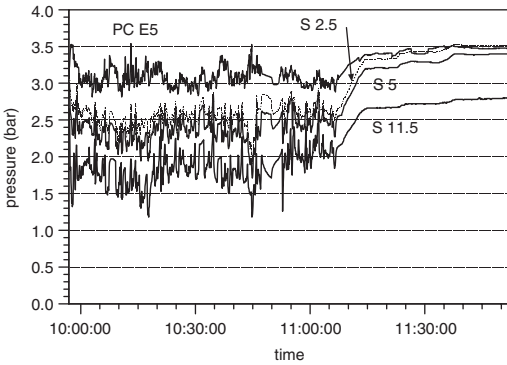


Figure 9. Ring 814 S pressures in the pressure chamber (PC) screw conveyor (S).

with the smoother pressure lines. PC E5 is the pressure in the pressure chamber at E5, see Figure 3. The other pressures are measured in the screw conveyor at respectively 2.5, 5 and 11.5 m from the entrance. These plots show two extremes that were found in the measurements:

- Ring 318 N: A considerable pressure drop between the pressure in the pressure chamber (PC E5) and the pressures in the screw conveyor. The pressure difference even increases during stand still.

- Ring 814 S: Only a small pressure drop that decreases during stand still.

In some other rings, where the pressures in the screw conveyor were checked, the pressure during and after excavation remained more or less constant. The high pressure drop measured at Ring 318 N between the entrance of the screw conveyor and in the screw conveyor itself indicates that there are grain stresses present in the muck close to the entrance. These grain stresses can cause arching in the pressure chamber. The influence of arching increases when excavation stops.

The situation of Ring 813 S occurs when there is limited or no arching in the pressure chamber. When that is the case the flow resistance in the screw conveyor decreases when the flow decreases after the end of excavation for that ring. Pressure can only be maintained by closing the valve on top of the conveyor.

Soil conditions were not very different for both situations (mostly sand), but more air was present in the samples taken close to Ring 318 N, compared with Ring 813 S.

3 DISCUSSION

3.1 Vertical gradient

The vertical gradient found in the pressure chamber of a slurry shield TBM is equal to the gradient that corresponds with the density of the slurry (Bakker et al., 2003). In the predictions made for these measurements it was assumed that this was also the case for an EPB shield. However, this is not found for this tunnel. Pressure gradients varied during drilling and this variation was much larger than can be expected from variations in densities. Measured vertical gradients were sometimes larger than 20 kPa/m. Assuming that such a gradient is a good indication for the density would mean that there would be rather dense saturated sand in the pressure chamber, which is quite unlikely.

From the results it is concluded that also the yield stress of the soil has an influence on the pressure gradient. This can also be seen from the pressure drop that is present at E5 compared to the pressures E4 and E6, see Figure 5 and Figure 10. At the lower end of the tunnel, the screw conveyor removes the mixture from the pressure chamber. This leads to a pressure drop due to the yield strength of this mixture.

Assume a layer of sand-water-foam mixture between the cutter head and the pressure bulkhead of the pressure chamber at L metre apart. The adhesion between the cutter head or the pressure bulkhead and the mixture is τ_a and the density of the mixture is ρ_m . In case of vertical flow, equilibrium of forces leads to the following equation:

$$\frac{dP}{dx} = \rho_m g \pm 2 \frac{\tau_a}{L} \quad (1)$$

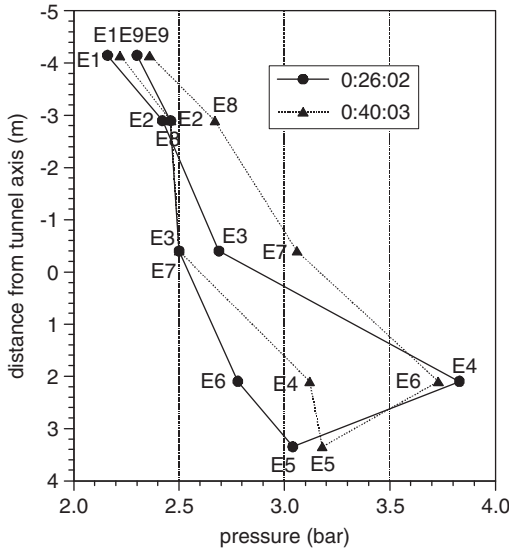


Figure 10. Ring 813 S. Distribution of pressures when the cutter head is rotating to the left (negative values) at 0:26:02 and to the right at 0:40:03.

Depending on the flow direction the pressure gradient can be $2\tau_d/L$ higher or lower than the pressure gradient corresponding to the density of the mixture. In case of a flow with a horizontal component as can be expected in the pressure chamber between E6 and E5 as well as between E4 and E5, the influence of the adhesion becomes even bigger.

There is no direct field data on the shear strength of the mixture in the pressure chamber, but from measurements in the laboratory it was found that this shear strength is one to a few kPa. This means that with an average density of the mixture of approximately 1500 kg/m^3 , the pressure gradient can vary as was measured depending on the direction of the flow. Lower values of the shear stress of 0.2 to 0.6 kPa were found from back calculation of the performance of the screw conveyor (Talmon & Bezuijen 2002). However, these values are likely to be lower than in the pressure chamber due to the pressure relief in the screw conveyor that leads to a higher porosity.

From a physical point of view the concept of adhesion as described here is probably too simple. Adhesion on flat iron surfaces can be less and the roughness, combined with the cohesion results in an apparent adhesion. However, also this apparent adhesion will result in the pressure gradient variations described here.

The vertical pressure gradient decreases after the actual excavation, during ring building. Foam injections executed during ring building are necessary to keep a stable boring face, but also lead to a decrease in

the average density of the mixture. The pressure loss is caused by ground water flow from the tunnel face to the ground water, a process driven by the excess pore pressure in the chamber (see also Bezuijen & Schaminée, 2001 and Bezuijen, 2002). The water that flows out is compensated with foam that contains only about 10% water and 90% air.

Consequence of the relatively low measured vertical gradient during most of the excavation cycle, compared to the gradient that corresponds with the density of the soil, is that the pressure gradient is lower than the soil pressure gradient. It is sometimes mentioned as an advantage of the EPB shield that there is a better 'match' with the pressure gradient in the soil when compared with a slurry shield. For the ground conditions encountered here this was not the case. The relatively high permeability sand (k is $5.8 \cdot 10^{-6} \text{ m/s}$ when Ring 318 N was drilled and 3.10^{-4} m/s during excavation of Ring 813 S) leads to expelling of water from the mixture. This reduces the density of the mixture. Together with the influence of the yield stress that leads to a further reduction of the vertical gradient the reduced density results in pressure gradients that are significantly lower than measured in a slurry shield (Bakker et al. 2003).

3.2 Pressure drop screw conveyor

Before the entrance of the screw conveyor a pressure drop of 1 bar or more was found for most of the rings, see Figure 8. This pressure drop was not expected. Given the strength of the muck, yield stress of about 3 kPa at maximum, the theory of extrusion of homogeneous plastic materials would apply, (Hill, 1986). For such conditions a pressure drop of about $dp = 5\tau_y = 15 \text{ kPa}$ is expected. An example of numerical pressure calculations in the mixing chamber, based on Bingham theory, is provided by Goeree 2001. The calculations of Goeree result in a comparable pressure drop as the extrusion theory.

A possible reason for the discrepancy is a thickening of muck in front of the entrance of the screw conveyor. The existence of such a phenomenon can also be the reason for difficulties encountered when sampling muck from the lowest sampling position through the pressure bulk head. Drained behaviour of the muck can lead to grain stresses.

A theory for distinction between drained and undrained behaviour was publicized by Winterwerp & van Kesteren, 2004. When the time-scale of drainage is shorter than the time-scale of deformation (= flow) of the muck, then compaction can occur. The key parameter is the so-called Peclet number that is defined by:

$$Pe = \frac{UD}{c_v} \quad (2)$$

with: U the characteristic velocity [m/s], D the characteristic length scale [m] and c_v the consolidation coefficient [m²/s].

The consolidation coefficient is defined by:

$$c_v = \frac{k}{\rho g m_v} \quad (3)$$

in which k is the permeability [m/s], ρ the fluid density [kg/m³] and m_v the compressibility [1/Pa].

At Peclet >10 the mixture displays undrained behaviour, and no thickening is expected. At Peclet <1 the mixture displays drained behaviour, and thickening might occur.

Measured permeabilities of muck are in the range: $2 \times 10^{-6} < k < 1 \times 10^{-4}$ m/s (Bezuijen, 2002). The air content in the muck determines its compressibility. At a porosity of $n = 0.5$ and a saturation of 0.5, the compressibility, at 2 bar (1 bar above the atmospheric pressure), is equated at: $1/m_v = 800$ kPa. As a result the consolidation coefficient will be in a range of $2 \times 10^{-4} < c_v < 1 \times 10^{-2}$ m²/s.

The characteristic length scale of the flow towards the screw conveyor equals the diameter of the screw conveyor $D = 1$ m. The characteristic velocity at the entrance of the screw conveyor is:

$$U = \frac{D_{TBM}^2}{D_{sc}^2} v_t \quad (4)$$

with: D_{TBM} the diameter of the tunnel and D_{sc} the diameter of the screw conveyor.

As a result the Peclet number is within the range: $5.4 < Pe < 270$.

It is concluded that muck properties are within the transition between drained and undrained behaviour. Only for the lowest permeabilities measured, the muck presumably will behave undrained. Under such conditions no segregation is expected to take place. The pressure build up at the entrance of the screw conveyor will disappear, flow control will be easier.

The theory described above showed that for these high permeable sands drained behaviour cannot be excluded. Such drained behaviour can lead to a decrease of the water content in the muck and porosity changes. Therefore it should be taken into account when designing an EPB for highly permeable soils. The theory is however, not more than partly the explanation for the observed phenomena in Figure 8 and Figure 9. As mentioned before, the soil conditions were not very different for both locations; only the water content was different. This would mean that at the location with the highest water content, the compressibility is lowest and the Peclet number is also lowest. Thus drained behaviour would be expected. Yet most arching (a result from porosity loss that could be caused

by drained behaviour) is found in the Ring with the highest air content in the muck, Ring 318 N.

The explanation is that soil is not a linear elastic material. The compressibility as mentioned above is only valid as long as there are no effective stresses. As soon as effective stresses occur (regardless whether this is caused by water flow or air compression) the soil will behave much stiffer, leading to a decrease of the Peclet number, thus drained behaviour.

4 CONCLUSIONS

From the study described in this paper we came to the following conclusions:

- While boring in sand with an EPB shield an important function of the foam is to increase the porosity of the sand to such a value that deformation is possible without or with only limited grain stresses. This is different from boring in clay where the lubricating is more important (Mair et al. 2003).
- The vertical pressure gradient is only to a certain extent influenced by the density of the mixture. Yield stress of the mixture also seems to have an influence.
- The vertical pressure gradient can be lower for an EPB using foam than for a slurry shield.
- Arching of sand before the entrance of the screw conveyor can lead to a considerable pressure drop before this entrance. This complicates the regulation of the pressure in the pressure chamber by means of the screw conveyor.

ACKNOWLEDGEMENTS

The laboratory tests were commissioned and supervised by BTL (Research foundation: Horizontal Drilling & Tunnelling) and COB (Centre for Underground Construction). The authors wish to thank these foundations for their permission to publish the results. The data on the Botlek Rail Tunnel presented here are derived from the COB-pilot project F300 in which the authors participate. The authors are very grateful to both COB and the builder of the tunnel BTC Botlek vof, with the granted opportunity to publish.

REFERENCES

- Bakker, K.J., Teunissen, E.A.H., Berg, P. van den, Smits M. Th. J.H., 2003, K100 research at the second Heineoord tunnel. *Proc. ITA 2003, Amsterdam*.
- Bezuijen, A. & Schaminée, P.E.L., 2001, Simulation of the EPB-shield TBM in model tests with foam as additive. *Proc. Int. Symp. on Modern Tunneling Science and Techn. Kyoto*.
- Bezuijen, A. Influence of soil permeability on the properties of a foam mixture in a TBM. *3rd Int. Symp. on Geotech.*

- Aspects of Underground Construction in Soft Ground, IS-Toulouse.*
- Bezuijen, A., Joustra, J.F.W., Talmon, A.M., Grote, B., Pressure gradients at the tunnel face of an Earth Pressure Balance shield. *Proc. ITA 2005, Istanbul.*
- BTL 62, van Seters, A.J., Bezuijen, A., Talmon, A.M., Caan en, C.P., Heijmans, R.W.M.G., 2000, From tunnel face to tunnel (In Dutch); *BTL-onderzoek 1995-1999; Compilatierapport Micro-Macro Tunneling M-0854.*
- Goeree, J.C., 2001, Numerical flow calculation of a Bingham-material in a 2D-model of an EPB (in Dutch), pt I&II, report no. 2000. *BT.5419. fac. Mechanical Engineering, Delft University of Technology.*
- Hill, R., 1986, The mathematical theory of Plasticity, *Oxford Science.*
- Joustra, J.F.W., 2002, Additional data analysis independent research project Botlek Rail Tunnel, the 'EPB-process' (in Dutch), *Delft University of Technology report. 2001.BT.5566.*
- Mair, R.J., Merrit, A.S., Borghi, X., Yamazaki, H. & Minami, T., 2003. Soil conditioning of Clay Soils. *Tunnels and Tunnelling International, April.*
- Talmon, A.M. & Bezuijen, A., 2002, Muck discharge by the screw conveyor of an EPB Tunnel Boring Machine, *3rd Int. Symp. on Geotech. Aspects of Underground Construction in Soft Ground, IS-Toulouse.*
- Winterwerp, J.C. & van Kesteren, W.G.M., 2004, Introduction to the physics of cohesive sediment dynamics in the marine environment, *Elsevier (pg 260).*

In-situ frost heave loads in artificially frozen ground for tunnelling

R.H.B. Rijkers

TNO-NITG/Netherlands Institute of Applied Geosciences, Delft, The Netherlands

B. Hemmen

GeoDelft, Delft, The Netherlands

N.M. Naaktgeboren

Ministry of Transport and Public Works/HSL-Zuid, Utrecht, The Netherlands

H. Weigl

Kombinatie Middelplaat Westerschelde, Terneuzen, The Netherlands

ABSTRACT: In the Netherlands the Westerscheldetunnel will be constructed with two tunnel bore machines and 26 connecting cross passages. The cross passages are built between the two main bored tunnels by using artificial ground freezing. During the construction phase of the cross passages an extensive monitoring program is carried out: (1) ground stress conditions and ground deformation and (2) deformation of the tunnel constructions – by measuring temperatures, frost heave loads and deformation. Measurements are taken in three different orientations: perpendicular, parallel and vertical to the cross passage with stress-monitoring stations and extensometers. Significant differences have been observed in loads and deformations, which are explained by different soil conditions. A significant variation in ground stresses has been monitored between the perpendicular and parallel direction with respect to the orientation of the freezing tubes. All separate phases of the construction activities of the cross passages (freezing, excavation, lining, thawing) are recognised clearly in the data.

1 INTRODUCTION AND OBJECTIVES

For the construction of the Westerscheldetunnel in the Netherlands 26 cross passages (or connections) are built between two parallel bored tunnels with artificial ground freezing (AGF) techniques (Hass et al., 2000). Special in-situ measurements of stress and deformation are carried out during the freezing period for the first two cross passages (DV1 and DV2) in order to evaluate the effects of the ground freezing technique. Due to the increase of volume of water to ice with 9% and ice lens formation frost heave loads are expected. The monitoring program includes measurements of stress and deformation development in the soil and the tunnel constructions.

The objectives of this study are (1) in-situ soil monitoring during period of artificial soil freezing, (2) evaluation of the frost heave loads to the tunnel due to soil freezing and (3) increase of knowledge on use of ground freezing techniques in soft soils for tunnelling.

2 WESTERSCHELDETUNNEL

2.1 Artificial ground freezing

The Westerscheldetunnel is located in the south-western part of the Netherlands below the estuarine river that connects to the port of Antwerpen (Belgium). In order to increase safety at the Westerscheldetunnel the two lanes in each direction are designed as separate tunnel tubes. These two parallel tunnel tubes are bored with inner diameters of 10.10 m. The total length of each bored tunnel tube is 6.6 km. To increase safety in the tunnel two bored tubes are connected with 26 cross connections at every 250 m. The cross passages are built from the inner side of the main tunnel tubes by using artificial ground freezing in order to make underground excavations possible. Artificial ground freezing techniques are used for both sandy soils and Boom clay because stiffness and permeability of all soil units in the trajectory is not considered to be sufficient for open excavation.

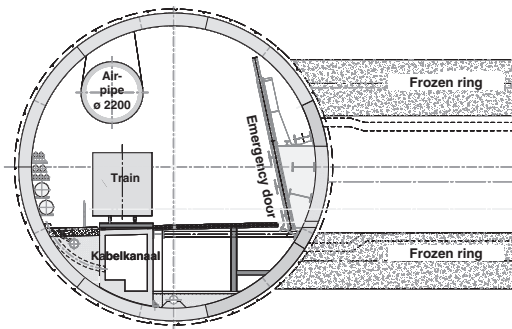


Figure 1. Situation of the western tunnel tube with the connection of frozen soil. The emergency door is opened after evaluation of the (frozen) ground temperature.

2.2 Construction of cross passages

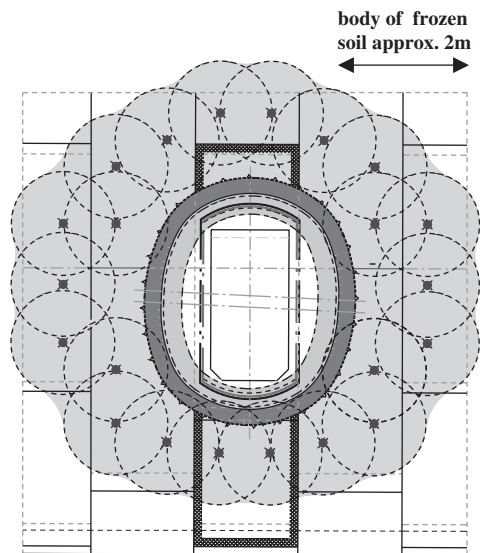
The 26 cross passages will be constructed in different ground conditions. Nine cross passages are made in sand, 11 in the stiff clay and 6 in mixed (sandy) soils. The cross passage has an elliptical reinforced concrete lining with an thickness of 400 mm, height of 2.75 m and width of 2.5 m. Outside these lining there is temporary shotcrete of 300 mm thickness.

In the main tunnel tubes five specials rings have been designed with a previously fixed and unchangeable sequence. In the middle ring steel segments replace two concrete segments. In these special enlarged steel segment the safety doors to the cross connection are constructed (Fig. 1). Twenty two freezing pipes are bored through special watertight connections in the specially prepared ring segments (Fig. 2). After closing the period of soil freezing (a minimum thickness of 2 m frozen ground) the excavation is started by the NATM-method. During the last phase the concrete lining of the cross passage is built and the freezing machine is stopped eventually for thawing the soil. During the excavation period the emergency door can be closed when a unsafe situation occurs.

2.3 Ground freezing machine

Ground freezing is performed as brine glaciation (NaCl_2) since a nitrogen glaciation in the tunnel was excluded for safety reasons. A freezing unit was developed for soil freezing at temperatures of the freezing tubes at approx. -38°C . This unit has a min. ammonia content of approx. 80 kg for a performance of 95 kW and numerous safety features. In a circular pattern 22 freezing tubes are bored with a distance of about 1.0 m to each other and parallel to the cross way axis (Fig. 2).

The freezing tubes are connected to the main pipe by means of a flexible pipe. The complete piping system includes approx. 3 m^3 brine. When starting the soil freezing system, the brine temperature at every brine



outer lining = shotcrete (250 mm) ● = freezing tube
inner lining = concrete cast in-situ

Figure 2. Cross section of a cross passage with the position of freezing tubes, frozen soil body, shotcrete (outer lining) and concrete cast in-situ (inner lining).

head on the starting side is measured in order to check whether the freezing tube works properly and whether the freezing capacity is distributed evenly.

2.4 Safety valve

The spatial and temporal development of the complete freezing body was checked permanently. The freezing body has a target thickness of $>2.00\text{ m}$ which was reached after approx. 26 days in sand at DV1 and after approx. 46 days in clay at DV2. Two diagonally arranged temperature monitoring devices controlled the formation of the frozen body. In order to avoid high pressure within the frozen body after closure of the frozen body (cylindrical formed), a draining possibility was installed near the axis of the cross passage. With this draining system water pressure in the ice-enclosed area was released in a controlled manner (an increase of water pressure was measured in sandy soil at DV1). In order to safeguard a water-tight connection between ice body and the tubings, approx. 26 temperature sensors, distributed in a plane, are distributed in the western tube. With these sensors it was possible to monitor the ice connection by temperature of the frozen soil. In addition, a 10 cm thick insulation is installed at the interior side of the tunnel tube. This insulation provided a faster connection of the ice body

Table 1. Geotechnical units at the cross passages DV1 and DV2.

Location	Geotechnical unit	Lithology	Geological formation	Age
Cross passage DV1	Z1	SAND	Naaldwijk Formation	Holocene
Cross passage DV2	BK1, BK2	CLAY, silty	Rupel Formation (Boom clay)	Oligocene

and warrants a longer remaining ice connection in case of a failure of the freezing system.

3 SOIL CONDITIONS

3.1 Soil profile and geotechnical characteristics

Soil freezing was carried out at cross passages DV1 and DV2 in sand and clay (Table 1). Figure 3 gives a soil profile based on several geological borings, cone penetration tests and geophysical bore hole measurements. Soils of three geotechnical units will be frozen for the first two cross passages: Z1, BK1 and BK2. Boom clay units (BK1 and BK2) dip slightly towards the north and are covered with young coastal sands (Z1). Note the large difference in plasticity and permeability between soil types at DV1 and DV2 (Table 2). The top of the Boom clay varies strongly due to erosion (Figure 3). The axis off cross passage DV1 is at 17,5 m-NAP and is constructed in loose sand of Holocene age (Z1 unit). The axis of cross passage DV2 is located at a depth of 28,7 m-NAP and is constructed in over-consolidated clay of Oligocene age (BK1 and BK2 unit). Both the top of the BK2 unit and the Z1 unit are characterised with a salt contents of 2000–13000 Cl⁻ mg/l. At both cross passages no significant ground water flow was recognised.

3.2 Frost susceptibility

Accordingly international standards of ISSMFE frost heave susceptibility of unit H1 (sand) is classified as 'negligible' and the overconsolidated clay of unit BK1 and BK2 as 'medium to strong' Frost heave susceptibility is the tendency of the soil to expand during soil freezing – due to the volumetrical expansion of water to ice with 9% – and the growth of ice lenses. Note the difference in BK1 and BK2 in clay contents.

3.3 Natural stress conditions

In-situ stress conditions of unfrozen soil have been measured with stress monitoring stations and have been compared with calculated theoretically soil stresses (Table 3). Calculated stress conditions are based on soil columns and volumetrical unit weights. Measured and calculated horizontal stresses match very well (Table 3). The measured vertical stresses

are significant lower than calculated values, probably due to the installation procedure of the monitoring equipment and remoulding of the soil.

4 GEOMECHANICAL BEHAVIOUR OF FROZEN SOIL

In sand the water contents shall freeze almost instantaneously due to the high percentage of free water. Clay shows a different behaviour in frozen state due to the strongly bonding forces between water and clay minerals. In clay a percentage of water will unfrozen at temperatures of –35°C. The grain size distribution also controls consequently differences in frost heave and strength development.

4.1 Frost heave and ice lenses

In freezing soil the formation water can segregate into ice lenses before it is frozen (Konrad & Morgenstern, 1981). As the result of growing ice lenses a water pressure gradient will develop that is depending on grain size and permeability of the soil (Penner, 1986). The thickness of ice lenses can range from < 10 μm to several cm's. The freezing expansion of clay is partly caused by ice lenses. The growth of the ice lenses is enhanced by the (slow) migration of water at this frozen front. That is the reason why soils with low permeability such as silts and clays are frost heave susceptible and (drained) sand is not. The process of migration of water due to freezing temperatures is referred as cryosuction. Konrad & Morgenstern (1981) have defined experimentally a linear relation between the frost heave rate h of a soil, the segregation potential SP_{θ} and the temperature gradient T :

$$h = SP_{\theta} \cdot grad T$$

This linear relation between temperature gradient and frost heave rate is experimentally been established with samples of the Boom clay from the tunnel trajectory (Fig. 4). Resulting SP_{θ} – values smaller than 0.5 m²/°C resulted in a low category of frost susceptibility. Following experiences in civil engineering with AGF works frost heaves were expected in the direction perpendicular on the freezing front or isotherms and not in the direction parallel to the axis the freezing tubes.

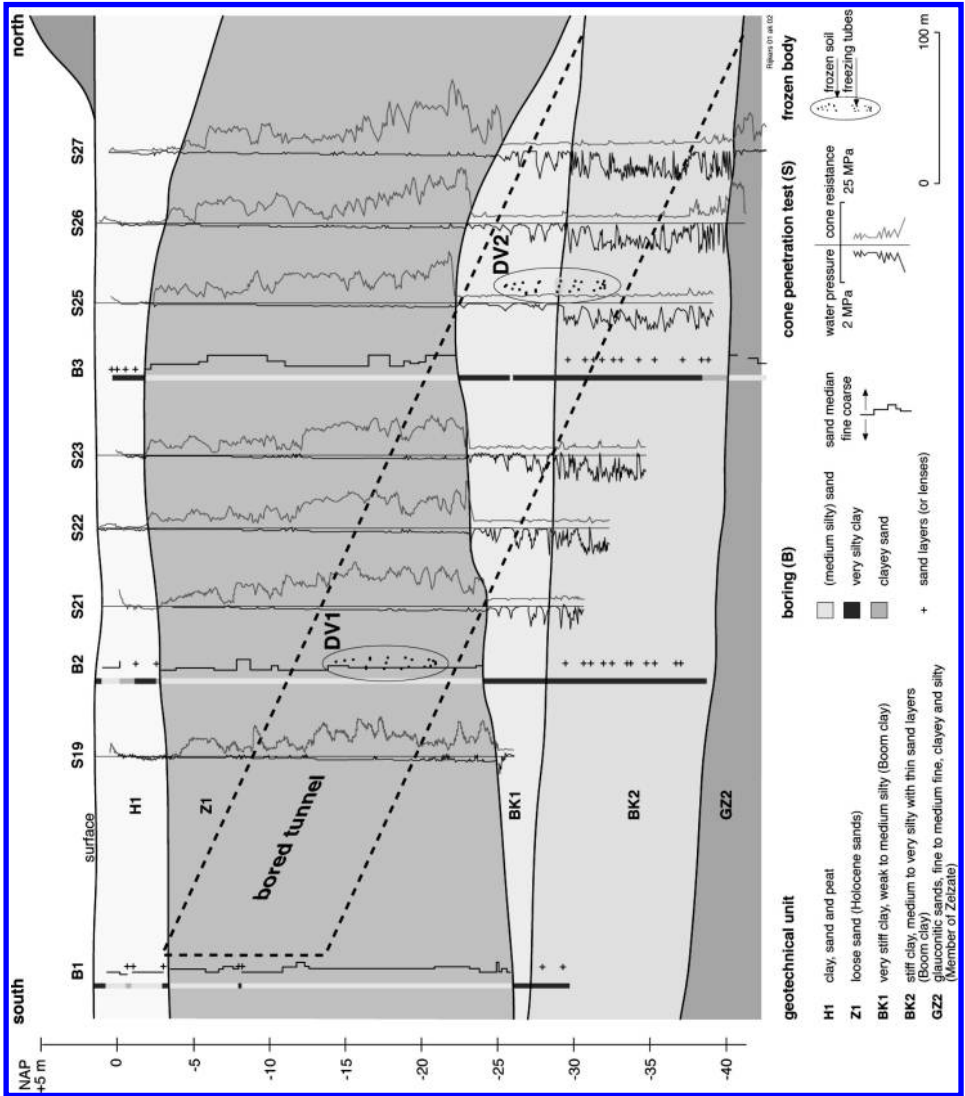


Figure 3. Soil profile with the position and depth of the cross passage DV1 and DV2. Soils of units Z1, BK1 and BK2 have been frozen during the construction of cross passages DV1 and DV2.

Three-dimensional frost heave behaviour of Boom clay has been experimentally investigated and reported by (Rijkers et al., 2000).

4.2 Creep

Creep theoretically decreases frost heave stresses that have developed in an initial stage in a ground freezing project. Assur (1963) states that creep of frozen soil is defined by temperature, time, load and material characteristics of soil. Creep processes are expected to occur in the frozen soils bodies at DV1 and DV2.

5 MONITORING PROGRAM

5.1 Monitoring equipment

In order to observe changes in stress, temperature and deformation a special monitoring program was designed. This program consists of water pressure recorders, stress monitoring stations, spade cells, temperature recorders, extensometers and inclinometers. The stress monitoring stations consist of three flat plates that record water pressure and temperature. The three plates can measure stresses directed parallel,

Table 2. Soil properties of geotechnical units Z1, BK1 and BK2.

Soil properties		Z1	BK1	BK2
Lithology	NEN5104	Fine SAND	Silty CLAY	Silty CLAY with sand layers
Clay contents (mean)	%	0	81.2	62.2
Sand contents (mean)	%	100	18.8	37.8
Water contents w	%	(22)	25.3	23.8
γ wet	kN/m ³		19.4	19.3
γ dry	kN/m ³	15.5		
Porosity p	%	~41	~50	~50
Permeability $k_{vertical}$	m/s	1.3–1.9E-4	1.5E-9–2.4E-11	(0.17E-9)
Permeability $k_{horizontal}$	m/s	–	2.7E-10–5.8E-8	–
$k_{vert.}/k_{hor.}$	–	–	~30	–
W_p plasticity limit	%	–	30	25
W_l liquidity limit	%	–	91	76
I_p plasticity index	–	–	61	51
Shear strength τ_{ovane}	kN/m ²	–	~220	~100
Salt contents	Cl ⁻ mg/l	3400–6600	2000–13000	<1000

Table 3. In-situ total stress σ and water pressure u at cross passages DV1 and DV2 measured by SM1 and SM4 (stress monitoring stations) before artificial ground freezing. The values between brackets are theoretically values based on depth and volumetrical unit weights of the soil column; $K_0 = 0.5$.

	σ vertical [kN/m ²]	σ horizontal // cross passage [kN/m ²]	σ horizontal ⊥ cross passage [kN/m ²]	u water pressure [kN/m ²]
Cross passage DV1 (SM 1) depth axis at 17,5 m-NAP	204 (309)	175 (153)	170 (151)	172 (168)
Cross passage DV2 (SM 4) depth axis at 28,7 m-NAP	310 (607)	289 (299)	291 (296)	279 (278)

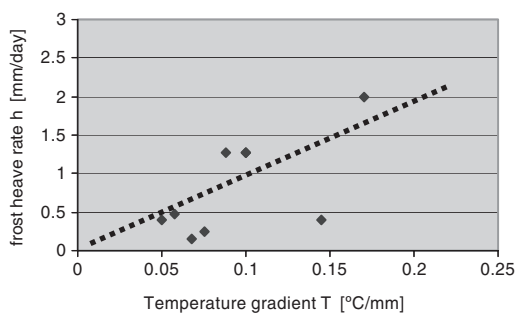


Figure 4. Frost heave rate vs temperature gradient of BK1/BK2 soil samples.

perpendicular and vertically with respect to the freezing tubes. The inclinometers have also been installed, but results are not discussed in this paper.

Extensometers are located at the top of the each cross passage and consist of four packers at different depth levels. The packers are fixed in the soil and

connected to the ground surface with bars. At the surface the shortening of the bars (distance between the packer and the surface) is measured. Water pressure recorders are situated on most of the instrument. During the complete period of ground freezing and thawing at cross passage DV1 and DV2 data was recorded.

Due to the large amount of recorded data and different data types, it is not in the scope of this paper to address all measurements. We restrict this paper to the highlights of stress monitoring stations (SM1 and SM4; Figs. 5–6) and extensometers (EX2 and EX3; Figs. 7–8) at cross connections DV1 and DV2. In Table 4 the reported data types are summarised.

6 STRESS AND DEFORMATION

6.1 Monitoring results

Data records of stress monitoring, extensometers and temperature data are given as time series in Figures 6–9. Stress is given in these graphs as absolute

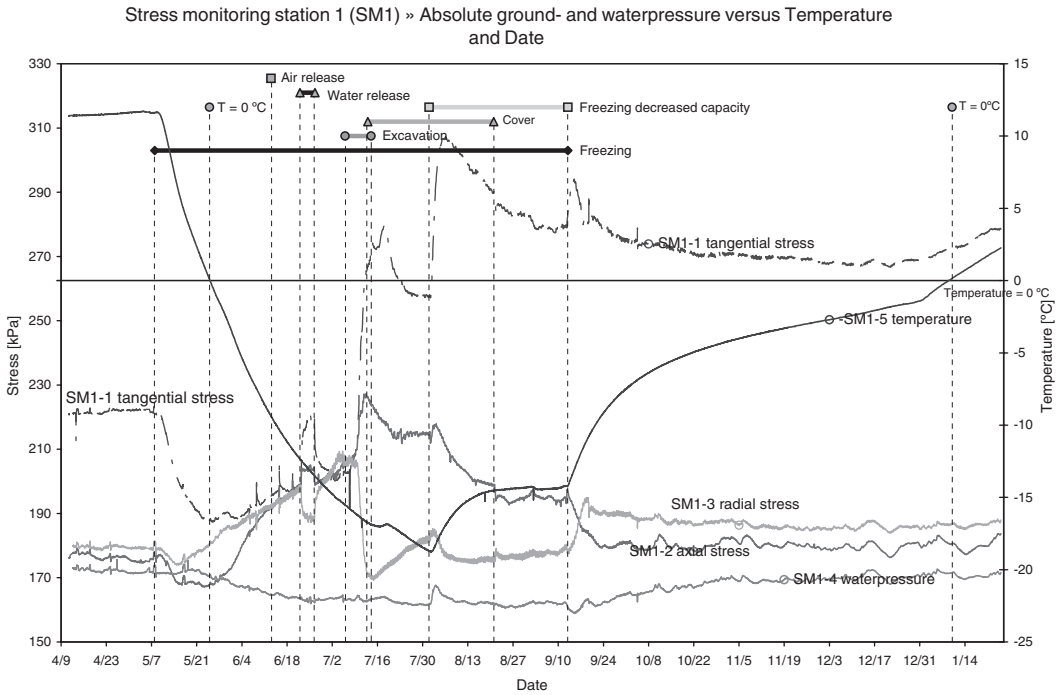


Figure 5. Measurements of stress monitoring station SM1 at cross passage DV1.

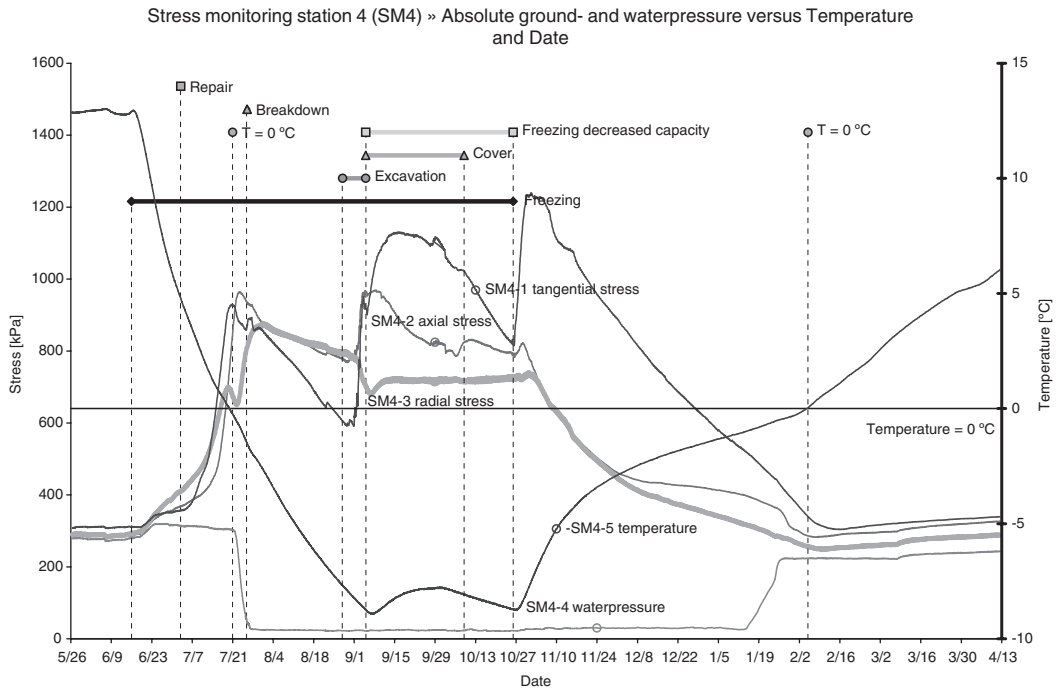


Figure 6. Measurements of stress monitoring station SM4 at cross passage DV2.

Extensometer 2 (EX2) » Absolute vertical deformation versus Temperature and Date

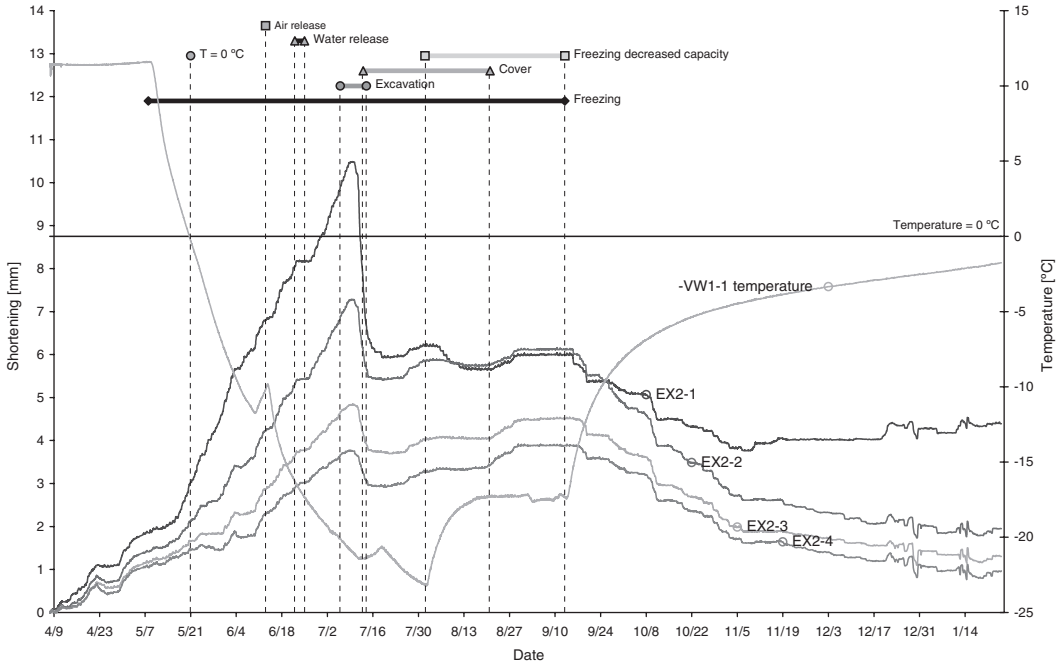


Figure 7. Measurements of extensometer EX2 above cross passage DV1.

Extensometer 3 (EX3) » Absolute vertical deformation versus Temperature and Date

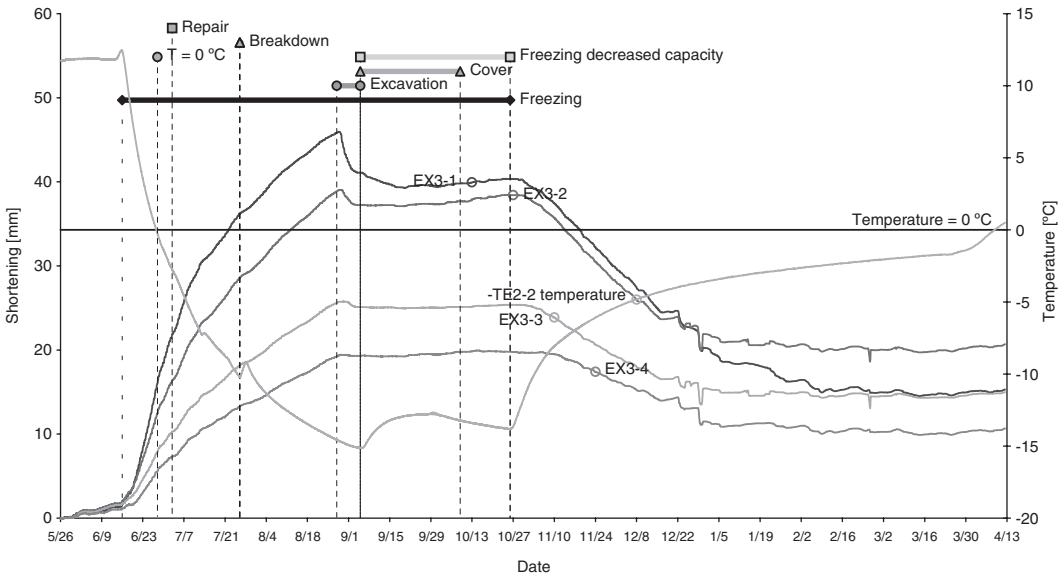


Figure 8. Measurements of extensometer EX3 above cross passage DV2.

Table 4. Characteristics and orientation of monitoring data of cross passage DV1 and DV2.

Data type	Orientation	Cross passage DV1			Cross passage DV2		
		Station	Data record	Soil unit	Station	Data record	Soil unit
Tangential stress	vertical	SM1	SM1-1	Z1	SM4	SM4-1	BK2
Axial stress	parallel to freezing tubes	SM1	SM1-2	Z1	SM4	SM4-2	BK2
Radial stress	perpendicular to freezing tubes	SM1	SM1-3	Z1	SM4	SM4-3	BK2
Water pressure	–	SM1	SM1-4	Z1	SM4	SM4-4	BK2
Deformation of soil above cross connection	vertical	EX2	EX2-1 to EX2-4	Z1	EX2	EX3-1 to EX3-4	BK1
Temperature	–	VW1	VW1-1	Z1	TE2	TE2-2	BK1

values. In the upper parts of the graphs main construction phases of the cross connections are given, such as freezing, excavation and covering.

6.2 Stress deviations from SM1 at DV1

When the freezing process starts the frozen front has not immediately reached the monitoring instruments (Fig. 5). Radial and axial stresses in the surrounding unfrozen soil (sand) decrease. From the moment where the freezing front reaches the monitoring instrument (temperature $<0^{\circ}\text{C}$), the instrument is part of the frozen soil. The frozen soil is expanding due to the continuing freezing process. Inside the frozen soil radial, axial and tangential stresses increase. Consequently the cylindrical frozen soil body is tightening.

The first construction phase is to excavate the heart of the cylindrical frozen soil body. Support to the frozen soil from inside is then removed. Axial and tangential stresses increase, while radial stress decreases. Shortly after excavations the frozen soil rises slightly in temperature, because the excavated area is in contact with relatively hot open air and hydration heat of the shotcrete. Temperature alternations cause deviations in the stiffness of the frozen soil and other equilibrium of stress distribution over the total cylindrical frozen soil. It leads to axial and tangential stress increase and radial stress decrease at the point of the stress monitoring stations.

The freezing process is continuing and the temperature in the total cylindrical frozen soil body decreases further. These actions provide radial and axial support from the inside. Radial soil stress increases, the frozen soil reacts against the shotcrete. Axial and tangential stresses decrease.

The freezing apparatus starts working with a lower capacity (33%). Temperature is increasing all over the frozen soil in a fast rate. Stress deviations also occur at a fast rate and stresses are redistributed over the frozen soil. The decrease in stiffness (due to temperature rise)

leads to a decrease in radial and axial stresses. An overall radial stress release leads to an overall tangential stress increase. After the fast increase the temperature stabilises causing a stabilisation of all stresses.

Finally, ground freezing stops and temperatures start to increase in the direction of the freezing point. The same process as freezing with a lower capacity recurs. There is one difference. Radial stress increases immediately after shutting the freezing apparatus. This reaction is probably caused by the redistribution of stresses over the frozen soil, with this difference that the total distribution of stiffness over the frozen soil is different as it was during the previous period of temperature increase. The final tangential stress increased with respect to the starting value. This is a result of the installation procedure of stress monitoring stations. The vertical stress after installation is less as the original vertical in-situ stress (Table 3). Probably because soil has been excavated via a pulse boring to install this type of instrument.

6.3 Water pressure deviations from SM1 at DV1

There are no large water pressure deviations while freezing in sand. The maximum amount of water pressure decrease is approximately -15 kPa . The sand is well drained and the decrease is a result of the chase of water during volume increase of frozen water.

6.4 Soil deformations from EX2 at DV1

In order to make installation of the instruments possible, soil is improved at both cross passages at ground level. Besides an extra cinder level is deposited. The extra load causes settlement to occur. In the beginning before the period of freezing this settlement is visible as a shortening of the packer bars.

After a while when the soil around the freezing tubes freezes and expands, packer EX2-1 reacts and shortening takes place (Fig. 7). Packer EX2-2 to EX2-4 reacts in a later stadium. The frozen front progresses

slowly. In the period of excavation the shortening drops (most for packer EX2-1 and respectively less for packer EX2-2 to EX2-4). The excavation causes a radial release and therefore a contraction of the cylindrical frozen soil body.

After this period deviations in deformation are low. Packer EX2-1 to EX2-4 show similar fluctuations conformable with radial stress observed at SM1. Further decrease in temperature causes a small expansion.

The freezing apparatus starts working with a lower capacity. Packer EX2-1 shows a small decrease in shortening followed by an increase. Packers EX2-2 to EX2-4 stabilise and increase. The freezing process continued although at a lower level. The frozen soil is still expanding.

Thawing leads to an overall decrease in shortening. The residual shortening is the result of the surface settlement for packer EX2-2 to EX2-4. Packer EX2-1 has a larger residual settlement. In fact this packer was the only one of EX2 packers inside the frozen soil.

6.5 *Stress deviations from SM4 at DV2*

All stresses increase strongly from the beginning after a frozen soil body (clay) starts forming (Fig. 6). Also tangential stress increases. The reason for this strong frost heave is the typical undrained character of clay. Water pressure increases with the same amount as the tangential stress. Radial and axial stresses increase conformable expectations, the freezing soil expands causing an stress increase in the surrounding unfrozen soil due freezing of the water contents of the clay and to ice lens formation.

From the moment the temperature drops under the freezing point, water pressure decreases in a fast rate to just above the vacuum pressure. Radial, axial and tangential stresses react and show a slight decrease. The water pressure is not as dominant any more as most of the water starts to freeze. Radial stress increases again to about a level where all three stresses start to decrease. This decrease in stress is due to creep or the volumetric contraction of ice at lower temperatures. Creep occurs at a certain level of temperature and stresses. The crystalline structure of the frozen water is not stable anymore and the soil more or less liquefies. At cross passage DV1 stresses in all principal directions increase in this period. The stress rate is much lower. Excavation leads to a radial release. Axial stress increases for the support from the heart is removed. The cylindrical frozen soil body contracts and tangential stress increases.

Just after excavation the periods of cover and freezing with lower capacity begins. Temperature increases for a period of time and decreases again after a while. Radial stress increases slightly while the freezing process is continuing, only at a lower rate. Tangential stress increases fast. These phenomena take also place at cross passage 1, where a temperature increase leads

to a fast tangential stress increase, caused by the redistribution of stresses and stiffness deviations in the cylindrical frozen soil body. The axial stress decreases also due to the redistribution of stresses over in the meantime covered cross connection. Finally, thawing does the same to the tangential stress as freezing with lower capacity. Tangential stress increases rapidly and due to a combination of creep and thawing the tangential stress is reduced to its original starting level. The axial and vertical stresses decrease by thawing. The total expansion stops and stresses decrease. The water pressure finds its original level at a temperature just below the freezing point.

6.6 *Deformations from EX3 at DV2*

The same soil improvement and cinder installation takes place at cross passage DV2. The same amount of settlement is visible in the beginning before the freezing period (Fig. 8). From the moment the freezing starts, expansion of the frozen soil body takes place. The difference between cross passage DV1 and cross passage DV2 is clear. The maximum shortening at DV1 is approximately 10 mm at packer EX3-1. The maximum shortening at DV2 is approximately 50 mm at packer EX3-1. Excavation leads to a decrease in shortening. The cylindrical frozen soil body shrinks. From this moment temperature increases and, but freezing continuous at a lower level. A smooth small expansion is the result. Thawing leads to the final decrease in shortening and all packers return to their original situation including the surface settlement. The residual shortening is large compared to DV1.

6.7 *Drainage of the frozen soil and insulation measures*

The average temperature evolution was the same as calculated for both cross passages. However, at the connection between the main tunnel tube and the frozen ring the temperature drops slower than expected. At the steel segments it is clear that the conduction of heat is high that proper insulation was necessary. At cross connection DV1 dry-ice was eventually used to maintain low temperatures at the connection between the steel segments and the frozen ring.

For drainage during soil freezing a borehole was used to control the water pressure inside the frozen body. Water expands when it is frozen, so in an undrained situation water pressure rises when the frozen ring is watertight (Fig. 9, point B). In the first part the increasing water pressure (Fig. 9, point A) gives an indication that the ring of frozen soil is watertight. In our case at DV1 monitored temperatures through the tunnel segments gives that soil was not frozen directly behind the segments. Another test was conducted with opening and closing the drainage tap (Fig. 9). Because the water didn't stopped we

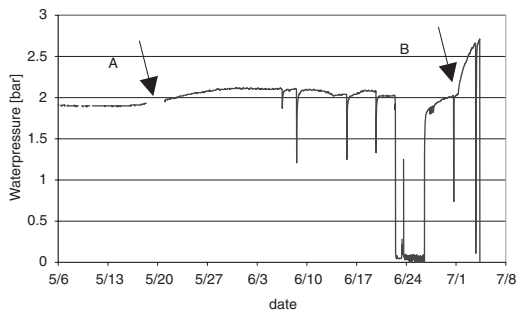


Figure 9. Development of the water pressure in the unfrozen cylinder at DV1.

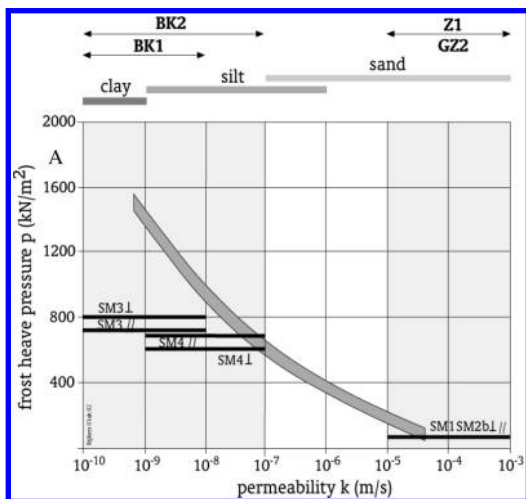


Figure 10. Measured (maximum) frost heave pressures at DV1 and DV2 versus permeability (adapted from Kofoed & Doran, 1996).

concluded that the frozen ring was not watertight and after one day using ‘dry-ice’ a significant rise of the water pressure occurs that proved the water tightness of the frozen ring.

At the cross passage DV2 it was not possible to drain the inner part of the frozen ring because of Boom clay with very low permeability. However, the drainage pipe was kept open to reduce ground pressure on the main tunnel segments.

7 FROST HEAVE LOADS AND TUNNEL DEFORMATION

During freezing activities tunnel convergence and offset of tunnel segments was measured (in the bored tunnel tube). Deformation and convergence of the main tunnel construction has been monitored during the freezing period. At cross passage DV1 (in sand) a maximum offset of tunnel segments of 4 mm was

observed. The deformation of the western tunnel at DV1 has been caused by the increase of ground pressure due to frost heave of 50 kPa measured in the direction parallel to the freezing tubes (SM1 SM2 \perp //; Fig. 10).

Frost heave pressure is defined as the increase of ground pressure due to soil freezing. The absolute measurements of frost heave pressures at DV1 and DV2 are higher (see Figs. 5–6).

At cross passage DV2 (in overconsolidated clay) the maximum offset of 20 mm was registered. Also corresponding measured frost heave values are significantly higher. In the direction parallel to the freezing tubes 680 kPa of frost heave stress has been observed that eventually caused 20 mm offset of the tunnel segments (SM3 SM4 \perp //; Fig. 10).

8 CONCLUSIONS

Frost heave loads and soil deformations have successfully been measured in (frozen) soil bodies of sand and clay during an artificial ground freezing activities. Frost heave pressures differ significantly between frozen sand and frozen clay bodies. All phases of construction of the cross passage are recognized clearly in the data.

ACKNOWLEDGEMENTS

We thank the organizations of KMW and COB for the permission publishing this paper. We also thank André Koers and Roel van de Kraan of TNO for preparing the drawings.

LITERATURE

- Assur, A. (1963) Creep of frozen soils. Proc. 1st Permafrost Int. In: *Conf. Nat. Acad. Sci. Publ.* Vol. 1287, pp. 339
- Hass, H.R. Jagow-Klaff & H.W. Seidel (2000) Use of brine freezing for the construction of the traverse galleries. In: *ISGF2000 – Frost action in soils* (ed. J.F. Thimus), Louvain-la-Neuve, pp. 289–294
- Kofoed, N. & S.R. Doran (1996) Storbælt Eastern Railway Tunnel, Denmark, Ground Freezing for tunnels and cross passages. In: *Geotechnical Aspects of Underground Construction in Soft ground*, Balkema Rotterdam 1996, pp. 391–398
- Konrad, J.M. & N.R. Morgenstern (1981) The segregation potential of a freezing soil, *Cndn Geotech. J.* 18, pp. 482–491
- Penner, E. & T. Ueda (1977) The dependance of frost heaving on load application – preliminary results. In: *Proc. Int. Symp. Frost Action in Soils, Lulea*, Vol. 1, pp. 92–101
- Rijkers, R.M. Naaktgeboren, H. Côté, J.-F. Thimus, M. Visschedijk (2000) Soil behaviour during artificial freezing – Part 2: Application in bored tunnels, In: *ISGF2000 – Frost action in soils* (ed. J.F. Thimus), Louvain-la-Neuve, pp. 237–242

Monitoring and modelling during tunnel construction

A. Bezuijen

GeoDelft Delft, The Netherlands

A.M. Talmon

WL/Delft Hydraulics

ABSTRACT: Tunnelling projects are often technologically challenging projects. Therefore it is not uncommon to perform quite some measurements during the execution of these projects. Measurements are performed to control settlements and/or control of the drilling process. Modern TBMs record all kind of data on the drilling process. This paper shows that analyzing the results of the measurements and modelling with relatively simple calculation models can lead to new insights in the tunnelling process and possible failure mechanism. Examples are presented, investigating the pressure distribution in front of, or at, the tunnel face and back-fill grouting.

RESUME: Les projets des tunnels creusés sont souvent technologiquement des projets de challenge. C'est pourquoi des mesures s'effectuent souvent pendant l'exécution de ces projets. Des mesures sont effectuées pour contrôler les tassements et/ou contrôler le processus de forage. Les tunneliers (TBM) modernes enregistrent tout genre de données durant le processus. Cet article montre que l'analyse des résultats des mesures et la modélisation par des modèles relativement simples peut mener à des nouvelles compréhensions du creusement des tunnels et des mécanismes de rupture possibles. Des exemples sont présentés, étudiant la distribution de pression au devant, ou au front de taille de tunnel et le remblayage par injection.

1 INTRODUCTION

The construction of bored tunnels started only recently in The Netherlands, in the nineties of the last century. Up to then it was expected that the soft soil in The Netherlands was not suitable for a cost effective construction of bored tunnels. With the start of the first bored tunnel projects it was decided to perform monitoring campaigns during each project. This research was initiated by the Dutch Ministry of Transport and Public works and the COB (the Centre for Underground Construction). These campaigns included prediction of the values that can be expected during the monitoring using state of the art calculation models, measuring before, during and after the passage of the TBM and evaluation of the data. This method has proven to be quite effective to acquire knowledge of the processes involved. The paper describes some measurements that led to a new or better description of processes that occur during tunnelling.

Measurements and modelling during 3 tunnel projects will be dealt with: the 2nd Heinenoord Tunnel, the first bored tunnel in The Netherlands, the Botlek Rail Tunnel and the Sophia Rail Tunnel. As will be described in the paper, insight was gained by prediction of the outcome of the measurements or by analyzing the measurements and performing

additional laboratory testing. This paper shows some of the measurements and describes briefly the mechanisms involved. A full description of the models used is not possible within the limits of this paper; reference is made in the literature for these models.

2 2ND HEINENOORD TUNNEL, PORE PRESSURES

Excess pore pressures have been predicted and measured in front of the tunnel face during drilling of the 2nd Heinenoord tunnel in saturated sand.

Before these measurements it was generally assumed that the bentonite slurry plasters the tunnel face. This is true after a stand still of several minutes, but not during excavation in saturated sand. The parameters presented in Table 1 were used in the predictions.

The set-up of the measurements is shown in Figure 1. Some pore pressure gauges are 'eaten' by the TBM. The original function of these pore pressure gauges was to investigate the influence of the cutting elements on the pore pressures in the sand.

The predictions showed however, that a penetration depth of 0.05 m is needed for full plastering and that between two passages of the elements (which take

Table 1. Soil conditions and slurry parameters during the drilling of 2nd Heinenoord tunnel.

Parameter	Value	Dimension
d_{15}	100	μm
Permeability	1.10^{-4}	k/s
Porosity	0.41	—
Viscosity slurry	$18 \cdot 10^{-3}$	$\text{Kg}/(\text{ms})$
Yield stress slurry	0.01	kPa
Face pressure above Pore press	50	kPa

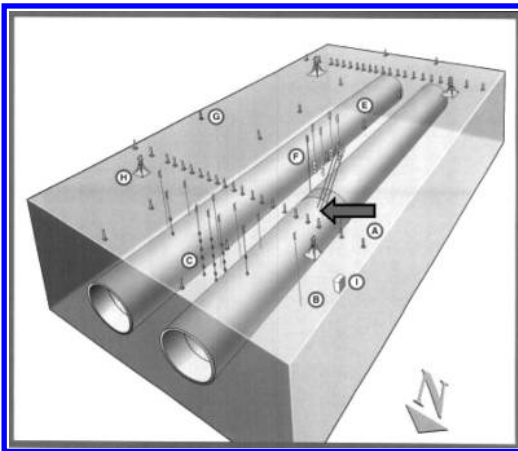


Figure 1. Artist impression measurement field 2nd Heinenoord Tunnel. The arrow indicates the pore pressure gauges in front of the TBM. Results of the gauge in the middle are used this paper. Drilling was from North to South (Bakker et al. 2003).

about 60 s) there could be no further penetration than 0.015 m, see Bezuijen et al. (2001). The lack of plastering of the tunnel face results in an excess pore pressure in front of the TBM. The course of the excess pore pressure on the tunnel axis was estimated assuming that specific discharge is the same all over the tunnel face. This is an approximation, in reality the discharge will be smaller in the center of the tunnel face compared to the areas further away from the tunnel axis. Although an approximation, it appeared that using the measured excess pressure at the tunnel face, the resulting formula could simulate the course of the excess pore pressure in front to the TBM very well, see Figure 2. It was realized that the measured excess pore pressure can influence the face stability (Bezuijen et al. 2001. Broere, 2001). This result had practical consequences during the construction of the Groene Hart Tunnel (a 15 m diameter tunnel for high speed trains), where at one location a surface load was applied to prevent a blow out (Aime et al. 2004).

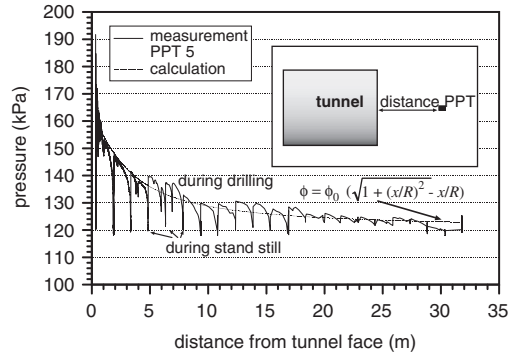


Figure 2. Measured excess pore pressure in front of a slurry shield and approximation.

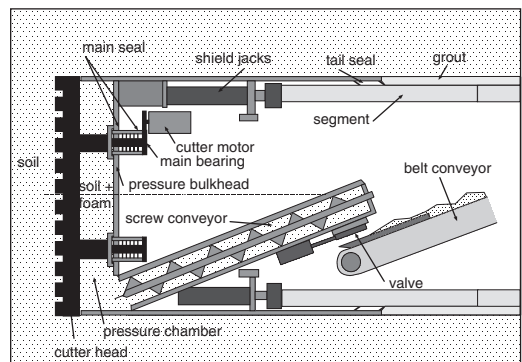


Figure 3. Principle of EPB TBM.

3 BOTLEK RAIL TUNNEL, TUNNEL FACE EPB

The Botlek Rail Tunnel, the second bored tunnel in The Netherlands, was made with an Earth Pressure Balance (EPB) shield TBM. The principle of such a TBM is shown in Figure 3. The soil is removed from the pressure chamber by a screw conveyor. The pressure drop from a few bars to atmospheric pressure is regulated with the screw conveyor and a valve or pumps at the end of the screw conveyor. The TBM can work without additives in clayey soils, but in sandy soil, as was present at the location of the Botlek Rail tunnel, it is necessary to condition the soil with additives. This is often done with foam. By injection of foam from the cutter head into the soil, the porosity of the sand is increased to a value above the maximum porosity, which facilitates excavation and also reduces the permeability (Bezuijen, 2002). Reduction of the permeability was of importance since the Botlek Rail tunnel passes on its deepest point through permeable Pleistocene sand ($k = 3.10^{-4} \text{ m/s}$).

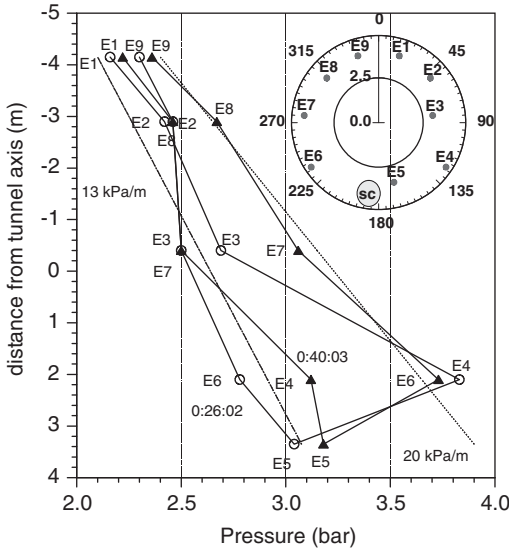


Figure 4. Example of non-hydrostatic pressure distribution measured at the Botlek rail tunnel. The rotation direction of the cutter head was reversed between the 2 measurements shown. The inset shows the position of the instruments and the position of the screw conveyor (SC) in the pressure bulkhead of the TBM.

An important aspect for the stability of the tunnel face and the limitation of surface settlements is the average pressure and the pressure distribution at the tunnel face. Therefore this pressure was measured at 9 locations on the pressure bulkhead. A non-hydrostatic pressure distribution was measured over the tunnel face where a hydrostatic pressure distribution was predicted based on results measured for a slurry shield, see for an example Figure 4. This figure shows two pressure distributions measured at different times and compares these with two hydrostatic pressure distributions. Clearly there are deviations from the hydrostatic distribution. There are differences between the pressures measured with the instruments on the right side of the TBM compared with pressures measured on the left side. This difference was attributed to the direction of rotation of the cutter head (Bezuijen et al. 2005^b).

It was found that the difference in vertical hydraulic gradient is likely to be caused by the yield strength of the muck in the pressure chamber. With no or hardly any yield stress in the muck the pressure distribution at the tunnel face is hydrostatic as was measured for a slurry shield TBM (Bakker et al. 2003). In presence of cohesion in the muck and adhesion to the TBM the vertical gradient can be written as:

$$\frac{dP}{dx} = \rho_m g \pm 2 \frac{\tau_a}{L} \quad (1)$$

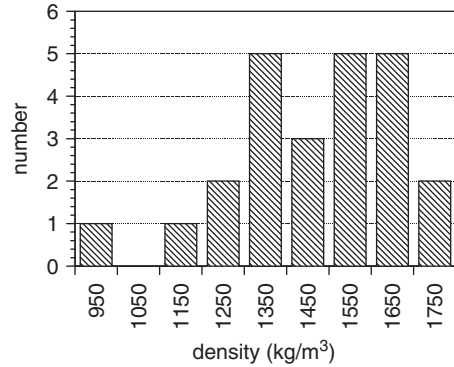


Figure 5. Distribution of muck densities measured in the pressure chamber (24 samples).

Where P is the pressure, ρ_m the density of the mixture, g the acceleration of gravity, τ_a the adhesion between the muck and the TBM and L the distance between the cutter head and the pressure bulkhead. Depending on the flow direction the pressure gradient can be $2\tau_a/L$ higher or lower than the pressure gradient corresponding to the density of the mixture. In case of a flow with a horizontal component, as can be expected in the pressure chamber between E6 and E5 as well as between E4 and E5, the influence of the adhesion becomes even bigger. Density in the pressure chamber was measured by taking samples through the bulkhead during drilling. The densities found are shown in Figure 5. Laboratory experiments have shown that the adhesion is 1 to a few kPa, with the densities measured and a L of approximately 1 m, this means that pressure gradients from 7 up to more than 20 kPa/m are possible.

Due to the foam injection that increases the porosity to values above the maximum porosity, there are no grain stresses in most of the pressure chamber, but it was found that there can be some grain stress close to and in the entrance of the screw conveyor due to drainage of the muck in that area (Bezuijen et al. 2005^b). This allows even negative pressure gradients, see Figure 4.

Analysing the measurements showed the influence of adhesion on the pressure distribution and the influence of drainage. These results mean that the pressure distribution on the tunnel face depends on more than the density of the slurry and that changes in this pressure distribution during the drilling process cannot be avoided.

4 SOPHIA RAIL TUNNEL, GROUTING

Another important part in the tunnelling process is the grouting of the tail void to fill up the space between the

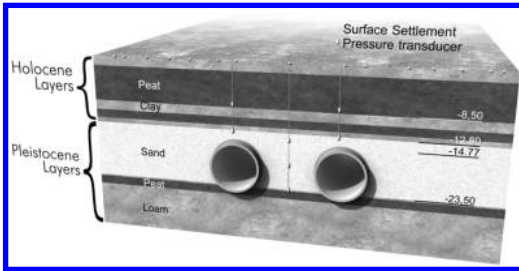


Figure 6. Cross-section of the Sophia Rail Tunnel and soil layering at the measurement location.

lining and the soil, see also Figure 3. The quality of the grouting process determines the position of the lining and is of major importance on the surface settlements. To get a better understanding of the grouting process, the grout pressures were measured in 2 rings during the boring of the Sophia Rail Tunnel. Soil conditions are rather uniform along a large part of this tunnel, see Figure 6.

In The Netherlands it is usual to prescribe the grouting pressures that have to be applied during the tunnelling in order to avoid excessive surface settlements. Furthermore it was tried to match the grout pressures to the total stress that exist in the soil before tunnelling also to minimize settlements.

A calculation model that describes the pressure distribution in the direct vicinity of the TBM was available before the start of the measurements. From calculations with this model it was possible to find the relation between injection strategy, yield stress of the grout mortar and the pressure distribution directly behind the TBM (Talmon et al. 2001). It was further realized that at a certain distance from the TBM the sum of the forces on the lining has to be zero and therefore the average pressure gradient is determined by the weight of the lining, more or less independent from the injection strategy.

A typical result from the grout pressure measurements is shown in Figure 7.

Figure 7 shows the pressure increase during drilling and a decrease during stand still. Conform the expectations the vertical hydraulic gradient decreases from nearly 19 kPa/m to below 7 kPa/m (Figure 8). This last value is close to the gradient that corresponds to the average weight of the tunnel lining and the auxiliary train (Bezuijen et al. 2004) and the higher gradients measured close to the TBM correspond with the values calculated with the flow model (Talmon et al. 2001, Bezuijen et al. 2004).

Analyzing the results, it was noticed, as mentioned already, that the grout pressure increases during boring and decreases during stand still. The reason for this appeared during grout consolidation tests to investigate how the grout mortar behaves under the applied

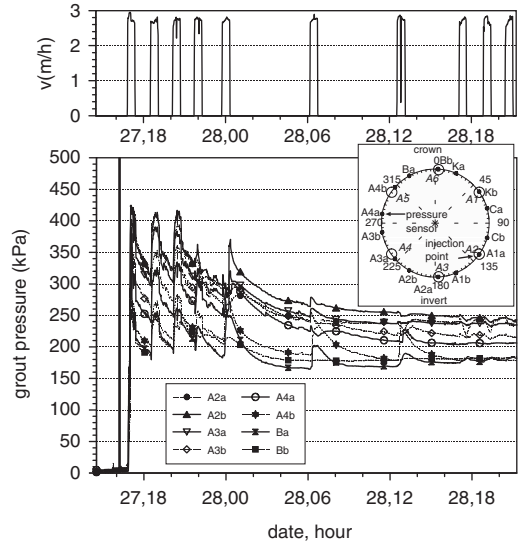


Figure 7. Sophia Rail Tunnel. Measured grout pressures and boring velocity. For clarity only the pressures measured on the left side are shown. The pressures increase during boring and decrease during stand still.

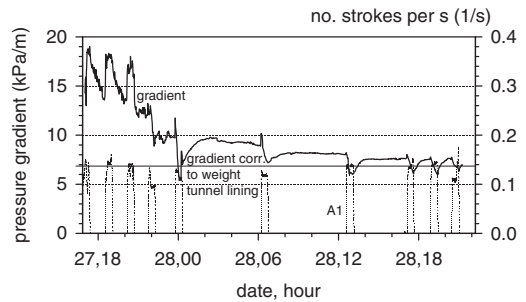


Figure 8. Measured vertical pressure gradient in the grout as a function of time, together with the no. of strokes per second for one of the grout pumps (these pumps are activated during boring).

pressure. Grout loses 3 to 10% of its volume when loaded with effective stresses up to 100 kPa. A grout consolidation test was developed to investigate the consolidation of grout, see Figure 9 and Figure 10. A test result is shown in Figure 11. After pressurizing the vessel the valve is opened and the grout starts to consolidate (sometimes described as bleeding). In the first part of the consolidation process the volume loss increases with the square root of time (Bezuijen & Talmon, 2003), see also Figure 11. This assumption is valid as long as the grain stress close to the impermeable plate is still negligible. When grain stresses develop, leading to a decrease in the measured pore pressure, the consolidation decreases to reach an end

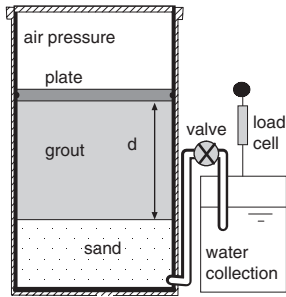


Figure 9. Grout consolidation, measurement principle.

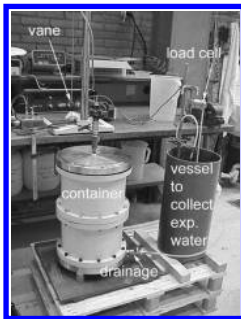


Figure 10. Grout consolidation, experimental setup.

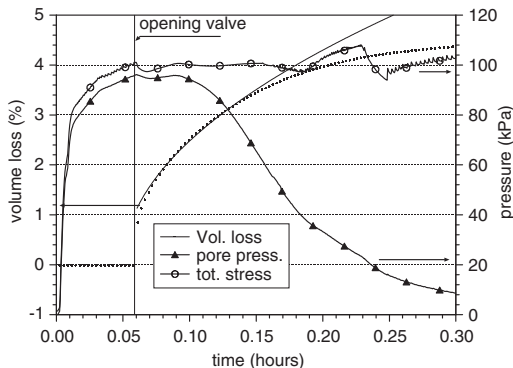


Figure 11. Result of consolidation test. Pore pressure and total pressure are measured on the impermeable plate.

value. The time necessary for grout consolidation is in most cases shorter than the time for hardening of the grout and then the consolidation is the dominant process for the increase of the yield stress in the grout over time.

In Figure 7 this decrease in grout pressure during consolidation is shown for one tunnel, but it is measured for a lot of tunnels that are bored in sand (Hashimoto et al. 2004). Consolidation of the grout leads to an unloading of the sand around the tunnel

lining because the sand reacts stiff during unloading, some volume loss leads to a significant pressure drop (Bezuijen & Talmon, 2003). Pressures restore however when drilling recommences. Pressures decay with distance from the TBM. This is caused by fluid loss, and is governed by yield stress and the thickness of the grout cake (Talmon & Bezuijen 2004). The grouting conditions directly behind the TBM are critical with respect to settlements. Here grout pressures and injected volume of grout are the governing parameters. Soil reacts less stiff during loading compared to unloading. Therefore different grout injection volumes lead to the same final grouting pressure, but to different settlements. From this it might be concluded that in controlling surface settlements it is more appropriate to control the volume of injected grout than the grout pressure once the injection pressures are within certain bounds.

The measured vertical hydraulic gradient also implies a loading on the lining. The longitudinal loading on the lining can be calculated using the beam equation (Bezuijen et al. 2005^a). Close to the TBM, where the pressure gradient is not yet in equilibrium with the weight of the tunnel, there will be buoyancy forces. It was found that these forces can reach critical values when the length over which the vertical gradient is higher than corresponding to the weight of the tunnel is too high. This can happen when the yield stress of the grout is too low and consolidation or hardening take too much time compared to the progress of the tunnelling process.

5 CONCLUSIONS

Several examples were shown where the combination of measurements and analyzing of the results led to new insight in some of the mechanisms of importance during the tunnelling process:

1. Excess pore pressures can occur at the tunnel face during the excavation process. These excess pore pressures decrease the stability of the tunnel face.
2. Pressure gradients at the tunnel face of an EPB are not only determined by the density of the slurry, but also by the yield stress of the slurry and the rotation direction of the cutter blade. This limits the possibilities to control the pressure gradient, which can be of importance when evaluating the soil deformation caused by the tunnel face.
3. The cause of the grout pressures and the grout pressure gradient as measured during tunnelling could be explained. Injection strategy determines the grout pressures just behind the TBM. At a larger distance these are dominated by the weight of the tunnel. Consolidation of the grout leads to a reduction in grout pressures at some distance from the TBM and the longitudinal loading on the lining can be coupled quantitatively to the grout properties.

ACKNOWLEDGEMENTS

The authors would like to acknowledge COB research at 2nd Heinenoord Tunnel, Botlek Rail Tunnel, Sophia Rail Tunnel and the contractors of these tunnels for permission to publish.

REFERENCES

- Aime R., Aristaghes P., Autuori P., Minec, S. 2004. 15 m Diameter Tunneling under Netherlands Polders, *Proc. Underground Space for Sustainable Urban Development (ITA Singapore)*, Elsevier.
- Bakker K.J., Teunissen E.A.H., Berg P. van den, Smits M. Th. J.H. 2003. K100 research at the second Heinenoord tunnel. *Proc. ITA, Amsterdam*.
- Bezuijen A., Zon W.H. van der, Talmon A.M. 2005^a. Laboratory testing of grout properties and their influence on backfill grouting. *Proc. ITA, Istanbul (submitted)*.
- Bezuijen A., Joustra J.F.W., Talmon A.M., Grote B. 2005^b. Pressure gradients at the tunnel face of an Earth Pressure Balance shield. *Proc. ITA, Istanbul (submitted)*.
- Bezuijen A., Talmon A.M., Kaalberg F.J., Plugge R. 2004. Field measurements of grout pressures during tunnelling of the Sophia Rail tunnel. *Soils and Foundations vol, 44, No. 1, 41–50, Feb.*
- Bezuijen A., Talmon A.M. 2003. Grout the foundation of a bored tunnel, 2003, *Proc ICOF 2003 Dundee*.
- Bezuijen A., Pruiksma J.P., Meerten H.H. van 2001. Pore pressures in front of tunnel, measurements, calculations and consequences for stability of tunnel face. *Proc. Int. Symp. on Modern Tunnelling Science and Techn. Kyoto*.
- Broere W. 2001. Tunnel Face Stability & New CPT Applications. Ph.D. Thesis, *Delft University of Technology, Delft University Press*.
- Hashimoto T., Brinkman J., Konda T., Kano Y., Feddema A. 2004. Simultaneous backfill grouting, pressure development in construction phase and in the long term. *Proc. ITA Singapore*.
- Talmon A.M., Bezuijen A., Aanen L & W.H. van de Zon, 2001. Grout pressures around a tunnel lining, *proc. IS-Kyoto 2001 conference on Modern tunnelling Science and Technology*, pp. 817–822.
- Talmon A.M., Bezuijen, A. 2005. Grouting the tail void of bored tunnels: the role of hardening and consolidation, of grouts, *Proc. TC28 Amsterdam (submitted)*.

Introduction to Grout Behaviour

Grout behaviour has got a lot of attention in tunnelling research performed at GeoDelft. Research on grout was nearly always performed in close cooperation with WL | Delft Hydraulics. The field measurements at the Second Heinenoord tunnel showed already the importance of grout pressures on the soil behaviour. A research programme was started, based on the results of these measurements, to get a better understanding in the measured grout pressures and grout pressure distribution.

The first paper in this chapter deals with centrifuge tests that are performed to investigate the influence of the grout pressures. In this test the grouting was simulated using a very high concentrated betonite slurry. The subsoil reaction and the reaction of a pile foundation were measured as a function of the grout pressure. It was shown that a surface settlement could be compensated for by increasing the grout pressure. However, settlement of piles very close to the tunnel could not be corrected by increasing the grout pressure.

The cooperation with WL | Delft Hydraulics led to a model that describes the flow of a Bingham liquid in an annulus and the resulting pressure distribution. This is the topic of the second paper. The importance of this work was that a prediction tool became available to make predictions for the field measurements on grout measurements that were planned during boring of the Sophia Rail Tunnel. This tool was also used to calculate the extra loading on the lining of the Green Heart Tunnel in case one of the grout injection points that bring grout in the tail void would fail.

The grout measurements for Sophia Rail tunnel are presented in the third paper. This paper shows the measurement results and explains the pressure gradients that were measured. It was shown that a bit further away from the tunnel the pressure gradients hardly depend on the injection strategy but on the weight of the tunnel. The pressure gradients in the grout can decrease to gradients lower than the gradient in the pore pressure. The grout pressure distribution close to the TBM corresponded with the calculation model described in the paper before. However, further away from the TBM the measured grout pressures were lower.

The paper just mentioned above focuses on pressure gradients but does not present an explanation for the absolute grout pressures measured. The measurements show that these have a characteristic course

of increasing grout pressure during drilling and a decrease during stand still. At a distance of 10 to 20 m behind the TBM the measured grout pressures are in the same order of magnitude as the pore water pressure for a tunnel drilled in sand. The mechanism that causes these pressures is explained in the fourth paper. It describes the soil grout interaction during consolidation or 'bleeding' of the grout and shows that the measured pressures can be described by assuming elastic unloading of the soil.

Grout pressure measurements performed in The Netherlands used relatively small pressure sensors and the measurements lasted a few days at maximum. The fifth paper deals with measurements performed in Japan during 180 days and with larger pore pressure gauges. The conclusions of these measurements for a tunnel bored in sand are however quite comparable to the conclusions from the Dutch measurements: The grout pressures decrease to values close to the pore pressure was also found in Japan for a tunnel bored in sand. This result leads to a considerable smaller ring loading on the lining than calculated using the Japanese code for this situation. Several codes, including the Japanese, assume a horizontal effective stress on the lining that is K_0 times the vertical effective stress and do not take into account the unloading of the soil by tunnelling. This unloading has reduced the effective stress around a tunnel bored in sand to values that are less than 10% of the original value. The original stress distribution in the sand around the tunnel has more or less disappeared due to the unloading of the sand.

The last 2 papers show the consequences of the measured grout pressures on the loading in the lining in longitudinal direction and the loading on the TBM. The first of the last two papers is more or less a summary from earlier papers and indicates how the stresses in longitudinal direction can be calculated using a numerical calculation scheme. In the last paper an analytical solution is worked out. From this solution it appears that the loading on the lining depends on the properties of the grout and of the soil. The model also predicts a considerable upward directed force on the tail of the TBM that is exerted by the buoyancy forces in the lining. This force was not always incorporated in the various numerical calculations, leading to a momentum in the lining calculated by numerical programs that differ to a very large extent from the momentum that was measured.

Modelling the grouting process around a tunnel lining in a geotechnical centrifuge

Modélisation du processus d'injection du revêtement d'un tunnel dans une centrifugeuse géotechnique

Henk E. Brassinga & Adam Bezuijen

GeoDelft, The Netherlands

ABSTRACT: The grouting process around a tunnel lining is modeled in a geotechnical centrifuge. A model grout is injected in a scaled model of a tail void. In different tests grouting is performed with pressures equal to 80 and 90% of the total vertical stress of the soil above the tunnel. At the end of the test the pressure is increased to investigate the maximum pressure that can be applied before this will lead to large soil deformations. Deformations of soil and settlement of adjacent pile foundations were studied. It was concluded that for fully loaded piles, the pile deformations exceeded the soil deformation. To decrease settlements afterwards high pressures were needed, easily leading to fracturing and in some case to further displacement of piles.

RESUME: Le processus d'injection autour du revêtement d'un tunnel est modélisé dans une centrifugeuse géotechnique. Un coulis modèle est injecté dans un modèle mesuré d'un espace annulaire. En différents essais l'injection est exécutée avec des pressions égales à 80 et 90% de la tension totale verticale du sol au-dessus du tunnel. A la fin de l'essai, la pression est augmentée afin d'étudier la pression maximale qui peut être appliquée avant que de grandes déformations du sol n'aient eu lieu. Des déformations du sol et de l'affaissement des bases adjacentes de pieux ont été étudiées. Il est conclu que pour des pieux avec une charge limite, les déformations de pieux ont excédés la déformation du sol. En limitant les déformations du sol plu tard de plus hautes pressions sont appliquées, causant des fractures dans le sol et en quelques pieux même un augmentation des déformations.

1 INTRODUCTION

The grouting of the lining is a critical process in shield tunnelling. Measurements, for example at the 2nd Heinenoord tunnel, (COB 1999) have shown that surface settlements are determined to a large extent by the quality of the grouting process. Grouting with a too low grouting pressure will lead to surface settlements, but a too high pressure can lead to a blow out of the grout and unpredictable deformations when the pressure is higher than the limit pressure that can exist in the soil at the depth of the tunnel. Furthermore a too low or too high grouting pressure can influence adjacent pile foundations.

The influence of tunnelling on surface settlement and pile foundations has been studied in a centrifuge (Bezuijen et al 1994, Loganathan et al 2000). In these studies the tunnelling process was simulated by a reduction of the volume of a model tunnel. However, with such a model it is not possible to find the maximum grouting pressure and it was found that the distribution of grouting pressure around the tunnel is of a major influence on the process. Therefore it was

decided that the grouting process in the tail void has to be modelled by injection of a model grout in a scaled tail void.

In a research project commissioned and supervised by COB and performed by GeoDelft, equipment was made to investigate in a geotechnical centrifuge the influence of the grouting process on soil deformations and deformations of adjacent pile foundations. This paper deals with the equipment made and shows results of the tests which were performed. In this paper attention is focussed on the measured surface deformations and pile settlements. The measured blow-out pressures will be dealt with elsewhere (Bezuijen & Brassinga 2001).

2 SCALE MODELS

In a geotechnical centrifuge the behaviour of soil can be studied in a scaled model. As the stress strain relation of soil is stress depending, and real soils are used as model material, the earth's gravity has to be enlarged. A model scaled 1:N has to be subjected to a

Table 1. Scaling factors in centrifuge tests.

Phenomenon	Prototype	Model
Volumetric weight	1	1
Dimension	N	1
Strain	1	1
Stress	1	1
Force	N ²	1
Time (consolidation)	N ²	1
Permeability	1	N

gravity level of N times earth's gravity to comply with the correct strains and stresses. Each phenomenon in the soil is scaled in a specific way. In Table 1 some scaling factors are given.

3 TEST SET-UP

To simulate the tunnelling process, it is essential that equipment can move horizontally through the soil. A device was developed to enable this, see Figure 1. A plunger below the model container can move an aluminium 'cart' over a distance of 400 mm. Equipment connected to the cart can be moved horizontally through a watertight seal in the model container. The system can operate in tests up to 150 g. The maximum load that can be applied is 100 kN.

To investigate the grouting process during tunnelling a so called tail void module was built. The module is shown schematically in Figure 2. An inner tube represents the lining. During the test, the outside tube, representing the TBM, is moved from the inner tube over a distance of 400 mm (on modelscale). During this process bentonite slurry is pumped through the supply system, connected with the outside tube, through the slits made in the inner tube. Bentonite slurry is injected by means of a plunger pump. The diameter of the outside tube is 130 mm, the diameter of the innertube is 125 mm. Some pore pressure gauges are placed at a distance of 200 mm behind the grout injection points, to measure the course of the pressure along the lining.

Bentonite slurry was used as a model grout. Slurry with 240 gr/l bentonite was used to get a liquid with a scaled viscosity and yield strength as a grout in such a way that the penetration process of the grout in the sand is properly scaled.

The processes studied, surface settlement and limit pressure, occur when the grout is still in the liquid phase and therefore the cementing of the grout was not modelled.

Model piles have been placed into the soil above and next to the tunnel. Different configurations were used in different tests. In this paper most attention will be

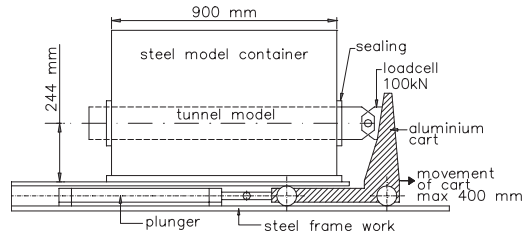


Figure 1. Side view test setup.

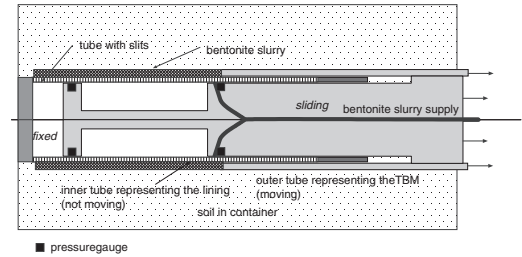


Figure 2. Sketch of the module made to simulate the grouting process.

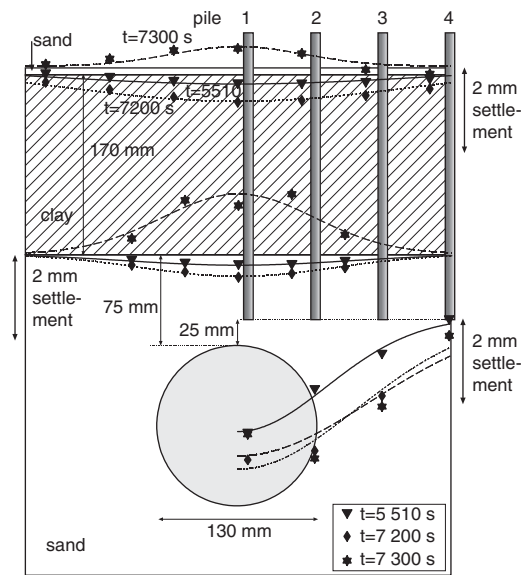


Figure 3. Test set-up for the OLS tests and results of the second test. Measured deformations and pile settlements at different times during the test and approximation with a gauss-curve.

paid to the OLS tests, as shown in Figure 3. The piles were located in such a position that after the outside tube was moved over 290 mm the grout injection points were just below pile 1, nearly straight above the tunnel.

0,01 mm/s without supplying bentonite, intended to cause a further decrease of the bentonite pressure. After the outside tube had reached maximum displacement (400 mm) the bentonite pressure was increased until the limit pressure was reached.

5 RESULTS

5.1 Measured pressures

The measured grouting pressures, the total horizontal soil pressure, the pore pressure in the soil during the experiment are shown in Figure 5. The pore pressure (p1) was measured in the sand layer, outside the influence of the tunnel. The grout pressures shown were measured 40 mm above (p3) and below (p4) the axis. The horizontal total pressure (p2) was measured at a distance of 10 mm from the tunnel, on the level of the axis of the tunnel. From this figure it turns out that the pore pressure in the sand around the tunnel hardly changes during the experiment. This means that the bentonite slurry which acts as a model grout hardly penetrates into the sand. The time during which the outside tube was moved under a controlled grouting pressure can be distinguished from the figure (from $t = 5100$ s until $t = 5510$ s), because during that stage there is some noise on the grouting pressures. Half way during this process the total pressure in the sand increases sharply (at $t = 5350$ s in Figure 5). At that time the end of the outside tube reached this pressure gauge. After the passage the pressure increase is caused by the model grout in the tail gap between the soil and the inner tube. Between $t = 5550$ s and $t = 6500$ s, while the moving and bentonite supply have stopped, the bentonite pressure drops because of the penetration of bentonite into the sand. Although the penetration is very small (see 5.3), the pressure drops because of the incompressibility of the bentonite. It can be seen that during the second stage of the displacement of the outside tube, also without bentonite supply, the grouting pressure drops to a level close to the pore pressure.

5.2 Pile settlements

The settlements of the piles are shown in Figure 6.

The piles were kept loaded to the ultimate bearing capacity after they were pushed into the sand during the test. Because of the limit state situation around the pile tip in the test, any extra shear stress in the sand will cause settlement of the pile tip. In practice the load will be less and therefore also the pile settlement caused by tunneling activities will be less. In the test pile settlement already occurs when the outside tube starts to move even though the tail void is still far away from the piles. Settling of Pile 1 and Pile 2 increase sharply when the tail void passes underneath

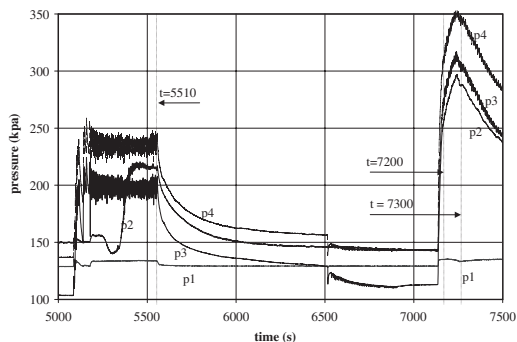


Figure 5. Measured pore pressure, grout pressures and total horizontal pressure.

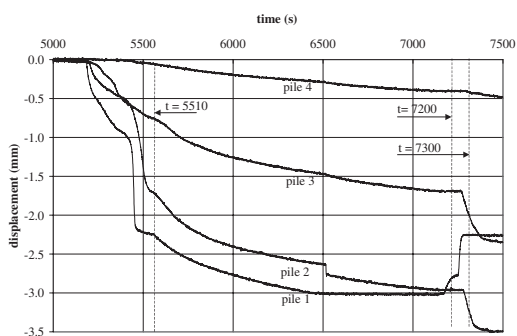


Figure 6. Settlements of piles.

the piles (approximately at $t = 5450$ s). From Figure 6 it is also clear that the displacement of piles at a larger distance from the axis of the tunnel decreases. At a distance of $1,5 D_{\text{tunnel}}$ the influence of the tail void on the behaviour of piles has almost disappeared.

During the 'consolidation' stage ($t = 5510$ s to $t = 6500$ s) settlement of the piles continues caused by the decrease of the bentonite pressure in the tail void. The settlement of the piles exceeds the settlement of the surface and of the sand, which is caused by a decrease of the strength of the soil around the pile tip.

From $t = 7200$ s, when the grouting pressure is increased, the settling of the piles goes on, except pile 1 which moves upward. Figure 3 shows that soil heave is measured over a larger area, but the soil failure leads to a further settlement of the piles 2 and 3. From Figure 3 and Figure 6 it can be deduced that the soil failure has a large influence on the settlements. There is still a settlement trough at $t = 7200$ s, but at $t = 7300$ s (at approximately the same pressure, but after soil failure) heave is created above the tunnel. Pile 1 moves upwards, but less than the surface and the top of the sand. The capacity of the pile is increased, apparently

in this case the soil strength does not decrease on top of the tunnel. Pile 2 and 3 both move downwards, while the surface and the top of the sand show heave. The loss of capacity of these piles has to be explained by loss of soil strength in the area next to the tunnel.

5.3 Inspection of the model after end of test

Figure 7 shows the model after removing the sand. From the inspection it turned out that the penetration depth of the bentonite into the sand was about 2 mm. The bentonite slurry remains around the tunnel due to the high yield stress. Reaching the limit pressure has led to the creation of lobes on both sides of the tunnel. At these locations a hydraulic fracture has occurred. This probably explains the decrease of the capacity of piles 2 and 3, placed aside of the tunnel.

The maximum pressure at which this fracture occurred was in between 2,2 and 2,5 times the vertical effective stress plus the pore pressure. More detailed information about this result will be published elsewhere (Bezuijen & Brassinga, 2001).

6 DISCUSSION

Surface settlements occur when the grouting pressure is less or equal to 90% of the vertical total stress. This means under the soil conditions tested it is insufficient to use grouting pressures that avoid failure of the soil, as for example can be calculated by (Leca & Dormieux 1990). It is really necessary to grout with a pressure that is equivalent to the original soil stress to minimize settlements. Increasing the grout pressure after settlement of the soil surface has occurred, has only a limited effect unless the pressure is increased to such a level that failure of the soil occurs. This is of course rather tricky because such high pressures can easily lead to a uncontrollable failure or blow-out of the grout.

The tests show that it is hardly to be avoided that heavily loaded piles will settle during tunneling in the neighbourhood of the pile tips. The moving of the outside tube of the model tunnel already led to settlement, probably due to shear stress that is exerted on the sand. This means that during tunneling not only the grouting process but also the TBM itself can have an influence on pile foundations. For the conditions present during these tests, the influence decreases significantly within a distance of 1 time the diameter outside the tunnel.

7 CONCLUSIONS

The tests lead to the following conclusions:

1. The grouting process can be modeled in a geotechnical centrifuge, not only by using a contraction



Figure 7. Model with bentonite after the test.

model but, more appropriate, also by really simulating the grouting process with a model grout.

2. The grouting pressure has to be equal to the total vertical stress at minimum to avoid surface and pile settlement. High grouting pressures in the soil are necessary to reduce significantly settlements that have occurred before. Such high pressures can easily lead to fractures.
3. Pile settlement will be significantly for the conditions tested on within 1 time the diameter from the tunnel. Pile settlement was sometimes reduced by high grouting pressures resulting in soil failure, but the tests showed that it is also possible, that such a process leads to further settlements.

ACKNOWLEDGEMENT

The research described in this paper is commissioned by CUR/COB. The authors want to acknowledge the permission from these foundations to publish the results.

REFERENCES

- Bezuijen A. & Schier, J van der 1994. The influence of a bored tunnel on pile foundations. Proc. Centrifuge 94. Rotterdam; Balkema.
- Bezuijen A. & Brassinga H.E. 2001. Blow-out pressures measured in a centrifuge model and in the field. To be published proc.IS-Kyoto 2001, Kyoto.
- COB 2000. Tweede Heinenoord tunnel, evaluatierapport K100-06, Gouda; CUR/COB (in dutch).
- Leca E. & Dormieux, L. 1990. Upper and lower bound solutions for the face stability of shallow circular tunnels in frictional material, Geotechnique 40, 581–606.
- Loganathan N, Poulos H.G. & Stewart D.P. 2000. Centrifuge model testing of tunnelling-induced ground and pile foundations. Géotechnique 50, No. 3, 283–294.
- Poel J.T. van der & Schenkeveld F.M. 1998. A preparation method for very homogenous sand models and cpt research, Proc. Centrifuge 98. Rotterdam; Balkema.

Grout pressures around a tunnel lining

A.M. Talmon & L. Aanen

Delft Hydraulics, Delft, The Netherlands

A. Bezuijen & W.H. van der Zon

GeoDelft, Delft, The Netherlands

ABSTRACT: At the rear of many tunnel boring machines an annular space is being created that has to be filled with grout. The grouting process is of importance with respect to subsurface settlements. The grouting pressures determine both the loading on the tunnel lining and the loading on the soil around the tunnel. Calculation models are presented to calculate the pressure distribution in the grout directly after the tunnel boring machine when grout flow determines the pressure and several meters from the tunnel boring machine when buoyancy forces dominate.

1 INTRODUCTION

The Dutch government has decided to invest increasingly in research and knowledge development in civil engineering. This has led to the establishment of the Delft Cluster.

GeoDelft and Delft Hydraulics, together with participating end-users, have initiated research to develop an understanding of the flow processes involved in grouting. The philosophy is to focus on the physics of the rheological processes, and to incorporate these in a mathematical model for the calculation of grout pressures around a tunnel lining.

During drilling of a tunnel the grout is being pumped in the annular space through a number of inflow-openings that are distributed over the circumference. This annular space is also called tail void. Typical 6 or less injection openings are used. From these injection openings, the principal grout flow takes place in tangential direction to fill the tail void, see Figure 1. The flow pattern is governed by continuity and differences in flow-resistance. This flow pattern is also influenced by time effects, because of ongoing hydration of cement and liquid loss.

An understanding of the fundamental behaviour of the grout in the tail void is needed in order to relate operational grouting conditions with grout pressures in the tail void. Therefore grout flow experiments were conducted first.

To control soil deformations and forces acting on the tunnel lining, the grout pressures in the first few meters behind the tunnel boring machine have to be matched carefully with the surrounding.

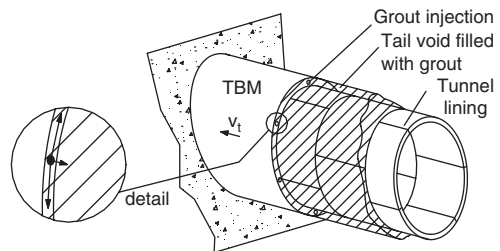


Figure 1. Schematization of grout flow pattern in the tail void of a tunnel boring machine (TBM) moving at an advance rate v_t . The grout is injected by six equally distributed injection openings. Dimensions not to scale.

2 MEASUREMENT OF GROUT FLOW PROPERTIES

2.1 Grout flow experiments

The behaviour of grout is complicated and depends on many factors. It is difficult to measure the rheological properties of grout mixtures. Small-scale experiments often fail because of the solid parts in the grout. Interpretation of the outcome of such experiments is difficult. One particular problem is that different types of small scale testing apparatus, that aim at the measurement of the same rheological properties, produce different results. Therefore prototype-scale experiments are set up where the flow conditions along the most important trajectories (streamlines) are simulated.

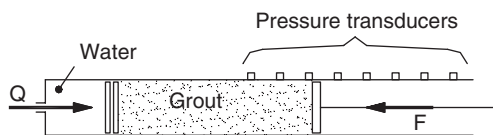


Figure 2. Set-up 1-D grout flow experiments. The grout is pressurized by a constant load acting on the piston at the right. The grout is pushed forward by water being supplied by means of a positive displacement pump. Dimensions are not to scale.

The experimental set-up consists of a circular pipe through which the grout is forced to flow, see sketch Figure 2. The diameter of the pipe is comparable to the dimension of the height of the tail void. The grout is pressurized by a piston (about 3 bar). A standard type grouting mortar and a two-component chemical grout (ETAC) are tested. Three different pipes have been employed: a smooth pipe to simulate the roughness of the tunnel lining, a rough pipe to simulate the surface of the undisturbed soil, and a smooth but permeable pipe to get rid of lubricating liquid films, sometimes being reported in the literature, Mannheimer (1983).

2.2 Composition and small scale rheological tests

The tested grouting mortar consists of a Portland cement paste (including a superplasticizer and some bentonite) and aggregates (coarse sand with a maximum particle diameter of about 4 mm). The typical mixture composition of the main ingredients is: water:cement:sand, 1/6, 1/12, 3/4 (weight ratio).

The two-component chemical grout mixture consist of chemicals, clay-sand and some air. It does not contain coarse aggregates, and is light weight. The mixture has the advantage of a quicker hardening and less volume reduction during hardening than conventional grout.

At the beginning of the experimental program some small scale consistency tests were conducted to determine the order of magnitude of the flow resistance of the grout and the time scale of rheological changes.

One of our goals was also to determine the relation between pressurization of the grout, liquid loss, and associated change of rheological properties. Due to experimental difficulties we did not succeed. However, according to McKinley & Bolton 1999 the liquid loss of cement grouts will lead to a consolidated layer at the grout/soil interface. Such a layer has a higher shear strength than the bulk of grout and a lower permeability. Consequently liquid losses will stop. We expect that such a consolidated layer does not significantly affect frictional characteristics of the grout flow in the tail void.

2.3 Results small scale rheological tests

Essential parameters to characterize grouts are yield stress and viscosity, Tattersall & Banfill 1983. Modelling as a Bingham fluid suffices. The time-dependency of these parameters has to be accounted for. A number of different apparatus were employed to measure those parameters: Brookfield rotoviscometer, Haake vane test, Torvane, slump test and pocket penetrometer. The order of magnitude of measured shear stresses are given below.

Brookfield rotoviscometer tests on conventional grout produced shear stresses up to 300 Pa before hardening commences. These results might be flawed by wall slip, Mannheimer 1983. Yield stresses obtained by Torvane tests and slump tests indicate yield stresses of about 1 kPa and higher. When also some recent literature data is considered, Pelova 1996 and Ferraris & de Larrard 1998, it is concluded that the yield stress of fresh mortars is of the order of 1 à 3 kPa. Workability of mortars is typically 4 hours.

Pocket penetrometer tests on the two-component chemical grout indicate yield stresses up to about 10 kPa before hardening commences. Vane tests produced yield stresses one order of magnitude smaller. The remolded shear strength measured by the vane test is of the order of 0.1 kPa.

2.4 Results grout flow experiments

The flow properties of the grouts have been tested in a pipe of 10 cm diameter and a measuring section of about 5 m length. Grout pressures are measured by 8 pressure sensors distributed over the length of the pipe. This set-up allows for the determination of time-dependent frictional properties of grout flow. The shear stresses on the wall are computed from the pressure drop between sensors.

The granulometric composition of the coarse sand fraction in the mortar is: $d_{50} = 1$ mm, $d_{10}/d_{60} = 0.2$. It was not possible to pump the grout mortar by means of the positive displacement pumps available. Consequently we devised a method in which the grout is confined between two pistons, much like the method reported by Ede (1957). The piston indicated on the right of Figure 2 provides backpressure, the other piston separates the grout mortar from clear water that is being pumped at a controlled flow rate by a positive displacement pump.

In case of the two-component chemical grout, the piston indicated at the left hand side of Figure 2 is discarded. A flange with a mixing nozzle is mounted. The two components are being injected by means of the mixing nozzle. Two positive displacement pumps were used to supply the two components.

A broad range of grout flow velocities (2 mm/s–100 mm/s) was tested. The smallest velocity is comparable to the advance rate of the tunnel boring machine

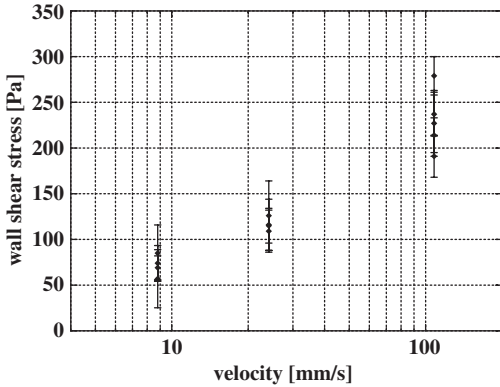


Figure 3. Example of data obtained from 1-D grout flow experiments: Portland type mortar, smooth pipe.

(TBM). Such velocities are expected at some distance from the injection openings. At outflow from the injection openings, and in supply pipelines, the velocities are about two orders of magnitude larger.

An example of the results of one of the test series is given in Figure 3. It concerns the flow of grout mortar in a smooth pipe. The wall stresses at three different grout flow velocities are given. The grout pressures varied in time and location. In the graph the results for the wall shear stresses obtained from different pairs of pressure sensors are given together with the root-mean-square values.

The results show that wall shear stresses are an order of magnitude smaller than the yield stress of the grout. It is concluded that a lubricating film has formed along the wall, the rheology of which will be governed by cementitious fluid in between the coarse grains of the grout.

We also observed that fluid loss due to pressurization of the grout strongly increases the flow resistance in case of a rough pipe (roughness 200 μm). This is due to grain contact between the grout and the rough wall. This means in practice that in case of fluid loss to the surrounding soil the shear stresses at the interface grout/soil will be of the order of the yield stress of the grout.

The grout flow experiments produced reliable data on the flow resistance as a function of flow velocity. These are, in combination with other data, input to the mathematical model for the calculation of grout pressures in the tail void.

3 CALCULATION METHOD

3.1 General features grout flow model

A 2-dimensional numerical model has been developed to calculate grout pressures as a function of the

number and position of the injection openings. The finite difference technique is used to solve the flow and pressure distribution. A shallow flow approximation is employed. The flow is averaged over the thickness of the grout layer. The thickness of the tail void is assumed constant. The flow resistance is caused by friction between the grout and the soil and between the grout and the tunnel lining.

Because fresh grouts are characterized by a pouring consistency (API 1967), no distinction is made between grain and fluid stresses. The rheological properties of the grout are modeled by a one-phase viscoplastic Bingham fluid. The rheological properties are a function of the time since injection.

The consequences of hydration of cement are accounted for by modelling the time-dependency of the rheological properties. The consequences of fluid loss from the grout to the surrounding soil are to be accounted for by modelling the associated time-change of rheological properties.

The normal stresses in the grout are assumed isotropic. Internal shear stresses in the grout, due to velocity differences with neighboring grid cells, are neglected. The surplus grout being injected to compensate fluid loss is not included in the continuity equations of the model.

The model calculates the distribution of grout pressures in an area covering the entire circumference of the tunnel lining over a distance of one or more tunnel lining segments adjacent to the rear of the TBM.

3.2 Grout flow model

The flow-field is calculated in a computational domain moving with the TBM. The flow velocity components with respect to the moving frame of reference are: V_s and V_n . The s-co-ordinate is parallel with the tunnel axis. The n-co-ordinate is directed tangential to the circumference of the tunnel lining. The origin of the coordinate system is at the rear of the TBM at the crest. These orthogonal velocity components satisfy continuity. Friction between the grout and the tunnel lining and the undisturbed soil is responsible for pressure losses in the tail void. In order to calculate wall friction, the flow velocity (U_s, U_n) with respect to these boundaries is considered:

$$U_s = V_s - v_t \quad , \quad U_n = V_n$$

with: v_t = advance rate TBM (during excavation).

The two momentum equations that relate grout pressures with frictional properties are:

$$h \frac{\partial p}{\partial s} = -2\tau_s \quad , \quad h \frac{\partial p}{\partial n} = -2\tau_n + \rho g \sin \theta$$

in which: h = thickness grout layer, p = grout pressure, ρ = density grout mixture, g = gravity, θ = inclination angle.

To calculate the wall shear stresses τ_s and τ_n , the shear rate of the grout flow at the walls has to be considered. This shear rate is, in analogy to laminar flow of Newtonian fluids in slit-geometry conducts, approximated by:

$$\frac{\partial u}{\partial z} = \frac{12U}{h}$$

The wall shear stresses are calculated by:

$$\tau_s = \eta \frac{12U_s}{h}, \quad \tau_n = \eta \frac{12U_n}{h}$$

in which: η = apparent viscosity

The rheological parameters of the Bingham model are the yield stress and dynamic viscosity. The relation between the shear rate and the shear stress is given by:

$$\tau = \tau_y + K \frac{\partial u}{\partial z}$$

with: τ_y = yield stress, K = dynamic viscosity.

The values of the parameters have been determined by the small scale rheological experiments and the grout flow experiments. For two-component grout special attention is needed for the influence of air on the parameters. Due to ongoing hydration and cementation of the grout, the resistance against deformation increases. The time-dependency has been modelled by an exponential function (depending on grout properties other functions can be chosen):

$$\tau_y = \tau_{y0} + (\tau_{y\infty} - \tau_{y0})(1 - e^{-t/T})$$

$$K = K_0 + (K_\infty - K_0)(1 - e^{-t/T})$$

in which: τ_{y0} = shear stress at $t=0$, $\tau_{y\infty}$ = shear stress at $t=\infty$, K_0 = dynamic viscosity at $t=0$, K_∞ = dynamic viscosity at $t=\infty$. In the model at $t=\infty$ asymptotic rheological values are reached. The validity of the model is however restricted to conditions where the grout is still workable.

The apparent viscosity η of a Bingham fluid is given by:

$$\eta = \frac{\tau_y}{\partial u / \partial z} + K$$

In case of extremely small velocities, the apparent viscosity has been limited to $\eta = \tau_y / 0.0001$ to obtain numerical stability.

In the mathematical model the wall shear stresses on the tunnel lining and the soil are assumed equal. To account for differences between these wall shear stresses, the rheological parameters at input should represent mean frictional conditions of both surfaces.

4 CALCULATED PRESSURE DISTRIBUTION DIRECTLY AFTER THE TBM

Two different injection strategies are simulated. One strategy in which six injection openings are distributed equally, and one strategy in which only three injection openings near the crest are employed. The three injection openings near the crest are located at 2, 10 and 12 hour positions. In case of six injection openings these are located at 2, 4, 6, 8, 10 and 12 hour positions. The input parameters are given in Table 1.

These rheological parameters are characteristic for typical mortars employed in tunnelling. The yield stress and dynamic viscosity are mean values of friction with the tunnel lining and the soil. The results are not very sensitive to the value of the dynamic viscosity because of creeping grout flow.

The calculated grout pressures are given in Figures 4 and 5. These calculations show that grout pressures in the first tunnel lining segment rings behind the TBM

Table 1. Typical operational conditions grout injection.

Parameter	Value
Outer diameter tunnel lining	$D = 10$ [m]
Thickness grout layer	$h = 0.15$ [m]
Drive speed TBM (continuous)	$v_t = 1$ [mm/s]
Soil pressure at crest tunnel	400 [kPa]
Yield stress at $t = 0$	$\tau_{y0} = 1500$ [Pa]
Yield stress at $t = \infty$	$\tau_{y\infty} = 2500$ [Pa]
Dynamic viscosity K at $t = 0$	$K_0 = 50$ [Pa s]
Dynamic viscosity K at $t = \infty$	$K_\infty = 75$ [Pa s]
Time scale rheology changes	$T = 14400$ [s]
Density of grout mixture	$\rho = 2000$ [kg/m ³]

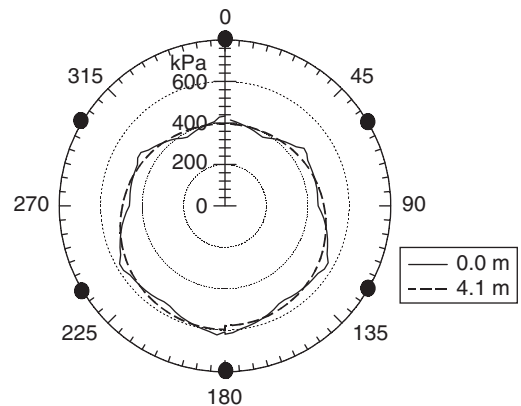


Figure 4. Calculated pressure distribution at rear of the TBM: 6 injection openings equally distributed. Pressures at 0 and 4.1 m behind the TBM.

are strongly influenced by the choice of active grout injection openings.

The pressure distribution is nearly static when grout is supplied by uniformly distributed injection openings, with locally higher values in front of the injection openings, with Figure 4. When a small number of injection openings is used, the grout has to cover longer distances. In that case the pressure distribution may be affected to such an extent that the static pressure contribution may be obscured completely, Figure 5.

The flow pattern is governed by continuity and differences in flow-resistance. Continuity determines the gross distribution of grout from the injection openings, differences in flow-resistance govern local flow. To explain the latter phenomenon consider a Newtonian fluid (=constant viscosity). Radial outflow will take place near injection openings. The drag due to the velocity difference between moving grid and stationary frictional boundaries (the walls) is everywhere the same in the tail void. Consequently this will not lead to deviations from radial outflow. The pressure field however will show under-pressures created by the advancing TBM. In case of shear thinning fluids, such as Bingham fluids, the viscosity is a function of the velocity difference with the stationary walls. Consequently the flow has the tendency to shift to regions where the velocity difference is largest. This is the case in a zone adjacent to the rear of the TBM. Consequently transverse flow will dominate.

When the forward movement of the TBM is halted to mount tunnel lining segments, the duration of the interruption of the grout injection is an important factor, because of ongoing aging of the grout. It is also possible to calculate consequences on grout distribution and pressure field. The sample computations given in Figures 4 and 5 do not include such interruptions.

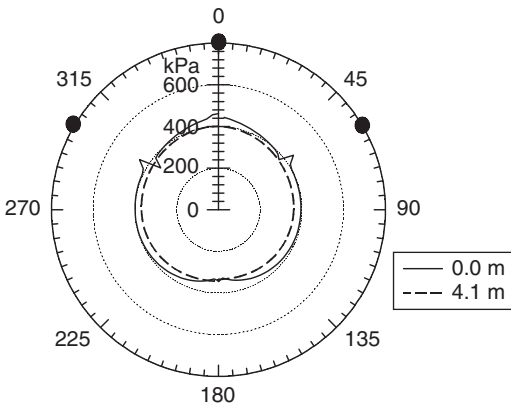


Figure 5. Calculated pressure distribution at rear of the TBM; 3 injection openings near the crest. Pressures at 0 and 4.1 m behind the TBM.

5 FIELD DATA, COMPARISON WITH CALCULATION RESULTS

The results from the finite difference model give insight how the injection pressure can influence the average value of the grouting pressure and how the pressure distribution directly after the TBM can be influenced by the number and position of the injection openings. However, the pressure distribution further from the TBM, but before the grout is hardened, is influenced by buoyancy and the stiffness of the tunnel lining and cannot be influenced by the number and position of the injection openings.

A nearly linear pressure distribution has been found in the grout further from the injection openings, Figure 6. However, the pressure increase with depth does not correspond with the density of the grout, but is less. This is caused by buoyancy forces acting on the tunnel lining.

The buoyancy of the tunnel lining induces side-ward and downward forces on the grout. Provided that opposing wall shear stresses are smaller than the yield stress of the grout, an upward movement of the tunnel lining is prevented. In the tail-void, the equilibrium of pressure gradient and wall shear stresses is given by:

$$\frac{\partial p'}{\partial h} = -\frac{2\tau_n}{h}$$

with: p' = deviation from static grout pressure.

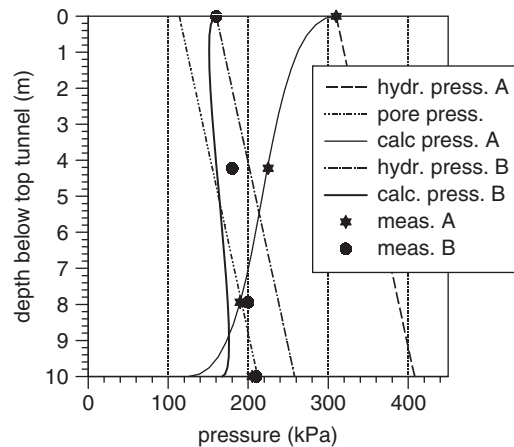


Figure 6. Measured and calculated grout pressures at two different times. (A) just after the TBM when the pressure and the position of the injection points dominate and (B), where the influence of the buoyancy force on the tunnel lining dominates the pressure distribution. Measured and calculated pressure are considerably lower than according to the hydrostatic pressure that is also presented in the figure.

Integration of p' and τ_n over the circumference gives:

$$\tau_n = -\frac{F}{D(D/h-1)}$$

with: F = net buoyancy force per unit length.

With these two equations it is possible to calculate grout pressures due to buoyancy. Figure 6 shows results of calculations compared with measured grout pressures for two situations.

For the situation (A) just after the TBM when the injection pressure and the position of the injection openings dominate, the yield stress is fitted to the measurement data to get the best agreement.

For the situation (B), where the influence of the buoyancy force of the lining dominates the pressure distribution, it was assumed that the buoyancy force is the only uplift force that has to be counteracted by the grout. In reality the clamping between various lining elements and the weight of the TBM will also influence the uplift force on the lining elements. Therefore the measurement points give a bit higher pressure than the calculation.

6 CONCLUSIONS

Relations between grout injection, the rheological properties of the grout and grout pressures in the tail void have been quantified.

It has been shown that it is possible to calculate the pressure distribution at the rear of the TBM, where filling of the tail void is most critical. It has also been shown that it is possible to calculate the pressure distribution farther from the TBM where buoyancy effects are important.

Our understanding of the fundamental behaviour of grout flow in the tail void will be verified by dedicated

monitoring of a railroad tunnel being constructed in the Netherlands.

Attention should be given to validation of the simplifications we allowed for in the 2-D model.

Special attention is needed with respect to rheological characterization of grouts, change of rheological properties, consequences of fluid loss and frictional properties at the grout/soil interface.

ACKNOWLEDGMENT

Project Organization Betuweroute (NS Railinfra-beheer), Project Organization High-Speed Line (HSL-Zuid), Nederlandse Bouwstoffen Combinatie, Delft Cluster.

REFERENCES

- API committee 116, Cement and Concrete Terminology, American Concrete Institute, Detroit, 1967.
- Ede, A.N. 1957. The resistance of concrete pumped through pipelines. *Magazine of Concrete Research*. vol. 9. no.27. pp 129–140.
- Pelova, G.I. 1996. BML-viscometer Measurements of rheological characteristics of fresh concrete: Preliminary experimental study. *Progress in Concrete Research; Annual Report Delft University*. vol. 5.
- Tattersall, G.H. & Banfill, P.F.G. 1983. *The Rheology of Fresh Concrete*. Pitman.
- Ferraris, C.F. & Larrard, F. de. 1998. *Testing and Modelling of Fresh concrete rheology*. NISTIR 6094. 62p.
- Mannheimer, R.J. 1983. Effect of slip on flow properties of cement slurries can flaw resistance calculations. *Oil, & Gas Journal*. Dec. vol. 5. pp 144–147.
- McKinley, J.D. & Bolton, M.D. 1999. A geotechnical description of fresh cement grout; filtration and consolidation behaviour. *Magazine of Concrete Research*. vol. 51. no. 5. pp 295–307.

Field measurements of grout pressures during tunnelling of the Sophia Rail Tunnel

A. Bezuijen

GeoDelft, Delft, The Netherlands

A.M. Talmon

Delft Hydraulics, Delft, The Netherlands

F.J. Kaalberg

Witteveen+Bos Consulting Engineers & North/Southline Consultants, Amsterdam, The Netherlands

R. Plugge

Fugro Ingenieursbureau b.v. Leidschendam, The Netherlands

ABSTRACT: During drilling, grout pressures were recorded on a tunnel lining measuring 9.5 m in diameter. Two tunnel rings were fitted with pressure gauges (14 gauges per ring). Measurements were performed for more than one day. Final hardening of the grout did not occur during this time. The lowest pressures were measured at the start of the drilling process after completion of the ring. Results show that the grout pressure distribution is dominated by injection during drilling, but this distribution changes when drilling stops and buoyancy forces start to exert an influence. The influence of buoyancy forces increases further away from the injection points. Bending moments in the tunnel lining also influence the gradient in the grout pressure distribution.

IGC: A10, C05, E13, K02

Keywords: Monitoring on site; Shield tunnelling method; Shear strength; Grouting; Vane shear test; Lining Rheology

1 INTRODUCTION

Since 1996, the Centre for Underground Construction (COB) in the Netherlands has initiated a substantial amount of practically-oriented field and desk research (Bakker et al 2001). One of the main issues in this research was settlement control and its prediction. As pressure control at the front of slurry type TBMs is generally properly controlled nowadays, the focus must now be on improving process control for backfill grouting in the annular tail void in order to increase settlement control. Research findings so far have shown an evident qualitative correlation between the quality of the grouting process in the annular tail void at the back of the TBM, and settlements. However, this correlation has not yet led to a quantified relationship. With plans underway to construct a metro tunnel under Amsterdam's historic city in coming years (Kaalberg et al 2001), the autonomic government policy for ongoing tunnelling research is given additional support.

COB therefore took the decision to define additional field and desk research at the Sophia Rail

Tunnel (4.2 km twin bore tunnel, external diameter 9.5 m). One of the main objectives of this research is to increase knowledge about the injection, flow and hardening process of the backfill grouting to obtain a more constant, reliable and predictable settlement control for future projects in urban environments worldwide.

Another main research topic is the behaviour of the tunnel lining during construction. Damage occurring at segmental joints is sometimes seen, originating primarily from joint design but presumably also from fluid grout loads in the annular tail void.

To tackle both these issues in a single field research project, two complementary ways of monitoring the grouting process were defined. The grout pressures at the back of the TBM were measured continuously, and one cross section was defined where building, surface and subsurface instrumentation are installed. Two tunnel rings (one in each tube) are also circumferentially fitted with grout pressure sensors in the lining.

The aim is to instantaneously analyse the grout pressure distribution around the tunnel, both behind the

TBM and at a greater distance. This information will later be used as input to further calibrate and validate earlier developed 4D FE models (van Dijk & Kaalberg 1998) for settlement prediction and lining calculations.

In this paper, the monitoring data of lining sensors for the first and second TBM passage are described and analysed, and grout pressures are calculated using a grout flow model.

2 THE SOPHIA RAIL TUNNEL

The Sophia Rail Tunnel is one of three bored tunnels along the Betuwe route. It consists of two single rail tubes with an outside diameter measuring 9.5 m, and a concrete lining with a thickness of 0.4 m. The tunnel crosses three polders and the River Noord (a branch of the River Rhine), and is located some 20 km southeast of Rotterdam. More information on the location of the tunnel and its design features can be found in Stive (1999).

The tunnel section where the measurements were performed was situated in the IJsselmonde Polder west of the River Noord, where the tunnel is at a constant depth. The polder is an agricultural area. A few houses are located close to the tunnel trace and the measurement location. These houses do not have deep foundations and have no influence on the tunnelling process.

At the location where the measurements were carried out, the 12-m-thick Holocene top layer consists of peat (2/3) and clay (1/3). The distance between the tubes is 10 m. Underneath the top layer is a medium density sand layer of Pleistocene sand measuring 10.7 m in thickness. Underneath this sand layer is the Kedichem layer, which consists of a layer of peat and silty clay at the measurement section. A cross-section of the tunnels and the soil layers is shown in Figure 1. Surface settlements were measured at various

locations in the same cross-section where the instrumented ring fitted with grout pressure transducers was placed. Piezometric head was measured using pore water transducers (see Figure 1 for the locations). The piezometric head appeared to be at the same level at different depths, approximately 1 m below the ground surface. The measured fluctuations in the piezometric head were less than 5 cm before drilling started. The overburden pressure at the crown of the tunnel is approximately 200 kPa.

The measured surface settlements above the instrumented ring were limited to less than 5 mm. At some locations, there was even a few millimeters of heave.

3 THEORY

Before hardening, grout can be described as a Bingham liquid. However, its properties change with time. Viscosity and yield stress increase. Talmon et al (2001) presented a flow model describing the pressure distribution around a tunnel lining caused by grout flow, and as a function of the discharge through the injection points.

However, a Bingham liquid can withstand shear stresses without flow (whereas a Newtonian fluid cannot). This means that also without flow, the hydrostatic pressure distribution is not necessarily present. In the case of grout around a tunnel lining, the lining will move upwards due to buoyancy forces. It can only move if the grout is pressed down. This will be prevented by the shear stresses between the soil and the grout. From our experiments and analysis of field measurements, Talmon et al (2001), we have concluded that the shear stress between concrete and grout is much smaller than the shear stress between soil and grout. The former can therefore be neglected. The relationship between shear stress and pressure caused by

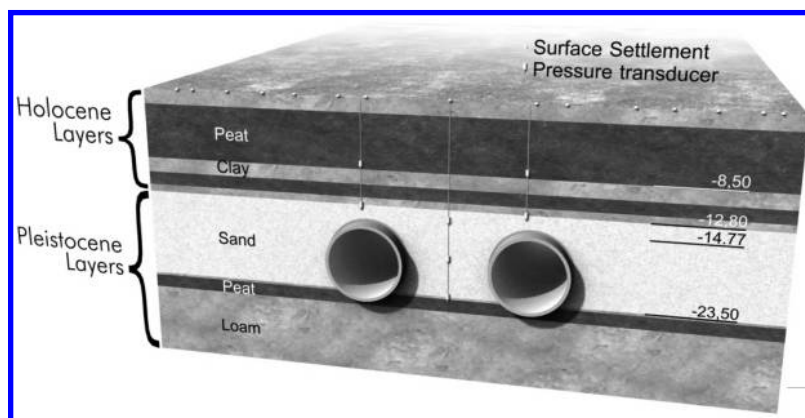


Figure 1. Cross-section of the Sophia Rail Tunnel and soil layering at the measurement location.

that shear stress can be derived from Figure 2, and results in:

$$\Delta P = \tau \frac{R}{s} d\alpha \quad (1)$$

where ΔP is the pressure change caused by the yield stress τ , R is the radius of the hole made by the tunnel, s is the thickness of the grout layer, and α the angle indicated in Figure 2. Assuming that the grout flows to the bottom of the tunnel from a location with a certain angle α , the total pressure drop by the yield stress is:

$$P = \tau \frac{R}{s} \alpha \quad (2)$$

This excess pressure that increases with α will result in a downward directed force on the tunnel. This compensates the buoyancy force K . For a small segment, it can be written as:

$$dK = PR \cos \alpha d\alpha \quad (3)$$

Combining Equations (2) and (3) and integration over the two half circles leads to:

$$\tau = \frac{Ks}{D^2} \quad (4)$$

Using this last equation, it is possible to calculate the yield stress that must be present to prevent upward movement of the tunnel lining until it touches the ceiling of the hole drilled due to buoyancy force.

If the actual yield stress τ is larger than the result of Equation (4), then there will be only limited movement

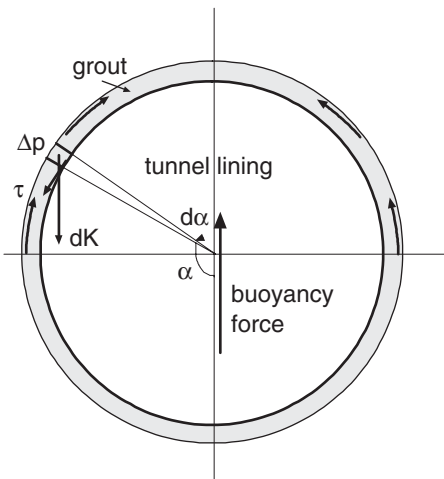


Figure 2. Scheme to calculate the pressure distribution due to buoyancy forces.

of the tunnel and Equation (2) using the result of (4) gives the influence on the pressure distribution. Without shear stress, the pressure will increase according to a hydrostatic pressure distribution. Equation (2) leads to a pressure that is highest on top of the tunnel, and which thus counteracts the hydrostatic pressure. The resulting pressure gradient will therefore be less than the hydrostatic gradient.

4 MEASUREMENT PROCEDURE

Several segments in one tunnel ring consist of an instrumented ring where pressure sensors were installed. The positions of the sensors in the ring are shown in Figure 3.

These pressure sensors in a stainless steel housing (see Figure 4) were permanently positioned using epoxy resin in holes drilled in the concrete segments. They can be used for measurements even after initial pressure monitoring. Before installation and measuring, a complete system test and calibration was carried out. One segment underwent a competency and waterproofing test by applying a pressure of 1 MPa for 24 hours. The remaining segments consequently

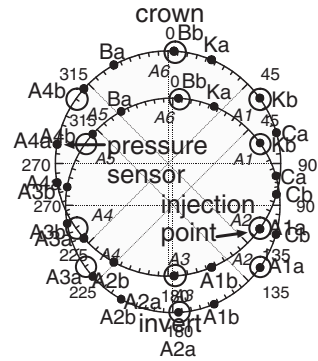


Figure 3. Distribution of pressure sensors in the lining and grout injection points on the TBM (with codes used in the graphs).

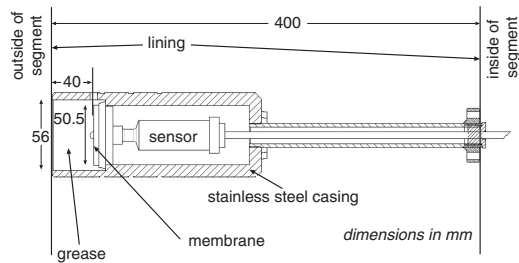


Figure 4. Cross-section of pressure sensor as mounted in the lining during the experiments.

underwent a competency and waterproofing test by applying a pressure of 0.25 MPa for 2 hours.

The pressure sensor is the Labom type DE1680-A4001-L19, with a measuring range of 1 MPa and an accuracy of 0.25% full-scale (2.5 kPa). The sensor consists of a flat membrane (50.8 mm diameter) placed on its outer surface. The membrane is placed 4 cm below the outer surface of the segment to prevent damage by the steel brushes at the end of the TBM shield as it passes by. To prevent airlocks, the space above the membrane is filled with the same grease used to seal the tail end.

During the measurements for the first tunnel tube, the sensors were sampled at 25 Hz. The relatively high frequency sampling of 25 Hz was used to measure possible high frequency events. Analysing the data, including Fourier transform, showed that such events were not present in the measurements. Therefore, a considerable data reduction of 1 of 500 samples could be used without loss of significant data. During the measurements for the second tunnel tube, the measuring frequency is reduced to 2 Hz.

The data acquisition system is based on an internal PC card (Keithley DAS 1802). This card controls the sensors and collects and archives the measured data. The internal PC card is connected to a signal conditioning box on which the sensors are connected. To reduce the risk of losing measurements, each sensor is connected to the signal conditioner box with a separate signal cable (instead of a bus system where one cable is used to connect all sensors). While the measurements are being taken, the results are presented online on a computer display in a graphical and tabular form. The

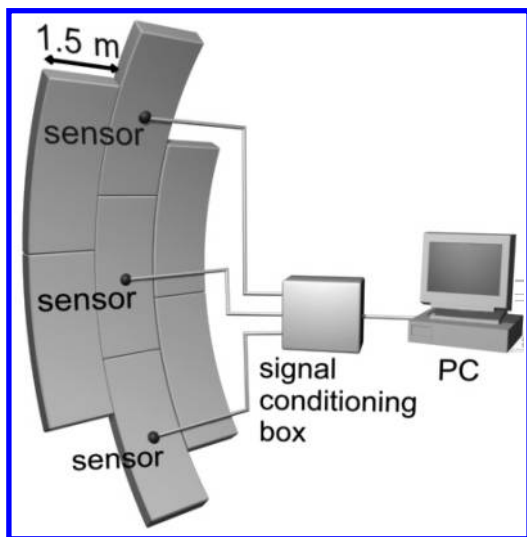


Figure 5. Outline of data measuring system (only 3 of the 14 sensors are shown).

measurement system used is shown schematically in Figure 5.

Data is recorded while the segment is still within the TBM shield. Measurements are continuously logged for 15 hours during the first phase, and for 30 hours during the second phase.

5 RESULTS

5.1 Pressures versus time and versus displacement

Measured grout pressures are shown in Figure 6 as a function of time together with the drilling velocity. The grout pressure is shown with respect to atmospheric pressure. The pressure is initially zero when the sensors are still in the TBM. Just before 06:00, the pressures become rather irregular as the instruments pass through the grease and brushes at the tail end of the TBM. There is a pressure jump at 06:00 as the instruments arrive in the tail void and the grout pressure is measured. This figure shows that grout pressures increase during drilling when grout is injected, but decrease during periods of standstill (probably due to dewatering of the grout into the soil).

Only half of the instruments are shown because the number of lines would lead to confusion if results from all the transducers were shown. Just before 05:00, the grout pressure transducers pass through the first tail brush. At approximately 06:00, they reach the grout.

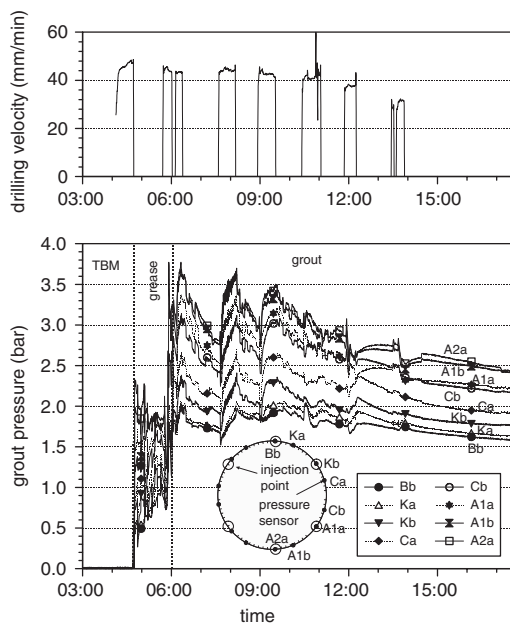


Figure 6. First tunnel tube: drilling velocity and measured grout pressures at the right side of the tunnel as a function of time.

After completion of drilling for that ring, the grout pressures decrease until drilling for the next ring starts at approximately 07:30. The segment width of a tunnel ring in the longitudinal direction of the tunnel is 1.5 m. In the decreasing pressure, a sharp rise or fall in pressure can be distinguished. Analysis of the measurements showed that this was caused by the ring building process. The rise or fall could be associated with movement of the plungers of the main jacks whilst the tunnel lining segments were being positioned.

What is remarkable is the dip in grout pressure, measured by all transducers just before drilling for a new ring started. The reason for this dip can be seen in Figure 7. This figure shows the drilling velocity and the number of strokes of the grout pumps per second as a function of displacement in the upper plot. It can be seen that when drilling started (the velocity jumps from zero to a certain value), the grout pumps do not start immediately. The first drilling is therefore carried out with too little grout, leading to a sharp decrease in the grout pressure. Once the pumps started, the grout pressure increases again.

5.2 Polar plots and gradients

Figure 8 shows the measured pressures at different times in a polar plot, and the distribution of pressures

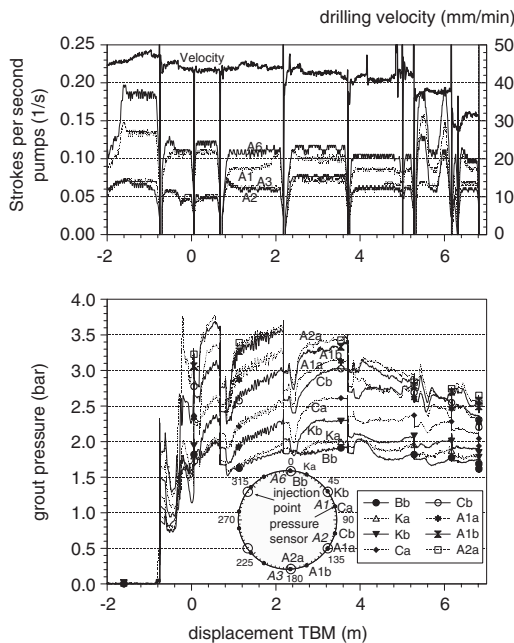


Figure 7. First tunnel tube: drilling velocity, strokes per second of the grout plunger pumps, and grout pressures as a function of the displacement (a moving average over 25 points was taken for the data on the plunger pumps to reduce data noise).

as a function of height. Actual drilling took place at 06:19:30 and 08:00:00, and there was standstill for the other points. The measurement time is presented, together with the time since the pressure transducers started to measure grout pressures (shown in brackets). Both plots showed that the pressure distribution is as expected. The pressure increases more or less linearly with depth. The pressure distribution is virtually the same on both sides of the tunnel, although there is some difference between both sides for the 07:00 measurement. What is remarkable is that the pressure gradient in the vertical direction is not constant in the measurements. The slope of the line in the lower plot of Figure 8 changes with time. The results shown in this paper are from measurements taken in one ring. This means that after installation, the same grout will be present during the measurement. If only the hydrostatic pressure in the grout determines the pressure distribution, then the gradient should be constant. However, more aspects play a role (see Section 3, Theory) and will be elucidated further in Section 7, Discussion. To investigate the gradients which did occur, the pressure gradient in the vertical direction was calculated using the least square method over all measurement points. The results are shown for the first tube in Figure 9, together with pump activity by the pump for grout

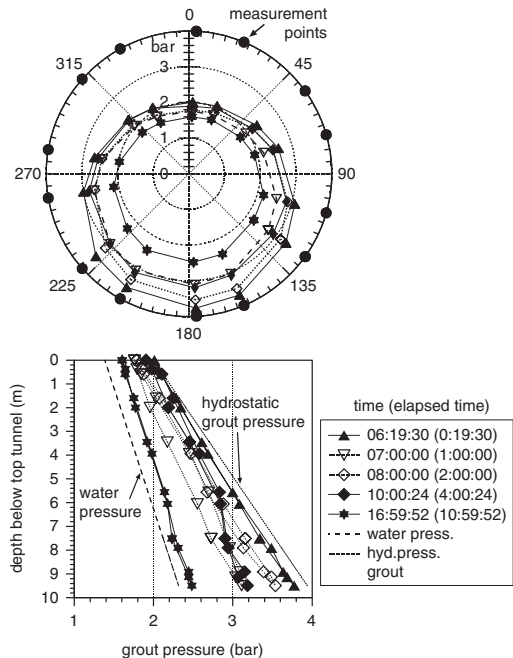


Figure 8. First tunnel tube: polar plots and pressures as a function of height at various time intervals. The lower plot also shows the water (pore) pressure and the hydrostatic pressure in the grout starting from 2 bar at the top as a reference.

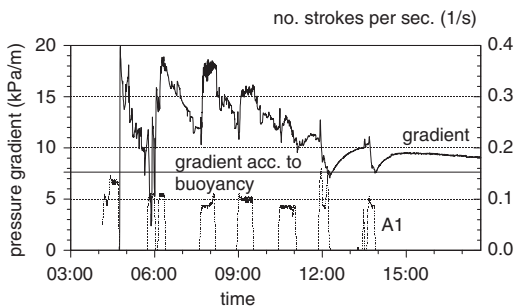


Figure 9. First tunnel tube: pressure gradient over the tunnel lining at one location, and pump activity for one of the injection points (A1) as a function of time.

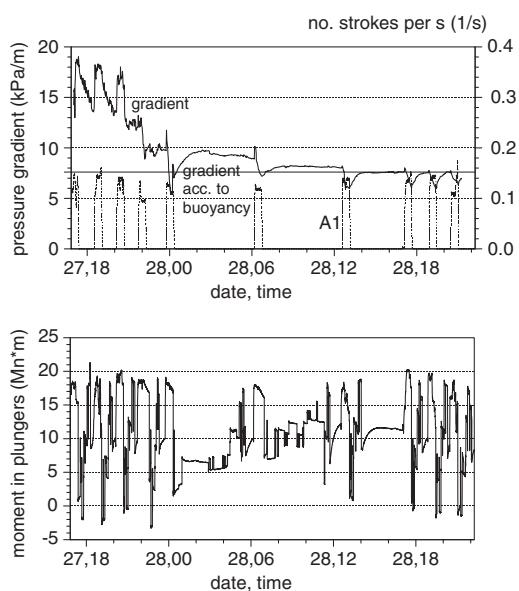


Figure 10. Second tunnel tube: pressure gradient over the tunnel lining at one location, and pump activity for one of the injection points (A1) as a function of time (upper plot). Momentum in vertical direction that is exerted on the lining by the plungers in the TBM (lower plot). A positive momentum means that the forces on the lower part of the tunnel are higher than on the upper part.

injection line A1 (the pump for A1 was selected to be reference when the pumps are on, although another pump could also have been chosen). The results show that the vertical pressure gradient generally decreases in time, and thus also as the distance between the TBM and the instrumented ring increases.

It is noticeable that up to 12:00 when drilling starts (and therefore activity from grout pump A1), there is a sharp increase in the pressure gradients. There is a

decrease for the last rings. Possible explanations are dealt with in Section 7, Discussion.

The gradients were also determined for the second tunnel tube. The results for this tube are shown in Figure 10. For the second tunnel tube, it was possible to take measurements over a longer period where more tunnel elements were placed. The date is also given because the measurement was performed over a two-day period. The results from this second tube were closely comparable to the results from the first tube, although the gradient resulted in even lower values. This will also be dealt with in Section 7, Discussion.

6 GROUT RHEOLOGY

The rheological properties of the grout are an important factor with respect to backfill grouting. The grout has to distribute uniformly around the tunnel lining, and has to provide resistance against uplift forces further behind the TBM. Grouts are basically hyper-concentrated two-phase solid-fluid mixtures, where fine cement, fly ash and other additives lower the permeability of the grout. Essential parameters characterising the flow properties of grouts are yield stress and viscosity. Modelling as a Bingham fluid suffices. The yield stress is the governing parameter in the tail void because of small flow velocities. The time-dependency of the yield stress has to be accounted for when back-filling. The yield stress of fresh grout mortars is typically in the range 1–3 kPa. This relates to failure of the grout interior. Workability of mortars is typically four hours.

The grout used at the Sophia Rail Tunnel is a grouting mortar made in accordance with specifications. With respect to frictional properties, the experiments described in this section showed that a distinction can be made between flow along smooth impermeable boundaries, and flow of pressurised grout along granular soil: along smooth impermeable boundaries, the flow of grout encounters little resistance (pipes, flexible hoses). This is due to the occurrence of a tiny lubricating liquid film.

Along soil boundaries, the friction is higher and is of the same order as the yield stress (this is our conclusion after analysing measured grout pressure distributions in tunnelling projects: Bezuijen & Talmon 2001 and Talmon et al 2001). A lubricating liquid film cannot develop as the grout pressure is higher than the pore pressure of the soil around the tunnel, and the liquid flows into the soil. As a result, the shear stress remains high and is governed by the internal failure mechanism of the grout.

Grout was collected from the production facility for rheological testing. The samples were taken just before the grout was sent to the TBM. The yield stress of the grout was determined by vane testing. The results of

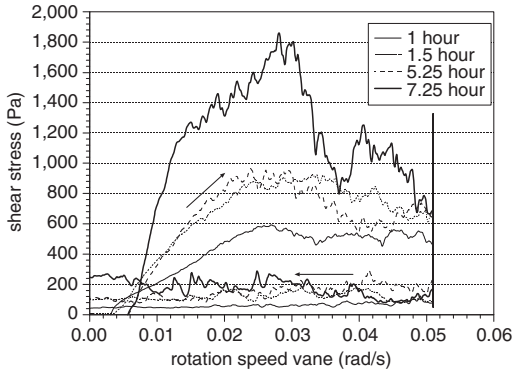


Figure 11. Registration of shear stresses measured by vane testing, peak values applicable to grout-soil interface, lower values applicable to grout-lining interface.

a number of consecutive vane tests on one sample are given in Figure 11. The rotational speed of the vane is given on the abscissa. The measured shear stress as measured with a rotoviscometer (Haake M1500, vane FL10) is shown on the ordinate of the graph. In the first part of the experiment, the rotational velocity of the vane increases linearly with time (from zero up to 0.05 rad/s in 1 minute). During this part of the experiment, the stress increases until a peak is reached. A breakdown of the grout's internal structure then commences because a slip plane is produced. This peak represents the shear stress required for characterising the yield stress at the grout-soil interface. In the second part of the experiment (when the rotational speed remains constant for 5 minutes), further breakdown of the internal structure in the slip plane occurs. In the third part of the experiment (when the rotational velocity decreases linearly to zero within 1 minute), the shear stress is constant. This shear stress is representative for the flow along smooth surfaces, such as the tunnel lining and pipe walls (the slip plane produced by the vane is smooth).

From Figure 11, it can be concluded that the final set of grout (hardening) commences after approximately 5.5 hours. After this time, the yield stresses increase quasi-linearly with time. During the first period of the final set (shown in Figure 11), the grout still has fluid-like properties that are quantified by increased rheological properties. In this case, the final set commences close to finalisation of drilling of the second ring following grout injection (transit of the grout from the production facility to the TBM takes about one hour).

Another way to obtain data on friction with smooth surfaces is by pipe-viscometer testing. The flow resistance of back-fill grouts was measured in a pipe-viscometer with an inner diameter of 100 mm

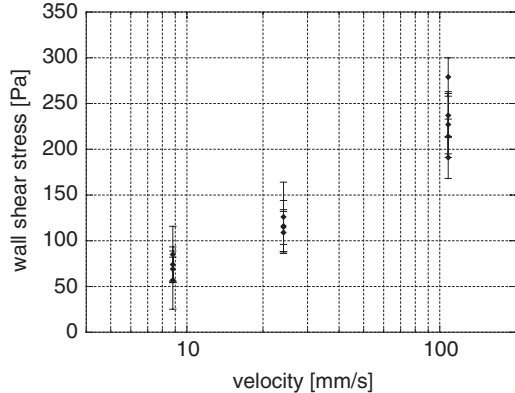


Figure 12. Example of data obtained from pipe-viscometer grout flow tests: portland-type mortar, smooth pipe, (see text).

(Talmon et al 2001). A range of grout flow velocities (2 mm/s–100 mm/s) was tested. The smallest velocity is comparable to the advance rate of the TBM. Such velocities are expected at some distance from the injection openings. In the immediate vicinity of the injection openings and in the supply pipelines, the velocities are approximately two orders of magnitude larger.

An example of results from one of the test series is given in Figure 12. It concerns the flow of grout mortar in a smooth pipe, fitted with pressure gauges. The graph depicts the results for the wall shear stresses obtained from different pairs of pressure gauges, together with the root-mean-square values.

The results show that wall shear stresses are an order of magnitude smaller than the yield stress of grouts. It can be concluded that a lubricating film has formed along the wall, the rheology of which will be governed by cement-like fluid in between the coarse grains of the grout. Consequently, such tests only produce data on flow resistance between the lining and the grout, and of course in supply pipes. The latter is important, because grout pressures in most TBMs are monitored using pressure gauges mounted on the supply lines.

Apart from hardening, the rheological properties of the grout can also be determined by fluid loss of the grout due to dewatering. Research is currently underway into ways of quantifying this dewatering and the influence on grout properties.

7 DISCUSSION

7.1 Total or pore pressures

When taking field measurements, it may be necessary to compromise between the ideal measurement location and a location where the sensors can survive.

Looking at the location of the membrane as shown in [Figure 4](#), two questions can be raised:

1. What is the influence of the grease between the grout and the membrane on the measurement results?
2. What is the pressure measured, a pore pressure or a total pressure?

Shear stresses that develop between the grease and the casing can influence the measurement results. However, we have no indication that this has happened. As can be seen from the measurement results, [Figure 6](#) and [Figure 7](#) also show small fluctuations that would not be present if the results were influenced by shear stresses. The stiffness of the casing and membrane is such that the pressure is transferred from the grout to the membrane without significant deformation of the grease. Such a deformation would be necessary before shear stresses can develop.

It is argued in literature that these relatively small pressure gauges only measure the pore pressures, and not the total stress. This particularly occurs when there has been some hardening of the grout. Special, relatively large sensors have been developed to measure the total stresses (Hasimoto et al 2002). However, the sensors used in the field tests described in this paper also measure total stresses. Due to the viscosity of the grease, it cannot penetrate into the grout along the grains of the grout. The stress on the grease is therefore the pore pressure exerted by the pore fluid and the grain stress exerted by the grains, i.e. the total stress. There was no bridging of the grout grains (which would lead to a lower effective stress near the sensor than elsewhere in the grout) due to the stiffness of the measurement device. If the pressure gauges only measured the pore pressures it would be impossible to measure a gradient lower than 10 kPa/m.

The arguments presented above are no real proof that the grease has no influence and that a total pressure is measured. This, however, was confirmed by the measurement results. The measurement results would be difficult to explain if the grease had exerted an influence or if only pore pressures had been measured.

7.2 Pressures

At the location of the instrumentation, the estimated effective pressure on top of the tunnel lining was approximately 200 kPa (2 bar) (Bezuijen & Talmon 2001). This is close to the grout pressure applied during drilling on top of the tunnel (instrument Bb in [Figure 6](#) and [Figure 7](#)). When drilling stops, the grout pressures decrease. This decrease is largest at the pressure gauges at the lower part of the tunnel. This will be the reason that the reported settlements at this ring were only limited.

The lower plot in [Figure 8](#) shows that the grout pressures are above the pore pressures at that location, although the difference is only small for the last measurement (time = 16:59:52). It also shows clearly that the measured pressures are always lower than the hydrostatic pressure in the grout if a 2 bar grout pressure is assumed at the top.

7.3 Gradients

The grout pressure on top of the tunnel is an important parameter that influences the surface settlement. The vertical pressure gradient is important for understanding the grouting process, but together with the absolute pressure, also determines the stress distribution in the soil. The latter is important for understanding soil-structure interaction for adjacent foundations.

The volumetric weight of the grout used was 21.5 kN/m³. In case the hydrostatic pressure determines the vertical pressure gradient, the gradient should be 21.5 kPa/m. As can be seen from [Figure 8](#) and [Figure 9](#), this value is never reached during these measurements. A likely reason for this discrepancy are the buoyancy forces explained earlier. When there is also still a grout flow however, the pressure distribution will not be a hydrostatic distribution (Talmon et al 2001). During drilling, the pressure distribution close to the TBM is governed by the grout flow from the grout injection points around the tunnel lining. If there is a downward directed flow, the pressure (corrected for hydrostatic pressures) has to decrease to maintain the flow.

The flow model described by Talmon et al (2001) was used to simulate the grout pressures. The parameters used are summarised in [Table 1](#). The density and rheological parameters of the grout were determined from samples taken from the construction site. The shear stress as determined with the vane tests was used to describe the friction between the grout and the soil. The result from the pipe flow tests was used for the friction between the grout and the lining. The distribution of grout injection flow rates over the six injection ports A1 to A6 (see [Figure 3](#)) has been read from the strokes made by the grout delivery pumps (see [Figure 7](#)). As a representative distribution, the following values were used: A1 = 0.2, A2 = 0.133, A3 = 0.133, A4 = 0.133, A5 = 0.2, A6 = 0.2, these values are relative to the whole flow rate, which is set to 1.0. Together with the flow resistance of the grout, this distribution governs the deviation of the pressure distribution from hydrostatic. The vane-measurement results (see [Figure 11](#)) revealed that the yield stress was 800 Pa up to a grout age of 5.5 hours. Once this age was reached, the yield stress began to increase. At an age of 7.5 hours, the yield stress was 1.8 kPa and increased with time. The input parameters of the flow model are listed in [Table 1](#). The results are given in [Figure 13](#) and show

Table 1. Parameters used in grout flow calculation.

Parameter	value	dim.
Diameter lining ($D = 2R$)	9.45	m
Thickness grout layer (s)	0.16	m
Density grout (ρ_{gr})	2190	kg/m ³
Yield stress at grout-lining interface, at injection	0.1	kPa
Yield stress at grout-soil interface, at injection	0.8	kPa
Onset hardening, time since injection	4.5	hour
Hardening rate grout	0.4	kPa/h
Grout pressure at top	1.8	bar
Drilling velocity	$7.2 \cdot 10^{-4}$	m/s

Table 2. Additional parameters used in calculations.

Parameter	Value	dim.
Thickness lining (sl)	0.4	m
Density concrete	2400	kg/m ³
Grout pressure at top	1.8	bar

The model described to calculate the influence of the buoyancy forces on the pressure distribution does not predict a constant vertical pressure gradient as measured. The gradient is assumed to be constant over the circumference (Equation (1) showed that $dP/d\alpha$ is constant) and would therefore vary over the tunnel height. The maximum gradient is found at 90 and 270 degrees (see Figure 8, upper plot). At these points, the gradient can be written as:

$$\frac{dP}{dz} = \rho_{gr} g - \frac{\tau}{s} \quad (5)$$

With ρ_{gr} the density of the grout and g the acceleration of gravity.

The additional parameters used in this calculation to calculate the gradient are presented in Table 2. The grout pressure at the top is now lower, because this pressure decreases when grouting stops.

Using these parameters, it can be calculated that the buoyancy force $K = 1239$ kN/m. Using Equation (4), this results in a shear stress τ of 2.22 kPa between the soil and the grout. Using these results and Equation (5), the maximum gradient is found to be 7.6 kPa/m if buoyancy forces only determine the gradient. This is less than the minimum gradient measured during standstill for the first tunnel tube (Figure 9). Therefore, it can be concluded that the measured gradient for that tube is also influenced by moments in the lining as it is fixed by the TBM on one side and the hardened grout on the other. For the second tube where the measurement interval is longer (Figure 10), the gradient during standstill is equal to the calculated buoyancy gradient.

These buoyancy calculations led to another result. The calculated shear stress is more than the yield stress measured (see Section 5: Results). This means that the tunnel would not be stable and would be lifted by buoyancy forces. Another way to look at the results is to determine the yield stress in the grout from the measurements. If the rheological properties of the grout are the same as for water, the gradient would always be 21.5 kPa/m with or without drilling. Assuming that the tunnel attempts to move upwards due to buoyancy forces, the minimum measured gradient results in a mobilized shear stress using Equation (5). This can be less than the yield stress, but not more. From using Equation (5) it can be concluded that a measured

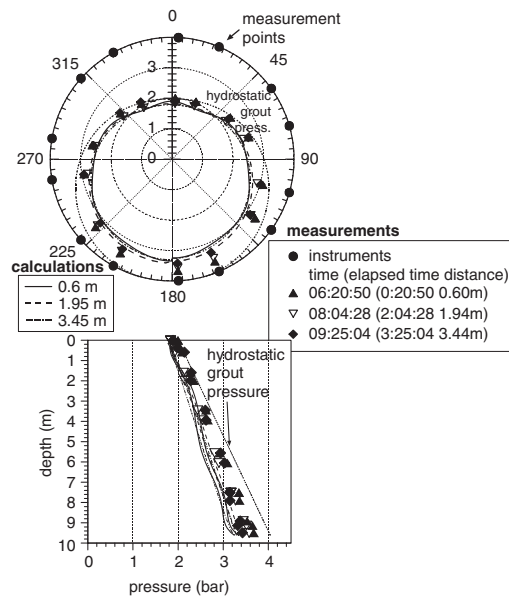


Figure 13. First tunnel tube: measured and calculated grout pressures compared during drilling (see text).

close correlation with measurements obtained during drilling. In Figure 13, the measurement legend shows the measurement time, the time elapsed since the grout pressure transducers entered the grout, and the distance to the back of the TBM. The distance to the back of the TBM is given for the calculations only. There is slight asymmetry in the calculation model. This results in a small pressure difference at 180 degrees in the calculated pressure in the polar plot. In the lower plot, this asymmetry results in two lines for each calculation (one for 0 to 180 degrees, and one for 180 to 360 degrees). This is an artefact of the numerical model only. The two lines are presented to show the accuracy of the solution procedure used.

gradient of 12 kPa/m around 08:00 (see Figure 9) corresponds with a minimum yield stress of 1.5 kPa. The minimum in the gradient measured just after 12:00 of 7.6 kPa/m means that the yield stress is then 2.2 kPa or more. These values for the yield stress are higher than measured with the vane. Possible reasons for these discrepancies are:

The rheological parameters are determined by atmospheric pressure. Dewatering in the field situation can lead to higher yield stress.

Based on flow experiments, the shear stress along the tunnel lining and the grout is neglected. It is possible that this changed in no-flow conditions.

From the measurements presented here, it appears too simple to state that the pressure distribution close to the tunnel is governed by the TBM and that buoyancy is dominant further away. The pressure close to the TBM is dominated by the grout flow during drilling, but is influenced more by buoyancy during standstill. The model presented on the buoyancy is purely 2-D. It only takes one ring into account and not the possible bending moment along the tunnel axis. This appeared to have a substantial influence close to the TBM. Further away from the TBM, however, the influence of the bending moment in the lining decreases during standstill and the gradient approaches the value calculated with Equation (5).

During actual drilling, the gradient is highest in the first lining elements that were placed after the instrumented ring. When the TBM is further away from the instrumented ring, however, the gradient is lowest during drilling. These low gradients can be seen around 12:00 and 14:00 for the first tunnel tube, and for the lining elements placed at 28,00:00 hour and later for the second tube (see Figure 9 and Figure 10). The high gradients in the grout pressure close to the TBM are caused by the injection strategy. An even distribution of grout over the lining will lead to a hydrostatic pressure distribution. There was no even distribution here as more was grouted to the top than to the bottom (see Figure 6). The pressure gradient was therefore slightly smaller than according to hydrostatic pressure. As distance increases from the TBM, the grout flow has virtually no influence on the pressure distribution. Buoyancy forces will be dominant for the pressure gradient in the grout, as well as forces exerted by the TBM on the lining, which can lead to lining movements and consequently a change in the pressure distribution e.g. if larger jack forces are used in the bottom part of the TBM to compensate for a tendency to penetrate too deeply because of its weight. These forces will induce a moment in the lining and will lead to lining movement until the pressures on top of the lining have increased to compensate for this moment. This latter effect leads to the extremely low pressure gradients measured during actual tunnel drilling. This is also shown in Figure 10. The lower plot shows the momentum exerted by the

TBM on the lining. This momentum is calculated using the pressures and positions of the 28 main hydraulic plungers used to push the TBM forward against the lining during drilling. The result is presented on the same time scale as the gradient in the upper plot. The plot shows that the momentum increases by drilling, meaning that larger forces are used at the lower half of the tunnel than on the upper half. It can be seen from the plots that a change in momentum does not directly influence the gradient in the grout pressure, but if the change is present over some time (as is the case during drilling), it will influence the grout pressure gradient.

8 CONCLUSIONS

The grout pressure measurements presented in this paper and comparison with calculations lead to the following conclusions:

1. Reliable measurements were obtained for the grout in the liquid phase and the start of the hardening phase. Measurements were taken over too short a period to provide data for the whole hardening phase of the grout. It is also uncertain whether the instrumentation used would survive the hardening phase.
2. It is likely that total stresses were measured, and this corresponds with the measurement results.
3. The grout pressures are not only influenced by the injection strategy and flow, but also by forces exerted on the lining during placing of segments or drilling.
4. Drilling commenced before start of the grout injection pumps. This led to a decrease in grout pressure at the start of drilling. This pressure decrease could be measured up to 5 m behind the TBM.
5. Injection strategy can influence the pressure distribution close to the TBM (<5 m) during drilling. During standstill and further away from the TBM, buoyancy forces and bending moments in the lining govern the pressures. This results in pressure gradients considerably lower than those determined according to hydrostatic pressure distribution in the grout.

ACKNOWLEDGEMENTS

The authors would like to acknowledge Project Organization High-Speed Line (HSL-Zuid), ETAC Grout Injection BV and Project Organization Betuweroute (NS Railinfrabeheer) for financing development of the computational model, HSL-Zuid, NS Railinfrabeheer, North/Southline of Amsterdam, and RWS (Public

Works Department of the Ministry of Transport and Public works) for financing the COB research at Sophia Rail Tunnel, and Tubecon (contractor for the Sophia Rail Tunnel) for their co-operation.

REFERENCES

- Bezuijen A. & Talmon A.M. 2001, Grout pressure measurements, Sophia Rail tunnel (*in Dutch, Delft Cluster Report 710504/10*),
- Talmon A.M., Aanen L. Bezuijen A. Zon W.H. van der. 2001, Grout pressures around a tunnel lining *Proc. Int. Symp. on Modern Tunneling Science and Techn. Kyoto*.
- Bakker K.J., Teunissen E.A.H. Berg P. van den, Smits M.Th. J.H. 2001, The Second Heinenoord tunnel; the main monitoring results, *Proc. XV ICSMGE, Istanbul*.
- Van Dijk B.F.J. & Kaalberg F.J. 1998, 3D geotechnical model for the NZ line in Amsterdam *Proc. NUMOG Udine*.
- Hashimoto T., Nagaya J. Konda T. Tamura T. 2002, Observation of lining pressure due to shield tunnelling, *3rd Int Symp. on Geotechnical Aspects of Underground Construction in Soft Ground, IS-Toulouse*.
- Kaalberg F.J., Hentschel V. Netzel H. and van Dijk B.F.J. 2001, Big Brother for TBM's, *Tunnels & Tunneling International Vol 33 (2001)1 pp. 20–23*.
- Stive R.J.H. 1999, Design features of the Sophia Rail Tunnel in the Betuweroute. *Tunnelling and Underground Space Technology, Vol 14, No.2, pp. 141–149*.

Grout the foundation of a bored tunnel

A. Bezuijen

GeoDelft

A.M. Talmon

WL/Delft Hydraulics

ABSTRACT: Grout pressures are influenced by consolidation. A test method has been developed to measure the consolidation properties of grout and a calculation model to quantify the influence of consolidation on the grout pressures. The consolidation of the grout and the properties of the surrounding soil determine the grout pressure decrease during stand still of the TBM and the final pressures.

1 INTRODUCTION

The foundation of bored tunnels is assured by grouting of the tail void surrounding the lining. The grouting determines the loading on the lining and is one of the influences that determine surface settlement. Looking at grout from a foundation point of view it is not a 'great' foundation material. Usually 30% more grout than the volume of the tail void has to be applied and after applying the grout its volume can be reduced with 5 to 10% due to bleeding caused by consolidation. Furthermore, the grout pressures as measured during grouting and afterwards are not very well understood.

Based on this situation it was decided by the COB (Centre of Underground Construction) in the Netherlands and Delft Cluster (a foundation in which the leading Delft Institutes on civil engineering co-operate) to perform field measurements and model tests on the grouting process.

Field tests were performed by instrumentation of one of the lining elements and measuring the grout pressures during boring and afterwards. The grout pressures during drilling could be explained by a flow model taking into account the Bingham flow properties of the grout and the hardening (Talmon *et al.*, 2001). It was shown that the buoyancy forces can explain the distribution of grout pressure around the tunnel after boring (Bezuijen *et al.*, 2002). When boring is halted, the grout pressures decay slowly due to fluid loss. Fluid loss and pressure decay are governed by consolidation. Remarkable is that the vertical gradient in the grout pressures decreases to values lower than the gradient in the pore pressures.

Grout consolidation tests, their results and interpretation are the subject of this paper.

2 TESTS PERFORMED

Tests have been performed to investigate the hardening and bleeding of conventional grout, see Figure 1 and Figure 2. In this test a grout layer of 0.2 m is loaded mechanically with a constant load of 1–3 bar. The expelled water is a measure of the consolidation of the grout. After several minutes of consolidation the sample was unloaded and the shear strength of the grout was measured at different locations in the grout. An example of results of such a test is shown in Figure 3 and Figure 4. Figure 4 shows the amount of expelled pore water as a function of time and the applied pressure. In this test a pressure of 300 kPa was applied. Pressure was relieved several times to be able to take the vane tests. Figure 4 shows the measured shear strength after various times that pressure was

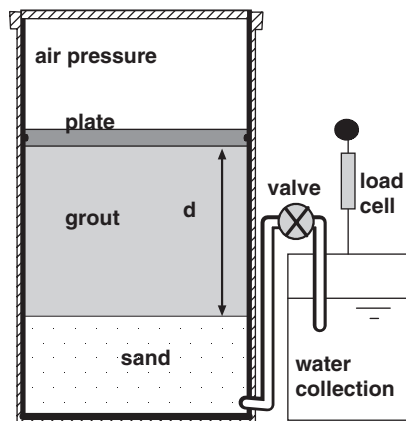


Figure 1. Measurement principle.

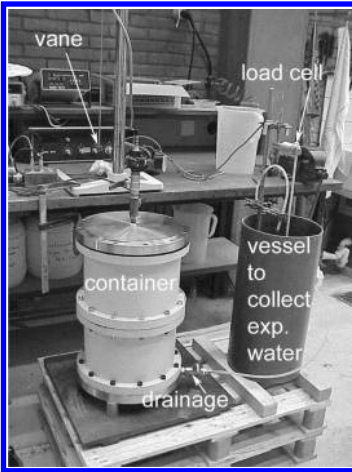


Figure 2. Experimental setup.

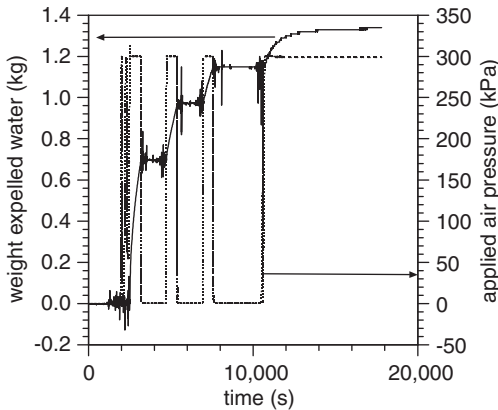


Figure 3. Test result expelled water as a function of time and applied pressure.

applied. In this test it was focussed on the lower values of the shear strength. Therefore only shear strengths up to 6 kPa were measured and presented in the plot.

The type of grout tested here was tested before at atmospheric pressure (Bezuijen *et al.*, 2002). In that test it appeared that the measured shear strength remained more or less constant until 5.5 hours and after that time the hardening of the grout started.

Comparing the result from the test at atmospheric pressure with the results of the tests at 1–3 bar over pressure it became clear that the increase in strength in the over pressure case is caused by consolidation of the grout and not by the hardening of the grout. To understand the grout properties just after injection in the tail void it is therefore necessary to understand consolidation. If the grout layer is consolidated it will have

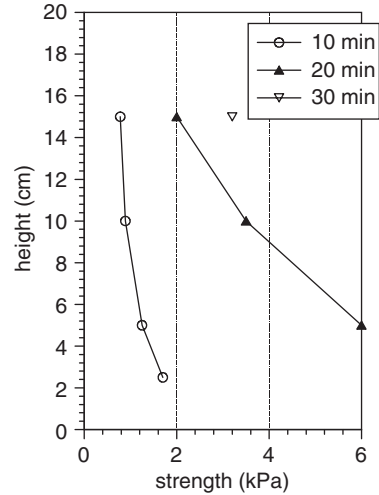


Figure 4. Strength development as measured with a vane.

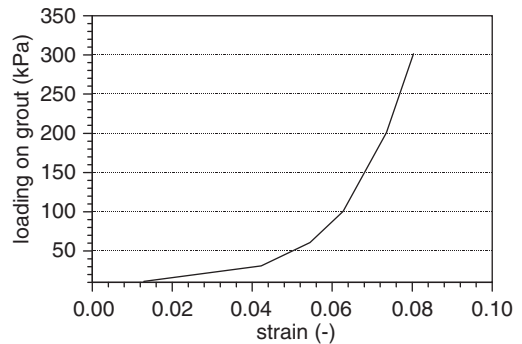


Figure 5. Example measured stress strain curve of grout in an oedometer test.

certain strength to act as a foundation for the tunnel lining, even before hardening of the grout commences. If it is not consolidated it is possible that the shear strength is too low to counterbalance the buoyancy forces of the tunnel. Another important consequence of consolidation is an increase of flow resistance, which directly affects the pressure distribution behind the TBM when drilling.

3 CALCULATION MODEL

3.1 General

During consolidation grout has a non-linear stress-strain curve. The curve as found in a standard oedometer test is shown in Figure 5. To implement such non-linear relations leads to a set of equations that can

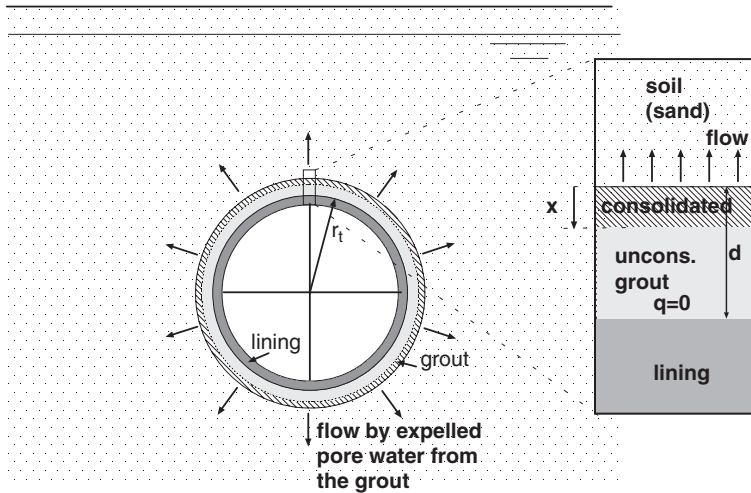


Figure 6. Sketch of consolidating grout around a tunnel lining and detail.

only be solved numerically, such a numerical simulation is described by Bezuijen (2003). Here we use a simplified approach, which appears within some limits suitable to describe the observed phenomena.

We assume that just after injection the grout behaves as a liquid. There will be no grain stress. Consolidation leads to the expelling of water and a decrease in porosity. It is assumed that the grain stress remains very small until a certain porosity. At that lower porosity the grains have contact with each other and the consolidation stops.

Such a description will be quite accurate when the amount of fines is limited, but will be less adequate in case a lot of clay mineral is present in the grout.

When a material as described above is subjected to 1 side consolidation (grout can only lose water into the surrounding soil, not to the lining). There will be a front of consolidated grout that moves from the surrounding soil to the lining.

3.2 Description of model, grout tests

Consider a part of the grout as it is applied around the tunnel, see Figure 6. Such a section is comparable with a section tested in the experiments described above. It is further assumed that the permeability of the sand is much larger than the permeability of the grout (the consequences of this assumption were analyzed in Bezuijen 2003 and it was shown that this assumption was true for a subsoil of clean sand). For such a situation the flow through the grout can be written as:

$$q = k \frac{\Delta\phi_1}{x} \quad (1)$$

With q the specific discharge through the consolidated grout, k the permeability of the grout, x the thickness of the consolidated grout layer and $\Delta\phi$ the pressure head difference between the non consolidated grout and the soil. The change in thickness of the consolidated grout layer is governed by the continuity equation:

$$q = \frac{n_i - n_e}{1 - n_e} \frac{dx}{dt} \quad (2)$$

With n_i the initial porosity of the unconsolidated grout, n_e the final porosity of the grout (after consolidation). Combining these equations lead to the differential equation:

$$\frac{x}{k} \frac{dx}{dt} = \frac{1 - n_e}{n_i - n_e} \Delta\phi \quad (3)$$

With the boundary condition that $x = 0$ at $t = 0$ and constant $\Delta\phi$ the solution is:

$$x = \sqrt{2k \frac{1 - n_e}{n_i - n_e} \Delta\phi t} \quad (4)$$

In an experiment it is possible to determine the initial and final porosity and by fitting the results of measurements to the results of the equation it is possible to determine the permeability of the grout.

3.3 Description of model, field situation

When grout is injected into the tail void with an excess pressure compared to the hydrostatic pressure, the situation is comparable with the situation in the test.

However, there is a difference: when the grout starts to consolidate this will lead to unloading of the surrounding soil, thus $\Delta\phi$ is not constant anymore. Again the real situation is a bit simplified and a cylindrical symmetric elastic unloading is assumed around the tunnel. In such a situation the relation between deformation and stress reduction can be written as (Verruijt, 1993):

$$\Delta\sigma = 2 \frac{\Delta r}{r} G \quad (5)$$

Where $\Delta\sigma$ is the change in pressure Δr the change in radius, r the radius of the tunnel and the grout and G the shear modulus of the soil around the tunnel. In case of a consolidating grout, Δr will be equal to the thickness of the water layer that is expelled from the grout. Using equation (2) and (5) this leads to the following relation between the pressure that is exerted on the grout as a function of the thickness of the consolidating layer:

$$P = \rho g \phi_0 - 2 \frac{G}{r} \frac{n_i - n_e}{1 - n_e} x \quad (6)$$

Where ϕ_0 is the difference in piezometric head between the grout pressure and the pore pressure in the sand, ρ is the density of water and g the acceleration of gravity. Combining the Equations (1), (2) and (5) leads to the differential equation that is valid for the field situation:

$$\frac{x}{k} \frac{dx}{dt} + \frac{2}{\rho g r} \frac{G}{r} x = \frac{1 - n_e}{n_i - n_e} \phi_0 \quad (7)$$

From this equation it can be concluded that consolidation can be limited by the stiffness of the soil. $dx/dt = 0$ when consolidation stops. For that situation it can be written:

$$x = \frac{\rho g r}{2G} \frac{1 - n_e}{n_i - n_e} \phi_0 \quad (8)$$

Thus a high shear modulus of the subsoil will lead to only a limited consolidation because the driving force for the consolidation, the excess pressure disappears due to unloading of the soil and a low shear modulus will lead to more consolidation of the grout.

The solution for differential Equation (7) with the boundary condition $x = 0$ at $t = 0$ is less straightforward than for Equation (3). It can be written as:

$$\frac{x}{k} \frac{dx}{dt} + Bx = C\phi_0 \quad (9)$$

with

$$B = \frac{2}{\rho g r} \frac{G}{r} \text{ and } C = \frac{1 - n_e}{n_i - n_e}$$

The solution for Equation (9) and the boundary conditions mentioned before reads:

$$x(t) = \frac{-t k B^2 - C \Phi \ln \left(C \Phi \text{LambertW} \left(\frac{e^{\left(\frac{t k B^2}{C \Phi} + \ln(-C \Phi) - 1 \right)}}{C \Phi} \right) \right) + C \Phi \ln(-C \Phi)}{B} \quad (10)$$

Where Φ is used instead of ϕ_0 .

The LambertW function in this solution is defined as:

$$\text{LambertW}(x) \cdot e^{\text{LambertW}(x)} = x$$

and the requirement that the function is analytical at $x = 0$.

4 COMPARISON WITH MEASUREMENT DATA

To compare the data from a grout consolidation test with the simulation, the measurement data without excess pressure (when the vane tests were taken) were removed from the data set. The remaining data were fitted to Equation (4). The results are shown in Figure 7.

It appears that in the beginning of the experiment the results fit quite well with theory. After approx. 2,000 s a deviation starts, because X becomes comparable to the grout thickness in the experiment (all grout is consolidated). From this result it can be concluded that the theory developed, although it has some simplifications, can be used to describe the behavior of consolidating grout.

5 CONSEQUENCES FOR FIELD CIRCUMSTANCES

Field measurements on grout pressures show an increase in pressure during boring and a decrease

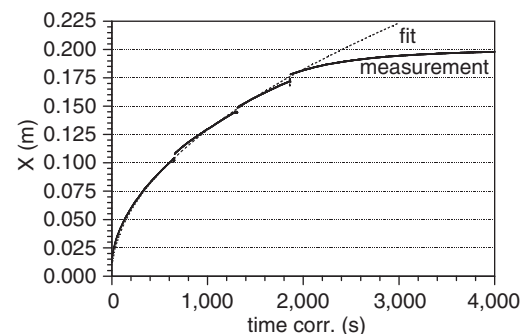


Figure 7. Experimental data on consolidation fitted to theory. X is the thickness of the consolidated layer.

during stand still of the TBM. The rate of pressure decrease is different in different field situations, see Figure 8. In this figure the rate of decrease seems comparable over the measurement interval, but that is not the case. The pressure decrease is much faster for the Botlek tunnel, as can be seen just after the peak, but movements of the TBM cause additional rises in the grout pressure in the shown time period.

It is likely that this pressure decrease is caused by consolidation of the grout. If this is the case, the stiffness of the subsoil has an influence, as can be seen from Equation (7), (8) and (10). A calculation was run for the situation at the Botlek Rail Tunnel using the parameters as presented in Table 1. The permeability of the grout after consolidation and the initial and final porosity were determined from the consolidation test. The shear modulus of the subsoil is an 'educated guess'. Using these values we found that only 0.039 m of the grout layer of 0.2 m consolidates and then the driving force has stopped. The course of the consolidation front and the pressure drop due to consolidation after the boring has stopped according to the calculation model is shown in Figure 9. The calculated pressures show qualitatively agreement with the measured pressure.

Table 1. Parameters used in calculation.

Parameter	value	dim.
radius tunnel	5	M
ϕ_0	10	m
G (soil)	90	Mpa
k (grout)	$4.7 \cdot 10^{-8}$	m/s
n_i	0.327	-
n_e	0.275	-

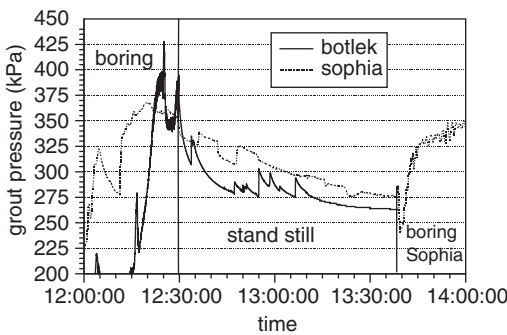


Figure 8. Grout pressure measured at the Botlek Rail tunnel compared with results from Sophia Rail Tunnel. Data is shifted so that drilling stops at the same point (first ring after the instruments came out of the lining). Pressure drop is about 10 times faster for Botlek.

The calculation was rerun with an much lower value of the shear modulus in the soil, 10 instead of 90 Mpa. In such a situation the grout pressure would remain more or less constant, which is obviously not in agreement with what is measured.

6 DISCUSSION

Consolidation of grout influences the grout pressures and a model is described, which presents the possibility to quantify this influence. Although some simplifications were necessary, it appeared that the model can describe the behavior in a consolidation test quite well. However, it should be emphasized that reality is more complex than the model. It is possible that the permeability of the soil is that low that it prevents consolidation. This can be the case when a tunnel is bored in impermeable clay, but also when a subsoil of sand is polluted with bentonite from the tunnel face. A cylindrical symmetric unloading was assumed for the subsoil, but this will not be the case. Due to buoyancy forces the tunnel will be pressed against the upper part of bored hole. This will lead to a continuous consolidation of the upper part of the grout. There will also be some consolidation during boring, which is neglected in this calculation method.

Consolidation will lead to a pressure decrease. In the calculations it is assumed that the pressures will decrease until the grout pressure is equal to the pore pressure in the soil. However, plastic deformation of the soil can prevent that such low pressures are reached. Low pressures are possible in case the subsoil consists of sand. Arching will then prevent a collapse. Low grout pressures were measured at the Sophia Rail Tunnel, see Figure 10. When boring stops, the pressures decrease to values very close to the pore pressure (the measurement at 16:59:52 in the plot). Values were closest to the pore pressure at the bottom of the tunnel.

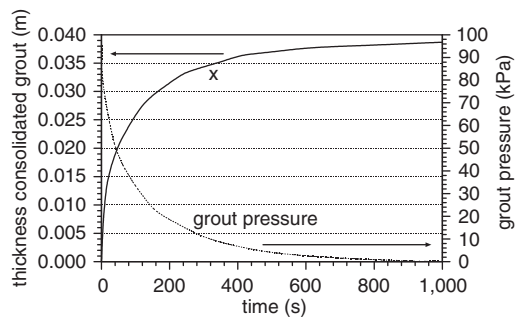


Figure 9. Calculated course of consolidation and pressure during stand still of the TBM. Parameters see text.

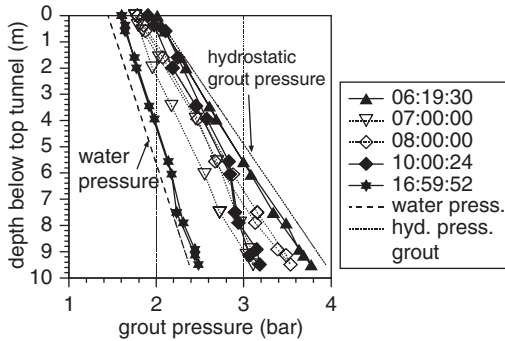


Figure 10. Measured grout pressures at the Sophia Rail tunnel. The pressure measured at 16:59:52 was measured several hours after boring has stopped.

7 CONCLUSIONS

A calculation model has been developed to quantify the influence of consolidation on the grout pressures. For conventional grout the consolidation determines the strength properties of the grout after injection. Increased flow resistance affects the pressure distribution around the tunnel lining and the increased strength of the grout reduces the stress in the tunnel lining due to buoyancy forces. The influence of hardening starts several hours after injection at a larger distance from the TBM.

The grout parameters necessary for the model can be measured with the consolidation test, as described.

For a tunnel bored in sand the normal situation will be that only a part of the grout consolidates before the grout pressures come nearly equal to the pore pressure. In such a situation the final grout pressure and thus the stress situation in the soil is not determined by the injection strategy but by the properties of the grout and the soil around the tunnel.

ACKNOWLEDGEMENT

Research was performed within the framework of the research on the Botlek and Sophia Rail Tunnel as initiated by COB (the Dutch center for underground construction). We acknowledge COB and its participants for their permission to publish the results and the members of the working groups for stimulating support.

REFERENCES

- Bezuijen A., Talmon A.M., Kaalberg F.J., Plugge R., 2002, Field measurements on grout pressures during tunnelling, 4th Int. Symp. on Geotechnical Aspects of Underground Construction in Soft. Ground – IS Toulouse, 23–25 October.
- Bezuijen A., 2003, Consolidation of grout, Theory. GeoDelft Report CO-403050/5, January.
- Talmon A.M., Bezuijen A., Aanen L & W.H. van de Zon, 2001, Grout pressures around a tunnelling, proc. IS-Kyoto 2001 conference on Modern tunneling Science and Technology, pp. 817–822.
- Verruijt A., 1993, Soil Dynamics, Delft University of Technology, b28.

Simultaneous backfill grouting, pressure development in construction phase and in the long-term

T. Hashimoto & T. Konda

Geo-Research Institute, Osaka, Japan

J. Brinkman & A. Feddema

GeoDelft, Delft, The Netherlands

Y. Kano

TAC Corporation, Okayama, Japan

ABSTRACT: Over the years it has become clear that simultaneous backfill grouting is of major importance to the design of the tunnel lining and TBM process control. Considerable research has been conducted in the last 20 years to get a grip on these two aspects. They are the key to successful settlement control, reducing the differential displacement between segments and rings, moments in the lining (in both ring- and longitudinal direction), and for optimisation of the tunnel boring process. In this paper a historical overview is given for simultaneous backfill grouting with the use of 2-component grout. An overview is given of the development of the grouting pressure with TAC (ETAC) grout in the construction phase and in the long-term, and the resulting bending moments in the lining.

1 INTRODUCTION

Simultaneous backfill grouting was carried out in shield tunnelling for the first time in 1982 in the construction of No. 4 line of the Osaka Subway in Japan. The conventional tunnelling method using mortar grouting had been expected to cause a ground settlement of 50–100 mm while tunnelling through very sensitive soft clay. The use of simultaneous backfill grouting kept the settlement in the range of 10–30 mm (Hirata, 1989). Since then, this method has been introduced in many regions of the world, such as Asia, Europe and America, reducing the settlement associated with shield tunnelling. The next step was the optimisation of the material properties of the grout.

Extensive research resulted in the development of a 2-component grout TAC (in Europe: ETAC) which gave:

- 1) A more efficient tunnel boring process because there is no clogging of the grout in the injection system
- 2) Fast, and uniform support of the tunnel lining (Hashimoto et al., 1997) (Hashimoto et al., 2002)
- 3) Settlement in the range of 0–15 mm, through of the better control of the grout injection.

A lining pressure meter with a large diaphragm (750 × 450 mm) was developed to accurately measure

the plastic backfill grouting pressure as well as the pressure acting on the lining after the grout hardening. By analysing the results of this monitoring, the mechanism of the lining pressures and their magnitude are now better understood (Hashimoto, 1993).

2 SIMULTANEOUS BACKFILL GROUTING METHOD WITH TAC AND ETAC

In Japan at present, the simultaneous injection method is usually performed with two grouting liquids. In recent years, this method has also been adopted on some projects in Asia and Europe. In Europe this type of grout is called ETAC and was developed in the Netherlands, using local materials and was first applied in the soft-ground EPB excavation of the Botlek rail tunnel (Feddema, 2001).

Figure 1 shows properties of TAC, 2-component grout. This system uses liquid A (cement, clay-sand, water and others) and liquid B (water-glass). After mixing of the two liquids, they become semi-solid (plastic state) in a few seconds, and keep this state for about half an hour. Then they become hard, generally 0.05–0.1 N/mm² by 1 hour. The gel- and hardening time can be set to meet specific project requirements.

Figure 2 shows typical equipment for simultaneous backfill grouting with TAC. The injection pipe

is attached to the tail of the TBM. If the two liquids are injected through one pipe, the pipe is often clogged due to the short hardening time of the liquids. Therefore, the pipe and the system were equipped with two extra mechanisms: one for mixing the two components just before entering the tail void and one for cleaning.

In the case of soft clay, a typical composition of backfill grouting is shown in Table 1, and Figure 3 shows an example of the ground deformation with this method.

3 DEVELOPMENT OF LINING PRESSURE

The pressure due to simultaneous backfill grouting starts acting on the circumference of the lining

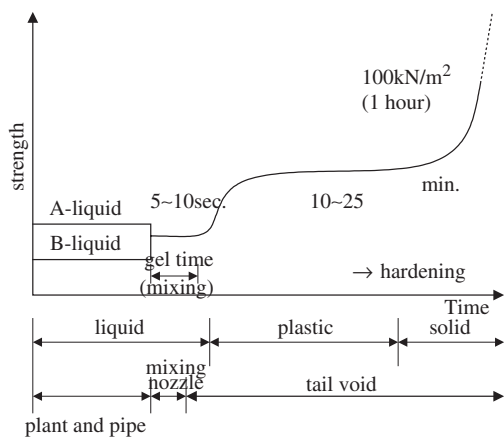


Figure 1. Properties of TAC two liquid grout.

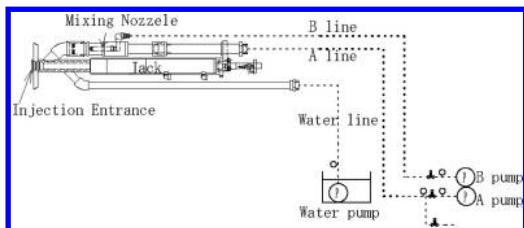


Figure 2. Equipment for simultaneous TAC grouting.

Table 1. Typical proportion of backfill grout for TAC grout.

A-liquid materials					B-liquid materials		Compressive strength (kN/m ²)		
Hardening material	Clay-sand material	Bubble forming Agent	Stabilizing agent	Water	Entrained Air	Regulated set agent	1 hour	1 day	28 days
270 kg	130 kg	0.5 kg	2.2 kg	630 Lit.	13.5%	100 Lit.	100–150	500	2500

immediately after the passage of the shield tail. The grouting pressure distribution becomes uniform shortly after the grouting because the grout is in the plastic state. With hardening, the grout holds the earth pressure and the water pressure in the ground and conveys them to the tunnel lining as shown in Figure 4. After the hardening of the grout, the lining pressure changes depending on the compression of the grout, the deformation of the lining, stress relaxation, and so on, and then reaches a steady value. The magnitude of the pressure change depends on the ground condition, e.g. hard or soft soil, and also on the magnitude of injection pressure. In the case of soft soil, the lining pressure approaches the initial stress with time regardless of the injecting pressure's magnitude. In the case of hard soil, lining pressure approaches the active earth pressure.

3.1 Development process of lining pressure and its change

3.1.1 Case on the Okawa Shield in soft clay (Hashimoto., 2001)

The construction was carried out with the slurry shield method; the TBM outer diameter was $\phi 7,150$ mm. The simultaneous backfill grouting method was implemented to fill the tail void. The overburden was approximately 15.3 m.

The excavated ground around the monitoring section was mostly Holocene clay, with strength increasing with increasing depth. The unconfined compression strength of the clay was approximately $c = q_u/2 = 50$ kN/m² and SPT N-value = 0–6. The ground was very sensitive with a high liquidity index ($I_L = 0.9$).

Figure 5 shows the soil profile and the tunnel position at a monitoring section. Major monitoring items were: earth pressure, water pressure and stress of the RC segments.

3.1.2 Observed lining pressure and earth pressure in the ground

Figure 6 shows the change in pressure with time during the tail passing, and for the following 2nd~6th

rings. The pressure during the tail passing showed a remarkable change in 4 phases as follows:

- 1) During the passing of the tail brush over the lining pressure meter
- 2) From the tail brush passing over the lining pressure meter to the end of excavation
- 3) Assembling the segments
- 4) After the process is completed

In the first phase, when the tail brush passed the lining pressure meter plate, the pressure (brush pressure included) decreased. The monitored value of the lining pressure when the tail brush completely passed the pressure meter corresponded to the backfill grouting pressure. This pressure was equivalent to the total overburden pressure (263 kN/m^2). In the second phase, the pressure decreased by $70\text{--}150 \text{ kN/m}^2$ when the tail brush passed beyond the plate. In the third phase, the pressure increased and slight change was recognized when retracting the jacks while assembling the segments. In the fourth phase, the pressure decreased. During tunnelling for the subsequent 2–5 rings, the lining pressure changed due to grouting and jack operation. A very steep inclination of 31% made it difficult to control the TBM jack operation. These difficulties caused fluctuation in the pressure on the lining. However, after the tail had passed the 6th ring, there was little further effect on the lining pressure due to the TBM excavation. Lining pressure distributions (a) after the tail passing, (b) five rings after tail passing, (c) one month after tail passing, and (d) six months after tail passing are shown in Figure 7.

In the first phase the pressure was distributed evenly all around the segment, however at the 5th ring, the pressure increased in the base of the ring because of the shore pressures required to steer the TBM.

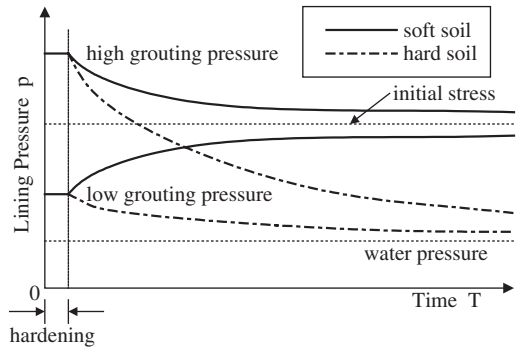


Figure 4. Conceptual figure on lining pressure change.

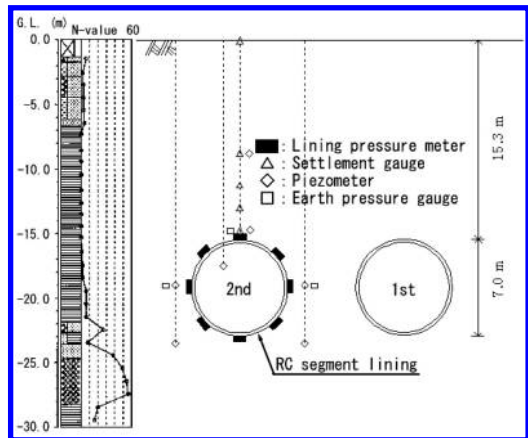


Figure 5. Soil profile at the monitoring section.

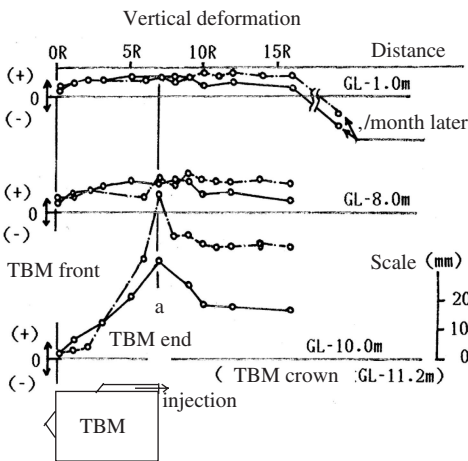
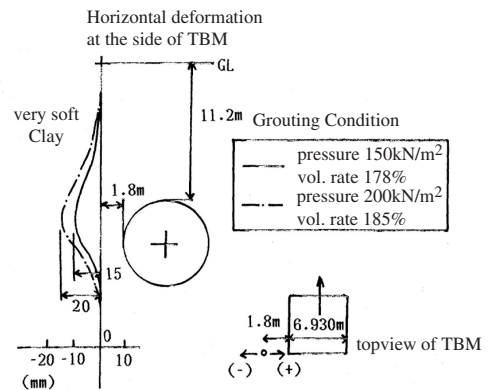


Figure 3. An example of backfill grouting pressure and deformation of ground (Nagata Shield).



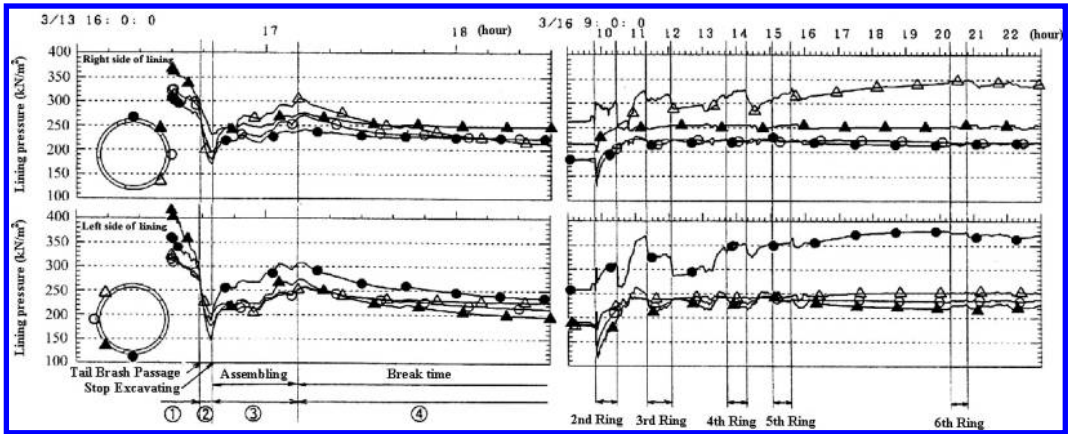


Figure 6. Lining pressure variation at tail passing and the 2nd–6th rings after the tail passing.

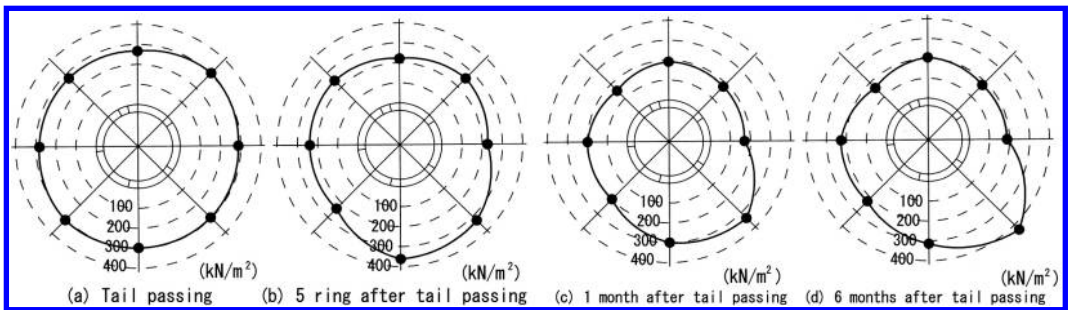


Figure 7. Lining pressure distribution at four phases.

3.2 Distribution of backfill grouting pressure

3.2.1 Tendency of distribution of backfill grouting pressure on lining

The pressure on the tunnel lining due to the backfill grouting is analysed here based on observation (Hashimoto, 2002). Figure 8 shows the notion used for each pressure p_{vg} , p_{hg} and p_{v0} , and parameters K_v , K_h .

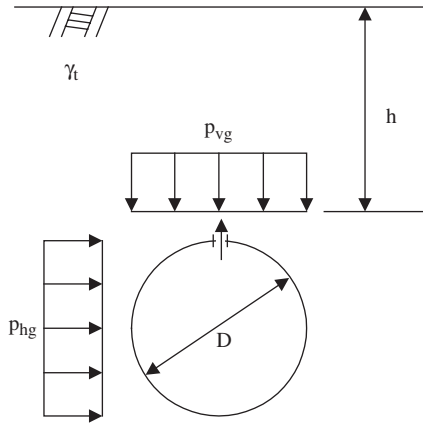
For the case grout is injected at one point a typical observation of lining pressure distribution due to backfill grouting pressure is shown in Figure 9. With simultaneous backfill grouting, generally, the pressure reaches a maximum just after grouting. This is because the backfill grouting pressure is increased at the last stage of thrust jacking in order to ensure a sufficient amount of backfill grout. The pressure tends then to decrease until the backfill grouting of the next ring starts. It begins to increase again under the influence of backfill grouting pressure of the next ring. The pressure tends to be large around grouting point just after backfill grouting. The farther from the grouting point, the smaller the pressure. The pressure distribution tends to become almost isotropic two days after the tail has passed.

3.2.2 Relation between vertical pressure and overburden pressure

Figure 10 shows the relation between $K_v = p_{vg}/p_{v0}$ and p_{v0} based on observed data. In soft clayey ground, many lining pressures observed two days after backfill grouting are distributed in the range $K_v = 0.75$ to 1.2, which is approximately the overburden pressure. In stiff clayey ground or in sand/sandy gravel ground, the pressure varies widely, but K_v is generally lower than 1. This reflects the common practice in stiff ground where ground settlement is not significant, that backfill grouting pressure is controlled based on water pressure and not overburden pressure.

3.2.3 Relation between horizontal pressure and vertical pressure

Figure 11 shows the relation between K_h and overburden pressure based on observed data. Many of the measurements, are in the range $K_h = 0.7$ –1.5, with an average value $K_v = 1$. That means the pressure distribution becomes more isotropic. K_h is affected by several factors, such as backfill grouting pressure, position, the loss of backfill grouting pressure behind lining, fluidity of grout, and so on.



p_{vg} = pressure on the tunnel crown
 p_{hg} = pressure at the tunnel spring line
 p_{v0} = overburden pressure ($p_{v0} = (\Sigma \gamma_t \cdot h)$)
 $K_v = p_{vg}/p_{v0}$
 $K_h = p_{hg}/p_{v0}$

Figure 8. Tunnel lining pressure due to backfill grouting.

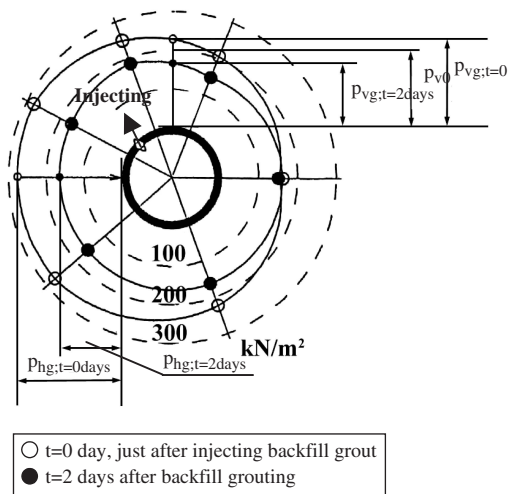


Figure 9. Lining pressure due to backfill grouting.

4 COMPARISON BETWEEN DESIGN AND OBSERVATION ON LINING PRESSURE

4.1 Conventional design method in Japan

In Japan, the conventional model and the full-circumferential spring model are usually used for designing shield linings. Figure 12 is a conceptual

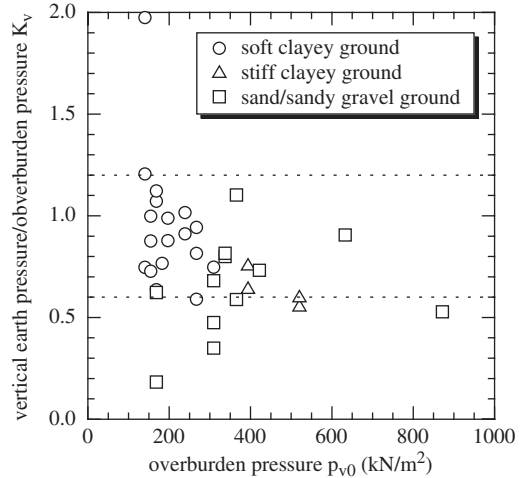


Figure 10. Relation between K_v and p_{v0} , 2 days after shield passing.

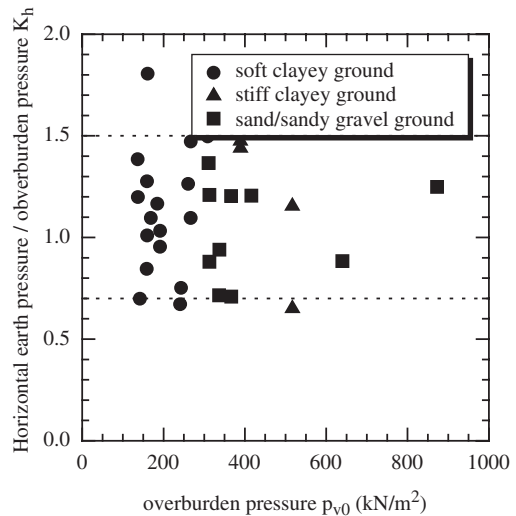


Figure 11. Relation between K_h and p_{v0} , 2 days after shield passing.

figure of the conventional model (Japan Society of Civil Engineers, 1996). This model is based on active earth pressure, water pressure and soil reaction (triangular distribution shape corresponds to the lining deformation).

In this design method, there are two different loading conditions depending on the amount of groundwater pressure. One is the total stress condition that is employed in soft clayey ground. The other is for the effective stress condition for sandy and stiff clayey ground.

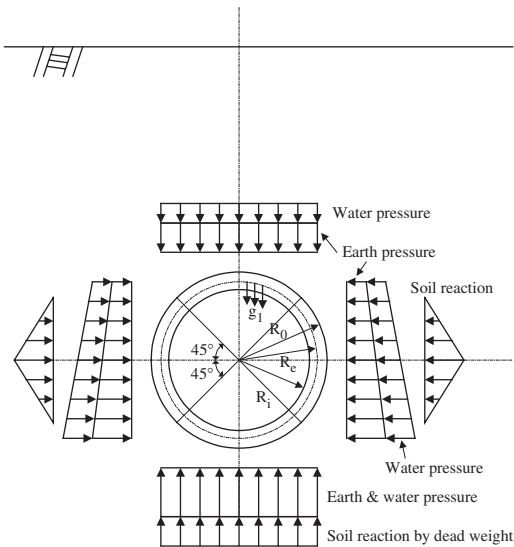


Figure 12. Conventional lining design method in Japan.

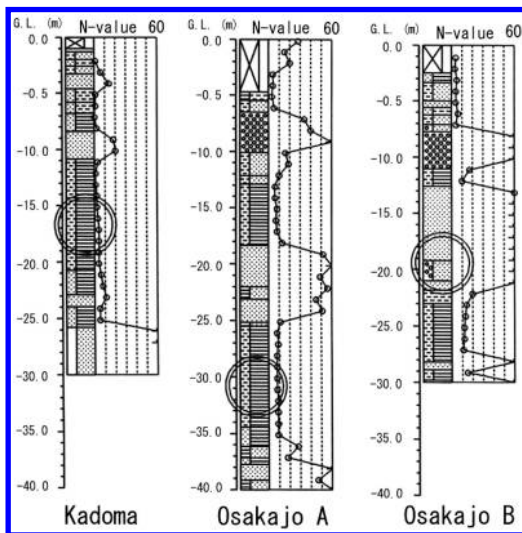


Figure 13. Soil profile at monitoring sites and locations of shield tunnels.

4.2 Simulation on coefficient of lateral earth pressure λ and coefficient of soil reaction k

To design the lining, member force will change depending on the combination of the deviator load which deforms segments (λ) and the soil reaction which prevents deformation (k). For the backanalysis presented in this section, the conventional method

was used. In the simulation various $\lambda - k$ combinations were applied in the calculations.

The presented monitoring locations are in Kadoma, Osakajo A, and Osakajo B (Hashimoto et al., 1997). Figure 13 shows the soil profile at monitoring sites and locations of shield excavation. Table 2 indicates each ground condition around tunnels.

The observed lining pressure at 3–5 meters after TBM passed in clayey ground at Kadoma and Osakajo A was approximately 50–70% smaller than the total overburden pressure. The vertical lining pressure was almost equivalent to Terzaghi's loosening pressure plus water pressure in sandy ground, such as at Osakajo B.

Parameters of the original design were $\lambda = 0.55$, $k = 10 \text{ MN/m}^3$ at Kadoma and Osakajo A, and $\lambda = 0.35$ and $k = 50 \text{ MN/m}^3$ at Osakajo B. In the original design, the bending moment at the tunnel crown largely depended on λ . As shown in Figure 14, a comparison between the observed bending moment and the result of parametric calculations for Kadoma and Osakajo A demonstrates that the calculated bending moment was close to the observations if λ is 0.7–0.8 under the total stress condition. The bending moment of the original design was 1.7 to 6 times larger than those observed. In the sandy ground of Osakajo B, the result of the original design calculated using $\lambda = 0.35$ and $k = 50 \text{ MN/m}^3$, was, under the effective stress conditions, five times as large as the observations. The backcalculated λ in this case is larger than 0.6 with $k = 50\text{--}90 \text{ MN/m}^3$. The results from these three cases show that the original design, using the conventional design model, seems to be conservative. It is necessary to improve and develop more rational design methods in the future.

5 CONCLUSION

With respect to ground deformations and lining pressures, the following results were obtained from in-situ monitoring in recent shield tunnelling constructions using 2-component simultaneous backfill grouting.

- 1) Simultaneous backfill grouting system is being widely adopted in shield tunnelling as it is very effective in reducing the ground deformation.
- 2) The large diameter lining pressure meter, developed by authors, enables monitoring of the long-term lining pressure as well as grouting pressure behind the TBM.
- 3) Lining pressure develops depending on the backfill grouting pressure during elapsed time. Generally a few rings behind the TBM the lining pressure distribution is uniform.
- 4) After the construction stage (few ring behind the TBM) the lining pressures do not change significantly in the long-term. This is based on observations, during 6 month.

Table 2. Soil characteristics.

		Kadoma	Osakajo A	Osakajo B
Liquid limit	w_n (%)	71.6	49.8 to 56.2	–
Plastic limit	w_L (%)	92.66	59.3 to 80.5	–
Grain size Distribution	w_P (%)	28.73	25.8 to 27.5	–
	gravel (%)	0	0.0	1 to 18
	sand (%)	1	0.4 to 0.9	72 to 87
	silt (%)	34	19.7 to 48.4	7 to 11
	clay (%)	65	50.7 to 79.7	5 to 8
SPT N-value		1 to 5	8.0 to 9.0	50+
Unconfined compressive strength	q_u (kN/m ²)	168 to 198	540	23

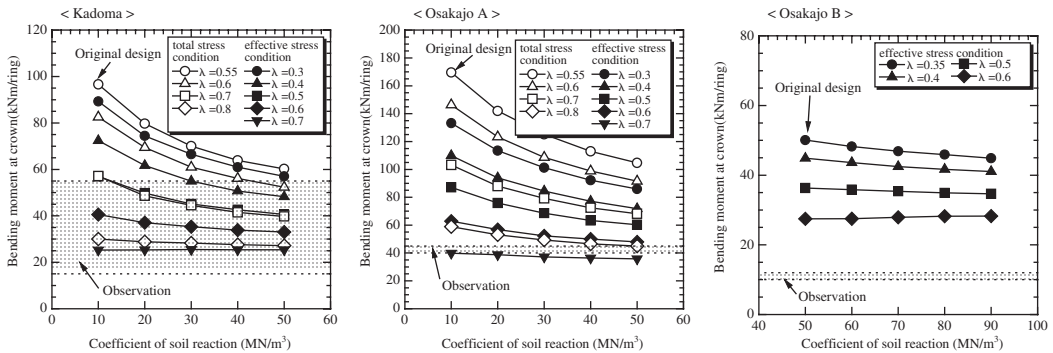


Figure 14. Comparison of bending moment between observation and parametric calculation with λ and k .

5) It is proved that a vertical earth pressure smaller than the overburden pressure and a coefficient of lateral earth pressure λ larger than λ based on the active earth pressure makes lining stress closer to the observations, even in Japanese conventional designs method.

REFERENCES

Feddema, A, Möller, M, Zon, W.H., Hashimoto, T, 2001. ETAC two-component grout field test at Botlek rail tunnel. Modern Tunneling Science and Technology, Swets & Zeitlinger, p.809–815.
 Japan Society of Civil Engineers, 1996. Japanese Standard for Shield Tunneling, the 3rd edition, p35. (in Japanese)
 Hashimoto, T, Yabe, K, Yamane, A, Ito, H, 1993. Development of oil pad type earth pressure transducer for shield tunnel segment. Proc. of 28th Annual Meeting of JGS, p.2055–2058. (in Japanese)

Hashimoto, T, Nagaya, J, Ohta, H, Shintani, T, Sugihara, K, 1997. Consideration of design earth pressure for shield tunnel based on measurement. Proc. of Tunnel Engineering, JSCE, Vol.9, p.37–42. (in Japanese)
 Hashimoto, T, 2001. Monitoring on lining pressure due to shield tunneling. IS-Kyoto, Modern Tunneling Science and Technology, Short Course, p.137–143.
 Hashimoto, T, Nagaya, J, Konda, T, Tamura, T, 2002. Observation of lining pressure due to shield tunneling. Proceedings of the Third International Symposium on Geotechnical Aspects of Underground Construction in Soft Ground – IS-Toulouse, p.119–124.
 Hashimoto, T, 2002. Experiences in monitoring in Japan for shield tunnels. Pre-proceedings of the Workshop Measuring and Predicting the Behaviour of Tunnels, p.125–145.
 Hirata, T, 1989. Study on behavior of cohesive soil in type shield tunneling work and on construction technique. Doctoral Thesis, Kyoto University, p.45. (in Japanese)

Grout pressures around a tunnel lining, influence of grout consolidation and loading on lining

A. Bezuijen

Geodelft, Delft, The Netherlands

A.M. Talmon

WL | Delft Hydraulics, Delft, The Netherlands

ABSTRACT: The influence of the grout properties on the grout pressure distribution around a tunnel lining is investigated. Initial yield stress of the grout and consolidation properties appear of importance. The consolidation properties are determined by means of element tests and appeared also to be influenced by the properties of the soil surrounding the tunnel. Field measurements have shown that grout pressures vary during the bore-cycle. Consolidation of the grout after injection in the tail void is one of the factors affecting the grout pressure distribution. The vertical pressure gradient in the grout decreases with increasing distance from the TBM. This decrease in gradient is important to determine the loading on the lining. It is shown that at some distance from the TBM the grout pressure is in most cases comparable to the pore pressure for a tunnel drilled in sand.

1 INTRODUCTION

Grout pressures around a tunnel lining determine the loading on the lining and are an important parameter to predict the settlement above the tunnel. Grout pressures have been measured in several projects (See for example Hashimoto et al. 2002, Koyama 2001). It was noticed (Hashimoto 2002) that the measured pressures are not in agreement with the design method used in Japan. The measured pressures were lower than predicted according to the design method when a tunnel was constructed in sand.

To increase the knowledge on the grout pressures these were measured systematically at 2 cross-sections of the Sophia Rail tunnel (Bezuijen et al., 2002 and Bezuijen et al., 2004). Apart from these measurements it was decided to perform element tests and model tests to acquire information on the properties of the grout and to develop calculation models (Talmon et al., 2001 and Bezuijen & Talmon 2003). The research was performed by the COB (Centre of Underground Construction) in the Netherlands and Delft Cluster (a foundation in which the leading Delft Institutes on civil engineering co-operate).

This paper will deal with measured grout pressures and consolidation of the grout during standstill of the TBM and will deal with some consequences for the loading on the lining and the pressure distribution in the soil.

2 MEASUREMENTS

2.1 *Field measurements*

Grout pressures were measured around two of the lining segments of the Sophia Rail Tunnel. The Sophia Rail tunnel is a tunnel constructed with a slurry shield TBM. The diameter of the tunnel is 9.55 m. It is situated in the western part of the Netherlands. The tunnel is covered with nearly 15 m soil at the location of the measurement and surrounded with Pleistocene sand. The soil consists of soft Holocene layers of clay and peat above the Pleistocene sand. See Figure 1. More details on the tunnel are presented by Stive (1999), more information on the measurement conditions can

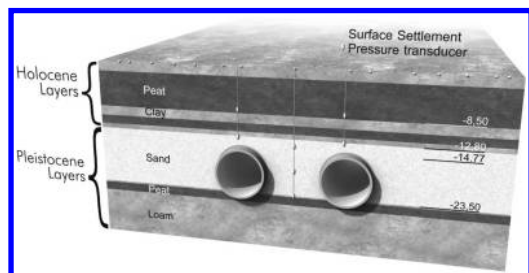


Figure 1. Cross-section of the Sophia Rail Tunnel, some of the instrumentation and soil layering at the measurement location. Depths are presented in meters below the surface.

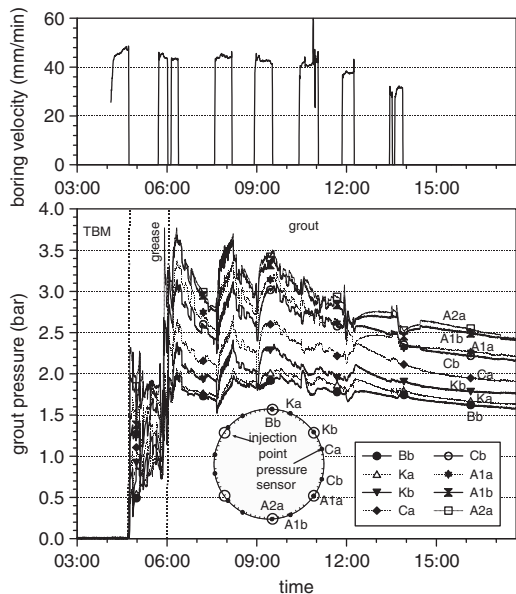


Figure 2. Position of instruments, boring velocity and measured grout pressures at the right side of the tunnel as a function of time.

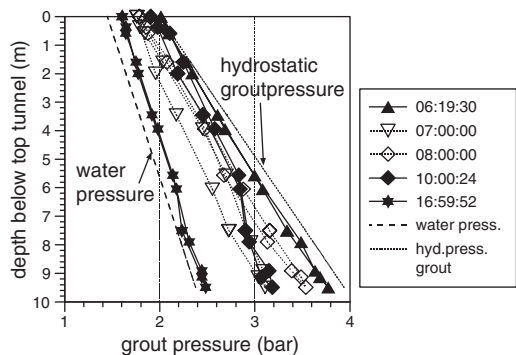


Figure 3. Measured grout pressures at the Sophia Rail tunnel. The pressure measured at 16:59:52 was measured several hours after boring has stopped.

be found in Bezuijen et al. (2002 and 2004). A result of the measurements is shown in Figure 2.

Figure 1 also shows the position of the various instruments placed in the soil surrounding the tunnel. However, this paper is focused on the measured grout pressures directly around the tunnel lining. The measurement results shown are comparable to results that have been found in other tunnel projects in the Netherlands. The grout pressure increases during drilling and decreases during stand still. The pressures are plotted as a function of depth in Figure 3. It is clear that

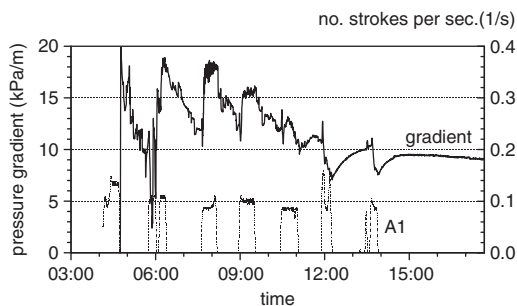


Figure 4. Pressure gradient over the tunnel lining at one location, and pump activity for one of the injection points (A1) as a function of time.

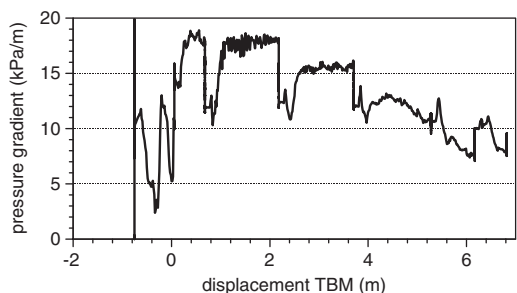


Figure 5. Pressure gradient over the tunnel lining at one location as a function of displacement of the TBM with respect to grout pressure sensors in the lining.

the pressure increases linearly with depth, but that the pressure as well as the vertical pressure gradient changes with time. This becomes even clearer when the average vertical pressure gradient in the grout is plotted as a function of time of distance from the TBM, see Figure 4 and Figure 5 respectively.

2.2 Element tests

Tests have been performed to investigate the hardening and bleeding of conventional grout, see Figure 6 and Figure 7. In this test a grout layer of 0.2 m is loaded mechanically with a constant load of 30–300 kPa overpressure. The expelled water is a measure for the consolidation of the grout. After several minutes of consolidation the sample was unloaded and the shear strength of the grout was measured at different locations in the grout with a vane. An example of results of such a test is shown in Figure 8 and Figure 9. Figure 9 shows the amount of expelled pore water as a function of time and the applied pressure. In this test a pressure of 300 kPa was applied. Pressure was relieved several times to be able to perform the vane tests. Figure 9 shows the measured shear strength

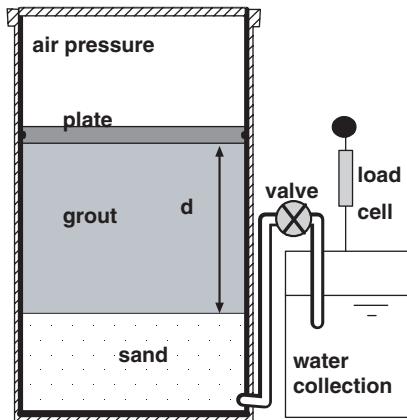


Figure 6. Measurement principle (grout loading by air pressure).

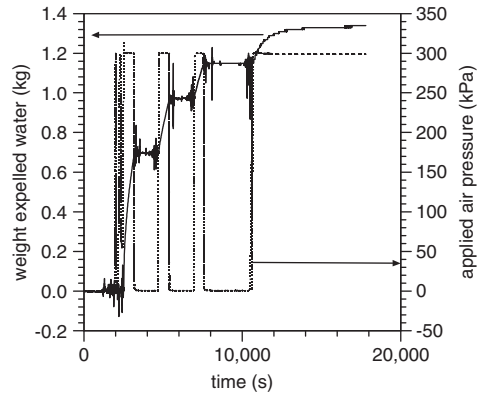


Figure 8. Test result expelled water as a function of time and applied pressure.

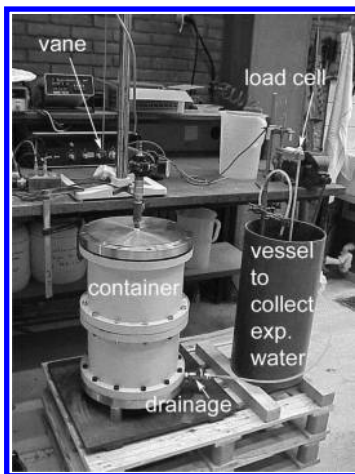


Figure 7. Experimental setup.

after various times that pressure was applied. In this test it was focussed on the lower values of the shear strength. Therefore only shear strengths up to 6 kPa were measured and presented in the plot.

The type of grout tested here, was tested before at atmospheric pressure (Bezuijen et al., 2002). In that test it appeared that the measured shear strength remained more or less constant until 5.5 hours and after that time the hardening of the grout started. For this grout it was therefore the consolidation and the resulting increase in grain stress that determines the increase in shear strength after injection of the grout. The influence of hardening is only limited. This result depends on the type of grout used and the pressure difference with pore water. The hardening time will be dominant for a grout that hardens quickly and has a long consolidation time.

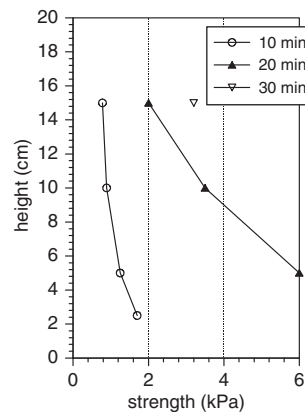


Figure 9. Strength development as measured with a vane.

3 INTERPRETATION

The decrease in the measured grout pressure in the field measurements during stand still is caused by bleeding (or consolidation) of the grout. It was shown by the element tests described before and calculations (Bezuijen & Talmon 2003) that applying a pressure on the grout at comparable conditions as in a tail void will result in a 5 to 10% of volume loss due to bleeding. The relative small volume loss leads to considerable decrease in pressure, because the surrounding dense sand has a high shear modulus for unloading. The principle is shown in Figure 10. Elastic deformation in the sand is assumed and a pressure decrease that is constant over the circumference of the tunnel (this last assumption is a simplification of the real situation, but it results in the order of magnitude of the deformation and grout pressure decrease). For such a situation the relation between x (the reduction of the grout thickness due to bleeding or consolidation of the grout, see

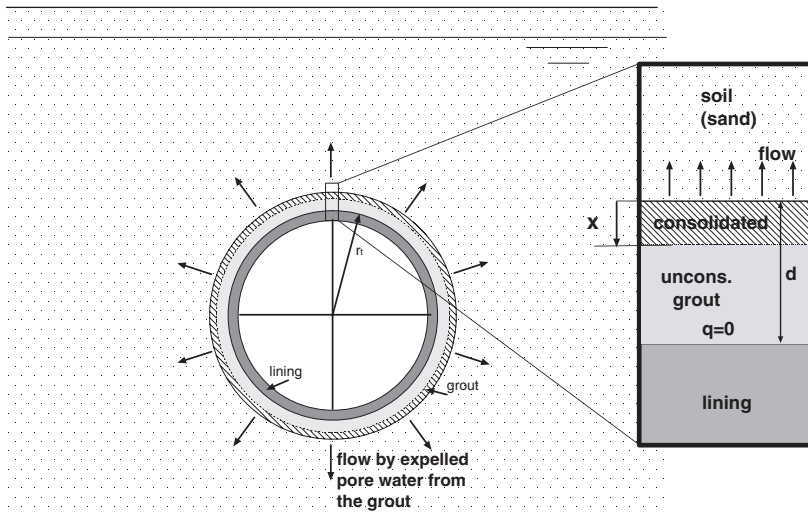


Figure 10. Sketch of consolidating grout around a tunnel lining and detail.

Figure 10) and the decrease in the grout pressure can be written as (Verruijt, 1993):

$$\Delta\sigma = 2 \frac{x}{r} G \quad (1)$$

Where $\Delta\sigma$ is the change in pressure, x the change in radius due to consolidation (see Figure 10), r the radius of the tunnel and the grout and G the shear modulus of the soil around the tunnel. In case of a consolidating grout, x will be equal to the thickness of the water layer that is expelled from the grout. A typical value of the shear modulus of dense sand for unloading is 50 to 100 Mpa. Assuming a tunnel radius of 5 m and 5% thickness reduction of the grout due to consolidation ($=0.01$ m for a grout layer with a starting thickness of 0.2 m), such a thickness reduction will lead to a pressure decrease of 200 to 400 kPa. Such a grout pressure reduction is sufficient to decrease the grout pressure to values close to the pore water pressure. Consolidation will stop when the grout pressure is close to the pore water pressure.

The dominant parameters for the rate of the pressure decrease in the situation tested in the element tests were the permeability of the grout and the shear modulus of the soil. The calculation method as described by Bezuijen & Talmon (2003) indicates that the permeability of the subsoil also influences the rate of consolidation in cases where this permeability is less than 50 times the permeability of the grout (10^{-7} to 10^{-8} m/s was found as typical permeabilities for the grouts tested).

The mechanisms that cause the changes in the vertical pressure gradient are described in detail in Bezuijen et al. (2004). Since grout can be described as a Bingham liquid with a certain yield stress, it is possible

that the vertical pressure gradient changes during the grouting process. Without yield stress, there can only be a hydrostatic grout pressure distribution and the density of the grout would purely determine the vertical pressure gradient. Due to the yield stress, the grout pressure in the tail void directly behind the TBM is governed by the injection strategy and the magnitude of the yield stress in the grout during drilling (Talmon et al., 2001). At a larger distance from the TBM the buoyancy forces and again the yield stress in the grout determine the vertical pressure gradient as will be explained below.

Assume, as a starting point, a hydrostatic pressure distribution in the grout with a pressure gradient that is determined by the density of the grout (2190 kg/m^3). In the field measurements for the Sophia Rail tunnel this corresponds to a vertical pressure gradient of approximately 21 kPa/m. The average density of a cross-section of the tunnel (the weight of the tunnel lining divided by the volume of the tunnel including lining) is much lower. A diameter of 9.45 m, a lining thickness of 0.4 m and a density of the lining of 2400 kg/m^3 results in an average density of the tunnel of 390 kg/m^3 . Assuming a linear increase with depth for the grout pressure, according to Archimedes' law, a cross-section of the lining would be in equilibrium for a vertical pressure gradient of 3.8 kPa/m. The gantry of the TBM adds additional weight and therefore vertical equilibrium with the buoyancy forces will be reached for a higher gradient (6.4 kPa/m), but in all cases the vertical hydraulic gradient for vertical equilibrium of a cross-section of the lining will be much lower than the hydrostatic pressure distribution in the grout and in most cases even lower than the gradient in the pore water.

A vertical pressure gradient as low as 6.4 kPa/m was not measured during the field measurements for the Sophia rail tunnel. This means that there will always be some loading on the lining. This loading will be transferred to the TBM and the part of lining where the grout is hardened. It is shown in Bezuijen & Talmon (2004) that there is a relation between the yield strength and the vertical grout pressure gradient. Without yield strength the vertical pressure gradient can only be 21 kPa/m for the conditions of the field tests. However, a lower vertical pressure gradient is possible when the yield strength increases.

Close to the TBM the yield strength in the grout is limited and therefore the vertical pressure gradient is relatively high. At a larger distance the gradient decreases to lower values due to the increased yield strength of the grout.

4 LOADING ON THE LINING

The measured vertical pressure gradient in the grout, behind the TBM, is higher than the gradient that corresponds with vertical equilibrium of a cross section of the lining during the measurement. This means that there is no vertical equilibrium in one cross-section of the lining and equilibrium has to be obtained by interaction between the lining elements. The lining reacts as a beam supported by the TBM on one side and the already consolidated or hardened grout at the other side. Vertical forces at the supports and moments in the lining will depend on the length over which the beam is loaded. The moment in longitudinal direction can be calculated using the beam equation:

$$EI \frac{d^4 y}{dx^4} = w \quad (2)$$

Where EI is the longitudinal bending stiffness of the tunnel (kNm²), x the length of the lining between the TBM and the hardened grout (m), y the vertical deformation (m) and w the vertical loading on the tunnel (kN/m). This equation can be solved analytically for various schemed boundary conditions. In our study we have measured the loading w (it can be determined from the vertical gradient, see Figure 5, or from all the grout pressures measured around the tunnel, see Figure 2 and Figure 3). A numerical solution is practical to use these measurement results as input for various loading situations. We used a finite difference solution. The differential equation can be written in finite differences for the point (i) on the beam:

$$EI \frac{y_{i+2} - 4y_{i+1} + 6y_i - 4y_{i-1} + y_{i-2}}{h^4} = w_i \quad (3)$$

Here is h the distance between the finite difference points and w_i the loading in that point. This equation

is valid for all points (i) on the beam. This leads to a matrix equation that can be solved in a spreadsheet.

Note that we use the measured pressures around the lining and it is therefore necessary to model the lining only. The soil interaction is included in the measured grout pressures and doesn't have to be modelled to simulate the reaction of the lining on the measured grout pressures.

Preliminary simulations have been run with the set of equations described above. If the distance over which high vertical gradients are present over the lining increases, this leads to an increase of the bending moments in the lining that is quadratic with this distance (as could be expected). However, it also became clear that the bending moments and deformation in the lining are influenced quite substantially by the boundary conditions at both sides on the lining. What is the reaction force and moment of the TBM on the lining and what is the boundary condition at the other end where the measurement ends. What boundary conditions have to be used, will be a subject for further research. In this research we will use the simple beam model described above to check the influence of various parameters. Furthermore 4-D finite element simulation will be used to study details of the TBM lining and lining soil interaction. A 2-D grout flow model is available to provide input pressures for these models (Talmon et al., 2001).

The preliminary calculations with the beam equation showed clearly that to reduce the forces on and the moment in the lining it is necessary to limit the length of the lining that is surrounded by not yet consolidated or not hardened grout. The measurements show clearly that the vertical gradient (and thus the loading on the lining) is highest directly behind the TBM, where the grout has the lowest viscosity and yield stress.

5 CONSEQUENCES FOR THE GROUT PROPERTIES

The grout applied influences the loading on the lining. In this paper we have only discussed the distribution of the loading perpendicular to the axis of the lining. For this loading it is of importance that the unsupported part of the lining (where buoyancy forces dominate) is as short as possible to reduce the moment in the lining and high vertical forces at the TBM and there where the grout is hardened. This can be achieved in 3 different ways:

1. The grout has a relatively high initial shear stress. In a situation with a high initial shear stress of the applied grout, the shear strength in the not yet hardened grout is already sufficient to prevent upward movement of the tunnel lining.
2. Subsoil and grout allow for a rapid consolidation of the grout, resulting in an increase of allowable shear

stress in the grout and as a result in only a limited unsupported length of the lining.

3. The grout used hardens quickly. This also leads to a limited unsupported length of the lining.

These 3 methods can be used for a tunnel made in sand. For a tunnel in clay the second option is not possible, because the low permeability of the clay prevents consolidation of the grout.

6 CONCLUSIONS

Results of field measurements on grout pressure decay during standstill of a TBM have been analysed in combination with the results of element tests. Grouts normally consolidate after injection into the tail void. This leads to a reduction of grout volume and to a decrease in grain stress of the surrounding soil.

It was found for several tunnel projects, where a tunnel was bored in sand, that the final pressure distribution around a tunnel was comparable to the pore water pressure and was more or less independent from the injection strategy. Only the initial pressure distribution directly behind the TBM can be influenced by the injection strategy.

Grout properties in combination with the soil properties influence the loading on the lining directly behind the TBM. It is therefore necessary to select a grout taking in into consideration the soil properties at the location and desired grout properties (yield stress, bleeding and hardening parameters).

ACKNOWLEDGEMENT

Research was supported within the framework of the research on the Botlek and Sophia Rail Tunnel as

initiated by COB (the Dutch centre for underground construction) and supported by ETAC grout injection BV. We acknowledge COB and its participants for their permission to publish the results and the members of the working groups for stimulating support.

REFERENCES

- Bezuijen A., Talmon A.M., Kaalberg F.J. and R. Plugge, 2002, Field measurements on grout pressures during tunnelling, *3rd Int. Symp. on Geotechnical Aspects of Underground Construction in Soft Ground – IS Toulouse, 23–25 October*.
- Bezuijen A., Talmon A.M., 2003, Grout the foundation of a bored tunnel, 2003, *Proc ICOF 2003 Dundee*.
- Bezuijen A., Talmon A.M., Kaalberg F.J. and R. Plugge, 2004, Field measurements on grout pressures during tunnelling, *Accepted for publication in Soils and Foundations*.
- Hashimoto T., Nagaya J., Konda T., Tamura T., 2002, Observation of lining pressure due to shield tunnelling, *3rd Int Symp. on Geotechnical Aspects of Underground Construction in Soft Ground, IS-Toulouse*.
- Koyama Y., Design Method of Shield tunnel – Present status and subjects-, *proc. IS-Kyoto 2001 conference on Modern tunneling Science and Technology*, pp. 29–38.
- Stive R.J.H., 1999, Design features of the Sophia Rail Tunnel in the Betuweroute. *Tunnelling and Underground Space Technology, Vol. 14, No.2, pp. 141–149*.
- Talmon A.M., Aanen L., Bezuijen A. and W.H. van der Zon, 2001, Grout pressures around a tunnel lining, *proc. IS-Kyoto 2001 conference on Modern tunneling Science and Technology*, pp. 817–822.
- Verruijt, A., 1993, Soil Dynamics, Delft University of Technology, b28.

Laboratory testing of grout properties and their influence on backfill grouting

A. Bezuijen & W.H. van der Zon

GeoDelft, Delft, The Netherlands

A.M. Talmon

WL | Delft Hydraulics, Delft, The Netherlands

ABSTRACT: Functions of tail void grout are described and necessary properties of the grout mortar to fulfil these functions are discussed. A simple model is derived to show the loading on the lining as a function of the mortar properties and the possible movement of the lining. When it takes a long time for the grout mortar to consolidate or to harden, this can lead to considerable forces in the lining of a tunnel as well as on the TBM as is shown with some example calculations in this paper.

1 INTRODUCTION

Back-fill grouting is a crucial process in TBM tunnelling. The grouting process determines the loading on the soil and with that an important part of the surface settlement. It also determines the loading on the lining. Field and laboratory measurements (Bezuijen et al., 2004, Bezuijen & Talmon, 2003) have revealed mechanisms that are of importance: the flow of the grout around the tunnel, the yield stress that determines the maximum resistance against the buoyancy forces and the influence of consolidation of the grout on the loading on the lining. The parameters necessary to describe these mechanisms are not given in the traditional grout tests and therefore a new test was developed.

The paper describes the functions of grout during and after injection in the tail void and the available and new developed laboratory experiments. A calculation method is presented that gives an indication about the loading along the lining. It presents some example calculations before ending with conclusions.

2 FUNCTIONS OF GROUT

2.1 General

Grout is injected in the tail void between the soil and the lining. In some cases it is injected through the lining, but most common is a grouting system that is constructed in the backside of the TBM and that can inject grout during drilling continuously, see Figure 1.

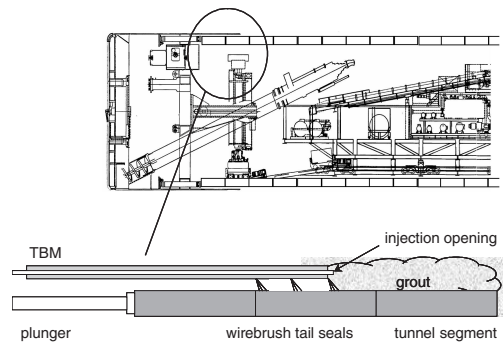


Figure 1. Sketch of TBM and detail of injections system.

The grout has different functions, as summarized by Shirlaw et al. (2004):

1. To ensure that there is uniform contact between the lining and the ground: The ground both loads the lining and provides resistance to distortion. Consistent filling of the tail void will avoid uneven loading.
2. To reduce the surface settlement over the tunnel: If the void is not filled with grout, the ground will move into the void, resulting in settlement. Typically, the volume of the tail void is in the range 3% to 16% of the internal volume of the tunnel. There can be high surface settlements if the grouting is ineffective, and the tail void closes as a result.
3. To hold the ring in place during shield advance: Soft ground and mixed face tunnel boring machines are typically advanced by thrusting off the installed

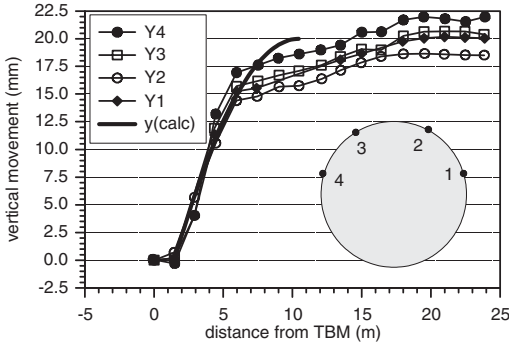


Figure 2. Rising of lining measured at 4 points on the lining after placement of lining segments (Sophia Rail Tunnel, The Netherlands) and calculated rising, see further text.

lining. If the lining is surrounded by liquid grout, then it can float upwards, See Figure 2. This can lead to stepping on the circumferential joint, birds' mouths developing on the radial joints, loss of plane and damage to the lining.

4. To carry the load transmitted to the lining by the shield back-up trailers.
5. To reduce seepage and loss of fine particles where the gasket is ineffective due to damage or because of stepping of the lining.

In addition to this, grout also has to provide sufficient resistance to overcome the buoyancy forces that occur in the first rings after the TBM. These buoyancy forces occur because the average density of lining and air that forms the tunnel is less than the density of the grout. This is comparable with what is mentioned under 3, but it can be compensated by reduction of the grout density as well as by an increase of the yield stress.

Some of these functions can only be taken into account by the construction of the TBM (sufficient grout injection points) or craftsmanship (taking care for open injection points, consistent filling of the tail void). However, for some it is possible to 'design' the grout. In this paper we will discuss the influence of the density, the initial yield stress, the consolidation properties and the hardening of the grout on the loading on the lining. It is focused on forces and moments along the lining. Ring loading is not taken into account.

2.2 Density of the grout and initial viscosity

The density of grout mortars usually varies from 1000 to 2200 kg/m³. The average density of the cross-section of tunnel lining and the air in the tunnel is in general around 400 kg/m³. This means that there will be a buoyancy force on the tunnel. This can lead to upward directed movement of the tunnel lining when it is released from the TBM. Furthermore it induces

stresses and moments in the TBM as will be explained later.

The grout mortar can be designed to minimize this buoyancy force by reducing the density and/or decrease the yield strength. The yield strength changes the pressure distribution over the lining. Assuming that the shear strength between the tunnel lining and the grout is small and the shear strength between the soil and the grout determines the pressure distribution, the relation between the yield strength and the maximum buoyancy force that can be compensated by the grout mortar can be written (Bezuijen et al., 2004):

$$F = \tau_y \frac{D^2}{s} \quad (1)$$

Where F is the maximum force per metre tunnel lining that can be compensated by the yield stress in the grout, τ_y the shear strength of the grout, D the diameter of the tunnel and s the width of the tail void. The buoyancy force K per metre lining exerted by the tunnel lining can be written as:

$$K = \frac{\pi}{4} D^2 (\rho_g - \rho_t) g \quad (2)$$

Where ρ_g is the density of the grout, ρ_t the average density of the tunnel (lining and air) and g the acceleration of gravity.

Equilibrium in a cross-section is reached when $F \geq K$. Such a situation can be reached when:

$$\tau_y \geq \frac{\pi}{4} s (\rho_g - \rho_t) g \quad (3)$$

This relation shows that a stable cross-section can be reached by using grout with high yield strength, or a low density or by increasing the average density of the tunnel (and/or dead weight or back-up train).

2.3 Properties along the lining

Although Eq. (3) looks rather simple, it is in a lot of cases not so easy to fulfil this equation directly behind the TBM due to other requirements on the grout mortar. The grout has to flow easily through the piping of the injection system and it has to fill the tail void completely and last but not least also costs play a role. These requirements quite often result in a grout mortar where Eq. (3) is not fulfilled directly after the TBM because the yield stress is too low. When this is the case, a part of lining directly after the TBM will have the tendency to move upward. However, this upward movement will be stopped by the friction forces between the lining elements still in the TBM on one side and the elements in the already hardened or consolidated grout on the other side. In such a situation it is necessary to know the hardening and consolidation properties of the grout as will be described later.

2.4 Consolidation and hardening

The yield strength of the grout mortar after injection will increase due to consolidation of the grout and hardening. It is of importance to have data to describe this strength increase because this determines for what length the tunnel lining has only limited support. Consolidation can lead to a strength increase for only a limited thickness of the grout layer (Bezuijen & Talmon 2003). This is the case when the tunnel is bored in stiff sand.

3 LOADING ON THE TUNNEL LINING

An example where Eq. (3) was not fulfilled is the Sophia Rail Tunnel (Bezuijen et al. 2004). The measured hydraulic gradient along a cross section of the tunnel lining is comparable to the average density of the tunnel at some distance from the TBM, there where the pressure gradient is more or less constant, see Figure 3, but increases close to the TBM. This leads to an upward directed loading on the tunnel lining close to the TBM until consolidation of the grout led to a yield strength that is high enough to overcome buoyancy forces further away from the TBM.

Using the pressure data during drilling it is possible to construct the load distribution on the tunnel for the part where the lining has the tendency to float. This loading can be used in a numerical program to calculate the shear forces and moments in the lining. The resulting shear forces and moments depend to a large extend on the moments and force exerted by the TBM. In this paper we focus on the influence of the grout and the influence of consolidation and hardening. We therefore assume a rather simple calculation model only to get an idea how the loading on the lining is influenced by the TBM induced moments and consolidation or hardening.

The lining is approximated to a beam that is fixed at the end where the grout is consolidated or hardened. Usually it is assumed that the lining rests on an elastic foundation. However, the measurements, Figure 3, show that forces on the lining are more or less constant at some distance (more than 9 m in the figure) from the TBM. Movement of the lining in the grout would lead to pressure variations in the grout that are not measured. This justifies this approximation.

The other end of the lining bears at the TBM. The TBM can exert a certain moment M on the lining. A loading distribution on the lining is assumed that increases linearly with the distance from where the tunnel lining is fixed in the consolidated grout. This is again only an approximation of the real loading that occurred, see Figure 3.

As can be seen from Figure 2, there is a certain permanent movement in the lining. With the boundary

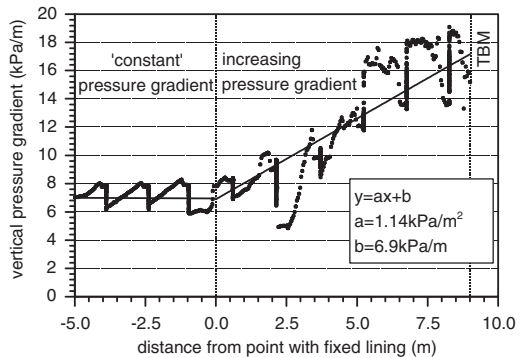


Figure 3. Example of gradient in the grout pressure as a function form the distance (0 on the X-axis represents the point where the lining is more or less fixed). The TBM is at 9 m). Results measured at Sophia Rail tunnel (Bezuijen et al., 2004).

conditions mentioned before it is possible to solve the beam equation:

$$EI \frac{d^4 y}{dx^4} = -q \cdot x \quad (4)$$

With the boundary conditions:

$$y(0) = 0, \frac{dy(0)}{dx} = 0, y(L) = A, \frac{d^2 y(L)}{dx^2} = \frac{M}{EI} \quad (5)$$

Where E is Young's modulus, I the moment of inertia, $x = 0$ the position where the grout is hardened, $x = L$ the other end of the lining connected in the TBM, A the vertical displacement of the lining with respect to the TBM, q the increase of the loading with distance x and M the moment the TBM exerted on the lining. For these boundary conditions the movement of the lining can be written as:

$$y(x) = \frac{x^2 (2qx^3 L^3 - 9xqL^5 + 120xA EI - 60xL^2 M + 7qL^6 - 360LA EI + 60L^3 M)}{240L^3 EI} \quad (6)$$

and the shear force (F_s) as:

$$F_s = 0.5qx^2 + \frac{3AEI}{L^3} - \frac{9}{40}qL^2 - 1.5\frac{M}{L} \quad (7)$$

Consequence of the assumptions is that F_s had to be 0 at $x = 0$ (a large F_s at $x = 0$ would be reflected in the measured pressure gradient, which is not measured).

With a length of the liquid zone of approximately 9 m and a tunnel with a diameter of 10 m, a beam equation cannot be more than an approximation, but as said before that is enough to get an idea of the importance of various parameters.

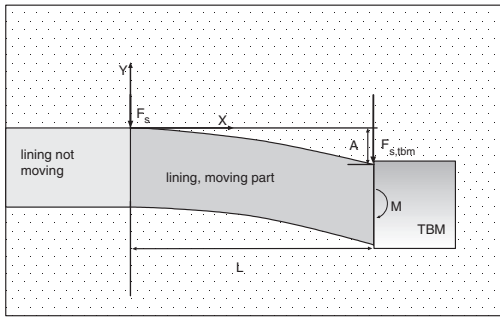


Figure 4. Definition sketch for calculating the loading on the lining.

4 LABORATORY TESTS

Shirlaw et al. (2004) emphasize the importance of performance tests for grout, since it is likely that also in the future most grout mortars will be tailor made from locally available constituent materials. They mention possible tests to test grout mortar:

- grading curves on individual constituents and the combined mix.
- Cube tests (compressive strength).
- Segregation of mortar components under gravity.
- Relaxation, height variations in time.
- Washout. Dissolving of the sample in water.
- Bleeding under pressure (Bariod filter press).
- Sump cone or Prepakt cone for workability.
- Cohesion or yield stress by a vane apparatus.
- Internal friction.
- Density of the grout.

More information on these tests is given by Shirlaw et al. (2004).

Comparing these tests with a definition of a performance test: A performance test is a test in which the product is used under actual service conditions, it must be concluded the test mentioned are no performance tests but index tests. Index tests are useful to compare different materials, but present limited information of the performance in service conditions.

The following properties are of importance to describe the behaviour of the grout just after the TBM that is the focus of this paper:

- the yield stress or cohesion this describe the loading on the tunnel, see Eq. (1).
- the density of the grout to determine the buoyancy forces, Eq.(2).
- the time necessary for the grout to consolidate or before hardening starts. This time and the drilling velocity determines L in the beam equations.

The first 2 parameters can be measured with index tests mentioned before. This is not possible for the

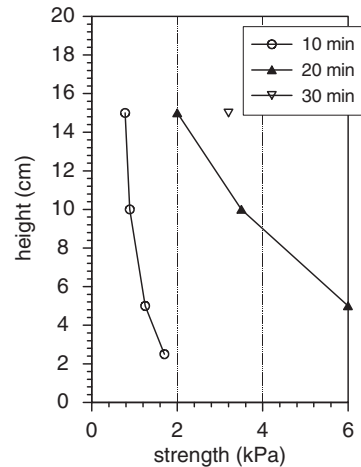


Figure 5. Strength development as measured with a vane during consolidation of grout.

third parameter and therefore a new developed test is described in the next section.

5 'FULL SCALE' CONSOLIDATION TEST

It is difficult to measure the consolidation of grout in a traditional oedometer test or filter press test, because the consolidation is fast compared to the consolidation of clay or peat, as will be shown later in this section. Furthermore it is possible that there will be hardening of the grout during the consolidation process. Therefore consolidation experiments have been performed in a cylindrical cell with a diameter of 0.3 m in which a grout layer was made of 0.2 m height, comparable to the average thickness of a grout layer in the tail void for tunnels with diameters in the range of 6 to 11 m.

The test set-up is described by Bezuijen & Talmon (2003). A result is shown in Figure 5 for a grout sample that was loaded with 300 kPa pressure. It shows that due to consolidation the strength of the grout increases considerably within 30 minutes. This time is much shorter than the time necessary for strength increase due to hardening of the grout, which was approximately 5.5 hours (Bezuijen et al., 2004).

Consolidation of grout, sometimes called bleeding, cannot be described by linear consolidation theory. It can be approximated quite well assuming it behaves as a grain-water mixture with little strength until the water is expelled from the grout and there is an effective stress between the grains. A description is presented in Bezuijen & Talmon (2003), see Figure 6. There it is also shown that the increase in yield stress of the grout corresponds with consolidation. This figure shows that the consolidation of a 0.2 m thick

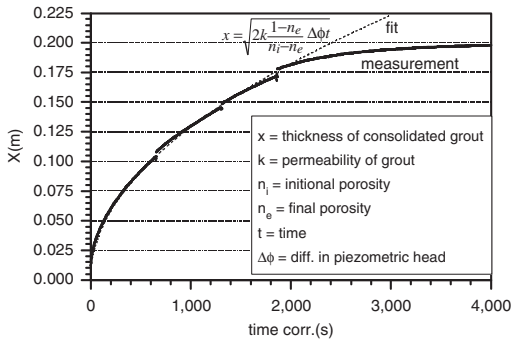


Figure 6. Experimental data on consolidation fitted with theory. x is the thickness of the consolidated layer.

grout sample takes 2000 s. A traditional oedometer test would last only 20 s, which is rather short to perform good measurements of the deformation and amount of expelled water and will not take into account possible hardening.

6 EXAMPLE CALCULATION

6.1 Sophia Rail tunnel

As example the measurements for the Sophia Rail Tunnel are used. The measured pressure gradients are already shown in Figure 3. In this figure the pressure gradient during drilling is most prominent; because then the TBM is moving and x is changing (the pressures were measured in one ring of the lining). The vertical points in the plot show the change in gradient during stand still. The constant value of 6.9 kPa/m is higher than the value that corresponds to the weight of the tunnel (4 kPa/m) but will also be influenced by weight of equipment in the lining. The value of q can be determined from a in Figure 3:

$$q = a.O \quad (8)$$

With O the cross-sectional area of the tunnel lining, q is 80 kN/m² for a tunnel with a diameter of 9.45 m as the Sophia Rail tunnel.

The momentum on the tunnel lining for the Sophia Rail tunnel as given in Bezuijen et al. (2004) is shown in Figure 7. Momentum is approximately 10 MNm during stand still and 18 MNm during drilling.

The stiffness of the lining is not well known. We used Eq. (7) to determine the stiffness. A very stiff lining will lead to a large downward directed shear force at $x=0$ and a flexible lining to an upward directed shear force, which are both not measured according to the pressure gradients in the grout. By adjusting the stiffness of the lining to $EI = 5.4 \times 10^7$ kNm² no shear

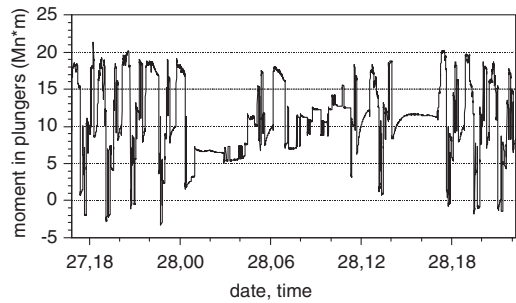


Figure 7. Momentum in vertical direction that is exerted on the lining by the plungers in the TBM. A positive momentum means that the forces on the lower part of the tunnel are higher than on the upper part.

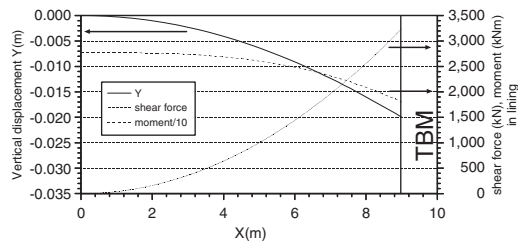


Figure 8. Results of calculation model. Calculated moments are divided by 10.

force is present at $x=0$. Results of this calculation are shown in Figure 8.

The calculated vertical displacement is also compared with the measured displacement in Figure 2 and showed reasonable agreement. This result means that the effective stiffness of the lining in liquid grout is less than normally assumed. It is possible that the segmented lining has more degrees of freedom than is assumed traditionally. It further implies that there is a considerable shear force present at the TBM that is counterbalanced by the weight of the TBM and the lining elements in the TBM. In this example a measured q was used, but this q is not the result from the grout properties only. For a situation with zero shear force F_s at $x=0$, the values of the parameters in Eq. (5) also determine q so that $F_s = 0$ for $x=0$, or to say it differently: not always all available shear stress in the grout is mobilized.

Consequence is that the influence of L (the length with linearly increasing grout pressure gradient) cannot be found by simply increasing L in Eq. (6) and (7). Assuming that the pressure gradient in the grout remains the same, it is also necessary to change q . Furthermore A has to be changed to fulfill the condition that $F_s = 0$ at $x=0$. The value A can be found by

Table 1. Parameters and results of beam calculations.

Parameter	Calc 1	Calc 2	dimension
Input			
L (length of ‘unsupported’ zone)	9	18	m
q (distributed loading near TBM)	80	40	kN/m ²
EI (stiffness of lining)	5.4×10^7	5.4×10^7	kNm ²
M (moment on TBM)	18	18	MNm
Result			
A (displacement of lining)	0.02	0.16	m
$M(x=0)$	28	57	MNm
$F_{s,TBM}$ (shear force at $x=L$)	3.2	6.5	MN

changing the boundary condition $y(L) = A$ to $F_s(0) = 0$ in Eq. (5) and solving Eq. (4) for these conditions leading to:

$$y(x) = -\frac{x^2(qx^3 - 10qL^3 - 60M)}{120EI} \tag{9}$$

and to a simple expression for the shear force $F_s(x)$:

$$F_s(x) = 0.5qx^2 \tag{10}$$

Eq. (9) for $x=L$ presents A as a function of q , L , M and EI , see the example below.

A calculation was run where L was increased with a factor of 2, see Table 1. It is clear that 18 m unsupported length leads already to totally unacceptable movement of the tunnel.

An interesting result is further that it appears that only with a finite value of A it is possible to get a condition of $F_s = 0$ for $x=0$. This condition is not always fulfilled in numerical calculations leading to shear forces in the lining that have no relation with reality.

A decreases quadratic with L therefore A can be minimized by using grout that acquire quickly a certain strength to develop the necessary shear strength. The ‘full scale’ consolidation tests described provide data on the consolidation properties. With the properties of the surrounding soil: shear modulus at unloading, permeability, it is then possible to calculate the time it takes before the necessary shear strength is available.

6.2 Variations

The calculation model presented in the section above, allows investigating the influence of various parameters. The loading on the lining close to the TBM exerted by the buoyancy force from the grout is $q \times x$ and thus 720 kN/m. Using eq. (1) and (2) it can be

Table 2. Influence of some variation in the parameters on the results of beam calculations.

Parameter	Calc 3	Calc 4	dimension
Input			
L (length of ‘unsupported’ zone)	9	9	m
q (distributed loading near TBM)	48	8.7	kN/m ²
EI (stiffness of lining)	5.4×10^7	5.4×10^7	kNm ²
M (moment on TBM)	18	18	MNm
Result			
A (displacement of lining)	0.017	0.015	m
$M(x=0)$	24	19	MNm
$F_{s,TBM}$ (shear force at $x=L$)	1.9	0.35	MN

derived that for such a situation $\tau_y = 0.5$ kPa (a bit lower than measured in the test shown in Figure 5 for fresh grout, but the maximum shear stress is a vector and therefore horizontal flow during injection decreases τ_y). It can be tested what will be the influence on the loading on the lining when this value is increased until 1 kPa. The loading on the lining reduces than to 432 kN/m close to the TBM and q to 48 kN/m². Another possible variation is to use the same shear stress (0.5 kPa) but to decrease the volumetric weight of the grout from 21 kN/m³ as it was for Sophia Rail Tunnel to for example 12 kN/m³. This will reduce the buoyancy force according to Eq. (2) to 78.3 kN/m close to the TBM, which, assuming again a linear increase in loading on the TBM, lead to a q of 8.7 kN/m². Table 2 shows results of calculation results obtained with the model described before.

As expected, both a larger shear stress in the grout and a lower density leads to a lower displacement of the lining, a smaller moment and shear force. Especially the reduction in shear force at $x=L$ is considerable. In this way the model can be used to get quantitative information on the influence of using a different grout.

Further research will focus on deformation and grout pressure measurements for different tunnels to see how general applicable the proposed model is.

7 CONCLUSIONS

The work described in the paper has led to the following conclusions:

- The thickness of a grout layer in a consolidation test has to be comparable to the thickness of the grout layer in the field if hardening and consolidation both has an influence.

- The stability of the tunnel in longitudinal direction depends on various parameters. The tunnel more or less 'seeks' the equilibrium conditions.
- A minimum grout strength is necessary for an equilibrium condition of the lining.
- The length of the insufficient supported zone is of crucial influence on the movement of the tunnel, the shear force at the TBM and the moments in the lining. Movements and moments can be reduced by reducing the length of this zone by changing the hardening or consolidation properties of the grout. Yield strength and density of the grout also influences the longitudinal loading on the lining.
- The model presented show quantitatively what is the influence of changing the grout parameters on the loading on the lining.

REFERENCES

- Bezuijen A., Talmon A.M., Kaalberg F.J. and Plugge R. Field measurements of grout pressures during tunneling of the Sophia Rail tunnel. *Soils and Foundations* vol. 44, No. 1, 41–50, Feb. 2004.
- Bezuijen A., Talmon A.M. 2003, Grout the foundation of a bored tunnel, 2003, *Proc. ICOF 2003, Dundee*.
- Shirlaw J.N., Richards D.P., Ramon P. and Longchamp P., 2004, Recent Experience in Automatic Tail Void Grouting with Soft Ground Tunnel Boring Machines. *Proc. ITA 2004, Singapore*.

Introduction to Model Testing

A number of model tests have been performed to study various aspects of tunnelling. Model tests were used for aspects that are difficult to test in the field. Testing can be difficult because controlled soil conditions are necessary or because a failure is needed to perform the test and such failure is in most cases not wanted in a real tunnel.

The first model test on shield tunnelling was performed several years before the first shield tunnel was made. The influence of tunnelling on an existing pile foundation was tested in a geotechnical centrifuge. The problem was seen as very important for the possibilities of shield tunnelling in Dutch cities. Among others the municipalities of Amsterdam and Rotterdam (the two largest cities in The Netherlands) contributed to this project. In the centrifuge the tunnelling process was simulated by a tube that could be decreased in diameter to simulate the volume loss. The soil conditions were comparable to the conditions present in the western part of The Netherlands; a soft clay layer was on top of a sand layer with densified sand. Loaded piles were located at various distances from the tube and the response of the piles on the volume loss of the tunnel was monitored. This setup has inspired various other researchers to perform comparable tests (Chen et al., 1999 and Jacobsz et al., 2002).

The face stability of the Second Heineoord tunnel was tested as a prediction of the real situation. The interesting part of this research was that the actual soil conditions were simulated in the test. This was done with 3 layers of sand with a varying density. As a prediction the test had only limited value because during the measurements it appeared that the minimum face pressure for a stable front is higher than according to the result of the test because of the presence of excess pore pressures in front of the tunnel face, see the chapter on field measurements. These excess pore pressures were not simulated in the model. For a situation without excess pore pressures the tests show a clearly the failure pattern that occurs in sandy subsoil.

Although a lot of attention was paid to the minimum pressure to prevent instability at the tunnel face, the first real problem in practice when drilling the

Second Heineoord Tunnel was an instability caused by too high pressures at the tunnel face leading to a blow out. The third paper in this chapter analyses this blow out and compared the results with the results of centrifuge tests where the grout pressures were raised until instability and plastic deformation occurs in the sand. Although there is thus a difference in geometry between the field measurements and the model tests, there is a reasonable agreement between the measured maximum pressures.

Another centrifuge research project was the face stability for a tunnel in soft clay. This test was not performed for a particular project, but was part of a research programme. The aim was to investigate what stability can be expected in very soft clay. The test results include the deformation as a function of the face pressure starting with very small settlements. The failure surface along the settlement trough that occurs at large deformations was determined by means of X-ray tomography. These results are published elsewhere (Kruse and Bezuijen, 1998).

Model tests on foam is the subject of the next two papers. The first of these two papers describes a model set-up to test different foams and to investigate the foam-sand interaction as it occurs in an EPB machine. While boring in sand an important function of the foam is to increase the porosity to a value higher than the maximum porosity of sand, so that the grain stresses become small. This finding is confirmed in the field measurements, which was the subject of a previous chapter. The screw conveyer is an important part in an EPB machine. A model was made to describe the flow of a sand-water mixture and the pressure drop in the screw conveyer.

The last paper deals with model tests that have been used in the design of the RandstadRail tunnel. This is a tunnel for a light rail system in Rotterdam. This tunnel is partly built in Holocene clay and the question was how the settling clay influences the loading on the lining. The results confirmed that the calculation method used is on the safe side. In the paper the results of the centrifuge tests are also compared with the results of Finite Element Calculations.

The influence of a bored tunnel on pile foundations

Adam Bezuijen & Joost van der Schrier

Delft Geotechnics, The Netherlands

ABSTRACT: The influence of a bored tunnel on an existing pile foundation has been investigated by means of model tests in a geotechnical centrifuge. Three tests were performed: one preliminary test with limited instrumentation for a tunnel in saturated sand and two tests with a soil model of sand with clay (layers) on top. The tunnelling was simulated by a model tunnel; a specially designed cylinder of which the diameter could be reduced. 6 piles were placed at different distances from the model tunnel and the load-settlement behaviour during reduction of the model tunnel diameter was monitored. The test results show that load-settlement behaviour was influenced by the horizontal distance from the pile to the model tunnel and the soil material that surrounded the model tunnel. Pile settlement was measured at larger distances from the tunnel when it was surrounded by sand. The settlement trough is measured as a function of the decrease in diameter of the model tunnel. The results from the settlement trough are compared with existing formulae of Peck and Verruijt.

1 INTRODUCTION

In regions with soft soil layers, most buildings are founded on piles to use the strength of stiffer layers at greater depth. In such a region it is likely that a bored tunnel, constructed for a metro or an underground part of a railway, will be founded in the same stiff soil layer as the pile tips of a pile foundation. During the boring process somewhat more soil is removed than the volume of the tunnel, leading to changes in the stress state of the soil. The influence of these changes on the bearing capacity of an adjacent pile foundation is of importance when a bored tunnel is planned in an urban area with many pile foundations. The interaction between loaded foundation piles and a tunnel under construction is difficult to model with (numerical) calculation programs, since it is a 3-dimensional problem and modelling the influence of the tunnel is only possible if the stress distribution around the driven piles is modelled properly. Therefore, this influence has been investigated in a model test in the geotechnical centrifuge of Delft Geotechnics (Nelissen, 1991). The tunnelling process was simulated by a model tunnel; a cylinder with the possibility to change the diameter in a controlled way. A decrease in the diameter of the model tunnel simulates the tunnelling process in which some more soil is removed than corresponds with the diameter of the tunnel. Six piles at different distances from the tunnel, loaded to 75% of their ultimate bearing capacity, were used to investigate the pile-tunnel interaction. In the tests, the diameter of the model tunnel was reduced and the settlement of the piles was monitored, as well as the depth and form

of the settlement trough at the soil surface. This paper describes the test set-up and the results of the tests. The consequences for practice are discussed.

2 TEST SET-UP

The prototype situation is a tunnel with a diameter of 7 m. This 7 m is in-between the diameter for a metro (6 m) and a single track railway tunnel (8–9 m). The prototype pile had a diameter of 0.4 m. A model scale of 1:40 was chosen.

A cross-section of the model is shown in [figure 1](#). It shows the soil model, the piles and the model tunnel. The soil model consisted of two layers of clay of 0.19 m, with a sand layer of 0.02 m in-between. The clay layers were preconsolidated. For handling the clay layers it was necessary to over-consolidate the top layers (1 and 2). The bottom layers (3 and 4) were normally-consolidated. The clay used in the tests was Speswite kaolin clay. The sand layer between the clay layers functioned as a drainage layer during the reconsolidation in the centrifuge. Three tests have been performed:

1. a preliminary test with a soil model of only densified sand with the same configuration of model tunnel and pile as shown in [figure 1](#), but with the centre of the tunnel and the pile tips 35 cm below the sand surface.
2. the 1st final test with the configuration of [figure 1](#) and the tunnel at the high position (position A in [figure 1](#)).

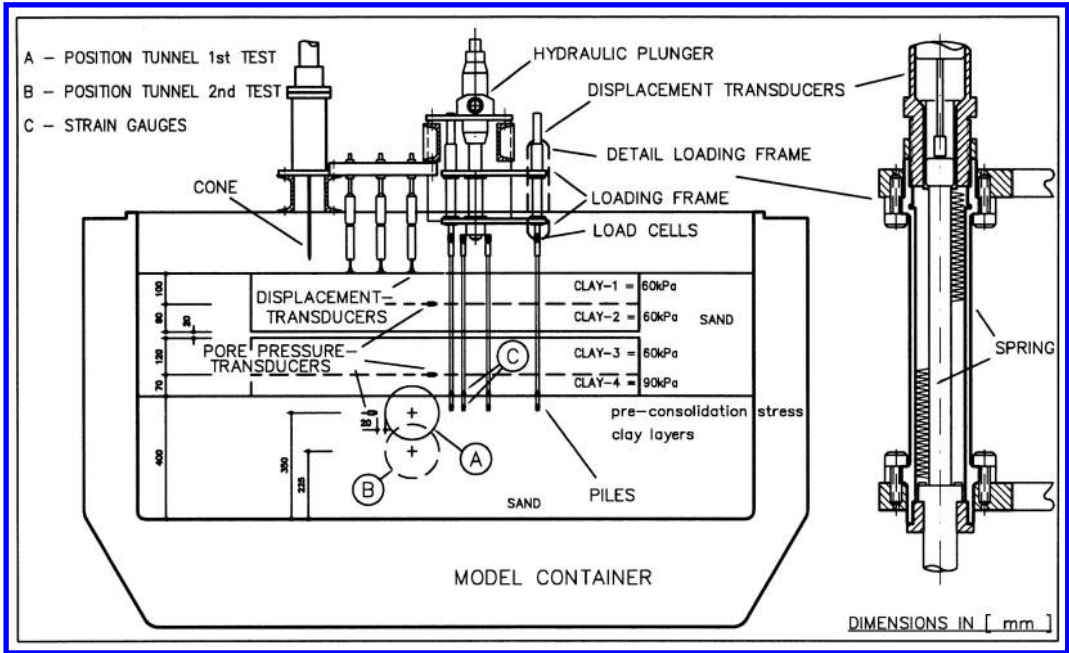


Figure 1. Cross-section through the centrifuge model.

Table 1. Properties of Speswhite kaolin clay and Eastern Scheldt sand.

<i>Properties clay</i>	
Unit weight constituent	26.1 kN/m ³
Liquid limit (LL)	69.0%
Plasticity index (PI)	31.0%
Plastic limit (PL)	38.0%
γ at W = 50%	17.0 kN/m ³
C_u/σ'_v	0.21
$I_r (=G/c_u)$	200
Friction angle ϕ	23°
Cohesion	0 kPa
<i>Properties sand</i>	
Unit weight constituent	26.5 kN/m ³
D_{50}	180 μ m
Friction angle at $D_r = 70\%$	45°

- the 2nd final test with the tunnel at the low position (position B in figure 1).

In all models the phreatic line was equal to the soil surface. The sand used is Eastern Scheldt sand, some properties of the clay and sand used are listed in table 1. After the tunnel was placed, the sand was densified by a vibration needle. Two piles were located at both 0.04 and at 0.08 m from the tunnel, one at 0.16 m and one at 0.32 m, resulting in a total of 6 piles. The positions of the piles were determined in a way to minimize group effects.

The piles were closed aluminium tubes with a diameter of 0.01 m. Forces on the piles have been monitored by a load cell on top of the piles and strain-gauges at 0.05 m and 0.01 m from the pile tip. The load cell on top of the pile measured the total load. The strain-gauge at 0.05 m was situated at the transition between sand and clay in the model and enables, knowing the load on top of the pile, to determine the friction of the clay along the pile shaft. The strain gauge close to the pile tip was used to monitor the tip force.

The piles were connected by springs to a loading frame. The positions of the piles in the loading frame can be seen in figure 2. The load on the piles could be controlled by a plunger on the loading frame. The springs had a stiffness of 0.1 kN/mm. The loading on the piles was calculated to be between 1.2 and 2 kN. With the springs chosen, a pile settlement of 1 mm implied a load reduction less than 10%. With the loading frame designed in this way it was possible to penetrate 6 piles with one plunger and to have a more or less force-controlled situation during the decrease in diameter of the model tunnel. The model tunnel consisted of 4 synthetic tunnel elements, placed on an aluminium core. By moving the core relative to the tunnel elements, the outer diameter could be varied (see figure 3). The entire model tunnel was covered by a rubber sack, which ensures watertightness and prevents intrusion of soil particles. The actual diameter of the tunnel was monitored by two displacement transducers mounted between the tunnel elements.

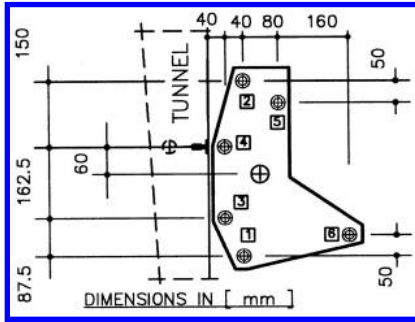


Figure 2. Top view on piles and loading frame.

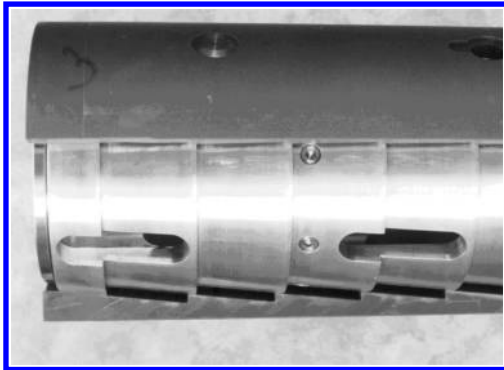


Figure 3. Detail of the model tunnel.

3 TEST PROCEDURE

The tests started with the model pile tips 15 mm above the actual testing position. The test procedure was as follows:

1. Reconsolidation of the clay model under its self weight at 40 g load. After 6 hours 95% consolidation was obtained.
2. When 95% consolidation was reached, a cone was penetrated in flight with a penetration speed of 0.15 m/s, comparable to the penetration speed in prototype.
3. The piles were penetrated to the actual testing position. This penetration was performed to acquire a stress state around the piles comparable to the stress state of a driven pile. The maximum penetration force was measured. Then the pile loading was reduced to 75% of the maximum penetration force to achieve a working load comparable with a heavy loaded pile in prototype. The reduction of load was not performed in the preliminary test.
4. The diameter of the tunnel was reduced continuously with the loading frame at a fixed position. The load-settlement curve of the piles was measured under the changed boundary conditions.

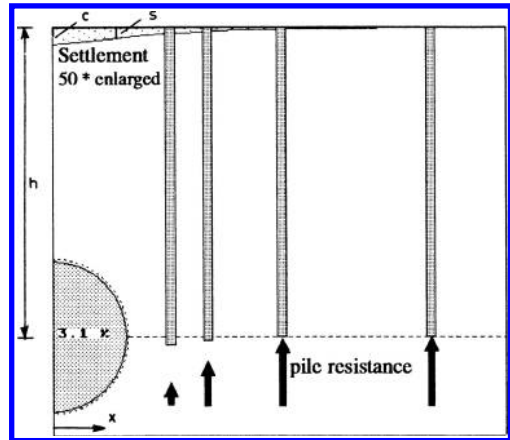


Figure 4. Results the preliminary test. The piles were all on the dashed line before the reduction of the tunnel diameter (all dimensions to scale).

5. The frame was pushed further to determine the ultimate loading capacity, after large pile settlement. This step was not performed in the preliminary test.

4 RESULTS

4.1 Overview

Results of the preliminary test are shown qualitatively in figure 4. In this figure the piles and tunnel are represented to scale. The number in the tunnel represents the relative decrease of the cross-sectional area of the tunnel. The measured settlement of the piles and the settlement trough are shown. This test showed large settlements of the piles close to the tunnel (much more than 1 mm) and, therefore, also a significant reduction in the pile resistance, as represented by the arrows below the pile. All piles had the same resistance before the reduction of the diameter of the model tunnel. The tests with clay layers above the tunnel show comparable results. The analysis of the results presented below focuses on the settlement trough measured above the tunnel and the pile settlement.

4.2 Settlement trough

The settlement trough at ground level was measured at two positions during the preliminary test and at three positions during the final tests (see figure 1). The results have been fitted with formulae presented by Peck and Verruijt. The formula of Peck (presented in Attewell et al. (1986)) is empirically based and written as:

$$s = ce^{-0.5(x/\sigma_s)^2} \quad (1)$$

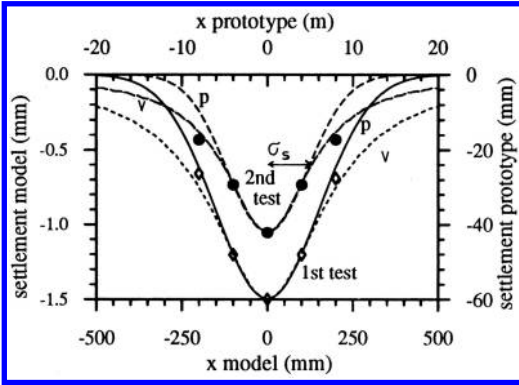


Figure 5. Settlement trough at 3% volume decrease of the model tunnel in the 1st and 2nd test. Measurement points (with the same values on the negative X-axis to impose a symmetric curve) and fits with the formulae of Peck (p) and Verruijt (v).

where s is the settlement, x the horizontal distance from the centre of the tunnel and c and σ_s are parameters defining the depth and the width of the trough. Attewell et al. also present relations for σ_s depending on the type of soil. Sagasetta (1987) has presented a calculation method to derive an analytical solution of the equations describing the deformation caused by a diameter decrease in an incompressible elastic half space. Based on this method Verruijt (1993) derived for a compressible elastic half space:

$$s = 2(1 - \nu) \frac{\Delta V}{\pi h} \frac{1}{1 + (x/h)^2} \quad (2)$$

where h is the depth of the center of the tunnel, ΔV the volume loss, V the total volume of the tunnel and ν the poisson ratio of the soil.

The equations can be fitted well with the measurement points (see figure 5). The mean values found for the parameters of equation 1 and 2 during the volume decrease are listed in table 2. From these results it appeared that the preliminary test and the second test – the tests where the tunnel was surrounded with sand – have comparable results for the settlement trough. The test with 1/5 of the model tunnel in clay has a wider settlement trough and a lower value of ν . The value of h , found when fitting the settlement trough to equation 2, is much less than the actual depth of the tunnel. This means, that although the equation for the settlement trough as derived by Verruijt can be reasonable, the soil is not behaving as an elastic material, as is assumed in the derivation of the formula, and plastic deformation occurs. This can also be concluded from the values of the poisson ratio. A value larger than 0.5 indicates, that there is an increase in volume of the material during deformation. This is not possible for

Table 2. Mean values of the parameters in equations 1 and 2 for the settlement trough.

parameter	prel. test	1st test	2nd test
σ_s (mm)	115	151	117
h (mm)	98	202	150
ν (-)	0.57	0.33	0.65

an elastic material. However, it is possible during plastic deformation and is well known for dense sand as dilatancy. Indeed it is found that the value of ν is only higher than 0.5 when the model tunnel is completely surrounded with sand.

This dilatancy of the sand around the tunnel can be measured in this model test because there is complete control of the tunnel volume. This is not the case when tunnelling is performed in the field. In field measurements, the volume decrease is measured from the settlement trough under the assumption that the volume taken at depth is equal to the volume of the settlement trough at ground level. Such a procedure is not always justified as appears from figure 5, which shows the settlement troughs for the 1st and 2nd test, both at 3% decrease of tunnel volume. Due to dilatancy of the sand in the 2nd test, the volume of the settlement trough is smaller than in case of the 1st test.

4.3 Pile settlement

Figure 4 shows that the volume decrease of the model tunnel has a distinct influence on the pile foundation leading to a reduction of the bearing capacity and consequently to pile settlement. As an example of the reduction in bearing capacity, the results of the 2nd test are presented in figure 6 as a function of the relative decrease in volume of the tunnel. For the piles at 0.04 and one at 0.08 m from the tunnel the reduction in bearing capacity is such, that the springs mounted on the loading frame reached their maximum stroke. This happened when the bearing capacity of the pile became less than appr. 0.9 kN, and no further settlement was possible. For these piles, ongoing soil deformation around the tunnel, by further decrease of volume, led to a rapid decrease in the bearing capacity. This result was also clearly demonstrated by the friction measured on the piles (see figure 7). The magnitude of the pile settlement is larger than the settlement of the clay, therefore positive friction developed on the piles. However, when the settlement of some of the piles stopped, negative friction developed, because the settlement of the soil continues. The pile settlement at 1% volume decrease of the model tunnel as measured in the 3 tests is shown in figure 8. In this figure, a mean value with deviation is presented for the locations with two piles at the same distance. A low value of volume decrease

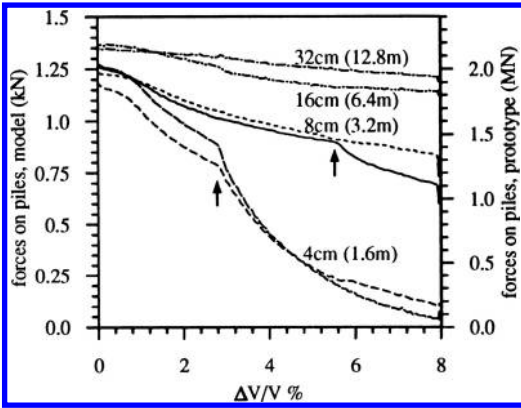


Figure 6. 2nd test: forces on piles during decrease in volume, the arrows indicates the point at which the settlement of the piles stops because the spring was pushed out completely (prototype distances between brackets).

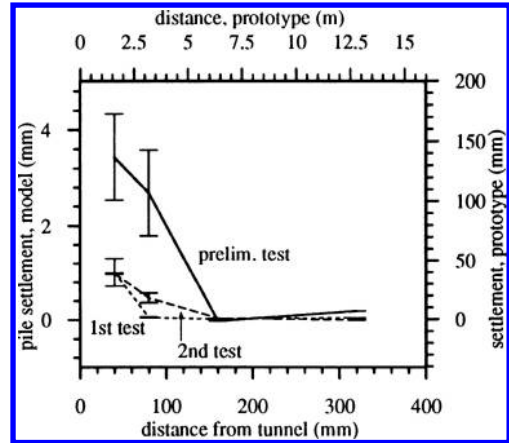


Figure 8. Pile settlement in the various tests at 1% decrease of tunnel volume. The settlement measured for the pile at 0.32m distance is not realistic, but the result of a small deformation of the loading frame.

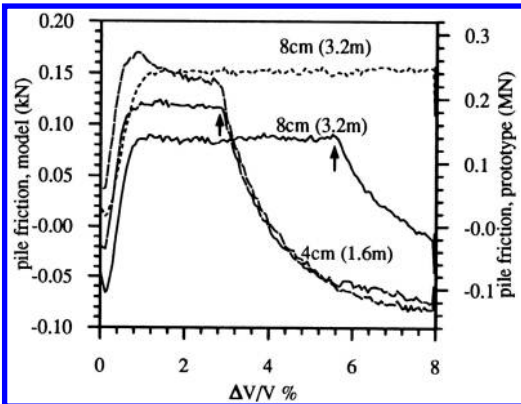


Figure 7. 2nd test: friction measured on piles.

was chosen because at a larger value the settlement is limited by the stroke of the springs in the loading frame.

From this figure, it is clear that the pile settlement was largest in the preparatory test. In this case the pile loading was larger relative to the bearing capacity of the pile. For the 1st test the distance, in which piles were influenced by the tunnel, is smaller than for the 2nd test. This appeared to be true for different values of volume decrease. In the preliminary test as well as in the 2nd test, the model tunnel was completely surrounded with sand. Deformations in this sand influenced the pile foundations at a larger distance. The following mechanism is proposed: the tunnel deformations cause a reduction of the horizontal stresses in the soil. This reduction reduces the bearing capacity of the piles. This is due to the fact that in case of driven piles

an important part of the bearing capacity is realized from the high horizontal stresses that develop during pile driving. In a stiff soil such as sand, a prescribed deformation leads to changes in stresses over larger distances and therefore to a reduction of horizontal stress over a larger distance.

5 CONCLUSIONS

The results of the tests as presented in this paper lead to the following conclusions:

1. A geotechnical centrifuge appears to be a valuable tool for studying the interaction between a bored tunnel and an existing loaded pile foundation.
2. The volume loss prescribed, by changing the tunnel diameter, can be more than the volume loss measured at ground level due to dilatation of the sand.
3. The width of the settlement trough is smaller in the tests where the tunnel is completely surrounded with sand (the preliminary and 2nd test). On the other hand the distance on which pile settlement can be measured is larger in these tests.
4. Pile settlement can be quite significant, if the volume loss is 1% or more and the distance between the pile and the tunnel is less than 1 tunnel diameter (0.175 m or 7 m in prototype). However, extrapolation of the results from the test makes it reasonable to assume that shorter distances, or larger volume loss are acceptable, in the case where the tunnel is placed for a less substantial part in the foundation layer.

ACKNOWLEDGEMENTS

The authors gratefully acknowledge the participants in this project, who provided the necessary funds:

- Municipal Management Amsterdam
- Public Works Rotterdam
- Nederlandse spoorwegen
- Bored tunnel combination:
 - Ballast Nedam Beton en Waterbouw BV, Hollandse Betonen Waterbouw BV, Structon Betonbouw BV, Ways und Freytag GA
- Dirk Verstoep BV
- van Hattum en Blankevoort
- Koninklijke van Drunen BV
- Delft Geotechnics
- Ministry of transport and public works
- de Weger Architects and Consulting engineers
- Ministry of Economic Affairs

The authors further acknowledge J. Out for the design of the equipment (model tunnel and pile loading frame), T. van Dijk, F. Kop and W. Löning for their assistance during preparation and testing.

REFERENCES

- Attewell P.B., Yeates J., Selby, A.R. (1986). *Soil Movements Induced by Tunnelling and their Effects on Pipelines and Structures*. Blackie, London. ISBN 0-216-91876-6.
- Nelissen H.A.M. (1991). *The Delft geotechnical centrifuge*, Proc. Int. Conf. Centrifuge '91, Boulder Colorado.
- Sagaseta C. (1987). *Analysis of undrained soil deformation due to ground loss*, Geotechnique 37, No. 3, 301–320.
- Verruijt A. (1993). *Elastostatics of a half space*. Lecture notes “Soil Dynamics”, University of Technology, Delft.

Shield tunnelling in saturated sand – face support pressure and soil deformations

J.W. Plekkenpol

Centre for Underground Space Technology, Gouda, The Netherlands

J.S. van der Schrier

Haskoning Consulting Engineers and Architects, Nijmegen, (formerly Delft Geotechnics, Delft), The Netherlands

H.J.A.M. Hergarden

Delft Geotechnics, Delft, The Netherlands

ABSTRACT: To support tunnelling activities in The Netherlands the Dutch government decided in 1994 to finance a five year research and development programme on tunnelling in soft soil.

One of the aspects to be studied is the determination of the appropriate slurry pressure to ensure full face stability in the case of slurry shield tunnelling. To determine the relation between support pressure and soil deformations in fully saturated sand, a model test has been carried out using the geotechnical centrifuge of Delft Geotechnics. Surface settlements and soil displacements close to the tunnel face were measured as a function of the applied support pressure and will be presented graphically.

In this paper the test set-up, testing procedures and final test results are given. The exact size and shape of the collapsed soil body is determined afterwards, and will be shown. The influence of arching in relation to face stability will be discussed.

The limit support pressure as determined from the centrifuge test is found to be slightly larger than the ground water pressure. The simple three dimensional model, proposed by Jancsecz and Steiner has been used to make a limit state calculation of the slurry pressure. The calculated limit support pressure is slightly larger than the ground water pressure at tunnel axis level. Comparison of these results with the test results shows reasonable agreement. It can be concluded that the three dimensional model as proposed by Jancsecz and Steiner is valid for the typical soil conditions at the site of the Second Heinenoord Tunnel.

1 INTRODUCTION

In 1994 an extensive research and development programme was initiated by the Dutch Government. To manage and coordinate this programme a Centre for Underground Space Technology (in Dutch COB) was established. In 1994, as part of the research programme, the detailed monitoring of two TBM tunnelling projects was started in order to gain experience with large diameter tunnelling in very soft soil. The first project is the Second Heinenoord Tunnel under the river Oude Maas and the second is the Botlek Railway Tunnel under the same river near Botlek to relieve the existing Botlek Bridge. From both projects the prototype behaviour is predicted using current methods and experimental research.

In the beginning of 1997 the boring of the first large diameter tunnel in The Netherlands, the Second Heinenoord Tunnel, has been started. The tunnel boring process is monitored continuously.

In this paper the results of predictions made with respect to tunnel face stability, using the geotechnical centrifuge of Delft Geotechnics, are presented and discussed. More detailed information of these prediction can be found in (Van der Schrier, 1996). The results will be used for comparison with the field measurements in the very near future.

2 PROTOTYPE SITUATION AT HEINENOORD

The river crossing consists of two tunnels with a length of 950 m. For the boring of the two 8.3 m diameter tunnels a slurry shield tunnel boring machine is used. The tunnels will be bored in holocene and pleistocene formations. The (upper) Holocene consists locally of sand and soft to very soft clay. The Pleistocene consists of dense sand. The boundary between Holocene and Pleistocene is located at a depth of approximately

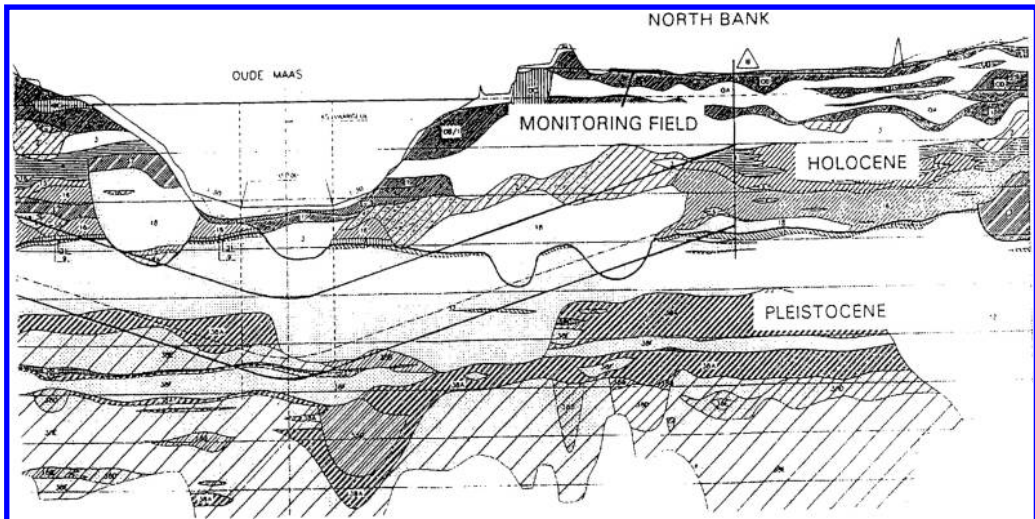


Figure 1. Longitudinal geotechnical profile of the Second Heineoord Tunnel.

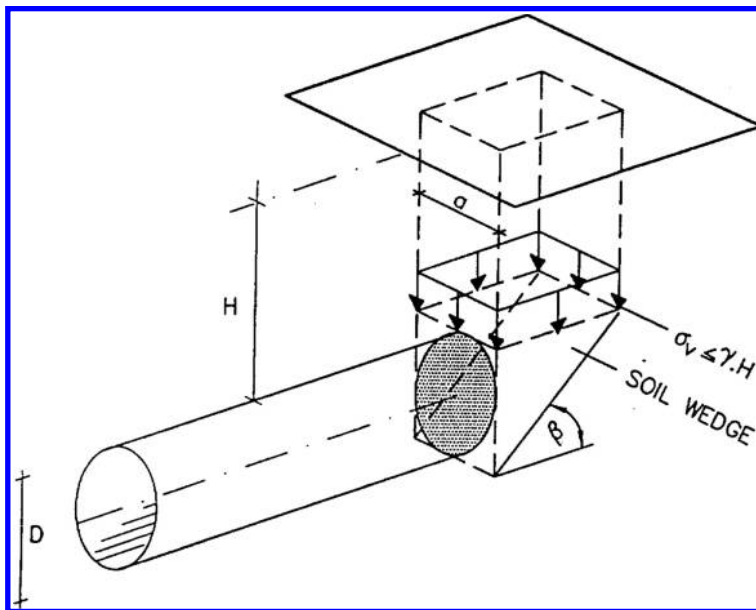


Figure 2. Three dimensional limit equilibrium model.

NAP -15 m (NAP is the Dutch reference level). The longitudinal (geotechnical) profile is shown in figure 1. The ground water level equals approximately NAP 0.0 m. Due to the high ground water level all layers can be considered as fully saturated.

At the North bank a $50 \times 75 \text{ m}^2$ monitoring field has been established. The predictions are valid for this monitoring field. The tunnel axis depth equals 15.5 m below surface level. At this location the soil consists of mainly sand.

3 PROBLEM DEFINITION

During the construction of the Second Heineoord Tunnel difficult soil conditions will be encountered. For safety reasons excessive soil deformations at the tunnel face and inward-flow of ground water should be avoided. Therefore, the appropriate support pressure has to be determined.

To determine this pressure and for a better understanding of the mechanics in front of the slurry shield,

the collapse mechanism should be known. This problem is three dimensional and can be studied by using a limit state design method, which has already been done by several authors. For a synopsis of the various analysis methods, reference is made to Balthaus (1989). Limit-state-design-based solutions have been proposed by Leca and Dormieux (1990). Leca and Dormieux (1990), Anagnostou and Kovári (1994) as well as Jancsecz and Steiner (1994) have the experience that the upper bound estimates are in close agreement with test results. Jancsecz and Steiner based their calculations on a simple three dimensional model (figure 2).

For a limit state calculation of the slurry pressure, it is most important to know the exact size and shape of the collapsed soil body. To establish the validity of the three dimensional model for the soil conditions as encountered at the site of the Second Heinenoord Tunnel, a centrifuge test has been carried out. This test gives information on the relation between the slurry pressure and the soil deformation at the tunnel face level as well as at surface level for typical Dutch soil conditions.

4 CENTRIFUGE TESTING

4.1 Why centrifuge testing?

The constitutive behaviour and the shear strength of soil materials depend on the effective stress level in the soil. The effective stresses are determined by the prototype geometry and the mass of the soil materials (submitted to the acceleration of gravity). In a 1:N scale model the dimension length is scaled down with a factor N compared to the prototype. As a result the stresses are far too low. In order to get reliable model test results, not only the mean effective stress in the model should be representative for the prototype under investigation, but also the distribution of stresses. When using the same soil material(s) in the model as present in prototype, this stress requirement in the soil model can be fulfilled by increasing the unit weight of the soil with a factor equal to the scaling factor by which the prototype is scaled down. By increasing the acceleration of gravity that acts of the model, similitude is obtained between model and prototype regarding the stress-strain relationship of the soil. This can be done by using a geotechnical centrifuge.

4.2 General scaling rules

From model laws it follows that for a first interpretation of test results the scaling rules in table 1 can be used. A geometrical scaling factor of 1:70 has been chosen. In most of the figures the dimension length is expressed in model quantities. To estimate this dimension in prototype terms the model quantity

Table 1. Scaling factors in centrifuge tests.

Quantity	Symbol	Prototype/ model	Scaling factor	SI-unit
Length	L	N	N_L	m
Stress	σ	1	N_σ	kN/m ²
Strain	ε	1	N_ε	–
Acceleration	g	1/N	N_g	m/s ²
Force	F	N ²	N_F	N

may be multiplied by the geometrical scaling factor ($N = 70$).

5 MODEL AND INSTRUMENTATION

5.1 Model boundary conditions

In order to obtain well defined test results, allowing for a direct and accurate comparison with current design methods, the following boundary conditions were adopted for the modelling of the prototype:

- In the centrifuge test only static equilibrium is investigated. The excavation process is not modelled and the tunnel module is fixed in place.
- The transition zone between the fluid in the working chamber and in the surrounding soil is impermeable to water.
- The initial horizontal effective stress equals almost half of the vertical effective stress.
- The volumetric mass of the support fluid equals 1000 kg/m³.
- The model scale equals approximately 70. The exact g-level was chosen in such a way that the model stresses at tunnel-axis level were representative for the stresses in the corresponding prototype.

5.2 Tunnel module

The tunnel module consists of a circular tube with a working chamber at the front side. The outer diameter of the tube equals 122 mm, the wall thickness equals approximately 6 mm. The working chamber is filled with support fluid. A schematic diagram is given in figure 3. In order to prevent the support fluid from escaping through the granular soil an flexible impermeable membrane is used. The membrane represents the mudcake that develops on the granular soil in the prototype. The mudcake is assumed to be impermeable. This is under prototype conditions not the case and a hydraulic gradient exists over the thickness of the mudcake zone. However, at low support pressures close to the phreatic water level, the influence of the hydraulic gradient on global stability is limited.

Support fluid can be pumped in and out the working chamber in order to control the support pressure.

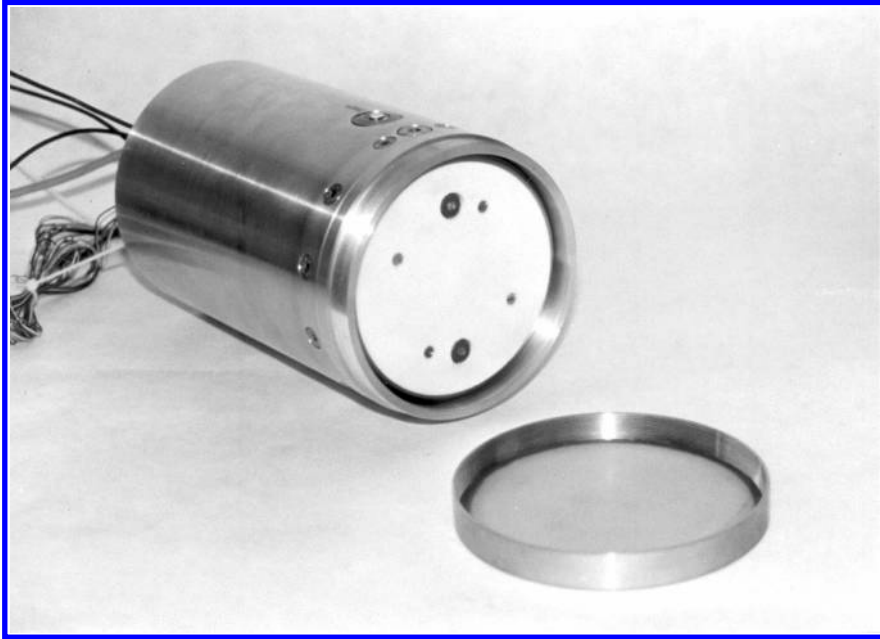


Figure 3. A schematic diagram of the tunnel module.

Active failure of the soil body in front of the tunnel face is simulated by a reduction of the support pressure (force controlled).

During spinning up of the centrifuge model, the soil stresses increase. In order to maintain face stability during this test phase, the tunnel face is supported mechanically. However, before the actual centrifuge test can be executed, the mechanical support must be removed, and the support pressure must be taken over by the support fluid. Therefore, to avoid soil collapse or excessive soil displacements inward the tunnel during this take over, the fluid pressure in the chamber is increased firstly. (Consequently, the load on the mechanical support decreases.) Since the normal stiffness of the mechanical support is limited, the tunnel face is pushed a few tenths of microns outwards. The effect of this outward displacement is negligible, since the soil reaction remains almost completely elastic. Once the contact between the mechanical support and the tunnel face is broken, the mechanical support is pulled back and the fluid is lowered to the level that was recorded just before the start of the taking over procedure.

5.3 Preparation procedure of the soil model

The model test was not only a benchmark test for the verification of (numerical) design methods, it was also meant as a mean to predict the prototype behaviour

Table 2. Geotechnical parameters used in centrifuge tests.

Layer number and location	Thickness d [mm]	Porosity n [%]	Relative density Dr(e) [%]	Angle of Internal friction ϕ [°]
1/under	183	35.1	98.5	44
2/middle	122	39.4	66.5	38
3/upper	160	41.8	46.5	34.5

at the Heinenoord location. Therefore soil properties must meet prototype properties as close as possible and must be known within sharp boundaries. Based on the results of the field and laboratory testing programme, conducted for the design of the Second Heinenoord Tunnel, and assuming a failure mechanism in accordance with Jancsecz, the relative importance of the individual soil layers was evaluated. It was then decided to model the prototype with three geotechnical units. For the soil Eastern Scheld model sand is used. The average particle size of this model sand (d_{50}) equals 155 μm . The uniformity d_{85}/d_{15} is 1.8. The geotechnical strength properties are given in table 2. All layers are completely saturated with water.

The first layer was densified to the minimum porosity that could be achieved within the model boundaries (approximately 35%). The soil layers 2 and 3 were

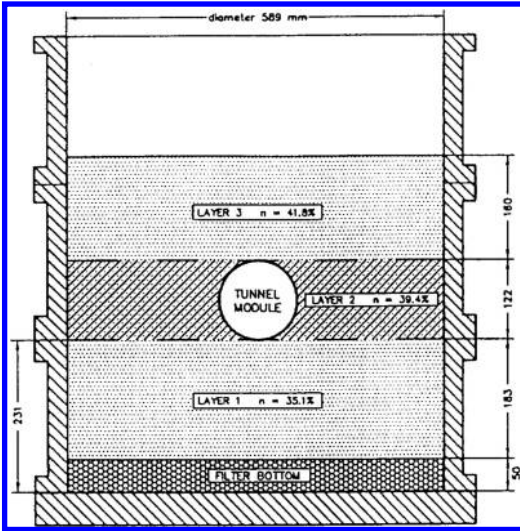


Figure 4. Section through the centrifuge model.

prepared in the loosest possible density (using the technique of raining under water), and then compacted dynamically till the desired porosity was achieved. For this purpose a number of shock waves was applied to the soil model (in a vertical direction), while a surcharge load was placed on top of the model. Schenkeveld e.a. (1996) has estimated the absolute accuracy of the porosity of the soil layers to be smaller than $\pm 0.6\%$.

The tunnel was placed in the model after preparation of the first soil layer. A section through the centrifuge model is presented in figure 4. The coloured marker layers, which will be used to determine the shape and size of the collapsed soil body are not shown.

The homogeneity of the soil layers is illustrated with figure 5. The model soil boundaries can be distinguished clearly in this figure. The smooth increase of the cone resistance with depth is a proof for the homogeneity of the soil model. Compared to prototype, the model cone resistance of soil layer 2 is on the average 5 MPa higher than the corresponding value in prototype. The cone of the model soil layer 3 is almost equal (in the zone just above the tunnel crown).

5.4 Instrumentation

During execution of the test the following quantities are measured: time, pressure in the working chamber, displacement of the membrane, ground water pressure and the displacements of the surface.

The slurry pressure in the working chamber is measured using a pressure gauge at tunnel axis height. This pressure represents the mean pressure on the tunnelling face (the distribution of the slurry pressure over

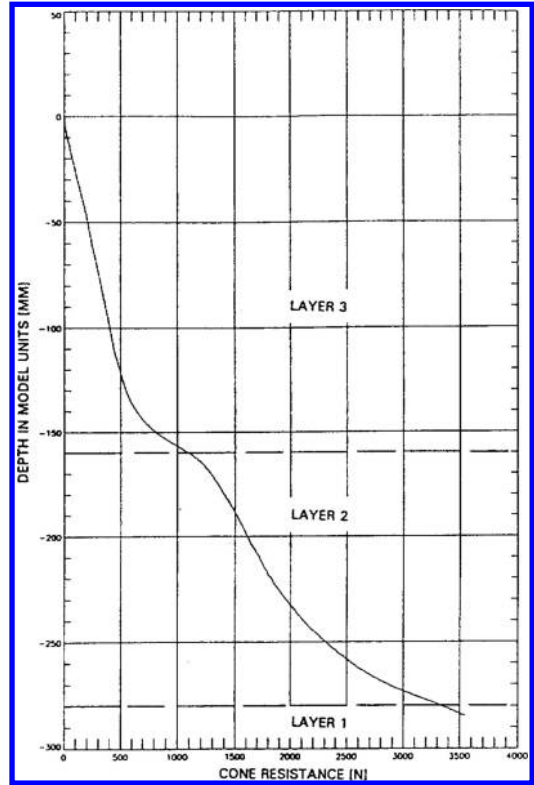


Figure 5. Cone resistant with depth of the soil model.

the height of the tunnel face is also known since the density of the support fluid is known as well). The ground water pressure is measured using a pore pressure transducer, which was mounted in the tunnel wall.

The horizontal displacements of the membrane of the tunnel module are measured at two locations. Both are located on a vertical line through the centre of the module at a distance of 32.5 mm (see figure 3). Surface settlements are measured at 25 locations. Those locations are mainly concentrated at positions just in front of the tunnel face.

5.5 Test procedure

The general test procedure is given below.

- Preparation of soil layer 1 (see preparation procedure).
- Installation of the tunnel module. At this stage the stability of the tunnel face is ensured by a mechanical support frame.
- Preparation of soil layers 2 and 3 (see preparation procedure).
- Spinning up of the geotechnical centrifuge.

- Taking over of the mechanical support of the tunnel face by slurry pressure (see tunnel module)
- Force controlled lowering of the face supporting slurry pressure till failure of the soil body occurs.
- Spinning down of the geotechnical centrifuge.
- Removal of the ground water, dismantling of the soil model and determination of the size and shape of the collapsed soil body.

6 OBSERVATIONS

6.1 Observations during testing

In figure 6 an overview of the test results is given. These test results are presented as a function of time. The line 'slurry pressure' represents the fluid support pressure in the working chamber at tunnel axis

level. At time $t=0$ sec, the tunnel face is still completely supported by the slurry pressure. This pressure reads 240 kN/m^2 . The water pressure at tunnel axis level equals 160 kN/m^2 . The initial horizontal effective stress needed for equilibrium is approximately equal to 80 kN/m^2 (at tunnel axis level). This value is almost equal to half of the vertical effective stress at the same level.

The amount of support fluid, which is pumped out of the working chamber, is given as the line 'volume of pumped-out slurry'. The linear shape proves the support to be well de-aired and shows that the pump rate is a constant during the execution of the test.

At the moment that the support fluid is pumped out of the working chamber, the support pressure decreases and as a result the rubber membrane starts to deform inwards the tunnel module. The support pressure reaches a minimum value at the moment

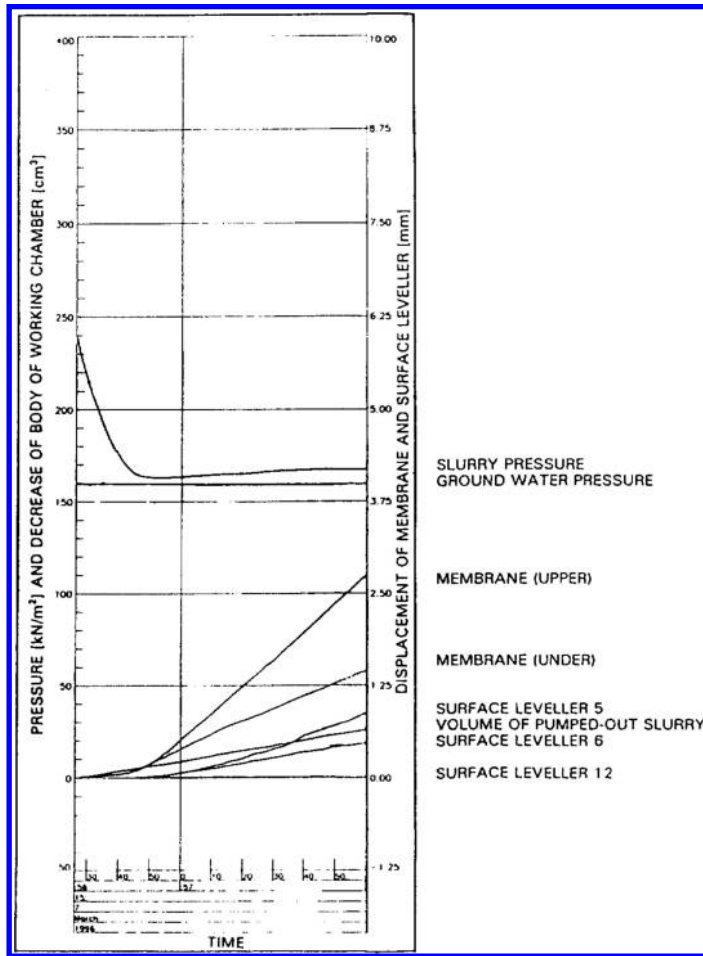


Figure 6. Overview of results of centrifuge test.

that the soil collapses. The support pressure is then approximately 165 kN/m^2 .

The displacements of the rubber membrane (tunnel face) at a distance of 32.5 mm below and 32.5 mm above the tunnel axis level are both given. These displacements start to differentiate after full collapse of the tunnel face. The largest displacements inwards the tunnel module are recorded below tunnel axis level.

In the same figure the lines 'surface leveller 5 and 6' show the soil displacements at surface level at 30 mm and 60 mm in front of the tunnel face respectively. Apparently, at tunnel depth soil displacements are recorded directly after pumping starts, while it takes some time before soil displacements are recorded at surface level. This is a proof for arching. The soil body between the tunnel face and surface level is more or less 'self bearing' till a minimum support pressure is reached. Then the soil collapses and large displacements occur. The largest displacements at surface level were recorded just in front of the tunnel face, at larger distances from this tunnel face the displacements appeared to become almost zero (see surface leveller 12 in the same figure). The size of the failure zone is limited (see also 6.2).

Complete failure (limit state) occurs at a support pressure of about 5 kN/m^2 above the ground water pressure at tunnel axis level. Till this moment the soil displacements are very limited. Depending on the exact stiffness and strength characteristics of the soil, these displacements are estimated at 5 to 10 mm for the prototype under consideration.

6.2 *Shape of the collapsed soil body afterwards the test*

Afterwards the test the ground water has been removed and the exact size and shape of the collapsed soil body has been determined by subsequently removing parts of the above and in front laying soil layers. Just by making vertical and horizontal cuts and using the information of the deformed coloured marker layers, it is possible to create a three dimensional profile of the collapsed soil body.

The photograph presented as figure 7 shows a section through the soil model. The pencil lays on the horizontal plane, which is located a few millimetres above tunnel crown level. The point of the pencil is heading towards the tunnel face. (If the tunnel module could move, it should move forwards in the direction of the photographer.) Just behind the point of the pencil a vertical outcrop through the model arises. The text board is located on top of the soil model.

On the vertical outcrop, thanks to the relative displacements of the coloured marker layers, the shape of the collapsed soil body can be distinguished clearly. On the horizontal plane, which happens to be a coloured marker layer too, the light area marks the boundaries of the collapsed soil body in the horizontal plane. The coloured marker layer is pushed downwards and original soil is now visible.

In a longitudinal direction the shape and size of the collapsed soil body have been determined graphically. The observed failure area is composed by putting all of the cross sections together. Figure 8 shows the failure

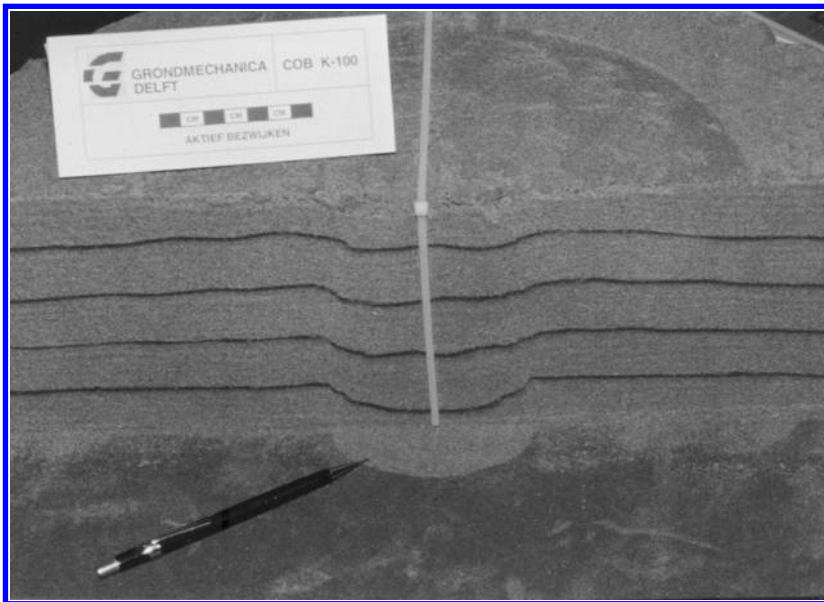


Figure 7. Size and shape of the collapsed soil body in front of the tunnel module.

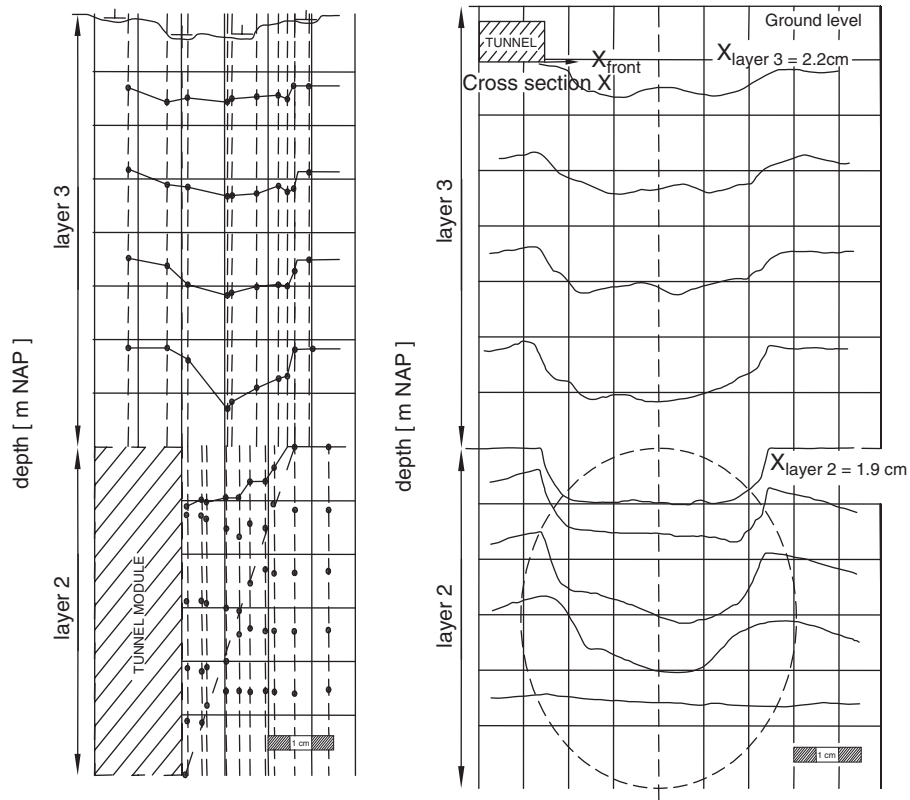


Figure 8. The shape and size of the failure zone in the longitudinal (left) and in a cross section (right) in front of the tunnel module.

zone. The thick dashed lines mark the boundaries of the failure area.

The shape and size of the soil body in the cross section, which lays approximately 2 centimetres in front of the tunnel module is presented graphically in the same figure (figure 8). In this figure the two ground layers are given and the position of the tunnel module is shown with dashed lines. The following things can be recognised from this figure. The magnitude of displacements in the coloured marker layers differ at various heights. Near surface level displacements are smaller than those occurring in front of the module. The boundaries of the collapsed soil body are slightly curved. The shape of an 'egg' has been developed.

7 LIMIT STATE CALCULATIONS

The three dimensional model, proposed by Jancsecz and Steiner, has been used to compare the test results with limit state calculations. This three dimensional collapse model consist of two parts: a silo wedge, the lower part, and a soil silo, the upper part (see

figure 2). The circular cross-section of the tunnel is approximated by a square whose sides are as long as the diameter D of the tunnel. The soil is idealised as a rigid-plastic material obeying the Mohr-Coulomb failure condition with cohesion c and angle of internal friction ϕ .

The parameters used in this calculation are presented below:

submerged unit weight:	$\gamma = 20 \text{ kN/m}^3$
angle of internal friction:	$\phi = 38^\circ$
cohesion:	$c = 0 \text{ kN/m}^2$
inner TBM diameter:	$D = 7.68 \text{ m}$
cover depth:	$H = 11.6 \text{ m}$

First the vertical pressure resulting from the soil silo and acting on the horizontal surface of the soil wedge has been calculated according to Terzaghi's solution. The size of the soil silo depends on the critical inclination angle β of the soil wedge. For $\phi = 38^\circ$ and $H/D = 1.5$ this inclination angle is 69° . The circumference of the horizontal plane of the soil silo (U) can be calculated at 21.1 m. The area of this plane (F) is 22.2 m². The resulting vertical stress $q_s(t)$ of the

prism at the interface between soil silo and soil wedge can be calculated at 32.7 kPa. With knowledge of β a three dimensional earth pressure coefficient has been derived: $K_{A3} = 0.16$.

The value of the limit support pressure at tunnel axis level has been calculated at 165 kPa. The water pressure at this level is 160 kPa. This means that the excess pressure that is necessary to retain equilibrium at this level (safety factor = 1) is very low: 5 kPa.

8 CONCLUSIONS

The geotechnical centrifuge has been used to examine the stability of the tunnel face in saturated sand. The relationship between face support pressure and displacements at the tunnel face and at surface level has been determined. From this relationship a few conclusions can be drawn. A slight reduction of the support pressure immediately results in displacements in front of the tunnel face. Due to arching in the above soil layer no surface settlements occur as a result of this reduction. Further reduction of the support pressure, almost equal to the ground water pressure leads to complete collapse of the soil body. Still the displacements at surface level are quite smaller than those in front of the tunnel face.

In the centrifuge test the transition zone between the fluid in the working chamber and the surrounding soil has been modelled as a membrane, which is a simplification of the reality. The infiltration of the slurry into the ground has not been taken into account.

After the test the ground water in the test set-up has been removed and the shape and size of the collapsed soil body could, thanks to the various coloured

markers, be determined precisely by making vertical and horizontal cuts in the dry ground model.

The simple three dimensional model, proposed by Jancsecz and Steiner has been used to make a limit state calculation of the slurry pressure. The calculated limit support pressure is slightly larger than the ground water pressure at tunnel axis level.

Comparison of these results with the test results shows reasonable agreement. It can be concluded that the three dimensional model as proposed by Jancsecz and Steiner is valid for the typical soil conditions at the site of the Second Heinenoord Tunnel.

REFERENCES

- Schrier, J.S. van der (1996): *Influence tunnel face stability, experimental prediction V10 Meetgebied Noord*, Report K100-W-037 / CO-358850/39, Delft Geotechnics (in Dutch).
- Schenkeveld, F.M. and Schrier, J.S. van der (1996): *Preparatie meerlagen grondmodel in de geocentrifuge*, Internal Report SE-50116/320/1, Delft Geotechnics (in Dutch).
- Balthaus, H. (1989): Tunnel face stability in slurry shield tunnelling. *Proceedings of the twelfth International Conference on Soil Mechanics and Foundation Engineering*, Rio de Janeiro, Balkema, Rotterdam, Volume 2, 775–778.
- Leca, E. and Dormieux, L. (1990): Upper and lower bound solutions for the face stability of shallow circular tunnels in frictional material. *Géotechnique* 43, 5–19 (in French).
- Anagnostou, G. and Kovári, K. (1994): The face stability of slurry-shield-driven tunnels. *Tunnelling and Underground Space Technology*, Vol. 9, No. 2, 165–174.
- Jancsecz, J. and Steiner, W. (1994): Face support for a large mix-shield in heterogeneous ground conditions. *Tunnelling '94*, The Institution of Mining and Metallurgy and The British Tunnelling Society.

Blow-out pressures measured in a centrifuge model and in the field

Adam Bezuijen

GeoDelft, The Netherlands

Henk E. Brassinga

GeoDelft, The Netherlands

ABSTRACT: A blow-out that occurred during the drilling of the 2nd Heinenoord Tunnel is investigated and the measured pressures are compared with measurements that were obtained during centrifuge experiments performed to investigate the maximum grouting pressure. Although geometry of the tunnel face is different from the geometry of the centrifuge tests, comparable results were obtained. It appeared that the pressure at which a blow-out occurred was equal to the pore pressure plus 2 to 3 times the vertical effective stress. This is more than what is often used as an upper boundary (pore pressure plus 1 time the vertical effective stress), but much less than according to some theoretical predictions.

1 INTRODUCTION

To prevent a blow-out at the tunnel face or during grouting of the tail void it is of importance to know the maximum pressure allowed. A blow-out that occurred during the drilling of the 2nd Heinenoord Tunnel showed that this is not only a theoretical risk.

In the shield tunneling practice it is generally accepted that the maximum allowable pressure at the tunnel face is equal to the pore pressure plus the vertical effective stress at the top of the tunnel. In theoretical studies, (for example Jancsecz & Steiner, 1994; Anagnostou & Kovári, 1994 and Leca & Dormieux, 1990) more attention was paid to the minimum allowable face pressure than to the maximum pressure.

In this paper the measurements during the blow-out that occurred at the 2nd Heinenoord Tunnel will be analysed and compared with measurements from centrifuge tests that were performed to investigate the maximum grouting pressure.

2 THEORIES ON MAXIMUM PRESSURE

Leca & Dormieux (1990) calculated the maximum pressure at the tunnel face. They elaborated the failure mechanism that a soil wedge breaks out due to high pressures at the tunnel face. However, the calculated maximum pressures according to their theory are much higher than values used in practice. The reason is that at the tunnel face the soil is loaded with a liquid and this will cause a fracture instead of a failure

by a wedge. The fracture is possible at much lower pressures.

Luger & Hergarden (1988) calculated the maximum pressure that can be used for horizontal directional drilling using the cavity expansion theory. Cavity expansion theory is regularly used to calculate the limit pressure in a spherical or cylindrical cavity. Also this limit pressure is too high to be used as the maximum allowable pressure during drilling. Luger & Hergarden stated that according to cavity expansion theory there is a zone of plastic deformation around a cavity. If this zone of plastic deformation exceeds the soil surface, it is likely that in reality failure will occur. Although Luger & Hergarden showed that reasonable results could be obtained using their theory, they also did not take into account that the soil is loaded with a liquid.

3 FIELD MEASUREMENTS

An instability of the tunnel face, caused by a blow-out occurred during the drilling of the 2nd Heinenoord Tunnel in the Netherlands. A tunnel with a diameter of 8.5 m was drilled below the river Old Meuse. At the moment of the blow-out the tunnel was covered with 4 m of Pleistocene sand with a friction angle of 36.5 degrees. The total cover, including this sand was 8.6 m of soil and above the soil 11 m of water, see [Figure 1](#) (in this schemed overall figure the pleistocene layer is thicker, the mentioned layer thickness is determined from data close to the blow-out). The soil above the sand consists of different materials, mostly relatively

soft soils, but also a layer of rip-rap and 1 m of sand. The top of the tunnel is 19.6 m below the water. The total stress at the top of the tunnel is calculated using the measured volumetric weights of the various soil layers is estimated to be 268 kPa. This corresponds with a total stress of 324 kPa at the centre of the tunnel. The effective stress is 73 and 87 kPa respectively. The face pressure before, during and after the blow-out is shown in Figure 2.

The strongly fluctuating pressures measured until approximately 2.65 hour after the start of that day indicate the drilling process. As usual during the construction of a bored tunnel the drilling was interrupted for the placing of a new ring. At 3.35 hour the cutting wheel was started again, leading to a small increase of the fluctuations in the pressure.

A relatively high face pressure was applied because lumps of clay were present in the mixing chamber. It was tried to remove these by a high pressure gradient over the discharge pipe.

At a pressure of 450 kPa at the tunnel centre the pressure suddenly dropped to 280 kPa. For some time it is tried to keep a certain face pressure by pumping bentonite. However, this was not successful and the pressure dropped to 260 kPa, close to the hydrostatic pressure (238 kPa). A hydraulic fracture occurred from the tunnel up to the river bottom, where a lot of

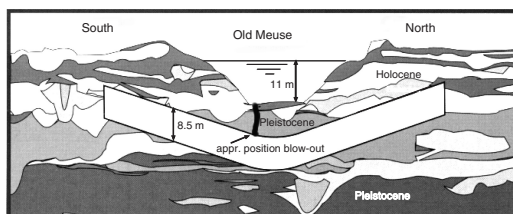


Figure 1. Schemed soil profile for the 2nd Heinenoord Tunnel and position blow-out.

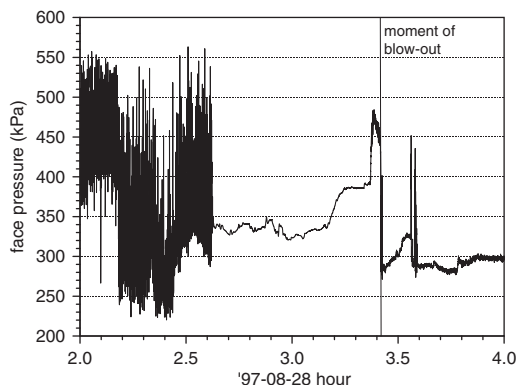


Figure 2. Face pressures measured at tunnel centre during blow-out 2nd Heinenoord Tunnel.

bentonite was found afterwards. The face pressure of 450 kPa was measured at the axis of the tunnel. The pressure at the top of the tunnel depends on the density of the slurry. Since drilling just started the density will be low, a value of 1200 kg/m³ is assumed. At the top of the tunnel, the face pressure during the blow-out was in that case 405 kPa and this is equal to the pore pressure plus 2.8 times the effective pressure.

These data were not obtained directly after the blow-out. Only time-averaged data over each ring were available at that moment. The averaged pressure was an average over the high pressure before the blow-out and the low pressure after the blow-out. From these data it was first concluded that the blow-out occurred because the total vertical pressure was just exceeded. Only when the time registrations became available, it could be concluded that the face pressures at the moment of the blow-out were much higher than they seem using the time averaged pressures.

In the evaluation it was suggested that it is unlikely that only the pressure causes the blow-out. The pressure was at a level of more than 450 kPa for several minutes and was actually decreasing at the moment of blow-out. It seems more likely that a combination of pressure and groundwater flow causes the failure. The bentonite forms a filter cake at the face when the drilling is stopped. This filter cake was destroyed as the drilling was started again, leading to an upward directed groundwater flow. This flow decreased the effective stresses, which together with the high pressure caused the blow-out, see also section 5.2.

4 CENTRIFUGE TESTS

Centrifuge tests have been performed to investigate the grouting process, see for more information about these tests Bezuijen & Brassinga (2001). In these centrifuge tests a tail void was created, with a minimum deformation of the soil around the model tunnel. The tail void was directly filled with a bentonite slurry to simulate the grouting process, see Figure 3.

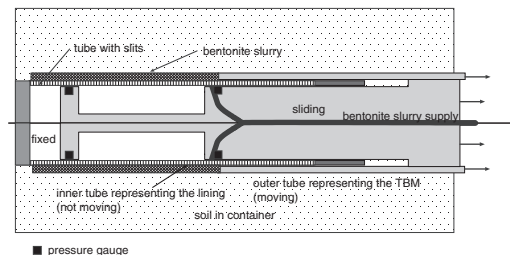


Figure 3. Sketch of the centrifuge module made to simulate the grouting process. Not to scale.

The outer tube in this figure simulates the tail of a TBM, it has a diameter of 130 mm. The inner tube represents the lining and has a diameter of 125 mm. The created tail void is 2.5 mm in the model.

After the filling of the tail void, the pressure in the bentonite slurry was increased until a blow-out occurred to investigate the maximum pressure that can exist in a soil when loaded with a liquid. Bentonite pressure was measured on several locations as well as the total pressure, pore pressure and soil movement at the surface. Three tests were run: one at 150 g in which the model tunnel was covered with sand and two at 40 g in which the model tunnel was covered with sand and clay.

4.1 First test

The first test was performed at 150 g. In this test the module simulates a very large tunnel with a diameter of 18.75 m. This test was performed to test the module at design conditions.

The bentonite concentration in the slurry was 230 gr/l. The soil model consists of sand with a relative density of 65%. 0.2 m of saturated sand is placed above the top of the tunnel, leading to an effective stress of 270 kPa at the top of the tunnel. At the end of the test the pressure is increased by pumping bentonite into the gap between the two tubes without moving the tubes with respect to each other. The result is shown in Figure 4.

In this plot the excess bentonite pressure above the water pressure is presented. It appears that the increase in bentonite pressure leads to an increase of the effective stress only (the pore pressure remains constant and the total soil pressure increases). Bentonite pressure was increased to the pore pressure plus 2.3 times the calculated effective stress at the top of the tunnel, but no real failure occurred. The pressure drop at the end of the test occurred because the test was stopped

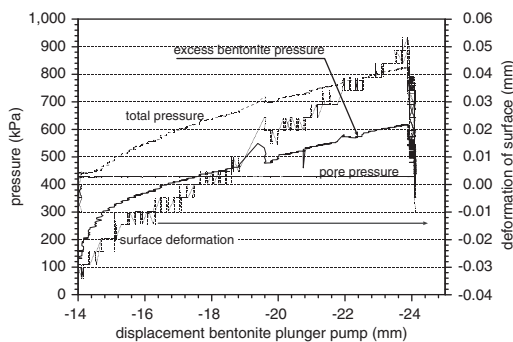


Figure 4. Pressures and deformation during first limit pressure test. Bentonite pressure is the excess pressure with respect to the pore pressure at the top of the model.

and the pressure was released. The deformation measured on the soil surface directly above the module is only limited.

After digging out the module, it was found that bentonite had spread below the module, but no soil failure was found. The bentonite was penetrated over a distance of only a few grains into the sand.

4.2 Second test

The second test was a test at a g-level of 40 g. The module was again surrounded with sand with a relative density of 65%. Bentonite slurry with a concentration of 160 gr/l was used. With this concentration the bentonite slurry has a yield stress of 100 Pa and a density of 1050 kg/m³. A sand layer of 77.5 mm is present above the tunnel. Above this sand there is a clay layer of 170 mm and the top of the soil model is 5 mm of sand. The water level is at the top of the sand layer of 5 mm. The effective stress at the top of the tunnel was in this test 87 kPa.

Again bentonite pressure was increased at the end of the test. The result is shown in Figure 5.

Also in this test the increase in bentonite pressure leads to an increase in the effective pressure only, and again the pore pressure remains constant. Here a failure of the soil around the tunnel is reached, because there is a maximum in the measured bentonite pressure. Failure was reached at a pressure of 190 kPa above the pore pressure, which is 2.2 times the effective pressure at the top of the tunnel. After the test the failure could be found in the bentonite as a line where the bentonite had penetrated into the sand and a fracture occurred, see Figure 6.

4.3 Third test

The third test was performed for the same conditions as the second test. The results are shown in Figure 7.

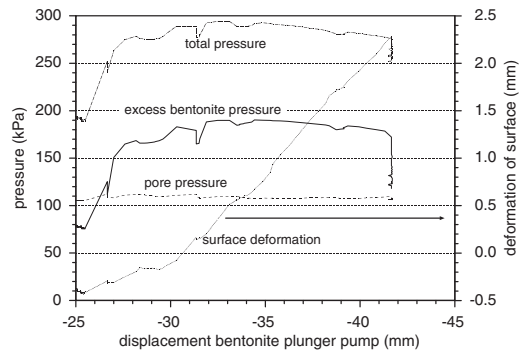


Figure 5. Pressures and deformations during the second limit pressure test. Bentonite pressure is the excess pressure with respect to the pore pressure at the top of the model.

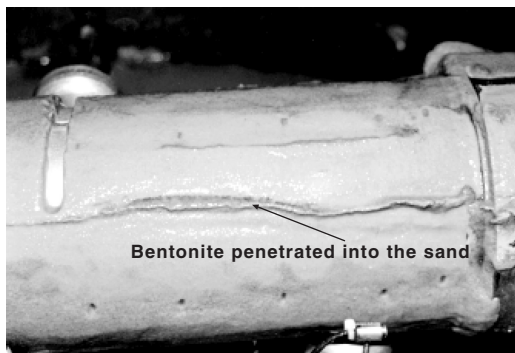


Figure 6. Grouting module after second test. Bentonite around the module after removing of the sand. Note the location where the bentonite has entered the fracture.

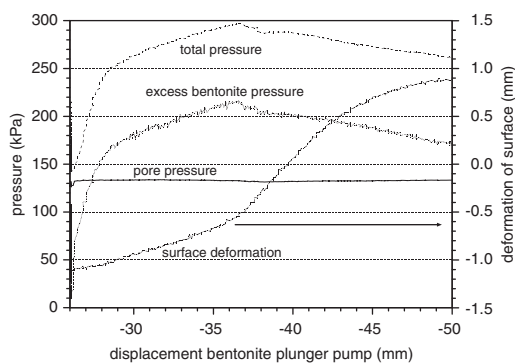


Figure 7. Pressures and deformations during third limit pressure test. Bentonite pressure is the excess pressure with respect to the pore pressure at the top of the model.

The results are more or less comparable with the results obtained from the second test, but a higher limit pressure is reached (215 instead of 190 kPa) and the test showed a clearer maximum in the pressure. The maximum pressure measured corresponds with the pore pressure plus 2.5 times the vertical effective stress.

5 DISCUSSION

5.1 Limit pressures without groundwater flow

The geometry of the tunnel face instability is different from the geometry of the grouting experiments in the centrifuge. Yet it appeared that comparable stresses (related to the effective stress) are necessary to initiate a failure.

2-D Finite element calculations were performed with the PLAXIS program as prediction for the 2nd

Table 1. Parameters used in numerical calculations.

Parameter	Speswhite clay	Sand med. dens.
γ_{wet} (kN/m ³)	17	19.6
c' (kPa)	1	8.3
Friction angle (deg)	23	37
Dilatancy angle (deg)	–	9
Poisson's ratio (–)	0.45	0.3
E_{50} (MPa)	1.5	58
K_0 (–)	0.53	0.4
n (–)	–	0.394
κ (–)	0.118	–
λ (–)	0.589	–
ν soft soil (–)	0.2	–

Table 2. Comparison between various experiments. Pressures at the top of the structures.

Test	g-level	$P - P_w$ (kPa)	σ_v (kPa)	$p - p_w/\sigma'_v$
Hein.	1	192	73	2.8
1st	150	620	270	2.3
2nd	40	190	87	2.2
3rd	40	215	87	2.5
PLAXIS	–	–	–	2.5

and 3rd experiment. The hardening soil model was used for the sand and for the clay the soft soil model was used (Plaxis, 1998). The parameters used in these calculations are presented in Table 1.

A finite element program normally does not present limit pressures, the maximum pressure for which a stable solution was possible is presented in the table. This pressure was found to be equal to the pore pressure and 2.5 times the vertical effective stress. The pressures found are also summarised in Table 2.

A finite element program normally does not present limit pressures, the maximum pressure for which a stable solution was possible is presented in the table. This pressure was found to be equal to the pore pressure and 2.5 times the vertical effective stress. The pressures found are also summarised in Table 2.

The finite element calculations did not take into account that loading is applied with a liquid, the possibility of fractures was not simulated. For the situations tested, this appeared to have only a limited influence. However, it seems likely that not taking into account the fact that loading occurred with a liquid, over-predicts the maximum possible loading at greater depth. The bentonite penetrated into the soil, as can be seen in Figure 6, showed that failure is localized to some areas as described for hydraulic fractures. From this it was concluded that localization of the strains in the soil could be the cause of the failure. This would

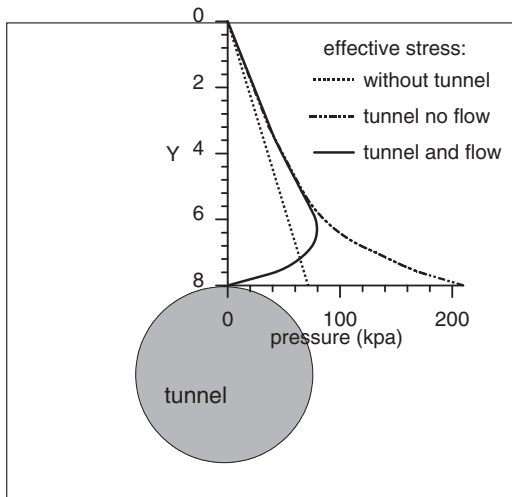


Figure 8. Sketch of the course of the effective pressure with and without groundwater flow (flow induced by the excess pressure on the tunnel face).

lead to a different failure criterion than simulated with the finite element calculations or the one suggested by Luger & Hergarden (1988).

The fracture pressure for competent rock and clay is determined from the pressure leading to tensile stresses larger than the tensile strength of the material in the rock (Andersen et al., 1993). Such a criterion cannot be used for sand. Assuming a Mohr-Coulomb constitutive model, the relation between the radial stress (σ_r) and the hoop stress (σ_θ) can be written as:

$$\sigma_\theta = \sigma_r \frac{1 - \sin \phi}{1 + \sin \phi} - 2c \frac{\cos \phi}{1 + \sin \phi} \quad (1)$$

where ϕ is the friction angle of the material and c the cohesion. It is clear from this formula that without cohesion the hoop stress (σ_θ) will always be positive and will only increase when the radial stress (σ_r) increases. This means that fractures in sand will not occur due to a negative hoop stress. It is likely, although not proven that fractures occur due to localization of strains. The first results of numerical calculations performed at our institute using a discrete element method to simulate the fractures point out in that direction. However, more work has to be done in that direction to be sure that the results of these calculations correspond with reality.

5.2 Limit pressures with groundwater flow

Very thick bentonite slurry was used in the centrifuge test. This slurry hardly penetrates into the soil

and therefore the increase in grout pressure did not lead to an increase in pore pressure in the soil, see Figures 4, 5 and 7. This was not the case during drilling of the 2nd Heineoord Tunnel. Measurements have shown that the pressure at the tunnel face causes excess pore pressures in the soil during drilling, see for example Bezuijen et al. (2001). These excess pore pressures can decrease the ultimate pressure at the tunnel face before a blow-out. This can be understood qualitatively using Figure 8.

Without groundwater flow an increase in pressure at the tunnel interface will lead to an increase in the effective stress. This increase will be at maximum close to the tunnel. In case the pressure is applied as a pore pressure (as seems to be the case at the tunnel face during drilling), the effective stress in the direct vicinity of the tunnel is only small. Effective stress will build up due to groundwater flow at some distance from the tunnel as is indicated in Figure 8. However, the mean effective stress from the tunnel to the soil surface will be less than in the situation without groundwater flow and therefore also the strength of the soil will be less. It is therefore more likely that a blow out will occur when there is a groundwater flow.

This may explain the blow-out at the 2nd Heineoord Tunnel. The plot of the pressures, Figure 2, showed that the blow-out occurred after the maximum pressure was reached. The blow-out occurred when drilling was just restarted after the placing of a ring of the tunnel lining. It seems likely that a combination of pressure and groundwater flow causes the failure. The bentonite forms a filter cake at the tunnel face when the drilling is stopped, see also (Bezuijen et al., 2001). This filter cake was destroyed as the drilling starts again, leading to an upward directed groundwater flow. This flow decreases the grain stresses, which together with the high pressure causes the blow-out.

5.3 Summarising

The various experiments showed comparable values of $(P_u - P_i)/\sigma'_v$ at which soil failure occurred. The difference between failure caused by too high front face or too high grouting pressures is only small. However, looking more in detail to the various experiments, it seems that various failure mechanisms are present. Further research has to show how general applicable the results obtained are and the relative importance is of the various failure mechanisms distinguished.

6 CONCLUSIONS

The maximum pressure that can be applied at the tunnel face or during grouting is investigated for a tunnel

made in sand. It was found that in a field test as well as in centrifuge tests the value of $(P_u - P_i)/\sigma'_v$ varies between 2 and 3. The highest value was found in a prototype blow-out of a tunnel face. This can be explained qualitatively from the geometry that was different from the geometry of the other tests.

It appeared that for the 2nd Heinenoord Tunnel, the prototype ring-averaged pressures indicate a much lower pressure for the blow-out than the actual values.

Various possible failure mechanisms could be distinguished. Hydraulic fracturing is of importance and groundwater flow seems to have an influence on the maximum pressure that can be applied. In spite of these different failure mechanisms, the pressures at which failure occurred are comparable in the various situations. Within the limits of this study it was not possible to derive how general applicable this result will be.

ACKNOWLEDGEMENT

The research described in this paper is commissioned by CUR/COB. The authors want to acknowledge the permission from these foundations to publish the results.

REFERENCES

- Anagnostou G. & Kovári K. 1994. The face stability of Slurry-shield-driven Tunnels. *Tunnelling and Underground Space Technology*, Vol 9, No.2. pp 165–174.
- Andersen K.H., Rawlings C.G., Lunne T.A. Trond & H. By. 1994. Estimation of hydraulic pressure in clay. *Can. Geotech. J.* 31. 817–828.
- Bezuijen A. & Brassinga H.E. 2001. Modeling the grouting process around a tunnel lining in a geotechnical centrifuge. *Proceedings of the 15th International Conference on Soil Mechanics and Geotechnical Engineering*. Held August 27–31, 2001 in Istanbul. Lisse: Balkema Publishers: 1455–1458.
- Bezuijen A., Pruiksma J.P. & Meerten H.H. van. 2001. Pore pressures in front of tunnel, measurements, calculations and consequences for stability of tunnel face. *Proc. Int. Symp. on Modern Tunneling Science and Techn. Kyoto*.
- Jancsecz S. & Steiner W. 1994. Face support for a large Mix-shield in heterogeneous ground conditions, *Tunneling '94*, 531–550.
- Leca E. & Dormieux L. 1990. Upper and lower bound solutions for the face stability of shallow circular tunnels in frictional material, *Géotechnique* 40, 581–606.
- Luger H.J. & Hergarden H.J.A.M. 1988. Directional drilling in soft soil: influence of mud pressure, *Proc. No-Dig '88, Washington*.
- User manual Plaxis, version 7, 1998, *Balkema Rotterdam*.

The stability of a tunnel face in soft clay

Adam Bezuijen

GeoDelft, The Netherlands

Adriaan van Seters

Fugro Ingenieursbureau, The Netherlands

ABSTRACT: The stability of a tunnel face in soft clay is investigated in centrifuge tests. The minimum front face pressure was measured and the deformations were monitored at both the clay surface and the tunnel face for various support pressures. The width of the settlement trough appeared dependent on the depth of the trough for as well a test in sand as for a test in normally consolidated clay with a cover diameter ratio of 0.6. The maximum surface settlement before failure of the clay in front of the tunnel increases exponentially with a decrease of the front face pressure. An analytical lower bound calculation method for the minimum allowable face pressure is compared with the results of the tests. It appeared that the calculation method results in much higher minimum allowable face pressures than measured in the tests. With respect to this aspect a bored tunnel in soft clay with a limited cover is feasible when the settlement requirements are not too strict.

1 INTRODUCTION

The drilling of several tunnels in The Netherlands has initiated research on tunnelling in soft soil conditions. Up to now these tunnels were constructed in sand for most of their length and therefore attention was focussed on the stability of the tunnel face in sand (see for example Bezuijen et al, 2001, Broere & van Tol, 2000, Broere, 2001).

In recent plans, for example for a light rail project in the city of Rotterdam, the possibility of a drilled tunnel is considered that is partly located in soft Holocene clay layers. One of the problems that occur for the construction of such a tunnel is the stability of the tunnel face during drilling.

This problem was envisaged in the research programme of BTL (Research Foundation: Horizontal Directional Drilling & Tunnelling) and the problem was studied in a centrifuge test. Starting point was the research performed by Davis et al (1980). This research suggested that in soft clay local instability of the tunnel face could be the governing mechanism that determines the minimum allowable front face pressure. A high minimum allowable front face pressure means that there is a risk of a blow-out and this would significantly hamper the possibility of drilling a tunnel in soft clay with a soil cover of less than one tunnel diameter.

This paper outlines the theory as presented by Davis et al and some results of FEM calculations. It further presents the set-up of the experiments, the results and conclusions.

2 THEORY

Davis et al (1980) reported on centrifuge tests to determine the stability of a tunnel face in clay. They present stability criteria to evaluate the test results. The proposed calculation method to calculate the minimum front face pressure for stability of the tunnel face is a combination of a global stability criterion and a local criterion. The global criterion is described with an analytical calculation using a lower bound and upper bound solution. The lower bound criterion presents for this situation the minimum pressure necessary to ensure a stable front face, the upper bound the minimum pressure below which there is certainly a collapse. For the use in a design the lower bound is of more importance and therefore will be elaborated further in this section. The lower bound criterion in a weightless soil, as presented by Davis et al can be written as:

$$\sigma_T = \sigma_s - 2s_u \left(1 + \ln\left(2\frac{C}{D} + 1\right)\right) \quad (1)$$

where: σ_s is the overburden pressure, σ_T the pressure at the tunnel face, which is supposed to be uniform, s_u the undrained shear strength and C and D the cover and diameter of the tunnel respectively. For a soil with a certain weight the stability criterion can be written as:

$$\sigma_T = \sigma_s + \gamma_c(C + 0.5D) - N_s s_u \quad (2)$$

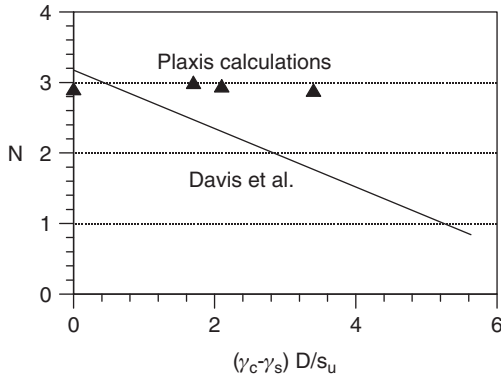


Figure 1. Plane strain situation comparison of analytical and numerical method.

Where:

$$N = 2 + 2 \ln \left(2 \frac{C}{D} + 1 \right) \quad (3)$$

The local stability is presented as a function of $\gamma_c D/s_u$ for constant pressure at the tunnel face, where γ_c is the unit weight of the soil. In case of a slurry shield this can be written as $(\gamma_c - \gamma_s)D/s_u$ with γ_s the unit weight of the slurry. Davis et al (1980) reported calculations in which it was found that in case of plane strain heading the heading was stable up to $(\gamma_c - \gamma_s)D/s_u = 5.63$ for $\sigma_T = \gamma_c(C + 0.355D)$. The stability of a circular heading (as in a real tunnel) will be equal or higher. Here this result for plane strain heading is also used for a circular heading. As a combination of the global and local criteria it is suggested to determine a lower bound criterion, to plot N for the weightless simulation and for the situation $(\gamma_c - \gamma_s)D/s_u = 5.63$ and to draw a straight line in between. The N value for $(\gamma_c - \gamma_s)D/s_u = 5.63$, $N = 0.84$, was obtained by combination of Equation (2), the relation $\sigma_T = \gamma_c(C + 0.355D)$ and $(\gamma_c - \gamma_s)D/s_u = 5.63$. This calculation is performed for the circular heading, using Equation (3) for the weightless situation and for the plane strain heading using the equation:

$$N = 2 + 2 \ln \left(\frac{C}{D} + 1 \right) \quad (4)$$

as was also proposed by Davis et al.

This calculation is a lower bound calculation and therefore it can be expected that for a certain value of $(\gamma_c - \gamma_s)D/s_u$ the N value is in reality higher than according to this figure resulting in lower collapse pressures (σ_T) and thus lower allowable minimum face pressures. However, with no other information available the lower bound calculation is used in design.

The research described here has the goal to get quantitative information about the differences between the collapse pressures (σ_T) according to the lower bound calculation and according to measurements.

2-D finite element calculations with the PLAXIS program (TEC, 1996) were run to check the stability calculation as proposed by Davis et al for the plane strain situation with $C/D = 0.8$ and as predictions for the centrifuge tests. The results are presented Figure 1 in comparison with the results of the method of Davis et al. The PLAXIS calculations showed for soft clay a different trend in the stability number N (with mostly higher values of N). This result would increase the possibilities for drilling tunnels in soft soil if it could be confirmed by tests.

3 TESTS PERFORMED

3.1 Test set-up

For these tests a model tunnel of 150 mm diameter is completely located in normally consolidated clay (this may not be very practical for a real tunnel due to settlement problems, but was studied here as an extreme case of a tunnel partly in clay). A cover/diameter ratio (C/D) of 0.8 and 0.6 was used in two tests. Before the tests in clay a test in sand was performed with also a C/D of 0.8. The test set-up for the test in clay with $C/D = 0.8$ is shown in Figure 2. The other tests had the same set-up, but no clay was present in the sand test and a thinner layer of clay above the tunnel was applied in the second clay test. A 0.9 m diameter inner container was used in which the tunnel was mounted and the soil model prepared.

Eastern Scheldt sand with a D_{50} of 155 μm was used. The sand bed on the bottom of the container was made by under water tamping of thin layers of sand. In this way a 100% relative density was reached with a porosity of 35%. This prevented settlement of the sand during the test. The sand around the tunnel was applied using the method described by Van der Poel & Schenkeveld (1998) and had a porosity of 42%. The friction angle of the sand used at this porosity is 36 degrees. Normally consolidated Spesswhite clay was used as a clay layer. The properties of this clay are summarized in Table 1.

The clay was prepared using hydraulic consolidation after installation of the clay as a slurry in the container. Hydraulic consolidation took place in the inner container with the tunnel in place. This procedure ensures an undisturbed tunnel face in front of the tunnel. The clay was reconsolidated in the centrifuge before the start of the test. The estimated value of s_u varied between 12 and 26 kPa (19.2 kPa at the tunnel axis) for the $C/D = 0.8$ situation and between 9 and 24 kPa (16.2 kPa at the axis) for $C/D = 0.6$.

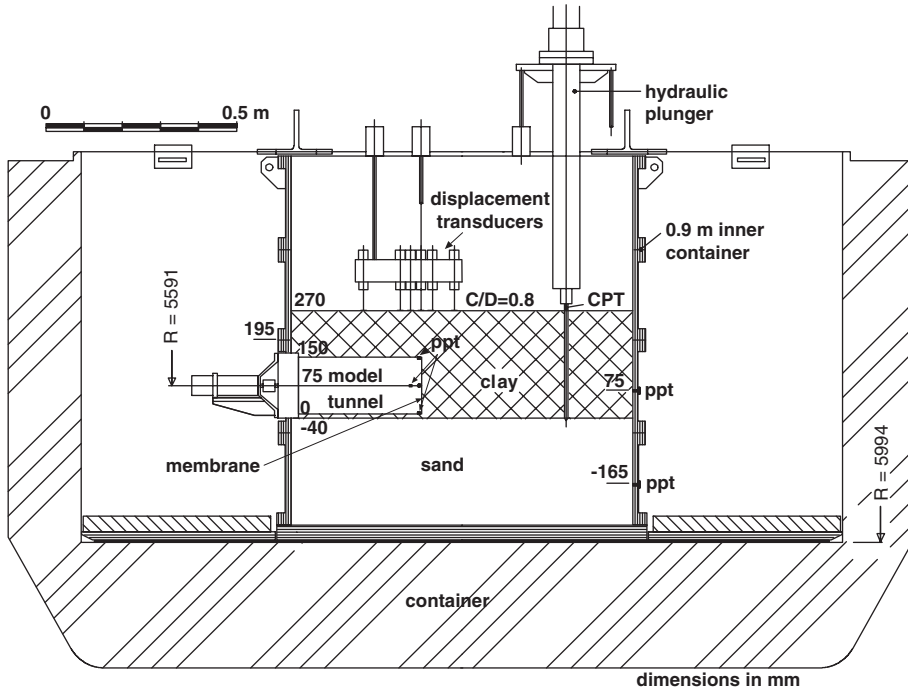


Figure 2. Test set-up.

Table 1. Properties of Speswhite clay.

Property	Value
unit weight constituent	26.1 kN/m ³
liquid limit	69%
plastic limit	31%
water content at $P_1 = 1 \text{ kPa}$	91%
s_u/σ'_v	0.22
γ'_1	4.76 kN/m ³
b	0.075

The tests were performed at 66 g, thus simulating a tunnel of 10 m diameter. The tunnel face was simulated with a membrane. A plunger and water supported the membrane during spinning up of the centrifuge. At the start of the test the pressure behind the membrane was increased up to a level high enough to prevent deformation by pumping sufficient water behind the membrane by means of an electrically driven plunger pump. Then the plunger was withdrawn. The pressure was then slowly decreased (by pumping water out) and deformation was measured at the tunnel face (at 7 locations) and at the ground surface (at 25 locations). The whole procedure of reduction of the face pressure lasted 3 minutes. This means that the stability of the front face and the deformations involved are tested for

an undrained situation in normally consolidated clay during the clay tests.

3.2 Preparation of clay layers

To obtain normally consolidated clay it is necessary that the slurry after consolidation results in a clay layer of the desired thickness without any trimming of the layer. It was therefore necessary to have a rather accurate prediction method to determine the thickness of the clay layer as a function of the amount of slurry used. The relation between clay volume and pressure for virgin compression as suggested by Den Haan (1994) was used, valid for large strains:

$$\frac{V}{V_1} = \left(\frac{P}{P_1} \right)^{-b} \quad (5)$$

Where V is the volume of the clay at pressure P , V_1 the volume at pressure P_1 (the reference pressure) with below water volumetric weight γ'_1 and b a coefficient. The pressure distribution cannot be calculated straightforward, because it will be a function of the weight of the clay layer above the layer considered. For a thin layer of clay it can be written:

$$dP = N_g \gamma'_1 dz \quad (6)$$

Where N_g is the ratio between the actual and normal (1g gravity), γ' the volumetric weight below water and z the depth below the surface. Equation (5) can also be written as:

$$\frac{\gamma'}{\gamma'_1} = \left(\frac{P}{P_1}\right)^{-b} \quad (7)$$

Combination of Equations (6) and (7) and integration results in a relation between pressure and thickness of the clay layer:

$$z = \frac{P_1}{N\gamma'_1(1-b)} \left(\frac{P}{P_1}\right)^{1-b} \quad (8)$$

This relation is valid as long as N_g is constant. This is not really the case in a centrifuge since N_g varies with z , but calculations have shown that in our case the influence on the relation between z and P is only small. Since the amount of clay powder is known, P at the bottom is known and z can be calculated. The parameter b was determined by means of small-scale centrifuge tests. γ'_1 is derived from the water content at P_1 (normally 1 kPa). The values found are presented in Table 1.

With the formulas it can be calculated that at 66 g a layer of 0.397 m slurry (with a water content of 100%) will consolidate to a layer of 0.28 m clay. An extra correction was necessary for this test because the volume of the tunnel will be the same before and after consolidation. The procedure was developed for these tests and appeared quite accurate. Also in other tests with different g-levels it showed to be able to present an accurate prediction of the final clay layer.

Figure 3 presents as an example the water content and γ' as a function of depth for the situation in these tests (g level 66 times gravity) calculated with the model described above assuming normal consolidation.

3.3 Test results

3.3.1 Maximum surface settlement

The maximum settlement at the surface was found with the displacement gauge 30 mm straight in front of the tunnel face for the sand test and 90 mm in front of the tunnel face for the clay tests. The maximum measured surface settlement at these locations is shown as a function of the pressure (σ_T) in Figure 4. The settlement is presented in prototype values (66 times the measured model values) for the test in sand and the test in clay with $C/D=0.8$. It shows the maximum settlement measured as a function of the pressure at the axis of the tunnel face. It was measured by applying an increase in volume loss at the tunnel face by pumping water from behind

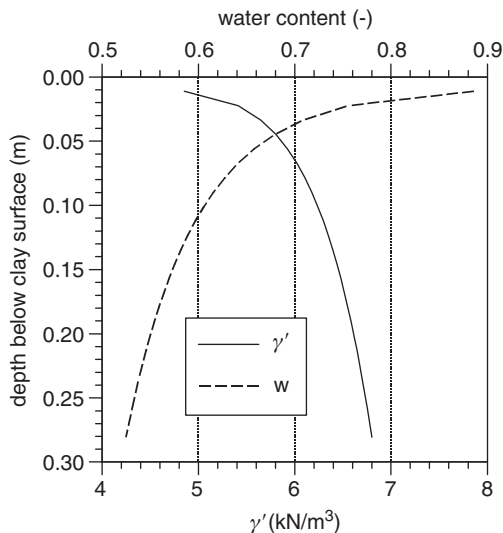


Figure 3. Calculated water content and γ' as a function of depth for the conditions during these tests.

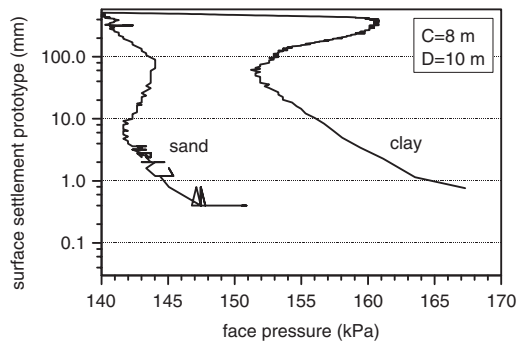


Figure 4. Measured maximum surface settlement as a function of the face pressure with increasing volume loss at the front face during the experiment. Prototype values for a tunnel face placed in sand and in clay.

the membrane. A logarithmic axis is used for the settlement.

The decreasing pressure from 165 to 152 kPa in the clay test shows an exponential increase in surface settlement (an approximately linear relation on the logarithmic scale). It is assumed that at a pressure of approximately 152 kPa a failure surface occurred. With this failure surface established, higher pressures were necessary to obtain a stable tunnel face. The resulting minimum in the face pressure was used for comparison with the calculated minimum pressure.

This minimum could be obtained because the position of the membrane of the model tunnel was volume

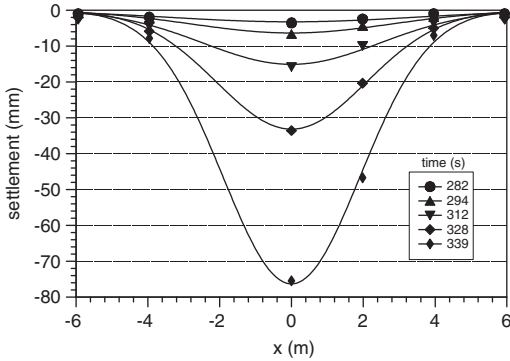


Figure 5. Surface settlements (prototype dimensions) at various times in the experiment with $C/D = 0.6$. Results fitted with a Gauss curve.

controlled. In a pressure controlled situation, as normally present in a tunnel, the minimum in the pressure would lead to a collapse of the tunnel face.

The curve for the sand test is comparable, but the minimum pressure has a lower value. Furthermore the minimum is reached at much lower settlement (61 mm in the clay test and 6.7 mm in the sand test), caused by the larger stiffness of the sand.

3.3.2 Settlement trough

The instrumentation did not allow for measuring the settlement trough perpendicular to the tunnel axis at the position of the maximum settlement trough. However, it was possible to measure the trough directly above the tunnel face. The data were fitted with a Gauss curve:

$$s = s_0 \exp\left(-0.5\left(\frac{x}{i}\right)^2\right) \quad (9)$$

where s is the settlement at a distance x from the axis of the tunnel, s_0 is the settlement at the axis and i is the parameter determining the width of the settlement trough. The settlement trough for the test with $C/D = 0.6$ is shown in Figure 5.

The results are used to determine the width of the settlement trough as a function of the amount of settlement. The measurement results were fitted to Equation (9) using a non-linear regression technique. The results are presented in Figure 6 in dimensionless units by dividing both the settlement and the measured i by the diameter of the tunnel. It appeared that a larger settlement leads to a smaller i especially for the test in sand and the test in clay with $C/D = 0.6$. The result for $C/D = 0.8$ is less clear.

Earlier experiments have shown an influence of the settlement on i for sand, but not for clay. Probably the

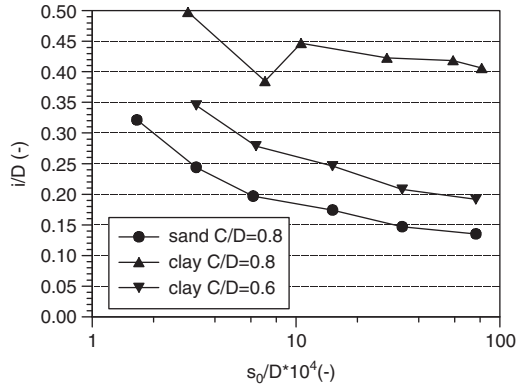


Figure 6. Width of the settlement trough (represented by the parameter i in Equation (5)) as a function of the amount of settlement.

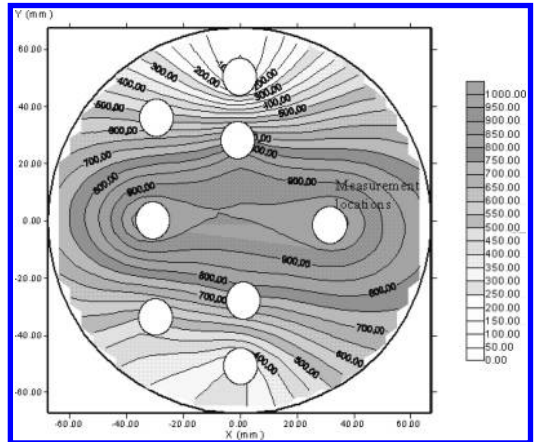


Figure 7. Measured soil deformation in microns at the tunnel face just before the moment of collapsing of the front face. Interpolated from measurement points indicated by circles.

influence found here has to do with the relatively small cover over the tunnel.

3.3.3 Deformations at the tunnel face

A result of the measurements at the tunnel face is shown in Figure 7. It shows the deformations of the tunnel face at minimum pressure (151.2 kPa) in the $C/D = 0.8$ clay test in model dimensions. The result shows that the reduction of face pressure leads to deformations of clay predominantly in the middle of the front face.

After the clay test with $C/D = 0.6$ the failure surface in the clay was determined using x-ray tomography. The results of this determination have been reported elsewhere (Kruse & Bezuijen, 1998).

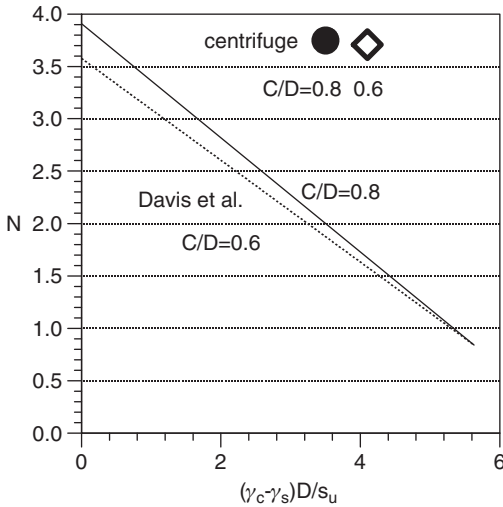


Figure 8. Comparison of the results of the analytical method with the results of centrifuge tests.

4 COMPARISON WITH CALCULATIONS

The measured minimum pressures in the clay tests were compared with the calculation method outlined in Chapter 2. Since the undrained shear strength varied over the tunnel face the average value (the value at the tunnel axis) was used in the back calculations. Figure 8 shows the stability lines according to theory and the measured minimum pressure just before a failure surface occurred (the minimum in the face pressure as shown in Figure 4).

It is clear from the figure that the N value measured is much larger than the value according to the calculation method. It should be larger because the calculation is a lower bound calculation. From Equation (2) it can be seen that a higher value of N means that a lower face pressure can be used and such a lower face pressure means that drilling can be performed at lower values of C/D .

As mentioned in Chapter 2, the calculation method is based on the combination of a global and local stability criterion. It seems that the stability factor is higher because the influence of the local stability criterion is overestimated in the theory. The PLAXIS calculations as well as the results of the centrifuge tests show stability numbers that are less dependent on $(\gamma_c - \gamma_s)D/s_u$ than according to the calculation method. It should be noted that 2 times a lower bound approximation is used for the calculation method: first to derive the minimum pressure in the weightless situation and second to combine the global and local instability. It is therefore not surprising that the measurements lead to higher stability numbers.

Table 2. Influence on N when a limited surface settlement is required.

max. surface settlement (mm)	face pressure (kPa)	N (-)
61	152	3.75
10	156	3.55
1	164	3.14

5 DISCUSSION ON THE RESULTS

Up to now the results of the calculations are compared with the measured minimum front face pressure necessary for stability. However, it appeared from Figure 5 that the minimum front face pressure in soft clay corresponds with relatively large settlements. A higher front face pressure will be necessary for limited settlement of the surface due to front face deformation. This limited settlement can be reached with a slightly lower value of the stability parameter. As an example it is calculated what is the influence on N , using Figure 5, if the settlement is limited to 10 mm or 1 mm. The result is presented in Table 2.

The results show that also in soft clay only a limited increase in pressure above the minimum pressure at the front face is needed to practically eliminate the settlement due to the front face deformations. Also when limited surface settlements are required the N value is still well above the value according to the analytical calculation method.

6 CONCLUSIONS

The centrifuge experiments in combination with the calculations described in this paper have led to the following conclusions:

1. A method has been developed to come to an accurate prediction of the thickness of a clay layer of normally consolidated clay depending on gravity and amount of slurry used.
2. The actual stability factor N as found in centrifuge tests is well above the value obtained from the lower bound calculation method.
3. The width of the settlement trough seems to decrease with larger surface settlements for a tunnel in sand and a tunnel in soft clay with a small cover.
4. The results indicate that a bored tunnel with a low cover/diameter ratio of about 0.6 can be constructed safely in soft clay with respect to the necessary front face pressure.

It is noted that other aspects of shallow tunnelling in clay, such as the forces on the lining and problems

that can occur with the steering of the tunnel boring machine have not been studied in this project.

ACKNOWLEDGEMENT

This study was commissioned and supervised by BTL (Research Foundation: Horizontal Directional Drilling & Tunnelling) and COB (Centre for Underground Construction). The authors wish to thank these foundations for their permission to publish these results.

The authors further acknowledge J. Out for the design of the equipment, Th.J. van Dijk, F.J. Kop and F.M. Schenkeveld for their assistance during preparation and testing.

REFERENCES

- Broere W. & Tol A.F. van 2000. Influence of infiltration and groundwater flow on Tunnel stability. *Proc. Int. Conf. on geotechnical aspects of underground construction in soft grounds*, eds. Kusakabe O. Fujita K. and Niyazaki Y.
- Broere W. 2001. Tunnel face stability & New CPT applications. *PHD thesis, Delft University of Technology*.
- Bezuijen A., Pruiksma J.P. & Meerten H.H. van 2001. Pore pressures in front of tunnel, measurements, calculations and consequences for stability of tunnel face. *Proc. Int. Symp. on Modern Tunneling Science and Techn. Kyoto*. Rotterdam: Balkema.
- Davis E.H., Gunn M.J., Mair R.J. & Senviratne H.H. 1980. The stability of shallow tunnels and underground openings in cohesive material. *Geotechnique* 30. No.4, pp 397–416.
- Haan E.J. den 1994. Vertical compression of soils. *PHD thesis, Delft University of Technology*.
- Kruse G.A.M. & Bezuijen A. 1998. The use of CT scans to evaluate soil models. *Centrifuge 98, Kimura, Kusakabe & Takemura (eds)*. Rotterdam: Balkema.
- Poel J.T. van der & Schenkeveld F.M. 1998. A preparation technique for very homogeneous sand models and CPT research. *Centrifuge 98, Kimura, Kusakabe & Takemura (eds)*. Rotterdam: Balkema.
- TEC (1996) PLAXIS-predictions for geo-centrifuge research, *BTL report 12, 13 Delft: Delft Hydraulics* (in Dutch).

Simulation of the EPB-shield TBM in model tests with foam as additive

Adam Bezuijen

GeoDelft, The Netherlands

Paul E.L. Schaminée

Delft Geotechnics, The Netherlands

ABSTRACT: Model tests have been performed to investigate the behaviour of a sand-water-foam mixture. A TBM with an earth pressure balance shield was simulated. Saturated sand was mixed with foam and the sand-water-foam mixture was removed with a screw conveyor. The properties of the mixture in the ‘mixing chamber’ and in the screw conveyor have been studied. Two different sands were tested with a d_{50} of 135 μm and 300 μm respectively and two different foams. Changing the sand had a significant influence on the result. The influence of the type of foam was less.

1 INTRODUCTION

Applying foam as an additive when drilling with an EPB-shield through sand is to a large extent still based on empirical experience. Properties of the foam are in most cases determined at atmospheric pressure (Woude van der 1996), or if not, at high pressure gradients (Condat 1998, Maidl 1995). In field conditions there can be a pressure of several bars, depending on the depth of the TBM and the position of the phreatic surface, but the pressure gradients will be limited.

To investigate the mechanisms involved, model tests have been performed. In these tests the relevant parameters were measured (penetration of foam in the sand, volumes, amount of removed mixture, pressures etc.). Two different sands were tested and two different foams. One foam was tested with two the different sands, the other with one sand only.

This paper deals with the set-up of the tests and the results of the measurements. The results are compared with other work on foam and conclusions are presented.

2 TEST SET-UP

2.1 Principle

Figure 1 shows schematically a TBM with an EPB shield, tunnelling through sand, using foam. During this process sand will be cut from the subsoil, moved into the working chamber and transported through the screw conveyor, influencing porosity, effective stress and pore pressure. The figure shows the assumptions that were used for the set up of the test.

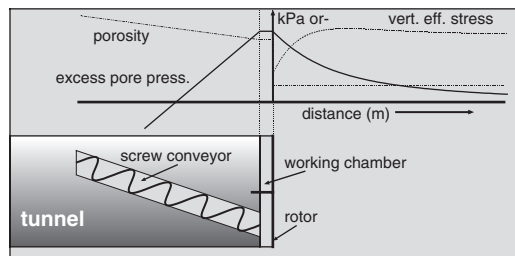


Figure 1. Sketch of course pore pressure, porosity and effective stress in front of a EPB shield.

During drilling there will be an excess pore pressure in the sand. This excess pore pressure was measured in the field in front of a slurry shield during drilling (Bezuijen et al. 1999). In the since the completion of these tests and the writing of the paper it is proven that this excess pore pressure is also present in front of a EPB shield drilling in sand using foam (Fugro 2000).

2.2 Model EPB

The most important part of the test set-up is shown in Figure 2. Not shown are the foam generator and a foam container from which the foam was released into the model container. Two types of test could be performed. In the set-up as shown on the left side of the figure mixing tests were performed. A sand-water-foam mixture was prepared and properties of this mixture (permeability, compressibility, yield stress) were measured. Results of this type of test are described in Bezuijen et al. (1999). This

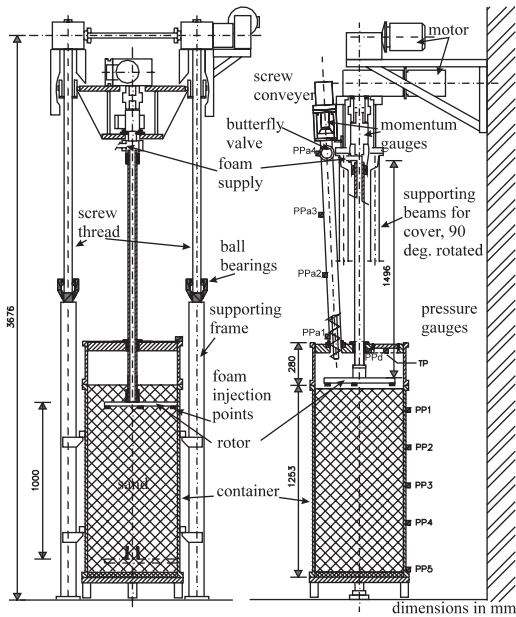


Figure 2. Test setup for both types of tests.

paper focuses on tests with the set-up shown on the right hand side of this figure. In these tests the drilling process is simulated including the removal of the mixture through the screw conveyer. Experiments were performed at a pressure 1 bar above the atmospheric pressure. Two different foams were used. Foam was prepared using equipment and recipe of the foam supplier. Foam expansion ratio was around 15 in the experiments. The expansion ratio was measured using a sample container. Most of the experiments were run with medium fine sand (250 μm), but 2 were run with fine sand (135 μm). Drilling velocity ranged from 0.2 to 1.4 mm/s.

Drilling direction compared to field conditions was changed from horizontal to vertical to have more control during the preparation of the soil sample. The procedure followed for sample preparation (Poel & Schenkeveld 1998) results in homogeneous and saturated sand. Properties of the sands used are summarised in Table 1.

2.3 Additional equipment

An overview of the set-up during a test is shown in Figure 3. Various components of the set-up will be described below.

The foam equipment from one supplier was the same as used in a TBM and has a much larger foam production than necessary for the model tests. Since it was not possible to reduce the foam production rate without effecting the quality of the foam and to increase

Table 1. Properties of the sands used.

Property	250 μm sand	135 μm sand
d_{10}	150 μm	90 μm
d_{50}	250 μm	135 μm
Permeability (at 40% por.)	$6 \cdot 10^{-4}$ m/s	$8 \cdot 10^{-5}$ m/s
Min. porosity	31.4	34.0
Max. porosity	44.7	46.9
Friction angle	33° (n = 42%)	41° (n = 41%)

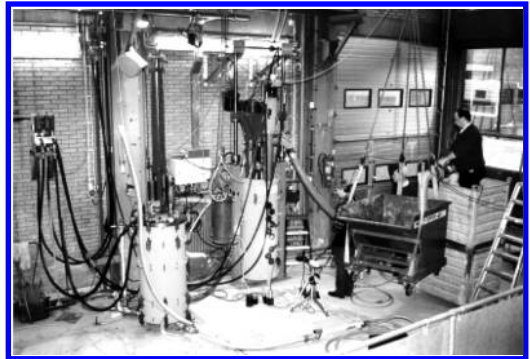


Figure 3. Overview of the set-up during a test. Left the foam supply vessel in the middle the sand container with the screw conveyer on top.

control of foam injection flow, it was decided to use a buffer container. The foam produced was led into a separate pressured container with a plunger before the start of the test. During the test the plunger pushed the foam from this container through the rotor in the container with the soil sample. The pressure in the buffer container is equal to the pressure in the sample container.

Another vessel (the outflow vessel) was used to control the hydraulic gradient in the sand. This gradient is of importance since it controls how much pore water the foam replaces and this determines the properties of the sand-water-foam mixture. In a field situation the gradient is a function of the diameter of the drilling and the pressure at the tunnel face (Bezuijen et al. 2001). Free outflow of water at the bottom of the sand container would lead to a gradient that is much too high compared with the field situation. Therefore the outflow vessel was connected to the bottom of the sand container and the discharge of water from the bottom of the sand container was controlled as a function of the drilling parameters, see Figure 4.

A startup vessel was used to start the drilling process. This vessel regulates the pressure in the screw conveyer before it is completely filled. At the start of the experiment, the pressure is constant over the screw

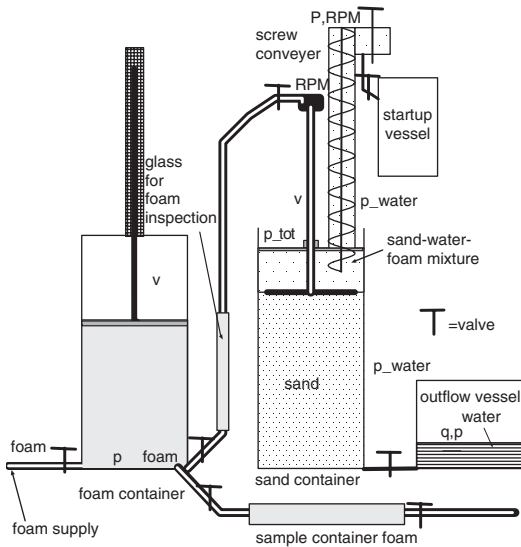


Figure 4. Schematic overview experiments. The letters present controlled variables. p = pressure, q = specific discharge, v = velocity, RPM = revolutions per minute (rotor and screw conveyor), p_{water} is the pore pressure measured in the sand and along the screw conveyor, see also Figure 2.

conveyor. The butterfly valve at the top of the screw conveyor will be closed. When the screw conveyor is partly filled, the pressure in the upper part of the screw conveyor will be less than in the ‘mixing chamber’ but probably still higher than atmospheric pressure. The pressure in the upper part of the screw conveyor is now regulated by the startup vessel in a way that the pressure in the mixing chamber remains constant. When the screw conveyor is sufficiently filled, the butterfly valve is opened and the angular velocity of the screw conveyor regulates the pressure, see also Figure 4.

When the drilling process was stable the total pressure in the mixing chamber remains constant by controlling the number of revolutions of the screw conveyor. Depending on the desired porosity of the mixture and the amount of pore water in the mixture, foam was supplied from the foam container.

3 MEASUREMENTS

Two test series were run. In the first test series (test-numbers 201–206) 250 μm sand and Condat foam was used. This test series was performed to acquire knowledge about the mechanism involved. In the second test series (test number 301–303) 250 and 135 μm sand were used and foam from Master Builders. In this series the influence of a different sand and a different foam was tested.

The measurements performed during the experiments are shown in Table 2. All instruments were

Table 2. Measurements during the tests.

Measured parameter:
The foam pressure in the foam container
Position plunger in the foam container
Position of rotor and top plate
Momentum on rotor
Rpm of the screw conveyor
Momentum of the screw conveyor
Total pressure of mixture against top plate
Pore pressure in mixture at top plate
Pore press. container location 1 until 5
Volume of water tapped from container
Pore press. screw conveyor loc. 1 until 4
Weight of the removed mixture

Table 3. Experiments performed. The replacement indicates the amount of the pore water which was replaced by the foam. Drilling velocity was decreased if torque on rotor increases. It was increased in test 302 only to test maximum velocity.

Exp. Nr	d_{50} sand [μm]	replacement [%]	drilling velocity [mm/s]	Remarks
201	250	100	1-0.25	velocity reduced to prevent high torque as 201
202	250	100	1-0.25	as 201
203	250	82	1-0.25	as 201
204	250	50	0.5-1	stable for 0.5 mm/s
205	250	50	0.5	
206	250	50	0.5	additive
301	135	50	0.5	final porosity set too low
302	135	50	0.5-1.2	stable up to high drilling speed
303	250	50	0.5	as 302 diff. sand. unstable

sampled with a sample frequency of 10 Hz and stored in a computer.

The process was visually monitored through 10 perspex windows with a diameter of 4.5 cm that were located in the sand container.

4 RESULTS

4.1 Description of tests

The experiments performed in the test series with a screw conveyor are summarized in Table 3.

The pressure drop in the screw conveyor was less than anticipated and therefore it was difficult to achieve a stable ‘drilling’ process in most of the tests. A stable drilling process means that the pressures in

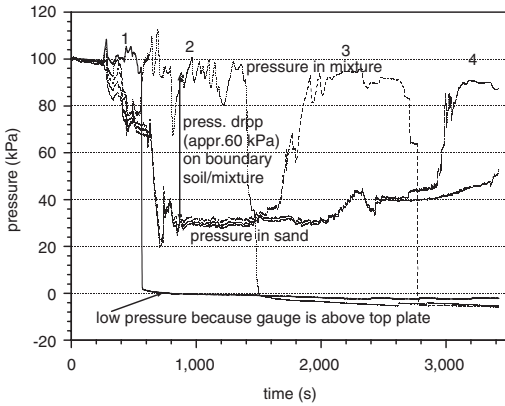


Figure 5. Pressures in model container Test 202. The numbers indicate the pore pressure transducers (PP# in Figure 2).

the mixing chamber and in the soil as well as the drilling speed are more or less constant. When the foam replaced a higher percentage of pore water, the drilling performance became better, because a larger pressure drop over the screw conveyor was possible. This is caused by adhesion of the mixture to the walls of the screw conveyor or by more cohesion in the mixture itself.

In Test 202 all pore water was replaced by foam. According to calculations performed for the Botlek railway tunnel (Talmon & Bezuijen 1999), such a complete replacement of the pore water during drilling is very unlikely in fine and medium coarse sand. However, it can occur during periods of stand still of the TBM. In such a situation a pressure drop can exist over the boundary soil-mixture as can be seen in Figure 5.

This figure shows the course of the pressure measured in the sand. The pressure at the top plate was 100 kPa. The pressure in the sand was 35 kPa. The pressure in the mixing chamber (between the rotor and the top plate) was approximately 90 kPa. For example PP 3 comes in the mixing chamber between 1700 and 2000 s. It remains at a high value until the top plate passes the PP. When this has happened (at t is appr. 2800 s for PP 3) the measured pressure falls down to atmospheric pressure (0 kPa in Figure 5).

In Test 204 the pressure in the mixing chamber remains constant over quite some time. Only when the drilling speed was doubled from 0.5 to 1 mm/s, the torque on the rotor increased and the stable drilling process was gone.

A rather strong additive was injected close to the inlet of the screw conveyor in Test 206. This additive increases cohesion as well as adhesion. However, due to this additive the properties of the mixture changes over the length of the screw conveyor (as was found from the pore pressure transducers), which made it

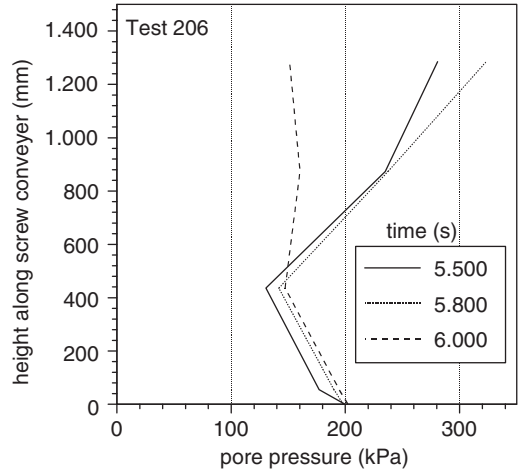


Figure 6. Test 206, pressure drop in screw conveyor.

again difficult to obtain a stable process. The influence of the additive is shown in Figure 6. Normally the pressure in the screw conveyor drops, see for example Figure 9. However, now the properties of the mixture changed in the screw conveyor and it becomes very difficult to push the highly viscous mixture through the half open butterfly valve, as a result the pressure increases near the butterfly valve (at a height of 1250 mm).

In the first test of the second series (Test 301) 135 μm sand was used, but the final porosity in the mixture was not adapted to the higher maximum porosity of this sand. As a result the torque on the rotor was too high. This was overcome in Test 302, which has a reasonable torque up to high drilling velocities. The drilling speed was increased during this test from 0.5 to 1.2 mm/s. At a velocity of approximately 1 mm/s it was possible to have the pressure drop of 100 kPa over the screw conveyor. The pressure drop over the butterfly valve is zero as can be seen from the result of pore pressure transducer 4 in Figure 7, which is located close to the butterfly valve. The drilling speed could be increased even further up to 1.2 mm/s. At that drilling speed the process became unstable. This will be discussed further in section 4.2.2.

Figure 8 shows the response of PP 2 on the passing of the rotor in Test 302. The passing leads to a fluctuation in PP 2. This fluctuation decreases in the mixing chamber. As was shown in Figure 5 for test 202, the pressure falls back to zero as the top plate passes PP 2. In test 302 only 50% of the pore water was replaced by foam, therefore no pressure difference on the boundary soil/mixture is found in this test, as was the case in all tests with less than 100% replacement of the pore water.

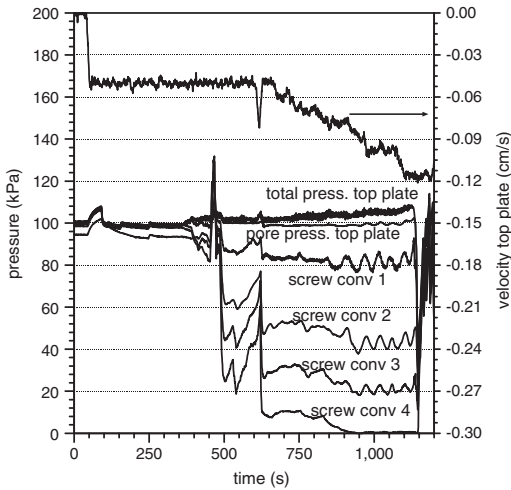


Figure 7. Test 302, drilling velocity pressures near top plate and in screw conveyor (numbers correspond to the numbers of PPa# in Figure 2).

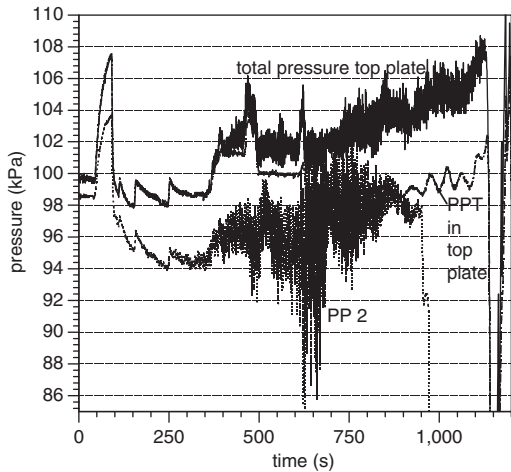


Figure 8. Test 302, total and pore pressure on top plate, Pore pressure in the sand at PP 2.

Test 303 was planned as a copy of the 204 test. It appeared however that drilling remains difficult for the 250 μm sand. No stable process was reached.

4.2 General results

4.2.1 Pressure drop screw conveyor

The pressure drop, as measured in the screw conveyor in the experiments 204 and 302 are compared, see Figure 9.

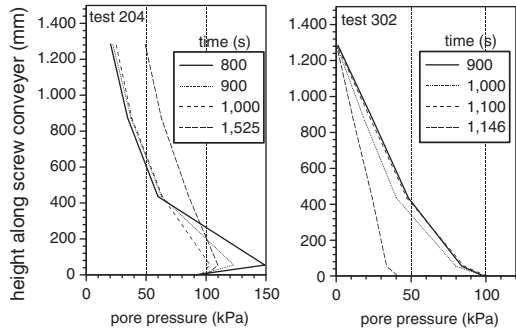


Figure 9. Pressure drop in the screw conveyor compared for 2 tests.

The experiments 204 and 302 were chosen because these had a constant pressure in the mixing chamber during a significant part of the experiment. It appeared that the pressure gradient in the screw conveyor is more or less constant during an experiment and over the height of the screw conveyor, with a small tendency to decrease higher in the screw conveyor. Experiment 204 shows a pressure peak at the entrance of the screw conveyor, at $t = 800$ s. An explanation for this jump is not found. A comparable course of the pressure in the screw conveyor was found in field measurements performed during the drilling of the 'Botlekspootunnel' (COB 2000). In experiment 302 the pressure at the bottom of the screw conveyor (in the mixing chamber) decreases until 40 kPa at $t = 1,146$ s. This is due to an instability, see Figure 10.

In experiment 204 the pressure is not zero (with respect to the atmospheric pressure) at the top of the screw conveyor, because the butterfly valve was not completely open in this experiment.

The more or less constant pressure gradient over the screw conveyor indicates that the friction between the material and the metal in the screw conveyor is more or less constant.

4.2.2 Learning from unintended events

The instability that occurred in Test 302 is analyzed more in detail in Figure 10.

This figure shows the results of various instruments at the moment of the instability. The cause of the instability was the volume control in the lower drain. At a constant drilling velocity, there should be a constant change in this volume as can be seen in the left side of the plot ($t < 1100$ s). However, after $t = 1100$ s the volume change decreases, the volume remains constant and even reverses, because the control system of the flow vessel could not cope with the relative high drilling velocities applied. The other lines in the graph show how the system reacts on such a change in

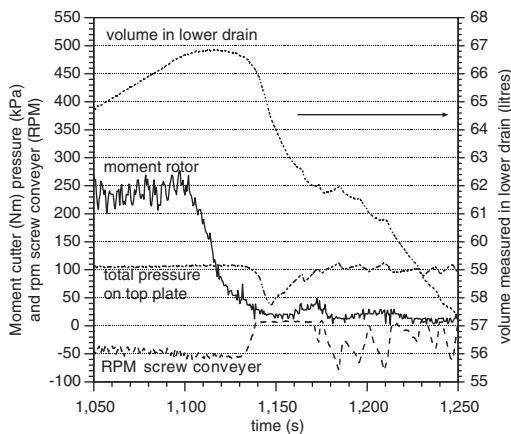


Figure 10. Course of various parameters during Test 302, see also text.

boundary condition. The stopping of the drainage leads instantly to a decrease in the moment of the rotor. Most likely this decrease is caused by the increase in the porosity of the sand in the mixture because less pore water is drained. Since the mixture is made at the rotor, where the foam is injected, the result is first measured at the rotor. When the mixture with the higher sand porosity reaches the screw conveyor it appears that it can flow through the screw conveyor more easily, with a smaller pressure drop over the screw conveyor. To keep a constant pressure in the container, the number of revolutions of the screw conveyor decreases to approximately zero. At that value the pressure in the container cannot be controlled anymore and therefore at approximately time = 1140 s, the pressure in the container starts to decrease sharply. The course of the instruments later in the experiment is influenced by manual intervention (closing the butterfly valve) and of less interest.

Although the instability was not a planned action, it showed clearly how sensitive the process is to changes in the amount of pore water in the mixture. A comparable situation as shown in Figure 10 can occur in a field situation when the permeability of the material decreases, resulting also in more pore water in the mixture.

4.2.3 Visual results

It appeared from monitoring the process through the glass windows that, in contrast with what is generally assumed, there is no penetration of foam in the sand in front of the tunnel face during drilling and when drilling stops penetration is limited to a few cm only. More penetration of foam in the sand can be reached, but needs a higher pressure gradient.

Since the pressure gradient in these experiments is comparable to the pressure gradient in field conditions, this means that also in field conditions the penetration of foam into the soil is limited. Penetration will not occur at all during drilling in medium and fine sand, because due to the low pressure gradients in combination with the limited permeability of the sand it will not even be possible to replace all the pore water by foam.

5 CONCLUSIONS

The conclusions of the tests series were that the foam has only a limited influence on the results. Drilling speed and the properties of the sand have higher influence. In agreement with field experiences, it was easier to perform drilling with an EPB shield in fine sand compared to drilling in medium fine sand.

The porosity of the sand in the mixing chamber is critical for the amount of torque on the rotor and the pressure drop over the screw conveyor. When the porosity of sand in the mixing chamber decreases to the maximum porosity of the sand, the torque on the rotor increases dramatically. (Due to the foam the porosity of the sand in the mixing chamber can be a lot higher than the maximum porosity). A too high porosity on the other hand leads to a decrease in the pressure drop over the screw conveyor, resulting in an unstable drilling process.

The penetration of the foam in the sand during drilling and during stand still seems different from what is generally assumed.

ACKNOWLEDGEMENT

This study was commissioned and supervised by BTL (Research foundation: Horizontal Drilling & Tunneling.) and COB (Centre for Underground Construction). The authors wish to thank these foundations for their permission to publish the results. The companies Condat and Master Builders supported this research by supplying foam and equipment and gave helpful advise on how to get an optimal result.

REFERENCES

- Bezuijen A., Schaminée P.E.L. & Kleinjan J.A. 1999; Additive testing for earth pressure balance shields. *Proc. XII ECSMGE*, Amsterdam.
- Bezuijen A. & Brassinga H.E. 2001. Modeling the grouting process around a tunnel lining in a geotechnical centrifuge. to be published *Proc. XIII ECSMGE 2001*, Istanbul.
- Bezuijen A., Pruiksmas J.P. & Meerten H.H. van 2001. Pore pressures in front of tunnel, measurements, calculations

- and consequences for stability of tunnel face. *Proc. Int. Symp. on Modern Tunneling Science and Techn. Kyoto*.
- COB 2000, Evaluation phase A MQ4, South tube, Front phase stability, mixture formation and soil transport, balance of forces and grouting (in Dutch), *COB doc, K300-W-018-02*.
- Condat 1998, Private communication.
- Fugro 2000, Botlek railway tunnel. Evaluation K300/GT. Stresses and deformations in subsoil (in Dutch). *Fugro report: M-0813*.
- Maidl, U. 1995, *Erweiterung der Einsatzbereich der Erd-druckschilde durch Bodenconditionierung mit Schaum*. Dissertation, Ruhr Universität Bochum.
- Poel J.T. van der & Schenkeveld F.M. 1998. A preparation technique for very homogeneous sand models and CPT research. *Proc. Centrifuge '98*.
- Woude van der S, 1996, *Conditioning of sand to increase the usability of an EPB*. TU-Delft Report part I and II, August.

Muck discharge by the screw conveyor of an EPB Tunnel Boring Machine

A.M. Talmon

Delft Hydraulics, Delft, The Netherlands

A. Bezuijen

GeoDelft, Delft, The Netherlands

ABSTRACT: A mathematical model for muck discharge by the screw conveyor of an Earth Pressure Balance (EPB) Tunnel Boring Machine is presented. The muck is modelled as a homogeneous plastic paste. The model considers momentum balances and kinematic conditions of muck flowing between the rotating screw and the barrel.

The mathematical model has been validated against laboratory scale experiments and field measurements during the construction of the “Botlek Rail Tunnel”. Major differences were found between the functioning of the screw conveyor in the laboratory tests and in the field. The adhesive properties of the muck are an important factor for controllability of muck flow rate and confinement pressure by the screw.

1 INTRODUCTION

Earth Pressure Balanced (EPB) shields are used on a regular basis in soft soil shield tunnelling and have proven their capabilities. Additives are necessary to use these shields in sandy subsoil. Foam has proven to be a successful additive in various projects. However, the governing mechanism that makes foam to a successful additive are not yet clarified, see also Bezuijen (2002).

The double-tube Botlek Rail Tunnel under the River Oude Maas near Rotterdam is the first bored rail tunnel in the Netherlands. An EPB shield tunnel-boring machine was used, see Figure 1. For more detail see Maidl (1999).

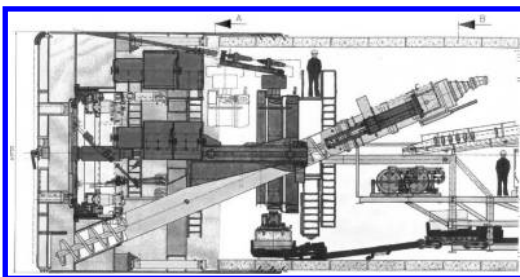


Figure 1. EPB machine Botlek Rail Tunnel.

Soft clayey layers are suitable for EPB shield tunnelling. In EPB tunnelling the soil is excavated under pressurised conditions to balance the tunnel face. In principle water or other substances do not dilute the soil. The earth paste is transferred via a screw conveyor from the pressurised chamber to the rear of the shield.

In the Botlek Rail Tunnel the transport of excavated soil from the working chamber is controlled by a combination of a screw conveyor, a hydraulically operated back gate (when necessary), two bulk pumps (when necessary), a conveyor belt and a hydraulic circuit. In cohesive soils, a pressure difference of some 3 bar can be controlled by the screw conveyor alone, Maidl (1999). In sand-layers the increased water permeability and internal friction will cause serious problems. Intensive soil conditioning with high density slurry or foam is required.

In an EPB tunnel boring machine the screw conveyor has to provide two important functions. First it transports soil out of the excavation chamber while the pressure decreases from the confinement pressure in the excavation chamber to atmospheric pressure at the discharge end of the screw conveyor. And secondly the confinement pressure in the excavation chamber is controlled by the operating conditions of the screw conveyor.

To investigate the mechanisms involved, model tests have been performed. In these tests the relevant parameters were measured (flow rates, pressures, etc.). The

set-up of the tests and some results of the measurements have been presented by Bezuijen and Schaminée (2001).

A mathematical model for the muck discharge by a screw conveyor is given in Section 2. The model is used for an analysis of the model tests and the screw conveyor in the TBM of the “Botlek Rail Tunnel”. The results are given in Section 3 and Section 4 respectively.

2 MATHEMATICAL MODEL SCREW CONVEYOR

The model was set up to relate muck discharge and confinement pressure with the rheological properties of the muck and the operational conditions of the screw conveyor. It is intended as a tool for prediction and analysis. The basic ingredients of the mathematical model are:

Kinematic conditions: flow rate of the muck, angular velocity of the muck, angular velocity of the screw, continuity.

Forces: angular momentum balance and longitudinal momentum balance. In these the shear stresses are assumed to be uniformly distributed over the screw, over the root of the screw and over the barrel. The direction of shear stresses over the barrel is variable, depending on operational conditions of the screw conveyor. The pressure difference over the blade is accounted for.

The muck is modelled as a homogenous plastic one-phase material. A definition sketch is given in Figure 2.

The geometry of the screw at the edge of the blade is given by, see Figure 2:

$$\tan \alpha_t = \frac{S}{\pi D} \quad (1)$$

with: S = pitch, D = diameter barrel, α_t = blade angle at the edge of the blade.

The characteristic flow rate of the screw is:

$$Q_{straight} = \frac{rpm}{60} S \frac{\pi}{4} (D^2 - D_r^2) \quad (2)$$

with: rpm = rotational frequency of screw conveyor [rotations/min], $Q_{straight}$ = flow rate when the muck moves in a straight line (e.q. without axial rotation). D_r = diameter of the root of the screw.

From kinematic conditions:

$$\tan \beta = \frac{\tan \alpha_t}{Q_{straight}/Q - 1} \quad (3)$$

with: Q = flow rate of the muck, β = direction of the flow adjacent to the barrel.

Muck rotation is in the same direction as the rotation of the blade for $Q_{straight} > Q$. The muck rotates in

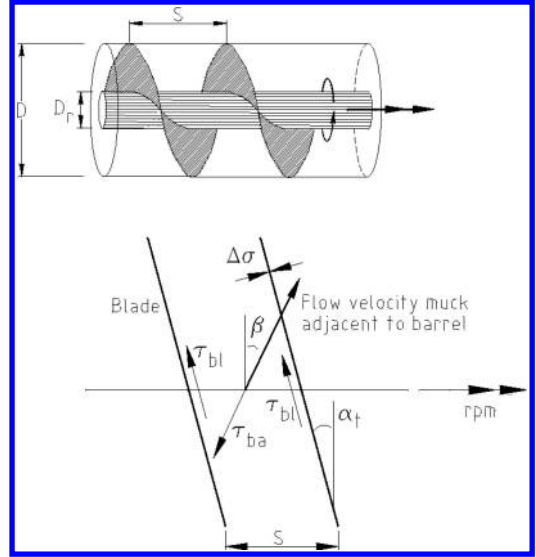


Figure 2. Definition sketch mathematical model screw conveyor, relating geometry, operational conditions and stresses.

opposite direction for $Q_{straight} < Q$. The mathematical expression for the pressure difference over the screw conveyor is (valid for $0 < \beta < 180$ degrees):

$$\Delta p = \frac{4L}{D - \frac{D_r^2}{D}} \left(\frac{1}{\pi} \left(1 - \frac{D_r}{D} + \frac{1 - (D_r/D)^3}{3 \tan^2 \alpha_t} \right) \tau_{bl} + \frac{\tan \beta \tan \alpha_t \tan \beta - 1}{[\tan \beta] \tan \alpha_t \sqrt{\tan^2 \beta + 1}} \tau_{ba} + \frac{D_r}{D} \sqrt{1 + \left(\frac{\pi D_r}{S} \right)^2} \tau_{rt} \right) \quad (4)$$

with: L = length screw conveyor, τ_{bl} = shear stress on the blade, τ_{ba} = shear stress on the barrel, τ_{rt} = shear stress on the root of the screw.

The pressure difference over the screw conveyor is a function of the flow rate of the muck (Q), the rotational velocity of the screw and the friction with steel surfaces. The direction of the flow ($\tan \beta$) is calculated by Equation (2) and Equation (3). Next ($\tan \beta$) is substituted in Equation (3) to calculate the pressure difference. In Figure 3a the dimensionless pressure difference over the screw conveyor is given as a function of the dimensionless flow rate $Q/Q_{straight}$ under the assumption that the friction at the blade is equal to the friction at the barrel and at the root.

Two curves are shown: one for the geometry of the screw conveyor in the model tests, and one for the Botlek Rail Tunnel. The graph shows that theoretically different operational transport modes are possible: passive confinement of pressurised muck in the excavation chamber for $Q/Q_{straight} > 0.75$ (in the

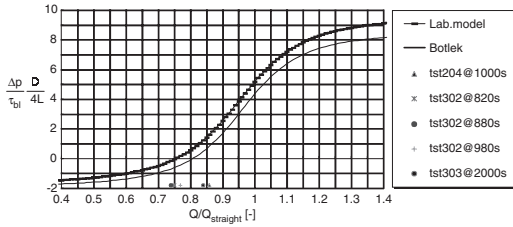


Figure 3a. Mathematical model screw conveyor (geometry model tests: $S/D = 0.70$ and $D_r/D = 0.45$, Botlek Rail Tunnel: $S/D = 0.63$ and $D_r/D = 0.22$). Dimensionless flow rates in model tests are indicated on the ordinate.

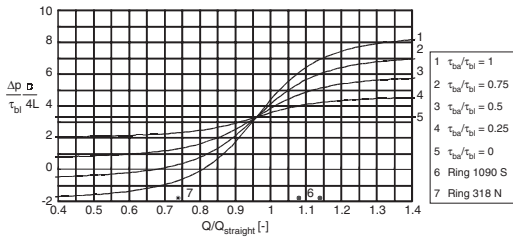


Figure 3b. Mathematical model screw conveyor: Botlek, variation of ratio τ_{ba}/τ_{bl} . Dimensionless flow rates for two situations being analysed are indicated on the ordinate.

laboratory model), or active extraction of muck from the excavation chamber for $Q/Q_{straight} < 0.75$. The later is referred to as ‘pumping action’. The calculated pressure difference is exclusive the static pressure. Some operational conditions, in which high-pressure differences have been measured, are displayed on the ordinate of the graph.

In practise a screw conveyor in a TBM might be equipped with additional foam injection ports, see for instance Maidl (1999). This additional foam might lower the friction with the barrel. The functioning of the screw conveyor under such a condition, according to Equation (4), is shown in Figure 3b. For $Q/Q_{straight} < 0.96$ the pressure difference between the entry and the exit of the screw conveyor increases.

A comparable situation results when a velocity dependent Bingham rheological flow model models the consistency of the muck. Then, for $Q/Q_{straight} > 0.5$, the velocity of the muck with respect to the blade is larger than with respect to the barrel. Consequently the shear stress on the blade is larger than on the barrel. The result is then comparable to Figure 3b.

3 LABORATORY EXPERIMENTS

Saturated sand was mixed with foam and the sand-water-foam mixture was removed with a screw conveyor, see Bezuijen and Schaminée (2001). The

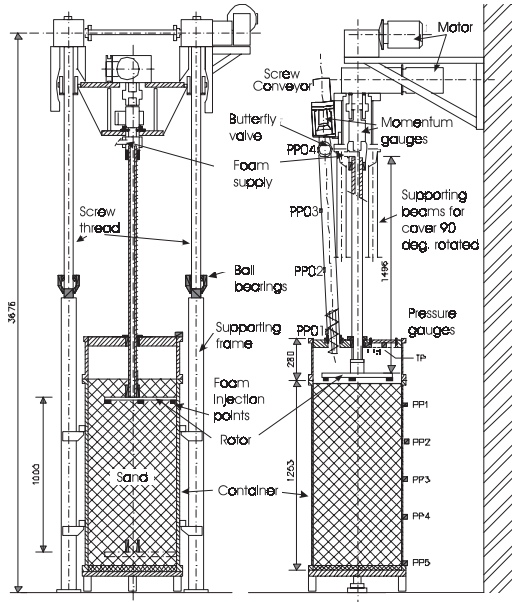


Figure 4. Set-up model test.

drilling direction, compared to field conditions, was changed from horizontal to vertical. The test set-up is shown in Figure 4. The internal diameter of the excavation chamber is 0.6 m. Not shown are a foam generator and a foam container from which the foam was released into the model container. The pressure in the excavation chamber was about 100 kPa. The specifications of the screw conveyor are: length barrel $L = 1.2$ m, diameter barrel $D = 107$ mm, diameter root $D_r = 48$ mm, pitch screw $S = 75$ mm, thickness blade ~ 2 mm. Substitution of these specifications in Equation (2) gives: $Q_{straight} = 0.031 * \text{rpm} [\text{m}^3/\text{h}]$. Some selected conditions where the screw conveyor controlled the discharge of muck are listed in Table 1.

Some examples of the measured pressure distribution along the screw conveyor are shown in Figure 5.

The operational conditions listed in Table 2 relate to $t = 1000$ in test 204, $t = 820, 880$ and 980 in test 302 and $t = 2000$ in test 303. The measured pressure difference includes 15 kPa static pressure.

The dimensionless muck flow rate $Q/Q_{straight}$ for the conditions above is displayed on the ordinate of Figure 3a. According to this model the operating conditions are in the region where the screw conveyor provides a positive pressure difference ($Q/Q_{straight} > 0.75$). This is in agreement with the measurements. The shear stress is back calculated from the dimensionless pressure difference read from the absciss of Figure 3a. The results are summarised in Table 2.

Table 1. Test conditions of the screw conveyor in model tests (at mean pressure in screw conveyor).

Parameter	Test 204	Test 302	Test 303
d_{50} sand [um]	250	135	250
Sand porosity	0.35	0.40	0.36
Drill vel. [mm/s]	0.49	0.73, 0.82, 0.96	0.31
FIR [-]	0.38	0.41	0.39
FER [-]	1:14.9	1:14.6	1:15.5
c_{sand} [v%]	48	45	50
c_{water} [v%]	13	14	9
c_{air} [v%]	39	41	41
rpm	24	32.5, 37, 43	18
Flow rate Q [m ³ /h]	0.63	0.90, 1.0, 1.24	0.41
Pressure drop [kPa]	90	100, 100, 100	65
$Q/Q_{straight}$	0.86	0.89, 0.88, 0.93	0.84

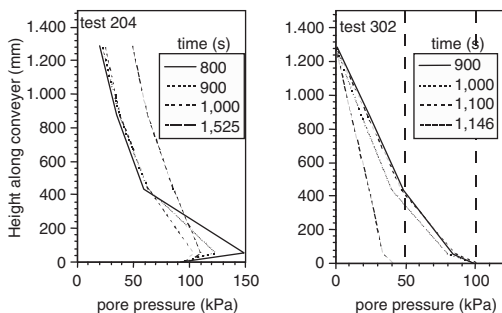


Figure 5. Measured pressure distribution over model screw conveyor.

Table 2. Functioning screw conveyor in laboratory tests.

Model test	$Q/Q_{straight}$	$\Delta p/\tau D/4L$ Math. model.	τ [Pa] Back calculated
test 204	0.86	1.6	1040
test 302	0.89	2.0	950
test 302	0.88	2.3	830
test 302	0.93	3.3	580
test 303	0.84	1.2	910

The results compare with vane tests at a mixture porosity of $n=0.52$: $\tau = 1.5$ kPa, see Bezuijen and Schaminée (2001) and Bezuijen *et al.* (1999).

4 SCREW CONVEYOR IN BOTLEK RAIL TUNNEL

The boring of the two tubes took place in the period 1999–2000. The geology of the subsoil and the main features of the tunnel are summarised by Maidl (1999).

4.1 Properties foamed soil

A number of samples was taken directly from the excavation chamber. The location where the samples were taken is at about half height of the bulk head 3.5 m from the centreline of the TBM. The cohesive properties of the muck were determined by means of a specially designed vane apparatus in the excavation chamber (the measurement took place during placement of lining segments, when the excavation was halted). The vane was located a few decimetres below the location where samples were extracted and at another location about 1 metre aside of the entrance of the screw conveyor.

The porosity of the samples was in the range 0.5 to 0.7, with extremes of 0.46 and 0.72. The volume percentage air in the samples (at ~3 bar in the excavation chamber) was in the range 25 to 35 v%. The measured porosity of the muck was higher than the maximum porosity n_{max} of the sand ($0.44 < n_{max} < 0.53$). For a homogenous muck there will be no grain contacts and the muck will be workable. Only in one test (Ring 341 North tube), out of a total of five of such tests, the measured porosity of the muck was smaller than n_{max} . The measured internal shear strength of the muck in the excavation chamber was within a range of 5 a 30 kPa.

4.2 Screw conveyor

The screw conveyor of the Botlek Rail Tunnel is shown in Figure 1. Technical specifications are: length barrel $L = 16$ m, diameter barrel $D = 1000$ mm, diameter root $D_r = 220$ mm, pitch screw $S = 630$ mm, thickness blade ~20 mm, max. rpm 22.4, max. flow rate 500 m³/h. The flow rate of muck transported in a straight line is calculated by: $Q_{straight} = 26.9 * rpm$ [m³/h]. The screw conveyor is equipped with a number of pressure gauges.

4.3 Analysis of the functioning of the screw conveyor

During the major part of the construction of the tunnel, the pressure drop along the length of the screw conveyor was about 150 kPa. At the same time a pressure drop of about 100 kPa was noticed in front of the screw conveyor. When the flow is regulated by the back gate, the pressure in the back of the screw conveyor is about 100 ka to 150 kPa. The pressure drop over the screw conveyor includes a static 70 kPa that is attributed to a height difference of 5.5 m.

An example of pressures measured during the excavation and during the positioning of tunnel lining segments is shown in Figure 6.

The pressure distribution over the length of the screw conveyor during the excavation is shown in Figure 7. From Figure 6 it is concluded that during standstill the muck at the entrance to the screw

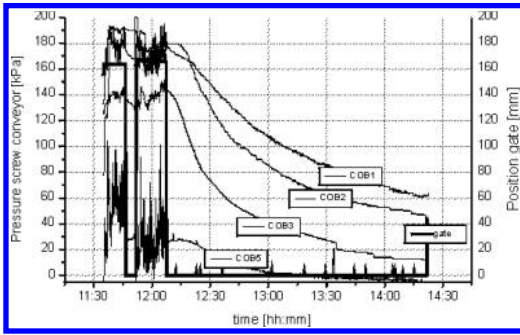


Figure 6. Botlek Rail Tunnel: pressure gauges along the screw conveyor as a function of time: South tube, Ring 1090. For $t > 12:10$ the excavation is halted and tunnel lining segments are placed.

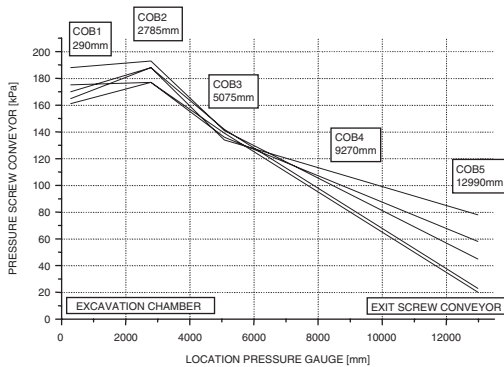


Figure 7. Botlek Rail Tunnel: pressure distribution along screw conveyor during excavation at different time-instances: South tube, Ring 1090.

conveyor is compacted, and may balance 1 bar. When the excavation recommences, the situation quickly restores itself to the former situation.

Two situations where typical high pressure differences were observed over the screw conveyor are discussed: Ring 1090 of the South tube and Ring 318 of the North tube. The average in situ porosity at Ring 1090 South tube was $n = 0.45$, and at Ring 310 of the North tube $n = 0.4$. The consistency of the muck was determined from samples obtained from the excavation chamber (Ring 1090 South and Ring 310 North). The flow rate of muck through the screw conveyor was calculated by two alternative methods: 1) From the in-situ porosity of the soil, the water content of samples and the volumetric air content of samples from the excavation chamber (the ideal gas-law was used to calculate the flow rate at the mean pressure level in the screw conveyor). 2) From the discharge by a slurry circuit that conveyed the soil out of the tunnel and the volume of air in the samples taken from the excavation chamber (also calculated at mean pressure level in the

Table 3. Operational conditions of the screw conveyor in the Botlek Rail Tunnel (at mean pressure in the screw conveyor).

parameter	Ring 1090 South tube	Ring 318 North tube
d_{50} sand [μm]	180	150
Drill vel. [mm/s]	0.96	0.31
c_{sand} [v%]	29	32
c_{water} [v%]	21	16
c_{air} [v%]	50	52
<i>rpm</i>	17.9	7.8
Flow rate Q [m ³ /h]	490 (from face) 530 (slurry circ.)	114 (from face)
Pressure drop [kPa]	150	200
$Q/Q_{straight}$	1.06 (from face) 1.14 (slurry circ.)	0.73

screw conveyor). The latter method is inaccurate at low drill velocities. In Ring 1090 South, foam was injected in the barrel. The operational conditions of the screw conveyor are summarised in Table 3.

The dimensionless muck flow rate $Q/Q_{straight}$ of the conditions above is displayed on the ordinate of Figure 3b. According to the model (in case $\tau_{bl} = \tau_{ba} = \tau_{rt}$) the dimensionless pressure difference for the operating conditions listed in Table 3 are: $\Delta p/\tau D/4L = 6$ & 7 for Ring 1090 South, and -0.8 for Ring 318 North. The back calculated wall shear stresses in Ring 1090 is 220 Pa. For the situation in Ring 318 North the outcome of this model-configuration is contradictory to the measurement.

When alternatively it is assumed that the friction between the muck and the blade is dominating, then the shear stress can be back-calculated from the curve $\tau_{ba}/\tau_{bl} = 0$ in Figure 3b, the result is $\tau = 450$ á 650 Pa.

These back-calculated shear stresses are an order of magnitude smaller than the shear stress measured by the vane tests in the excavation chamber.

5 CONCLUSIONS

Conclusions are:

- 1) Two rheological properties of the muck have to be discerned: friction with steel surfaces (adhesion) and internal friction (cohesion). The former is relevant to the functioning of the screw conveyor as a flow and pressure regulator. The latter is probably governing the pressure drop that occurs at the entrance of the screw conveyor and the pressure build-up in front of the back gate, when in use. Typical confinement pressures of 3 bar were balanced. This compares with the situation in Japan, where two-stage screw conveyors are used to deliberately create sand plugs for pressure confinement, Babendererde (1991).

- 2) We have found major differences between the functioning of the screw conveyor in the laboratory model tests and in the field at the TBM of the Botlek Rail Tunnel. At the TBM, large differences were found between cohesion and adhesion. In the laboratory tests these differences were only about a factor of two. Explanations for differences are:
- The porosity of the muck at Botlek was significantly higher than in the laboratory tests. This could have led to poor adhesion properties.
 - Foam injection in the barrel could have impaired the functioning of the screw conveyor.
 - The velocity difference between the blade and the muck is larger than the velocity of the muck with respect to the barrel. If the muck were viscoplastic the friction in the screw channel is the governing factor, as was found at Botlek Rail Tunnel.
 - The screw channel might be clogged.
- 3) The injection of smaller quantities of foam should be considered in future tunnelling projects to produce a muck with a lower porosity than at Botlek. The muck will become more stable and the controllability of the muck flow rate and the confinement pressure are expected to improve. The functioning of the screw conveyor will improve when the adhesive properties are improved. According to the mathematical model, the highest-pressure differences will be attained at slow rotation of the screw.
- 4) To further improve the control of the muck pressure in the excavation chamber, the attention should be directed towards developing foams and injection recipes that provide higher friction between the muck and steel parts.

ACKNOWLEDGEMENTS

The laboratory tests were commissioned and supervised by BTL (Research foundation: Horizontal Drilling & Tunnelling) and COB (Centre for Underground Construction). The authors wish to thank these foundations for their permission to publish the results. The data on the Botlek Rail Tunnel presented here are derived from the COB-pilot project F300 in which the authors participate. The authors are very grateful to both COB and the builder of the tunnel BTC Botlek vof, with the granted opportunity to publish.

Data-analysis was conducted by J.F.W. Joustra MSc, B.J.H. Grote MSc, R. Peters MSc, S. Rodenhuis BSc, and B. Hoogzaad MSE. GeoDelft and Delft Hydraulics invested company research budgets.

REFERENCES

- Babendererde, S., 1991, Tunnelling Machines in soft ground: a comparison of slurry and EPB shield systems, *Tunnelling and Underground Space Technology*, vol.6, no. 2, pp.169–174.
- Bezuijen, A., 2002, The influence of permeability on the properties of a foam mixture in a TBM 4th Int. Symp. on Geotechnical Aspects of Underground Construction in Soft Ground – IS Toulouse 2002.
- Bezuijen, A., Schaminée, P.E.L. & Kleinjan, J.A., 1999, Additive testing for Earth pressure balance shields. Proc. 12th European Conf. on Soil Mechanics and Geotechnical Engineering, Amsterdam. June 1999. Rotterdam, Balkema, 1999, volume 3, pp. 1991–1996.
- Bezuijen, A. & Schaminée, P.E.L., 2001, Simulation of the EPB-shield TBM in model tests with foam as additive, proc. IS-Kyoto 2001 conference on Modern tunnelling Science and Technology.
- Maidl, U., 1999, Design Features of the Botlek Rail Tunnel in the Betuweroute, *Tunnelling and Underground Space Technology*, Volume 14, No. 2, p. 135.

APPENDIX I. NOTATION

D :	diameter barrel
D_r :	diameter root screw
L :	length screw conveyor
n :	porosity
Δp :	pressure difference over screw conveyor (excl. static)
Q :	muck flow rate
$Q_{straight}$:	flow rate when muck moves in a straight line
S :	pitch screw
α_r :	blade angle at edge of blade
β :	direction of the flow adjacent to barrel
τ_{ba} :	shear stress on barrel
τ_{bl} :	shear stress on blade
τ_{rl} :	shear stress on the root of the screw

Geotechnical centrifuge tests to verify the long-term behaviour of a bored tunnel

H.M.A. Pachen & H.E. Brassinga

Engineering Department Rotterdam Public Works, The Netherlands

A. Bezuijen

GeoDelft, The Netherlands

ABSTRACT: Building the Rotterdam section of RandstadRail involves the construction of two bored single-track tunnel tubes in the city area of Rotterdam, each with an outer diameter of 6.5 m and a length of 2.4 km. On several parts of the alignment the tunnel tubes are located at the transition of soft Holocene clay to stiff Pleistocene sand. It is expected that the top of the soft Holocene layers will settle 1.5 m due to consolidation and creep during the lifetime of the construction. Therefore the external loading on the tunnel lining will increase. The time dependent additional loading has been analyzed analytically as well as numerically. Physical modeling, using the Delft GeoCentrifuge, was performed in order to verify the design approach. The paper presents the results of the centrifuge tests and the findings of the back analysis using the finite element techniques.

1 INTRODUCTION

RandstadRail is a future light-rail link between Rotterdam, The Hague and Zoetermeer in the Netherlands. Building the Rotterdam section of RandstadRail involves the construction of 2 single-track shield tunnels in Rotterdam, each with an outer diameter of 6.5 m (Figure 1) and a length of 2.4 km, using a slurry shield TBM.

2 GROUND CONDITIONS

The geotechnical profile of the Rotterdam city area consists, starting from surface level (at 1 m above the reference level NAP), of a shallow toplayer of anthropogenic sand, 15 m of soft Holocene layers (peat and

organic clay), overlying the Pleistocene sand layer, which has a thickness of about 20 m. The water level is about 2 m below NAP. Some soil classification parameters are given in Table 1.

The stress dependent stiffness of the soil layers is determined with oedometer tests, and given below (symbols are explained at the end of the paper):

Peat:	$E_{oed} = 500 \cdot \left(\frac{\sigma'_v}{p_a} \right)^{0.8}$
-------	--

Organic clay:	$E_{oed} = 1700 \cdot \left(\frac{\sigma'_v}{p_a} \right)^{0.8}$
---------------	---

Pleistocene sand:	$E_{oed} = 40000 \cdot \left(\frac{\sigma'_v}{p_a} \right)^{0.5}$
-------------------	--



Figure 1. Two single track tunnels of 6.5 m diameter.

3 TUNNEL DESIGN

Tunnelling will be performed in the Pleistocene sands over a substantial part of the alignment. However, nearby the Station Statenweg and the connections to the existing (metro- railway-) lines the over-burden is very shallow and the lining is predominant located in the soft organic clay layers. Each segment is provided with 2 constructive dowels and sockets to bridge the

Table 1. Soil properties Rotterdam city area (mean values).

	h (m)	γ_{sat} (kN/m ³)	w (%)	PI (%)	c_u (kPa)	K_0 (-)	OCR (-)
Top layer	1	18	—	—	—	—	—
Peat (Holocene)	5	10.5	450	—	40	0.4	1.2
Organic clay (Holocene)	10	13.5/16.5	90/55	50/40	40/30	0.5	1.3
Sand (Pleistocene)	20	20	—	—	—	0.5	1.0

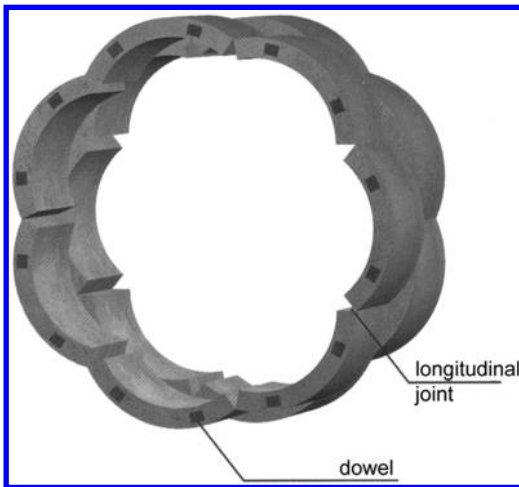


Figure 2. Concrete lining segments with constructive dowels and sockets.

ring joints (Figure 2) in order to reduce the deformation of the lining and therefore to secure the water tightness.

The design is based on two single track tunnels with an internal diameter of 5.8 meters each and a concrete lining of 0.35 m thickness. The lining consists of 7 pre-cast concrete segments and 1 keystone. The segments have a width of 1.5 m.

4 LONG TERM SETTLEMENTS

During design lifetime of the tunnel (100 years) the soft layers will settle due to consolidation and creep. A regular sand supply on ground level is necessary in order to maintain the surface at a fixed level. To study the settlement behaviour of the organic clay and peat layers, extensometer gauges were installed. Some results are plotted in Figure 3.

From the extensometer measurements and the levelling data of the manhole covers of the sewerage system in this part of the city over the past 20 years, it was concluded that a yearly settlement of 15 mm at the

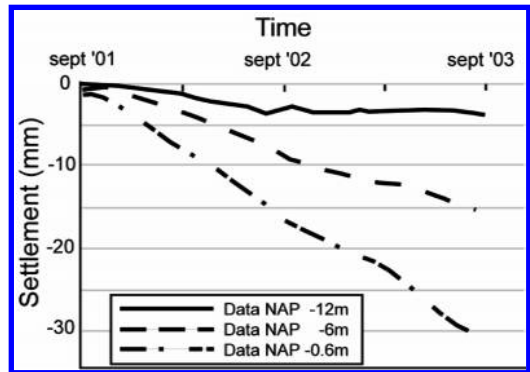


Figure 3. Extensometer measurements.

surface and 2 mm over the height of the tunnel is to be expected. The Pleistocene sand will not settle.

5 FORCES ON THE LINING DUE TO LONG TERM SETTLEMENT

Because the tunnel is a relatively stiff element the forces in the lining will increase due to long term settlements. The vertical force on the crest will exceed the vertical overburden pressure. The time dependent extra force, called negative skin friction, was analysed analytically assuming a linear stress strain relation. Using the stress distribution function of Airy the vertical and horizontal additional stresses Δp_v and Δp_h were determined (Pachen & van Zanten 2002). For an embedment of 135° (see Figure 4) and a Poisson ratio of 0.33. The solutions are:

$$\Delta p_v = \frac{0.5 * u_0 * E_{oed}}{R} \quad (1)$$

$$\Delta p_h = \frac{0.06 * u_0 * E_{oed}}{R} \quad (2)$$

6 GEOCENTRIFUGE MODELLING

In order to verify the analytical solution two physical model tests were performed in the GeoCentrifuge at GeoDelft.

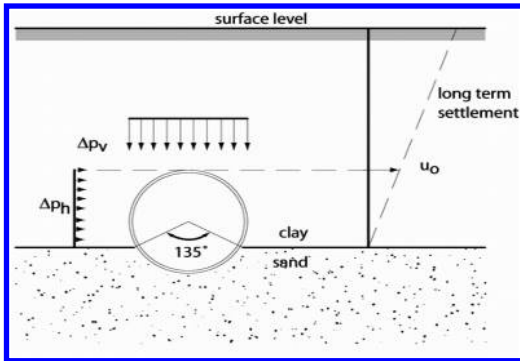


Figure 4. Loading due to negative skin friction on a bored tunnel (mechanism adopted from analytical modelling).

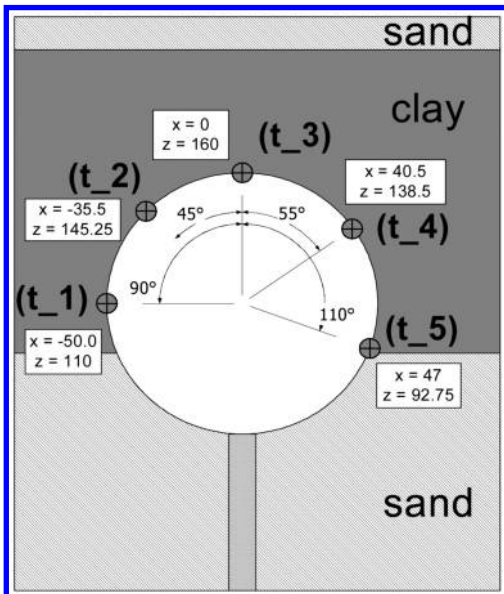


Figure 5. Positions of instrumentation on the model tunnel. A total pressure and pore pressure gauge was mounted on each position.

6.1 Test set up

The model was built at a scale of 1:65. The model tunnel was made of an aluminum tube, placed in a strongbox and supported by an aluminum strip. The lower part of the tunnel was embedded in a dense sand layer (135°). The tube was instrumented with pore pressure gauges and total pressure gauges, see Figure 5.

After placement of the tunnel in the sand, a layer of Spesswhite clay slurry with a water content of 94% was applied. The first part of the centrifuge tests was the self weight consolidation of the clay. The thickness of the clay layer after the self weight consolidation

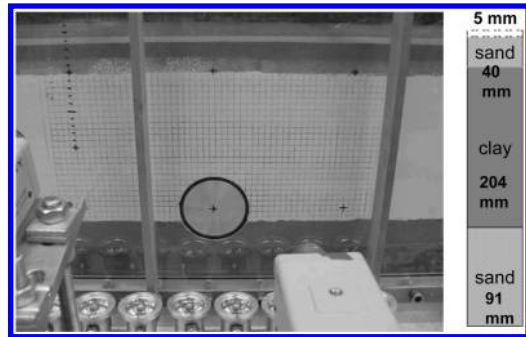


Figure 6. Set-up of the centrifuge tests and different soil layers.

was 10 m at prototype scale (test 1) and 9 m in test 2. On the model tunnel, in the sand and in the clay layer pore pressure and total stress transducers were installed. The front of the strong box consisted of a Perspex window, through which a grid, applied on the clay, was observed with 2 video cameras. The set-up before the test, is shown in Figure 6.

After self weight consolidation had taken place in the GeoCentrifuge, a sand layer was applied on top of the clay in flight. This sand layer caused an overburden pressure of about 55 kPa. After consolidation of the clay a second layer of sand was applied with the same thickness, leading to further consolidation of the clay layer. In the second test a sand layer of 1.3 m (prototype scale, 0.02 m in the model) was applied on the clay before self weight consolidation to increase the stress level in the clay with approximately 13 kPa (tests were performed in saturated conditions). As in the first test also two extra sand layers were applied after self weight consolidation of the clay. Since creep effects can not be scaled in a centrifuge test, these tests are only valid for the consolidation effects on the tunnel.

In the tests it was investigated whether the deformation pattern was influenced by wall effects at the glass wall. Some colored spaghetti was put through the clay layer from the backside to the glass wall. After the test it was found that the spaghetti was still straight, indicating that wall effects had only little influence on the results.

6.2 Test results

In Figure 7 the deformation of the clay at the end of the consolidation of the first sand layer (test 2) is shown.

Figure 8 shows the measured vertical soil stresses during the test at the crest of the tunnel and at the same level in the clay at 220 mm from centre of the tunnel. The vertical stress at some distance from the tunnel was calculated from the total stress transducers that were placed between the sand layer at the bottom of the model and the clay layer.

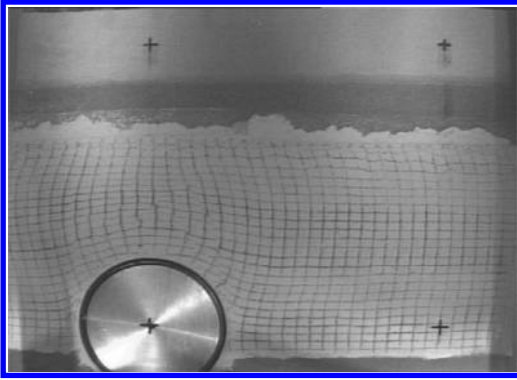


Figure 7. Deformed grid after test 2.

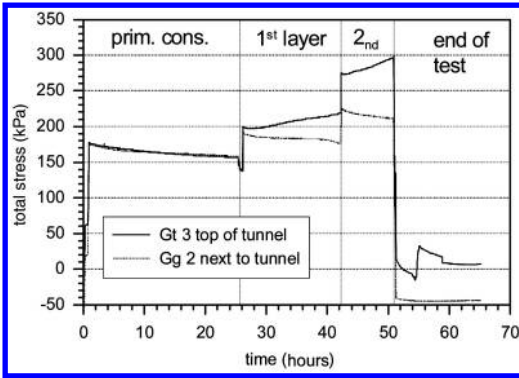


Figure 8. Test 2: Measured soil stresses on the tunnel and in the clay at 220 mm from the tunnel axis.

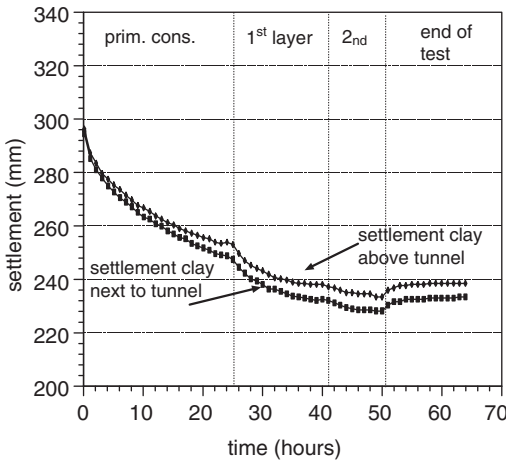


Figure 9. Test 2: Measured surface settlements during the test just above the tunnel and 220 mm next to the tunnel axis (model dimensions). Settlements determined from video images.

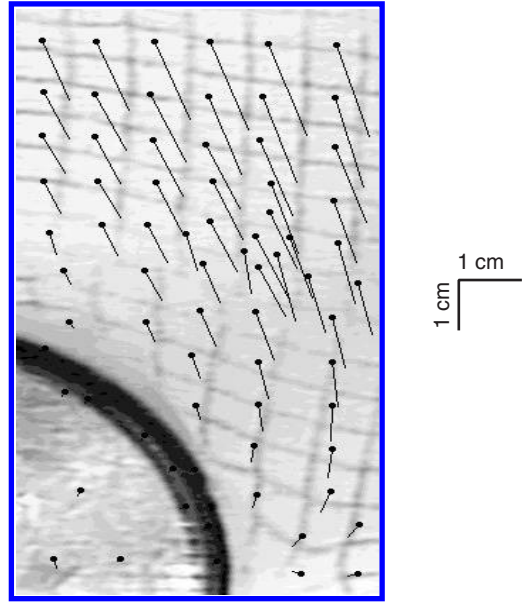


Figure 10. Deformation of clay around the tunnel as determined by image processing. The dot is the original position, the end of the line the position at the end of the test.

The increase of the soil stress on top of the tunnel (Gt3) compared to the stress in the clay (Gg2) at some distance from the tunnel during the consolidation of the two sand layers shows how the presence of the model tunnel led to an extra increase in the total stress compared with the free field situation, the difference was approximately 90 kPa at the end of the test. It appeared that during primary consolidation both pressure gauges measured the same total stress, but after applying the sand layers the stress on top of the tunnel increases more than the stress in the clay at some distance from the tunnel. This indicates that during primary consolidation when the clay is still very soft the ‘negative friction’ hardly influences the result, but the influence increases as the clay has gained some stiffness.

Surface settlements were a bit less just above the tunnel compared to the settlements at 220 mm from the tunnel axis, see Figure 9, but the difference is only small.

Deformations in the clay were measured using image processing, see Figure 10 that shows the direction of the deformation around the tunnel as determined from the grid on the clay before and after the test. It appears that, apart from the vertical deformation, there is horizontal clay deformation away from the tunnel axis in the clay above the upper fourth part of the tunnel and a horizontal deformation to the tunnel in the clay lower beside the tunnel.

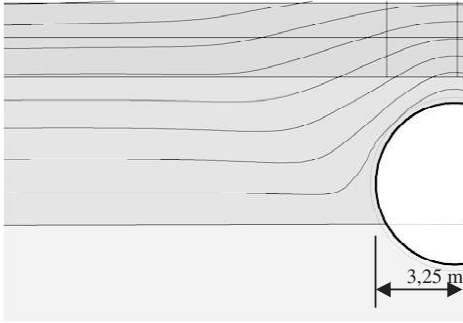


Figure 11. Deformation of clay around the tunnel; contourlines from FEM calculations.

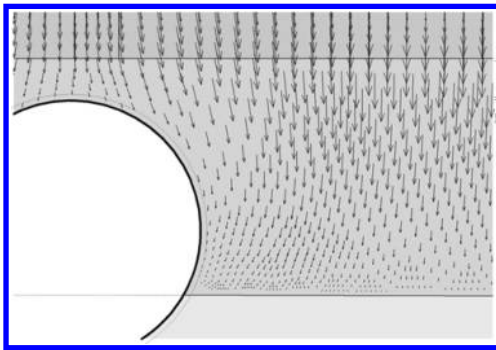


Figure 12. Deformation of clay around the tunnel; increments from FEM calculations.

7 BACK ANALYSIS

By means of a FEM model the results from the tests were analysed. In the numerical model both self weight consolidation and the consolidation after applying the two sand layers was simulated. The soil model used was the Plaxis Hardening Soil Model (HS; see Brinkgreve et al.). The material parameters were determined from Constant Rate of Strain (CRS) tests and CU triaxial tests on samples of the Spesswhite slurry.

Figure 11 shows the contour lines of the deformations as calculated with the FEM model and Figure 12 the deformation increments in the FEM mesh, both after application and consolidation of two sand layers. When the deformation pattern of the FEM-calculations is precisely compared with the findings of the centrifuge measurements, see Figures 7 and 10, it is evident that the negative skin friction mechanism for the numerical and physical modelling is quite similar.

Figure 13 shows the measured and calculated total radial stresses on the upper part of the tunnel (test 2).

The stresses coincide rather well. The differences between calculation and measurement are explained

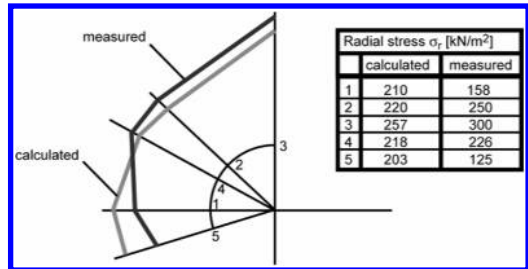


Figure 13. Measured (GeoCentrifuge) and calculated total radial stresses (FEM-method) on the tunnel lining.

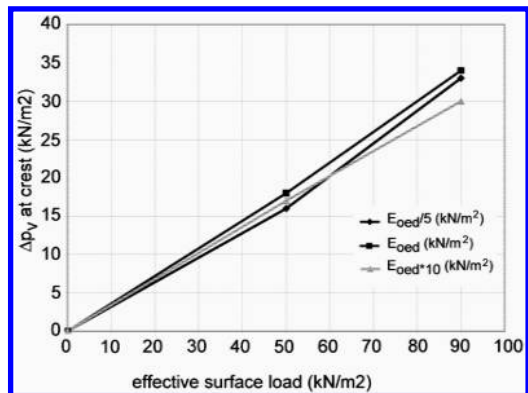


Figure 14. Vertical additional load Δp_v versus effective surface load for a variation of the soil stiffness E_{oed} and a geometry in accordance with the GeoCentrifuge tests.

by the rigid (aluminium) support under the model tunnel.

From the results of the back analysis it was concluded that the HS model in Plaxis is suitable to calculate the stresses around the tunnel.

The calculated effective radial stresses and shear stresses around the tunnel were used to determine the vertical (Δp_v) and horizontal components (Δp_h) of the additional stresses. In this way a comparison between the linear elastic solution (Eq. (1) and Eq. (2)) and the FEM-analyses could be made.

From these calculations it was concluded that Δp_v decreases more or less linearly towards the outside of the tunnel. The horizontal component Δp_h increases approximately linearly from the axis to the top of the tunnel. This result contradicts the elastic solution where both Δp_v and Δp_h result in constant values. Obvious, in the FEM-model, the soil arches on the stiff Pleistocene sand next to the tunnel.

The relation between the soil stiffness E_{oed} and the additional load due to negative skin friction was determined from the back analysis of the GeoCentrifuge tests. Results from calculations with a variation of 50 times E_{oed} are shown in Figure 14. It was concluded

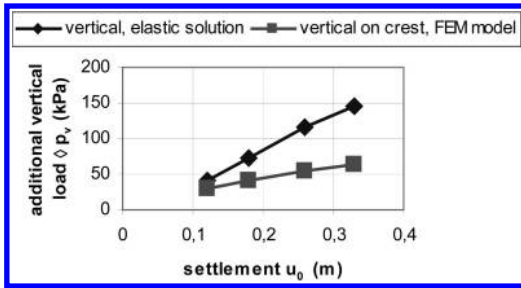


Figure 15. Vertical additional load Δp_v and settlement u_0 for the location Station Statenweg; elastic approach versus FEM scheme.

that the negative skin friction (end of consolidation value) is independent of E_{oed} . As u_0 is directly related to E_{oed} , this is in agreement with the elastic solutions Eq. (1) and (2), except for the factors given. For a specific geometry the negative friction can be regarded as only dependent on:

- the effective surface load (submerged value);
- the rate of embedment of the tunnel;
- the stiffness ratio of the soil and the tunnel lining.

Using the FEM Plaxis scheme the vertical component of the negative friction was determined at the location of the Statenweg Station. The ground conditions of this location and details of the lining properties are given in paragraphs 2 and 3 of this paper. The additional vertical stress was calculated as a function of the settlement u_0 of the undisturbed clay at crest level. For the results see Figure 15. It is evident that the negative friction is not limited by full plasticity in the calculated range. The difference with the elastic solution is increasing with increasing settlement over the height of the tunnel.

8 CONCLUSIONS

When tunnel tubes are located at the transition zone of soft to stiff soil layers, long term settlements of the soft layers lead to additional loads on the tunnel lining.

As expected, the additional loads affect the vertical effective stresses on the tunnel lining. The study revealed that a change of the horizontal stresses has to be accounted for as well.

The analytical linear elastic approach according the stress distribution function of Airy (see Eq. (1) and (2)) appears to be conservative.

A more sophisticated elasto-plastic soil model is needed to simulate the centrifuge tests. With the finite element approach, using the Plaxis Hardening Soil model, the centrifuge test results can be simulated well. The difference with the elastic solution is increasing with increasing settlement (see Figure 15).

The negative skin friction force at the end of the consolidation phase appears independent of the soil stiffness. When the stiffness increases, the deformation around the tunnel decreases but the rate of soil loading increases. For a given soil stratification and tunnel dimensions the end of consolidation value of the negative skin friction loading depends only on the effective surface loading.

A plastic upper bound for the negative skin friction was not found, neither in the GeoCentrifuge nor in the back analyses with the finite element model. The additional loading on the lining increases nearly linear with the long term settlements due to consolidation and creep and therefore the tunnel loading increases steadily in time.

REFERENCES

- Pachen, H.M.A. & van Zanten, D.C. van, 2002. Prediction of long term behaviour of a bored tunnel in soft soil. *Proc. Sec. Int. Symp. On Geotech. Aspects of Underground Constructions in Soft Ground Toulouse*, Balkema; Rotterdam.
- Pachen, H.M.A., Brassinga, H.E. & Bezuijen, A., 2003. Geotechnical centrifuge tests to predict the loading conditions on a bored tunnel due to consolidation settlements. *ITA Proc. (Re)Claiming the Underground Space Amsterdam*, Swets & Zeitlinger Lisse.
- Brinkgreve, R.B.J. et al., Plaxis 2D version 8, Balkema; Rotterdam.

The following symbols and abbreviations are used in this paper:

γ_{sat}	: saturated unit weight	[kN/m ³]
w	: water content	[%]
PI	: Plasticity Index	[–]
σ'_v	: effective vertical stress	[kPa]
c_u	: undrained shear strength	[kPa]
Δp_v	: vertical loading due to negative skin friction forces on tunnel lining	[kPa]
Δp_h	: horizontal loading due to negative skin friction forces on tunnel lining	[kPa]
u_0	: vertical soil displacement at crest level; determined outside the sphere of influence of the tunnel	[m]
E_{oed}	: constrained modulus of elasticity	[kPa]
E	: modulus of elasticity	[kPa]
p_a	: atmospheric pressure	[kPa]
R	: radius of tunnel tube	[m]
K_0	: coefficient of horizontal earth pressure at rest	[–]
OCR	: overconsolidation ratio	[–]
CPT	: Cone Penetration Test	

Introduction to Numerical Analysis

Tools for numerical analysis have improved quite a lot in the last decade. This can be seen clearly when the 2-dimensional element meshes of the first papers are compared with the 3-dimensional meshes of the last papers. Also the possibilities to apply the boundary conditions that can be expected (staged construction, loading on soil and lining during various phases) has been improved. Yet it is still not straight forward to make a successful numerical simulation of the tunnelling process. Still there are boundary conditions that play an important role, but are not clarified up to now, for example the interaction between the TBM and the lining and the influence of the grout consolidation on the pressure distribution. Furthermore because of the limited deformations involved, it is of importance to have stress strain relations for small strain conditions that are often not available. The papers in this chapter indicate what progress is made at GeoDelft.

The first paper was made several years for the first large diameter shield tunnel was made. The research was triggered by the construction of a 3 m diameter tunnel for water control that was made using the shield tunnelling technique. The article shows in general what were by then the challenges in the numerical simulation process of the tunnels and presents some results specific for the 3 m diameter tunnel.

The second paper deals with a 2-dimensional simulation of the tunnelling process for a tunnel in sand underneath soft clay. The tunnelling is simulated using volume contraction in the tunnel and the soil is modelled with the Mohr-Coulomb model. The results show the deformation patterns, the stress distribution and the plastic zone.

The third paper in this chapter presents finite element calculations performed for the Second Heinenoord Tunnel to check contractor's calculation method for the loading on the lining. It is shown that the 'bedded beam' model used by the contractor does not always lead to safe results compared with the results of finite element calculations.

The first GeoDelft publication with a 3-dimensional calculation on tunnelling was in 1997. In this calculation the tunnel face stability was analyzed using a modified Cam clay model (the 'Egg-Cam clay model') that is also described in this paper. No constant factor was found between results of 3-dimensional and 2-dimensional calculations, which means that 3-dimensional calculations are necessary to simulate 3-dimensional phenomena.

A three dimensional calculation simulates tunnel and surrounding soil in 3 dimensions. It is also possible to include the time dependent tunnelling process. This is nowadays sometimes called a 4 dimensional calculation. An example of such a calculation is presented in the fifth paper. The method was used to simulate the boring of the 14.5 m diameter Green Heart Tunnel in the Western part of The Netherlands.

Although 3 and 4-dimensional calculations were performed at the turn of the century, it remained rather demanding calculations when it comes to computer time and memory usage. The last contribution in this chapter showed how this can be reduced by introducing some simplifications in the mesh geometry and the soil layering. This enables the possibility to run the simulation on a personal computer.

Introduction to Miscellaneous

This chapter deals with papers that do not fit within the other chapters. These are overview papers and some papers that deal with a cut and cover tunnel that was built in The Hague (the Tram Tunnel). The papers of the Tram Tunnel, the first three papers in this chapter, show that tunnelling in The Netherlands, with its high water table in the soil at most of the locations, can become a struggle with the ground water. Permeability of what should be impermeable and clogging of what should be permeable has resulted in some problems during this project.

The fourth paper of this chapter presents some tunnel projects from the past (before 1994), a problem that occurred during micro-tunnelling and some “open tunnel solutions”. By that time several concepts were worked out that could be an alternative for shield tunnelling. Two of these concepts are the “open tunnel solutions”. Time has learned afterwards that these concepts hardly have been used.

The fifth paper emphasizes possible risks of underground construction and stresses the value of research. It is shown on economic principles that the annual

turnover of the building market in The Netherlands and cost reduction that can be achieved justified far larger budgets for research than by then was common practice (and still is).

An overview how the “innovation circle” has been used in tunnelling research in The Netherlands is presented in the fore last paper in this chapter. This “innovation circle” assumes that progress in an empirical science as geotechnics needs a combination of field testing and monitoring, calculations and model testing. The contributions in the various chapters of this book also showed that GeoDelft have been active in all aspects of the innovation cycle.

The last paper deals with two aspects of shield tunnelling where pore pressures and pore water flow are found to be important. These aspects are mentioned already in other papers in earlier chapters, but this contribution presents a summary for these aspects. It deals with the excess pore water pressure in front of the drilling face that can influence the face stability and the consolidation of the grout that results in an unloading of the surrounding soil.

Constructing underground: influencing geotechnical equilibrium

Berg, P. van den, Schrier, J. van der & Hergarden, H.J.A.M.

Delft Geotechnics, Research Engineering, Delft, The Netherlands

ABSTRACT: Building underground structures in soft soil affects the geotechnical equilibrium. During and after the construction process, information is required on the magnitude of the stress changes and the corresponding deformations which are induced in the soil. Therefore, the strength- and stiffness characteristics of the total system, consisting of the structure interacting with the surrounding soil, should be understood. Nowadays, soil-structure interaction problems are analysed adequately by use of a finite element method. However, special care should be taken with respect to the input parameters and the way they are determined. In this paper attention will be paid to the application of the finite element method when simulating soil-structure interaction in soft to very soft soil. As an example, the results are presented for a simulation of the construction of two 3 meter diameter tunnels bored in soft soil in the Netherlands.

1 INTRODUCTION

Constructing an underground structure causes interaction between the structure and its environment. This environment may include existing buildings, roads, pipelines etcetera. Unfortunately, in the western part of the Netherlands, where the call 'go underground' is heard most loudly, the subsoil consists mainly of soft to very soft soil under the ground water level. Under these conditions the interaction between structure and soil is complicated and may be critical for the design. Clearly, the interaction must be investigated.

Soil-structure interaction problems can be simulated by using a finite element method. However, basic knowledge of both the finite element method used and the soil mechanics is required to interpret the calculation results properly. In this paper attention will be paid to the use of a finite element method, and the input parameters required, to simulate the soil-structure interaction correctly under the geotechnical conditions as encountered in the western part of the Netherlands. By way of illustration, a short review is given of the geological history of the area under consideration.

2 THE GEOLOGICAL HISTORY OF THE WESTERN PART OF THE NETHERLANDS DURING THE QUATERNARY: A SHORT REVIEW

With respect to the subject one could say that the geological history of the Netherlands starts about thirty seven million years ago. Caused by local movements

within the European plate, a SE-NW orientated rift fault system is developing in the southern part of the present Netherlands.

The sea level varies in time, but most of the area stays below sea level. Sediment is brought in from the hinterland by the ancient river Rhine and centres of deposition are developed within the areas of subsidence.

Seven million years ago the delta of the ancient river Rhine starts growing and the main centre of deposition shifts north-west. An uplift of the hinterland starts. Apart from that, some three million years ago, an extensive delta is developing in the northeast of the present Netherlands as the sea retreated from the North-German lowlands.

Almost two million years ago the main centres of deposition shift further northwest, towards the present North Sea. Due to an increased sediment supply caused by the uplift of the hinterland and a change in climate, the Rhine-Meuse delta in the south and the delta of the North German-Baltic river system in the north, expand rapidly. Both deltas form one single large delta which covers an area much larger than the present area of the Netherlands. The sea level varies, the sea level is relative low during the glacial periods and relative high during the interglacial periods. During times of high sea levels the present west-coast is below sea level and marine clays are deposited, but generally speaking sediments related to (braided) river systems dominate (coarse sands and gravels during glacial periods and windblown sands during inter-glacial periods). In fact, a long period of sedimentation predominantly related to an open marine environment (marine clays) has come to an end.

At the beginning of the holocene period (some 10000 years ago) the last sea level rise starts and the tidal zones reach the south west of the Netherlands again. Peat formation starts nearby the floodplains. These peat layers are sometimes overlain by marine clay and are sometimes eroded by the sea.

About 5000 years before present, the rate with which the sea level rises is decreasing and, also due to a positive sedimentation balance, a coastal barrier system is developing. At the top of this coastal barrier, dune forming starts. In the areas behind the coastal barrier, out of reach of the aggressive sea, thick peat layers are formed.

Starting some 3000 years before present the sea starts attacking the coastal barrier and about 1000 years ago the coastal barrier has partly disappeared. Locally sediments fall prey to the sea, but in the early middle ages mankind intervenes and starts coastal protection. In the seventeenth century land is even reclaimed from the many lakes, which had been formed naturally and by human action due to peat extraction.

By now, the top-section of the stratigraphy of the western part of the Netherlands consists of roughly 20 m peat and soft to very soft clay laying on top of a thick layer of sand, coarse sand and gravel.

3 ON THE STIFFNESS OF SOIL

In order to determine deformations and stresses under working loads the stiffness of the material plays a very important role. This is especially true for the behaviour of underground structures in soft soil. The soil-stiffness in relation to the stiffness of the structure defines the mechanical behaviour of the soil-structure interaction system. Since the soil-stiffness is difficult to measure and also because a number of definitions exist in the literature, in this paragraph a short review of the so-called 'soil-stiffness' will be given.

In finite element analyses, Youngs' modulus E and Poisson's ratio ν are the input parameters to define the elastic behaviour of the soil. A number of tests exist to derive these parameters, but most of them do not give Youngs' modulus directly. For 3 types of tests it will be indicated how to derive the Youngs' modulus.

Table 1 gives an overview of values for the Youngs' modulus E for a number of different soil types. These values are rough values, but rather typical for Dutch circumstances. The Youngs' modulus E can be derived from an oedometer test, a triaxial test or, for instance, a pressuremeter test.

In an oedometer test, the modulus is derived from the curve representing the relationship between the settlement of the test specimen and the vertical pressure exerted. Since the rigidity of the circular ring around the sample does not allow any lateral displacement,

Table 1. Rough values for Youngs' modulus E (MN/m²) for different soil types.

Soil type	Youngs' modulus MN/m ²
soft peat	0.5–1.0
peat	1.0–3.0
soft clay	1.0–2.0
clay	2.0–4.0
sandy clay	3.0–6.0
preconsolidated, stiff clay	4.0–10.0
clayey sand	5.0–15.0
loose sand	5.0–15.0
medium dense sand	15.0–30.0
dense sand	30.0–50.0
gravel	60.0–120.0

a 'constrained' modulus is measured. The relationship between this modulus (E_c) and Youngs' modulus (E) is:

$$E_c = \frac{E(1-\nu)}{(1+\nu)(1-2\nu)} \quad (1)$$

where: ν = Poissons' ratio.

In the case of fine sand, it is recommended to use a value of about 0.3 for Poissons' ratio ν . For clay and peat, Poissons' ratio strongly depends on the loading rate: at high rates, the material behaves undrained. This implies that the volume of the material is constant and thus Poissons' ratio will be (nearly) equal to 0.5. Drained behaviour of the same material results in ratios between 0.2 and 0.3.

Youngs' modulus can be directly derived from a triaxial test. Assuming the material is homogeneous and isotropic, Hooke's law gives:

$$\varepsilon_v = 1/E[\sigma_v - 2\nu\sigma_h] \quad (2)$$

where: ε_v = vertical strain of the sample
 σ_v = vertical stress applied on the top of the sample
 σ_h = lateral pressure.

The pressuremeter test permits in-situ measurement of soil-stiffness. In this case, problems associated with sample-disturbance (clay and peat samples) or the re-building of samples in the test-apparatus (sand) do not exist. The test is performed by expanding a cylindrical cavity in the ground. The test probe is pushed into the soil and, after reaching the required depth, a cylindrical rubber membrane is inflated. The pressure as well as the volume increase are measured. During the elastic phase of the test (when plasticity effects can be neglected), Youngs' modulus can be derived as follows:

$$E = (1+\nu) \frac{(p-p_o)r_o}{r-r_o} \quad (3)$$

where: r = current radius of cylindrical hole
 r_o = initial radius of the hole

- p = pressure applied
- p₀ = initial horizontal soil-stress
- ν = Poisson' ratio.

There exist also other methods to derive Youngs' modulus, as for instance a 'plate bearing test' or correlations with the cone-resistance as measured by a Dutch cone penetration test.

The large number of tests illustrates the fact that the term 'the stiffness of the soil' at its own, is not precisely defined. For a good understanding, additional information is needed. It is essential to know in what way the parameter was derived. In addition, since any modulus of elasticity is stress dependent, differs with the rate of deformation and varies with the stress path followed (soil reacts for instance stiffer when it is unloaded compared with the case in which the soil is loaded for the first time), it is most important that the test conditions during the determination of the modulus of elasticity do agree with the circumstances that will occur in the actual situation.

4 MODELLING SOIL-STRUCTURE INTERACTION PROBLEMS

The analysis of soil-structure interaction problems is complicated. Mostly two or even three dimensions have to be taken into account, a number of construction phases has to be distinguished and, in addition, the soil behaviour is highly non-linear and rate dependent. So, up to 10 or 20 years ago, one was obliged to use empirical or semi-analytical models. Since a number of assumptions and modifications had to be made, in many cases this may have resulted into 'too safe' constructions.

For instance, in the analytical models developed to calculate stresses and strains in tunnels, large diameter culverts and pipelines, the interaction between soil and construction has not been incorporated yet into one combined model. The vertical loading and the horizontal and vertical reaction of the soil are determined by a separate model, and after that applied to the construction. In this manner, the interaction between construction and soil is highly schematized. Normally, aspects such as the increase of the bedding angle and the horizontal support with increasing deformation, and also the smoothness or roughness of the outside of the construction are not taken into account.

At the present stage of development, finite element models can be used to give a better prediction of the behaviour of underground structures. The major advantage of a finite element method is that it is capable to consider the soil-structure interaction as one integral problem to be solved. The following aspects can be taken into account:

- smoothness or roughness of the structure
- the presence of bentonite or other fluids

- non-circular geometries of the construction
- a layered soil-profile
- time-dependent effects such as creep and consolidation
- a full 3-dimensional approach.

Evaluating these effects, it is concluded that more sophisticated models are advantageous when compared to the option of applying and/or modifying existing models.

In modelling soil-structure interaction problems by using finite element models, three types of elements have to be distinguished: elements to model the behaviour of the soil, the structure and the interface between soil and structure (see Figure 1). Since introducing the last mentioned elements into a finite element model is a very recent development. The mechanics of these elements will be worked out in the next paragraph.

In fact, two mechanisms can be distinguished at the interface: the contact-gapping mechanism and the frictional shearing mechanism. The interface behaviour can be described in terms of a relation between the normal and shear forces, t_n and t_s, and the normal and shear relative displacements across the interface, Δu_n and Δu_s. The relation between t_n and Δu_n, the contact-gapping mechanism, is modelled by a very stiff spring to simulate contact up to a specified maximum normal force.

If the normal force exceeds this maximum value a discrete 'gap' arises between the construction and the soil and the normal force reduces to zero. Generally the friction mechanism, is described as follows: up to a specified shear stress level, depending on the normal stress at the interface, 'elastic' shearing-behaviour is assumed. If the shear stress exceeds the specified shear stress level, plastic slip deformation occurs at the interface. In that case the maximum shear stress t_{max} can be defined by the Coulomb friction model:

$$\tau_{\max} = a + \sigma_n \tan \delta \quad (4)$$

where:

- a = the adhesion between soil and structure
- σ_n = the normal stress at the interface
- δ = the interface friction angle.

5 SOIL STRESSES AROUND UNDERGROUND STRUCTURES

The initial state of stress in the soil, before starting construction, can be characterized by the volumetric weight of the soil (γ), the depth (z) and the lateral pressure ratio (K₀).

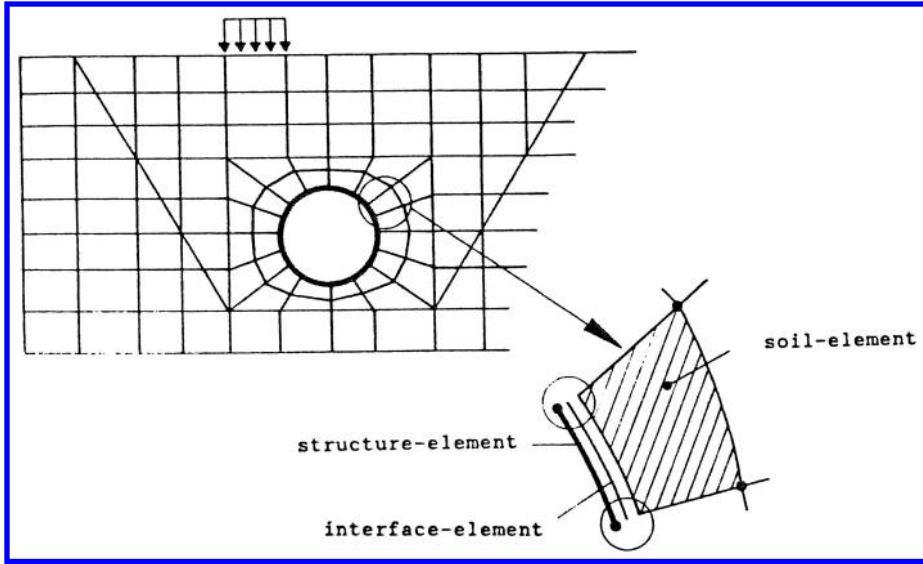


Figure 1. Schematization of finite element model for soil-structure interaction problems.

This ratio is defined as the quotient of the horizontal (principle) effective stress σ_1 and vertical effective stress σ_3 :

$$K_0 = \sigma_1 / \sigma_3 = \sigma_1 / (\gamma z) \quad (5)$$

Introducing the initial state of stress into a model in a correct way is very important. After introducing the initial stresses into the model, all stress points in a diagram relating the isotropic stress to the deviatoric stress are located on the 'K₀-line'. An example is given in Figure 2. Since the difference between the 'K₀-line' and the failure envelope of the material is a rough measure of the load bearing capacity, introducing the initial stresses into the model is necessary to get reliable results.

When starting the construction phase, it is important to introduce the stiffness of the soil into the model in a proper way. In most cases, the interest is not only focussed on the safety against complete failure of the construction, but also on the deformation in and around the structure, for instance the settlement of the soil surface. These aspects are dominated by the deformation parameters of the soil (see paragraph 3).

The stiffness of the soil can be used as a part of the load bearing capacity. Very flexible structures, for instance large diameter thin-walled steel culverts, can only be applied when the surrounding soil has a certain stiffness (Van den Berg, 1990).

The culvert deforms due to the soil dead weight above the structure, and during deformation a horizontal reaction is created, necessary to get a new equilibrium between soil and structure.

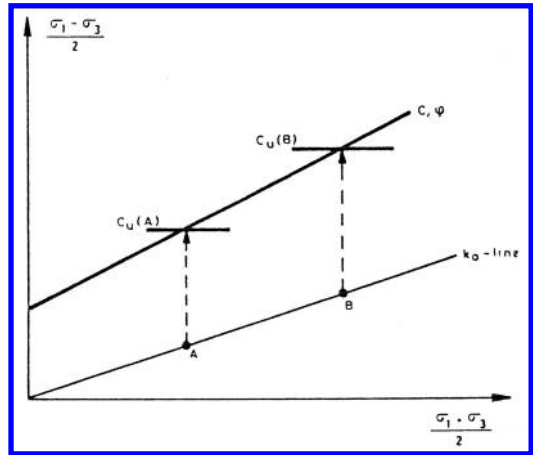


Figure 2. Initial state of stress in the soil and failure envelope.

Rigid structures (made of concrete for instance) are supposed to carry the load by themselves. If the structure is stiff relative to the surrounding soil, peak stresses will increase since rigid members attract stresses. On the other hand, if the structure is capable to deform a bit, the directions of the principle stresses rotate, a stress arch may develop and the soil around the structure may become partly self-supporting (arching). There is, however, a difference when looking to the soil-stresses around a smooth and a rough structure under comparable conditions. For instance, above a smooth culvert the stress arch will develop more clearly than around a rough culvert. In the case of a

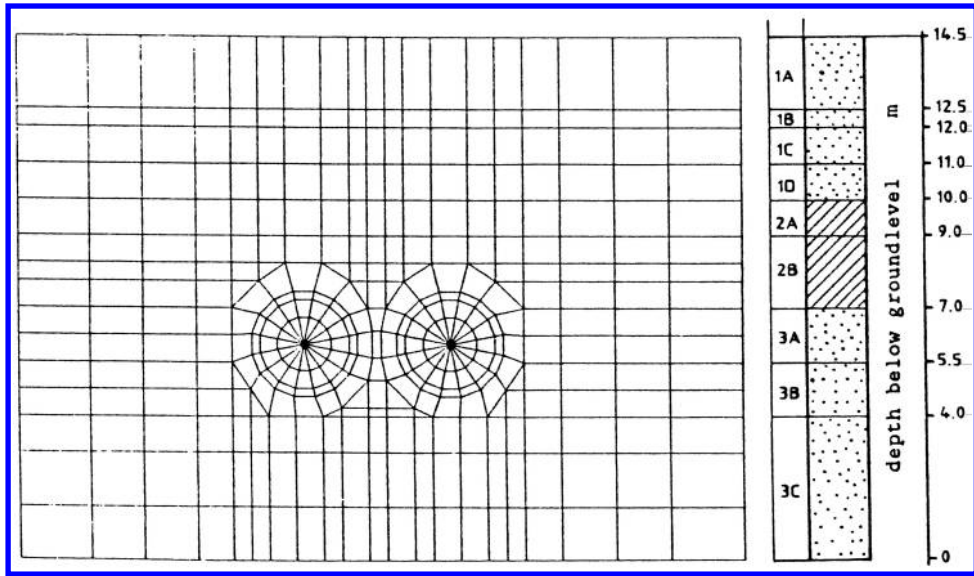


Figure 3. Finite element model to investigate the influence of two bored tunnels on the surrounding soil.

rough culvert the contribution of the shear stresses at the interface becomes more important, and a larger part of the load is transferred to the culvert itself.

After construction, time-dependent effects may have influence on the stresses around a structure. Especially in soft soil layers (clay and peat) consolidation and creep will occur. Drainage effects due to consolidation and creep, but also due to rainfall and movement of the groundwater level, will have influence on the behaviour of the soil and the occurring stresses.

6 TWO 3-M DIAMETER TUNNELS IN AARLE-RIXTEL

In the southern part of the Netherlands two tunnels with a diameter of 3 meter have been bored in soft soil using a shield tunneling technique. An extensive description of the project, the measurements carried out and the results of finite element calculations can be found in (Van der Schrier, et al., 1991).

In this paragraph the attention will be focussed on the influence of the construction of the culverts on the surrounding soil. A two-dimensional plane strain finite element model has been used to investigate this influence. The model is presented in Figure 3.

The process of tunneling will cause some settlement of the surface. This is also indicated in Figure 4. In this figure, the soil displacements are presented at the end of the construction of the second tunnel (the first tunnel has been completed already). As can be seen, the soil displacements are not symmetrical. This is caused

by the fact that the soil above the first tunnel, which was constructed at the left side of the second, has been influenced. Due to the construction of the first tunnel, the stress state is not virgin anymore. After the construction of both tunnels, the settlement profile at the surface will be slightly asymmetrical.

The stresses in the soil are strongly influenced by the tunneling process. This is illustrated in Figure 5. As can be clearly seen, a stress arch has been developed around the tunnel. The directions of the principle stresses rotate and the vertical stresses above the tunnel strongly decrease. Next to the tunnel the stresses increase. Since the second tunnel will be installed within this area (the dashed line in Figure 5), the load on the second tunnel will be relatively large. Furthermore, because the construction of the second tunnel will partly disturb the stress arch around the first one, the load on the first tunnel will increase also.

The influence region can be estimated from Figure 5. For the case presented, the stresses in the soil change due to the tunneling process up to about two diameters above the tunnel and one diameter next to the tunnel. It can be concluded that, in this case, the interaction between the two culverts would have been negligible if they were constructed at a distance between them of at least one tunnel-diameter.

7 CONCLUDING REMARKS

- It is demonstrated that in modelling soil-structure interaction problems, a finite element model can be used adequately. The interaction between soil and

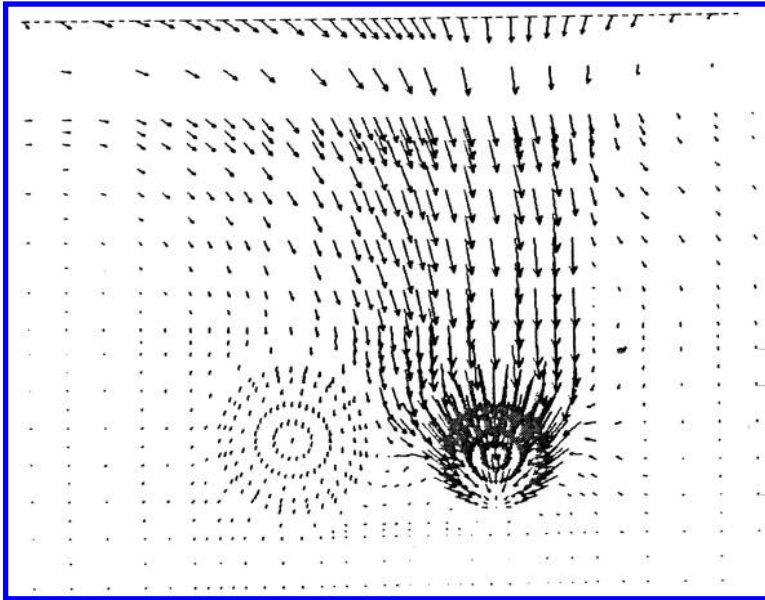


Figure 4. Soil displacements at the end of the construction of the second tunnel.

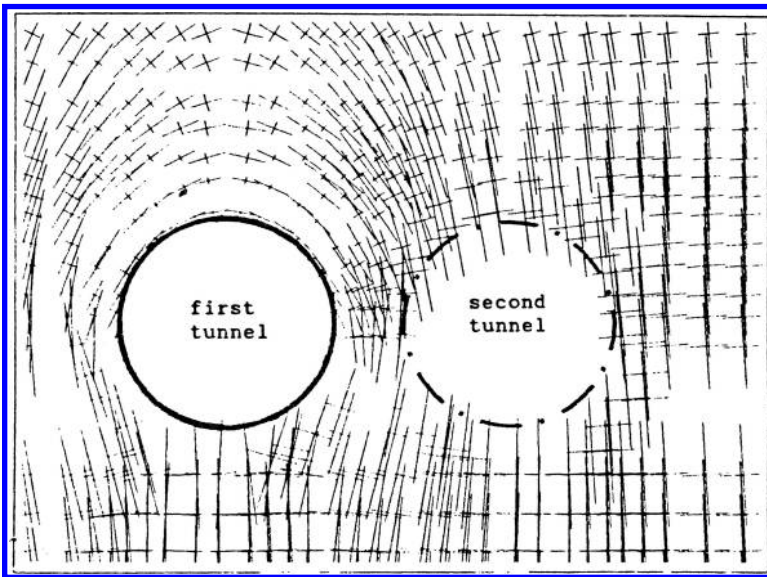


Figure 5. Stresses around a bored tunnel.

structure is considered as one integral problem and can be solved.

- Using a finite element technique, the region influenced by an underground construction process, can be determined. If the region of influence overlaps with the region of influence of an existing structure,

an interaction with the existing structure will start and must be investigated.

- Since at present time the interest is not only focussed on the safety against failure, but also on the deformation and stresses around the structure due to working loads, the stiffness of the soil is a

very important parameter. However, 'the stiffness of the soil' is not a precisely defined parameter and therefore special attention is needed to determine this parameter.

- To determine 'the stiffness of the soil', a number of tests can be used, it should be realised that each of them delivers another stiffness parameter.

The following points are most important:

- the test conditions during the determination of the stiffness parameter must agree with the circumstances that will occur in the actual situation (stress level, stress path and deformation rate).

- the test used to determine the stiffness parameter must be in accordance with the calculation method in which it is used.

REFERENCES

- Van den Berg, P., Zorn, N.F. (1990) "Numerical analysis of flexible culverts in layered soils", Pipeline and Design and Installation Conference, ASCE, Las Vegas, March 25–27, 1990, pp. 383–397.
- Van der Schrier, J.S., Hergarden, H., Van den Berg, P. (1991) 'Aanleg duikers in Aarle-Rixtel levert gegevens voor simulatie', Land + Water, Nr. 5, mei 1991, pag. 58–61.

Stress distribution due to tunnel excavation

A.J. Grashuis & J.A.M. Teunissen

Delft Geotechnics, The Netherlands

ABSTRACT: This paper studies the effects of stress distribution on adjacent constructions such as pile foundations due to volume loss in the tunnel boring process. A specific case is discussed of a relative deep tunnel in a sand layer covered with clay. Due to the volume loss a change of horizontal stresses is observed. Increase as well as decrease of horizontal stresses occurs depending on the location and the amount of volume loss. This is of particular importance for constructions which foundation depends on the stress state, such as tension piles. The mechanism resulting from a deep tunnel is different from the mechanism resulting from a lower overburden. These mechanisms are noticed and discussed.

1 INTRODUCTION

The most common methods for subsurface construction are the cut-and-cover method in soft soils and direct cutting in hard soils like rock. In densely populated areas, like big cities, transportation takes place more and more through tunnels. The lack of surface space, the inconvenience with surface activities for constructing, and the still increasing demand for transport leads to the need for more sophisticated methods for constructing tunnels. The shield boring machine for such a situation is of current interest in The Netherlands. The effects of tunnelling in soft soils on adjacent constructions and foundations are of practical interest (Fujita, 1989). This paper describes the stress distribution due to tunnel excavation. It is especially directed to effects on pile foundations. For surface settlements much more is already known (Attewel, et al., 1986).

The excavation for constructing tunnels is a complicated three dimensional problem (Peck, 1969). It consist of several components: the excavation at the front, the frontpressure, the overcutting, the placement of the tunnel segments and the backfill grouting. The aspect of tunnelling which has most effect on the surrounding environment is the reduction of volume. It is caused by the smaller lining in comparison to the cutting diameter. Study of this effect is presented in this paper after performing plane strain simulations.

In section 2 the problem is defined. In section 3 the method of solution is presented. Results of the simulation are given in section 4. These are discussed in section 5. The paper closes with conclusions in section 6.

2 PROBLEM DESCRIPTION

The geological situation in The Netherlands can be characterized as follows. The soil stratigraphy consist

of holocene soft clay and peat layers from surface to a depth of 15 m to 25 m, on top of a relatively stiff pleistocene sand layer which is used as a foundation layer for piles. The undrained shear strength of the clay is around 10 kPa and the volumetric weight of saturated peat can be lesser than 11 kN/m³. Furthermore the groundwater table is close to the surface. Many pile foundations and several existing tunnels are present, which are obstacles for additional to be designed tunnels which should be constructed with the shield boring technique.

This paper presents a pre-design of an 8 m diameter tunnel which is located with its top at 27 m below surface. The large overburden is due to its location close to a waterway to be crossed. A sand layer follows after 23 m of soft clay layers from surface to 4 m above the top of the tunnel. In Table 1 the used soil parameters for this case are given. It is assumed that the water table is present at surface.

Of particular interest is the development and behaviour of the stresses near the tunnel due to excavation and its construction, because an existing construction is close to this new designed tunnel. For the existing construction tension piles are used to resist the uplift forces caused by the water pressure at the bottom of it. For a good and stable behaviour of the tension piles the horizontal stresses, which cause the necessary friction between pile and surrounding soil, are

Table 1. Used soil parameters.

Soil-type	Level m	E MPa	ν_i/ν -	φ'/ψ°	c' kPa	γ' kN/m ³
Clay	+5 to -18	1-5	0.45/0.4	25/0	5	7
Sand	<-18	25	0.35/0.3	35/5	0	10

very important. The purpose of analyzing this case is to investigate the effect of tunnel excavation on the surrounding soil.

3 METHOD

The calculation is performed with a finite element code developed for non-linear geotechnical problems (Teunissen, 1991). In the analysis a Mohr-Coulomb model has been used. The elastic behaviour is described by a linear-elastic model with the parameters Young's modulus (E) and Poisson's ratio (ν). The strength parameters in the Mohr-Coulomb model are the friction angle (ϕ'), the dilatancy angle (ψ) and cohesion (c').

The calculation is performed as a drained analysis. This implies that the pore pressures are neglected, which for clay is only acceptable for simulation of long term effects. The tunnel is modelled without any special interface behaviour between the tunnel and the surrounding soil.

The used finite element mesh (consisting of 2539 nodes and 926 quadratic triangle and quadrilateral elements) is given in figure 1, together with the dimensions. For reasons of symmetry, only half of the tunnel and soil is modelled.

The calculation is performed with a conventional constant stiffness method.

The calculation is divided into two stages:

1. the initial stress build up,
2. the volume reduction in small calculation steps.

It is assumed that the weight balance of the tunnel is zero: its initial weight (i.e. effective body force of sand) equals the after construction weight including the uplift force caused by water pressure. In this paper presented amount of volume reduction is the

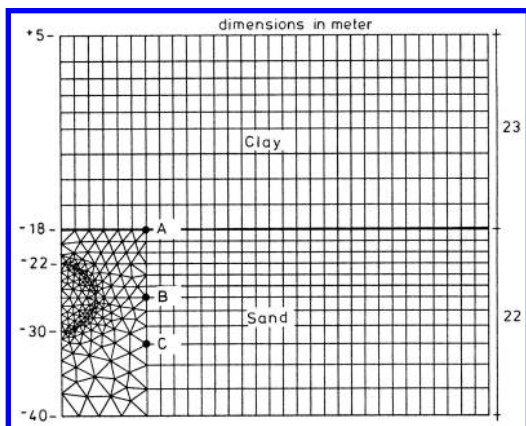


Figure 1. Used finite element mesh.

direct volume loss around the tunnel and not as it is measured from surface settlement. Determination from surface settlement may include other geometrical effects resulting from the occurrence of compression or extension of the soil. The volume loss in the calculation is applied by a force controlled compression of the tunnel. This means that the tunnel is not fixed in the soil, but is able to move vertically if the reaction forces in the surrounding soil force the tunnel to do this. Not taken into account is the deformation of the tunnel itself. Its shape remains exactly circular.

4 RESULTS

The applied volume loss ranges in small steps from 0 to 2.63% of the initial tunnel volume. After 2.63% volume loss the base of the tunnel moves 22 mm upwards and its top 84 mm downwards. This means that the tunnel axis moves as a whole slightly downwards (21 mm) due to the behaviour of the surrounding soil. Settlement troughs at horizontal levels +5 m, -6 m and -18 m after 0.53% and 2.63% volume loss are presented in figure 2. The volume of the settlement troughs is slightly lower than the applied volume loss which means that some expansion of the soil occurs. From figure 2 it seems also that close to the sand layer a trough with a smaller width and steeper slope is present compared with the troughs in the clay layer.

Of importance is the behaviour close to the tunnel. At a vertical 10 m from the tunnel axis displacements and stresses at three locations are recorded, see figure 1 for the locations A (above the tunnel), B (besides the tunnel) and C (under the tunnel). Figure 3 presents the horizontal displacements and figure 4 the development of the horizontal stresses at the three mentioned locations during applying the volume loss. Initially the soil moves horizontally towards the tunnel,

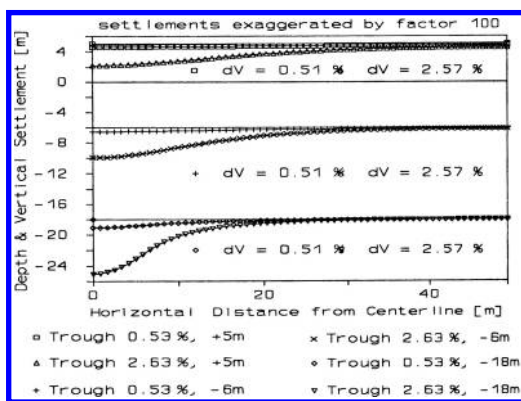


Figure 2. Settlement troughs after 0.53% and 2.63% volume loss.

however after about 1% volume loss for location B a drastic change in the moving direction takes place. For the horizontal stress a decrease can be seen, the largest for location A. For location B, after an initial decrease of horizontal stresses, an increase occurs. In section 5 the possible causes for this behaviour is discussed.

For comparison, some results at the beginning stage of the volume loss and at the end of the calculation are given in the figures 5 and 6 in an area close to the tunnel. Figure 5 presents the velocity field (incremental displacements) between a volume loss of 0.26% to 0.53% (figure 5a) and between 2.37% to 2.63% (figure 5b). The drastic change in direction of the nodal displacements is clearly shown. The stress state after 0.53% volume loss is given in figure 6a, and after 2.63% in figure 6b. The horizontal stresses σ_{xx} and the vertical stresses σ_{yy} after 2.63% volume loss is presented in the figures 7a and 7b. Above and under the tunnel a horizontal stress build up results and besides the tunnel a vertical stress build up. From the figures 6 and 7 the development of arching can be seen.

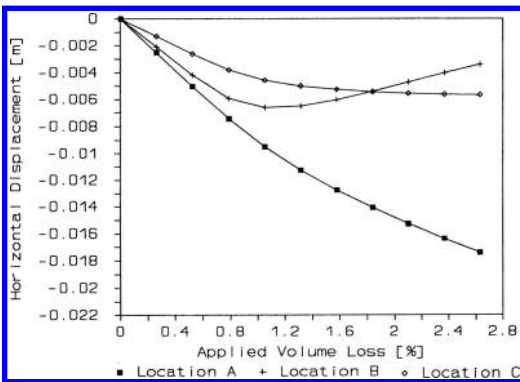


Figure 3. Development of horizontal displacements at three locations.

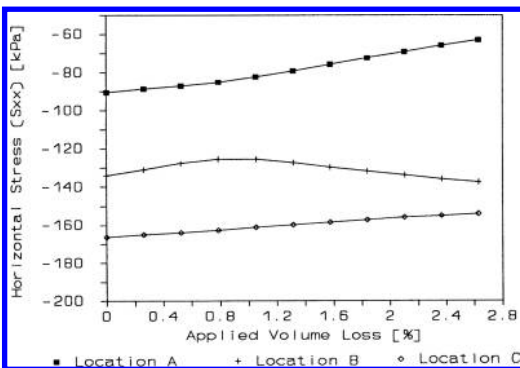


Figure 4. Development of horizontal stresses at three locations.

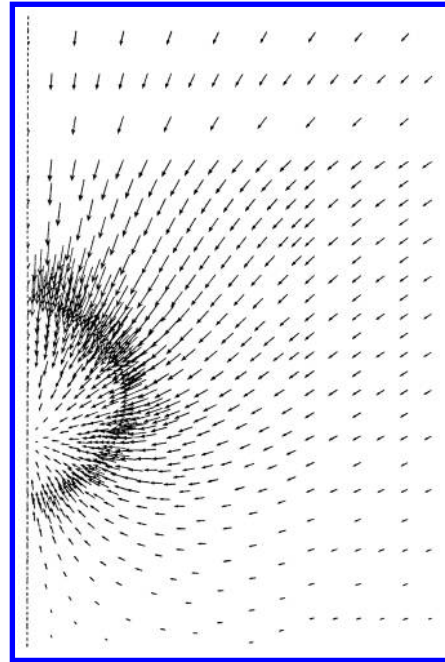


Figure 5a. Incremental displacements between 0.26% to 0.53% volume loss.

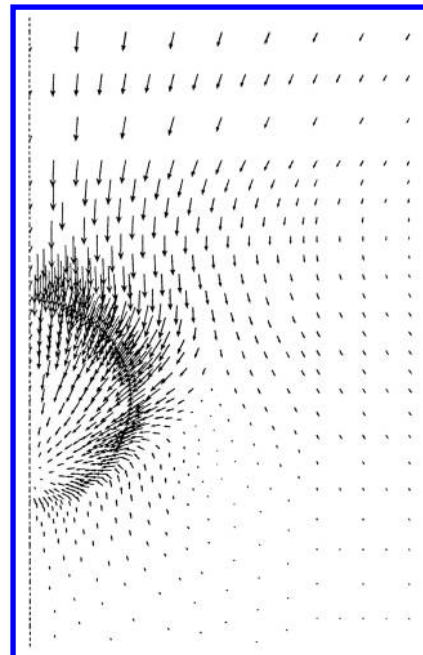


Figure 5b. Incremental displacements between 2.37% to 2.63% volume loss.

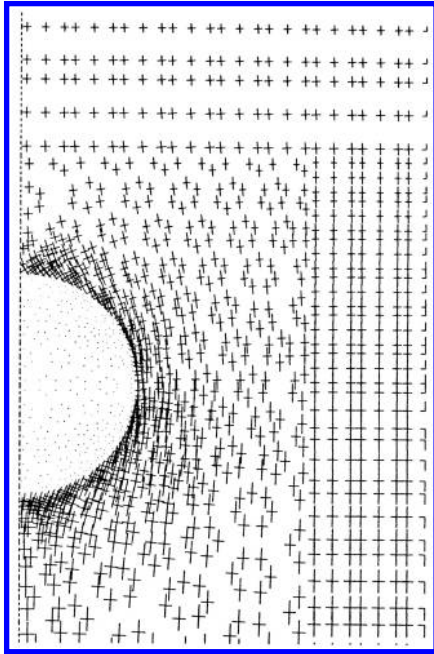


Figure 6a. Stress state after 0.53% volume loss.

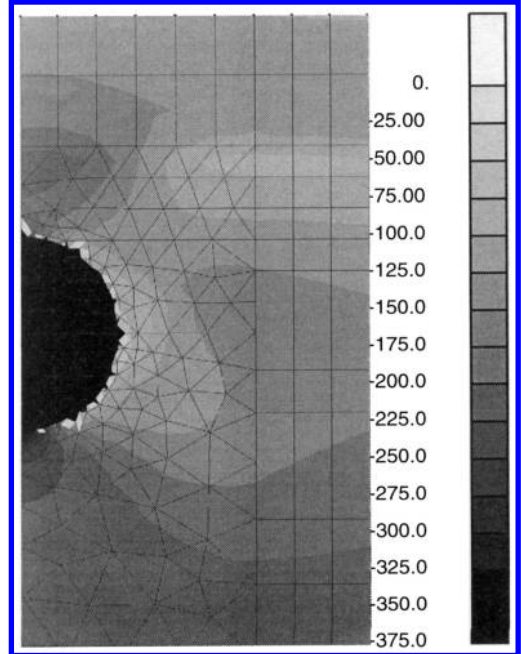


Figure 7a. Horizontal stresses σ_{xx} [kPa] after 2.63% volume loss.

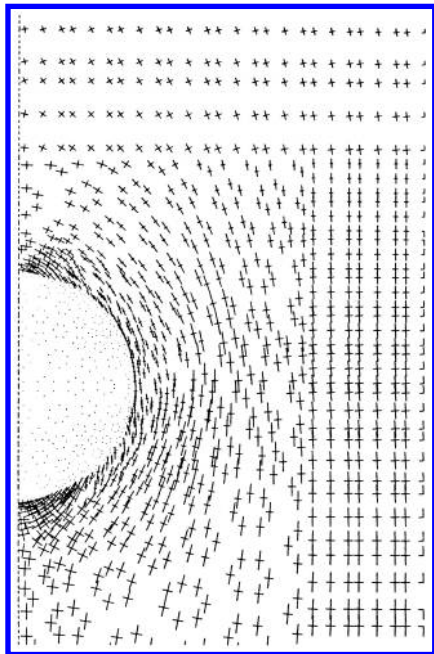


Figure 6b. Stress state after 2.63% volume loss.

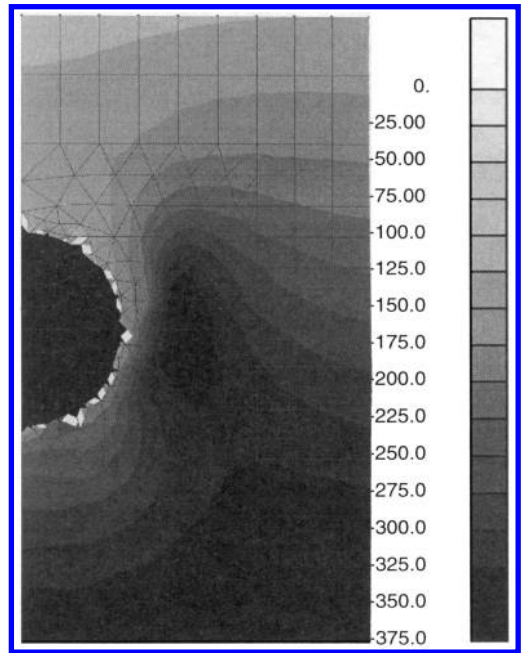


Figure 7b. Vertical stresses σ_{yy} [kPa] after 2.63% volume loss.

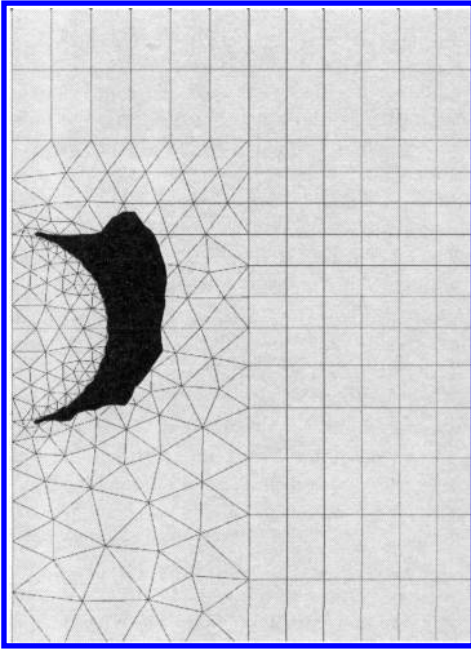


Figure 8. Area of plasticity (in black) after 2.63% volume loss.

5 DISCUSSION

The results show that the effect of the applied volume loss can be divided into two parts.

The first part up to about 1% volume loss can be characterized as an elastic response to an initial amount of volume loss. The reaction of the surrounding soil is a flow of soil particles in the direction of the tunnel where space is created. Plasticity is not yet present and due to the created space a decrease of stresses occurs. The decrease of horizontal stresses at location B is about 7%. Additional simulations result in a decrease locally of about 25%.

The second part of the volume loss starts from about 1% volume loss. Comparison of figure 5a with figure 5b shows a drastic change of the direction of displacements. For location B for instance, it results in a flow away from the tunnel instead of a flow towards the tunnel before, see figure 3. Locally the direction of displacements changes over 90°. A strong arching around the tunnel develops also during this part of volume loss, see figure 6a and 6b. A further inspection of this case shows local plasticity around the tunnel. This area of plasticity is slowly increasing during increasing volume loss, see figure 8 for the area of plasticity after 2.63% volume loss.

The arching band and the area of plasticity are both located within half a diameter around the

tunnel. Therefore it is concluded that the arching band reaches its ultimate stress state.

Close above the tunnel the flow is separated in a part which remains active on the tunnel (up to a vertical at about 0.75 times the tunnel radius besides the tunnel) and a part which is moving besides the tunnel and is active on the soil mass just outside the arching band, see figure 5b.

6 CONCLUSIONS

In other almost similar performed tunnelling simulations, the mentioned behaviour of a drastic change in flow direction near the tunnel was not noticed. The principal difference with the case presented here is the smaller overburden. So the depth of the tunnel and thus the resulting overburden is presumably a key factor in the development of mechanisms in the soil. In case of a low overburden (say 1 to 2 times the tunnel diameter), usually a plastic shear band occurs starting from the tunnel and developing to the surface with a steep slope (between 70° and 90° with the horizontal) in case of an overburden consisting of sand layers, and a flat slope (between 40° and 60°) in case of less stiffer clay layers. The main part of deformation takes place direct above the tunnel. For the case presented in this paper diffuse plasticity occurs around the tunnel and it does not reach the surface due to the large overburden.

Additional calculations were carried out with different soil parameters and also including an interface layer between tunnel and surrounding soil with smooth and rough conditions. All calculations resulted in similar effects as described in this paper.

The effect of volume contraction of the tunnel results in the effect of soil moving to the tunnel. This effects gradually a larger area around the tunnel if the tunnel has a low overburden. Then a marked area above the tunnel with shear zones from the tunnel upwards develops. If the location of the tunnel is deep, geometrical effects become important. Above the tunnel is still the weakest area in comparison to soil next to or below the tunnel. But the soil massive above the tunnel will move down and will simultaneously push the soil next to the tunnel away. The overburden will remain elastic.

Some constitutive aspects such as nonlinear compressibility of the soil may influence this behaviour. Preferably this should be done with a Cam-Clay type of model with inclusion of undrained behaviour for clay. For sand a stress and load dependent model could be used (loading with a higher modulus of elasticity, unloading with a lower one). This has not been performed in this study. It can improve the quantitative data.

Of importance is also to incorporate the behaviour of the lining during volume loss. A non-circular deformation of the lining will occur. This is still a topic of research.

REFERENCES

- Attewell, P.B., Yeates, J., Selby, A.R., 1986. Soil movements induced by tunnelling and their effects on pipelines and structures. *Blackie and son Ltd.*
- Fujita, K., 1989. Special lecture B: Underground construction, tunnel, underground transportation. *Proceedings of the 12th international conference on soil mechanics and foundation engineering, Volume 4: 2159–2176*, Rio de Janeiro.
- Peck, R.B., 1969. General report: Deep excavations and tunnelling in soft ground. *Proceedings of the 7th international conference on soil mechanics and foundation engineering*, Mexico.
- Teunissen, J.A.M., 1991. Users manual finite element code PLUTO. *Delft Geotechnics*.

Soil loads acting on shield tunnels: comparison between bedded beam model and finite element calculations

J.T. van der Poel & H.J.A.M. Hergarden

Delft Geotechnics, The Netherlands

H.R.E. Dekker

Ministry of Transport and Public Works, The Netherlands

ABSTRACT: The Ministry of Transport and Public Works of The Netherlands has ordered the construction of a large diameter bored tunnel at Heinenoord. The tunnel will have an outer diameter of 8.3 m and will be the first large diameter shield tunnel in The Netherlands. The tunnel will be bored in soft soil conditions. For the design of the tunnel lining, calculations have been performed with the bedded beam model. A comparison between these calculations and finite element calculations has been made. It was concluded that soil stresses acting on the lining and behaviour of the lining according to the finite element calculations was different from the bedded beam model with respect to the influence of the water pressures (buoyancy of the tunnel) and the modulus of subgrade reaction.

1 INTRODUCTION

In 1994 and 1995 a design was prepared for the first large shield tunnel to be driven in The Netherlands, the Second Heinenoordtunnel. The tunnel contains two tubes with an outer diameter of 8.3 m and a lining thickness of 0.35 m. The tunnel crosses the Oude Maas river. Delft Geotechnics has executed the soil investigation for this project and has provided geotechnical recommendations. The design has been made by the TCH contractor combination on behalf of the Dutch Ministry of Transport and Public Works. The TBM is of the Slurry Shield type.

The soil conditions in the western part of The Netherlands differ at various locations from soil conditions in the surrounding countries. The top layers can be characterised as very soft and the ground water table is mostly high. Therefore extensive research has taken place and will be executed in the near future to investigate the applicability of foreign design methods for Dutch soil conditions. In this paper some results are presented of research, that has been executed by Delft Geotechnics.

Results will be presented with respect to the geotechnical parameters used in the bedded beam model to determine stresses in and deformations of the tunnel lining. Special attention is given to:

- effective soil stresses acting on the lining after construction of the lining;

- the determination of the modulus of subgrade reaction and distribution of the subgrade reaction of shallow tunnels;
- effective soil stresses on tunnels situated in soil, which is liable to settlement.

For this research 2D finite element calculations have been executed for two situations at the Second Heinenoordtunnel and a hypothetical situation, representing a Dutch soft soil profile. These calculations will be discussed in this paper.

2 CALCULATION MODEL

The calculation model, that has been used by the TCH to determine bending moments, shear forces and normal forces in the lining is the version of the bedded beam model developed by Wayss & Freytag. Two parallel lining rings are modelled, where each ring contains 7 elements with a width of 1.5 m and a thickness of 0.35 m. The second ring is rotated over half the segment length in comparison with the first ring. The two rings are connected by a “shear spring”. The principle of this model is given in [Figure 1](#).

The subgrade reaction and the effective soil stresses are schematised in accordance with ITA and Duddeck (1980). This means that for shallow tunnels, no subgrade reaction is taken into account at the top of the

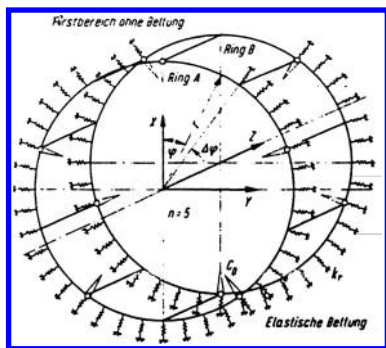


Figure 1. Wayss & Freytag's bedded beam model.

lining over a total angle of 90 degrees. The fact that the vertical effective stress acting on the bottom of the lining is taken equal to the original vertical effective stress at the top of the lining, suggests that no stresses in the lining are generated due to decompression of the soil below the lining. The buoyancy is eliminated from the calculation, in accordance with Erdmann (1983), by assuming a sine distribution of the water pressures.

3 ANALYSED SOIL PROFILES

In this paper analyses will be discussed of tunnels in 3 soil profiles. The first two profiles were obtained from the Heinenoord project. The first profile is found at the northern starting point of the shield tunnel. The top layer mainly consists of loose sand, followed by firm peat and peaty clay layers with an undrained shear strength of about 50 kPa. These layers are lightly over consolidated. Below these layers a dense to very dense sand layer is found. The tunnel is located mainly in the peat and clay layers, while the bottom rests on the dense sand layer. The spacing between the tubes at this location is half the outer tunnel diameter. The ground water table is at approximately 4 m below ground surface.

The second profile is situated at the river crossing. During high tides and/or high river flow a water level of approximately 14 m above the river bed occurs. At this location the soil above, adjacent to and below the tunnel is dense to very dense sand. The spacing between the tubes equals about 1 diameter. These two soil profiles are given in Figure 2. A detailed description of the soil parameters and layer thickness is given in section 4.

Additional calculations have been executed for a typical Dutch soft soil profile. The top 10 m consist of very soft peat and peaty clay layers, with an undrained shear strength increasing from approximately 3 kPa at ground surface to approximately 12 kPa at 10 m depth. The ground water table is located at approximately 0.8 m below ground surface. The saturated unit weight of these layers varies from 10.2 kN/m³ of the peat

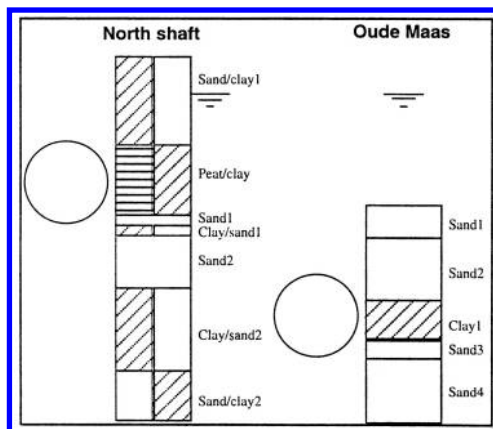


Figure 2. Soil profiles Second Heinenoordtunnel.

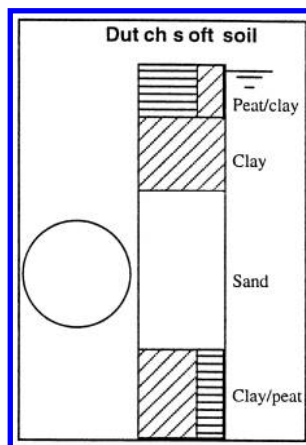


Figure 3. Dutch soft soil profile.

layers to 14.5 kN/m³ of the clay layers. The average unit weight of the soft layers is about 12 kN/m³. Below the soft layers a very dense sand layer is found with a thickness of about 12 m. Below the sand layers a stiff clay layer is found with an undrained shear strength of approximately 150 kPa. In this profile two tubes with an outer diameter of 9.8 m and a lining thickness of 0.45 m was modelled. The profile is visualised in Figure 3.

4 CALCULATIONS

The aim of the calculations was to simulate the stress changes in the soil due to the tunnelling process for the normative situations. The calculations were 2D finite element calculations performed with the Pluto package which has been developed by Delft

Table 1. Soil parameters northern shaft Second Heinenoordtunnel (1).

Soil type	Top of layer (m to NAP)	Unit weight (kN/m ³)	E (kPa)	ν (-)
sand/clay1	+4.5	17	7000	0.28
peat/clay	-5.2	14.5	3300	0.28
sand 1	-12.9	20	41000	0.25
clay/sand 1	-14.0	15.5	6000	0.30
sand 2	-15.0	20	47000	0.26
clay/sand 2	-20.5	19.7	25000	0.27
sand/clay 2	-29.4	20	40000	0.26

Table 2. Soil parameters northern shaft Second Heinenoordtunnel (2).

Soil type	Top of layer (m to NAP)	ϕ' (degr.)	c' (kPa)	K_0 (-)
sand/clay 1	+4.5	27	1	0.55
peat/clay	-5.2	22	4.5	0.55
sand 1	-12.9	34	0	0.55
clay/sand 1	-14.0	22.5	3	0.55
sand 2	-15.0	34	0	0.45
clay/sand 2	-20.5	29	4	0.45
sand/clay 2	-29.4	32	2	0.45

Geotechnics. In the calculations, the following process was modelled:

- first, the unit weight of all soil layers is applied, to generate the initial stress state in the soil layers;
- after that, the first tube is installed in the mesh;
- the unit weight of the concrete lining is applied, the effective weight of the excavated soil is removed and the water pressures acting on the tube, including the buoyancy force, is applied;
- finally, a second tube is installed in the same way as the first tube.

For the calculations, performed for the design of the Second Heinenoordtunnel, use has been made of a Mohr-Coulomb failure criterion for all soil layers and a linear elastic stiffness until failure. The stiffness of the soil layer below the tunnel has been increased in comparison with the measured values to incorporate a relatively stiff behaviour under decompression. The soil layers and soil parameters are given in Tables 1 and 2 for the calculation, executed for the situation just behind the northern shaft, and in Tables 3 and 4 for the calculation, executed for the situation at the Oude Maas crossing.

In these tables E is Young's modulus, ν is Poisson's ratio, ϕ' is the angle of internal friction, c' is the effective cohesion and K_0 is the coefficient of effective horizontal stress at rest.

The top level of the tubes near the northern shaft is NAP -5.1 m and the bottom level NAP -13.4 m.

Table 3. Soil parameters Oude Maas crossing Second Heinenoordtunnel (1).

Soil type	Top of layer (m to NAP)	Unit weight (kN/m ³)	E (kPa)	ν (-)
sand 1	-10.7	20	7500	0.30
sand 2	-15.0	20	24000	0.26
clay 1	-21.8	19.5	9500	0.27
sand 3	-26.0	20	19000	0.26
sand 4	-28.0	20	50000	0.26

Table 4. Soil parameters Oude Maas crossing Second Heinenoordtunnel (2).

Soil type	Top of layer (m to NAP)	ϕ' (degr.)	c' (kPa)	K_0 (-)
sand 1	-10.7	30	0	0.40
sand 2	-15.0	34	0	0.40
clay 1	-21.8	28.5	5	0.40
sand 3	-26.0	32.5	0	0.40
sand 4	-28.0	32.5	0	0.40

The spacing between the tubes was 4.4 m. The ground water table is taken at NAP +0.4 m.

The top level of the tubes at the Oude Maas crossing was NAP -19.4 m and the bottom level NAP -27.7 m. The spacing between the tubes is 8.3 m. The water level in the river is taken at NAP +0.5 m.

To incorporate the effect of reduced lining stiffness due to segmentation a Young's modulus of the lining of 12 GPa was used, which is approximately 30% of the concrete stiffness. The unit weight of the concrete lining has been taken 24 kN/m³. A full bond between tunnel and soil was assumed.

4.1 Results northern shaft

At the northern shaft a water pressure of 56 kPa was acting on the top of the tubes and 139 kPa at the bottom of the tubes.

In Figure 4 the effective, radial soil stresses acting on the lining at the end of the calculation are given for the first tube to be installed and the second tube to be installed.

The results show a horizontal ovalisation of the tunnel i.e. the horizontal diameter increases and the vertical diameter decreases due to deformation of the tubes. Some influence was found of the buoyancy of the tunnel. Due to the buoyancy some soil reactions are mobilised at the top of the tube, which enlarges the horizontal ovalisation. The difference in the (vertical) water pressure acting on the top of the tube and the (horizontal) water pressure acting on the side of the tube at centreline causes a relative vertical ovalisation. The dead weight of the tube and the effective soil stresses cause a relative horizontal ovalisation.

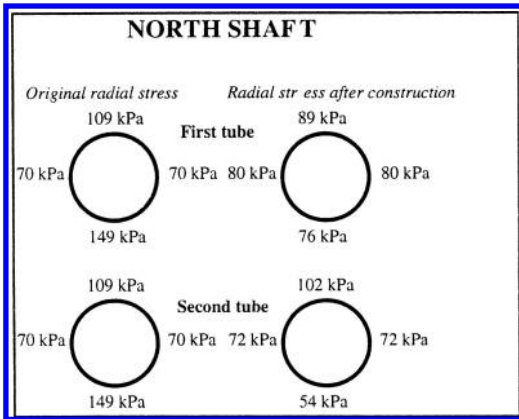


Figure 4. Effective radial soil stresses before and after tunnel installation at northern shaft.

In the calculations an uplift of the tunnel of approximately 20 mm is found. This uplift is partially caused by swelling of the soil layers below the tunnel due to decompression as a consequence of the removing of the effective soil weight in the tubes. Because the layers directly below the tunnel are sand layers, it is likely that this part of the uplift has already occurred before hardening of the tail void grout.

A distinct interaction was found between the two tubes, although the spacing between the sides of the tubes was more than 0.5 times the outer tunnel diameter. Due to horizontal ovalisation of the first tube, the effective horizontal stresses increase at the location of the second tube before installation of this tube. This results in lower horizontal deformations of the second tube in comparison with the first tube and therefore lower bending moments. A horizontal ovalisation of the first tube of approximately 2 times 9 mm was found and approximately 2 times 5 mm of the second tube. Due to the buoyancy of the second tube, vertical effective stresses on top of the first tube are reduced. Also the distribution of the stresses acting on the first tube changes due to the installation of the second, tube which causes an increase of the maximum bending moments in the continuous beam model by approximately 10%.

4.2 Results Oude Maas crossing

At the Oude Maas crossing a water pressure of 199 kPa was acting on the top of the tubes and 282 kPa at the bottom of the tubes.

In Figure 5 the effective, radial soil stresses acting on the lining at the end of the calculation are given for both tubes.

In this calculation a horizontal ovalisation of the tube was found of approximately 2 times 6 mm. The

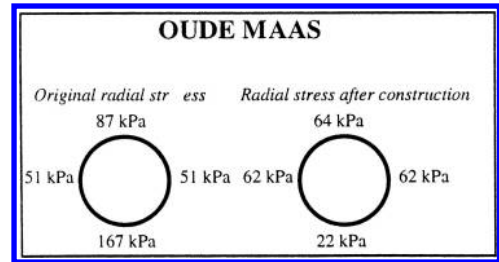


Figure 5. Effective radial soil stresses before and after tunnel installation at Oude Maas crossing.

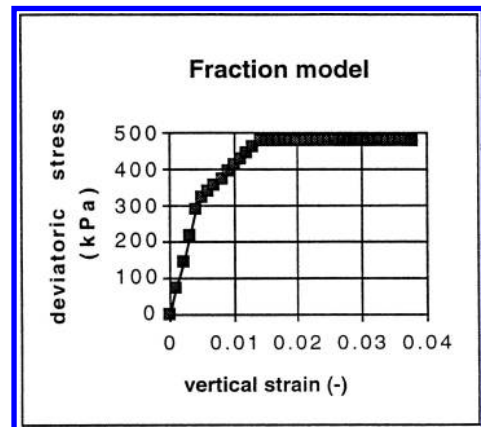


Figure 6a. Results of triaxial test simulated with 2 parallel Mohr-Coulomb fractions.

bedded beam model would predict a vertical ovalisation. Due to the buoyancy and the dense layer overlying the tunnel, a horizontal ovalisation was found. The spacing between the tubes was 1 outer tube diameter. No noticeable interaction between the tubes was found. The uplift of the tubes was about 20 mm. Due to the buoyancy force effective soil stresses at the bottom of the tunnel reduces to a low value of 22 kPa.

4.3 Results Dutch soft soil profile

The calculations for the Dutch soft soil profile have been executed with more advanced soil models. The clay and peat layers were analysed with the modified Cam-clay model. For the sand layer a trilinear model was used containing two parallel Mohr-Coulomb fractions in order to make a more adequate schematisation of the behaviour under triaxial conditions. This is visualised in Figure 6a.

Young's modulus for deviatoric stresses between 0 and 50% of the maximum deviatoric stress is equal to the sum of the Young's moduli of both fractions; Young's modulus for larger deviatoric stresses is equal to the Young's modulus of the second fraction.

Table 5. Soil parameters Dutch soft soil profile (1).

Soil type	Top of layer (m to NAP)	ϕ' (degr.)	c' (kPa)	K_0 (-)
peat/clay	-1.1	21	3	0.65
clay	-6.0	22.5	5	0.60
sand	-13.0	35	0	0.50
clay/peat	-27.8	29	10	0.70

Table 6. Soil parameters Dutch soft soil profile (2).

Soil type	Unit weight (kN/m ³)	κ (-)	λ (-)	ν (-)
peat/clay	11	0.40	1.6	0.2
clay	14	0.14	0.55	0.2

Soil type	Unit weight (kN/m ³)	E_1 (kPa)	E_2 (kPa)	ν (-)
sand	20	55000	17000	0.30

Soil type	Unit weight (kN/m ³)	κ (-)	λ (-)	ν (-)
clay/peat	20	0.009	0.055	0.35

The magnitude of the soil parameters, used in this calculation, is given in Tables 5 and 6.

In these tables κ represents the swelling index and λ the compression index. E_1 and E_2 represent Young's modulus of the first and second fraction. For the shallow peat/clay layer and the clay layer an OCR of 1.05 has been applied; for the deep clay/peat layer an OCR of 1.6 was adopted.

The ground water table was taken at NAP -1.9 m. In the deep sand layer the piezometric head is approximately 3 m higher than the ground water table.

The concrete tube has a diameter of 9.8 m. The top level of the tubes was NAP -16.2 m and the bottom level NAP -26.0 m. The spacing between the tubes was 9.8 m. To incorporate the effect of reduced lining stiffness due to segmentation a Young's modulus of the lining of 10.8 GPa was used, which is approximately 1/3 of the concrete stiffness. The unit weight of the concrete lining has been taken 24 kN/m³. A full bond between tunnel and soil was assumed.

In this situation the vertical effective stress at the top of the tubes is low, so the safety with respect to buoyancy is low. In Figure 6b the radial effective stresses before and after the installation of the tunnel are given.

The results indicate a horizontal ovalisation of the tubes. Because the loading is relatively low, the calculated horizontal deformation is less than 1 mm. A vertical deformation of approximately 20 mm was found. Significant decompression of the soil below

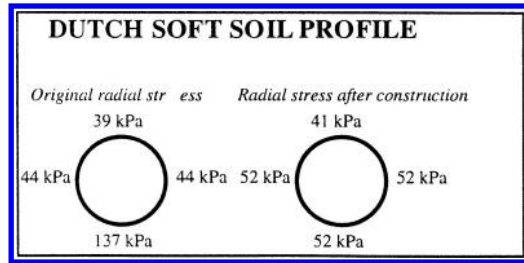


Figure 6b. Effective radial soil stresses before and after tunnel installation for Dutch soft soil profile.

the tubes occurs due to the removal of the effective soil weight in the tubes and the buoyancy force.

The effect of decompression due to volume loss before hardening of the tail void grout is not modelled here. The soil below the tubes consists of stiff clay with a very low permeability of approximately 10⁻¹¹ m/s. Calculations show that the vertical deformations of the tunnel due to decompression of the clay occurs predominantly within a period of approximately 2 years. Therefore the clay layer below the tunnel will behave almost undrained before hardening of the grout, so most of the swelling will occur afterwards.

The vertical effective stress at the top of the tubes is increased, despite the horizontal ovalisation. This is caused by the buoyancy of the tubes. The increase in vertical effective stress at the top is low (about 2 kPa). The vertical effective stresses at the bottom of the tubes is almost equal to the sum of the original vertical effective stress at the top of the tunnel and the stresses, caused by the dead weight of the concrete lining. Because a full bond between tube and soil was assumed, a shear stress at the side of the tunnel of almost 20 kPa was generated. If the influence of the shear stresses is removed, the distribution of the stresses is almost in accordance with the assumptions of the bedded beam model for shallow tunnels.

To obtain quantitative information of the modulus of subgrade reaction due to horizontal ovalisation, a horizontal, outward deformation of 20 mm was imposed on the two nodes at the level of the centreline of the tube at the end of the aforementioned calculation steps. The calculated deformations and stress changes at the interface between lining and soil have been used to determine the magnitude of the modulus of subgrade reaction. The results are given in Figure 7.

The results show that the modulus of horizontal subgrade reaction at the sides of the tubes is lower than the expected value of E_{oad}/R , where E_{oad} the oedometer modulus represents and R the radius of the tube (Ahrens, 1982). In this case only 65% of the expected value was calculated. This may be caused by the limited thickness of the sand layer above the top of the tunnel (3.2 m) in comparison with the tube diameter. This type of calculation has been executed for

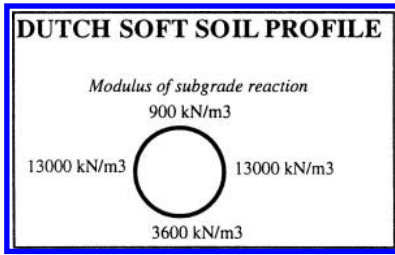


Figure 7. Calculated modulus of subgrade reaction.

several soil conditions. In general, for shallow tunnels a modulus of horizontal subgrade reaction is found of between $0.5 E_{oed}/R$ and E_{oed}/R .

The modulus of vertical subgrade reaction at the bottom of the tubes is relatively low. In the calculations the behaviour of the deep clay/peat layer was described with the modified Cam-clay model. This means that stiffness and settlement/swelling is proportional with the isotropic effective stress. Although the soil below the tunnel behaves as relatively stiff, over consolidated soil, the stiffness reduces with decreasing isotropic effective stress.

4.4 Tunnel in soil liable to settlement

For the Dutch soft soil profile an analysis has been made of the consequences of applying a tunnel with the aforementioned dimensions, which is partially located in the soft layers. This situation occurs just behind shafts in order to limit the depth of the shafts. In that case the weight of the soil overlying the tunnel is insufficient to withstand buoyancy of the tunnel. One of the solutions is to increase the weight of the overlying soil by placing a sand fill or replacing the soft layers by sand. Placing of a sand fill on ground surface causes significant settlement. Also, the soil around the tunnel would be compressed significantly, even if excess pore water pressures are almost eliminated by using vertical drainage and a certain preload time. For instance due to a sand fill with a thickness of 3 m and a preload time of 1 year, using vertical drains, a settlement after installation of 0.20 m due to secondary compression would be expected at the top of the tunnel and almost no additional settlement of the deep sand layer, assuming that half of the 9.8 m diameter tunnel is located in the soft layers. Because the bottom of the tunnel is located in very dense sand, the bottom of the tunnel will not follow the vertical deformation of the soft layers. The consequence is a high load at the top of the tunnel and/or large deformation of the tubes.

Removal of the soft layers would be a better solution. However, if all soft layers would be removed and replaced by sand, flooding of the polder would

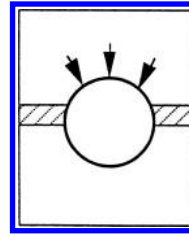


Figure 8. Tunnel in soil, liable to settlement.

occur, because the piezometric head in the deep sand is higher than ground surface. Therefore approximately 1 m of soft, impermeable layers will have to remain. The solution, in which all soft layers except for the deepest 1 m are removed and a preload during 1 year is applied, still leads to a differential settlement between the soil at the top of the tunnel and the dense sand of approximately 30 mm.

Due to the differential settlement between the soil at the top of the tunnel and the dense sand, additional vertical effective stresses are generated at the top of the tubes (see Figure 8). If the tunnel would be infinitely stiff, the total effective stress on top the tubes can be larger than the neutral soil loads, due to arching. A fair estimation of the additional deformation of 30 mm by the modulus of subgrade reaction determined for a situation with a sand fill overlying the tunnel. The calculated additional stress corresponds with the stresses obtained from Leonhardt's method (ATV, 1978), applied for dimensioning of pipelines in soil which is liable to settlement. The sum of the original vertical effective stress and the additional vertical effective stress due to settlement has to be applied in the bedded beam calculation. Due to ovalisation of the tubes, calculated with the bedded beam model, the loads at the top of the tunnel may reduce.

5 CONCLUSIONS

Some remarks were placed on the bedded beam model, based on experiences obtained from results of finite element calculations. The results show that the buoyancy force may be important for the design of the lining. Also, neglecting the subgrade reaction at the top 90 degrees of the tubes is not always conservative. Various calculations show that the modulus of subgrade reaction may be significantly lower than according to the bedded beam formulae. It is concluded that the performance of finite element calculations for normative situations is recommendable in order to determine the modulus of subgrade reaction and to investigate complex phenomena.

REFERENCES

Ahrens, H., Lindner, E., Lux, K-H.

Zur Dimensionierung von Tunnelausbauten nach den
“Empfehlungen zur Berechnung von Tunneln im Lock-
ergestein (1980)”, Die Bautechnik, 1982

ATV-Regelwerk

Richtlinie für die statische Berechnung von
Entwässerungskanälen und -leitungen, 1978

Duddeck, H.

Empfehlungen zur berechnung von Tunneln in Lock-
ergestein (German), Die Bautechnik, 1980

Erdmann, J., Duddeck, H.

Statik der Tunnel im Lockergestein – Vergleich der
Berechnungsmodelle (German), Bauingenieur, 1983

ITA

Guidelines for the Design of Tunnels.

3D analysis of soft soil tunnelling

Analyse tri-dimensionnelle du tunnelage en sols tendres

Suzanne J.M. van Eekelen & Peter van den Berg

Delft Geotechnics, Delft, The Netherlands

Klaas-Jan Bakker

RWS-Bouwdienst, Utrecht and Delft University of Technology, Delft, The Netherlands

Fred Jonker

CUR, Gouda, The Netherlands

ABSTRACT: The Egg-Cam clay model is based on the Modified Cam clay model. With this model it is possible to control the K_0 -prediction for one-dimensional compression. The Egg-Cam clay model is used for the analysis of a tunnelling problem. The influence of the slurry pressure on the stability of the tunnel face and the deformations in the surroundings of the tunnel were the main subjects of study.

RESUME: Le model Egg-Cam clay a été developé du Modified Cam clay model. Avec ce model il est possible de controller la prediction K_0 pour la teste de compression dans une dimension. Le model Egg-Cam clay est utilisé pour l'analyse du probleme de tunnelage. L' influence du slurry pressure sur le stabilité du front du tunnel et les deformations autour du tunnel sont été les sujets principaux de l'etude.7

1 INTRODUCTION

In the crowded western part of the Netherlands, it is important to have a good insight in the influence of tunnelling on the surroundings. The existing 2D finite elements models are not sufficiently equipped to model this typical 3D problem. Especially the effects around the tunnel face are purely 3 dimensional.

A research program has been carried out with the purpose to develop complete 3D models which are specifically suitable for the analysis of soil-structure problems in general and tunnelling problems in particular. Within this study, (3D) constitutive models have been defined and implemented in the finite element program DIANA. One of these models is the Egg-Cam clay model, which is a moderated version of the Modified Cam clay model.

This model will be described in the first part of this paper. In the second part of the paper this model will be used for the analysis of a tunnelling problem. The influence of the slurry pressure on the stability of the tunnel face and the deformations in the surroundings of the tunnel were the main subjects of study. Sandy layers have been modelled with the Mohr-Coulomb model, and clay and silt layers have been modelled with the Egg-Cam clay model.

2 THE EGG-CAM CLAY MODEL

The advanced constitutive model for clay is based on the Modified Cam clay model. For a description of this model the reader is referred to Roscoe and Burland (1968), Britto and Gunn (1987) and Muir Wood (1990). The Modified Cam clay model gives, at service load, good predictions of deformations, not only under compression, but also under shear. However, the stresses are not always described properly. Under one-dimensional compression the horizontal stresses (and thus the $K_0 = \sigma'_h / \sigma'_v$) are too high. With the Egg-Cam clay model it is possible to control the predicted K_0 -value for one-dimensional compression.

The difference between the Modified Cam clay model and the Egg-Cam clay model is the shape of the yield locus. The yield locus of the Modified Cam clay model is an ellipse, while the yield locus of the Egg-Cam clay model consists of two half ellipses, see [Figure 1](#). To be precise, the yield function of the Modified Cam clay model is cut on the top into two pieces. The right part is replaced by another half ellipse with a horizontal axis of variable length. At the top of the two ellipses, where they touch each other, the tangent of both ellipses is horizontal. The left part of the yield locus remains the same as in the Modified Cam clay

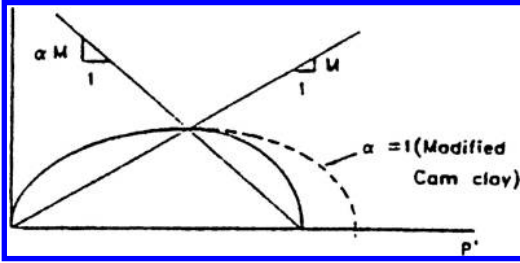


Figure 1. The Delft Egg model.

model. The parameter which defines the shape of that part is $M = (6\sin \varphi)/(3 - \sin \varphi)$. To define the shape of the right side of the ellipse, a new parameter is introduced: α .

The Modified Cam clay model is still a special case of the Egg-Cam clay model ($\alpha = 1$). Later we will see that this parameter α is not a new material parameter which has to be determined. If we assume some value for K_0 , or for example a relationship between φ and K_0 , α turns out to be dependent on a few other Modified Cam clay parameters. The yield function of the Egg-Cam clay model is:

$$f_{egg} = q^2 - M^2 \left[\alpha^2 p' \left(\frac{2\alpha}{\alpha+1} p'_{c,egg} - p' \right) - \frac{\alpha^2(\alpha-1)}{\alpha+1} p'_{c,egg} \right]^2 = 0 \quad (1)$$

where

$$\begin{aligned} p' &\leq \frac{\alpha}{\alpha+1} p'_{c,egg} - \alpha = 1 \text{ (Mod. Cam clay)} \\ p' &> \frac{\alpha}{\alpha+1} p'_{c,egg} - \alpha > 1 \text{ and } p'_{c,egg} = \frac{\alpha+1}{2\alpha} p'_{c,mcc} \end{aligned} \quad (2)$$

2.1 One-dimensional compression, the parameter α

Suppose a one-dimensional compression test (oedometer test). A clay sample is loaded vertically, while horizontal deformations on the boundary of the sample are forced to be zero. The vertical stresses in the sample are defined by the vertical force divided by the surface of the sample. The horizontal stresses in the sample are defined by $K_0 = \sigma'_h/\sigma'_v$. Since the nineteen-forties several researchers have tried to find a relationship between K_0 and the internal friction angle φ . These researchers have carried out many experiments, the results of which were collected by Kumbhojkar et al. (1993) and drawn in Figure 2. It is clear that Jaki's formula $K_0 = 1 - \sin \varphi$ (Jaki, 1944) is a good fit through these experimental data.

When a one-dimensional compression test is simulated with the Modified Cam clay model, vertical stresses are prescribed, and horizontal stresses are calculated K_0 can be determined. The K_0 -prediction of the Modified Cam clay model can be expressed explicitly

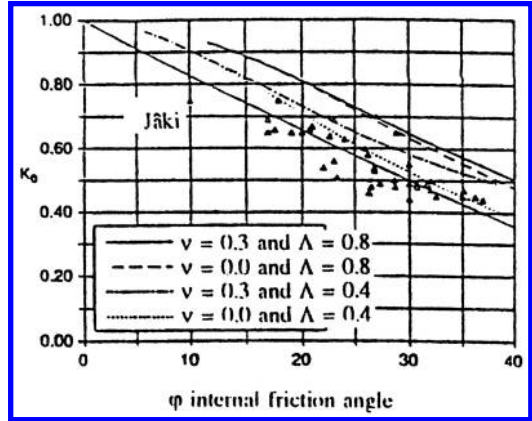


Figure 2. K_0 -predictions of the Modified Cam clay model compared with experimental data for clay.

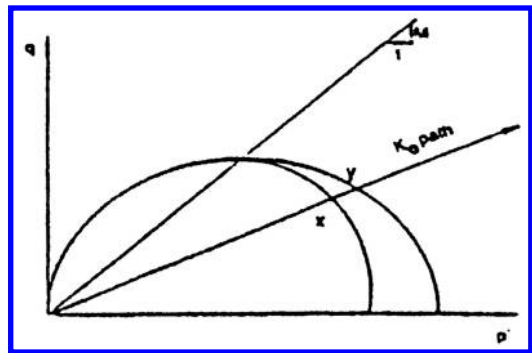


Figure 3. The K_0 -prediction depends on the slope of the yield surface at the intersection with the K_0 -path.

as a function of v , φ and $\Lambda (= (\lambda - \kappa)/\lambda)$ and is drawn in Figure 2. For the lower values of v and Λ the K_0 is better than for the higher values of v and Λ , but in all cases K_0 is too high.

The K_0 -prediction of the Modified Cam clay model depends on the slope of the yield locus at the point that the ellipse is crossed by the K_0 -path. The steeper the ellipse at that point, the lower the K_0 -prediction of the model. Figure 3 shows that the slope of the K_0 -path (point X) is steeper than the slope of the Modified Cam clay model at point Y. So, it can be expected that the K_0 -prediction of the Egg-Cam clay model will be lower than of the Modified Cam clay model. The top line in Figure 4 shows the K_0 -prediction of the Egg-Cam clay model with $\alpha = 1$, which is the same as the Modified Cam clay model. The prediction of the Egg-Cam clay model with $\alpha = 1.9$ lies lower in the figure. This proves that the higher the α , the lower lies the K_0 -line in the figure. If we assume some value for K_0 (for example

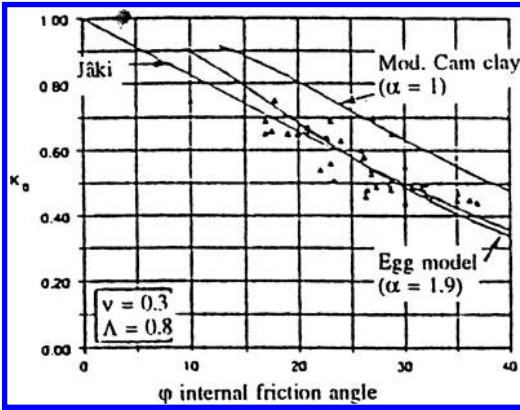


Figure 4. K_0 -predictions of the Egg-Cam clay model.

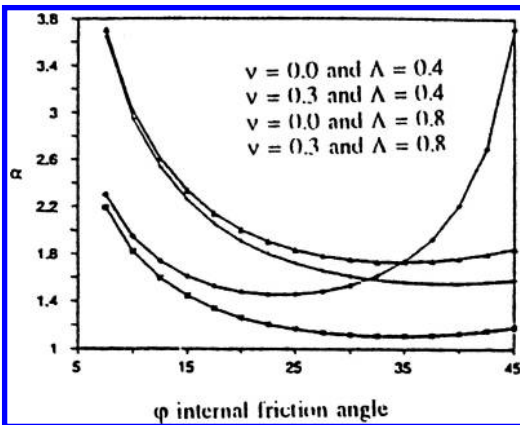


Figure 5. The values for α which have to be used to get the K_0 -predictions $K_0 = 1 - \sin \varphi$.

$K_0 = 1 - \sin \varphi$), we can calculate the factor α from ν , φ , $\Lambda (= (\lambda - \kappa) / \lambda)$ and α (Van Eekelen et al., 1994).

Figure 6 shows experimental data of Graham et al. (1983). From this paper it can be concluded that the Egg yield locus agrees better with the experimental data than the Modified Cam clay ellipse.

2.2 Conclusions

The Egg-Cam clay model is an advanced version of the Modified Cam clay model. An additional parameter α has been introduced to control the K_0 -prediction. This parameter α turns out to be dependent on other conventional material parameters.

3 3D ANALYSIS OF A BORED TUNNEL

This study considers a specific aspect of tunnel boring, using shield tunnelling techniques. For a slurry shield

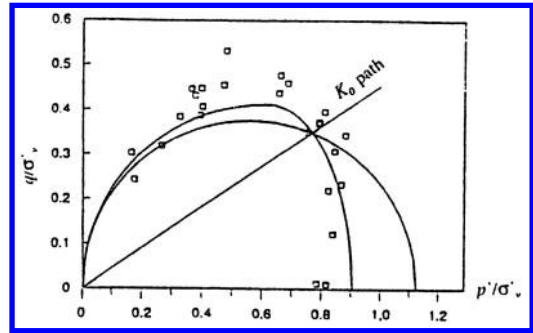


Figure 6. Experimental data of Graham et al. (1983), the Egg, and Modified Cam clay.

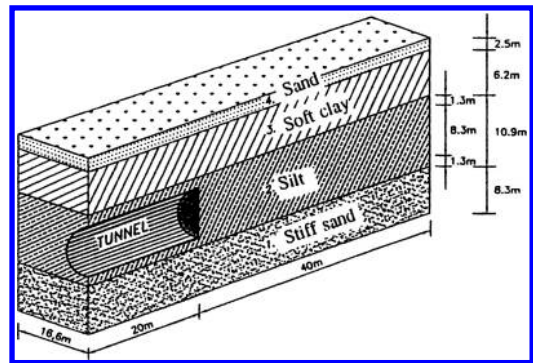


Figure 7. Soil profile.

it is very important to know the relation between the slurry pressure at the front, the stability of the front and the deformations in the surroundings. This typically 3D problem will be modelled 2D and 3D.

Figure 8 gives definitions of several pressures at the tunnel face.

The soil profile is representative for the situation near the Second Heinenoordtunnel, which is being built near Rotterdam in the Netherlands. The soil profile (Figure 7) is modelled by a 3D element mesh with 8 noded cubic elements, and a 2D element mesh with 8 noded quadrilateral elements. This 2D mesh is a longitudinal cross-section of the tunnel. In a plane strain situation it is a long, continuous opening in the soil, with a height equal to the diameter of the tunnel.

The model has four layers. The two sandy layers have been modelled with the Mohr-Coulomb model, and the clay and silt layers, have been modelled with the Egg-Cam clay model. The behaviour of all layers is assumed to be drained. Table 1 gives the material parameters which are used in the calculations.

The results of the calculations have been compared results in which all layers were modelled with the Mohr Coulomb model.

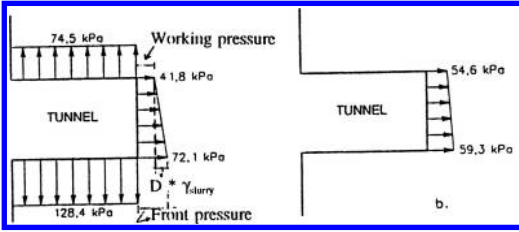


Figure 8. Phase 1 and 2 of the calculations.

Table 1. Material parameters which are used in the calculations.

Parameter	Stiff sand		Soft clay		Sand
	MC	Egg	Egg	MC	
φ	35	26	22.5	30	°
ψ	5			0	°
c	0			0	kPa
E	150			10	MPa
ν	0.3	0.33	0.35	0.32	—
γ_{wet}	21.5	16.5	14		kN/m ³
γ_{dry}				16.5	kN/m ³
n_0		0.61	0.76		—
OCR		1.2	1.3		—
λ		0.036	0.425		—
κ		0.007	0.085		—
α		1.85	1.97		—

The calculations have been carried out in 3 phases:

1. The initial stresses, caused by the soil weight are generated. On the tunnel lining a boundary pressure which is equal to the soil stress is introduced. (see Figure 8a).
2. The (horizontal) pressure against the front is adapted, in order to simulate the slurry pressure on the front. We assume that the pressure in the centre of the tunnel (56.95 kPa) is kept constant and the gradient is defined by $\gamma_{slurry} = 11 \text{ kN/m}^2$ (see Figure 8b).
3. The slurry pressure is
 - a. increased down to active failure
 - b. decreased up to passive failure

3.1 Results

Figure 9 shows the maximum horizontal deformation at the tunnel face as a function of the working pressure. All lines in Figure 9 start at the starting working pressure of 54.64 kPa (which is the end of calculation phase 2). The 8 lines correspond with the 2D and 3D calculations, active and passive failure, calculations in which all layers have been modelled with the Mohr Coulomb model (MC) and calculations in which the two soft layers have been modelled with the Egg-Cam clay model (Egg).

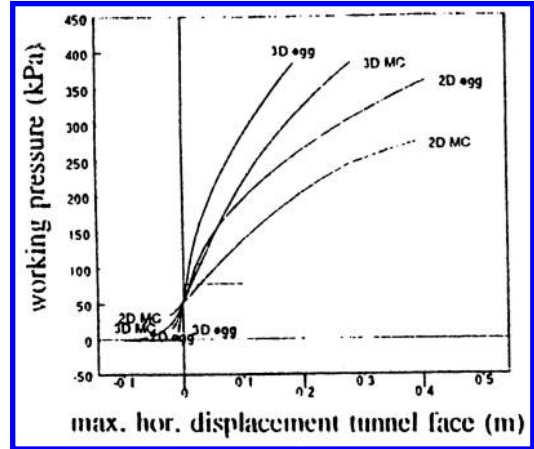


Figure 9. Maximum horizontal deformation tunnel face.

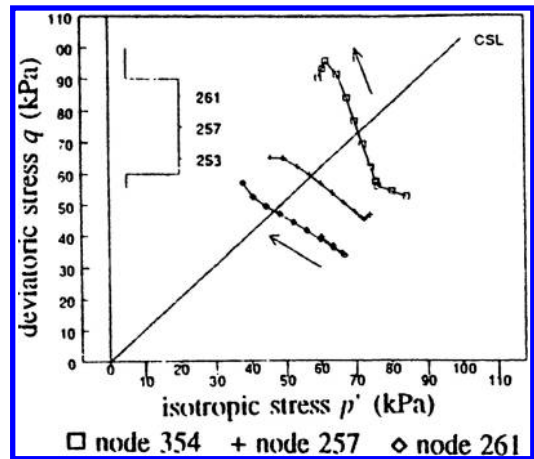


Figure 10. Egg-Cam clay model: stress paths of three modes at the tunnel face during decreasing front pressure.

The deformations during lowering of the front pressure are quite small. Even with a working pressure of the front pressure are quite small. Even with a working pressure of 0.0 kPa, the 3D tunnel face remains stable.

The 3D calculations behave stiffer than the 2D calculations: In the 2D calculation a long, continuous opening in the soil is modelled.

In the right part of Figure 9, the Egg-Cam clay calculations behave stiffer than the Mohr Coulomb calculations due to the stress-dependent stiffness of the Egg-Cam clay model. If the front pressure is increased, the Egg model behaves stiffer than the Mohr Coulomb model.

The left part of Figure 9 shows the same as the right part: the Egg model behaves stiffer as the Mohr Coulomb model. Figure 10 and Figure 11 give an explanation. The figures show the stress paths of three

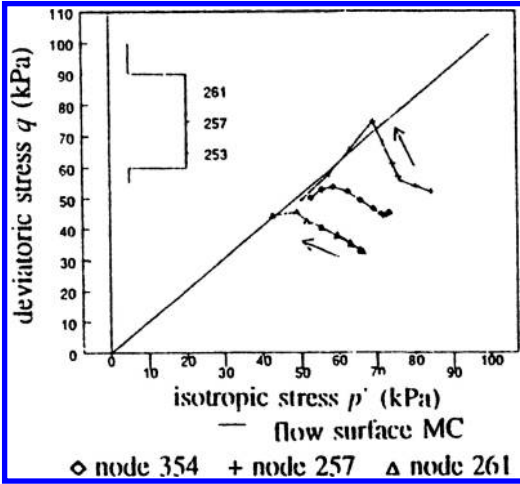


Figure 11. Mohr Coulomb model: stress paths of three nodes on the tunnel face during decreasing front pressure.

nodes at the tunnel face during lowering the front pressure. During this phase, the horizontal stress σ_h decreases, while the vertical stress σ_v remains more or less the same, thus $q = \sigma_v - \sigma_h$ increases, while $p' = (\sigma_v + 2\sigma_h)/3$ decreases.

Both figures give the same diagonal: for the Mohr Coulomb model this is the yield locus, which can not be crossed by a stress path. As soon as the stress path reaches the yield locus, the behaviour is perfectly plastic and consequently, less stiff.

For the Egg model the diagonal is the Critical State line (CSL). Now, the stress paths can intersect this line, as long as the stress state falls within the ellipse. During this phase, the Mohr Coulomb model already behaves plastic and less stiff. When the stress path reaches the yield locus (the Egg), softening occurs. The calculations have not been carried out far enough to see major softening. Only local softening occurs (node 253). In the calculations the interface between tunnel and soil is taken smooth. Figure 12 shows that the deformations in front of the tunnel face cause too much circular movement above the tunnel lining. For future analysis it is recommended to introduce a good tunnel-soil interface model.

Figure 12 also shows that the deformations at the tunnel face are considerably larger than the deformation at ground level. In the 3D calculations this difference is even larger.

Figure 13 and Figure 14 give the deformations at the tunnel face for the 3D calculations. The results show that the maximum deformations at the tunnel face for the 2D calculations are 1.7 to 2.4 times larger than for the 3D calculations (Figure 15).

Figure 16 compares the maximum ground level settlement calculated by the 2D and the 3D model.

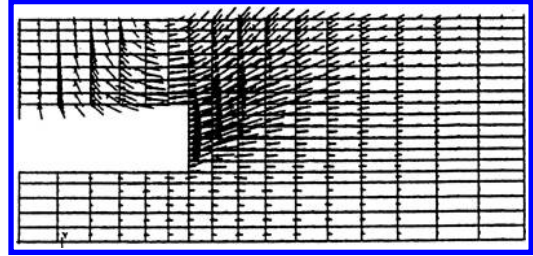


Figure 12. Deformation pattern under working pressure 15.64 kPa.

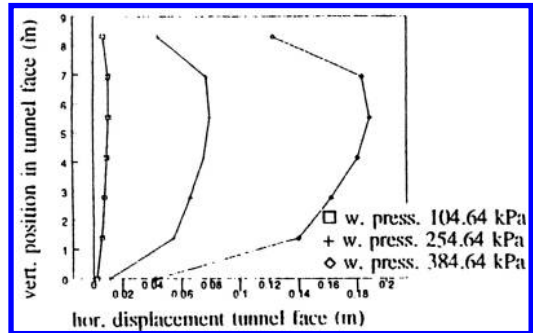


Figure 13. Deformation tunnel face during increasing the front pressure (3D).

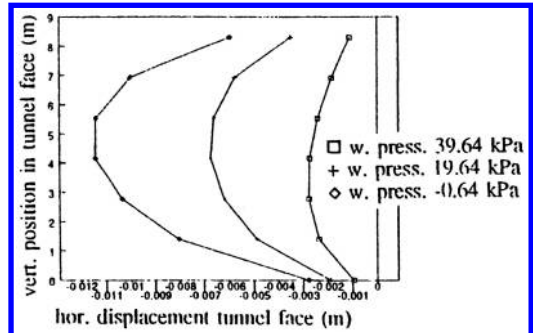


Figure 14. Deformations tunnel face during decreasing front pressure (3D).

The difference between the 2D and 3D calculations is, for realistic pressures, between a factor 5 and 8.

Figure 17 and Figure 18 show the deformations at ground level straight above and parallel to the tunnel. The deformations at the left part of the figures, straight above the tunnel, are very large. This is mainly caused by the smooth tunnel-soil interface. The deformations at the right part of the figures are more realistic. The maximum settlement is found at a distance from the tunnel face of about one to one and a half times the tunnel diameter.

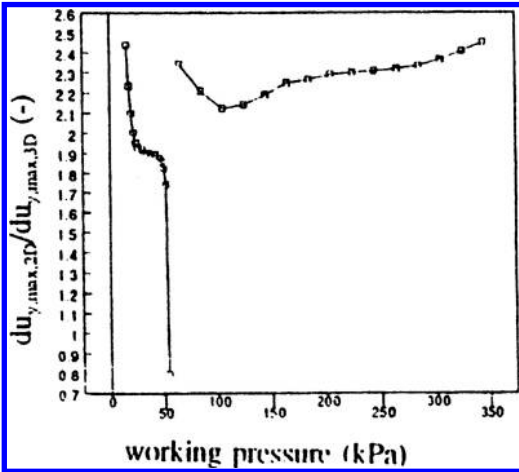


Figure 15. Relation between 2D and 3D calculation: comparison between maximum deformations of the tunnel face (2D/3D).

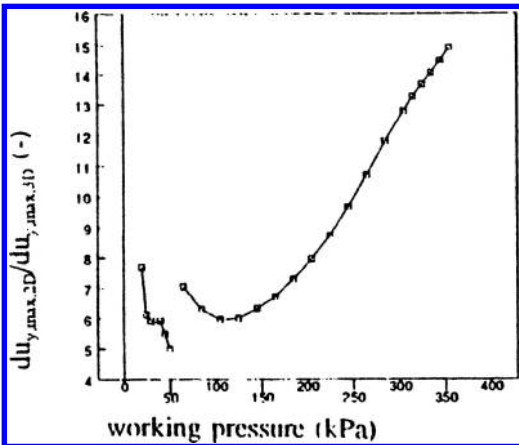


Figure 16. Relation between 2D and 3D calculation: comparison between maximum deformations at ground level (2D/3D).

3.2 Conclusions

The differences between the results of the Mohr Coulomb model and the Egg-Cam clay model are mainly caused by the stress dependent stiffness of the Egg-Cam clay model.

The deformations which are found during decreasing the front pressure are quite small. For the specific soil profile analyzed, even with a working pressure of zero, the tunnel face remains stable.

It is not possible to find a constant factor for the difference between 2D and 3D tunnel calculations. The factors found in this study differ between about 2 and 8.

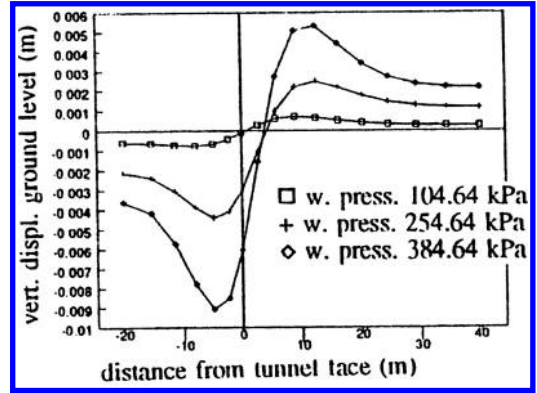


Figure 17. Deformation at ground level, straight above and parallel to the tunnel, increasing front pressure (3D).

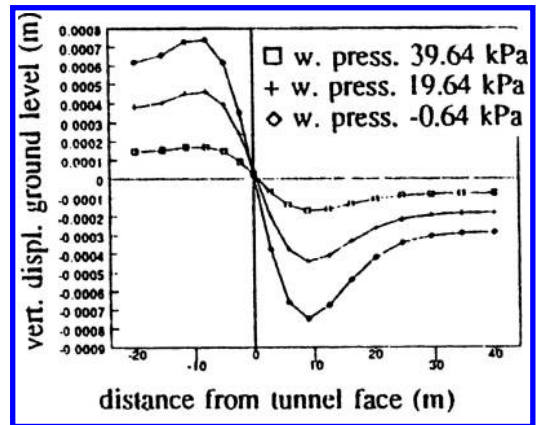


Figure 18. Deformation at ground level, straight above and parallel to the tunnel, decreasing front pressure (3D).

For the analysis of the front stability the 2D analysis gives a more conservative value for the ultimate working pressure (and a such a save estimate). Whereas, the 3D analysis gives a more realistic prediction of the deformations.

4 NOTATION

- E Young's modulus
- f yield locus
- K_0 σ'_h/σ'_v
- M Shape factor for Cam clay ellipse/slope of the critical state line
- OCR overconsolidation ratio
- p' $\frac{1}{3}(\sigma'_{xx} + \sigma'_{yy} + \sigma'_{zz})$ effective isotropic stress, axial symmetry: $p' = \frac{1}{3}(\sigma'_a + 2\sigma'_r)$
- p'_c isotropic preconsolidation stress

- q deviatoric stress:

$$q = \sqrt{\frac{1}{2}(\sigma'_{yy} - \sigma'_{zz})^2 + \frac{1}{2}(\sigma'_{xx} - \sigma'_{zz})^2 + \frac{1}{2}(\sigma'_{xx} - \sigma'_{yy})^2 + 3(\tau'_{xy}{}^2 + \tau'_{yz}{}^2 + \tau'_{zx}{}^2)}$$
axial symmetry: $q = \sigma'_a - \sigma'_r$
- α shape parameter of the Egg-Cam clay model, which defines the shape of the right side of the yield surface
- γ unit weight of soil
- κ swelling index (defines the slope of the swelling line)
- λ compression index (defines the slope of the line which gives the relationship between $\ln p'$ and v for a virgin compression test)
- ν Poisson's ratio
- σ stress
- φ internal friction angle
- subscripts:
 v vertical
 h horizontal

ACKNOWLEDGEMENTS

The work presented in this paper is financially supported by the Dutch Centre for Civil Engineering Research and Codes. This support and the fruitful

discussions with members of the committee C94 are gratefully acknowledged.

REFERENCES

- Britto, A.M. and Gunn, M.J. (1987). Critical state soil mechanics via finite elements. *Ellis Horwood Series in Civil Engineering*
- van Eekelen, Suzanne, J.M., van den Berg, Peter (1994b). The Delft Egg model, a constitutive model for clay. *Proceedings of the First International DIANA Conference on Computational Mechanics, to be held October 24–25, 1994, Delft, The Netherlands*
- Jáki, J. (1944). A nyugalmi nyomás tényezője, ('The coefficient of earth pressure at rest') *Magyar Mérnök és Építész-Egylet Közlönye (J. of the Union of Hungarian Engineers and Architects)*, 355–8
- Kumbhojkar, Arvind S. and Banerjee, Prasanta K., (1993). An anisotropic hardening rule for saturated clays. *International Journal of Plasticity*, Vol. 9 861–888
- Roscoe, K.H., and Burland, J.B. (1968). On the generalised stress-strain behaviour of 'wet' clay, *J. Heyman and F.A. Leckie (eds.), Engineering plasticity (Cambridge: Cambridge University Press)*. 535–609
- Wood, David Muir, (1990). Soil Behaviour and Critical State Soil Mechanics. *Cambridge University Press* 1990

Three dimensional numerical simulation of tunnelling

J.A.M. Teunissen & J. Brinkman

GeoDelft, Delft, The Netherlands

P.S. Jovanovic

Project Organization High Speed Line, Project Office North Holland, (Holland Railconsult), The Netherlands

ABSTRACT: In this paper a novel approach is followed to model the boring process by a convection analysis. In this simulation the tunnel is fixed and the soil moves in axial direction in the direction of the tunnel. The advantage of such an approach is that stress history of the soil is followed and it gives marked improvement to the existing calculation methods in performance. The method is used to simulate the boring of the 14.5 m High-Speed Line (HSL) Green Heart tunnel in Holland.

1 INTRODUCTION

For the design of the tunnel lining for the High-Speed Line (HSL) tunnel a three dimensional finite element model has been developed to simulate the stresses in the lining [Leendertse 2001]. From practical experience follows that the assembling stage is the most critical phase in the construction process. However, due to the inability to take into account all aspects that play a role in the complex situation that exists during tunnel driving and segment erection, many tunnel designers only consider the service-ability stage ('final situation') and try to minimize the effects of (unknown) assembling stresses by optimizing lining design and execution procedures. Although minimizing assembling stresses is an essential thing to do, thinking unintended stresses can be eliminated this way is an illusion. It would be very useful if one could predict these stresses, so the tunnel lining could be designed to resist them. In order to overcome these kind of problems Project Organization High Speed Line South developed a three dimensional FEM model for the lining in which typical assembling is involved.

In this model the soil has been modelled with independent linear elastic springs. The characteristics of these springs have been determined on a plane strain deformation situation based on a horizontal ovalization of the lining. This approach entails a number of limitations because the boring of the tunnel is an essential three dimensional problem with effects of frontstability, overcutting, the conical shape of the shield, the grouting at the tail end, the shear force

between the soil and the shield, the change of the constitutive properties of the grout in time and the uplift of the shield and the tunnel due to the water pressure (Archimedes). In order to estimate the magnitude of these effects a three-dimensional model has been developed that is focussed on the soil behavior. This three-dimensional simulation is performed to give accurate predictions of the stresses, ground surface displacements and the soil deformations. The results of this 'soil' calculation can be compared with the 3D detailed lining calculation. So the effect of the simplification of the soil to springs can be quantified. Further these calculations serve as a model for the interpretation of the monitoring data.

The three dimensional numerical model is set up to model the boring process by a steady state analysis. In this simulation the tunnel is fixed and the soil moves in axial direction in the direction of the tunnel and the TBM face. The advantage of such an approach is that stress history of the soil is followed. Distinction should be made between large displacements and large deformations. The modelling of bored tunnels is a problem with small deformations and progressive process of soil removal and building. A small deformation approach with convective terms for such problems is more than sufficient. It is an alternative to simulations of progressive building stages. This kind of simulations requires complex input data and considerable more computational effort.

In this paper the first results of the calculations based on the small deformation approach with convective terms will be presented. The simulations

involve a mesh of in total 25298 nodes and 22768 elements. The calculations are based on the design properties.

2 PROBLEM DESCRIPTION

The boring of the tunnel is simulated at a point where the center of the tunnel is placed at NAP -27.8 m and the ground surface level on NAP -1.2 m. This section is considered to be representative for the tunnel boring of the Green Heart Tunnel. The cover on the tunnel is 19.35 m and consists of soil partly clay (10.8 m) and partly sands (7.35 m). The tunnel and the lining are considered to be horizontal. The layers of the soil are taken horizontal.

The boring of the tunnel will be simulated in several stages. This includes the loading scheme for the TBM and the construction of the lining. The TBM and the building constructions for the lining are shown in figure 1.

The simulation does not only include the static analysis but it is aimed to model the progress of the

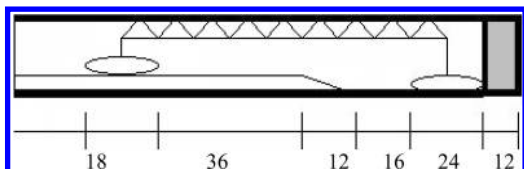


Figure 1. TBM and the lining with the building constructions.

tunnelling process by moving the soil towards the tunnel. This is realized by moving the stresses and the other integration point data stepwise towards the TBM. The size is linked to the elemensize in the longitudinal direction of the tunnel. The (element) size is 2.0 m for this problem.

3 GEOMETRY

Section km 28.000 of the HSL is the starting point for the calculations. The tunnel is modelled by a mesh of a length of 152 m, a width of 50 m and a depth from NAP -1.20 m to NAP -70 m. In front of the tunnel is a length of 34 m.

The TBM and lining is modelled for a length of 118 m. This model involves the complete construction of the lining as shown in figure 1. The mesh with used groups is shown in figure 2. The length of the TBM is

Table 1. Definition of the different groups.

1	Clay (code 12) top at -1.2 m NAP
2	Clay (code 6) top at -6.0 m NAP
3	Sand (code 22) top at -12.0 m NAP
4	Sand (code 34) top at -25.0 m NAP
5	Sand (code 38) top at -36.0 m NAP up to the bottom of -70.0 m NAP
6	Soil element next to the TBM
7	Grout in the liquid area
8	Stiff grout next to the lining behind the liquid area
9	Shell elements describing the TBM
10	Shell elements describing the lining

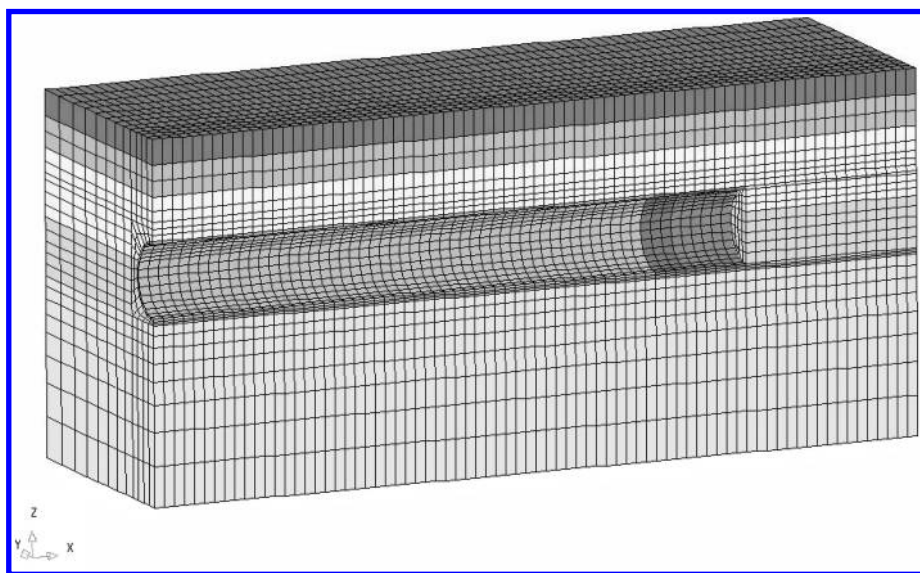


Figure 2. Used finite element mesh.

12.0 m. The TBM and the lining have been modelled with 4-noded shell elements.

The soil is modelled with 8 noded volume elements with a constant volume (B-bar method) [Hughes 1987]. The shell elements are 4-noded Mindlin-Reissner elements integrated with reduced transverse shear terms [Hughes 1987].

4 MATERIAL PARAMETER

4.1 Soil parameters

The material parameters are based on a somewhat simplified soil profile. Not all layers [Brinkman 1998] are taken into account in the finite element calculation. The material parameters for loading have been used, except for layer 38. The first two layers represent clay in the Holocene. The other layers represent the Pleistocene. The volume elements have been used with a simple Mohr-Coulomb material model. This constitutive model should be improved for capturing unloading and reloading behavior of the soil.

The groundwater level is -1.85 m NAP. The potential in the sand is -2.25 m NAP. The small difference in the potential for the sand has not been included in the calculations.

4.2 Grout

At the moment of this numerical analysis the type of grout and the number of injection points to be used was not known. The characteristics of the grouting process of the first tube of the Botlek tunnel project have been used.

The grout is injected directly behind the TBM. Over a length of 6.0 m the grout is in a (semi-) liquid state. The thickness of the grout layer is 0.185 m. The grout is injected in 6 active points (located at 2, 4, 6, 8, 10 and 12 hour). Grout is injected with a certain pressure between the lining and the soil. At first the grout is liquid and later grout becomes stiff. The grout in the calculation is of the same type as Botlek grout type 1.

Over the 6 m where the grout is (semi-) liquid the grout pressure on the soil and on the lining is modelled by prescribed pressures acting on both sides of the layer of elements modelling the grout. The grout pressure at the top at 6 m behind the TBM was for this first analysis taken identical to the vertical soil pressure. The detailed grout pressure distribution around the lining for the 6 m of (semi-) liquid grout was calculated in a separate HSL research program [Talmon 2001]. In this research program a 2-dimensional numerical flow analysis was performed. In this approach the rheological properties of the grout are modelled by a one-phase viscoplastic Bingham fluid. The rheological properties are a function of the time since injection.

The Young's modulus of liquid grout is taken a factor 1000 lower of solid grout.

4.3 Shell parameters

The lining and the TBM are modelled with shell elements, which are connected directly with each other. This is a limitation in respect to the 3D-lining model.

The diameter of the lining is 13.9 m. The thickness of the lining is 0.60 m. The Young's modulus is 13×10^6 kPa. This value is based on the effect the segments have on the global stiffness and follows from the long-term stiffness of concrete of 21×10^6 kPa reduced with a factor 0.65 for the segments. The Poisson ratio is 0.2. The mass density of the concrete is 24 kN/m^3 .

The TBM is modelled with shell elements with the same diameter as the lining. The 10 mm overcut and the 10 mm difference in radius between the front and the back of the TBM, have not been included in these calculations. The length of the TBM in the simulation is 12.0 m. For the TBM the stiffness and the thickness of the shell have been increased. The weight of the TBM is 18953 kN. The centre of gravity is 4.4 m behind the front of the TBM.

5 METHODS OF CALCULATION

There are several methods to calculate the boring process of tunnels. These methods are:

- the construction stage by stage of the tunnel in the Finite Element simulations
- Arbitrary Lagrangian and Eulerian (ALE) approach
- a Finite Element approach with convection.

Modelling the bored tunnel in a stepwise construction is possible in two different approaches. In the first approach the progression of the boring is omitted. The different loading conditions are applied on the TBM and the lining. This is the oldest and the most simple approach to solve the problem. In such an approach the progression of the boring process is not included. This is done in the second approach. In such an approach the loading conditions move forward for each new ring of elements in the lining. This requires a complex input for the Finite Element program.

The ALE approach comes forward from structural engineering. This is used to study for instance the behaviour of metal forming processes. A possible way of using these programs is by an Eulerian approach. In this spatial calculation mode the material moves through the mesh. These methods are generally intended for large deformations and large displacements. The boring of a tunnel is a small deformation problem (except for the flow of the grout). The strains in the soil remain small. So this method although applicable for this kind of problems has more capabilities than needed.

The Finite Element approach with convection is a semi Eulerian approach in a small deformation

context. In this approach the material moves through the mesh i.e. the displacements and all data related to the material such as the stresses. The convection can be related to the displacements found in the analysis and thus the direction of the convection is not fixed. The direction of the convection can also be prescribed. This approach has been followed in this study. Along the direction of convection the displacement and the stresses can be convected stepwise by element or more gradual by interpolation. The stepwise convection has been used in this study. This approach has resemblance to the stage construction of the tunnel but it is for computational point of view more straightforward.

6 SIMULATION SCHEME

The calculation is built up in several stages up to simulate the boring of the tunnel.

In the 1st stage the weight of the soil is applied. This is done without generating displacements.

In the 2nd stage the lining is given its stiffness and the weight of soil in the lining is replaced by the weight of the lining. The soil gets the proper stiffness. The front pressure is applied. The pressure at the top is 331 kPa (based on total pressure) and the gradient is 12.0 kN/m³ for each meter. It is based on the waterpressure with an additional 150 kPa at the top of the TBM.

In the 3rd stage the resulting pore pressure (Archimedes) is applied on the lining and the TBM.

In the 4th stage the shell elements of the TBM are made stiff and the weight of the TBM is applied. Also the reactions of the front pressure are put on the TBM.

The TBM and lining is modelled for a length of 118 m. This model involves the complete construction of the lining as shown in figure 1. The mesh with used groups is shown in figure 2. The length of the TBM is 12.0 m. The TBM and the lining have been modelled with 4-noded shell elements.

In the 5th stage the weights of the building constructions in the lining are applied these are the two wheel sets of the TBM train and the ballast construction in the tunnel.

The lining is loaded from 52.0 m after the TBM with 348 kN/m' ballast. From 40.0 m to 52.0 m after the TBM a linear transition exists from zero loading to ballast loading. The stiffness of ballast construction is not included in the simulation. The total load on the first set of wheels is 8501 kN. The width of the rails is 6.2 m over a length of 24.0 m.

The total load on the second set of wheels is 5372 kN. This is applied on the lining distributed in length over 18.0 m and over the same width as the ballast construction on the lining.

In the 6th stage the pressure of the grout is applied. This pressure is acting in radial direction on both the soil and the lining.

In the 7th stage the convection is applied. This is done in such a way that all the material has moved along the lining.

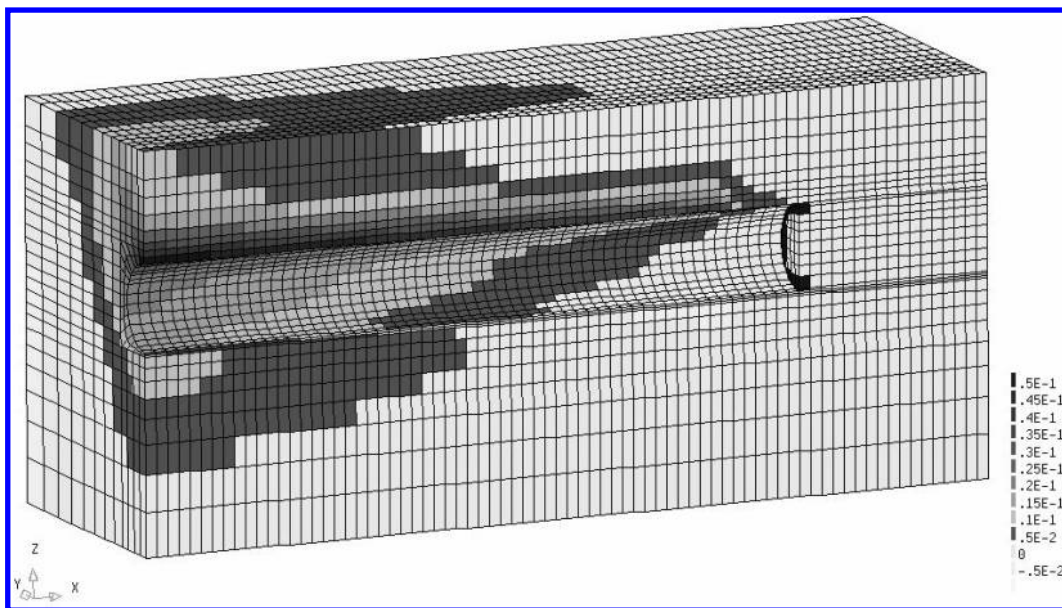


Figure 3. The vertical displacements after convection [m].

The calculations are performed with PLUTO [Teunissen 1991]. In this program special facilities have been build for the convection of stresses and displacements.

In the convection mode the program calculates an equilibrium state given the external forces and the internal stresses. After a step the internal stresses are moved in this case with the stepsize of one element i.e. 2 m towards the TBM. And simultaneously the displacements are moved with 2 m. The displacements of the incoming soil are set to zero. This creates an unbalance with the non-moving external forces that will be corrected in the following step.

7 RESULTS

In the 1st stage the weight of the soil is applied. The stiffness parameters are chosen in such a way that the displacements remain small (less then 0.1 mm). This implies that this situation can be used as Reference State.

In the 2nd stage the lining is given its stiffness and the weight of soil in the lining is replaced by the weight of the lining. The front pressure is applied. The lining is lighter than the surrounding soil and as a result decreases the vertical stress below the lining. The vertical stress distribution near the TBM shows this reduction.

In the 3rd stage the resulting pore pressure is applied on the lining. The tunnel moves upward except at the

TBM. There the soil at the front gives shear resistance to the TBM. As a result the effective stress decreases below the tunnel.

In the 4th stage the shell elements describing the TBM are made stiff and the weight of the TBM is applied. It can be seen that the TBM is moving downward. Far from the TBM the soil is slightly moving upward. The vertical stress below the TBM increases.

In the 5th stage the weights of the building constructions in the lining are applied these are the two wheel sets of the TBM construction train and the ballast-way in the tunnel. The vertical displacements at the end of the tunnel are the significant. The loading of the wheel set near the TBM has only little effect. The ballast in the tunnel has significant more effect then the wheel loading and the weight of the TBM.

In the 6th stage the pressure of grout is put on. The grouting has a considerable local effect on the soil around the tunnel. The pressure is high that the vertical stresses below the tunnel increases. The grout layer itself is pushed aside. The grout volume to push the ground is not controlled. In this case the grout pressure is controlled. Three-dimensional effects limit the area of influence.

There is heave at the surface directly due to the grouting process.

In the 7th stage the convection is applied. This has been done in such a way that all the soil moves along the lining. This plasticity is generated near the liquid grout. There is a development of the plasticity at the

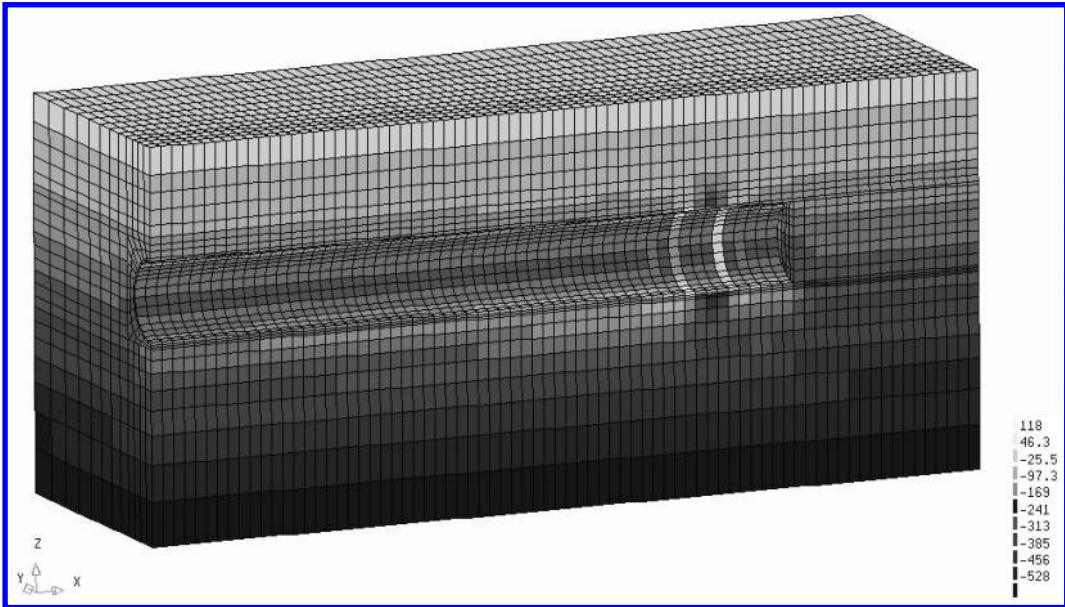


Figure 4. The vertical stress distribution after convection [kPa].

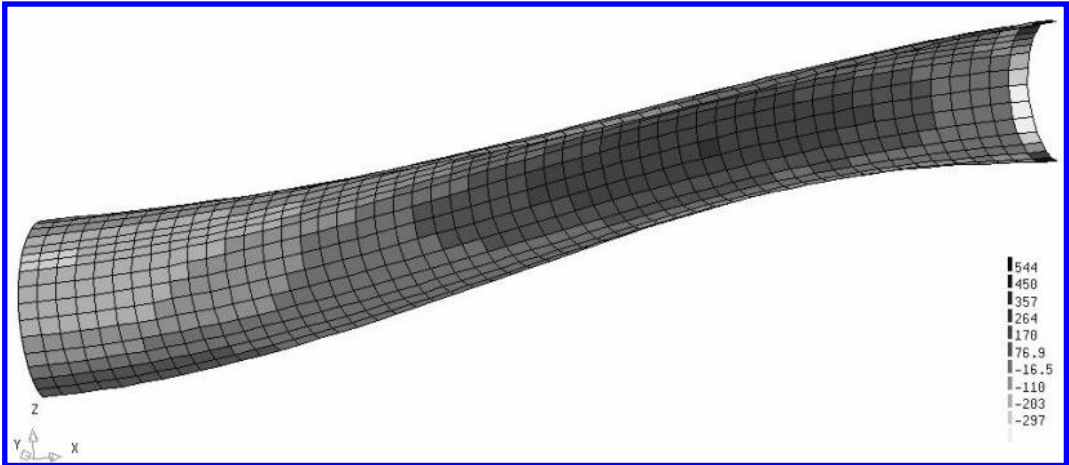


Figure 5. The moments on the radial plane in the lining [kNm].

top and slightly at the bottom of the lining during the convection process. This extends over the whole lining during the convection. This plasticity evolves from the grout pressure. The grout pressure is rather high for this case. The convection leads to tilting of the lining. At the TBM side it is moving up and at the other side it is moving down.

The vertical stress distribution is shown in figure 4. It can be seen that there is an increase of vertical stress near the liquid grout where the grout pressures are put on. Below the lining is a decrease of vertical stress.

The moments on the radial plane of the lining are shown in figure 5. The total length of the modelled lining 106 m. The liquid grout acts on the lining on the first 6 m (i.e. 3 element rings). All the results are presented in a deformed mesh. The lining and the TBM are directly connected with each other this leads to substantial moments near the TBM. The sign of the moments in the tunnel change over the distance of the lining.

The vertical displacements are shown in figure 3. The grouting zone starting 12 m behind the TBM face induces the heave.

At the surface maximum heave of 10 mm is found. This heave is the primary result of the (high) grout pressures used.

The grout pressure leads to uplift of the surface. The maximum rise is not directly above the tunnel but it is slightly away from the centre line. The maximum heave is found more accentuated outside the tunnel axis when the soil moves through the mesh. Above the tunnel the surface comes down. This effect although small creates a different surface trough as the Peck curve [Peck 1969] as can be seen in figure 5.

The convection shows a development of stresses and of plasticity around the lining. This is not found with the simulation of the grouting process only. The grouting process has a considerable impact on the development of the stresses on the lining.

There may be an effect of the boundary conditions on the solution. This is still subject of research. Especially the conditions at the front of the TBM and at the tail end seem somewhat to close and may effect the results. The tail end is important due to the rigidity of the lining. The quality of the solution may increase if the front and tail boundaries are moved away.

REFERENCES

- Brinkman J., 1998. Geotechnical Aspects *High Speed Line Organization Symposium Groene Hart Bored Tunnel Report September 8th 1998*, pp 9–10, Amsterdam
- Hughes T.J.R., 1987. Finite Element Method, *Prentice-Hall International*, Englewood Cliffs, New Jersey
- Leendertse, Jovcanovic & Bakker, 2001. Measures for riskcontrol on ‘Green Heart’ Tunnel. *To be presented on the International IABSE Conference on Safety, Risk and Reliability – Trends in Engineering, Malta 21–23 March 2001*
- Peck R.B., 1969. Deep excavations and tunnelling in soft ground, State of the art report, *Proceedings of the 7th International Conference on Soil Mechanics and Foundation Engineering*, pp 225–290, Mexico 1969
- Talmon A.M., Aanen A., Bezuijen A. & Zon W.H. van der, 2001 Grout pressures around a tunnel lining. *To be presented at IS-Kyoto 2001 30 Oct – 1 Nov 2001*
- Teunissen J.A.M., 1991. Analysis of plasticity and non-coaxiality in geomaterials, *PhD Thesis at the Technical University of Delft*

Simplified three-dimensional numerical modelling of shield tunnel advancement

Modélisation numérique tridimensionnelle simplifiée de l'avancement du tunnelier

A.R. Koelewijn

GeoDelft (formerly Delft University of Technology), Delft, The Netherlands

A. Verruijt

Delft University of Technology, Delft, The Netherlands

ABSTRACT: For shield tunnelling in urban areas with a soft subsoil, reliable prediction tools are indispensable. A three-dimensional finite element model is presented which can be used to simulate phased tunnel advancement using an ordinary computer only. In this planewise model, a significant reduction of the computational requirements is achieved by introducing some restrictions regarding the geometry and the material behaviour. With a comparatively simple input, this model enables a three-dimensional phased analysis of the tunnel boring process with slurry or EPB shields. It has been applied to the Second Heinenoord Tunnel near Rotterdam. Although the magnitude of the surface settlements is overestimated, the shapes of the time-dependent settlement troughs and the relative rate of increase of the settlements are reasonably well calculated in the simulation. For the bending moments and the normal forces in the tunnel lining a reasonable agreement is found between measured and calculated values.

RÉSUMÉ: La construction d'un tunnel foré dans un région urbain demande des techniques d'analyse sûres. Ici un modèle d'éléments finis 3D est présenté, qui permet de déterminer les déplacements et les contraintes dans le sol autour d'un tunnel foré si la géométrie du réseau des éléments soit indépendante du coordonné dans la direction de l'axe du tunnel. La solution des équations numériques se fait par une méthode itérative, d'une couche d'éléments à une autre, d'afin que l'analyse peut être effectué avec ordinateur PC. Le modèle a été utilisé pour l'analyse du second tunnel de Heinenoord. Bien que les déplacements de surface sont un peu surestimés, l'aspect général et le développement des déformations agréent bien avec les mesures réelles. Les forces et les moments dans le matériau du tunnel sont aussi prédits par le modèle avec assez de précision.

1 INTRODUCTION

The importance of shield tunnelling techniques for the construction of underground infrastructure in densely populated areas with a soft subsoil is still growing. Because of the sensitivity of these areas to any disturbance caused by tunnelling activities, there is a clear need for reliable methods to predict the deformations and stress changes in the soil and to determine the forces and bending moments in the tunnel lining.

In the present design practice, for bored tunnels often use is made of two-dimensional finite element analyses, analytical models and relationships based on experience in similar projects. In some cases three-dimensional finite element analyses are carried out. It will be clear that each of these methods has its

drawbacks. In a two-dimensional analysis, for instance the influence of the excavation face and arching effects related to the limited length of the zone behind the shield in which fresh (i.e. unhardened) grout is present cannot be included. Analytical models do not account for heterogeneity of the soil, while empirical formulas can only be applied successfully if enough knowledge has already been gained on projects which are indeed similar. Most three-dimensional finite element analyses of shield tunnelling are still associated with excessively high computational requirements, both in terms of memory and in terms of calculation time. Moreover, with many of the commercially available three-dimensional finite element packages, it appears that erroneous data is quite easily entered by geotechnical experts involved in the design of

bored tunnels, as they are usually familiar only with two-dimensional finite element analyses, which involve less complicated modelling aspects.

At the Delft University of Technology, a simplified three-dimensional finite element model has been developed by which the advancement of a shield in soft soil can be simulated using an ordinary personal computer only (Koelewijn 2001). The input requirements of this new model correspond to the input required for a few number of two-dimensional finite element analyses. Procedures have been developed to enable an automated simulation of the phased construction of a bored tunnel. The model has been applied to a bored tunnelling project near Rotterdam, for which field measurements of surface settlements and bending moments and normal forces in the tunnel lining are compared with calculated values.

2 PLANEWISE 3D FINITE ELEMENT MODEL

From the notion that three-dimensional finite element analyses are practically always carried out using a brick-shaped finite element mesh with equal cross-sections in at least one direction, it has been decided to develop a new three-dimensional finite element model in which this repetition of cross-sections is exploited as much as possible in order to reduce the memory requirements. As a result, three-dimensional problems requiring a rather large number of finite elements, like for instance shield tunnel advancement, can be analysed using equipment commonly available in engineering practice. Meanwhile, the calculation time remains within acceptable limits.

In the model, a three-dimensional finite element mesh is constructed on the basis of a limited number of cross-sections, each with the same division into elements. Corresponding elements in different input sections do not need to be of the same size and shape, as shown in Figure 1. The constructed mesh typically consists of a large number of blocks of finite elements with parallel planes between these blocks. The properties of the volume elements are attributed to the element nodes which are all located in these parallel planes.

Because of the above restrictions regarding the topology of the mesh, all calculation data can be arranged in a planewise manner. Thus the stiffness

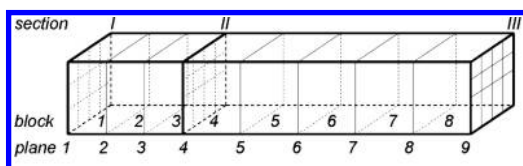


Figure 1. Example mesh with input sections, blocks with elements and calculation planes.

matrix which needs be solved will exhibit the same structure for each plane. In practice, the properties of a large number of parallel planes will be equal to each other. Now by creating and storing data of unique planes only, a significant reduction of the calculation requirements can be achieved in comparison with conventional finite element models where all mesh data is stored after first being created. Although it will help to reduce the storage requirements, the material properties of corresponding elements in different input sections do not need to be equal to each other, nor do the planar coordinates or the boundary conditions of corresponding nodes need to be equal.

For the calculation itself an iterative procedure is adopted, in which the parallel planes are solved one after the other using a sparse direct solver at the level of a plane. Details on the solution method and some basic characteristics of the model regarding memory requirements, calculation times and accuracy of the solution are given in Koelewijn (1999).

For most practical situations, a significant reduction of the calculation time is achieved at the cost of an error of less than one percent due to the iterative solution method. This error can be considered as negligible in comparison with the accuracy of geotechnical parameters usually available during design.

A further reduction of the calculation time can be achieved by adopting the iterative GMRES* scheme (Golub & Van der Vorst 1997) using the planewise iteration scheme as a preconditioner. This requires some more memory, but even then for practical calculations the total amount of memory can be less than with existing iterative solvers, like for instance the Conjugate Gradient method.

In the model, the well-known Mohr-Coulomb model has been implemented to account for soil plasticity. Both drained and undrained material behaviour can be simulated. Consolidation cannot be simulated in the model, because this requires a regular reformulation of the global stiffness matrix and because this would introduce different submatrices for initially equal parallel planes. Thus, the advantages of this new planewise model over a conventional three-dimensional finite element model would be lost. In combination with the rather simple input of mesh data, the model may easily be used by geotechnical engineers familiar with two-dimensional finite element analyses to quickly perform three-dimensional calculations, especially in situations in which parameters required for more advanced soil models are still lacking.

3 MODELLING OF SHIELD TUNNELLING

To facilitate the analysis of shield tunnelling, dedicated procedures have been developed to enable a

more or less automated simulation of shield tunnel advancement. Attention has been focused on the modelling of tunnelling using slurry or earth pressure balanced (EPB) shield types, which are the most common types of machinery used for tunnelling in soft soils below the groundwater table. For a three-dimensional finite element analysis of shield tunnelling, four distinct phases may be discerned, as indicated in Figure 2.

The first phase extends to the excavation face. The soil ahead of the face is mainly influenced by the loading conditions applied at this face. The support pressure applied at the excavation face is modelled by a horizontal pressure which increases in depth.

Behind the excavation face, the soil elements inside the shield are deactivated. The shield itself is modelled as a ring of very stiff elements (with properties of steel) with another ring of elements representing the concrete lining inside. The conical shape of the shield is accounted for by application of a certain amount of contraction to the nodes along the circumference of the shield. This results in a loss of volume around the shield without fixing the tunnel in space.

At the tail of the shield, where in reality grout is injected during shield advancement, the properties of fresh cement grout are assigned to the ring of finite elements which represented the shield in the second phase. The volume of grout material to be injected is simulated using the same procedure as applied to simulate the conical shape of the shield, although at this location usually an expansion will be prescribed. It has been decided to simulate the grouting process by means of a strain-controlled procedure rather than a stress-controlled procedure, because usually the amount of volume to be placed in the shield tail gap is better known than the actual pressure at the grout-soil

interface during injection, especially when the tunnel is yet to be built. Shortly after injection of the grout, the hardening process will start. During hardening a certain amount of shrinkage will take place. This is again modelled by means of the procedure simulating contraction.

After hardening, the tunnel may be considered to be completed. The properties of the 'grout' elements are replaced by those of hardened grout.

The advancement of the shield is simply modelled in a discontinuous manner, by simulating the location of the shield a number of blocks farther in the mesh at each subsequent calculation step. Alternatively, shield advancement may be modelled as a continuous process, as for instance shown by Komiya et al. (1999). However, this requires far more computational power than available on ordinary personal computers. It therefore falls well beyond the scope of application of the planewise three-dimensional finite element model described here.

4 APPLICATION TO THE SECOND HEINENOORD TUNNEL

The second tunnel under the Oude Maas river near Rotterdam has been commissioned by the Dutch government as a bored tunnel in order to obtain experience with shield tunnelling in Dutch soft soil conditions. The tunnel actually consists of two tubes with an external diameter of 8.3 metres and a length of about 950 metres. Boring activities started in January 1997 and were completed in July 1998. The tunnel is situated in strongly heterogeneous soil conditions, as shown in Figure 3. Because of the experimental character of this project, an extensive research program has been set up to predict and monitor various aspects related to the construction of this tunnel, as described by Bakker et al. (1999).

The model has been applied to simulate the first passage of the Northern monitoring area, for which the soil profile and the geotechnical parameters to be used with the Mohr-Coulomb model are given in Table 1. Because of the permeability of each of these soil layers, a fully drained analysis was carried out. All input data has been taken from technical reports prepared for the Dutch Centre for Underground Construction (COB) before the construction of the tunnel started, in order to provide a clear parameter set to be used for all predictions. Further details are given in Koelewijn (2001).

The finite element mesh used in the simulation is shown in Figure 4. It consists of 100 blocks of 920 elements each, i.e. 92,000 elements in total, and covers the full length (75 m) of the Northern monitoring area. As the length of each ring of precast concrete lining

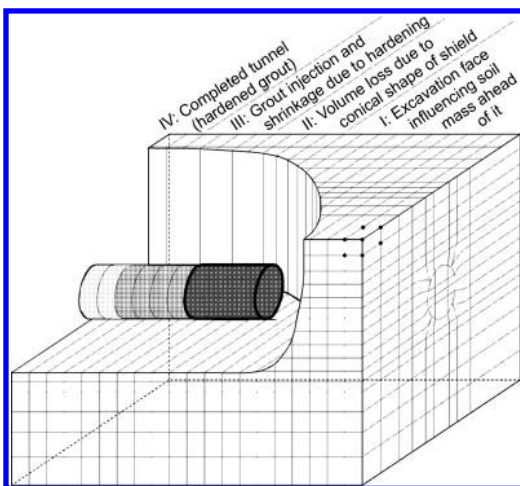


Figure 2. Phases in shield tunnelling.

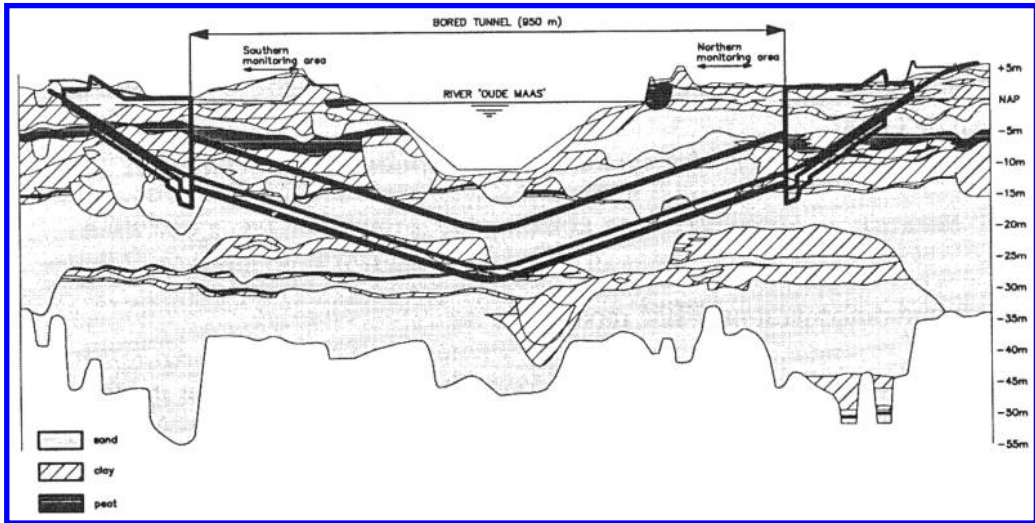


Figure 3. Geotechnical profile of the Second Heinenoord Tunnel in longitudinal direction (from Van Jaarsveld et al. (1999)).

Table 1. Soil profile and geotechnical parameters for the Northern monitoring area.

Layer type	Top of layer (m)	γ_{sat} (kN/m ³)	K_0	G (kPa)	ν	ϕ (°)	c (kPa)
Clay and sand	+2.70	17.2	0.58	1440	0.34	27	3
Sand, locally clay	-1.50	19.5	0.47	7400	0.30	35	0.5
Sand with clay	-5.90	19.0	0.47	7100	0.31	33	0.5
Sand, locally clay	-9.90	20.5	0.45	11,400	0.30	36.5	0.5
Sand, gravel	-17.15	20.5	0.50	17,100	0.30	36.5	0.5
Clay, locally sand	-20.75	20.0	0.55	4500	0.32	31	7
Sand	-25.10	21.0	0.55	22,800	0.30	37.5	0.5
Clay, locally sand	-26.60*	20.0	0.55	4500	0.32	31	7

* The bottom of this layer is at -29.20 m below the reference level.

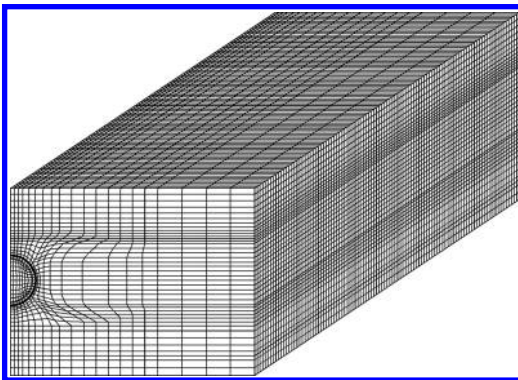


Figure 4. Finite element mesh used to calculate the first passage of the Northern monitoring area.

segments equals 1.50 m, each block of finite elements covers half the length of a lining ring.

For the simulation itself first an initial stress field has been generated by application of gravity loading to the mesh in which the tunnel was not yet present. After gravity loading, all horizontal stresses have been recalculated using the values for the lateral earth pressure coefficient given in Table 1, to account for the slight overconsolidation of the soil layers. Next, shield advancement has been simulated in 22 calculation steps in which the shield has been advanced over 58 blocks (43.5 m). With a simulated shield length of 8.25 m and a grout hardening zone (phase III in Figure 2) of 10.5 m, the completed tunnel length at the end of the simulation comprised 33 blocks (24.75 m).

The calculation has been performed on a personal computer with a Pentium-II processor and 236

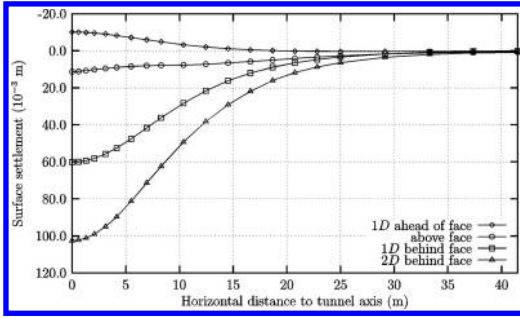


Figure 5. Calculated transverse settlement troughs for several positions of the excavation face.

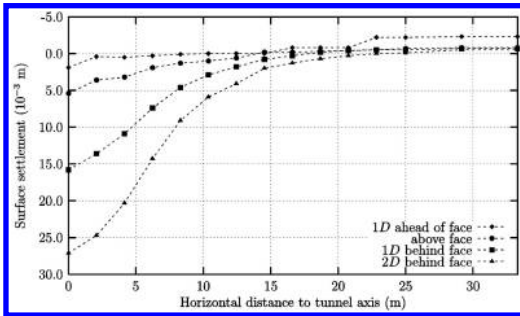


Figure 6. Measured transverse settlement troughs during the first passage of the Northern monitoring area for several positions of the excavation face.

Megabytes of internal memory available. The calculation time was within acceptable limits.

The calculated transverse settlement troughs for several positions of the excavation face are shown in Figure 5. In front of the shield some heave is calculated, but above and behind the excavation face the surface settles. At a distance of two times the outer diameter of the tunnel behind the excavation face, the surface settlements are nearly at their maximum value. The measured transverse settlement troughs for comparable positions of the shield with respect to the line of measurement are shown in Figure 6 (Van Jaarsveld, 1997). The measured maximum surface settlement increased to 32 millimeters after some time. No heave has been measured, but otherwise comparable graphs are found. However, the values of the calculated settlements are roughly four times larger than the measured values. This is likely to be related mainly to the values of the shear modulus used in the calculations, which is related to primary loading, whereas the use of much higher values would have been more appropriate to account for unloading/reloading behaviour at comparatively small strains.

The values of the bending moments and the tangential normal forces in the tunnel lining are much more in

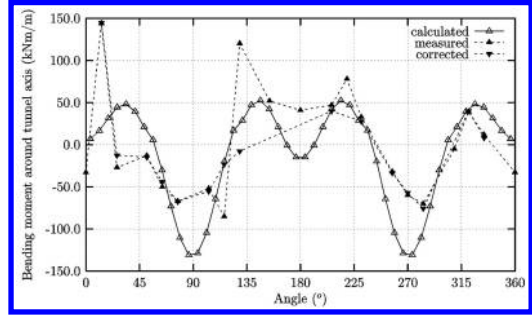


Figure 7. Calculated and measured bending moments in the tunnel lining.

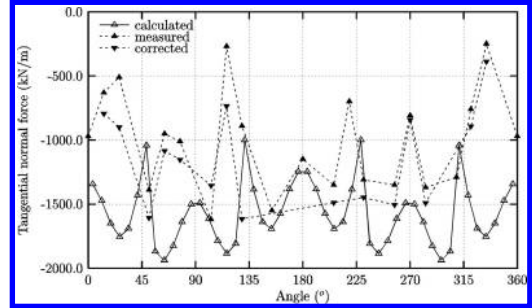


Figure 8. Calculated and measured tangential normal forces in the tunnel lining.

agreement with the measured values, as shown in Figures 7 and 8. In these figures, both the initially reported values as given by Blom and Van Oosterhout (1997) and the values corrected for temperature effects and supposedly erroneous signals as submitted by Bakker (2000) are given.

It is expected that the use of a higher shear modulus for the soil to improve the values calculated for the surface settlements will not have much influence on the values calculated for the bending moments and the normal forces in the lining, as the latter are mainly determined by the weight of the overlaying soil and the properties of the lining itself.

5 CONCLUSIONS

To analyse the influence of shield tunnelling on the soil a three-dimensional analysis of the tunnel boring process is desirable. By introducing some restrictions regarding the geometry and the material behaviour, a significant reduction of the computational requirements may be achieved. This enables a three-dimensional finite element analysis of shield tunnel advancement using an ordinary personal computer. In the planewise three-dimensional finite element model described in this paper, the tunnel boring process using

slurry or EPB shields can be modelled by a limited number of consecutive phases.

The resulting model has been applied to the Second Heineoord Tunnel near Rotterdam. Although the magnitude of the surface settlements is overestimated, the shapes of the time-dependent settlement troughs and the relative rate of increase of the settlements are reasonably well calculated in the simulation. For the bending moments and the normal forces in the tunnel lining a reasonable agreement is found between measured and calculated values.

ACKNOWLEDGEMENT

The research described in this paper has partially been supported by PLAXIS B.V.

REFERENCES

- Bakker, K.J. 2000. Personal communication.
- Bakker, K.J., Boer, F. de & Kuiper, J.C. 1999. Extensive independent research programs on second Heineoord Tunnel and Botlek Rail Tunnel. In F.B.J. Barends, J. Lindenberg, H.J. Luger, L. de Quelerij & A. Verruijt (eds), *Geotechnical Engineering for Transportation Infrastructure, Proc. XIIIth European Symp. on Soil Mechanics and Geotechnical Engineering, Amsterdam, Netherlands, 7–10 June 1999*: 1969–1978. Rotterdam: Balkema.
- Blom, C.B.M. & Van Oosterhout, G.P.C. 1997. Tweede orde evaluatie tunnelconstructie Tweede Heineoordtunnel – Deel 1. Technical Report K100-W-061. Gouda: Centrum Ondergronds Bouwen.
- Golub, G.H. & Vorst, H.A. van der 1997. Closer to the solution: Iterative linear solvers. In I.S. Duff & G.A. Watson (eds), *The state of the art in numerical analysis*: 63–92. Oxford: Clarendon.
- Jaarsveld, E.P. van 1997. Evaluatie geotechnische metingen meetgebied Noord (1e passage). Technical Report K100-W-059. Gouda: Centrum Ondergronds Bouwen.
- Jaarsveld, E.P. van, Plekkenpol, J.W. & Messemackers van de Graaf, C.W. 1999. Ground deformations due to the boring of the Second Heineoord Tunnel. In F.B.J. Barends, J. Lindenberg, H.J. Luger, L. de Quelerij & A. Verruijt (eds), *Geotechnical Engineering for Transportation Infrastructure, Proc. XIIIth European Symp. on Soil Mechanics and Geotechnical Engineering, Amsterdam, Netherlands, 7–10 June 1999*: 153–159. Rotterdam: Balkema.
- Koelwijn, A.R. 1999. Memory-efficient 3D FE-analysis in geomechanics using a planewise model. In G.N. Pande, S. Pietruszczak & H.F. Schweiger (eds), *Numerical Models in Geomechanics – NUMOG VII, Graz, Austria, 1–3 September 1999*: 323–328. Rotterdam: Balkema.
- Koelwijn, A.R. 2001. *Numerical analysis of soft soil tunnelling*, PhD thesis, Delft University of Technology.
- Komiya, K., Soga, K., Akagi, H., Hagiwara, T. & Bolton, M.D. 1999. Finite element modelling of excavation and advancement process of a shield tunnelling machine. *Soils and Foundations* 39(3): 37–52.

Souterrain The Hague: clogging of groundwater wells above a gel layer during construction of an underground tram station

H.J. Luger & E.E. van der Hoek
GeoDelft, Delft, The Netherlands

A.F. van Tol
Delft University of Technology, Rotterdam Public Works, The Netherlands

ABSTRACT: An injected silicate gel-layer (soft-gel) was used to reduce water inflow into the building pit of the Station Spui in the Souterrain in The Hague. Excessive clogging of wells which hindered dewatering is explained by chemical processes originating from the gel-layer. Chemical and mechanical counter-measures are considered. The final testing, design, installation and performance of a successful dewatering system by means of gravel piles are described.

1 INTRODUCTION

The Souterrain in The Hague is divided into “tunnel-parts”, where a cement grout-layer is provided to restrict the inflow of water and stations, where an injected silicate gel-layer is used for the same purpose. Experiences with the cement grout layer are reported in a companion paper (Kruit 2003). This paper deals with Station Spui in the middle part of the tunnel. Station Spui has an area of ca. 4000 m² and a width which varies from 15 to 25 m. Diaphragm walls go down to 28 m depth. The construction of Station Spui consists of two diaphragm walls providing lateral support, a covering roof and internal floors, as shown in Figure 1. Pre-installed vertical anchors ensure stability of the future tunnel floor.

Inflow of water into the building pit is restricted by a silicate gel-layer, at the base of the walls. This gel-layer had been formed by permeation grouting based on a dilute solution of sodium-silicate and sodium-aluminate. Dewatering was planned to take place by means of deep filters with underwater pumps as shown in the middle of Figure 1.

When the construction was delayed for a period of more than two years there was concern about the durability of the gel-layer, which was not intended as a permanent barrier. This concern was amplified when gradually the effectivity of the deep filters declined.

In order to continue dewatering small filter tubes with 2 inch diameter and 3 m filter length were placed along the diaphragm wall at 6 m intervals. The filters were situated both above (Fig. 1, left side) and below (Fig. 1, right side) a peat layer with low permeability.

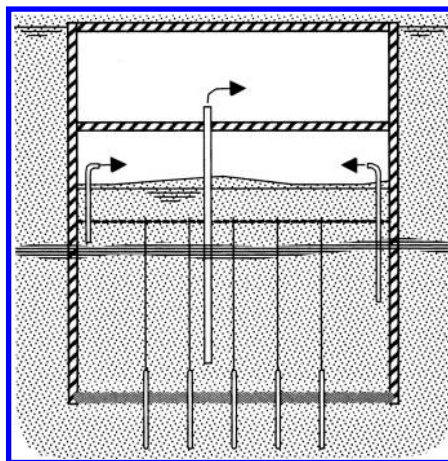


Figure 1. Cross-section of Station Spui during construction.

The small filters along the diaphragm walls proved to be very short lived: while initial yield was good it decreased to practically zero within days. Without the peat layer the solution would be to dewater at the ground surface within the tunnel. However, the low permeability of the peat layer made it necessary to extract the water below the peat layer.

This was due to two phenomena, which would be caused by excess water pressures under the peat:

- instability (uplift) of the peat layer and the overlying sand;

- reduction of the passive resistance of the soil within the building pit, which would lead to over-loading of the diaphragm wall.

It was concluded that clogging of the formation soil around the filters occurred. Because of the length of the construction period which was still to come the short-lived filters would be inadequate to continue and finish the work.

2 INVESTIGATING THE CLOGGING

In order to resolve the construction problems the clogging mechanism was studied. Most common clogging mechanisms are (NOBIS 1998):

- Soil particle migration
- Precipitation of iron (or manganese) oxide
- Growth of biomass.

Mostly the clogging of wells for dewatering building pits or production of drinking water occurs because different water qualities are mixed. Mixing of aerobic (oxygen-rich) water and anaerobic water is known to cause problems (KIWA 2000). The oxygen can cause precipitation of dissolved iron and/or may induce biomass growth. To commence and enable analysis of the process in the tunnel a number of laboratory tests were performed on locally retrieved ground and groundwater samples including:

- Soil permeability tests and sieve analyses.
- Chemical analyses of ground and groundwater.
- Physical (density and viscosity) testing of the groundwater.

The tested soil was taken from below the peat layer between 7.0 and 13.6 m below excavation level, right in the zone where filters experienced clogging. The performed laboratory tests showed the samples to consist of a medium fine to coarse sand. The deepest samples contained some silt. The permeability varied from 7.8×10^{-6} m/s to 1.3×10^{-5} m/s. The groundwater retrieved from the clogged wells showed a remarkable dark color, almost like that of black tea or cola.

The chemical composition the ground and groundwater was comparable with normal sandy soil and groundwater characteristics. Except that high:

- pH (8.9–10.1),
- silicon and sodium concentration and
- dissolved organic carbon (DOC) concentration were found in the groundwater.

These high pH and high silicon and sodium concentrations found in the groundwater are caused by the silicate-gel layer. The viscosity was comparable with normal water 5.5 mPa/s (at 25°C) and a density of 1003 kg/m³.

The above results showed that the usual clogging mechanisms were not present. In the sandy soil particle

migration is not expected to cause clogging in such a short time at such a low flow rate: Clogging due to particle migration occurs generally after a few years of high flow in drinking water wells (KIWA 1984). The iron concentration in the retrieved groundwater remained high, which indicated that no iron precipitation occurred. The composition, viscosity, density and in particular the high pH level of the groundwater do not indicate biomass growth.

Besides these common clogging mechanisms also the influence of bentonite was investigated because bentonite was used in the tunnel construction for the drilling of the anchor rods and the support of the diaphragm wall excavation. A test with methylene blue coloring showed that no bentonite was present in the groundwater taken from the clogged wells.

To study process of clogging further laboratory tests were performed. Comparative tests studying the development of permeability with time were performed with the groundwater of the clogged wells using the soil from the construction site as well as a standard reference sand (Baskarp sand).

The clogging could be simulated using both the groundwater and soil from construction site in two days of testing at a small gradient. Using the standard soil no clogging appeared and the permeability remained 2×10^{-5} m/s. In the laboratory clogged material some electron microscopic analyses were performed.

Electron microscopic analyses showed that the particles were attached to each other (Fig. 2) and covered by a coarse precipitate. EDAX analyses of the precipitate show no iron, but the presence of carbon (20%), oxygen (30–40%), sodium (8%), silicon (25–40%) and some calcium (2–6%).

The EDAX analyses were compared with chemical analyses of the original (unclogged) soil. The carbon

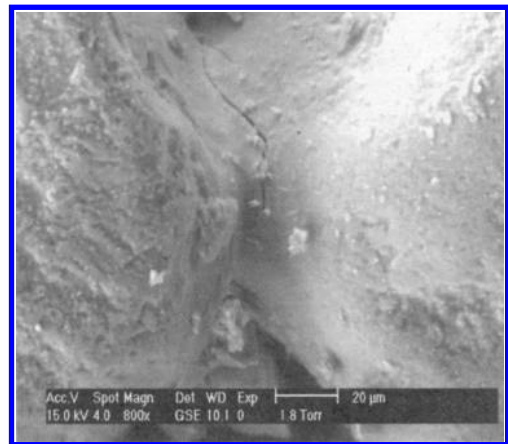


Figure 2. EM evidence of deposition between particles.

had to originate (partly) from organic sources and appeared only after clogging. The precipitated material was found all over the surface of the particles and contained silicon and carbon.

The following mechanism was proposed. The injected gel-layer is causing a very high pH level (above pH 13) in the surrounding ground and groundwater. During the upward water flow through the formation from the gel-layer to the wells the pH level decreases due to mixing and chemical interaction with the formation through which the water flows. This is in particular the case near the peat layer, which has a low pH (4–5). At high pH inorganic complexes or organic matter is known to dissolve while at lower pH it will precipitate again. The precipitated matter will build-up and clogs the pores the quickest where groundwater flow rate is the highest, i.e. just around filters.

The electron microscopic analyses indicate that organic matter instead of inorganic complexes is the cause of the clogging. To confirm this hypothesis laboratory test were performed on the brown groundwater from the clogged well. Organic matter precipitate when salt is added. This was observed also in the brown groundwater adding an abundant amount of sodium chloride. The influence of pH was tested. The pH of well water was stepwise decreased by adding acid. It turned out that at very low pH (values between pH 1 and pH 2) precipitation occurred and a clear fluid with brown deposition resulted, as shown in Figure 3. It is known that precipitation of inorganic complexes will occur at higher pH and therefore these inorganic complexes are not the driving agents in the investigated clogging process. For humic acids (present in the organic matter) it is known that these materials precipitate much slower, but that abundance (or addition) of calcium salts increases the precipitation rate. This behavior was indeed found after adding calciumchloride (CaCl_2).

Although in this specific case the gel-layer was old and injected several years ago because of delay in the

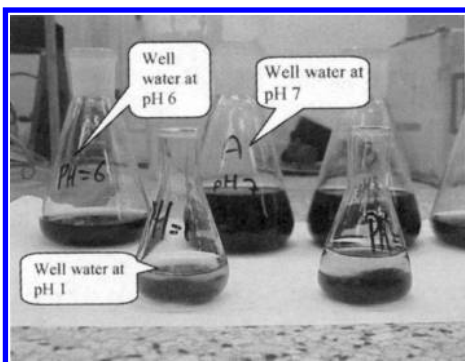


Figure 3. Precipitation and solution of organic matter depending on acidity of the well water.

construction process, it was expected that this effect could occur and would have occurred more often in connection with grouted silicate gel-layers.

Indeed it was found that the behaviour at Station Spui was not unique and that two other (Schuil-ing, Brons, pers. comm.) unpublished cases of clog-ging above silicate gel-layers had occurred in The Netherlands. One of these other cases was influenced by the presence of a shell layer in which the calcium was causing the organic material to precipitate.

3 SOLUTIONS

3.1 Chemical approach

To lower the water table in Station Spui different solutions were formulated. First different options were considered to prevent the clogging process. The clog-ging process consists of two steps

1. the dissolution of organic matter and
2. the precipitation in or nearby the filters.

The best solutions would be to prevent the dissolution of the organic matter or to remove the organic matter. Because the underlying gel-layer should not be affected the pH could not be lowered. Chemical oxidation of the organic matter seemed to be difficult because the high pH is not favorable for oxidation with peroxide or permanganate. This was confirmed in a laboratory test where addition of permanganate did not show enough degradation to warrant a verification test in the field.

Therefore, increasing the pH in the whole sand formation was proposed, preventing and even reverting precipitation of organic material near the filters. Laboratory tests confirmed the increased permeability of a clogged soil after injection with caustic soda. The idea was applied in a prototype scale test infiltration and washing with a high caustic solution. However, results of both an in-situ prototype test and laboratory tests showed a secondary precipitation and clogging mechanism. This secondary process is now believed attributed to be the dissolution and later precipitation of the silica matrix, especially because very high concentrations of caustic solution (pH 14) were used.

Another solution was to retrieve the water just above the gel-layer where the pH was still high and no clogging due to precipitation was expected.

However, in order to place (short filter) wells just above the gel-layer precise information of the actual gel-layer depth (which is uncertain since local heterogeneity determines the position of the gel around each injection point) was required. Furthermore there was concern about the influence of localized pumping, very close to the gel-layer, on the gel-layer integrity. Therefore this solution was not implemented, and not even tested.

3.2 Mechanical approach

Early in the project, already before the chemical investigations into the clogging mechanism were started, it was recognized that the main issue was the decrease of piezometric levels below the peat layer.

To reduce these pressures simple piercing of the peat layer was considered. In order to investigate the possibility of piercing the peat layer with gravel columns a preliminary field test was performed with nine small diameter (0.13 m) gravel columns. The gravel columns were provided with a filter pipe in order to monitor the achieved flow rate. Extra observation wells were installed within the test field to measure the resulting drawdown of the water level. The behavior of these gravel columns with internal filter was very similar to the filter pipes installed earlier along the diaphragm walls: within days the water production dwindled to negligible flow rates.

In hindsight this was no surprise. The gravel used in the gravel columns was far too coarse to act as a geometrically closed filter around the filter pipe. While initially the gravel may have been clean of sand the water flow will have transported sand grains into the gravel pores, and the resulting formation around the filter pipe was no better than the formation around the filter pipes which were not placed in gravel columns. The decrease in permeability which was attributed to the clogging of the sand by precipitated organic material occurs then similar to the other filters.

If clogging within the formation is a process which develops with time and is directly related to the amount of water which passes, the surface of the filter construction will determine the potential production of a given well.

Therefore three other filter piles were constructed with larger filter areas. They had a diameter of 0.3 m and extended 1.5 m below the peat layer, giving a filtersurface of approx. 1.5 m². The granular material in these piles was much finer than the gravel used previously. The grainsize of this material ranged from 1 mm to 2 mm, which was sufficient to ensure a geometrically close filter. Above the peat layer the filter column was closed off with a PVC liner (Fig. 4, filter type A). This enabled a regular and accurate measurement of the filter capacity by performing rising head tests. One of these test piles remained intact for several months and the decrease in filter capacity was recorded (GP1 in Fig. 5).

It was recognized that a simple (passive) gravel pile like type A in Figure 4, but without the PVC-liner, had a drawback in practice. During excavation the gravel pile would intersect the excavation slope and would destabilize the slope by the outflow of water from the filter. In view of this, and to enable better dewatering of the layer above the peat, a filter-column with a possibility for active dewatering was designed (type

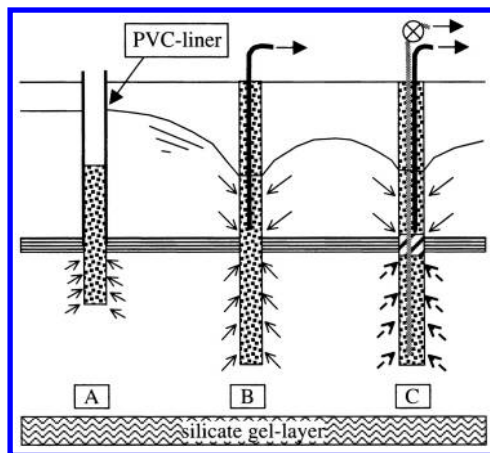


Figure 4. Different filter types.

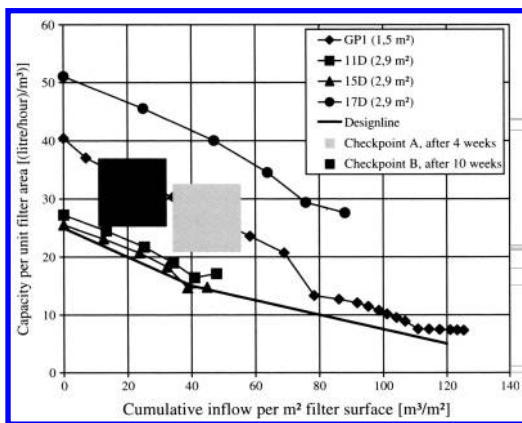


Figure 5. Prototype filter test results.

B in Fig. 4). In order to prolong the lifetime of the filter it was also designed to penetrate further below the peat-layer, which doubles the filter inflow surface.

The main problem that remained was the ongoing decrease of the filter capacity since water started flowing as soon as the filter was made and the formation clogging progressed. Especially since it could not be guaranteed that the filters were all made just before they had to start dewatering. Some filters had to be made weeks before they were actually needed, and the risk that some other delay would occur could not be neglected.

In view of this a filter type C was designed, as shown in Figure 4. This filter type is provided with two internal filter tubes surrounded by a granular filter. The zone above the peat layer is separated from the zone below the peat layer by means of an impermeable clay plug. The filter tube, which extends below the peat layer, under the clay plug, can be closed off by means

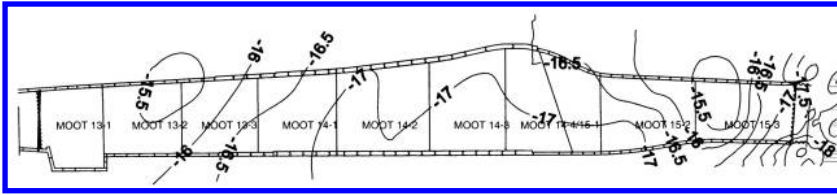


Figure 6. Depth of peat layer.

of a valve. The result of this is that when the valve is closed no water will flow through the formation around the filter. Therefore, until the filter is actually needed no degradation of the filter due to clogging of the surrounding formation will take place and maximum capacity will be available when it is most needed.

Before implementing such a dewatering system a prototype test was performed. Apart from three gravel piles with PVC lining, out of which one was closely monitored during a long period, a total of ten type B and type C piles were installed to monitor their performance. Out of these three type C piles, (Nr. 11D, 15D and 17D) were most closely monitored.

The test results are depicted in Figure 5. In order to compare the results for piles with different inflow areas and for piles over which a varying differential head was acting the results have been normalized.

The capacity (m^3 per second) was divided by the inflow area of the gravel pile and by the differential head, which acted over the filter. The resulting normalized capacity has then the dimension of s^{-1} . Since the clogging of the formation around a filter is not just a function of time but depends on the amount of water which has flowed through the formation it is logical to use the total inflow (m^3), normalized with respect to the inflow area of the gravel pile (m^2) as a history parameter.

The test results of the piles show initial capacities ranging from 25 to 52 ($1/\text{hr}$)/ m^3 and similar behavior with respect to the decrease of capacity with time. Since the installation of these first series of piles was not without problems, (one had to drill against the excess water pressures under the peat layer) the difference in the initial capacity was considered to be as much due to in-situ heterogeneity as to differences in installation procedure. On basis of this the lower bound of the capacity curve of the test piles was taken as achievable design capacity.

There were other important observations during the period of prototype testing of the wells:

- the piezometric levels reacted very fast on changes in the suction of the piles;
- large differences occurred in piezometric levels over relatively short distances.

4 NEW DEWATERING SYSTEM

4.1 Dimensioning

The total inflow into Station Spui was recorded and remained fairly constant at 400 m^3 per day during the period that the dewatering system was designed. The sand formation, both above and below the peat layer had a permeability of 1 m/day . On basis of the leakage is the average resistance of the gel-layer was calculated to be 40 days, which was the same as the back-calculated resistance of the peat layer. The required drawdown of the piezometric level varied from place to place in Station Spui. While the requirements for the diaphragm wall were known beforehand the requirements for vertical stability of the peat layer and the overlying sand varied with the position of the peat layer (see Fig. 6) and the locally required excavation depth.

On basis of these data separate maximum water pressures were determined for each of the sections of the station. While the conservative designline of Figure 5 was used it was considered prudent to build the system with an full extra safety: Apart from the so-called primary piles, placed at 1 pile per 12 m^2 density, a secondary system was installed at a 1 pile per 14 m^2 density. This extra safety was deemed necessary because later placement of more piles was not feasible.

4.2 Implementation

Piles were constructed by means of wash borings using a "lost" drillhead with nozzles and an external return flow. No serious problems were encountered with the drilling through the excess water pressures under the peat layer. It was however noticed that pile drilling and dewatering before placement of lateral struts caused displacements, after which placement of the struts was brought forward in the construction schedule, while the dewatering was postponed as much as possible.

4.3 Monitoring and performance

As explained the rapid reaction of pore pressures on loss of vacuum and the local variability of the excess pore pressures called for a spatially dense and frequent automated monitoring of the piezometric levels.

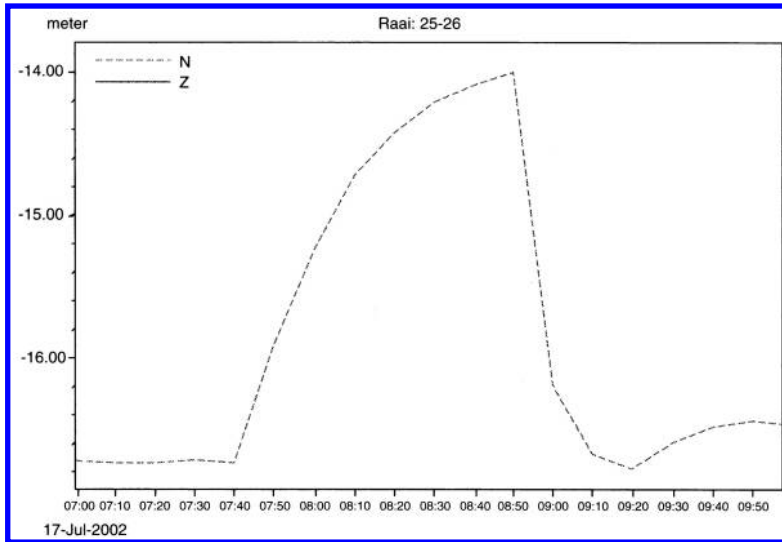


Figure 7. Pore pressure rise of 2.7 m in 70 minutes.

Typical margin between maintained and maximum allowable piezometric levels was 1 to 1.5 m.

Figure 7 shows the quick reaction of pore pressures to a loss of vacuum, where groundwater level rose at a rate of more than 4 m per hour.

Another interesting feature is the response of the pore pressures to the drilling of the gravel piles. Upon penetration of the peat layer the water pressures caused by the drilling could be felt as far as 30 m from the drilling location. On a daily record the number of installed piles could easily be counted.

Often an oscillatory behavior was observed. This was caused by a loss of vacuum, subsequent decrease of the pumped flow with a rise of waterlevels as a consequence, followed by a decrease in waterlevels after a vacuum had been build up again. From these types of measurements the insight was obtained that in this case manual (less frequent) monitoring might have been deceiving and dangerous and would not have provided the understanding of the dewatering system which was obtained now.

The performance of the dewatering system and the gradual degradation of the wells fell within the range that was found during the prototype filter tests. The large squares in Figure 5 give the estimated performance of the dewatering system after 4 and 10 weeks operation. Overall the system had a more than adequate capacity: It appeared that the average resistance of the gel-layer had remained better than estimated and that localized weak spots caused the most water inflow. In one of these areas also the secondary system had to be switched on in order to achieve sufficient dewatering.

5 CONCLUSIONS

Despite the fact that at least two similar cases had occurred in the Netherlands the clogging mechanism related to the release of caustic soda from a grouted silicate gel-layer was a surprise to those involved in this project. This emphasizes the need for recording and dissemination of field experiences among designers and builders.

The caustic soda release from the silicate gel-layer leads to a high pH level in the groundwater, which in turn may lead to solution and precipitation of organic materials (humic acids). Precipitated solids transported by groundwater will cause clogging effects, in particular in areas where high specific discharges are present, i.e. around extraction filters and wells.

Prototype and lab tests with chemical countermeasures involving artificial increase of the pH level in the groundwater had unwanted side-effects, apart from safety and water discharge considerations.

Clogging in the soil formation around the filter is a function of the cumulative specific discharge through the formation and can therefore be counteracted by increasing the inflow area of the filters as long as the dewatering system has to be operational over a limited span of time. Filter columns with a suitable (gravel or sand) filter layer providing a large enough filter inflow area proved adequate for the dewatering of the building pit: The clogging mechanism was not prevented, but could be coped with thanks to the large filter area available.

The automated monitoring, by means of relatively closely spaced standpipes, of the performance of the

dewatering system was indispensable in this situation: Water pressures could rise to critical levels within 1–2 hours (incompatible with manual logging) and did vary over relatively short distances (5–10 metres).

REFERENCES

- Brons, 2001, personal communication.
- KIWA, 2000, Kennisdocument Putten(velden) 9/2000, 22.2237.015.
- KIWA, 1984, Ervaring met diepinfiltratie, KIWA mededeling 79.
- Kruit, J., J. de Jong, M.G.A. van den Elzen and Th.A. Feijen. (2003), Souterrain the Hague: re-design construction method and recent experiences with grout layers. Proceeding of ITA World Tunneling Congress, Amsterdam, 12–17 April 2003.
- NOBIS, 1998, Implementatie beslissystematiek ontwerp en onderhoud van infiltratie- en onttrekkingsmiddelen NOBIS 98–108.
- Schuilig, 2001, personal communication.

Souterrain The Hague: imperfections in jet-grout layers

A.F. van Tol

Delft University of Technology, Rotterdam Public Works, The Netherlands

J.B. Sellmeijer

Geodelft, The Netherlands

ABSTRACT: Since several years horizontal jetgrout layers, consisting of short overlapping columns are used to ensure the vertical stability of building pits and trenches. At the Tramtunnel project in The Hague a considerable part of the building pits had such jetgrout arch. This layer appeared to be not fully watertight. In recent years there have been several, nearly catastrophically events with these jetgrout screens. This was one of the reasons for Delft University of Technology and GeoDelft to start a research work on the design criteria and the reliability of a jetgrout layer as a groundwater barrier. The safety approach that was introduced is that a covering sand layer of a certain thickness is necessary. This paper reviews the required thickness of a covering sand layer. First a theoretical consideration was made to analyze the stability of a sand prop in a hole. In addition experiments were carried out to determine the governing parameters. Finally the field observations of the Tramtunnel project in The Hague are compared with the results of the theoretical and experimental research.

1 INTRODUCTION

For some time now, horizontal jetgrout screens consisting of short overlapping columns have been used to ensure the vertical stability of building pits and trenches. The advantage of a jetgrout screen or a jetgrout layer is the fact that these injected bodies have enough strength to function as a structural part of the building pit for example as an arc. For the vertical stability it is possible, at least from a structural point of view, to locate this jetgrout screens just below the excavation. In recent years, there have been several, near-catastrophic events involving these jetgrout screens, which were intended to act as a water barrier under the building pit or trench. At the Tramtunnel project in The Hague a considerable part of the building pits had such jetgrout arch. This layer appeared to be not fully watertight, which was detected unfortunately only during excavation when groundwater and sand were flowing into the building pit. Nevertheless the average permeability of these screens, determined with pumping tests, was satisfying. To continue tunnel construction the design of the building pit had to be changed drastically (Kruijt et al., 2003). Similar events have arisen in projects in Cairo, Berlin and Bilbao.

This was one of the reasons for the Delft University of Technology to begin research into the design criteria

and the reliability of a jetgrout screen as a groundwater barrier. The research focused on two aspects: the reliability of jetgrout screens (Tol, 2001a), and the consequences of imperfections in jetgrout screens, the subject of this paper.

According to the actual state of the art, all injection layers show imperfections. This means that the percolating water should be discharged in a controlled manner using a drainage system in the soil above the jetgrout layer, without the risk of erosion. A covering sand layer of a certain thickness is therefore necessary. In this research, an analytical model for the stability of the soil in a flow channel in the jetgrout screen was developed. In addition, analytical experiments (scale 1:5) were carried out to verify the model and to estimate the governing parameters. On the basis of this research, it is possible to determine the minimal thickness of the covering sand layer and the most important design criteria. Finally the field observations of the Tramtunnel project in The Hague are compared with the results of the theoretical and experimental research.

Earlier research followed also this approach, (Bieberstein et al., 1999). In their study the governing failure mechanism is the complete reduction of effective stress at the top of the hole and in the covering layer due to the seepage pressure. In the present research a more critical failure mode for the hole was found.

2 ANALYTICAL SOLUTION

2.1 Equilibrium of the soil in the hole

It is assumed that an imperfection in the jetgrout screen is filled with sand. A difference in pore pressure is created across the grout layer when the construction pit is pumped empty. This leads to groundwater flow through the sand-filled hole. In a stationary situation, the seepage pressure acts as a uniformly distributed load over the height of the soil prop in the hole in the grout layer. In a hole with a constant cross-section and filled with uniform sand, a constant gradient across the hole occurs.

The water pressure drop over the construction pit consists of three areas: the area outside the pit, the grout layer and the area inside the pit. The resistance over the grout layer is much bigger than the ones in the other areas as long as the hole is filled with sand and has a small diameter. Therefore, the pressure drop in the other areas is neglected. This is a conservative estimate for the stress state in the hole. Calculations with groundwater models confirm the assumption.

If the construction pit is pumped empty, a large pressure drop is present over the grout layer. Such, that the equilibrium of the sand in the hole may be jeopardised. To estimate the danger of loss of stability, a limit equilibrium calculation is performed. Along the edge of the hole the maximum possible shear stresses are mobilised. Figure 1 shows the stresses acting on a soil element in the hole.

The following differential equation can be established from the vertical equilibrium of this element:

$$\frac{d\sigma'_z}{dz} - \frac{K \tan \delta}{A/O} \sigma'_z = (\gamma_{\text{sat}} - \gamma_w) - i\gamma_w \quad (1)$$

with:

- γ_{sat} – density of saturated soil
- γ_w – density of water
- A – surface area of hole cross section
- O – circumference of hole cross section
- K – horizontal earth pressure coefficient
- σ'_z – vertical effective stress
- σ_z – vertical total stress
- δ – friction angle between wall and soil
- i – gradient across hole

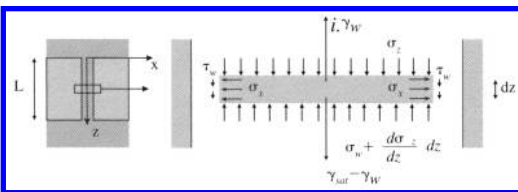


Figure 1. Equilibrium of a soil element in the hole.

Equation (1) needs one boundary condition to be solved. The purpose of this calculation is to determine under which conditions the danger of loss of stability is avoided. This will be formulated later. Meanwhile, a yet unknown stress σ'_L at $z = L$ will be introduced.

This gives the following description of the effective stresses over the height of the hole (also see Sellmeijer, 1999):

$$\sigma'_z = [i\gamma_w - (\gamma_{\text{sat}} - \gamma_w)] \frac{1 - e^{-\frac{K \tan \delta}{A/O}(z-L)}}{\frac{K \tan \delta}{A/O}} + \sigma'_L e^{-\frac{K \tan \delta}{A/O}(z-L)} \quad (2)$$

The expression is only meaningful, if $i\gamma_w > \gamma_{\text{sat}} - \gamma_w$. If not, the dead weight of the sand in the hole is heavy enough to withstand the gradient. Therefore, the vertical effective stress consists of two positive contributions. Hence, a stress on top of the hole is required to assure stability.

The minimum required stress on top of the hole is found substituting $\sigma'_L = 0$. At that stage the sand has lost cohesion at the bottom of the hole. Indicating the stress on top of the hole by σ'_0 , it follows:

$$\sigma'_0 = [i\gamma_w - (\gamma_{\text{sat}} - \gamma_w)] \frac{1 - e^{-\frac{K \tan \delta}{A/O}L}}{\frac{K \tan \delta}{A/O}} \quad (3)$$

Figure 2 shows the pore pressures, the total stresses and the effective stresses over the height of the hole.

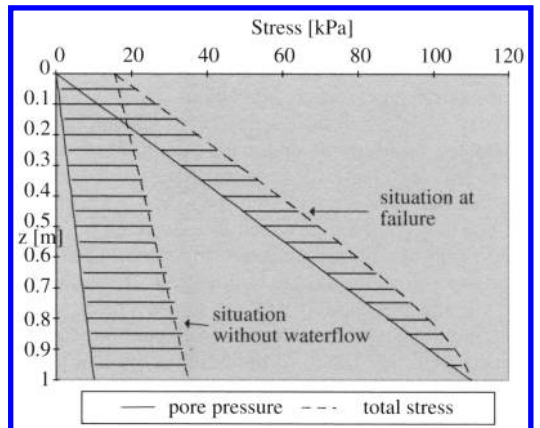


Figure 2. Stress state in a hole without seepage and at point of failure due to seepage.

Figure 2 shows both the stress states at the moment of failure as well as the initial stress state, without seepage.

2.2 Evaluation

Equation (2) describes the stress state in a hole in a jet-grout layer. For the solution given, three aspects need to be considered.

1. The hydraulic gradient over the hole at the point of failure is far more than 1, so that the seepage pressure would normally lead to liquefaction. This does not occur because an additional vertical force arises in the equilibrium of forces, in the form of developed shear stresses acting at the wall of the hole. Moving upwards, the soil prop fixes itself. This phenomenon is similar to traditional arching in granular materials.
2. Increasing the hydraulic gradient over the hole reduces the effective pressure on the lower side of the hole to nil at a certain moment. Then there is just equilibrium in every cross-section over the height of the hole. Further reduction of effective stress on the lower side of the hole means that the lower section can no longer develop shear stresses. As the maximum shear stress has already developed across the remaining part of the soil column, the entire soil column will then be forced out of the hole.
3. A condition for achieving the stress state described is that the upper side of the hole is stable. The covering layer must exert a certain minimum effective stress. If this is not the case, there is no reactive force to the flow pressures on the upper soil section. The flowing water then carries the particles away and the hole will be worn away from the upper side. The presence of a covering layer above the grout layer is therefore essential. The flow pressure in the covering layer will quickly fall due to the rapidly widening flow pattern, so that the particles there are stable.

3 EXPERIMENTAL RESEARCH

3.1 Test set-up used

Two types of tests were carried out, whose aims were: to test the developed analytical model on experimental data; to determine the two remaining unknowns, namely: the size of the maximum shear stresses to be developed in the hole; the maximum effective pressures developed in the covering layer at failure.

In the first series of tests, only the hole in the grout layer was modelled. In the second series, both the hole as well as the covering layer were modelled. Separating the failure behaviour of the hole and the covering layer allows a controlled description of the stability of soil

in the hole, without influence from the covering layer. The link is made, though, in the second tests series. There was no soil under the grout in either test series.

A cylindrical tube was used for modelling the hole in a jetgrout layer, measuring 100 mm in diameter, 550 mm in length, and made from Plexiglas lined with sand (see Figure 3). Pore pressure devices were fixed to the tube wall. Water can flow into the lower part of the tube at varying pressure. Excavation and pumping out of the construction pit in the field is modelled by slowly increasing the pore pressure differential across the tube.

The covering layer was not included in the first series of tests. The presence of effective pressure on the upper side of the hole is essential, as stated earlier. For this reason, a movable filter was fitted on the upper side of the sand column, permeable for water and impermeable for sand. Different loads could be placed on top of this. In the second series of tests, a larger cylinder was fitted above a similar tube, measuring 600 mm in diameter, 400 mm in height, and in which pore pressure devices could be placed at the axis point. Both the tube (the hole in the grout layer) and the larger cylinder were filled with sand. Pore pressure was then increased over time, until failure occurred.

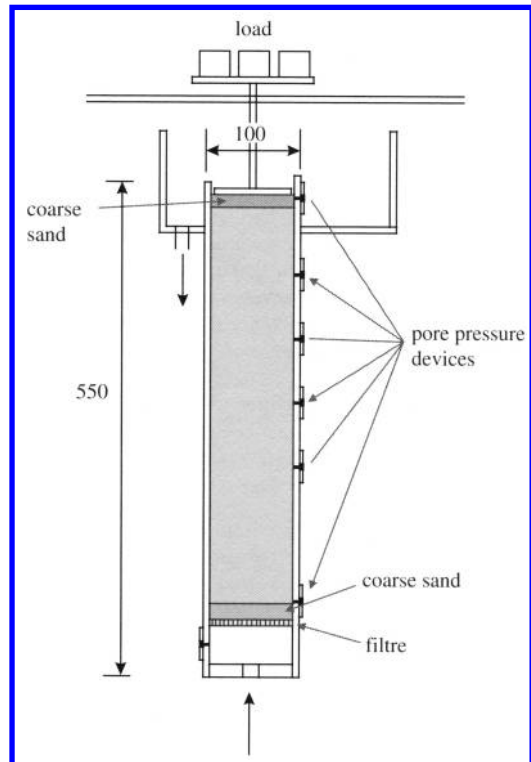


Figure 3. Test set up.

3.2 Observed failure mechanism

In the experiments carried out, a failure mechanism occurred which followed different phases over time. The different phases can be described as follows:

1. Crack formation: As pressure gradually increases, horizontal cracks form at the point where the pressure first builds up. This is often above the sand filter.
2. Fluidisation and compression: The section between the lower side of the set-up and the upper side of the crack becomes fluid. The sand column (above the crack) becomes somewhat compressed from the lower side. This increases the density of the sand above the crack. The upper side of the sand column has not yet been affected.
3. First shift of upper column: When the pore pressure is increased at a certain moment, the entire sand column moves upwards. The maximum movement of the upper side amounts to a few millimeters. This shift mobilizes the wall friction along the entire height; this results in sufficient resistance to prevent further column movement.
4. Stable situation as pressure increases further: Once friction has developed over the entire height, the sand column remains stable as the pore pressure increases. In this way, the load can be increased considerably.
5. Failure mode (1): At a certain moment, the pore pressure is so large that the shear stress, which has developed no longer, offers sufficient resistance to a sand column shift. The column then slowly moves up. This movement continues until the entire sand column is pushed upwards. During this shift, the sand in the lower side of the column is completely stable. The water underneath the sand column is perfectly bright, no particles fall back against the flow.
6. Failure mode (2): The entire stable sand column is forced out of the hole.

3.3 Test series

In the first test series, different sets of parameters were tested. Table 1 gives an overview of the range of the

Table 1. Overview of tested parameters.

Parameters	Lower limit	Reference test	Upper limit
Top load [kN]	1	3	6
Porosity [-]	0.34	0.38–0.40	0.44
Wall friction [°]	12.5°	0.8φ	φ
Length [m]	0.25	0.50	0.50
Grain size sand	Fine	Fine	Coarse

parameters that were varied. Most of the tests were carried out with sand glued at the inner wall of the Plexiglas tube. Some had 100% sand in these tests while others only 80% of the inner surface, leaving small vertical zones without sand so that the behaviour of the sand fill in the tube could be observed. The angle of wall roughness in these tests was supposed to be 0.8ϕ . A few tests were carried out with a tube without a sand liner, with a roughness $\delta = 12.5^\circ$.

3.4 Determining remaining unknowns

As stated earlier, determining the two remaining unknowns (the maximum shear stresses in the hole and the effective stress to be mobilised in the covering layer at failure) was one of the reasons for performing the experiments. As equation (2) determines the vertical effective stress in the soil in the hole the unknown parameter is $K \text{ tg } \delta$. Figure 4 gives the values of $K \text{ tg } \delta$ as a function of the porosity, found in the experiments. It appears that there are two branches, one for medium to loose sands with a $K \text{ tg } \delta$ value between 0.4 and 0.5 and one for dense sands with a $K \text{ tg } \delta$ value of 1.0–1.2. This corresponds to an active and passive condition in the hole at failure along a vertical wall.

The fact that the values of $K \text{ tg } \delta$ at the point of failure in those experiments with a 80% to 100% sand liner in the tube are similar for medium and loose sand can be explained by the compression of the sand column from underneath, before actual failure occurs. In Figure 4 only the experiments without a sand liner in the Plexiglas show a considerable lower value for the friction.

The second unknown is the influence of the covering layer on the failure behaviour, or the maximum effective stresses that the covering layer can deliver. If this is modelled as a cone pushed upwards in this layer the tests indicate that the apex of this cone is about 8° . If the maximum stress is back-calculated from friction

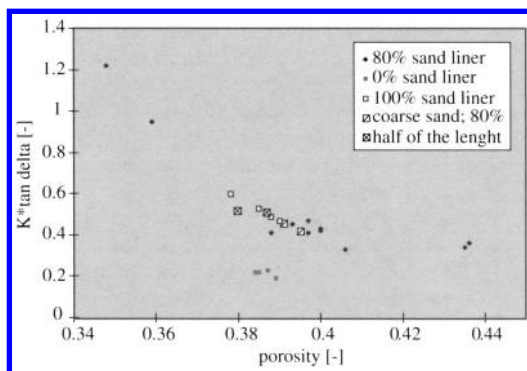


Figure 4. Results from the experiments, $K \text{ tg } \delta$ versus the porosity.

along a cylinder with a diameter D , based on effective vertical stress in the covering layer multiplied by a $K_r \text{ tg } \phi$ it appears that the horizontal earth pressure coefficient $K_r = 0.27$.

4 DESIGN

4.1 Design chart

The required vertical stress σ'_0 at the top of the hole in a jetgrout layer is specified in (3). It is copied here. Note that A/O is expressed as the diameter of the hole: $1/4 D$.

$$\sigma'_0 = [i\gamma_w - (\gamma_{\text{sat}} - \gamma_w)] \frac{1 - e^{-\frac{4K \tan \delta}{D} L}}{\frac{4K \tan \delta}{D}} \quad (4)$$

The available vertical stress $\sigma'_{z;r}$ at failure, in case a cone is pushed upwards in the covering sand layer with thickness d is:

$$\sigma'_{z;r} = (\gamma_{\text{sat}} - \gamma_w) \left(1 + \frac{2}{D} d \cdot k_r \cdot \text{tg } \phi \right) d \quad (5)$$

In this equation the seepage pressure (in the covering layer) is neglected. The experiments confirmed this assumption. Bieberstein (1999) and Sellmeijer (1999) did use an approximation for the excess pore pressure in the covering layer.

In Figure 5 both equations 4 and 5 are depicted for an increasing hole diameter, different gradients and thickness' of the covering layer. Other parameters are fixed and the design values are giving in the figure. Figure 5 (Tol et al. 2001b) presents the required thickness of a covering sand layer. The overall safety factor $\eta = 2$ is applied to the height of the covering layer. For the parameters design values are used: $K_d \text{ tg } \delta = 0.32$, $\gamma_{\text{sat}} = 18.2$, and i as shown in Figure 5. The thickness of the grout layer is equal to $L_d = 1.25$ and the friction

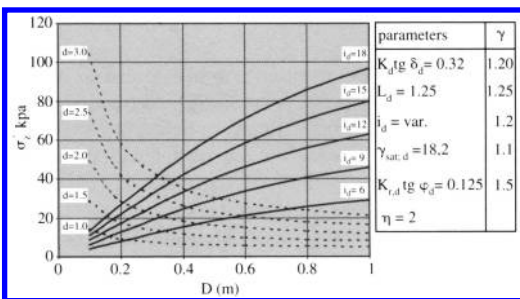


Figure 5. Required cover as function of the hole diameter. Required thickness d of a covering sand layer as function of gradient i_d .

in the covering layer is calculated with $K_r \text{ tg } \phi$ equal to 0.125. It should be noted that the design method presented is valid for homogeneous soil in the hole and the covering layer.

The required height of the covering layer can be determined, for the used set of parameters with the curves in Figure 5. If for example a hole diameter of 0.2 m is chosen and a gradient $i_d = 12$ then $\sigma'_z = 17.4$ kPa and the required thickness of the covering layer d is 1.5 m (the continuous curve for $i_d = 12$ intersects the dotted curve for $d = 1.5$ at $D = 0.2$).

4.2 Conclusions

The following conclusions can be drawn:

- there is considerable resistance to failure when there is a sufficiently large, effective pressure on the upper side of a hole. This means that a gradient between 10 and 15 can be resisted.
- a long hole, or a thick grout layer, without ground coverage can only resist a hydraulic gradient of about 1 and is therefore far less favourable than a hole in a much thinner grout layer with some ground coverage, even if this is quite small.

Design calculations can in principle be performed using equation (2). Failure occurs when the effective stress at the bottom of the hole equals nil: ($\sigma'_z = 0$ at $z = L$) giving equation (3) and the required effective stress at the upper side of the hole (σ'_z at $z = 0$), which determines the required thickness of the covering sand layer. All parameters are known in this equation, except for the factor $K \text{ tg } \delta$, which was determined in the experiments.

The available effective stress from the covering layer can be determined using equation (4). The unknown factor k_r was also determined in the experiments.

It should be noted that the presented design method is valid for homogeneous soil in the hole and the covering layer. Heterogeneous soil can have a negative influence on the stability. Especially a thin clay layer in the upper part of the hole requires a thicker covering layer.

4.3 Design approach

To design a jetgrout layer as a water barrier, it is important to realise that imperfections will always occur and that they can lead to a failure mechanism as described in this paper. A safe design can be achieved by using a sufficiently thick covering layer above the grout layer. A design approach for such a jetgrout layer may be as follows:

- using the probability model described by Tol (2001a), the hole with the largest surface area is defined, with a required probability of failure such as 1 in 10,000;

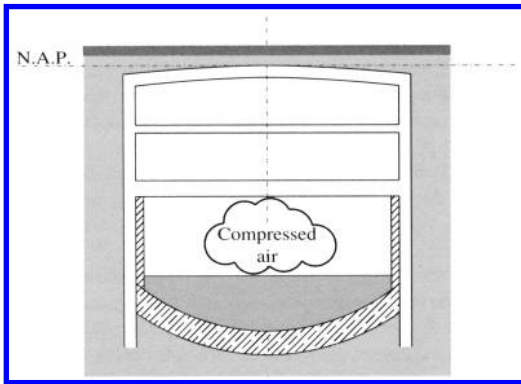


Figure 6. Cross-section of the Tramtunnel with the chamber for compressed air.

- using the model for hole stability described in this paper the required thickness of the covering layer for a hole with this diameter is determined;
- although the seize of the hole is determined with a probabilistic model it is recommended to calculate the thickness of the covering layer with design values of the parameters and to apply a safety factor to the thickness of the covering layer.

4.4 Evaluation

Following the serious problems that occurred in March 1998, it was decided to change the working method and, in particular, the design of the building pit with the grout arch, in such a way that the last part of the excavation is carried out under compressed air. The original design was already based on the so-called wall-roof method, where first the retaining walls and then the roof are constructed.

The tunnel is excavated and constructed under the roof. A cross-section is shown in Figure 6. According to the redesign the compartment under the lowest floor is constructed as a compressed air chamber. To reduce the enormous costs of the work under compressed air, it was decided to excavate 3.25 m under the lowest floor at atmospheric conditions. In this situation, the stability of the sand prop in expected holes in the grout arch is achieved based on the above-mentioned analyses.

Before the start of excavation, a drainage system is installed with wells close to the walls.

During the atmospheric excavation, several boils developed that were controlled and repaired under compressed air by additional grouting. According to the analyses based on homogeneous soil, however, such boils could not occur in this stage. In fact, the soil just above and at the level of the grout arch is not uniform. Several thin clay layers are present in the covering layer. This could explain why actual conditions were worse than analysed. If a clay layer is present in the covering sand layer and the drainage system is installed above this clay layer, then excess pore pressure will build up between the grout layer and the clay layer if there are holes in the grout layer. If the hydraulic resistance of the clay layer considerably exceeds the resistance of the grout layer, then the excess pore pressure may rise to such a level that the effective stresses at the top of the hole in the grout layer are too small and the sand prop in the hole loses its stability.

The conclusion regarding the stability of sand props in a jetgrout layer is that a drainage system should be installed as deep as possible, and at least below the lowest silt and clay layers.

REFERENCES

- Bieberstein, A., Herbst, J. & Brauns, J. (1999), *Hochliegende Dichtungssohlen bei Baugruben-umschliessungen*, Geotechniek (1999) nr 2.
- Kruijt, J., Jong, J.J. de & Elzen, M.G.A. van den & Feijen, Th.A. (2003), *Souterrain the Hague: re-design construction method and recent experiences with grout layers*. Proceeding of ITA World Tunneling Congress, Amsterdam, 12–17 April 2003.
- Sellmeijer, J.B. (1999), *Safe excavation level above jetgrout arch*, Report GeoDelft CO-390471/8, annex 1, in Dutch (1999).
- Tol, A.F. van, Riel, A.J.E. van & Vrijling, J.K. (2001a), *Towards a reliable design for jetgrout layers*. Proc. of the XV International Conference on Soil Mechanics and Foundation Engineering, Rotterdam, Balkema, 2000.
- Tol, A.F. van, Koster, S., Ramler, J.P.G., Vrijling, J.K. & Verruijt, A. (2001b), *Imperfections in jetgrout layers*, Proc. XV International Conference on Soil Mechanics and Foundation Engineering (Togrol et al., ed.), Balkema, Rotterdam, 2001, pp. 1883–1886.

Souterrain The Hague: scouring in case of sand boils through a jet-grout layer

D.R. Mastbergen & W.G.M. van Kesteren

Delft Hydraulics, The Netherlands

A.F. van Tol

Delft University of Technology, Rotterdam Public Works, The Netherlands

ABSTRACT: Since several years jetgrout layers, consisting of short overlapping columns are used to ensure the stability of building pits and trenches. At the Tramtunnel project in The Hague a considerable part of the building pits had such jetgrout arch. In recent years there have been several, nearly catastrophically events with these jetgrout screens due to the inflow of groundwater and sand into the building trench. This paper presents a method to assess the amount of water and sand flowing through a hole in a jetgroutlayer, the possible influenced zone in the surrounding and the available time for countermeasures.

1 INTRODUCTION

1.1 The jet grout construction method

Since several years horizontal jetgrout layers, consisting of short overlapping columns are used to ensure the vertical stability of building pits and trenches. The advantage of a jetgrout screen or a jetgrout-layer is the fact that these injected bodies have enough strength to function as a structural part of the building pit for example as an arch [van Tol, 1991, 2001 and Brons, 1994]. For the vertical stability it is possible, at least from a structural point of view, to locate such a grout arch just below the excavation. At the Tramtunnel project in The Hague over a considerable length the building pits were provided with jetgrout arches (see Fig. 1).

1.2 Problem definition

These grouted layers appeared to be not fully watertight, which was detected unfortunately only during excavation when groundwater and sand were flowing into the building pit [Tol, 2001 and Kruyt, 2003]. In recent years there have been several, nearly catastrophically events with jetgrout screens that were supposed to function as a water retaining structure under the bottom of a building pit or trench.

This was one of the reasons for project management of the Tramtunnel and Delft Hydraulics to start research on the possible scour under a grout layer in case of sand boils. The question to be answered, posed within the framework of risk control, was to determine the consequences of sand-carrying well if

it does develop. Within this context, the consequences of a sand-carrying well through the grout arch in the Tramtunnel project in The Hague were considered. The question was how much soil is transported from under the grout arch into the pit and over what time period. This question is extremely relevant as the answer indicates how much time is available to stop the flow, for example by activating a drainage system or pumping water in the construction shaft. In the case of the Tramtunnel the building shaft was adapted after the event of sand boils in such a way that as soon as a well is detected the shaft is closed and compressed air pressure is applied [Kruyt, 2003]. It may take 3–4 hours in this case to apply sufficient air compression to stop the well. The situation considered here is concerns the time

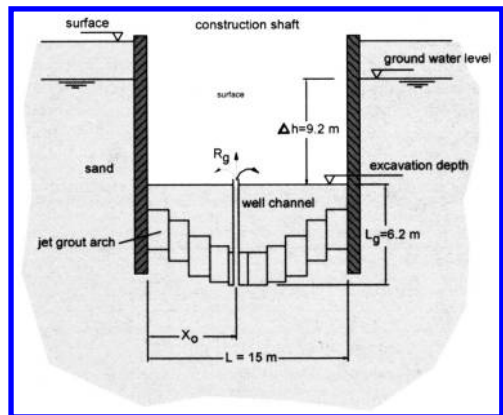


Figure 1. Construction shaft with jetgrout floor Tramtunnel.

span from moment a sand boil is actually present and a well channel has formed, until detection and subsequently application of air pressure (about 3–4 hours).

2 ANALYSES OF GROUNDWATER FLOW

2.1 Maximum flow rate or discharge capacity assessment

Given the hydraulic gradient, diameter, length and the hydraulic roughness of the vertical well channel in the grout arch and the sand layer, the maximum flow rate of the well can be computed quite simply. The maximum flow rate or discharge capacity would establish if the water under the grout arch would be available unrestrictedly (in analogy with the outflow from a water tank).

Assuming the channel well as a pipe flow, in which the available potential pressure gradient will be fully consumed by flow acceleration and hydraulic friction, the maximum flow rate can be computed with:

$$Q_m = \pi R_g^2 u_0 = \pi R_g^2 \sqrt{\frac{2g\Delta h_g \frac{\rho_w}{\rho_m}}{\left(1 + f_0 \frac{L_g}{D_0}\right)}}$$

in which:

- Q_m = maximum flow rate well in m^3/s
- R_g = radius well channel in m
- u_0 = maximum stationary flow velocity in the well channel in m/s
- Δh_g = available hydraulic pressure gradient in m
- ρ_m = sand–water mixture density, in kg/m^3
- ρ_w = water density ($1000 kg/m^3$)
- L_g = length of channel in m
- f_0 = Darcy-Weibach hydraulic friction coefficient (about 0.05–0.1)

Due to the imposed increase of compressed air pressure in the shaft in the case of an emergency (enabled after about 1 hour), the hydraulic pressure gradient reduces the maximum flow rate until the flow is finally stopped completely (after another 3 hours).

The total volume of water flowed into the Tramtunnel shaft and the maximum amount of sand transported through the well follows from integration of the maximum flow rate in time, given the compressed air pressure emergency management scenario, knowing that a maximum of about 30% by volume of the total flow may consist of pure sand particles. At higher concentrations the sand–water mixture will show increasing internal flow resistance.

The maximum flow rate is defined strongly by well diameter. However, the groundwater flow computations (next paragraph) show that the flow

rate is defined by the permeability and the well area principally. So the assumption of unlimited water availability is certainly NOT true, and the well diameter turns out to be of no importance.

2.2 Groundwater flow and hydraulic gradient computation

The ground water flow through the well can be computed numerically or in an analytical way (as applied here), given the geometry and the hydraulic gradient due to the ground water level difference, present from the moment the excavation of the construction shaft has achieved the designed depth and the water has been pumped away (see Fig. 2).

The water permeability of the local sand soil, a very important parameter in this case, follows from sand grain size distributions, but has been determined on the site with pumping tests also ($k = 1 \text{ à } 5 \text{ m/day} = 1 \text{ à } 5 \times 10^{-5} \text{ m/s}$).

The hydraulic gradient was computed analytically with a potential flow model analysis by superposition of point source and drain terms in an axial-symmetric schematisation. The flow resistance in the well channel is neglected, if this is true will depends on flow rate and well channel diameter and will be verified later.

To obtain a constant potential at the tunnel wall (on distance x_0 resp $x_0 - L$) a number of sources were mirrored.

The solution for the potential flow now reads:

$$\psi = \sum_{n=-\infty}^{\infty} \frac{-m(x - 2nL - x_0)}{\sqrt{(x - 2nL - x_0)^2 + y^2 + z^2}} + \frac{m(x - 2nL + x_0)}{\sqrt{(x - 2nL + x_0)^2 + y^2 + z^2}}$$

$$\phi = \sum_{n=-\infty}^{\infty} \frac{-m}{\sqrt{(x - 2nL - x_0)^2 + y^2 + z^2}} + \frac{m}{\sqrt{(x - 2nL + x_0)^2 + y^2 + z^2}}$$

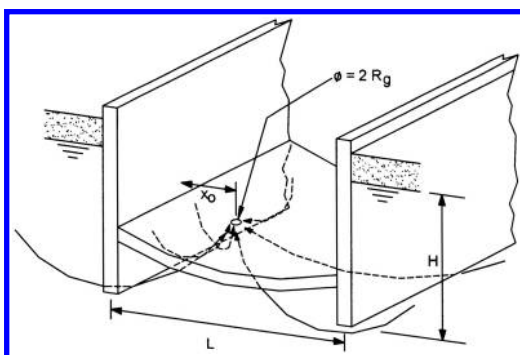


Figure 2. Groundwater flow to well in grout arch Tramtunnel.

with the source strength m :

$$m = \frac{2Q}{4\pi k} = \frac{Q}{2\pi k}$$

Solving this system of equations results in a solution for the flow rate and the hydraulic gradient as a function of the radial distance from the well (note that the gradient is infinite at the well boundary, but the average value is defined anyway) and the finite circular well radius R_g .

The potential flow function reads at the place of outflow:

$$\phi_0 = -\frac{\pi m}{2 R_g} = \frac{Q}{4kR_g}$$

Assuming a homogeneous permeability distribution in the sand soil, the ground water flow through the well can be computed with:

$$Q = kiA$$

in which:

Q = groundwater flow rate through the well in m^3/s

k = permeability in m/s

i = averaged hydraulic gradient

A = interstice surface area through which the groundwater enters the well, in m^2

with initially: $A = \pi R_g^2$.

The hydraulic gradient in the centre of the well reads:

$$i_0 = -\frac{2\phi_0}{\pi R_g}$$

The average value from which the flow rate can be computed reads half this value. The hydraulic gradient concentrates to the boundary interstice contours of the well just below the grout arch.

Since the main contribution to the pressure gradient occurs close to the well, in the schematisation the permeability and the source radius R_g define the flow rate principally.

Computations show with a radius of not more than 1 meter and a permeability of maximum about 5 m/day, that the flow rate is limited. The total volume of water flowing into the construction shaft in the time period from initiation until detection of the leak and taking effect of emergency measures (closing work space, putting up air pressure) is very limited. The occurring flow velocities near the well are so small that hardly any sand particles will be moved, let alone that a scour hole will develop.

Even in the case that groundwater flow concentrates into erosion channels and “piping” occurs (Sellmeijer, 1988), the flow rate remains restricted and flow velocities are not able to erode the channels considerably.

3 SCOURING

3.1 The breaching mechanism

The flow rate through the well increases considerably when the area over which the ground water enters the well increases. Notwithstanding the fact that the flow rate initially is too small to cause severe scour near the well, retrogressive erosion can take place, creating an interstice waterlayer between the grout arch and the sand soil (see Fig. 3). The increase of this interstice area, flow rate and the total volume of water and sand flowing into the shaft in a certain time span, are defined directly by the retrogressive erosion process (see Figs. 6 and 7).

This important but not generally recognized erosion mechanism, known as “breaching” [see van den Berg et al., 2002], occurs in densely packed fine sand and results in an autonomous slowly retrograding steep slope. Due to the dilatancy properties of the sand, water underpressures develop and the breach can remain stable for a while.

3.2 Wall velocity

The breaching process is known from dredging related processes, in the case of sand suction and cutting and has been investigated at Delft Hydraulics. The retrogression or “wall” velocity can be derived from a dynamic stability analysis of the sand grains and is defined by geotechnical properties uniquely [Breusers, 1974 and Van Rhee en Bezuijien, 1992] and reads, derived here with hydraulic gradient included:

$$v_{wal} = \frac{i + (1 - n_0)\Delta \frac{\sin(\varphi - \alpha)}{\sin(\varphi)}}{\Delta n/k_f}$$

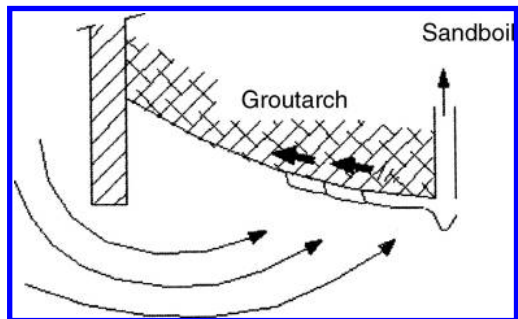


Figure 3. Stage 1: creation of interstice by retrograding small breaches.

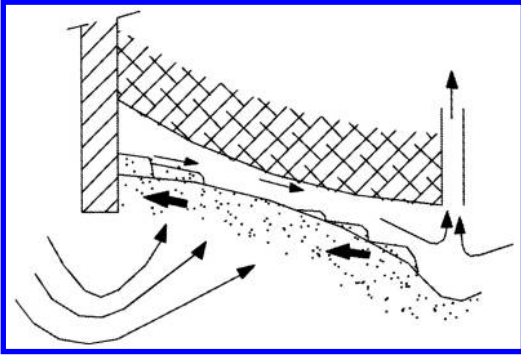


Figure 4. Stage 2: scour and equilibrium bed slope establishment.

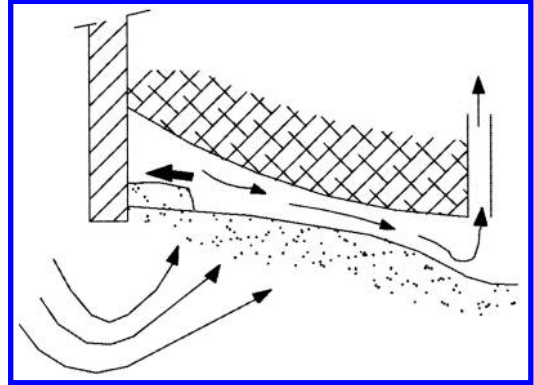


Figure 5. Stage 3: further development of scour hole.

in which:

- v_{wal} = wall velocity in m/s
- n_0 = porosity sand layer
- i = hydraulic gradient (negative in the case of out-flowing pore water)
- Δ = relative density sand grains in water (= 1.65)
- Δn = porosity increase from actual to loose condition
- k_l = permeability of loosely packed sand in m/s
- α = breach slope angle (maximum 90°)
- φ = natural angle of repose of the sand (about 37°)

In the case no groundwater flow is present $i = 0$ and the maximum retrogression velocity develops for a vertical “wall” (with $\alpha = 90^\circ$). No more breach retrogression occurs for a slope gentler than the natural equilibrium slope.

Due to a negative hydraulic gradient the equilibrium slope (at which $v_{wal} = 0$) will decrease. For full fluidization circumstances equilibrium slope reduces to zero. In the case of a positive gradient (f.i. shear dilatancy) the equilibrium slope increases. Retrogressive small breaches will be active until an equilibrium situation is established (see Figs. 6 and 8).

Initiated by the removal of at least the fine fractions of the sand particles from the soil beneath the well channel, a small initiating sand surface disturbance develops, which will axially and retrogressively propagate along the grout arch (Figs. 4 and 5). Breaching is enhanced by gravity and the present hydraulic gradient, but is NOT principally powered by an eroding flow velocity, as is the case with f.i. piping in dykes. This process therefore will initiate already at very low flow velocity, far beyond the Shields threshold for sand particle traction (as is the case with “piping”). The flow rate in the vertical channel should only be sufficient to allow the particles to move along and overcome fall velocity.

So the radius of the ground water receiving area R_g , initially equal to the channel well radius, gradually increases, until finally the side walls of the

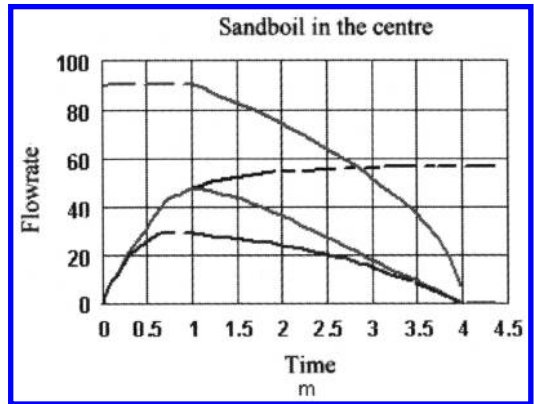


Figure 6. Flow rate development in time.

construction shaft are reached (after about 1 hour). Further increase will, from that moment, take place only in linear direction along the tunnel axis.

4 CALCULATION RESULTS

In Figure 7 is indicated the computed flow rate development in the case of the Tram Tunnel shaft, following 4 different scenario's, based on an available pressure difference of 9.2 m (Fig. 1) and a permeability of 5 m/day. Four different scenario's are given:

- 1 groundwater flow development with constant hydraulic gradient, achieving finally a value of $57 \text{ m}^3/\text{hour}$;
- 2 groundwater flow development with decreasing pressure difference due to applied air compression, after 1 hour a maximum value of $48 \text{ m}^3/\text{hour}$ is achieved, successively decreasing until after 4 hours sufficient air pressure is achieved;
- 3 groundwater flow development with decreasing pressure difference due to applied air compression

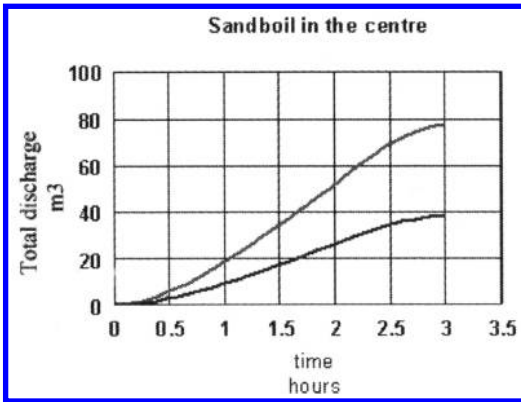


Figure 7. Maximum volumes water and sand transported in 3 hours.

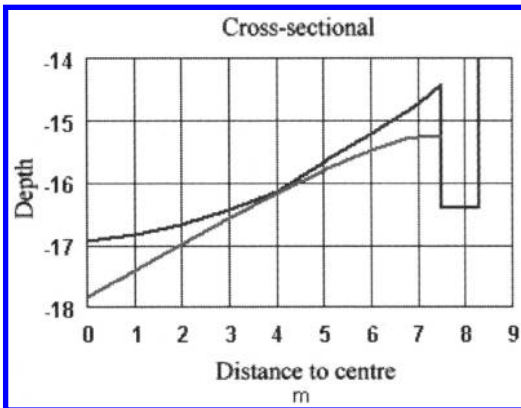


Figure 8. Equilibrium bed slope just below the grout arch of the Tramtunnel (well in centre $x_0 = 7.5$ m; $k = 5$ m/day and $L = 15$ m).

and taking into account friction pressure losses in the well channel (if sufficiently small), reducing maximum to $30 \text{ m}^3/\text{hour}$ with a channel diameter of 0.08 m;

- 4 maximum flow rate, if supply of groundwater would be unrestricted, resulting in a maximum of $90 \text{ m}^3/\text{hour}$ for a channel diameter of 0.08 m.

The total amount of water and sand scouring, transported through the well into the Tramtunnel shaft can be computed now from flow rate and maximum sand concentration in the flow (about 30% sand by volume), see Fig. 7.

The formation of small sand producing breaches will continue until an equilibrium sand bed slope has established everywhere, defined by the local hydraulic gradient. The equilibrium slope can be computed, resulting in the total volume of sand to be scoured and the maximum sand bed lowering at the toe of the

shaft walls. If the sand bed regresses below this level a severe risk for large subsidence and damage to the construction will arise. Figure 8 shows the computed sand bed for the well in the centre of the construction shaft ($0 = \text{centre of shaft}$). From this computed equilibrium sand bed, the total sand scour volume can be determined and the final sand bed lowering beneath the grout arch (about 1 m in the centre and about 0.75 m at the sides near the shaft walls).

If flow velocity near the sand bed at the well is sufficiently large, a scour hole near the well will develop further, until finally an equilibrium scour depth has been achieved, defined by flow velocity and sand properties.

5 CONCLUSIONS AND RECOMMENDATIONS

The total volumes of water and sand flowing through the well into the construction shaft of the Tramtunnel are defined by the ground water flow conditions below the arch, especially the interstice area and the sand properties (permeability).

It seems that with a hydraulic gradient such as that found at the Tramtunnel, the discharge capacity (maximum flow rate) of the hole does not form a limit, not even for small diameter (<0.10 m).

Due to retrogressive breaching, the interstice layer between grout arch and sand bed can develop immediately and continually, enabling the ground water flow to increase rapidly (assuming a permeability of 5 m/day). Successive scour results in an equilibrium bed slope, defined by sand properties and hydraulic gradient. Since flow velocities may be increased sufficiently further scouring beneath the well may occur until a final depth is achieved.

The time span from well formation to detection and operational measures such as compressed air application (about $3-4$ hours) strongly defines the total volume of water and sand transported through the well. Early detection therefore is important to manage the consequences adequately.

With a permeability of 1 m/day the resulting flow rates are so small that scouring is negligible. The influence of this parameter therefore is strong and in-situ measurements are recommended.

REFERENCES

- Berg, J.H. van den, Gelder, A. van & Mastbergen, D.R. (2002), *The importance of breaching as a mechanism of subaqueous slope failure in fine sand*, *Sedimentology*, 49: 81–95.
- Breusers, H.N.C. (1974), *Bull. Int. Ass. Eng. Geol.*, 10, 65–66.
- Brons, K.F. (1994), *Jetgrouten, sterk wapen in arsenaal funderingen*, Brons, K.F., *Land en Water*, 34 (4), 53–55.

- Kruyt, J., Jong, J. de, Elzen, M.G.A. van den & Feijen, Th.A. (2003), *Southern the Hague: re-design construction method and recent experiences with grout layers*. Proceeding of ITA World Tunneling Congress, Amsterdam, 12–17 April 2003.
- Rhee, C. van, Bezuijen, A. (1992), *Influence of seepage on stability of sandy slope*. *Jo of Geotechnical Engr.*, Vol. 118, No. 8.
- Sellmeijer, J.B. (1988), *On the Mechanism of Piping under Impervious Structures* (Thesis), LGM-Medelingen, No. 96, October 1988.
- Tol, A.F. van, Koster, S., Ramler, J.P.G., Vrijling, J.K. & Verruijt, A. (2001), *Imperfections in jetgrout layers*, Proc. XV International Conference on Soil Mechanics and Foundation Engineering (Togrol et al., ed.). Balkema, Rotterdam, 2001, pp. 1883–1886. Suction of Sand.
- Tol, A.F. van (1991), *Civiele Techniek*, 46 nr. 3, pp. 16–25, *Jetgrouting als alternatief voor grondwaterkering (Ground-waterbarriers constructed by jet grouting)*. Theoretical Hydrodynamics, L.M. Milne-Thomson, Macmillan Press Ltd., 5th Edition, 1968.
- CUR (1992), *Kunstmatig onder water gestorte zandlichamen* CUR rapport 152, Gouda.

The use of the underground space in deltaic areas

Frans B.J. Barends

Delft Geotechnics, The Netherlands

Wim L. Leendertse

Ministry of Traffic, Bouwdienst, Utrecht, The Netherlands

ABSTRACT: The Netherlands is a deltaic area, pre-eminently. The geological stratification consists of typical soft to very soft soils, particularly in the western part. The land surface is flat and the ground-water table is high. For underground construction these conditions are not favourable. Yet, more than twenty tunnels are built, some of them under difficult circumstances crossing large waterways, and few metro lines are built in the cities Amsterdam and Rotterdam. The call for underground solutions to divert the growing traffic congestion and the need for space to save the landscape, natural environment or to promote urban development becomes stronger. The state of the art of underground construction in the Netherlands is illustrated and the national plans for the future are unfolded in this contribution.

1 GEOLOGICAL HISTORY OF NETHERLANDS, A TYPICAL DELTA

The Netherlands are located at the boundary of the North Sea Basin, which is subject to subsidence. During the Quaternary Period the basin was filled with fluvial, marine and aeolian sediments. In Northwestern Europe the Quaternary Period consists of two era's: the Pleistocene and the Holocene Epoch.

The Pleistocene Epoch, 2.5 million to 10 thousand years ago, is marked by several glaciations and interglaciations, with low and high mondial sea levels. Sedimentation was caused successively by fluvial processes and marine processes, resulting in a stratification of alternating sand and clay layers, and locally silty sand or sandy loam.

Aeolic deposits are found as river dunes, so-called "donken", consisting of medium sand, sometimes more than 10 meter thick, meandering through the underground, difficultly to detect.

During the Holocene Epoch, from 10 thousand years until present, a significant temperature rise caused a drastic sea level rise. Sea and river deposits from that period contain a large variety of sediments. In the western part of the Netherlands on the edge of the North Sea Basin sea and river deposits cover completely the Pleistocene formation; it is called the Westland Formation (Figure 1). In the eastern part rivers have cut a trench in the Pleistocene deposits; it is filled with fluvial deposits, referred to as the Betuwe formation.

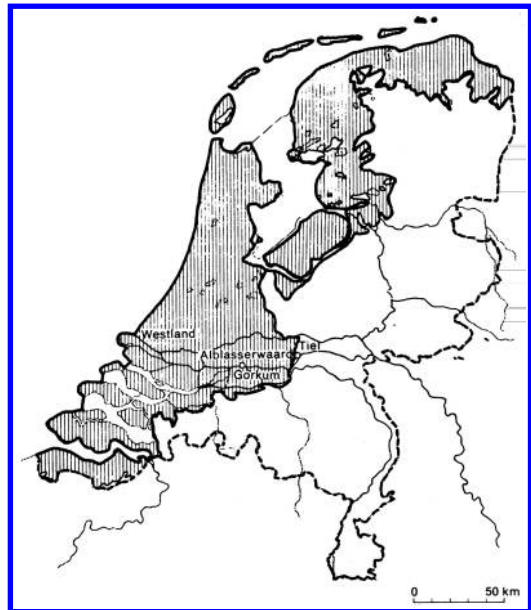


Figure 1. The Westland Formation in the Netherlands.

The Westland formation consists of dune and beach deposits, marine deposits (sandy clay, sand), peri-marine deposits (clay, peat and sand gullies) and organic deposits (peat).

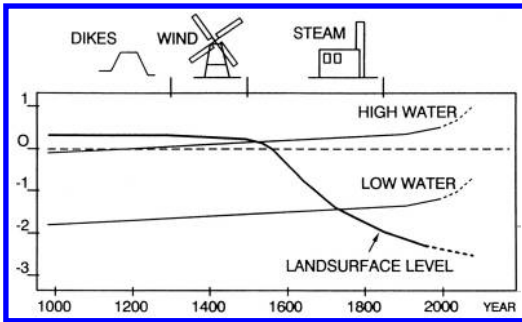


Figure 2. Polder land subsidence in the Netherlands.

The thickness of the Westland formation varies 5 to 15 meter. The Betuwe formation consists of flow belt deposits (gravel and sand), bank deposits (fine sand) and flood basin deposits (clay, and peat). In the southwestern part, the province Zeeland, the Holocene formation is thin and the sand layers are relatively thick and loosely packed.

Many large cities in the Netherlands are located in the western part. At present 24 railway and high-road underground tunnels and metro lines are realised crossing rivers, canals and other main lines in the infrastructure. For underground building the characteristics of the Pleistocene and Holocene deposits are important, i.e. the permeability of the sand layers and the deformability of the soft layers. A particular problem is the strong variation in the Holocene formation.

2 HYDROLOGICAL AND GEOTECHNICAL ASPECTS

The western part of the Netherlands is won from the sea by earthen walls, later polders were reclaimed by dewatering using windmills and dikes. As a consequence the soft soil layers are shrinking, the land surface subsides, and more effort is required to keep the land dry. This process went on for centuries, enhanced drastically when steam and diesel power became available. At present most of the reclaimed land is significantly lower than the sea level (Figure 2). The permanent dike defence system and the entire road and railway system are situated on soft compressible soil, subject to settlements (consolidation and creep), which are non-uniform due to the heterogeneous subsoil stratification. Almost all buildings are founded on piles reaching the more solid Pleistocene sand deposits. For the Rotterdam high buildings piles reach a length of 40 meter.

Pore pressures changes in the sand layers due to tides, artificial dewatering, river discharges, and changes in the surface load (embankments) have a direct effect on adjacent clay and peat layers. Compaction is generated, which causes differential

settlements and additional negative skin friction to existing pile foundations leading to building damage.

Therefore, two problems occur related to the geological profile, particular to underground building in deltaic areas, to wit, leakage in sand deposits and settlement/instability in the weak soil layers. A special matter is the relatively high permeability which causes sizable discharges, unexpected when knowledge about the subsoil is missing. Another special matter is the long term deformation behaviour, i.e. creep. Settlements may continue for decennia, both vertically and horizontally.

Special methods are developed to handle the time-dependent ground water effect for dike and road design, making use of clever measuring techniques to determine essentially global the geohydrological and geotechnical characteristics representative for the heterogeneous subsoil, and a new comprehensive method is developed to account for consolidation and creep in a practical manner [1].

The collection of soil data for these sediments (stratification, mechanical/chemical properties) requires special investigation methods. In the Netherlands two unique field methods are developed and applied with success for many years. One is the CPT (Figure 3a), which is superior to SPT for soft/medium soil. It becomes more and more popular in other parts of the world now. The other one is the continuous sampler (Figure 3b) developed at Delft Geotechnics, a special boring technique which can core without disturbance up to a depth of 20 meter and more. Recently, also geo-electric methods are promising because of the improvement in interpretation by using modern fast computer techniques. In this manner a vast and special experience on field investigation and interpretation methods is gained in the Netherlands, which is valuable for design and evaluation of environmental effects of underground building.

3 CARE FOR THE ENVIRONMENT

National and provincial interests mostly dominate realisation plans for the infrastructure in the Netherlands, although these plans do have an important impact on the social situation of the local population and the environment as well. As mobility and care for transport capacity to the Dutch Mainports are issues of national interest besides the concern of a durable, liveable society, it is inevitable to also incorporate local and environmental aspects in the discussions about alternative solutions for the infrastructure.

Recently studies are performed on the arguments and aspects which play a role in the decision process about underground or aboveground construction of the infrastructure. It appeared that for railroad projects in rural areas the Figure 3. The CPT probe and the



Figure 3. The CPT probe and the continuous sampler.

continuous sampler investment costs are far dominant. A striking example is the recent outburst of discussions about the Betuwe-line, the rail connection of the main port Rotterdam to Germany. It also appeared that

for railroad projects in densely populated areas (within city borders) not investment costs alone, but also environmental care, safety and possible re-use of land are to be considered.

The four track railroad tunnel in the city of Rijswijk, which is under construction, illustrates the fact, that re-use of land for city planning purposes was the particular issue. The discussion on the intended four-track passage through the city centre of Delft will probably end up in a tunnel solution as well.

The environmental issue was much earlier pronounced in the planning of highroad projects. The first to be mentioned is the passage of A27 through an authentic landscape of willow bush of Amelisweerd near the city of Utrecht, some 15 years ago. As a passage was realised as an open tunnel with special measured against traffic noise (Figure 4). More recent is the even deeper open tunnel passage of highroad A2 near Best and Vucht, a section of 6 kilometre realised in 1991.

The two tables on the next page show according to the studies of the national Dutch Working group "Underground Traffic Infrastructure" the main arguments to include the underground alternative as a hundred percent competitive solution for urban or rural areas. Moreover, for the decision process the various environmental aspects are classified and their relevance is obvious.

The choice between under or above ground solutions is strongly dependent on the local situation. It is recommended to incorporate environmental and aesthetic aspects during the entire project development. A solid and well weighted decision is more than the exclusive selection from a limited number of alternatives. For an integral design the purpose should be that solutions are given which satisfy technical and economical requirements and fulfil the social demands.

4 SUBSURFACE USE IN THE NETHERLANDS

In the Netherlands, as in other densely populated coastal and deltaic areas, a serious conflict is arising between care for environment, economics and social demands of the growing population. The government tries to establish a balance between economic development on one side and the creation of a durable, liveable society on the other side. The effective use of the enormous potential on subsurface space seems to inspire a solution.

The use of the subsurface is not new for the Netherlands. In a typical deltaic country, such as the Netherlands, dominated by natural and artificial waterways the tradition is applying tunnelling methods apart from bridges to cross these waterways. Until 1994 some 50 kilometre of highroad and railroad tunnels were completed.

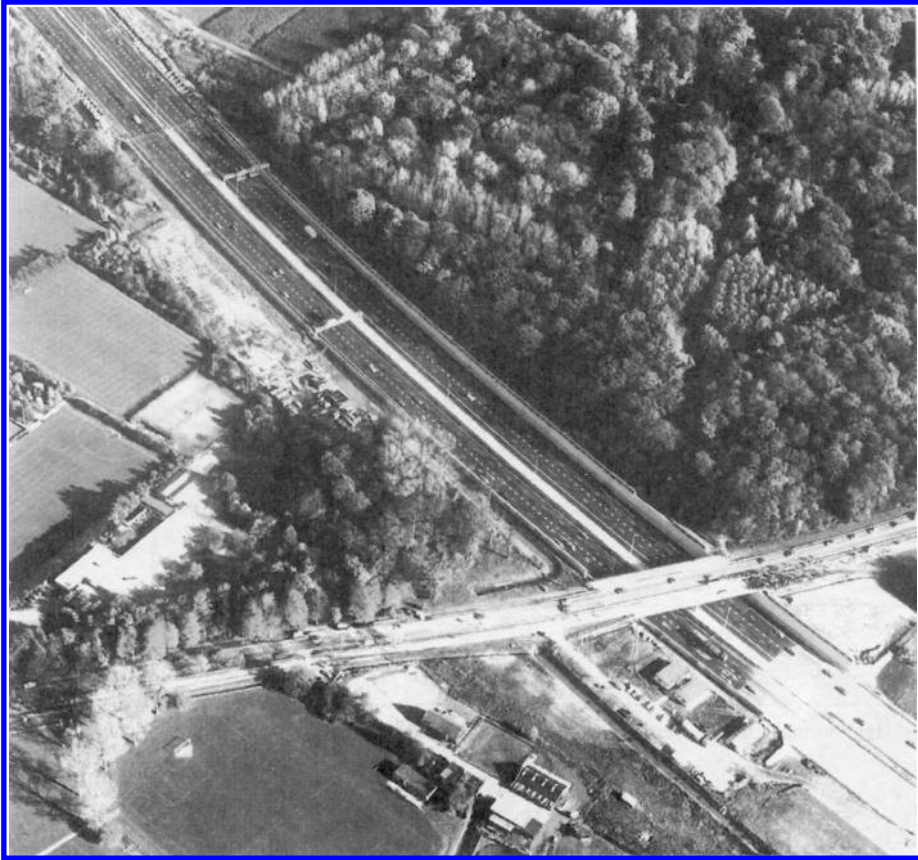


Figure 4. A nature saving open tunnel through Amelisweerd.

The first real tunnel was the Maas-tunnel crossing de Nieuwe Maas in the city of Rotterdam. Based on the principle of immersion of prefabricated tunnel elements as developed in the United States (the first tunnel built by this method was the Michigan Central railroad Tunnel in 1910) the construction of the Maas tunnel started in 1937 and finished in 1942. Rattling machine guns and flying bombs dominated most of the construction period. Celebration was understandably postponed until after the War on 19 May 1945.

Except for the Velsen tunnel most of the major highroad and railroad tunnels in the Netherlands were constructed by the principle of immersion of tunnel elements. Figure 6 gives an overview of all the tunnels completed so far in the Netherlands.

Quite different construction methods were used for the construction of the Rotterdam and Amsterdam subway-lines. In 1968 Princess Beatrix opened the first subway-line from Central Station to Zuidplein in Rotterdam. At that time it was the world shortest metro-line with a length of 3 kilometre and only

seven stations, but the soil conditions are exceptionally difficult.

Between 1970 and 1981 the east-west metro line linking the suburb of Bijlmermeer to the Central Station of Amsterdam was completed. About 20% of the total length of 18 kilometre is built under the old inner city. The tunnel tube was constructed by the so-called "pneumatic caisson" method.

Enormous concrete caissons were erected on ground level, and immersed by excavation of the subsoil under high pressure. The future for Amsterdam promises a modern underground central station where bus, train and metro meet.

In 1971 a start was made with the construction of the east-west line on the right bank of the Nieuwe Maas. Most of the line from Marconiplein till Kralingse Zoom, about 8 kilometre, is situated underground. The construction method was the so called "open trench" or "cut-and-cover" method.

The actual tunnel construction was completed in a temporary trench made of sheet piling and a concrete floor. In Figure 7, a traject from Marconiplein to

MAIN REASONS TO CHOOSE A SUBSURFACE ALTERNATIVE	
Rural Areas	<ul style="list-style-type: none"> - landscape - ecology - noise - loss of precious objects - disturbance in land use
Urban Areas	<ul style="list-style-type: none"> - use and social aspects - noise - safety and risk - air pollution (road projects) - loss of habitats and precious objects

CATEGORIES	ASPECTS
Natural Environment	<ul style="list-style-type: none"> - landscape - water and subsoil quality - ecology
Habitational Environment	<ul style="list-style-type: none"> - vibration and noise - air pollution - safety and risk - social aspects of the environment - social aspects of the use
Land Use	<ul style="list-style-type: none"> - living - working - recreation - agriculture - environmental development
Durableness	<ul style="list-style-type: none"> - environmental quality - energy and use of spare raw materials

The architectural drawing shows a cross-section of an underground station. The ground level is marked with '0'. Below the ground, there are several levels: a level at -1, a level at -2, and a level at -3. The station structure includes a large central hall with a vaulted ceiling, supported by columns. There are also smaller rooms and service areas. On the right side, a surface building with a gabled roof and arched windows is shown. The drawing uses hatching to indicate different materials and levels.

Figure 5. The underground as a city-friendly solution.
The future central station in Amsterdam.

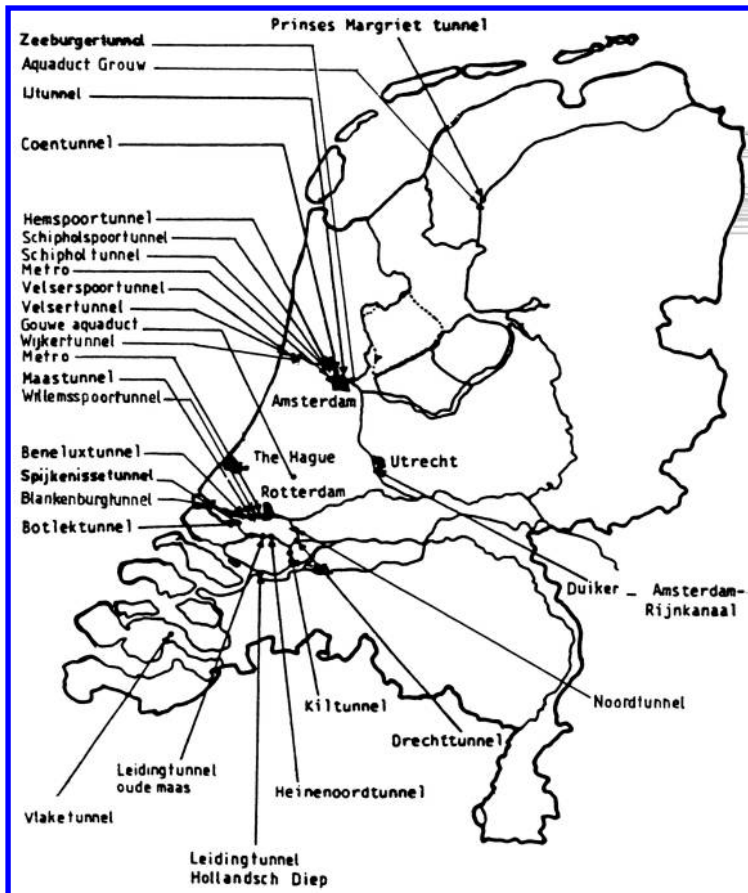


Figure 6. Map of existing tunnels in the Netherlands.

Dijkzigt, it is clarified that the “open trench” method has an immense impact on the surroundings; it actually cuts bluntly through the city, obstructing local mobility (traffic, shopping) seriously. At present the Rotterdam metro-system, above and underground, is with more than 40 kilometre and 38 stations the largest network in the Netherlands.

Apart from an impressive amount of highroad and railroad tunnels some 300,000 kilometre of pipelines are completed in the Netherlands, for gas, water, sewerage and other transport. The pipelines connect the port of Rotterdam, our industrial Mainport, with other industrial areas like Antwerp, Zeeland and the western part of Noord-Brabant. The gas fields in the north of the Netherlands provide gas for cooking and heating to every household through a nation-wide pipe network.

Of special interest is the 700 meter long freshwater transport tunnel crossing the Hartel Canal near Rotterdam (completed 1988). This was the first major diameter tunnel in the Netherlands built by the shield boring method under an existing waterway.

Until now the shield-tunnelling method has not been applied on large scale in the Netherlands. But this is due to be changed. Two experimental tunnel projects are in preparation, the Heinenoord traffic tunnel and the Botlek railroad tunnel, both will be bored with a diameter of 8 metre with a machine as shown in Figure 8. This will enhance experience and specific knowledge on large diameter shield-tunnelling in extremely soft soil. Execution of both tunnels will start in the mid of 1995.

Concerning transport the use of the subsurface in the Netherlands will increase. The Dutch government intends to invest 5 to 8 billion US\$ for the next 15 to 20 years in the construction of new highroad and railroad tunnels; an average investment of 350 million US\$ per annum, 10% of the total investment in infrastructure each year.

Some other interesting facts in the Netherlands can be mentioned concerning underground living, recreation and storage. The School of Art in Maastricht is realised completely underground, and nearly



Figure 7. Tunnel trench through the heart of Rotterdam.

invisible from the surface. It contains educational facilities and a complete theatre. A similar example is the underground Governmental Archives in Den Bosch. The construction of the underground water purification station Dokhaven in Rotterdam is shown

in Figure 9. Finally, some other underground structures realised or planned in the soft Dutch subsoil are:

- Museonder, an underground museum (completed)
- Large parking palace under the Malieveld in the Hague (completed)

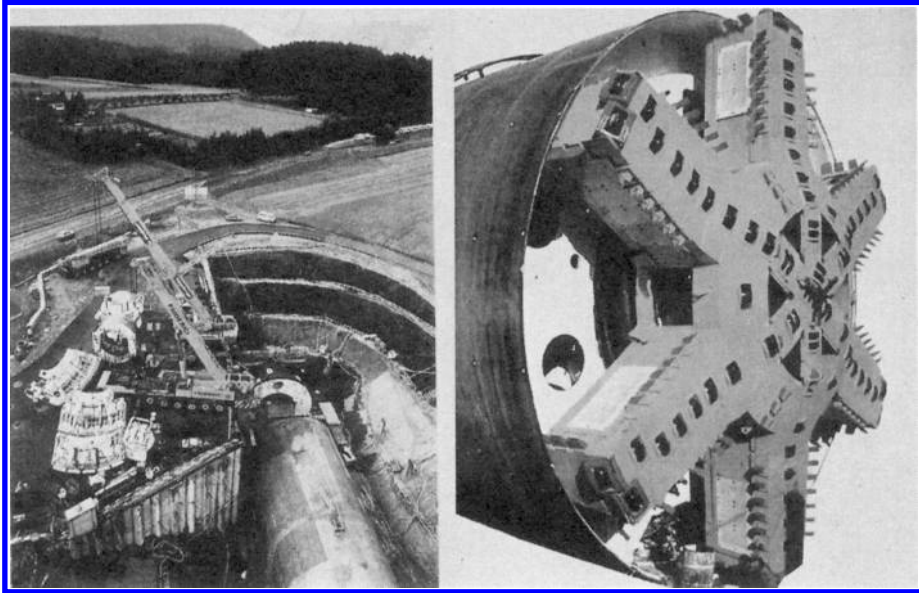


Figure 8. The head of a large tunnel boring machine.



Figure 9. The situation of Dokhaven station.

- Underground storehouse for the shopping centre in the Hague (construction)
- Nuclear waist disposal in underground salt domes (plan)
- Underground energy storage (plan).

5 LESSONS FROM THE PAST

Underground construction in soft soil is realised by one of three methods, the open excavation method, the immersion method, or the shield boring method [3].

5.1 From open excavation to cut-and-cover

The advantage of the open excavation method is that the underground structure with its foundation is build directly in its final position. Costs are relatively low because no auxiliary constructions are required to build the tunnel. For undercrossing waterways special measures are to be taken. The method is then applicable in successive separate excavations and if temporarily lowering the ground-water table is possible.

In the western part of the Netherlands the water table is just below the surface, which means that for open excavation the water has to be lowered significantly. The investigation of this matter is very important. When it becomes clear that drainage will seriously damage the environment, other construction methods, not requiring drainage, should be considered, using cofferdams, sheetpiling or diaphragm walls in conjunction with underwater concrete floors.

In 1930 a combined road and railway tunnel was planned under the North Sea Canal (salty water). This canal was opened in 1876 and linked the harbour of Amsterdam to the North Sea. The construction was stopped during the war, and plans were reviewed afterwards: only a motor vehicle tunnel was to be build, the Velsen tunnel. It would cut through a clay layer at 16 meter depth which separated the salty and fresh ground water regimes. Dredging a trench would disturb the deep fresh ground water quality seriously, so an open excavation method in parts sealed off by a cofferdam, allowing ship passage through the canal, was chosen. The excavation reached 25 meter below surface and a

double dewatering system was installed (Figure 10). The tunnel was opened in 1957.

The geological profile shows thick permeable sandy and silty sandy layers separated by a clay layer. A well test in 1937 provided the geo-hydrological characteristics. The first excavation in 1941–1942 showed that the deep drainage caused more siltation and water pressure drop at a larger distance than foreseen, but the drastic drawdown in the top layer causing large damage was totally unforeseen. Unfortunately, 1953 became a unique dry summer. Finally, the drainage caused more than 100 claims for siltation, grass field and flower desiccation, building damage (up to 30 cm settlement) and 150 trees died from siltation. This experience gave rise to reconsider the construction method.

Because of adverse environmental effects the open excavation method is hardly applicable any more in the Netherlands. A suitable method avoiding temporarily lowering the water table is the open-trench method or the cut-and-cover method, examples of which are given in the previous chapter.

5.2 The immersion method

The principle of the immersion method is based on construction of individual tunnel elements at separate locations (dock). The elements are then transported and immersed in a trench dredged in the waterway which is to be crossed.

As described in chapter 4, the method was applied in the Netherlands for the first traffic tunnel, the Maas tunnel in Rotterdam, which was opened in 1942. Because of the success and the enormous technical and financial advantages, this method became very popular for large tunnel projects under waterways.

Even though the immersion method does not require an open excavation, a drained construction dock is needed. The drainage system for the construction dock for the Vlakte tunnel project, completed in 1975, in the province Zeeland (Figure 11), caused an unexpected large environmental effect due to the strong inhomogeneity of the geological stratification. Claims for agricultural and building damage reached 3 million US\$, being 12% of the total project cost. A positive point is that new techniques for improving

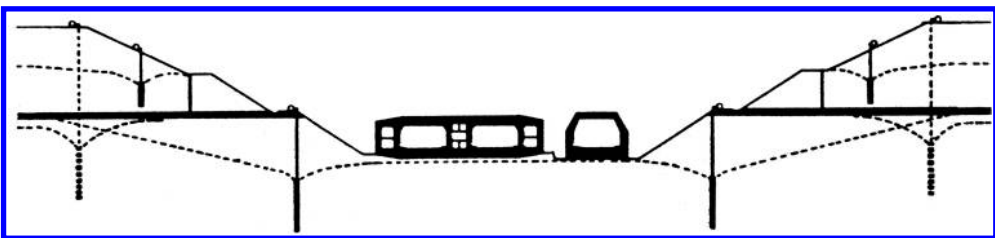


Figure 10. Water drainage system for the Velzer tunnel excavation.



Figure 11a. Environmental damage, settlements; Vlakte tunnel project.



Figure 11b. Environmental damage, desiccation; Vlakte tunnel project.

concrete strength (cooling system) and for the foundation (sand flow method) were applied with great success.

In the same period, the drainage system for the construction of an aqueduct under the Princes Margriet Canal near Sneek in province Friesland, which passes through a semi-confined three-aquifer system (Figure 12), caused even 5 million US\$ of damage and repair cost for building and agriculture. The original

prognosis for the drainage system, 32 wells and 1880 m³/hr, had to be increased to 48 wells and 2400 m³/hr. Settlements caused an additional damage of 0,3 million US\$ to gas and water pipes.

As to avoid this experience a watertight sheet was applied for another aqueduct, the Grouw tunnel, under the same canal, completed in 1992. During installation erosion and sand migration under the sheet caused tear and repair took an extra year and an extra 5 million



Figure 12. The Margriet tunnel in operation.

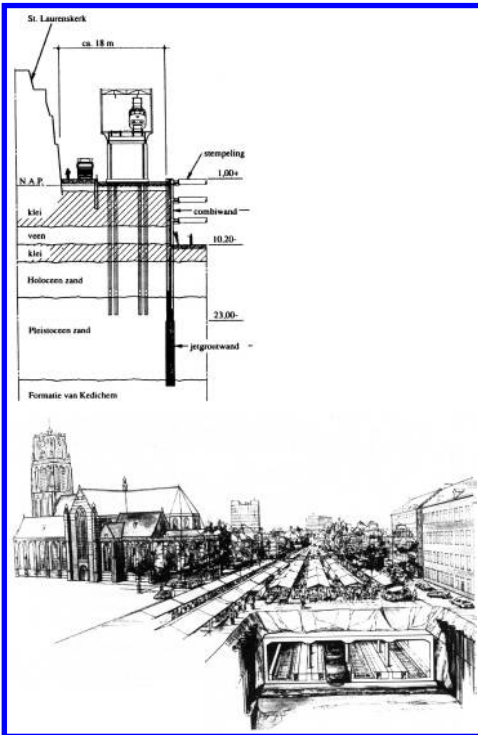


Figure 13. Cross-section and design; Willemspoortunnel project.

USS. Thus, working with a water-tight sheet is possible but requires very careful operation.

A recent example of special protection against the effects of drainage is the Willem Railroad Tunnel in Rotterdam, which runs through the city centre closely along existing buildings, one of which is the monumental St. Laurens Church, build in 16th century and founded on wooden piles. For that section not only a return drainage was implemented, but also the sheet piling of the excavation were prolonged by bentonite diaphragm walls to a deeper clay formation and the construction pit bottom was sealed off by a chemical injection (Figure 13). In this manner the local water-table lowering caused by the dewatering system was reduced significantly. No damage occurred. The tunnel is since 1992 in operation.

In another occasion grouted anchored sheetpiling was used to conduct the waterway during construction of the Gouwe aqueduct (Figure 14). Although calculated and designed with the best means and experience, the anchors broke. The development of horizontal soil stresses (creep) in soft soil is a matter that needs more investigation.

In conclusion, in the deltaic area in the Netherlands the environmental effect caused by dewatering systems for open excavations are sometimes underestimated due to insufficient investigation of the geo-hydrological situation. The geological inhomogeneity and non-uniformity should be better assessed, and the method of pumping tests require a longer duration to determine the proper characteristics. It deserves to improve these investigations, since alternative methods, which do not require drainage are

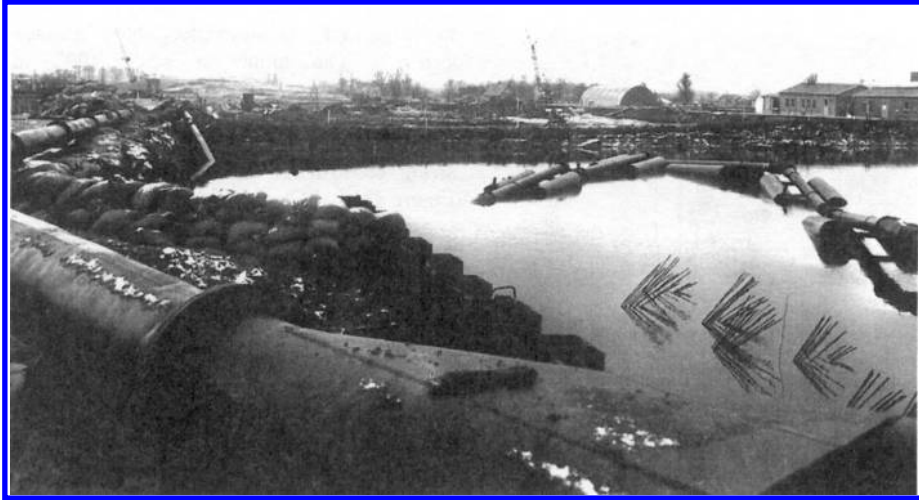


Figure 14. Sheet piling anchor failure at the Gouwe aqueduct project.

expensive, and, last but not least, unexpected damage during construction is even more expensive.

5.3 The shield boring method

The shield boring method uses special boring equipment to build a tunnel underground. The application depends on the geological composition of the subsoil. For conditions like those in the Netherlands the slurry or mixed shield method and the earth pressure balance shield method can be considered.

The slurry shield method uses a bentonite suspension under pressure in the compression chamber of the drilling system. In clayey soils the bentonite is partly replaced by the available clay. This type of boring is reliable and suitable for dutch conditions. However, because of environmental conditions the bentonite must be separated from the excavated soil afterwards and removed.

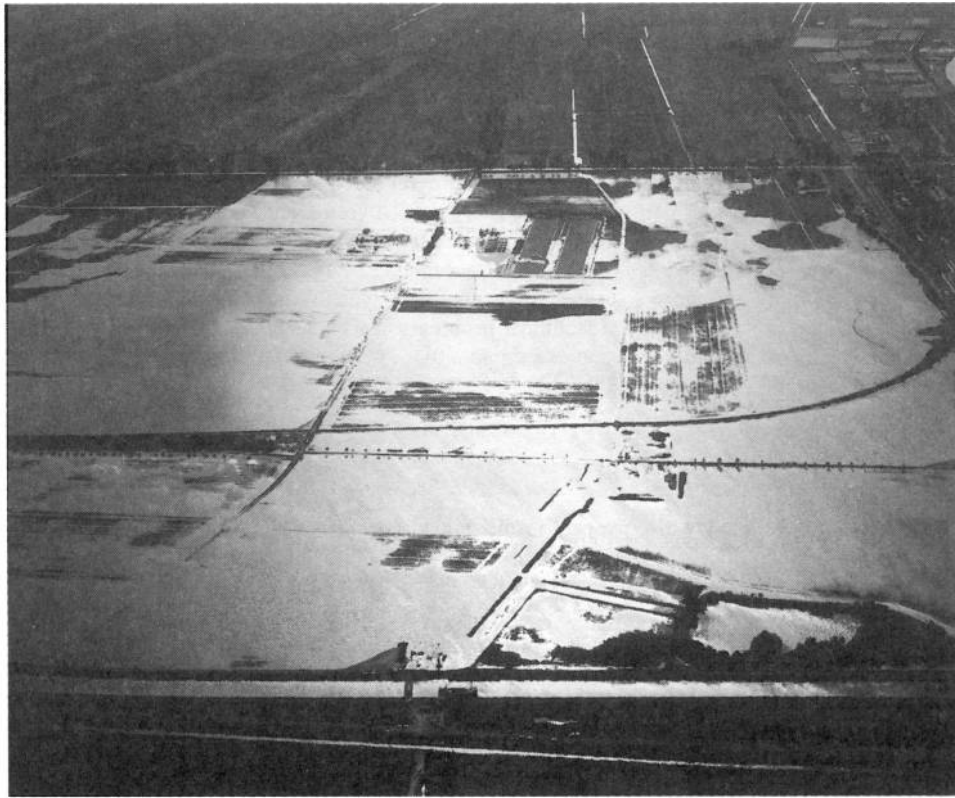
The earth pressure balance shield method uses pressure on the front face. The pressure should be in balance with the mechanical equilibrium, while removing soil. If the pressure is too large the drill moves out of line, too much soil removed leads to subsidence.

Abroad (Japan, USA, Germany) the tunnel boring in soft soils is applied for some time. Only recently the method was applied in the Netherlands: the Hartel Canal water transport tunnel, diameter 1.870 meter length 684 meter, completed in 1988, and the Zuidwillemsvaart Syphon, two tubes of 115 meter length and 2.5 meter diameter, completed in 1990. A mixing shield and earth pressure balance shield method were applied, respectively.

For small diameter tunnels more experience is gained in the Netherlands. Horizontal boring and directional drilling, using pneumatic systems, is a known practice for gas and water pipes under dikes, waterways and roads. Also in this case great care with the geo-hydrological situation is required.

In 1993 horizontal boring under the highroad A12 and the railway near Zoetermeer showed two problems. One concerns the start of the drilling, which may deviate as soon as the heavy drill leaves the start construction pit due to low bearing capacity and creep of the subsoil. It is not easy to correct afterwards. The other problem occurred when a short period too much soil was removed compared to the shield advancement and a significant subsidence (15 cm) took place. The advices: the drilling equipment should be improved by the installation of a back-pressure sensor to the excavated soil directly behind the compression chamber.

Another unlucky experience the same year took place during horizontal boring for a gas pipe under the Wildevanck Canal in the province Drenthe, a diameter of 1.5 meter over a length of 150 meter, through a fine loosely packed sand layer, maximum cover under the canal 2.3 meter. The boring under the canal was almost completed when suddenly the first dike failed. The entire area inundated rapidly, and the work and equipment was seriously damaged (Figure 15). The probable reason is the development of a sand migrating pipe directly under the dike, made possible by slightly over-excavation (earth balance shield method). The canal level being 2.6 meter above surface caused this erosion mechanism that in due time resulted in dike failure and complete liquefaction of the sand layer under the canal.



Copyright: Aerophoto Eelde

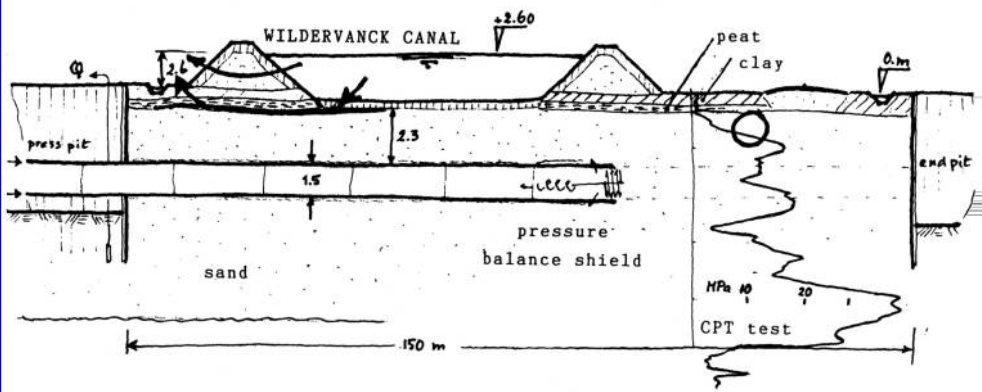


Figure 15. Inundation after dike collapse during underboring operation.

Building tunnels in open construction pits in densely populated urban areas with intensive economic activity and mobility, is more and more regarded as extremely annoying and inconvenient. Often during construction roads must be diverted and existing underground lines relayed. Traffic jams and long

periods of access restrictions to shops cause financial suffer. Also the environmental impact, social acceptance, noise hindrance, and aesthetic values become more and more a serious condition for the construction methods. The shield tunnel techniques have advantages, technical problems can be

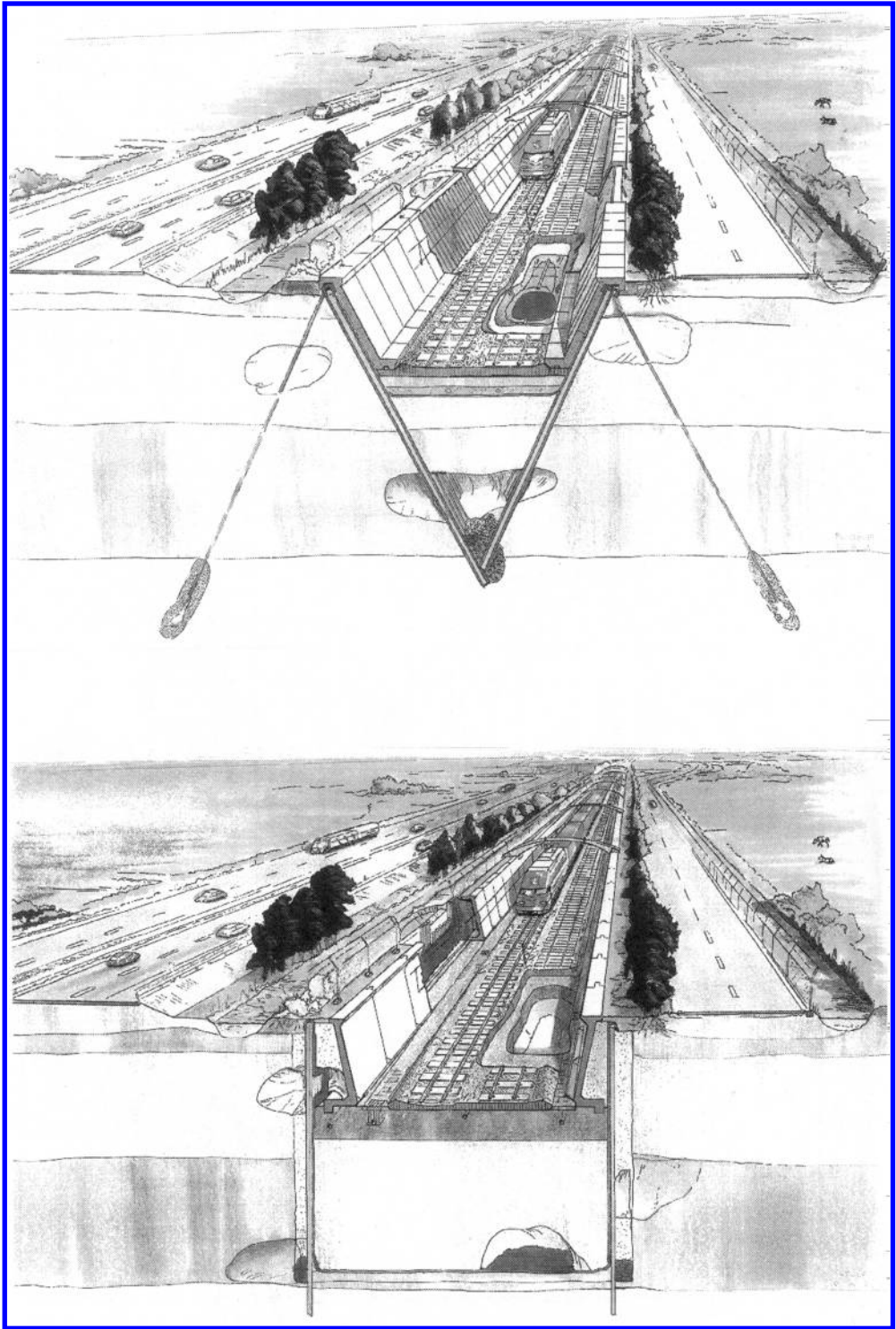


Figure 16. The V-polder concept and the U-polder concept.

Table 1. A research program for underground construction.

Part of the program	Project	Target
I BORING IN VERY SOFT SOILS To gain experience and knowledge on shield-tunnelling in typical Dutch soft soils; to gain insight in the risks of boring	1 Practical research tunnel boring methods	* Knowledge about boring process, risks and validation of existing instruments
	2 Environmental aspects of boring	* Knowledge on ground separation and use of bentonite
II RECONNAISSANCE, PREDICTION AND MONITORING Development of reliable reconnaissance, prediction and monitoring instruments for tunnel construction in soft soils, in order to reduce risks	1 Shallow detection	* Detection up to about 2 meter deep to detect cables and small pile-lines
	2 Deep detection	* 3D-detection down to 50 meter to observe obstacles and to investigate the soil stratification and composition
	3 Monitoring the front of the boring process	* Development of a front-monitoring systems
	4 Vibrations	* Prediction of vibrations; determination of vibration criteria
	5 Numerical simulation models for underground construction	* Development of prediction models for the (environmental) impact of boring; development of prediction models for the soil-structure interaction
III ECONOMIC TUNNEL CONSTRUCTION Optimization and renewing of tunnel construction techniques for soft soils in order to reduce costs	1 Boring tunnels and pile-lines	* Knowledge on dig and ground mixing techniques
	2 New boring technology	* Research towards new boring techniques for soft soils
	3 Industrial trench building	* Research for optimal trench-techniques and cut and cover techniques for soft soil
	4 Robotizing tunnel construction	* Research for possibilities of automation and robotizing of construction, management and maintenance of tunnels
	5 Soil improvement techniques	* Optimization and improvement of ground improvement technique for Dutch soils
IV CONSTRUCTION, MANAGEMENT AND MAINTENANCE Achieving the optimum results for the user, the manager and the surroundings Development of reliable reconnaissance, prediction and monitoring instruments for tunnel construction in soft soils, in order to reduce risks	1 Safety of tunnels during calamities	* Improving insight in the risks of calamities in tunnels (explosion and fire) * optimization of tunnel construction in relation to calamities * Definition of norms and risk levels
	2 Safety and risks of tunnels for the users	* Improving insight in the risks of use of tunnels * Optimization of tunnel construction in relation to calamities * Definition of norms and risk levels
	3 Integral design and integral selection procedures	* Integral tuning of the process of design, construction, use, management and maintenance * Optimum selection of the underground infrastructure with regard to the user, the manager, the surrounding and economic analyses
	4 Management and maintenance	* Uniform management, maintenance and monitoring system for tunnels
	5 Reliability	* Definition of a coherent set of design rules and reliability demands for tunnels
	6 Planning and environment	* Development of models, guide lines and norms for spatial quality (value of use, aesthetic value), for social environmental aspects (visual hindrance, city development, building noise), for landscape and ecology, for air quality (long tunnels, norms, ventilation system, cleaning systems), for noise, for ground and ground water (disturbing soil stratification, use of bentonite), for social aspects of use and labour conditions (transport toxic materials), and for the durability

surmounted, and the tunnel boring method will eventually become a competitive alternative to open excavation and immersion methods in the soft Dutch soils.

6 RESEARCH FOR THE FUTURE

The essential question is which research will indeed contribute to promote underground construction in those situations where it is best. Costs of underground solutions are relatively high, existing methods do not always comply with the demands, and the applicability for typical soft soil conditions is yet more risky, particularly for tunnel boring methods.

Under supervision of the Dutch national working group "Underground Traffic Infrastructure" over 100 specialists from governmental institutes and private companies investigated in 1992 and 1993 the pro's and contra's to above, on, in and underground construction of road and railway connections in the Netherlands [2]. Missing knowledge was listed and translated into a comprehensive research programme.

All aspects which may play a role were systematically considered according to typical project phases: initiative phase, definition phase, design phase, construction phase, and exploitation phase.

For every aspect possible problems were evaluated and compiled into problem clusters. The information is collected in a database together with additional data on costs, time, priority and spin-off. In this manner problem clusters and their coherence could be assessed. The most urgent problem clusters were indicated and relevant research proposals could be defined.

The knowledge infrastructure was evaluated with regard to the existing experience, the availability of specific knowledge (whether operational or not), and the interest for the individual element of the knowledge infrastructure. These elements comprise: governmental institutes and authorities, (private) research institutes, universities, engineering and consulting companies, contractors and manufacturers, research coordinating bureaus and professional organisations.

The complex working field of underground construction, is typically multi-disciplinary. The following disciplines relevant to realising the underground traffic infrastructure are recognised: civil, mining, mechanical, electro-technical, mathematical and chemical engineering, but also economy, laws, planning, and social, cultural and environmental sciences.

Using the collected information and considering the benefits of each research proposal a kind of ranking priority was settled by engineering judgement from various points of view (disciplines), mainly focusing on the decrease of risks in design, finance, execution and exploitation, on optimising the construction concepts, on the decision process for the trace, and on the development of new technologies for monitoring during and after construction.

For the research proposals various disciplines have to work together. Most of the required knowledge is available, but in fragments in the various elements of the knowledge infrastructure. A solid coordinating institution is necessary to interrelate the available knowledge and the different disciplines. This can be achieved in a national centre for underground science, which exist in several countries. In the Netherlands this centre can be connected to an existing research centre, which has a well developed network and a good experience for multi-disciplinary and private-public financed research.

A special chair "underground technology" at the Technical University of Delft is suggested to promote the third dimension in civil engineering and to realise a multi-disciplinary approach involving the various faculties.

There is a need for space for the validation of new techniques. A strong argument is made for so-called "experimental facilities", which provide an opportunity to develop new knowledge and to test new ideas. The experimental facilities are laboratory facilities in technical institutes and universities and, more important, facilities during the execution of large tunnel projects at different locations. In such situations one is able to try out various techniques in a realistic set up.

The research proposals which are of highest importance are compiled and clustered in a "research programme for the future", shown in the table on the next pages. A frame for cooperation between different institutes is suggested and the required budget is estimated. At the moment the Dutch Cabinet has assigned US\$ 20 million for enforcing the knowledge infrastructure for underground construction, the industry is willing to contribute with another US\$ 10 million in the coming five year, and the Ministry of Traffic has chosen two pilot projects: a slow traffic tunnel and a railway tunnel, for both a boring method will be applied in soft soil stratification (clay, peat and sand).

At present also two alternative trench building concepts are tried out: the V-polder concept and the U-polder concept (Figure 16). The V-polder is a drained area ("polder") between two sheet piles in a V formation; the U-polder applies a impermeable sheet in a U-form. If all works well, the state of the art on underground construction and on soft soil tunnelling in particular may proceed a significant step forward in the near future in the Netherlands.

REFERENCES

- Dike Technology Engineering Handbook, Cie Boertien I, TAW, 1994
- "Ondergronds over Wegen" (Dutch), SOVI report, CUR, 1993
- Tunnels in the Netherlands. Holland Book Sales, Helmond, 163 pg, 1990

Unseen features jeopardise underground construction

F.B.J. Barends

*Delft Geotechnics, Delft, The Netherlands, Technical University Delft, CiTG CT,
Geotechniek, Delft, The Netherlands*

SUMMARY: For underground construction the soft and wet soil conditions in The Netherlands are not favourable. Yet, more than twenty tunnels are built, under difficult circumstances. The soil-structure interface and the local soil stratification gave sometimes rise to sudden unforeseen uncontrollable progressive erosion. A trace back to the cause elucidates possibilities to detect such risks in time. Existing tools and facilities are evaluated for their use in such circumstances. Some new ideas and lessons from the past are outlined. It pays off to enlarging our knowledge. Fortunately, the research programmes COB-2 will give ample opportunity.

Keywords: Underground, Soil structure interaction, Failure, Detection, Prediction, Experience, Tunnel

1 INTRODUCTION

Not more than three decennia ago engineering in the building sector was based on safety, uncertainties were covered by wide safety margins (practical intuition, based on historical events). Since then our knowledge about material behaviour grew, and at present the incorporation of uncertainties (risks) are not anymore taboo. They are to be considered in the context of the probability of extreme events and of life cycle. This called for an integral approach, for multi-disciplinary co-operation and functional analysis.

Risk engineering is such a modern approach that fits in the so-called design and built contracts which are becoming the fashion for large infrastructure projects. Which risks may occur? What is their value (consequence*probability)? And who is the 'owner' (risk sharing)? Since in the process of construction (and use) not all assumptions are sure, it is economic and safe to minimise negative effects, to buy them off, or accept them. In this respect the engineer should be able to quantify risks. What do we know? What are our facilities? Particularly in new fields, outside our common experience, unforeseen events are likely to occur. Such a field is the underground construction in soft low lands, the western part of the Netherlands.

The underground is, by nature, a source of uncertainty. How much we do know about the stratification, about the intrinsic properties with respect to mechanical and chemical behaviour, and about the in-situ state with regard to stresses and residual strength. The importance of these uncertainties is underscored by the fact that 40% of structural damage is due to malfunctioning of the foundation and/or the soil;

the annual investments in building in the Netherlands reach beyond 85,000 million guilders. Projects may show an uncertainty of the order of 10%: for large infrastructural projects the risk is even higher, up to 15% of the total cost. If 3% is related features that can be prevented by additional investigation and research, then it is worthwhile to invest (a part of) $40\% \cdot 0.03 \cdot 85,000 = 1,025$ million guilders in risk prevention in the building sector related to soils. But only if we can prove to be successful. How good are we?

Prediction and detection techniques are the tools for a risk assessment; these tools must be adapted and improved for that purpose. Risk assessment quantifies jeopardising events, which may arise during construction and use of underground structures. It allows optimisation in design, construction and maintenance. We can also learn from good cases, even more from bad cases, and from pilot projects where specific effort is put into observation and understanding of the processes and mechanisms involved. In this paper we will focus on the borders of our capability in predicting and preventing (un)foreseen risks, on lessons to learn and opportunities to take.

2 WHAT ARE OUR CAPABILITY BORDERS?

2.1 *Detection*

Our knowledge and experience of soil behaviour is based on detection, prediction, validation and, non the least, failures (malfunctioning). It is essential to know before hand as accurate as required the soil stratification, the existing underground infrastructure

Table 1. Possibilities of NAT (non-destructive detection technique).

Type NDT	Depth	Piles <i>hole</i>	Stone <i>boulder</i>	Peat <i>lence</i>	Clay <i>lence</i>	Loam <i>lence</i>	Silt <i>lence</i>	Gravel <i>bed</i>	Gas <i>pocket</i>	Sand <i>type</i>
From surface or borehole <i>vertical</i>										
CPT + coring	N-F	+?	+!?	+?	+?	+?	+?	+!	+?	+
Seismic	M-F	?	?	?	?	?	?	+?	+?	?
Electro-magnetic	N-M	-	-	+?	-	-	?	?	-	-
Ground radar	N	+?	+?	-	-	-	-	-	?	-
Geoelectric	M-F	-	-	+	+?	?	+?	?	+?	?
Out from TBM <i>horizontal</i>										
CPT + geoelectric	N-F	+?	+!?	+?	+?	+?	+?	+!	+?	+
CPT (+ coring)	N-F	+	+!?	+?	+?	+?	+?	+!	?	+
Ground radar	N	?	?	-	-	-	-	+	?	?
Seismic	M-F	?	?	-	?	?	?	+	-	?

N: near 1–5 m, M: medium 5–20 m, F: far, more than 20 m, ?: probability, +: applicable, -: inapplicable, !: damage

(cables, pipelines, and their purpose), existing foundations (type and condition). Furthermore, the essential mechanical properties (stiffness and strength), the state of stress in relation to the design and execution, obstacles (boulders, gravel lenses, dumped litter, gas pockets), and particular places where leakage, liquefaction, blowouts, slope failure, etc. may occur.

A category of depth of the soil in western Netherlands with respect to detection techniques for the building sector is:

- Shallow (Near): less than 5 meter
- Deep (Medium): from 5–20 meter
- Very deep (Far): more than 20 meter

The common approach is the bore hole method. In the Netherlands CPT was applied already decenia ago; it became popular abroad. It provides point data. The interpolation/extrapolation between soundings is a subjective matter. It fits in a risk assessment approach. It is, however, common to reduce sounding activities drastically (saving cost) and lean on expertise and experience (also subjective). One easily misses local differentiation, which sometimes appears to be essential. Recent innovation in the CPT technique is more related to bio-chemical aspects.

The non-destructive technique by wave energy reflection from the surface or in boreholes is the other way. In recent years great progress has been achieved with microwaves (ground radar) and elastodynamic waves (seismic waves). The high-energy electro-magnetic waves with the radar technique (di-electric soil resistance) cannot be used in clay, brackish and salty zones. The damping is crucial. For the seismic technique the surface wave (and interface waves) is a disturbing phenomenon in the shallow (and sometimes the deep) zone. The resolution (the smallest size to detect) is about 25% of the wavelength. Long waves penetrate deeper, but detect less. Small

waves, with higher frequencies show stronger damping. A detection technique that provides us with proper information about the state (stress, strength) is not available. Much improvement and innovation is yet to be done (see Table 1).

2.2 Prediction

The risk assessment requires facilities suitable to quantify expected behaviour; in other words simulation by numerical models and physical scale models. Physical scale models are important to recognise mechanisms and phenomena, but the extrapolation to the site, in fact the quantification, is limited because of scaling effects. Furthermore, the model cannot obtain the exact state, since we do not know it, and the non-linear soil behaviour cannot precisely be simulated. The geocentrifuge technique can meet the non-linear aspect to some extent (absolute stress dependence) and it can handle complicated situations, i.e. 3-dimensions and soil-structure interaction (Figure 1). The size of the model is limited, and the material used is prepared (artificial). Much knowledge about the applicability of this facility is obtained the last 20 years.

Numerical models, which show a great improvement due to the seemingly unlimited computer power, have their specific limitations as well. The most essential one is the mathematical description of soil behaviour; be aware, it is a fancy! Only selected processes are modelled in an approximate manner (small strains, undrained or drained), and then only the moment of malfunctioning can be simulated, not the failure itself (consequence). The controlling parameters are to be obtained from detection, and most of them cannot be obtained directly. Modelling soil anisotropy, stratification variability, soil-construction interaction, and the sequence of different phenomena (bifurcation, liquefaction) is practically almost

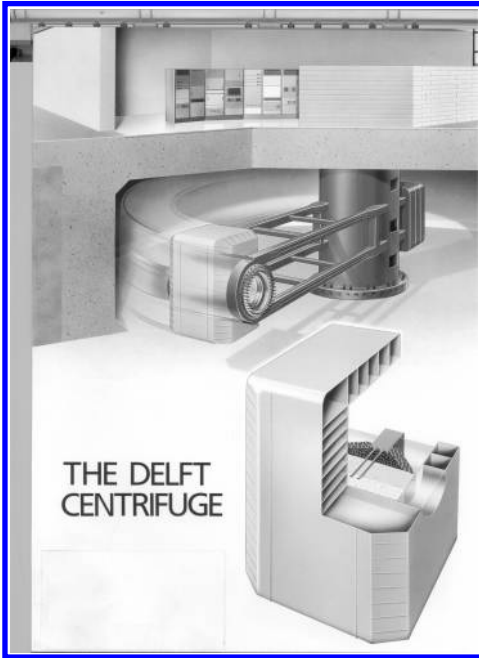


Figure 1. Geocentrifuge facility.

impossible. Moreover, three-dimension modelling has still its limitation.

2.3 Experience

Lessons learned from failures in the past are the hard way. Since optimisation is continuously asked in gradually more complicated situations, more failures will occur, if we do not anticipate and update our knowledge permanently. This is especially true for the soil aspect. In the field of geotechnics our knowledge and facilities are far from complete. In contradiction to concrete and steel construction the soil is a given fact; we do not make a particular soil, such as high quality steel or concrete prefabricated elements of well-controlled quality. Massive soil mixing (cement mixing) is rarely applied in the Netherlands because of the costs. Whether the quality can reach the one in use for concrete is a matter of investigation.

Underground works disappear from the sight, while aesthetic structures rise on top, in full sight. Decay is noticed and restored. What happens underground is unseen. Therefore, the underground works should be solid, less vulnerable to decay or malfunctioning, risks cannot be tolerated.

Our experience in foundation engineering and soil construction works is for a large part empirical. We did learn from mistakes, but when a failure happens, details usually vanish in the chaos that remains. Moreover, nobody likes to be rhetoric on his failure! When

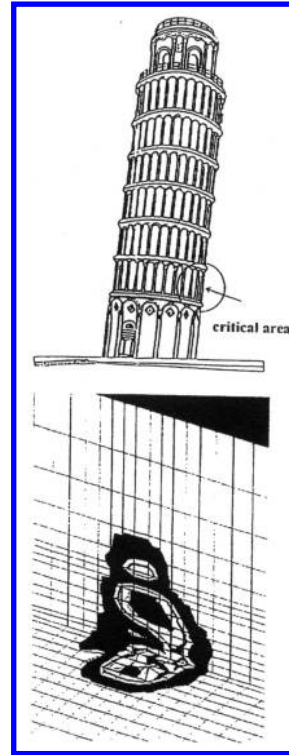


Figure 2. The Pisa Tower, plastic zones after putting counter weight.

a situation is critical, the correct counter measures are difficult to find. A typical example in this respect is the Tower of Pisa (Figure 2), where already 14 committees of experts have tried to put it right. The last news is, the rescue operation will start in late 1998, provided the Italian government can decide on the budget allocation.

In the Dutch situation, soft soils with high water table, a frequently returning cause is loss of stability due to the interaction of ground water, either along structure-soil interfaces or at places of loosely packed sand. Another typical cause is loss of stiffness in soft clay and peat; if the surcharge is high continuous slow plastic behaviour and large settlements are triggered which may take years. A typical example is the dike at Langerak in the Alblasserwaard. Maintenance becomes a burden. That is why the HSL (high-speed railroad) will be founded on piles reaching the stiff Pleistocene sands.

In the national research programme (COB-2) parallel pilot projects are foreseen in the execution of large infrastructure projects. They will give a firm step forwards in the validation of our expertise and experience (Heinenoord tunnel).

2.4 Conclusion

Detection techniques are promising, but several essential soil parameters at a site cannot be measured directly. The resolution of NDT is yet limited (see Table 1). There is ample opportunity for innovation.

Prediction techniques are promising, but they are not complete; numerical and physical scale modelling may show more impetus when used mutually complementary.

Our experience is yet mostly empirical. Validation by pilot projects becomes possible (COB-2). Proper expert information in the ICT-environment will become soon a commodity (ICT = information and communication technology). But we should temper our expectations; comprehension and association cannot be digitised. ICT is an expert support; it will not replace expertise.

A new approach is risk assessment, which uses the available deterministic tools and the detected parameters, but more information is required: the variability of the geology (heterogeneity), the variance in parameters, the stochastics of the loading and the uncertainty of models. The outcome is then a margin of the possible result and, what is important, also the partial contribution of each of the specific uncertainties. The outcome, therefore, gives automatically the priority for improvement.

Our effort should focus on detection methods and simulation methods according to probabilistic techniques. The approach is really different, since all significant failure modes, essential stochastic features and their correlation's should be included, as well as the required margin (safety), which is based on the customer's wishes or the nation's safety demands. This is the way to optimising profoundly. It gives the direction to where we should extend our borders.

3 LESSONS LEARNED AND NEW IDEAS

3.1 General view

A comprehensive review of the Dutch history in sub-surface construction (tunnels, pipelines, underground public facilities) and in the various methods and their shortcomings is presented in the symposium held on the occasion of the 20-years jubilee of the Ingeokring of the Royal Geological and Mining Society of the Netherlands, 3 June 1994 in Delft (Barendse & Leendertse, 1994).

Since that time the Heinenoord traffic tunnel (a pilot project) has been completed, successfully constructed with TBM (8 m diameter slurry-shield). The metro extension in Amsterdam (Noord-Zuid lijn) is under construction and in The Hague the underground shopping-metro area in the centre approaches its completion. Tunnel pilot projects for the HSL and the

Betuwe railroad, and a tunnel under the Westerschelde are being prepared.

1998 is the final year of a five-year national research program (COB-1) in which many parties, involved in the field of tunnelling and underground construction, participated (a budget of 70 million guilders for 30%–50% subsidised by the government). Many aspects have been studied. The knowledge is collected in a large number of reports, which cover logistics, environment, safety, mechanics, detection, prediction, testing, etc. At present a new research agenda is being prepared for the following five years (COB-2).

3.2 Recent events

During the first passage of the TBM under the river Maas a sudden blowout occurred in the Heinenoord project, which forced a delay of several weeks. The probable cause is a geological imperfection in the top layer formation due to the removal of one or more anchor piles, which were used for the construction (immersion method) of the existing highroad tunnel several years ago. This weak spot (filled with sand?) caused a drastic shield pressure drop and drilling stopped. Peat gas pockets could have caused similar problems. How to detect such spots in time, remains an important question.

In the underground project in The Hague a sudden failure of the drainage system caused delay and damage. At a certain location leakage was increasing drastically, but it was not noticed in time. A large central drainage system was designed with sufficient extra capacity, even the excess local water leakage. The spot itself collapsed and the drainage ran out of hand. The tunnel section had to be inundated in order to make repair possible.

3.3 Challenging problems

Problems in the tunnel-boring sections in the Amsterdam metro-project are related to negative influence on existing pile foundations. The local stress state may be affected such that the structures on top will be damaged. In the Heinenoord experimental tunnel project a test pile field was placed and investigated for this purpose. Also predictions have been performed with numerical and physical models (geocentrifuge, Figure 1), which showed the sensitivity of bearing capacity in relation to an at certain distance passing TBM.

This stress/deformation influence is a complicated problem. It is typically three-dimensional. Moreover, the influence of water/consolidation is not to underestimate. Measurements at the Heinenoord project have revealed that before the shield significant pore pressure increments occurs. If this is not accompanied by a similar total stress increase, which is

obviously not the situation in all directions, effective stresses may decrease and soil strength (shear resistance) may become insufficient causing unwanted deformations or even local failure. How to control these phenomena out from the TBM?

3.4 *A scouting eye*

Pilot borings for large diameter tunnels and horizontal directional drilling can be realised by the use of a horizontal borehole datalogger ('tracker'). The concept was elaborated within the COB-research programme. A test for a span of 100 m at 8 m depth was promising.

A cone can be instrumented with sophisticated facilities to scan the area, horizontally out from the tunnel front, before the shield ('prick nose'). This has been recently applied for a 2.5 m diameter jacketed tunnel. The trial was so successful that more measurements, particularly at locations of uncertain geological stratification, were executed. In ten tests into the sand layer a rare claybody (old water pit?) and a PVC-pipeline were found. The results are still to be worked out (Van Deen, 1998).

3.5 *TBM as a source*

Another idea is proposed: to use the TBM as a seismic source and to use surface detectors in a sophisticated way. This has been applied for the Heinenoord TBM within the COB-research program. Results are promising (Fokkema, 1998).

3.6 *Physical models*

In the frame of the collective research program COB the geocentrifuge at Delft Geotechnics has been applied for various predictions. The special equipment for a specific centrifuge test is usually an important part of the budget. A set of auxiliary equipment, specific for tunnelling (mini-TBM, with special devices), has been collected and developed to save cost for new tests.

3.7 *Numerical modelling*

The performance of advanced numerical models is promising. Various calculations have been worked out, prediction as well as postdiction. A co-operation with a Japanese consultant (GRI/Osaka-GD/Delft) for tunnels is settled, in particular the support with advanced numerical simulations (Dutch sophisticated calculation models: PLUTO and DIANA). The accuracy of such simulations can be best shown on the problem of the leaning Tower of Pisa, one of the best benchmarks for such an evaluation. In 1994 led blocks were placed on the higher part of the foundation slab in order to reduce the tilting. The weight of the led

increased the tower weight by 4% and decreased the tilt moment by 10%. The outcome was unsure. Prediction of three-dimensional behaviour by Delft Geotechnics in 1993, using Camclay soil behaviour, showed an inclination of 5.42° and a reduction of 0.12° due to the counter weight. The additional settlement was calculated 1.90 mm. Other predictions by the University of Rome (Calabresi c.s., using American model CRISP) showed a reduction of 0.08° to 0.16°. Knowing that the 1994-leaning is 5.48° and the measured outcome of the led weight is a tilt reduction of 0.094° and an additional settlement of 2.09 mm, gives us strong confidence that such models, if calibrated well and fed with proper data, are capable of simulating the initial state and special effects in complicated situations, fairly well. In Figure 2 three-dimensional simulated plastic zones are shown of the 1994-state. The practical result is simply: a well calibrated rotational incremental spring stiffness: $(2.8 \pm 1.0)10^5$ MN-m/rad, and vertical incremental spring stiffness: $(5.0 \pm 2.9)10^3$ MN/m valid for a range of about 0.25° (Jamiolkowsky, 1994). This is used for the evaluation of further restoration activities.

3.8 *The role of ground water*

A comparison of failure cases shows that for most situations there exists a significant static (ground)water loading. In many cases an unseen interior erosion process took place along existing interfaces, which ultimately caused a sudden progressive collapse. Only in some situations signals were noticed, mostly shortly before the collapse, and sometimes the signals were not immediately understood as a forewarning, because the proper behaviour for quite some time. Investigations afterwards often show that the situation is caused by a combination of several unfavourable factors, such as local low relative density directly beside a rigid structure, a large static pore pressure drop, internal migration or regressive erosion (piping), and induced (small) deformations. Monitored data of the development of unexpected failure is seldom. It is, of course, a problem to account for the unexpected during the design and construction, or the operation phase.

It is remarkable that the ground water is such a common factor in failure. It may gradually change the local conditions, stimulated sometimes by large pressure drops. This process takes place slowly, seemingly unimportant. A deep building pit is usually wet (at least in the Netherlands), if not from rain then from normal leakage (through sheetpiling). So, local erosion by ground water is hardly noticed. Mostly it is self-healing or stays limited, nothing happens, nobody knows something could have happened. However, denly a progressive process starts, and in short time a disaster develops.

It is yet possible to see this process in time. We should be able to pinpoint before hand the most

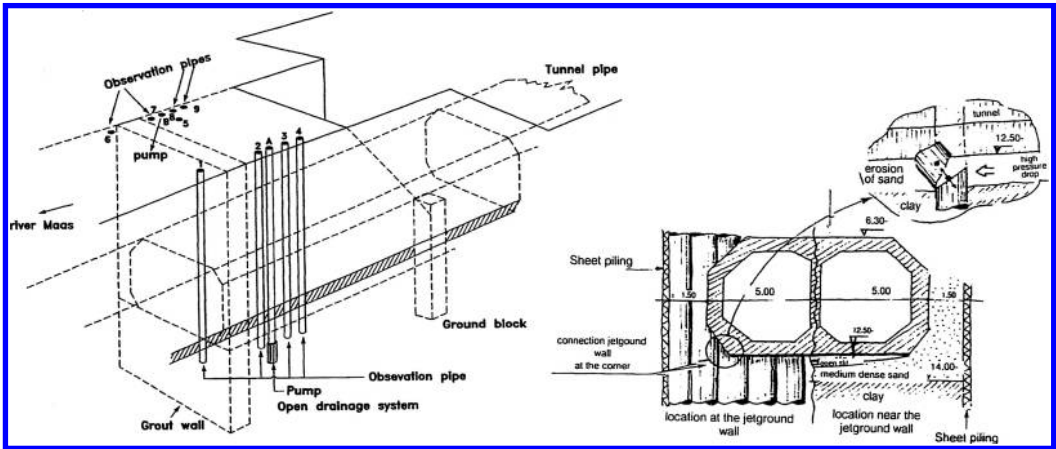


Figure 3. Metro-station building pit over an existing and operating metro tunnel, near the river Maas.

sensitive locations. A suitable monitoring procedure can give proper information and it can show the moment when counter measures are required. The collapse of a temporary retaining wall at the metro-station project at the Wilhelmina Pier in Rotterdam, is such an example.

4 LEARNING FROM A POSTDICTION

4.1 A typical collapse

In 1995 a grout-column retaining wall protecting a deep building pit near a river, collapsed suddenly after months of proper behaviour. A new metro station is being built around an existing metro tunnel while train services are uninterrupted. Investigations revealed that a combination of several factors gradually caused a critical situation: leakage, consolidation, erosion, piping, pump failure, column fracture. By chance pore pressures have been measured continuously, and afterwards, they show the unseen gradual process of local deterioration, which took place along the interface of the existing metro tunnel and the subsoil.

It is worthwhile to mention, that, if the erosion process would have taken two month more, probably nothing would have happened, as then the construction phase would not allow for.

4.2 The Wilhelmina metro station

The metro tunnel itself is built in the sixties applying the sink-in-trench method using prefabricated tunnel segments of 10 m*6.2 m*90 m. The foundation consists of special vibropiles with their heads lifted under water by jetgrout after placement of the segments. The tunnel leads the metro under the river Maas in Rotterdam. It operates properly.

In 1994 construction operation started to make a large underground metro station at the Wilhelmina Pier, Rotterdam, in the river bank, while the metro services are uninterrupted; a complicated engineering task. The metro station has been opened officially by the Dutch Minister of Traffic, Public Works and Water Management in spring 1997. It is the deepest metro station in the Netherlands (Figure 3).

4.3 Construction stage

The building pit reaches a depth of 11.5 m. One should keep in mind that the soil is very soft and the water level is stationary high. To prevent leakage several measures have been taken, such as grouting the slit under the existing tunnel (an opening of more than 15 cm was found), installing a solid retaining combi-wall, a deep pumping system and around the existing tunnel a wall of grout-columns of 1.8 m diameter by the VHP-grouting technique. Under the tunnel the closure was realised by boring a thin pipe through the tunnel at night. A sketch of the situation is shown in Figure 3.

To test the water tightness of the grout-column retaining wall a local shallow pumping system is placed. It has been in operation during the construction. Measured pore pressures show the development of the unseen process (Figure 4). During November 1994 until February 1995 the system functioned well; no clear evidence was observed that anything would go wrong. Several safety systems around and in the tunnel worked properly. No excessive displacements occurred.

4.4 Unexpected problems

However, in February 1995 after five month of correct behaviour, water inflow was noticed, a pump broke

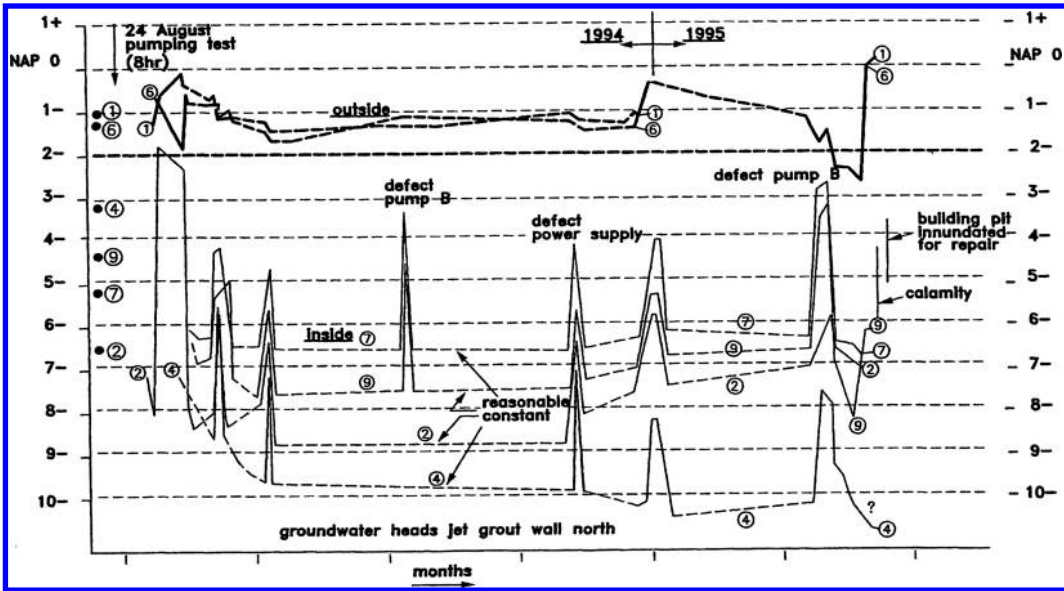


Figure 4. Measured pore pressures at the water tight grout-column retaining wall.

down, quite some sand inflow was noticed, and after a temporary repair the grout-column wall locally collapsed and the mud and water inflow could not be stopped. Finally, the building pit had to be put under water in order to repair the grout-column wall properly.

4.5 Investigation

During the investigation afterwards all possible causes have been considered, such as seepage under and around the wall, leakage through the walls, stability and strength, flow under the existing tunnel, functioning of the pumping systems, climatic effects (rain, high river levels), vibration due to building activities (pile driving), inhomogeneity of the subsoil, and the quality and control of applied materials and construction methods.

The conclusion is that an unfortunate combination of several factors led to the critical situation, and that it was hardly possible to understand that something was going on. The grout-column retaining wall was correctly functioning. Some minor leakage was noticed already from the beginning, but this could be handled easily by the installed pumping system. Since the wall had to function temporarily, the leakage was acceptable. This is usual practice for temporary structures.

The leakage and a probably small deformation of the deeper clay layer due to the deep pumping system (head drop of about 12 m), may have given place to regressive erosion of the sand under the existing tunnel (piping), which is founded on piles in the sand layer

underneath the clay. Small water and sand inflow could hardly be noticed during the excavation and construction works (open pit, it rained regularly). It is assumed that with time the sand directly behind the wall under the tunnel at the sides was eroded, and that under the large water pressure drop (about 10 m), in the absence of local soil support, some parts of the grout-columns fractured, giving rise to a strong mud flow.

4.6 Valuable measurements

It is a coincidence that during the entire period the pore pressures in eight observation pipes, installed in the critical zone, have been monitored. This information gives valuable insight afterwards (Figure 4).

Firstly, a pumping test with a duration of 8 hours was considered to have reached a sufficiently steady state. However, the permanent response of the same situation is significantly different. A pumping test of 8 hours is too short. The standard practice to shorten pumping tests to save cost and time is not advised.

During October to the end of December everything worked properly. At the new-year recess, something went wrong with the pumping system, and in January the pore pressure field has slightly changed. A groundwater flow simulation afterwards shows the difference in the corresponding porous flow pattern (Figure 5): the leakage is more pronounced around pump B. Unfortunately, pump B collapsed in the beginning of February. Additional pumps, quickly installed, could not solve the problem. They may have increased porous flow and erosion.

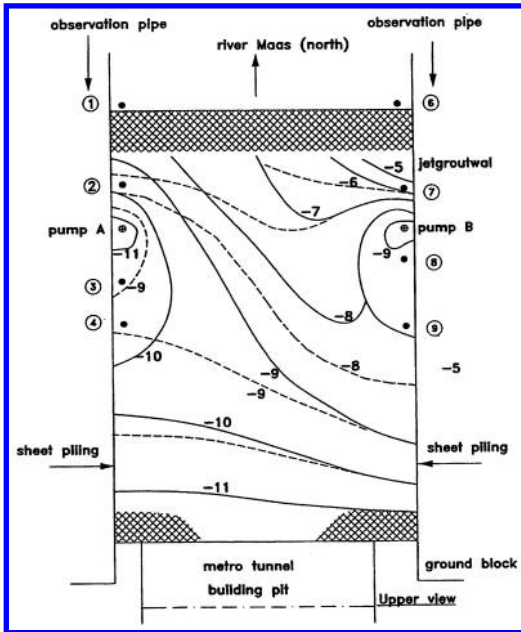


Figure 5. Flow pattern changes due to unseen leakage-induced erosion.

It is to be said that the changes in the pore pressures and porous flow pattern, noticed during the investigations afterwards, were at the time not alarming at all. Everything looked in order. No particular significant leakage or mudflow from under the tunnel was observed. The grout-column retaining wall was properly designed and its strength in combination with the soil support was sufficient. So, one may argue who ever could or should have known before hand, that such a failure would take place.

4.7 Conclusion

Finally, it is learned from this example that it is worthwhile to continuously monitor the pore pressures around a building pit wall, which retains a large water pressure, particularly when in contact with existing structures. The silent erosion process, mostly occurring along interfaces between soil and structures or between different soil types, may be noticed before a failure will occur, and proper counter measures can be taken in time.

5 VALUES AND EXPECTATIONS

5.1 Value of research

Does research pay off? Is it worthwhile to invest in innovation? The answer is a strong and firm yes! The

cost of delay in a construction process or of repair after malfunctioning are very high in comparison to the cost invested in research, even if a successful R&D-product is not always guaranteed. Is it necessary to prove that research is useful? In fact, not! But it is justified to do; money can be spend only once.

In Annex I a statistical analysis is elaborated on the financial interest of applied research products, based on a limited number of practical cases (R&D-projects by Delft Geotechnics). The emphasis is on the cost of R&D product and implementation versus the cost reduction by their application to a specific case. The products are representative for the field of geotechnical engineering (special CPT, numerical model, pollution detection, piping, monitoring, etc.). The result of the evaluation is that R&D cost is only 2.2% of the benefit (savings) due to the use of it, including the unsuccessful R&D trials (only 10% success is assumed, 50% would be more realistic; this is not important!). It, however, does not include the cost for the proper ambience: general facilities, education, and knowledge maintenance to be able to do R&D, and the cost of implementation in a specific project. If we include this, the percentage would be at least twice: 4.4% (interest 2300%).

In the introduction it was stated that any budget under 1025 million guilders is worthwhile to invest in R&D, to prevent some of the annual damage cost in the building sector related to geotechnical aspects. The present annual public investment in the geotechnical R&D sector is estimated to 12 million. With 4.4% this will in average produce $12/0.044 = 273$ million project cost savings per year by R&D implementation. In comparison to the budget of 1025 million, this 273 million is only 25% of what would be economically profound.

In conclusion, we can state that public R&D-investment in geotechnical sector is 75% too low; 48 million should do. It may save up to 1,000 million. This is significant. For the coming period the government plans to invest yearly 9,000 million guilders in the infrastructure and transport (MIT report: more-year-program infrastructure and transport, Dutch Ministry of Traffic and Water Management) and there is an extra 12,000 million for budget exceedence¹ on projects in execution and new initiatives. Investment in R&D in geotechnics gives a profit far better than any financial market (2300%).

¹ The Betuwe railroad estimated at 2,500 million in 1990 is now estimated to cost over 9,000 million, and some economists state that it will rise even to 15,000 million. Such boost of costs is for a significant part due to political developments (saving environment, granting local demands, choosing for innovative methods), and for another part to underestimation of uncertainties. The project is still subject of a vivid discussion.

5.2 COB-research agenda 1999–2003

The agenda of the research program COB-1: 1995–1998 has been outlined (Barends & Leendertse, 1994). Much of the goals and foreseen innovations have been achieved. In the Netherlands a solid base for a knowledge infrastructure for underground construction has been founded, due to this collective, open, and precompetitive program. In the new research program COB-2: 1999–2003 the main topics are:

- technology program (missing knowledge elements, required R&D).

REFERENCES

COB (*Centrum Ondergronds Bouwen*) CUR/COB Büchnerweg 1, PO Box 420, 2800 AK Gouda, The Netherlands, tel.: 031-(0)182 540 660, email: cob@cur.nl

- Delft Geotechnics. (1993) *Pisa-Toren berekening & validatie PLUTO-3D*, report: SE-57013 (in dutch)
- Fokkema, J.T. (1998) *Seismic NDT from TBM to surface*. Technical University Delft, CiTG, Geosciences, Delft, private communication
- Jamiolkowsky, M.B. (1994) *Leaning Tower of Pisa, description of the behaviour*. Lecture KIVI Geotechniekdag, 3 Nov. 1994, Utrecht
- Van Deen, J.K. (1998) *Application of the scouting eye (speurneus)*, Delft Geotechnics, Delft, private communication
- Van den Berg, P. (1998) *COB-2 Research program*, Delft Geotechnics, Delft, private communication

ANNEX I Interest of R&D investment in the geotechnical sector

The following table shows the benefit of 12 research projects implemented in practice (source Delft Geotechnics).

Case	Field	Foundation		Dynamics		Underground		Environment		Dikes		
I Investment	0,2	0,6	1,4	0,07	0,4	0,1	0,1	0,1	0,2	0,2	1,5	1.0
S Savings	10			0,25		0,1	1,0	0,5/j	250	1,4	150	
U Use		0,2	10		100			10		100		1400
B Benefit	50	0,3	3	3,5	250	1	10	50	1250	250	100	1400

I, S, U in MFI; **B = (S ∨ U)/I**; **I**: invested R&D without overhead; **S**: direct savings in a project; **U**: indirect savings (if without R&D) The average investment $I_m = 0.486$ MFI (million guilders). The exceedence $P_{B>X}$ can be elaborated:

	<i>Chance</i>	<i>Effect</i>
$P_{B<1} = (1 - P_{B>1})$	0.08	No benefit
$P_{B=1}$	0.08	Even
$P_{B>0}$	1.00	All cases
$P_{B>1}$	0.84	Benefit
$P_{B>10}$	0.58	Fair benefit
$P_{B>100}$	0.42	High benefit
$P_{B>1000}$	0.08	Extreme benefit

Statistical elaboration yields:

$$P_{B>X} = 0.9 - 0.109 \ln(X) \quad \text{or}$$

$$X = \exp(8.28 - 9.2P_{B>X})$$

So, 50% of the cases with R&D application will have benefit of $B > 39.7$. It means that a profit of $39.7I$ in 50% in building projects is achieved, or in average at least 19.3 MFI (a lower limit!).

The unsuccessful cases (they cost money):

$$P_{B<=1} = (1 - P_{B>1}) = 1.0 - 0.9 = 0.1$$

The value per case of applied R&D is therefore defined by:

$$V = \int_0^{0.9} PXIdP - \int_{0.9}^{1.0} (1 - P)XIdP$$

with $P = P_{B>X}$

Elaboration gives, assuming $I = I_m$:

$$V = (46.5 - 0.038)I_m = 22.58 \text{ MFI} \quad \text{and}$$

$$B_m = 46.46$$

The cost of unsuccessful cases (no profit) is very small (maximum $0.038I_m$). This gives automatically also the effect of non-implemented R&D studies; they will not cost more than unsuccessful ones. If we assume that 10% of the R&D studies will be implemented, The effect will be that for each project 10 R&D trials are not implemented, or $0.38I_m$; so, the value becomes per case:

$$V = (46.5 - 0.38)I_m = 22.41 \text{ MFI} \quad \text{and}$$

$$B_m = 46.12$$

The cost of unsuccessful R&D is negligible. The profit is high because of the cost of infrastructure projects is high. The relevance of R&D is trivial; the researcher's zest to application is sufficient for success.

Managing soil deformations due to tunnelling in the Netherlands

J. Brinkman

GeoDelft, Delft, The Netherlands

ABSTRACT: All the work that has been and will be done in the field of soil deformations in the Netherlands can be put in a risk management perspective. In early nineties the bandwidth for prediction and controlling tunnelling was far too large to start tunnelling in the sensitive ancient inner cities of the Netherlands. One can say that to narrow this bandwidth a risk management process was started by visiting Japan in 1991. In 2002 the bandwidth has been narrowed to such an extent that tunnelling the North-South Metro Line in the sensitive ancient city centre of Amsterdam is feasible. In this process the “innovation circle tool” has been applied. For two examples the innovation circle will be given: for grouting and for EPB face stability. A brief overview on soil deformation research in the Netherlands in relation to the different tunnelling projects is given. Finally a general overview is given for the present Dutch situation, this is an interpretation of design procedures of the different projects from a risk management point of view.

1 INTRODUCTION

Over the last decade the Netherlands has invested considerable effort in tunnelling. In the early nineties the idea of the appliance of large diameter shield tunnels in the Netherlands was born from the shortage of space, the increasing road congestion and the growing economy. At that time, on the initiative of J. Kruizinga, a Dutch delegation under the leadership of Prof. A. Verruijt visited Japan. In Japan an enormous number of shield tunnels in relative similar alluvial soil conditions was already been constructed. A few years later it had decided that the first large diameter shield tunnel in the Netherlands would be constructed: the second Heinenoord tunnel. At this point of time only limited knowledge about shield tunnelling was present in the Netherlands. Germans mainly did the design and construction of the second Heinenoord tunnel and even the TBM was built in Germany.

In 1994 a nation-wide foundation was formed with the Centre of Underground Construction (COB). The government sponsored this initiative because to gain knowledge and experience in the field of tunnelling of soft soil was important for the Netherlands. Among the COB members are contractors, engineering consultancy companies, universities, research institutes and governmental organisations.

In this paper first the settlement control is put in an overall view on the Netherlands risk management control perspective over the last 10 years. Hereafter is dealt with deformation control in the different project phases.

2 RISK MANAGEMENT ON SOIL DEFORMATIONS DUE TO TUNNELLING

All the work that has been en will be done in the field of soil deformations can be put in a risk management perspective. In early nineties the bandwidth for prediction and controlling tunnelling was far too large to start tunnelling in the sensitive ancient inner cities of the Netherlands. One can say that to narrow this bandwidth a risk management process was started by visiting Japan (figure 1). In 2002 the bandwidth has been narrowed to such an extent that tunnelling the North-South Metro Line in the sensitive ancient city centre of Amsterdam is feasible. In this process the “innovation circle tool” has been applied. This is a balanced continues innovative circle of field

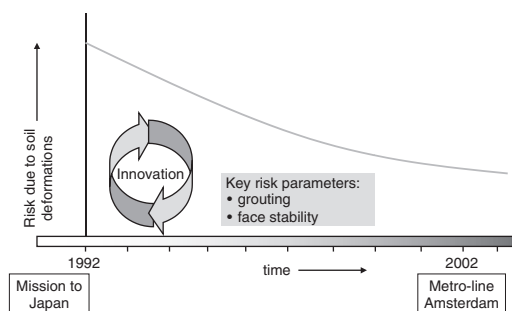


Figure 1. Reduction of risk due to soil deformations as a function of time.

observation, numerical modelling and model tests, resulting in a lower risk level.

3 KEY RISK PARAMETERS FOR SETTLEMENT CONTROL

Relatively soon in the Heineoord shield tunnel project it became clear that the tunnelface and the grouting process were the two key risk parameters in the settlement risk management. Considerable research has been conducted in the years after to get a grip on these aspects. As they are the keys to successfully reducing the bandwidth of settlements. For two examples the innovation circle will be given: for grouting and for EPB face stability.

The innovation circle for grouting (figure 2):

1. The only way to get a good match between FEM calculations and the measured soil deformations of the Heineoord tunnel was the introduction of grout pressures in the calculations. For the grout pressure 4 hypothetical grout pressure distributions were used. The type of distribution around the tunnel and the change in time was the important factor [COB 2000].
2. The next step was the development of the DC-grout-pressure distribution calculation model [Talmon 2001].
3. Model test were parallel to the development of the calculation model conducted. The aim of the tests was to get a better understanding of the physical properties of the grout flow and the change in physical properties due to water dissipation and hardening. Also a joint research with Japan was conducted which resulted in the appliance of ETAC grout in the second tube of the Botlek tunnel [Feddema 2001].
4. In the Botlek shield tunnel grout pressures and soil deformations were measured. With 2D FEM

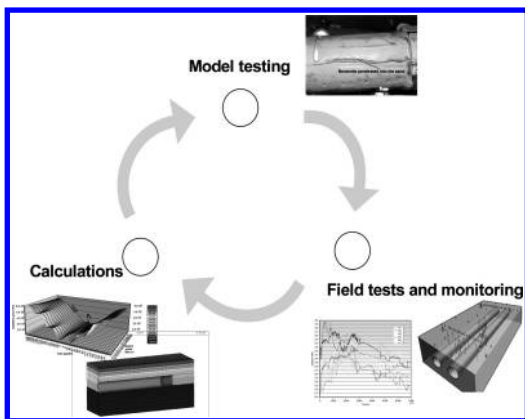


Figure 2. Innovation circle for grouting.

model based on the grout-pressures predictions, postdictions and back analyses were made. The same was done with the DC grout-pressure distribution model.

5. From risk management prospective the grout pressure is still a key risk parameter. In 1999 a joint Delft Cluster and COB research program for the Sophia Tunnel was started. In this program the DC-calculation model is further improved, model test are conducted and field measurements are done [Bezuijen 2002a]. The aim is the use of the grout pressure distribution in a 4D FEM model in which the progress of the tunnelling is incorporated. With this model the soil displacements can be predicted. These deformations can then be used for the impact analysis ground deformations on buildings. This research is conducted in close relation to the North-South metro line as they are going to use the results in their risk management system.

For the Heineoord shield tunnel the face stability for a slurry shield has been researched. This has resulted in the detection of a new significant mechanism of the build up excess pore pressure in front of the TBM [Bezuijen 2001 and Broere 2000 & 2001]. This new mechanism has been incorporated in a calculation model that is now used in daily practice. An EPB shield has been used for the Botlek tunnel and there is not much knowledge in the Netherlands about face stability for an EPB. As face stability is a key risk parameter this research was conducted by the contractor and COB. In figure 3 an innovation circle has been drawn for this problem.

The innovation circle for EPB face stability:

1. Model experiments conducted using foam, simulating the drilling with an EPB shield [Bezuijen 1999 & 2001]

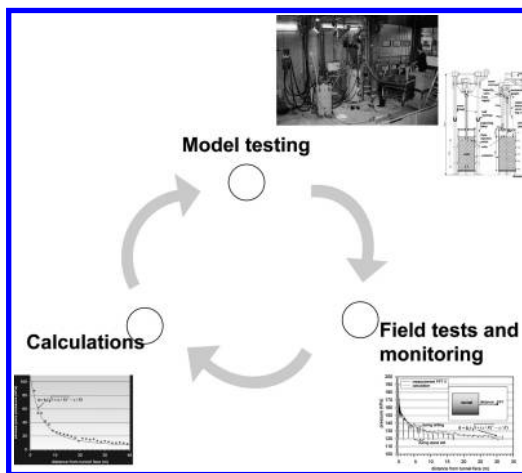


Figure 3. Innovation circle for EPB face stability.

2. Based on the results a calculation model was suggested
3. In the field in front of the Botlek EPB shield also excess pore pressures were present [Fugro 2000]
4. Based on this the calculation models of have been further developed [Bezuijen 2002b].

4 OVERVIEW OF RESEARCH

In figure 4 a brief overview on soil deformation research in the Netherlands in relation to the different tunnelling projects is given. This overview is not intended to be complete but to give a good impression.

5 PROJECT PHASES

In the different project phases of a tunnelling project, different approaches to handle soil deformations are used. Of course each project has its project specific demands. So a more general overview is given for the present Dutch situation, this is an interpretation of design procedures of the different projects from a risk management point of view. In figure 5 a general idea is given of the development of risk during a project.

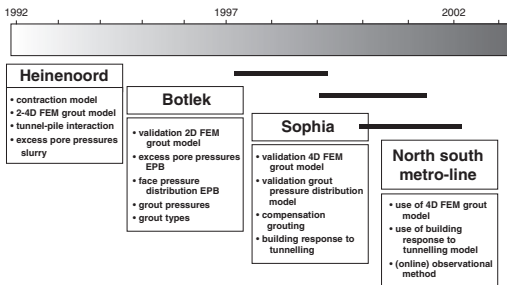


Figure 4. Research on soil deformation in relation to tunnel projects.

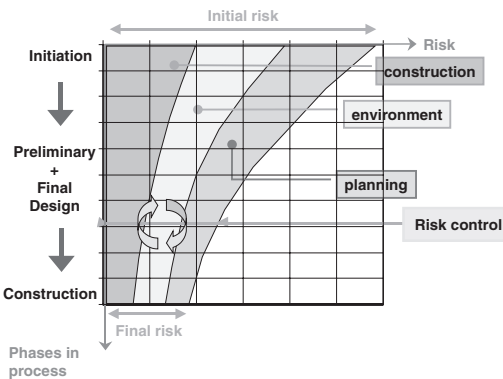


Figure 5. Development of risk in a project.

In this simplified example the risk is built up from 3 components; construction, planning and environment (like politics, imago and permits). The project phases are the initiation, preliminary design and final design and construction phase. These phases will be described in detail below. To get a risk reduction risk control should be applied. In each phase the risk analysis has its place, see figure 6.

5.1 Initiation phase

At the start of a project not everything is known like alignment, soil conditions, TBM type, diameter and the sensitivity of the surroundings. At this time the bandwidth in costs is far higher than in the construction phase.

In this phase empirical relations found in literature and the experience with another tunnelling project in the Netherlands is used (COB Experience database). In this way it is possible to get a quick insight in what to expect. This means that the bandwidth in expected settlements is large in this phase and the knowledge of its impact on the surroundings small.

To optimise the investigation/design process and make it possible to answer the different questions in the further phases a first risk analysis is made. Most of time this is done by putting some experts on the different fields together in a room and let them decide what the project specific risks are (quantified in time, money, and imago). By doing so in the early stage of a project one can make a risk management control strategy for the key risk parameters in the different project phases.

5.2 Preliminary design

In this phase the first soil investigation results are available and there are more details known. So from the experience database a more narrow selection can be made of what to expect. In this phase the first 2D FEM models are applied to see what deformation are to be expected under specific project conditions. And

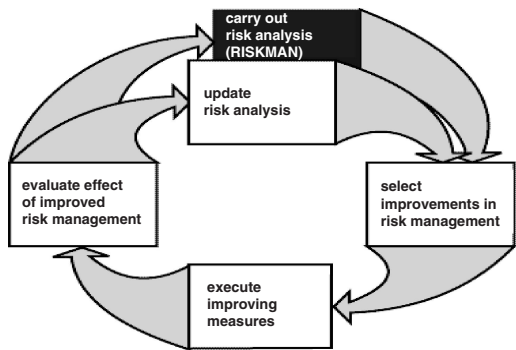


Figure 6. Riskman-cycles [RISKMAN 2002].

of course the risk analyses are updated with the latest information. From this the strategy for the next steps is derived. Sometimes this means that special research has to be conducted to manage specific risks.

5.3 Detailed design

In this phase most commonly 2D FEM calculations are performed for all the bored sections. The results of these soil calculations are sometimes also directly used in the design of the lining. For the location with a high risk profile there are 4D FEM [COB 2000 & Teunissen 2001] analyses conducted. In this phase grout model test are conducted and grout is designed to meet to project requirement. This means that an optimal grout pressure distribution has to be designed. And of course the risk analyses is updated with the latest information.

5.4 Construction phase

Part of the detailed design phase is setting up a monitoring philosophy for the construction phase based on risk management. Some parts of the design can still be so sensitive that the optimal way to manage it is the appliance of an observational method. To get a good idea what bandwidth in soil deformations are to be expected for instance a level 2 probabilistic approach can be applied. In this probabilistic approach the 2D-grout model can be used as the bases for finding the deformation bandwidth. The soil properties (Youngs modulus, angle of internal friction, soil weight and groundwater pressure) and the grout pressure are the stochastic parameters. This analyses result in a bandwidth of settlements for each boring section. The same type of probabilistic analyses can be applied on the face stability. From this analyses sections with higher changes on face instabilities are detected. These analyses make it possible to monitor the key risk parameters for relevant mechanisms at the relevant locations and optimise the monitoring. Further a strategy how to use this information in the tunnel boring process management can be made. In some cases the needed reaction time can be so short that it leads to an online monitoring system option like in the North-South metro line tunnel has integrated in the tunnelling process.

5.5 Evaluation phase

In this phase the observations and the experiences are summarised in reports put in the COB tunnelling experience database. Back analyses are made and new tunnelling models are tested to improve the prediction models for the next project.

CONCLUSIONS

The development of knowledge in the field of tunnelling over last decade has reduced the risk related to soil deformations.

The alternate use of field observation, model test and calculation models (innovation cycle) has proven to be a powerful tool in increase the knowledge and there by reducing the risk.

REFERENCES

- Bezuijen A. 2000. Model experiments using foam, simulating the drilling with an EPB shield, *GeoDelft report CO-51010*.
- Bezuijen, Adam & Brassinga, E., 2001a. Blow-out pressures measured in a centrifuge model and in the field *Proc. Int. Symp. on Modern Tunneling Science and Techn. Kyoto*.
- Bezuijen, Adam, Pruiksm, P. & Meerten, H. van, 2001b. Pore pressures in front of tunnel, measurements, calculations and consequences for stability of tunnel face *Proc. Int. Symp. on Modern Tunneling Science and Techn. Kyoto*.
- Bezuijen A, Talmon A.M, Kaalberg F.J. and Plugge R. 2002a. Field measurements on grout pressures during tunnelling *Proc. 4th Int. Sym. on Geotechnical Aspects of Underground Construction in Soft ground, Toulouse*.
- Bezuijen A. 2002b. The influence of soil permeability on the properties of a foam mixture in a TBM *Proc. 4th Int. Sym. on Geotechnical Aspects of Underground Construction in Soft ground, Toulouse*.
- Broere W., Tol A.F. van 2000. Influence of infiltration and groundwater flow on Tunnel stability. *Proceedings International Conference on geotechnical aspects of underground constructions in soft grounds*.
- Broere W. 2001. Tunnel Face Stability & New CPT Applications. Ph.D. Thesis, *Delft University of Technology, Delft University Press*.
- COB 2000, Tweede Heineoordtunnel Evaluatie rapport report *K100-6 COB, Gouda*.
- Feddema A, Möller M., Zon W.H. van der and Hashimoto T. 2001. Geo Research Institute, Osaka, Japan ETAC two-component grout field test at Botlek rail tunnel. *Proc. Int. Symp. on Modern Tunneling Science and Techn. Kyoto*.
- Fugro 2000, Botlek railway tunnel. Evaluation K300/GT. Stresses and deformations in subsoil (in Dutch). *Fugro report: M-0813*.
- Riskman 2002 Riskman-cycles www.riskman.nl
- Talmon A.M, Aanen A, Bezuijen A. & Zon W.H van der, 2001. Grout pressures around a tunnel lining. *Proc. Int. Symp. on Modern Tunneling Science and Techn. Kyoto*.
- Teunissen J.A.M., Brinkman, J. 2001, Three dimensional numerical simulation of tunnelling *Proc. Int. Symp. on Modern Tunneling Science and Techn. Kyoto*.

Influence of pore pressure at tunnel face

Einfluss des Porenwasserdrucks auf die Stabilität der Tunnelbrust

A. Bezuijen

GeoDelft, Delft, Niederlande

GeoDelft, Delft, The Netherlands

ABSTRACT: The influence of groundwater flow in front of a tunnel face is investigated for a tunnel bored in saturated sand. It is shown that groundwater flow hampers the plastering of the bentonite slurry in front of a slurry shield. Consequences for the stability of the tunnel face for minimum and maximum face pressure are discussed. Groundwater flow increases the minimum allowable pressure and decreases the maximum allowable pressure and thus decreases the 'pressure window' that can be used by boring a tunnel.

Groundwater flow also has an influence during the grouting process for a tunnel drilled in sand. The consolidation of the grout, determines the pressures on the lining. Consolidation of grout is measured in an element test. Traditional calculation methods over predict the stresses on the lining for a tunnel drilled in stiff sand (up to a factor of 5) by not taking into account the consolidation of the grout.

RÉSUMÉ: Für den Bau eines Tunnels wurde der Einfluß der Grundwasserströmung auf die Stabilität der Tunnelbrust untersucht, der in gesättigtem Sand gebohrt wurde. Grundwasserzufluß hemmt die Filterkuchenbildung der Bentonitsuspension vor dem Hydroschild. Die Konsequenzen für die Stabilität des Tunnelbrust bei minimalem und maximalem Stützdruck werden beschrieben. Der Grundwasserzufluß erhöht den kleinsten zulässigen Stützdruck und verringert den größten zulässigen Stützdruck. Folglich wird der Bereich des anwendbaren Stützdruckes (das 'Stützdruckfenster') verringert, mit dem der Tunnel gebohrt werden kann.

Die Grundwasserströmung hat auch Einfluß während das Einbringen des Verpressmörtels. Die Konsolidation des Verpressmörtels bestimmt den Druck auf die Tunnelwandung. An einem Tunnelement wurde die Konsolidation des Verpressmörtels getestet und gemessen. Traditionelle Berechnungsmethoden überschätzen die Spannungen auf die Wandung eines in steifem Sand gebohrten Tunnels (bis zum 5-fachen Wert), wenn die Konsolidationswirkung des Verpressmörtels nicht beachtet wird.

1 INTRODUCTION

The soil is incorporated in the design of tunnels by calculating the soil pressures that are exerted on the tunnel and pressures necessary to have a stable tunnel face. Pore pressures are taken into account, but generally only a hydrostatic pressure distribution is assumed. However, the construction of a tunnel uses liquids pressurized with pressures different from the hydrostatic pressure: bentonite slurry at the tunnel face and grout mortar at the tail void. This will lead to excess pore pressures. Knowledge of these excess pore pressures appears to be of importance for the stability of the tunnel face and the final pressures on the lining.

This contribution describes the origin of the excess pore pressures in front of the tunnel face and also deals briefly with the influence of water flow in the grout mortar on the final pressures on a tunnelling.

2 PORE PRESSURES AT THE TUNNEL FACE

2.1 Background

Shield tunneling started only recently in the Netherlands, the soft soil conditions and the high water table in most of the country are difficult conditions for this technique. The first tunnel bored was the 2nd Heineoord tunnel, just south of Rotterdam. To increase the knowledge of the processes involved when boring a tunnel in soft soil, a measurement campaign was set-up. Part of this campaign was measuring the pore pressures in front of the tunnel face.

2.2 Measurements

Pore pressure gauges (PPTs) were mounted in the tunnel track as a part of the measurement campaign.

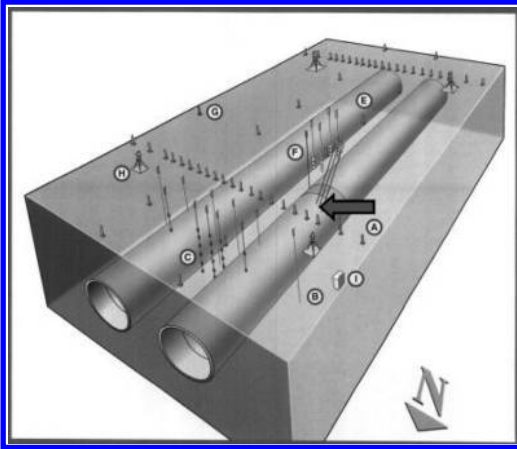


Figure 1. Artist impression measurement field. The arrow indicates the pore pressure gauges in front of the TBM. Results of the gauge in the middle are used this paper. (Bakker et al. 1999).

The total instrumentation, measuring deformations and pressures, in one of the measurement fields is shown in Figure 1. The PPTs in the tunnel track were in use until their destruction by the TBM. Results will be discussed for a PPT located in sand. Excess pore pressures were measured in front of the TBM during drilling. However, the pore pressure decreased until hydrostatic pressure when the drilling stopped.

The result of one of the gauges is shown in Figure 2. When the TBM reaches the PPTs, the passing of the cutters on the TBM can be seen in the measured pore pressures as variations in the pressure. The pressure decrease during a stand still can be seen in the 3-D plot, Figure 3, where the pressure is presented as a function of both the distance from the tunnel and the time. From this plot it is clear that when there is no progress in the drilling (the distance remains constant) the pressure decreases. The pressure starts to increase when drilling started then the distance between the gauge and the tunnel decreases.

The measurements show that there is a plastering of the tunnel face by bentonite when drilling stops, but that there is no plastering during drilling. The reason for that will be explained in the next section.

2.3 Pressure calculations

If there is no plastering of the tunnel face at all, it is possible to calculate the excess pore pressure by means of groundwater flow computations. The actual 3D boundary value problem reduces to a rather simple problem if we calculate the pressure in front of the tunnel at the tunnel axis, assuming a constant excess pore pressure over the tunnel face, a homogenous soil and no influence of the surface. For such a situation

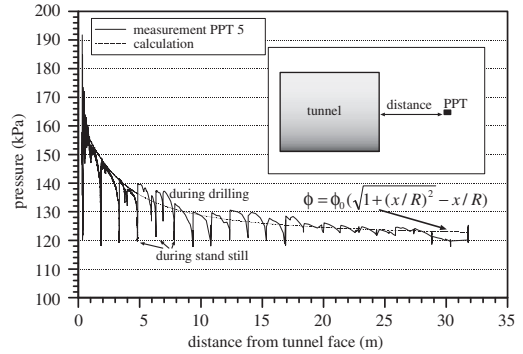


Figure 2. Measured excess pore pressure in front of a slurry shield and approximation.

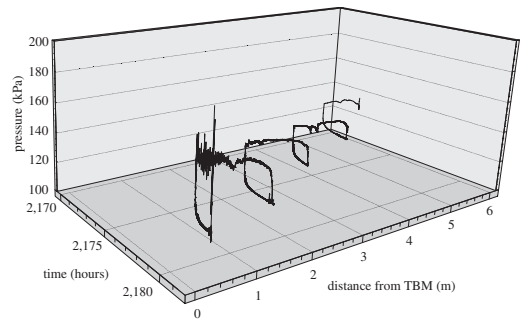


Figure 3. 3D presentation of the measured excess pore pressure in front of a slurry shield.

the solution of the piezometric head at the tunnel axis leads to:

$$\phi = \phi_0 (\sqrt{1 + (x/R)^2} - x/R) \quad (1)$$

Where ϕ is the excess piezometric head above the hydrostatic level at a distance x from the tunnel face. ϕ_0 the excess piezometric head at the tunnel face and R the radius of the tunnel. This solution is plotted with the measurements in Figure 2 and showed good agreement.

With this solution it is also possible to understand why the bentonite at the tunnel face cannot provide plastering during drilling. The hydraulic gradient in front of the tunnel can be calculated by taking the derivative of Equation (1). At the tunnel face ($x=0$) this leads to the equation with i the hydraulic gradient. The pore water velocity (v_p) in front of the tunnel can be written as:

$$i = \phi_0 / R \quad (2)$$

with i the hydraulic gradient. The pore water velocity (v_p) in front of the tunnel can be written as:

$$v_p = \frac{ki}{n} \quad (3)$$

where k is the permeability of the sand and n the porosity. When a tunnel with a diameter of 10 m (5 m radius) is drilled in sand with a permeability of 10^{-4} m/s and a porosity of 40% (average values for this tunnel), the velocity of the pore water will be $2.5 \cdot 10^{-4}$ m/s. Bentonite cannot penetrate faster than the velocity of the pore water. If the drilling advances with 1 mm/s, this means that the drilling goes faster than the bentonite penetrates. Bentonite will penetrate, but every time a cutter of the rotor passes, it will take away all bentonite and there is no possibility to form a filter cake.

This means that the excess pore pressure measured is not caused because the bentonite does not plaster well enough. It is caused because drilling goes faster than bentonite penetration into the sand for this tunnel.

2.4 Plastering

When drilling stops, a filter cake will build up due to the mud spurt and consolidation of the bentonite slurry (Bezuijen 1997). Using the results of experiments (Huisman 1998) and the permeability of the soil, it is possible to derive the course of the pressure in the soil just in front of both the tunnel face and the slurry cake when drilling stops. At the axis close to the tunnel face there will be 1-dimensional flow. In that situation the pressure, written as a piezometric head, in front of the tunnel due to the mud spurt (the most important mechanism) can be written as:

$$\phi_{ms} = \frac{x\psi + nk_{ws}\phi_0 + k_s(\phi_0 - \Gamma x)}{x\psi + nk_{ws} + k_s} \quad (4)$$

where ϕ_{ms} is the piezometric head in the soil in front of the tunnel face, ϕ_0 is the piezometric head at the tunnel face, x the distance the bentonite has penetrated into the soil, n the porosity, k_{ws} the permeability of the consolidated slurry, k_s the permeability of the soil for slurry, Γ the ratio between applied piezometric head and final penetration of the bentonite slurry as measured in a plastering test, in which bentonite penetrates into a sand sample using a predefined pressure difference (Huisman, 1998). ψ is the 1-dimensional flow resistance in the soil in front of the tunnel without bentonite (caused by groundwater flow only) and is defined as:

$$q = \psi(\phi_{ms} - \phi_\infty) \quad (5)$$

with q the specific discharge and ϕ_∞ the piezometric head at a large distance from the tunnel ($=0$ when the

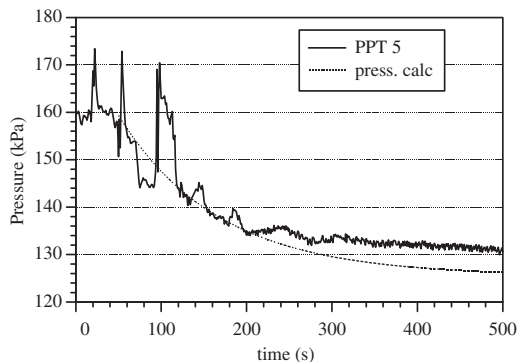


Figure 4. Measured and calculated pressure in the soil in front of a tunnel face during a stop in the drilling when a filter cake is built.

other values are presented as excess values). Since the thickness of the bentonite layer that penetrate into the soil during the mud spurt is very small compared to the dimensions of the tunnel, this layer can be neglected to determine ψ . Using equation (2) and Darcy's law $q = k \cdot i$ it is found:

$$\psi = k / R \quad (6)$$

x in Equation (4) varies with time and is determined by the amount of slurry that has flown into the soil and can be solved using the equation:

$$\frac{dx}{dt} = \frac{q}{n} = k_s \left(\frac{\phi_0 - \phi_{ms}}{x} - \Gamma \right) \quad (7)$$

To check the validity of these equations the results of PPT 5 measurements were used during the last drilling stop before the gauge was destroyed by the TBM. The result is shown in Figure 4 together with the result of a calculation using the measured Γ (133) and $\phi_0 - \phi_\infty = 3.5$ m, $n = 0.4$, $\psi = 2.5 \cdot 10^{-5}$ 1/s, $k_s = 5 \cdot 10^{-5}$ m/s and $k_{ws} = 2.5 \cdot 10^{-8}$ m/s. The result showed reasonable agreement apart from pressure peaks that are present in the measured signal, probably because the rotor is still turning. Analysing laboratory results Huisman (1998) found that better agreement between measurements and calculations could be obtained if also the blocking of the pores by bentonite particles is taken into account by an empirical blocking factor. These field data do not clearly prove the need for such a factor.

3 CONSEQUENCES FOR STABILITY

Calculation methods for the stability of the tunnel face normally do not take into account the influence of excess pore pressure on the stability. It is generally assumed that the pressure at the tunnel face

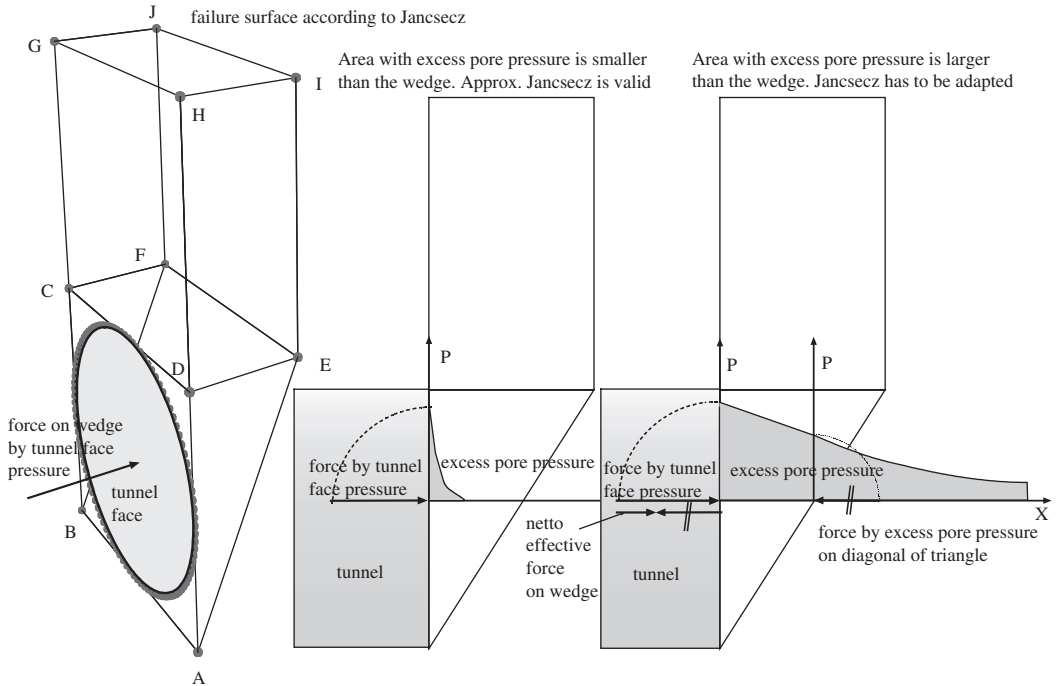


Figure 5. Sketch, influence of pore pressure on stability tunnel face. What is mentioned about the approach of Jancsecz is also valid for the other “wedge shaped solutions” mentioned in the text.

is directly applied to the grains, which means that implicitly a perfect plastering is assumed. Using the wedge shape failure mechanism as suggested by Horn (1961), Anagnostou & Kovári (1994) and Jancsecz & Steiner (1994), the influence of the excess pore water can be explained, see Figure 5. The figure shows a 3 dimensional plot of the failure surface and two 2 dimensional cross-sections. In the left 2 dimensional cross-section the situation as assumed in the various calculation methods is presented, the cross-section at the right presents the situation with excess pore pressures in the sand. Stability is obtained because the tunnel face pressure supports the triangle column ABCDEF.

It is clear that this support is less effective in the situation with excess pore pressure. As indicated in the figure, the net force to support the triangle is less. On the other hand, the excess pore pressure will also create a vertical gradient over the block CDEFGHIJ resulting in a reduction of the force from this block on the triangle.

To investigate the influence of the excess pore pressure on the stability, the analytical calculation methods as described by Anagnostou & Kovári (1994) and Jancsecz and Steiner (1994) has been adapted by Broere (2000) and as described in CUR/COB (2000). Both models showed comparable results, a

significant increase in the minimum allowable tunnel face pressure to achieve a stable front.

Numerical calculations (Bezuijen et al., 2001) have confirmed the results of these analytical calculations.

4 CONSEQUENCES FOR MAX. PRESSURE

The section above has dealt with the consequences for the face stability at minimum pressure. However, depending on the situation it is possible that the excess pore pressure influence the maximum allowable drilling pressure. An example of such a situation is discussed below.

In view of the excess pore pressures measured at the 2nd Heineoord tunnel it was decided to determine the possible risks of these excess pore pressures for another Dutch tunnelling project. The hypothesis that there might be a large risk involved arises from the geohydrological conditions in this polder area of Holland: relatively high piezometric levels compared to a low surface level. Calculations were made to check this in the design phase for a large tunnel project (14.9 m diameter) crossing a deep polder (Surface level = SL - 5 m; groundwater head average = SL - 3.5 m, maximum = SL - 3 m). The depth of the tunnel is shown in Figure 6. In the normal

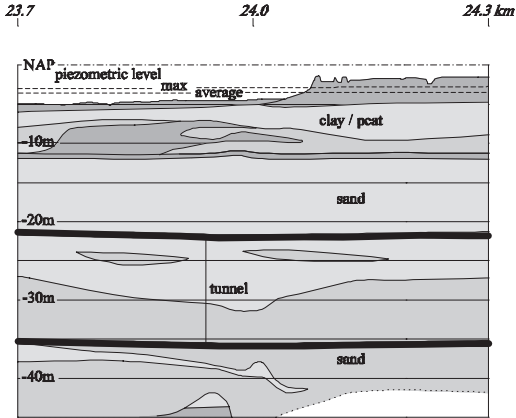


Figure 6. Geotechnical profile tunnel in polder.

situation the weight of the (semi)confining top soil layer, consisting of only 7 m of peat and soft clay, just equals the upward forces from the groundwater underneath. A surplus of water pressure can disturb this vulnerable equilibrium state (bursting of the top layer).

The minimum slurry pressures, which are needed for a stable tunnel face during drilling were for this situation calculated using the analytical model of Broere (2000). As minimum excess pore pressure in front of the cake a value of 28.3 kPa was determined (2.83 m surplus water head).

The slurry pressure can only be transmitted to the groundwater in the period that the slurry cake is cut from the soil face by the rotating cutting wheel of the TBM. As argued before, there will be no cake formation during drilling and drilling of one ring takes between 0.5 and 1.5 hours. However, the water pressure will not adapt directly to the slurry pressure during drilling due to the time dependent damping effect in the groundwater aquifer caused by the elastic storage capacity.

The groundwater effects just below the (semi)confining top were calculated with the finite difference groundwater program MODFLOW. The $10 \times 5 \text{ km}^2$ axial symmetrical model was multilayered (13 anisotropic model layers for the aquifer) and the input was: flow resistance top aquifer $c = 10000$ days, total transmissivity aquifer $kD = 1600 \text{ m}^2/\text{day}$, storage capacity $S = 1 \cdot 10^{-3}$ [-], anisotropy factor $kh/kv = 3$.

The calculated surplus water pressure depended on the duration of the drilling period as shown in Figure 7. The calculated extra water head below the confining layer is 1.05 m. The calculation results led to the conclusion that the stated hypothesis concerning bursting risk is true. Measures to overcome problems, e.g. by monitoring and adaptation of the drilling procedure or even hydrological solutions must be considered in this situation.

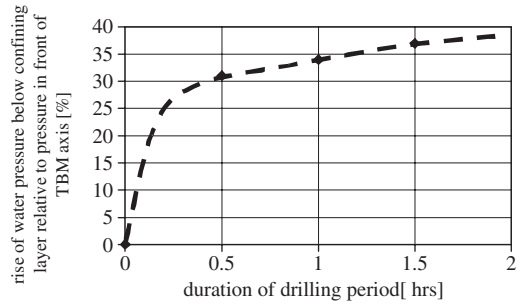


Figure 7. Calculated pressure build up when drilling starts.

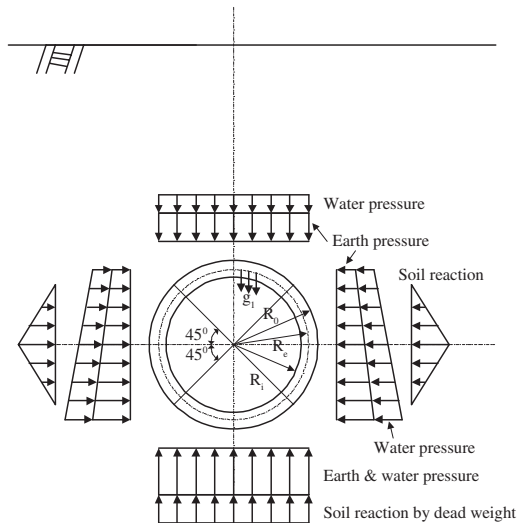


Figure 8. Conventional lining design method in Japan (from Hashimoto et al. 2004).

5 PORE PRESSURES AND GROUTING

5.1 Description

Grouting of the tail void is a critical process during the boring of a tunnel. It determines the loading on the lining of the tunnel and on the soil around the tunnel. Changing the grouting procedure can make the difference between a problematic and a successful project. Grout pressures to be applied are part of the regular design calculations for a tunnel project. Calculations are based on the stress distribution in the soil before the tunnelling starts, see for example Figure 8.

However, it was found that for a tunnel in sand the measured pressures around the lining at some rings from the TBM are close to the pore pressure (Bezuijen et al. 2003) and furthermore that the measured loading on the tunnel in sand is much lower than calculated, see Figure 9 (Hashimoto et al. 2004).

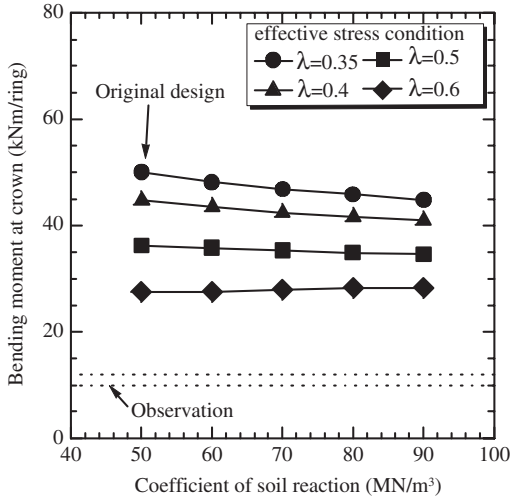


Figure 9. Discrepancy between design and calculation. The point to which the arrow points is the original design for a tunnel in sand. Changing of parameters does not result in a better fit.

To understand this behaviour it is necessary to look more into detail into the properties of the grout mortar. This mortar is injected as a liquid. As long as it is a liquid there will be no direct interaction between de soil and the tunnel lining. The average grout pressure will be determined by the pore pressure plus the grain stresses and the pressure distribution in the grout by the properties of the grout and the weight of the lining (Bezuijen et al. 2004).

Due to the excess pore pressure in the grout it will consolidate and loses its water to the soil around the tunnel. The speed of consolidation depends on the permeability of the grout in case the tunnel is bored in sand but on the permeability of the subsoil for a tunnel bored in less permeable subsoil as clay. This consolidation leads to a volume reduction of the grout and therefore also to a reduction of the effective stresses in the soil. A sandy soil will react very stiff to unloading and therefore a small reduction of the grout volume (a reduction of 5 to 10% of the grout volume was measured in consolidation tests), leads to a considerable reduction of the effective stresses in the sand and thus also to a reduction of the loading on the tunnel.

5.2 Measurements

5.2.1 Laboratory measurements

It is difficult to measure the consolidation of grout in a traditional oedometer test, because the consolidation is fast compared to the consolidation of clay or peat. Furthermore it is possible that there will be hardening of the grout during the consolidation process. Therefore consolidation experiments were performed

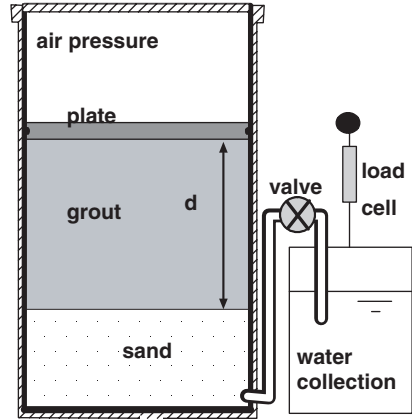


Figure 10. Measurement principle.

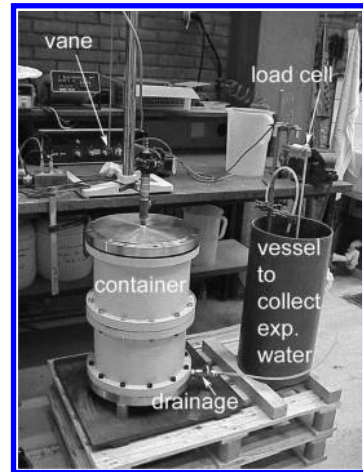


Figure 11. Experimental setup.

in a cylindrical cell with a diameter of 0.3 m in which a grout layer was made of 0.2 m, comparable to the average thickness of a grout layer in the tail void for tunnels with diameters in the range of 6 to 11 m.

The test set-up is shown in Figure 10 and Figure 11. The grout sample is loaded with air pressure to the desired pressure. The test measures the consolidation properties of the grout assuming relatively permeable subsoil and consolidation in one direction (water can flow into the soil not to the lining of the tunnel). The flow resistance of the sand is much lower than that of the grout. After several minutes of consolidation the sample was unloaded and the shear strength of the grout was measured at different locations in the grout.

An example of results of such a test is shown in Figure 12 and Figure 13. Figure 12 shows the amount of expelled pore water as a function of time and the applied pressure. In this test a pressure of 300 kPa was

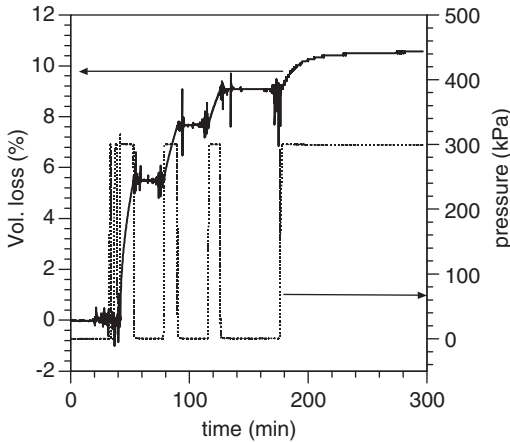


Figure 12. Test result: volume loss as a function of time and applied pressure.

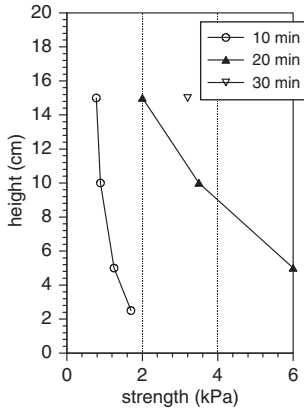


Figure 13. Strength development as measured with a vane.

applied. Pressure was relieved several times to be able to take the vane tests. Figure 13 shows the measured shear strength as a function of depth after for different times of applied pressure. In this test it was focussed on the lower values of the shear strength. Therefore only shear strengths up to 6 kPa were measured and presented in the plot.

The type of grout tested here was tested before at atmospheric pressure (Bezuijen et al. 2002). In that test it appeared that the measured shear strength remained more or less constant until 5.5 hours and after that time the hardening of the grout started.

Comparing the result from the test at atmospheric pressure with the results of the tests at 1–3 bar over pressure it became clear that the increase in strength in the over pressure case is caused by consolidation of the grout and not by the hardening of the grout. To

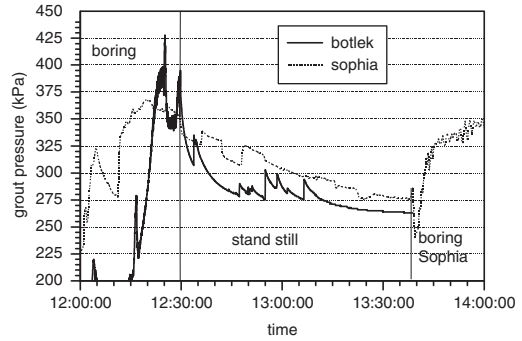


Figure 14. Grout pressure measured at the Botlek Rail tunnel and the Sophia Rail Tunnel. Data is shifted so that drilling stops at the same point (first ring after the instruments came out of the lining).

understand the grout properties just after injection in the tail void it is therefore necessary to understand consolidation. If the grout layer is consolidated, it will have certain strength to act as a foundation for the tunnel lining, even before hardening of the grout commences. If it is not consolidated it is possible that the shear strength is too low to counterbalance the buoyancy forces of the tunnel. Another important consequence of consolidation is an increase of flow resistance, which directly affects the pressure distribution behind the TBM when drilling.

Consolidation of grout, sometimes called bleeding, cannot be described by linear consolidation theory. It can be approximated assuming it behaves as a grain-water mixture with little strength until the water is expelled from the grout and there is an effective stress between the grains. A description is presented in Bezuijen & Talmon (2003).

5.2.2 Field tests

Grout pressures during injection and after injection were measured during tunnel projects in the Netherlands. Characteristic results are shown in Figure 14.

The grout pressure increases during drilling and decreases to values that are close to the pore pressure of water during stand still due to consolidation of the grout and decrease of the effective stress due to unloading of the soil.

The pressure distribution around the tunnel, measured on the lining appears to increase linearly with depth. However it is not a hydrostatic pressure distribution, see Figure 15. The gradient varies in time and decreases to values below the gradient of the pore water. This is caused by buoyancy forces exerted by the lining and the yield stress in the grout (Bezuijen et al. 2004).

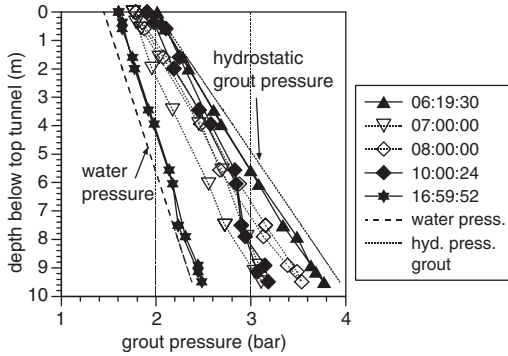


Figure 15. Measured grout pressure distribution at the Sophia Rail tunnel at various times. The pressure measured at 16:59:52 was measured several hours after boring has stopped.

6 CONCLUSIONS

It is shown that the measured excess pore water pressures in front of the tunnel face are mainly caused by the groundwater flow conditions much less influenced by the slurry properties. During stand still plastering occurs. The formulation for this plastering, presented in this paper, presents reasonable results, but needs the input of plastering experiments. The excess pore pressures during drilling have consequences for as well the minimum and maximum pressures that can be allowed at the tunnel face.

The average pressure on the lining due to grouting reduces to values close to the pore pressure several rings after the TBM for a tunnel made in sand. This is caused by the volume loss due to consolidation in the grout. The pressure gradient around the tunnel is determined by the buoyancy forces in the lining. Due to these mechanisms the resulting stress distribution around the lining can differ considerably from the results of traditional calculations.

More in general it can be said that ground water flow and the resulting pore pressures needs attention when drilling a tunnel below the water table.

ACKNOWLEDGMENT

HSL-Noord, COB, Delft Cluster.

REFERENCES

- Anagnostou G. & Kovári K. 1994. The face stability of Slurry-shield-driven Tunnels. *Tunnelling and Underground Space Technology*, Vol 9. No. 2. pp 165–174.
- Bakker K.J., Boer F. de, Kuiper J.C. Extensive independent research programs on 2nd Heineoord tunnel and Botlek Rail tunnel. *Proc. XII ECSMGE, Amsterdam*, 1999.
- Bezuijen A. 1997. Plastering and mud spurt during drilling (in Dutch). BTL-report 27.
- Bezuijen A., Pruiksmá J.P., Meerten H.H. van, 2001. Pore pressures in front of tunnel, measurements, calculations and consequences for stability of tunnel face. *Proc. Int. Symp. on Modern Tunneling Science and Techn. Kyoto*.
- Bezuijen A., Talmon A.M. 2003. Grout the foundation of a bored tunnel, 2003, *Proc ICOF 2003 Dundee*.
- Bezuijen A., Talmon A.M. 2004. Grout pressures around a tunnel lining, influence of grout consolidation and loading on lining. *Proc. ITA 2004, Singapore*.
- Bezuijen A., Talmon A.M. Kaalberg F.J. and R. Plugge, 2004. Field measurements on grout pressures during tunnelling, *Soils and Foundations vol, 44, No 1, 41–50, Feb*.
- Broere W., Tol A.F. van, 2000. Influence of infiltration and groundwater flow on Tunnel stability. *Proc. Int. Conf. on geotechnical aspects of underground construction in soft grounds*, eds. Kusakabe O. Fujita K and Niyazaki Y.
- CUR/COB 2000, Directive for the design of drilled tunnels for roads and tunnels. *final report commission L500* (in Dutch).
- Hashimoto T., Brinkman J., Konda T., Kano Y, Feddema, A., 2004. Simultaneous Backfill Grouting, Pressure Development in Construction Phase and in the Long-Term, *Proc. ITA 2004. Singapore*.
- Horn N. 1961. Horizontal Erddruck auf senkrechte Abschlussflächen von Tunnelröhen. *Landeskonferenz der Ungarischen Tiefbauindustrie*. pp. 7–16.
- Huisman M. 1998. Static plastering, Theory and experiments, *BTL-report 34, WL | Delft Hydraulics J1384* (in Dutch)
- Jancsecz, S. Steiner, W., 1994. Face support for a large Mix-shield in heterogeneous ground conditions, *Tunneling '94*, 531–550.